DCT 204

An Investigation of Continuous Compaction Control Systems

By

CHRISTOPHER MEEHAN
FARAZ SADEGHI TEHRANI

Department of Civil and Environmental Engineering
College of Engineering
University of Delaware

July 2009

Delaware Center for Transportation
University of Delaware
355 DuPont Hall
Newark, Delaware 19716
(302) 831-1446

The Delaware Center for Transportation is a university-wide multi-disciplinary research unit reporting to the Chair of the Department of Civil and Environmental Engineering, and is co-sponsored by the University of Delaware and the Delaware Department of Transportation.

DCT Staff

Ardeshir Faghri
Director

Jerome Lewis
Associate Director

Ellen Pletz
Assistant to the Director

Lawrence Klepner
T^2 Program Coordinator

Matheu Carter
T^2 Engineer

Sandra Wolfe
Senior Secretary

DCT Policy Council

Natalie Barnhart, Co-Chair
Chief Engineer, Delaware Department of Transportation

Michael Chajes, Co-Chair
Dean, College of Engineering

Delaware General Assembly Member
Chair, Senate Highways & Transportation Committee

Delaware General Assembly Member
Chair, House of Representatives Transportation/Land Use & Infrastructure Committee

Michael Gamel-McCormick
Dean, College of Education and Public Policy

Harry Shenton
Chair, Civil and Environmental Engineering

Ralph Reeb
Director of Planning, Delaware Department of Transportation

Stephen Kingsberry
Director, Delaware Transit Corporation

Shannon Marchman
Representative of the Director of the Delaware Development Office

James Johnson
Executive Director, Delaware River & Bay Authority

William Osborne
Executive Director, Transportation Management Association

Delaware Center for Transportation
University of Delaware
Newark, DE 19716
(302) 831-1446

TABLE OF CONTENTS

Appendix

LIST OF TABLES

LIST OF FIGURES

ABSTRACT

Continuous Compaction Control (CCC) systems have demonstrated great promise for improving the efficiency of field compaction and revolutionizing the compaction control process. To evaluate the effectiveness and reliability of CCC systems in the State of Delaware, a field study was performed on a local soil (a poorly graded sand with silt), with compaction being performed using an MDP-CMV equipped compactor. A variety of in-situ test methods that are currently used for compaction control were also performed as compaction progressed in the study, for purposes of comparison with the CCC results. Comprehensive analyses were performed on the data obtained from the field study using various statistical techniques.

As a first step, basic statistical analysis was performed on the recorded in-situ testing values. In general, it was concluded that there was significant scatter in the measured in-situ test results, which made it difficult to make a precise judgment on the quality of compaction. However, based on the dry unit weights measured by the nuclear density gauge (NDG), the quality of compaction was determined to be in an acceptable range, according to current DelDOT specifications. In addition, the measured water contents indicated that in general the compaction was performed on the dry side of the optimum moisture content.

Statistical analysis of the CCC roller data illustrated a promising trend for MDP and CMV values as the compaction progressed: MDP values decreased and

CMV values increased as the number of passes increased. It was also realized that MDP values contained less variability than simultaneously recorded CMV values.

The ordinary kriging method was employed to determine the magnitude of CCC values at the same locations as the in-situ tests that were conducted. Comprehensive analysis of different models showed the appropriateness of the Rational Quadratic model for predicting the MDP values and the Exponential, Spherical, and Linear models for predicating the CMV values. Maximum lags of ~ 1.5 m (3.0 ft) and ~ 3.0 m (10 ft) were also selected as the optimum lag distances for kriging the roller data.

Univariate regression techniques were applied to the in-situ data and kriged CCC values to identify possible relationships between the data sets. It was discovered that point-by-point comparisons did not yield strong relationships between the data. However, taking the average values of each lift and pass into consideration in the regression analyses yielded much stronger correlations between the in-situ testing values and the kriged CCC data. MDP values showed stronger correlations with in-situ testing data than did CMV values. The GeoGauge did not yield strong correlations with CCC values. Strong correlations were also identified between the CCC and in-situ testing values versus the water content of the compacted soil. Therefore, it was decided to include the effect of water content in the analysis using multiple regression methods. The results showed a great improvement in the relationship between average kriged CCC values and corresponding in-situ testing data, which confirmed the effect of water content on the measured CCC and in-situ testing values.

Chapter 1

INTRODUCTION

Recent technological advances for real time monitoring and control of compaction field equipment during construction show significant promise for improving how soils and asphalts are compacted. Implementation of Continuous Compaction Control (CCC) systems and Intelligent Compaction (IC) systems can revolutionize how soils and asphalts are compacted in the field, improving the quality of compaction and the long-term performance of roadways and other geotechnical structures while reducing the need for continuous technician monitoring during compaction. Although true Intelligent Compaction systems are only in their early stages of technological development, Continuous Compaction Control systems have been widely used in Europe throughout the 1990's and have been studied by some state DOT's in the United States in more recent years.

Successful adoption of CCC technology requires careful calibration, validation, and demonstration of utility with commonly used soils. There is a need to calibrate this technology for local soils in the state of Delaware, a need to demonstrate the utility of this technology to local contractors to ensure that it is successfully adopted, and a need to show engineers at the Delaware Department of Transportation (DelDOT) the improvements in compaction monitoring and construction quality that can result when this technology is used. To address all these demands, a DelDOT-sponsored research project was begun at the University of Delaware in the fall of 2007. In the first phase of this project, a comprehensive literature review was performed to assess the current "state of practice" and "state of the art" with respect to IC and CCC system technologies and performance. In the second phase of this project, a five-day field study was planned and performed utilizing a roller-integrated CCC system in conjunction with a number of in-situ compaction quality control methods, in order to evaluate the effectiveness of two CCC technologies (MDP and CMV) for use with compaction of local soils. In the third phase of the study, the recorded CCC values and measured in-situ test results were statistically compared to assess the abilities of the CCC system for performing quality control of the compaction process with respect to the abilities of other currently employed in situ quality control methods.

The goal of this thesis is to present the results from the aforementioned research project, providing a detailed description of the activities that were performed from the beginning to the end of this project. In Chapter 2, a summary of the most pertinent literature that was reviewed will be presented. In Chapter 3, the Delaware field study that was performed will be explained in detail. Preliminary evaluations of the measured in-situ test data and recorded CCC values will be described in Chapter 4 and Chapter 5, respectively. Chapter 6 will focus on the use of kriging methods for robust statistical interpolation between measured CCC data points. In Chapter 7 and Chapter 8, regression analysis techniques will be introduced to investigate and identify potential relationships between in-situ test measurements and the corresponding CCC values. Finally, Chapter 9 will present the most significant conclusions from this research, and will provide recommendations for future research in this area.

Chapter 2

LITERATURE REVIEW

2.1 Compaction

Compaction is a process where mechanical energy is applied to particle mixtures, to densify the material by minimizing the air voids that are present (Holtz and Kovacs 1981). In civil engineering, a wide variety of particle mixtures such as soil, asphaltic concrete, or recycled material mixtures (such as reclaimed concrete, crushed glass, shredded or ground tires, etc.) are commonly used in the construction of many large structures, due to their relatively low unit cost as a building material and/or their widespread availability. In all of these cases, proper compaction improves the engineering properties of the compacted material.

The focus of the literature review in this chapter will be on the compaction of soil for use as a civil engineering construction material. However, many of the concepts and principles discussed will have equal applicability to other types of particle mixtures that are used in civil engineering construction. In general, there are several improvements to the engineering performance of a soil that can be achieved through compaction:

- Detrimental settlements can be reduced or prevented.
- Soil strength can be increased.
- Bearing capacity of pavement subgrades can be improved.

- Undesirable volume changes caused by swelling and shrinkage can be controlled.

The most frequently used method for compaction of medium- to large-area soil fills or engineered earth structures is roller compaction (Figure 2.1a and 2.1b). Small hand compactors such as walk-behind compactors (Figure 2.1c) and jumping-jack tampers (Figure 2.1d) are more common for small-area fills or detail work on large projects (such as compaction around pipes or other existing utilities, near retaining wall faces, etc.).

Figure 2.1 Different types of compactors: a) Pad-foot or tamping-foot roller, b) Smooth-drum vibratory roller, c) Walk-behind vibratory compactor, and d) Jumping-jack tamper

There are various parameters that determine the compactibility of different soils and the appropriate type of roller that will work best for compaction of a given soil. The primary soil factors that contribute are (Adam and Kopf 2004):

- Soil grain size distribution, maximum grain size, grain shape and degree of non-uniformity
- Soil moisture content
- Permeability of soil (both water and air permeability can affect the process)

The primary compaction machine parameters that contribute are (Adam and Kopf 2004):

- Total weight of roller and static drum load in static and dynamic compaction
- The following parameters in dynamic compaction:
  - Direction of resulting dynamic contact force
  - Excitation frequency
  - Theoretical drum amplitude
- Surface shape and diameter of drum

2.2 Fundamentals of Vibration Theory

Before proceeding to the main portion of this literature review, it is timely to define some basic concepts in vibration theory. This will make future discussion of vibratory soil compaction processes clearer.

Frequency (*f*, Hz) is the number of occurrences of a repeating event per unit time.

Angular frequency (ω, rad/s) is defined as the rate of change in the orientation angle during rotation (Equation 1):

$$\omega = 2\pi f \tag{2.1}$$

Period (T, s) is the duration of one cycle of a repeating event. The period is the reciprocal of the frequency.

Phase (ϕ, radians) of an oscillation or wave is the fraction of a complete cycle corresponding to an offset in the displacement from a specified reference point at time t = 0.

The **Harmonic** of a wave is a component frequency of the signal that is an integer multiple of the fundamental frequency. For example, if the fundamental frequency is f, the harmonics have frequencies f, $2f$, $3f$, $4f$, etc. The harmonics have the property that they are all periodic at the fundamental frequency, therefore the sum of harmonics is also periodic at that frequency. Harmonic frequencies are equally spaced by the width of the fundamental frequency and can be found by repeatedly adding that frequency. For instance, if the fundamental frequency is 25 Hz, the frequencies of the harmonics are: 25 Hz, 50 Hz, 75 Hz, 100 Hz, etc.

Subharmonic frequencies are frequencies below the fundamental frequency of an oscillation at a ratio of $1/x$. For example, if the fundamental frequency of an oscillator is 440 Hz, sub-harmonics include 220 Hz (1/2) and 110 Hz (1/4).

Amplitude (mm) is the magnitude of change in the oscillating variable, with each oscillation, within an oscillating system.

2.3 Compaction Methods

Static compaction, kneading compaction and dynamic compaction are the three general techniques that are used for soil compaction (Holtz and Kovacs 1981). There are also a number of other compaction techniques that fall under the subheading of dynamic compaction, such as vibratory compaction, oscillatory compaction and Vario compaction, which are explained in more detail in the following sections.

2.3.1 Static compaction

During static compaction, the weight of a compactor is distributed over a designated contact area, applying a static pressure to a particular surface. Figure 2.2 shows an example of a typical static compactor.

Figure 2.2 Pneumatic rubber-tired static roller compacting a clay soil (From Boulanger 2002)

The compaction process is primarily driven by the contact pressure of the roller, as it is this applied pressure that presses soil particles together, effectively reducing the volume of voids in the soil. Adequate compaction by static rollers is normally achieved only in the upper layers of a compacted material, as the effect of static compaction is typically limited to low depths (Adam and Kopf 2004). Suitable materials for static compaction include fine-grained soils such as silty and clayey soils and bituminous materials like asphalt (Adam and Kopf 1998).

2.3.2 Kneading compaction

In the case of cohesive materials, pressures applied using static compaction may cause rapid buildup of excess pore water pressure without allowing rapid pore pressure drainage or dissipation. This "undrained" response to loading often makes it quite difficult to reduce the volume of air voids in a soil, resulting in inadequate soil compaction. To overcome this limitation, a technique known as "kneading compaction" is employed, through which the compactor kneads and remolds compacted materials to enhance the removal of the air-voids to achieve the appropriate densification. Pad-foot drum rollers, polygonal drum rollers, and sheepsfooted compactors are classified in this category (Adam and Kopf 2004). Figure 2.1.a, provided earlier, shows an example of a pad-foot roller. The materials most suitable for kneading compaction are cohesive fine-grained soils such as clayey soils (Adam and Kopf 1998).

2.3.3 Dynamic compaction

Dynamic compaction is a technique used to compact granular materials such as sandy and gravelly soils by applying a periodic dynamic impact. Using this approach, a dynamically excited drum delivers a rapid succession of impacts to the underlying surface, where the resulting compression waves and shear waves are transmitted through the material to set the particles in motion. This periodic excitation reduces the effect of internal soil friction by changing the nature of particle to particle contacts within the soil mass, facilitating the rearrangement of individual soil particles into a tighter, more stable particle arrangement (corresponding to a lower void ratio and higher density). The resulting increase in the number of contact points and planes between the grains leads to higher stability, and lower long-term settlement behavior (Adam and Kopf 2004). Vibratory compaction and oscillatory compaction are two types of dynamic compaction (Adam and Kopf 1998). Recently, a Vario roller has also been introduced by Bomag, which is an alternative for vibratory and oscillatory rollers (Brandl and Adam 2004).

2.3.3.1 Vibratory compaction

The drum of a vibratory roller is excited by rotating an eccentric mass along a shaft on the drum axis (Figure 2.3). The rotating mass sets the drum in a circular translatoric motion, i.e. the direction of the resulting force corresponds with the position of the eccentric mass. Compaction is achieved mainly by transmitted compression waves in combination with the effective static drum load. Consequently, the maximum resulting compaction force is almost vertical with a slight inclination (Brandl and Adam 2004).

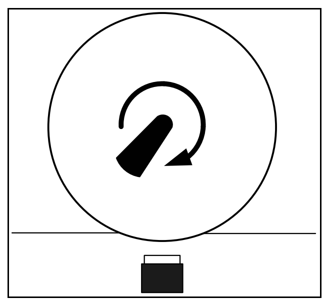

Figure 2.3 Excitation of vibratory roller drum and dynamic compaction effect (compression) (modified from Brandl and Adam 2004)

The most significant parameters in vibratory compaction are the total weight of the roller drum, the excitation frequency, and the theoretical amplitude of the drum. Modern rollers are usually equipped with two vibratory frequencies commonly referred to as the "low" and "high" frequencies, and two amplitudes, commonly referred to as the "small" and "large" amplitudes. The speed of the roller during compaction usually ranges between 2 to 6 km/h (~ 1.5 to 4 mph), and is another parameter affecting the quality of the compaction (Brandl and Adam 2004).

2.3.3.2 Oscillatory compaction

In some cases, vibratory rollers are so powerful that, during compaction, soil or asphaltic mix aggregates are fractured, the asphalt mat cracks (for compaction of asphaltic concrete), and/or damage to nearby buildings and underground utilities occurs. To resolve this issue, oscillatory compaction has been introduced (Figure 2.4). In oscillatory compaction, the drum of the roller oscillates horizontally (parallel to the surface that is being compacted). The applied horizontal oscillation is caused by two opposite rotating eccentric masses, whose shafts are arranged on opposite sides of the axis of the drum. The resulting motion of the roller causes the soil to be dynamically loaded in a horizontal direction, in addition to the vertical static load that is applied by the dead weight of the drum and the contributing roller frame. These cyclic and dynamic horizontal forces result in additional soil shear deformation; dynamic compaction is achieved mainly by transmitted shear waves. Investigations have revealed that oscillatory rollers operate in two conditions depending on roller and soil parameters. If the applied force exceeds the friction force (including the adhesion) at the soil-drum interface, the drum starts slipping. During slipping the compaction effect is reduced; however, the surface is “sealed” by this slip motion. Consequently, oscillatory rollers are mainly employed for asphalt compaction. Oscillatory rollers are also often used in the vicinity of sensitive structures, because the emitted vibrations are significantly lower than those of traditional vibratory rollers (Thurner and Sandström 2000, Brandl and Adam 2004).

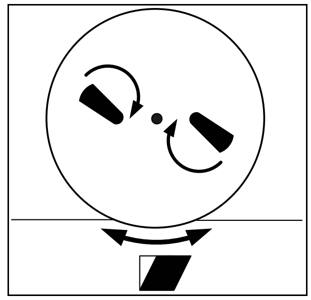

Figure 2.4 Excitation of oscillatory roller drum and dynamic compaction effect (shearing) (modified from Brandl and Adam 2004)

2.3.3.3 Vario roller

The Vario roller was developed by Bomag Americas, Inc (Bomag) in the late 1990's. In a Vario roller system two counter-rotating exciter masses which are concentrically shafted on the axis of the drum cause a directed vibration. The direction of the excitation can be adjusted by turning the complete exciter unit in order to optimize the compaction effect for the corresponding soil type (Figure 2.5). If the exciter direction is vertical or horizontal, the compaction effect of the Vario roller can be compared with that of vibratory or oscillatory roller, respectively. Therefore, Vario rollers can be used as a substitute for vibratory and oscillatory compactors (Brandl and Adam 2004).

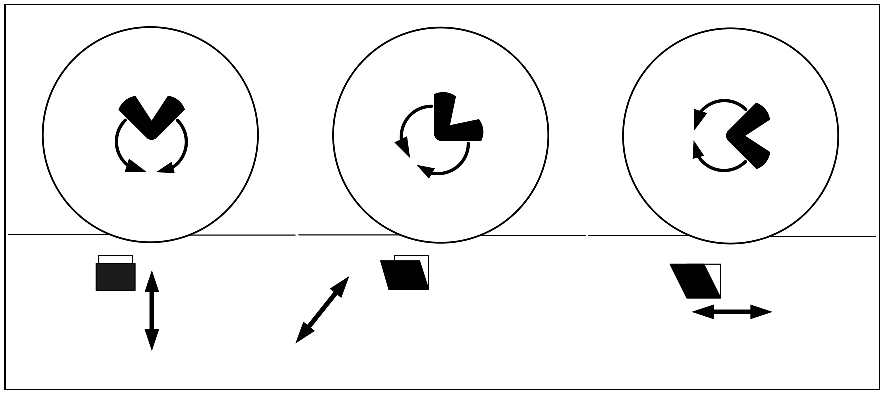

Figure 2.5 Adjustable excitation direction of a Vario roller drum and specific compaction effect (modified from Brandl and Adam 2004)

The Vario roller has another advantage over conventional vibratory compaction equipment, which is that it has been proved that vertically directed force is more effective in increasing the density in deeper layers (Figure 2.5.a) compared to the conventional radially vibrating roller, which generates vibration by means of a single, eccentrically-weighted, rotating horizontal shaft located inside the roller drum, as shown in Figure 2.3 (Uchiyama et al. 1998). After Vario compaction in the vertically-directed mode, the dry density in deeper layers of the soil and the CBR (California Bearing Ratio) are found to be higher than those for soil compacted using a traditional radially vibrating roller. The hypothesis used to explain this observation is that the radially directed force amplifies the kneading action between the drum and soil, generating a hard surface shell layer incapable of transferring the compacting force into deeper layers, while the vertically directed forces with less kneading action can influence the deeper layers and compact the whole soil layer efficiently (Uchiyama et al. 1998).

Deep dynamic compaction is another ground improvement technique that is used to improve soil; this technique is typically not used as part of the placement process for an engineered fill, and is consequently neglected here since it is out of the scope of this literature review.

2.4 Quality Control and Quality Assurance Methods

The most common approach to quality control in road construction is to carry out a series of periodic in-situ tests (Briaud and Seo 2003). Evaluation of the quality of the compaction is based on the engineering properties of the compacted soil including strength and density.

The most common density-based quality control methods consist of measurements of in situ density and moisture content using the nuclear density gauge, sand cone equivalent test, and water balloon method. Recently, some other density-based methods have been added to this list, most notably the electrical density gauge (EDG) and time domain reflectometer (TDR), which rely on correlations between electrical properties of the soil and in situ density and moisture content.

The most common strength-based methods attempt to generate representative measurements of the in-situ modulus or stiffness of the soil. The elastic modulus E [FL^{-2}] is defined as the quotient of stress to strain in the elastic part of the stress-strain curve of a material. The stiffness k [FL^{-1}] is defined as the ratio of the force applied on a boundary through a loading area divided by the displacement experienced by the loaded area. The elastic modulus is a fundamental soil property, while the stiffness is affected by both the soil response and the test approach that is used, as it depends on the size of the loaded area. Therefore, for an elastic material, the stiffness measured with one test will be different from the stiffness measured with another test if the loading areas are different (Briaud and Seo 2003). The most commonly utilized strength-based in-situ test methods are the: plate load test (PLT), falling weight deflectometer (FWD), light weight deflectometer (LWD), dynamic cone penetrometer (DCP), Clegg-impact hammer, and soil stiffness gauge or GeoGauge (Mooney and Rinehart 2007).

In addition to the methods mentioned above, many state DOTs use static proof-rolling as another technique for quality assurance and final acceptance of earthwork compaction. Using this approach, a heavy truck (e.g., loaded water truck or dump truck) is driven at walking speed along the alignment. Quality assurance agents walk alongside the truck looking for signs of inadequate compaction such as cracking and excessive settlement. Problematic areas are identified and reworked until the acceptance criteria are met. Vibratory compaction has been proven to be a more effective proof rolling technique than static proof rolling, as it has an easier time identifying potentially weak zones (Mooney and Rinehart 2007).

2.5 Limitations of the Conventional Methods

The current state-of-practice for compaction quality assurance and/or quality control (QA/QC) relies primarily on process control (lift thickness and number of passes) or end-result in-situ testing techniques to ensure that adequate compaction and proper moisture control has been achieved (White et al. 2005).

Traditionally, compaction has been carried out by means of a 5-15 ton roller running over a fixed number of passes (5-10 passes) per layer, often resulting in relatively non-uniform compaction (Thurner 1993). For vibratory rollers, during this process their vibration frequency and amplitude are kept constant while the roller operator controls the roller's speed (Thurner and Sandström 2000, Sandström and

Pettersson 2004). The degree of non-uniformity in the engineering properties of a compacted soil lift is therefore dependent on a combination of roller parameters (e.g. linear load, vibration frequency, vibration amplitude and roller speed) and on soil parameters (e.g. layer material, layer thickness and characteristics of the soil beneath the lift that is being compacted). This non-uniformity will cause differential settlements in the final construction (Thurner 1993).

The in-situ testing techniques mentioned in Section 2.4 provide only moderately accurate measurements of the properties of the compacted material (Thurner and Sandström 1980). The relatively local area of test influence and the limited effective depth of these control methods (20-60 cm (0.6-2.0 ft)) are not sufficient enough to represent the real volume of compacted soil (Adam 1997, Thurner and Sandström 2000). Therefore, it is not possible to detect all weak zones in the compacted area using the traditional techniques. This may lead to non-uniform compaction, followed by differential settlement, low bearing capacity and some cracks in the final construction (Adam 1997). In addition, the in situ methods discussed above are somewhat time consuming and can be relatively expensive (Thurner and Sandström 1980, Adam 1997).

2.6 Continuous Compaction Control and Intelligent Compaction

Continuous compaction control systems (CCC) and intelligent compaction (IC) were introduced to the compaction industry in an attempt to address the limitations of commonly used in situ QA/QC tests stated above, In this portion of the literature review, the history and evolution of CCC and IC systems is presented followed by a detailed description of different systems used in the new technology as well as the theoretical background of different CCC/IC systems.

2.6.1 Background

The first attempts to measure, record, and monitor vibration-integrated measurements during compaction were performed with vibratory plates in the 1930s (Mooney and Adam, 2007). Initial research development of roller integrated measurements occurred in 1974 when Dr. Heinz Thurner of the Swedish Highway Administration performed field studies with a 5-ton tractor-drawn Dynapac vibratory roller instrumented with an accelerometer (Thurner and Sandström 2000). A miniature roller that travelled behind the compacting roller was used to record vibrations in the area surrounding the large roller. Additionally, triaxial geophones were buried in the ground in order to measure ground vibrations. Simultaneous recordings from all sensors were analyzed and it was realized that the accelerometer on the roller recorded significant changes in the time history of the sensor signal (Thurner and Sandström 2000). These tests indicated that the ratio between the amplitude of the first harmonic of the recorded acceleration and the amplitude of the excitation frequency could be correlated to the compaction effort and the stiffness of the soil measured by the static plate load test. In 1975, Dr. Thurner founded the Geodynamik Company with partner Åke Sandström to continue development of the roller-mounted compaction meter. In cooperation with Dr. Lars Forssblad from Dynapac, Geodynamik developed and introduced the compaction meter and the compaction meter value (*CMV*) in 1978. The *CMV* is described in more detail in section 2.8. This new approach to compaction monitoring was introduced at the "First International Conference on Compaction" held in Paris, France in 1980 (Thurner and Sandström 1980, Forssblad 1980). Subsequently, many of the roller manufacturers (e.g., Caterpillar, Ingersoll Rand, and Sakai) adopted the Geodynamik *CMV*-based system for further research and installation on their construction equipment (Mooney and Adam 2007).

In the late 1980s, Bomag developed the OMEGA value and corresponding Terrameter. The OMEGA value provided a continuous measurement of compaction energy, and at the time served as the only CCC alternative to *CMV*. In the late 1990s, Bomag then developed a measurement value E_{vib}, which provides a measure of dynamic soil modulus (e.g., Kröber et al. 2001). Ammann followed suit with the development of a soil stiffness parameter k_s (Anderegg and Kauffmann 2004). These E_{vib} and k_s parameters signaled an important evolution towards the measurement of more mechanistic soil properties, e.g., soil stiffness and modulus (Mooney and Adam 2007). In the early 2000's, Caterpillar developed an alternative CCC system based around machine drive power (MDP) consumption, which provided a means for assessing the effectiveness of compaction in fine-grained materials – soils where vibratory compaction is traditionally not that effective.

To enhance the field application of CCC technology, Geodynamik developed a compaction documentation system (CDS) in 1989, which was intended to help the driver to optimize the compaction process, assist the contractor in a quality pre-test, and document compaction results (Thurner 1993).

In the 1990s, vibratory roller technology became much more sophisticated when Bomag introduced the Vario control roller with counter-rotating eccentric masses and servo-hydraulic control of the vertical centrifugal force (see Figure 2.5). Likewise, Ammann introduced the Ammann Compaction Expert (ACE) roller with servo-hydraulic two-piece eccentric mass and frequency control (Figure 2.6). Other manufacturers such as Caterpillar and Dynapac followed suit (Mooney and Adam 2007).

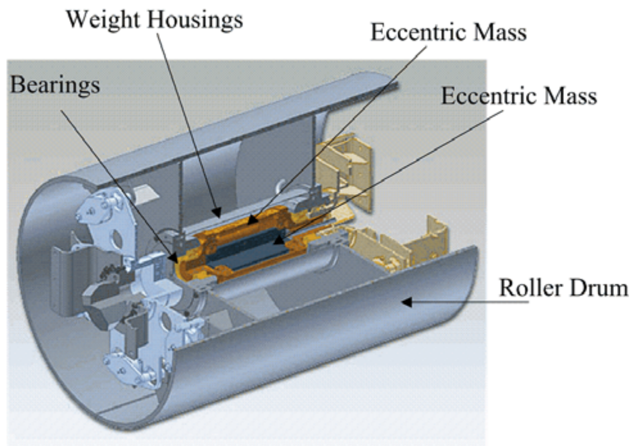

Figure 2.6 Ammann two-piece eccentric mass assembly and variable control of eccentric force amplitude and frequency (modified from Ammann brochure)

The introduction of servo-controlled vibratory drum technology has catalyzed a new initiative termed intelligent compaction, where the vibratory force amplitude and/or frequency are automatically adjusted to improve roller performance and compaction. The first prototype of a GEODYNAMIK "Intelligent Compaction Machine, ICM" was on display in 1992 (Sandström and Pettersson 2004). In the following years afterwards, development has continued but a product has not been made broadly available to the construction community (Sandström and Pettersson 2004). Currently, the so-called "intelligence" of available intelligent compaction equipment is limited. Most rollers can now automatically decrease the vertical vibration force when a jumping (double jump) mode is sensed (see section 2.7).

Furthermore, some rollers (e.g., Bomag, Ammann) have the ability to automatically reduce the eccentric force amplitude when a user-defined threshold measurement value has been reached. In a broader sense however, it can be stated that intelligent compaction is in its early stages and considerable advances are anticipated towards achieving truly intelligent compaction over the next decade (Mooney and Adam 2007).

2.6.2 Description of CCC/IC Technology

The primary purpose of continuous compaction control and intelligent compaction systems is to enhance the final quality of the compacted material. Quality in compaction of unbound soil layers means achievement of both uniform compaction and sufficient bearing capacity. Efficient compaction requires compaction to be concentrated in areas where further compaction is useful (where there is the potential to further increase the bearing capacity). Efficient compaction reduces the overall compaction time for a given lift of soil, while effectively avoiding under-compaction (which causes a higher risk of settlement problems) as well as overcompaction (which wastes time and has the tendency to crush aggregates) (Thurner 1993). "Ideal" compaction on a given project can be characterized by the following factors (Brandl and Adam 2004):

- Compaction optimization
- Compaction documentation, which is essential not only for site acceptance but also for quality control and long-term risk assessment.
- Compaction control

2.6.2.1 Definition of CCC and IC systems

Continuous Compaction Control (CCC) systems are data acquisition systems installed on compaction equipment that continuously collect real-time information about the operation and performance of the compactor (Thurner and Sandström 1980, Adam 1997, Adam and Brandl 2003). For vibratory compactors (see Sections 2.8.1 to 2.8.5), the data that is often collected includes the vibratory frequency, the amplitude of the roller drum, and the speed of the roller (Adam 1997). For machine drive power based systems (see 2.8.7), the engine gross power of the compacting roller is typically recorded, in addition to other properties such as roller speed, roller acceleration, and the slope angle (White et al. 2005).

Intelligent Compaction (IC) is a machine-driven process whereby CCC data is interpreted and used in real-time to adjust the operation of the compactor in an attempt to optimize the compaction process and to achieve more uniform soil compaction (Adam and Brandl 2003, Anderegg et al. 2006). As an example of this process, on a typical granular-soil compaction project, IC optimization begins by compacting the soil using high amplitude and low frequency vibratory energy for the initial compactor passes, which encourages effective compaction of the layer to deeper depths. As the compaction progresses, in order to avoid crushing soil aggregates and to encourage compaction of more surficial soil layers, the IC system raises the excitation frequency and decreases the amplitude automatically using a machine feed back loop in conjunction with the CCC system (Anderegg and Kaufmann 2004).

2.6.2.2 Different parts of a CCC system

As mentioned in 2.6.1, CCC systems were initially developed for vibratory rollers. A vibratory CCC system is composed of three fundamental elements: the vibratory roller, the underlying material that is being compacted, and a data recording system. In addition, a real-time global positioning system (GPS) is essential for identifying the locations of the recorded data points that are measured by the CCC system.

2.6.2.2.1 Roller

The roller itself is the integral measuring tool in a CCC/IC system. There are various parameters in vibratory rollers that are used to measure the degree of compaction such as excitation frequency, drum amplitude, the weight ratio between the effective weight of the frame and drum, and the speed of the roller (Adam 1997).

As mentioned in 2.2, amplitude is a nonnegative scalar measure of the magnitude of oscillation. The amplitude of the roller is dictated by the position of the eccentric masses inside the roller (Camargo et al. 2006). Adjustment of the amplitude is performed via an eccentric shaft and a tube mounted coaxially in relation to the shaft, each producing half of the centrifugal force. The die relative position of these two components to one another is continuously adjustable by means of a differential gear so that any desired eccentricity of the unbalanced mass ($m_e r_e$) between 0 and the maximum can be obtained (Anderegg and Kaufmann 2004). When the weights are 180° opposite each other, amplitude is at the minimum and if the weights are aligned with each other, amplitude is at the maximum (White et al. 2008).

Frequency is the number of oscillations per unit time. The frequency of the drum can be adjusted to optimize compaction of a specific soil type. The continuous variation of the frequency is achieved by changing the pivoting angle of the vibropump (Anderegg and Kaufmann 2004). Matching the frequency of the drum with that of the underlying soil increases the efficiency of compaction (Anderegg and

Kaufmann, 2004). However, others believe that altering drum frequency may lead to increased maintenance and a reduced operational life for the roller (Camargo et al. 2006).

The speed of the roller dictates how much energy, per unit length of soil, is delivered to the underlying soil layer (Camargo et al. 2006). It should be constant during compaction to give the best results. As an example, a higher *CMV* is obtained by driving at a lower speed (Forssblad 1980).

The travel direction of the roller also influences the roller measurements. In some cases, a higher degree of compaction is achieved via reverse direction (driving the roller backwards) rather than forward direction, because the transmission of the dynamic compactive force to the soil occurs at a more favorable angle to the soil surface (Forssblad 1980).

2.6.2.2.2 Material

The type of material that is being compacted plays a key role in the efficiency of the compaction process. In general, there are three broad categories of soil, which are compacted using different approaches. In cohesionless soils, dynamic compaction is generally the most effective approach to achieving efficient, acceptable compaction. Cohesive soils should be compacted using tamping foot, pad foot, or sheepsfooted static rollers, since dynamic compaction of cohesive soils typically causes buildup of excessive pore water pressure and subsequently poor compaction. In stabilized soils, shrinkage is problematic which causes large cracks in the road pavement; consequently, these soils should not be subjected to heavy compaction, and are best compacted using pad-footed compactors (Chang et al. 2009). CCC can find those cracks and prevent damages in the upper layers (Adam 1997).

The best materials for compaction using vibratory CCC technology are well graded coarse-grained soils consisting of primarily sands and gravels (Adam 1997). Poorly graded sands and gravels also work relatively well. The compaction of coarse-grained soils containing a larger proportion of fine grains, such as silty sands or clayey sands, does not work as well, as the compaction process is strongly influenced by the water that is present in the soil voids. For these soils, if the moisture content varies in the neighborhood of the optimum moisture content, CCC can play an effective role in the compaction process. As an example, in fine-grained materials, the *CMV* decreases when the water content exceeds the optimum water content (Forssblad, 1980). Vibratory CCC approaches generally do not work well for heavily cohesive soils like silts or clays, unless CCC is performed at moisture contents close to the plastic limit of the soil; the same issue noted above with respect to the undrained soil response is present in an even stronger fashion for these soils (Adam and Kopf 1998).

In terms of lift thickness, research has shown that thicker lifts of material can be more efficiently compacted using CCC/IC technology (McVay and Ko 2005; Camargo et al. 2006).

2.6.2.2.3 Recording System

Early research into CCC systems showed that various indices incorporating drum acceleration amplitude and the amplitude of its harmonics (i.e., multiples of the excitation frequency) could be correlated to soil density and underlying stiffness (Forssblad 1980). This approach forms the basis of many onboard compaction “meters” used today (Thurner and Sandstöm 2000, Sandstöm and

Pettersson 2004, Mooney and Rinehart 2007). Various recording systems are comprehensively presented in section 2.8.

2.6.2.2.4 Global Positioning System (GPS)

If measurements made by an IC/CCC roller are linked to the corresponding measurement point coordinates (and associated time stamps) supplied by the GPS system, the compaction process can be recorded and presented in a graphical form in real time (Anderegg et al. 2006). Typical GPS set ups consist of a external reference station (commonly referred to as the "base station") which includes real-time kinematic GPS (RTK-GPS), a GPS-antenna and a radio modem transmitter (Figure 2.7a). The system also utilizes a mobile data recording and analysis station that is attached to the roller, which includes on-board RTK-GPS, a GPS-antenna, a radio modem transmitter and a computer (Figure 2.7b). The third part of the GPS system is a visual monitoring station, which consists of a computer with a radio modem receiver (Figure 2.7c).

Figure 2.7 GPS system; a) base station, b) GPS equipped roller, c) monitoring station

The “base station” GPS receiver, which must be located relatively close to the area that is being compacted, is often referenced to a global coordinate system for projects that necessitate precise positioning controls. Positioning errors accumulate between the ground-based GPS receivers and the satellites, which have to be corrected in order to display precise location coordinates in real time (the RTK portion of the GPS). These correction messages are sent to the GPS in the mobile stations by a radio modem transmitter to correct its position. A computer fixed on the operator’s console displays the travel locus of the roller or the number of passes, and records these input data, while simultaneously transmitting its position to the monitoring station (Nohse et al. 1999). The in-situ tests that are conducted for quality control are also registered together with the current GPS position, which allows observing a correlation between the in-situ test results and the respective values measured by the CCC/IC roller (Anderegg et al. 2006).

2.6.3 Benefits of CCC/IC technology

The primary advantage of CCC/IC systems is that they provide instantaneous and continuous measurements of the properties of a compacted material, while also providing complete coverage of the entire compacted area. A second significant benefit of these systems is that they can potentially provide more uniform compaction with a fewer number of passes, resulting in a more optimum expenditure of time and energy on a project site (Thurner and Sandström 1980, Anderegg and Kaufmann 2004).

After conducting several projects in Europe, a comparison between projects that utilized CCC equipped compactors and the those which utilized conventional compaction equipment and traditional in-situ tests showed that by using new technology, the costs for construction work increase slightly while the costs for external control tests and repair were reduced significantly (Adam 1997). In addition, using CCC/IC systems showed that the overall lifetime of the compactors could be increased because of the reduction in vibrations and mechanical loads (Anderegg and Kaufmann 2004).

Another significant potential benefit and area for cost savings with CCC/IC systems is that they have the potential to significantly reduce the required quantity of conventional QA/QC tests (such as sand cone equivalent or nuclear density gauge tests) on a given project, which typically require skilled operators and impose additional time and costs to the project (Camargo et al. 2006). Recent research has shown that newer QA/QC tests such as dynamic cone penetrometer (DCP) or light weight deflectometer (LWD) may be more appropriate for independent comparison and evaluation of CCC roller data (Camargo et al. 2006).

In summary, the benefits of CCC/IC systems are classified in two categories:

1- Improved compaction control

- Full coverage of compacted area
- More uniform compaction
- Providing real-time soil modulus/stiffness for compacted area
- Spotting weak zones

2- Increased compaction efficiency

- Avoiding overcompaction
- Decrease in number of passes

- Higher adaptability (thin/thick layers, soft/stiff subbase)
- Decreasing the number of conventional proof tests

Continuous compaction control and intelligent compaction have also been criticized in some cases. The most commonly referenced drawbacks are as follows (Petersen et al. 2006):

- Require the use of sophisticated/sensitive equipment in a rugged environment
- Can require additional operator training
- Require more expensive equipment than conventional compaction
- Need RTK GPS for precise compactor location

2.7 Operation Modes of Vibratory Roller

When a given vibratory roller is compacting, five modes of operation may occur, which can influence the dynamic compaction values distinctively (Table 2.1) (Anderegg and Kaufmann 2004). Generally, soil stiffness influences the operating condition of the drum, but roller parameters also contribute (Brandl and Adam 2004).

Table 2.1 Operating modes of a vibratory roller drum

<table>
<tr><th>Drum-soil interaction</th><th>Cycle [1]</th><th>Operating condition</th><th>Application of CCC</th><th>Soil stiffness</th><th>Roller speed</th><th>Drum amplitude</th></tr>
<tr><td>Contact</td><td>1</td><td>Continuous Contact</td><td>Yes</td><td>Low</td><td>Slow</td><td>Small</td></tr>
<tr><td rowspan="4">Partial loss of contact</td><td>1</td><td>Partial uplift</td><td>Yes</td><td rowspan="3">↓</td><td rowspan="3">↓</td><td rowspan="3">↓</td></tr>
<tr><td>2 (4)</td><td>Double jump</td><td>Yes</td></tr>
<tr><td>2 (4)</td><td>Rocking motion</td><td>No</td></tr>
<tr><td>-</td><td>Chaotic motion</td><td>No</td><td>High</td><td>Fast</td><td>Large</td></tr>
</table>

[1] Cycles are specified as a multiple of the excitation cycle, $T = 2\pi/\omega_0$.

Continuous contact happens in the early stages when the soil stiffness is very low, i.e. in the case of uncompacted or soft clayey layers (Adam 1997, Brandl and Adam 2004).

Partial uplift and *double jump* are the most frequent modes of operation during vibratory compaction. The distinction between these two conditions is that the double jump mode contains more excitation cycles (Adam 1997).

Rocking motion is the other mode that occurs when the stiffness of the soil increases. As the roller runs into this mode, the drum axis is no longer vertical and the drum starts rocking (Adam 1997, Brandl and Adam 2004). Bouncing (double jump) and rocking are not desirable modes since they tend to have a loosening effect on the top layer of the soil and the roller loses its maneuverability. The only difference between bouncing and rocking is a phase shift of 180° that occurs between the subharmonic vibrations of the right and left edges of the drum. The theory predicts rocking if the natural frequency of the rocking motion is lower than that of the vertical vibration; otherwise, bouncing will occur (Anderegg and Kaufmann 2004).

Chaotic motion is the last one, which occurs on soils with a very high stiffness (Adam 1997). At this point, the roller is not maneuverable any more (Brandl and Adam 2004). The chaotic behavior of the vibratory roller originates from the nonlinearity and occurrence of subharmonics during compaction. In a chaotic mode of vibration, the dynamic behavior of the roller may be unstable and erratic. To prevent this condition, one solution can be to reduce the power of excitation by increasing the static moment $m_e r_e$ (see 2.8) (Anderegg and Kaufmann 2004).

In summary, as the soil stiffness increases, the drum goes into the later modes of vibration (rocking and chaotic), which make the continuous compaction control process inaccurate and unreliable (Adam 1997). Among the previously discussed modes of operation, continuous contact, partial uplift, and double jump can be described theoretically by a one-degree-of-freedom interaction system while the rocking motion and chaotic motion require a more sophisticated multi-degree-of freedom system (Brandl and Adam 2004).

2.8 Principal Theories of Operation of CCC/IC Systems

There are various recording systems that have been introduced into the CCC/IC industry over the years, which are briefly reviewed in 2.6.1. In this section, these recording systems are discussed in more detail. In the first few sections, vibratory-based systems are reviewed and at the end, a machine drive power-based system is described.

All of the following vibratory-based systems that are discussed consist of a sensor set containing one or two accelerometers attached to the bearing of the vibratory roller drum, a processor unit, and a display to visualize the measured values. The sensor continuously records the acceleration of the drum. The time history of the acceleration signal is analyzed in the processor unit in order to determine dynamic compaction values with respect to specific roller parameters (Brandl and Adam 2004).

2.8.1 Compaction Meter Value (CMV)

The drum of a vibratory roller exposes the soil to repeated blows – one per cycle of the vibration. These blows can be considered analogous to a repeated dynamic plate load test of the soil. It can be shown that the force amplitude F of the blows is proportional to the first harmonic of the vertical acceleration. The vertical displacement z_d during the blow can be approximated by the amplitude of the double integral of the fundamental acceleration component (Sandström 1993, Adam 1996, Thurner and Sandström 2000). Therefore, it is relevant to express the "cylinder deformation modulus" E_c as the ratio of the applied force and the corresponding displacement:

$$E_c = C_1 . \frac{F}{z_d} = C_2 . \omega^2 . \frac{\hat{a}(2\omega_0)}{\hat{a}(\omega_0)} \qquad (2.2)$$

where, C_1 and C_2 are constants, ω = fundamental angular frequency of the vibration, $\hat{a}(2\omega_0)$ = Amplitude of the first harmonic of the acceleration response signal, and $\hat{a}(\omega_0)$ = Amplitude of the exciting frequency (Thurner and Sandström 2000).

Using the general framework of Equation 2.2, engineers at Geodynamik (Thurner and Sandström 1980) developed a roller measurement value called Compaction Meter Value (*CMV*). *CMV* is calculated by dividing the amplitude of the first harmonic of the acceleration signal by the amplitude of the exciting frequency (Equation 2.3).

$$CMV = C \cdot \frac{\hat{a}(2\omega_0)}{\hat{a}(\omega_0)} \qquad (2.3)$$

where, C = A constant value chosen to empirically scale the output *CMV* values to an easier-to-interpret range. Using C = 300 has become a commonly accepted and standardized approach for calculating *CMV* values from measured vibratory roller data (Sandström and Pettersson 2004).

Thurner and Sandström tested the *CMV* equation shown above on compacted soils at a range of different densities and stiffnesses. It was observed that if the drum of the roller moves on a very soft zone, then there was no first harmonic.

In this case, *CMV* was approximately zero. When the drum moves over a loose, coarse-grained material (beginning of compaction) the amplitude of the first harmonic will be low and consequently *CMV* will remain at a low value. As compaction progresses, the amplitude of the first harmonics becomes relatively high and the corresponding CMV values increase.

The ratio of $\hat{a}(2\omega_0)/\hat{a}(\omega_0)$ is a measure of nonlinearity. In a truly linear roller-soil system, a roller with an excitation frequency of 30 Hz (a reasonable value) would produce a 30 Hz drum acceleration response and $\hat{a}(2\omega_0)/\hat{a}(\omega_0)$ would equal zero. However, because the roller-soil system is nonlinear, the drum acceleration response is distorted and is not purely sinusoidal. (The response of soil to vibratory compaction is actually nonlinear elastic-plastic, and because a partial loss of contact occurs, the contact surface varies nonlinearly during each cycle of loading). Fourier analysis can reproduce a distorted waveform by summing multiples of the excitation frequency. Therefore, the ratio $\hat{a}(2\omega_0)/\hat{a}(\omega_0)$ is a measure of the degree of distortion or nonlinearity (Mooney and Adam 2007).

From an analytical stand point, the value of *CMV* is determined by performing spectral analysis of the measured vertical drum accelerations over two cycles of vibration (Figure. 2.8). The reported *CMV* values are the average of a number of two-cycle calculations. Geodynamik typically averages the values over 0.5 sec; however, this can be modified as needed. *CMV* precision is governed by a 1% distortion resolution of the accelerometer. By using Equation 2.3 with $C = 300$, a 1% acceleration distortion equates to a $CMV = 3$ or ± 1.5. However, Geodynamik reports less reliability for *CMV* when recorded values are below 8-10 (Mooney and Adam 2007).

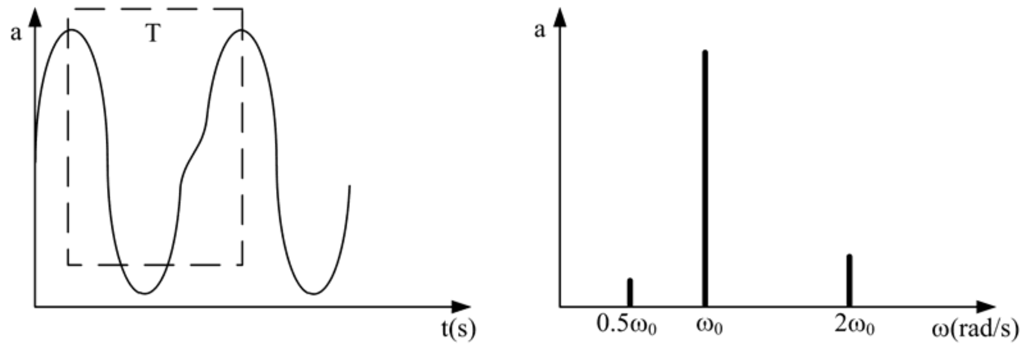

Figure 2.8 Method to determine CMV involves spectral analysis (right) of two cycles of vertical drum acceleration time history data (left) (modified from Mooney and Adam 2007)

Another control value that is commonly used in Compactometer systems is the Resonant Meter Value (*RMV*), which is proportional to the quotient of the amplitude of the half frequency of the acceleration signal divided by the amplitude of the exciting frequency (Equation 2.4). A non-zero *RMV* indicates that the drum is not in the mode of continuous contact (Adam 1997).

$$RMV \sim \frac{\hat{a}(0.5\omega_0)}{\hat{a}(\omega_0)} \tag{2.4}$$

where $\hat{a}(0.5\omega_0)$ = Amplitude of subharmonic acceleration caused by jumping, i.e., the drum skips every other cycle, and $\hat{a}(\omega_0)$ = Amplitude of the exciting frequency.

Currently, Dynapac, Caterpillar and Ingersoll Rand (via Geodynamik equipment) are utilizing a Compactometer system for CCC roller monitoring (Mooney and Adam 2007).

A compaction meter for oscillatory rollers has also been developed that is based on a measurement of the horizontal acceleration of the center axis of the drum. When the drum is operating at frequencies above the resonance frequency, and there is no slip, the amplitude of this signal is a function of soil stiffness as well as the roller parameters. This stiffness value, called the Oscillometer Value (*OMV*), is not sensitive to moderate variations in the excitation frequency. When there is slip between the drum and soil, the signal processor of the oscillometer uses a special algorithm to calculate the *OMV*. This calculation is based solely on the time intervals during which the soil and the drum move together without slipping (Thurner and Sandström 2000, Sandström and Pettersson 2004).

2.8.2 Compaction Control Value (CCV)

In an attempt to improve upon the Compaction Meter value, the Japanese company Sakai has introduced a continuous compaction value (*CCV*), which considers the first subharmonic ($0.5\omega_0$) and higher-order harmonics in addition to the fundamental and first harmonic (Mooney and Adam 2007).

$$CCV = \left[\frac{a(0.5\omega_0) + a(1.5\omega_0) + a(2.5\omega_0) + a(3\omega_0)}{a(2.5\omega_0) + a(3\omega_0)} \right] \times 100 \tag{2.5}$$

2.8.3 OMEGA

In 1988, Kröber from the American-German company Bomag, developed the OMEGA value and incorporated it into the Terrameter system (Mooney and Adam 2007). The OMEGA value provides a measure of the energy transmitted to the soil. The concept is illustrated by the schematic of the roller compactor and the forces acting on the drum in Figure 2.9. Here, F_s is the force transmitted to the soil, which is determined by summing the static force (roller weight), drum inertia and eccentric force $m_0 e_0 \omega^2$ while ignoring the effect of frame inertia (Adam 1997).

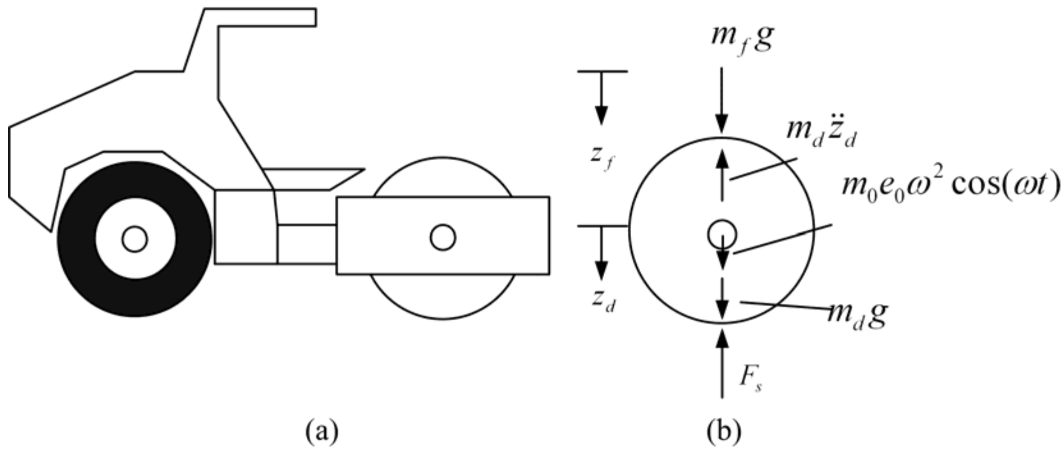

Figure 2.9 One-degree-of-freedom lumped parameter model representation of vibratory compactor (modified from Mooney and Adam 2007)

The drum acceleration $\ddot{z}_d$ is measured in two perpendicular directions. An accelerometer provides the time history of the drum acceleration. The OMEGA value is determined by integrating the transmitted force F_s and drum displacement z_d time history over two consecutive cycles of vibration to consider the operating condition of double jump (Adam 1997):

$$OMEGA \sim W_{eff} = \oint_{2T} \left[-(m_d)\ddot{z}_d + (m_d + m_f)g + m_0 e_0 \omega^2 \right] \dot{z}_d dt \tag{2.6}$$

where, $\dot{z}_d$ =Drum vertical velocity (m/s^2), m_d = Drum mass (kg), m_f = Frame mass (kg) , m_0 = Mass of the rotating eccenter (kg), e_0 = Eccentricity (m), ω = Circular frequency (rad/s), g = Gravitational acceleration (9.81 m/s^2), and W_{eff} = Absorbed energy by soil (N·m).

Like *CMV*, OMEGA values increase as drum behavior transitions from continuous contact to double jump. Consequently, under similar operating conditions, OMEGA values increase with increasing soil stiffness. Upon entering the double jump mode, a sudden drop in OMEGA values occurs, followed by a continued increase with increasing soil stiffness within the double jump mode (Adam 1997). OMEGA values correlate well to soil stiffness, provided that a linear transformation between dynamic compaction values is performed. However, this conformity is valid only for values within a particular mode of drum vibrational behavior. The correlation between *CMV* and OMEGA is approximately linear within the operating conditions of continuous contact and partial uplift (Brandl and Adam 1997).

2.8.4 Stiffness (k_s)

In the late 1990s, Ammann introduced a roller-determined soil stiffness parameter k_s (Anderegg 2000). Using this approach, the roller free body shown in Figure 2.10 is treated as a lumped parameter model to represent the vertical kinematics of the soil-drum-frame system. Within this framework, the soil behavior is modeled using a Kelvin-Voigt spring-viscous dashpot model (Mooney and Adam 2007). As shown in Figure 2.10, the roller can be subdivided into two separate pieces, the frame and the drum, where the frame is supported using an elastic suspension element whose behavior is modeled using stiffness k_t and damping c_t. The subgrade behavior can then be modeled as a spring with stiffness k_s and a viscous damper connected in parallel, having a damping constant c_s . In conjunction with the drum, this creates the spring-mass-dashpot vibration system, which describes the characteristics of a dynamic compactor (Anderegg and Kaufmann 2004). This model is valid provided that the excitation frequency is well above the resonance frequency for the frame-suspension elements (Anderegg et al. 2006).

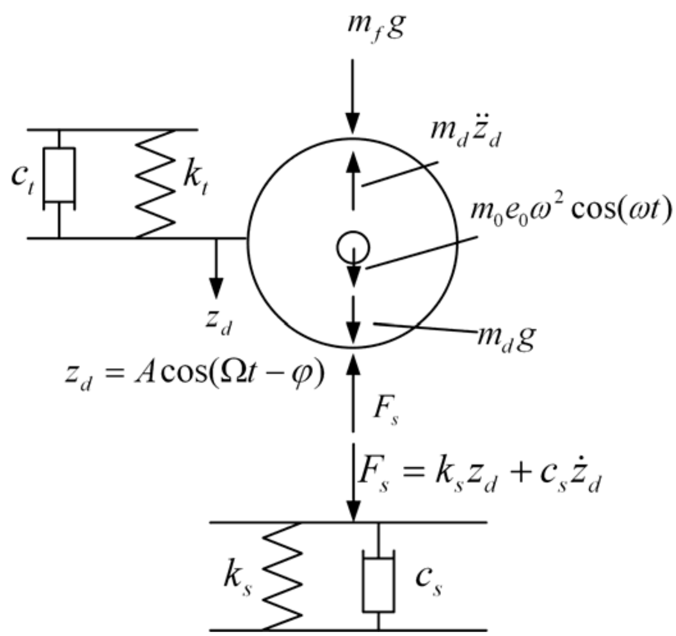

Figure 2.10 Simplified model for roller-soil interaction

As the compaction progresses, the stiffness increases and the damping decreases. Assuming constant machine parameters, the vibration behavior of the system varies accordingly and this can be used as a measurement indicator value in a continuous compaction control system. The steady-state dynamic behavior of the soil-machine system is described by the following equations (Anderegg and Kaufmann 2004):

$$F_s = -m_d \ddot{z}_d + m_0 r_0 \omega^2 \cos(\omega t) + k_t (z_d - z_f) + c_t (\dot{z}_d - \dot{z}_f) + m_d g \qquad (2.7)$$

$$0 = -m_f \ddot{z}_f + k_t (z_f - z_d) + c_t (\dot{z}_f - \dot{z}_d) + m_f g \qquad (2.8)$$

where, F_s is soil-drum interaction force,

$$F_s = k_s z_d + c_s \dot{z}_d \qquad \text{if } F_s \geq 0 \qquad (2.9)$$

$$F_s = 0 \qquad \text{else} \qquad (2.10)$$

where, f = Frequency of excitation (Hz), m_0r_0 = Eccentric moment of unbalanced mass (kgm), k_s = Soil stiffness (MN/m), c_s = Soil damping (MNs/m), k_t = Suspension stiffness (MN/m), c_t = Suspension damping (MNs/m), t = Time (s). The other parameters used in Equations 2.7 through 2.10 have been defined previously (for Equation 2.6). In the equations above, the subscripts d and f denote drum and frame, respectively.

The nonlinearity caused by drum lift-off can be recognized by the occurrence of additional frequency overtones that correspond to integral multiples of the excitation frequency. As an example, subharmonic vibrations may occur at harmonic frequency multiples of 1/2, 1/4, 1/8. etc. of the excitation frequency (Anderegg and Kaufmann 2004). As shown in Figure 2.11, this characterization makes use of the time progression of the soil reaction force F_s or the frequency analysis of the drum motion z_d:

$$z_d = \sum_i A_i \cos(i\Omega t - \phi_i) \tag{2.11}$$

where, A_i is the amplitude at frequency if and ϕ_i is the phase lag between the generated dynamic force and the part of the drum displacement with frequency if (Anderegg and Kaufmann 2004). Depending on the operational status, the vibration displacement has one or more frequencies: Permanent drum-ground contact, linear: i = 1; Periodic loss of contact, nonlinear: i = 1, 2, 3; Bouncing or rocking: i = 1/2, 1, 3/2, 2, 5/2, 3

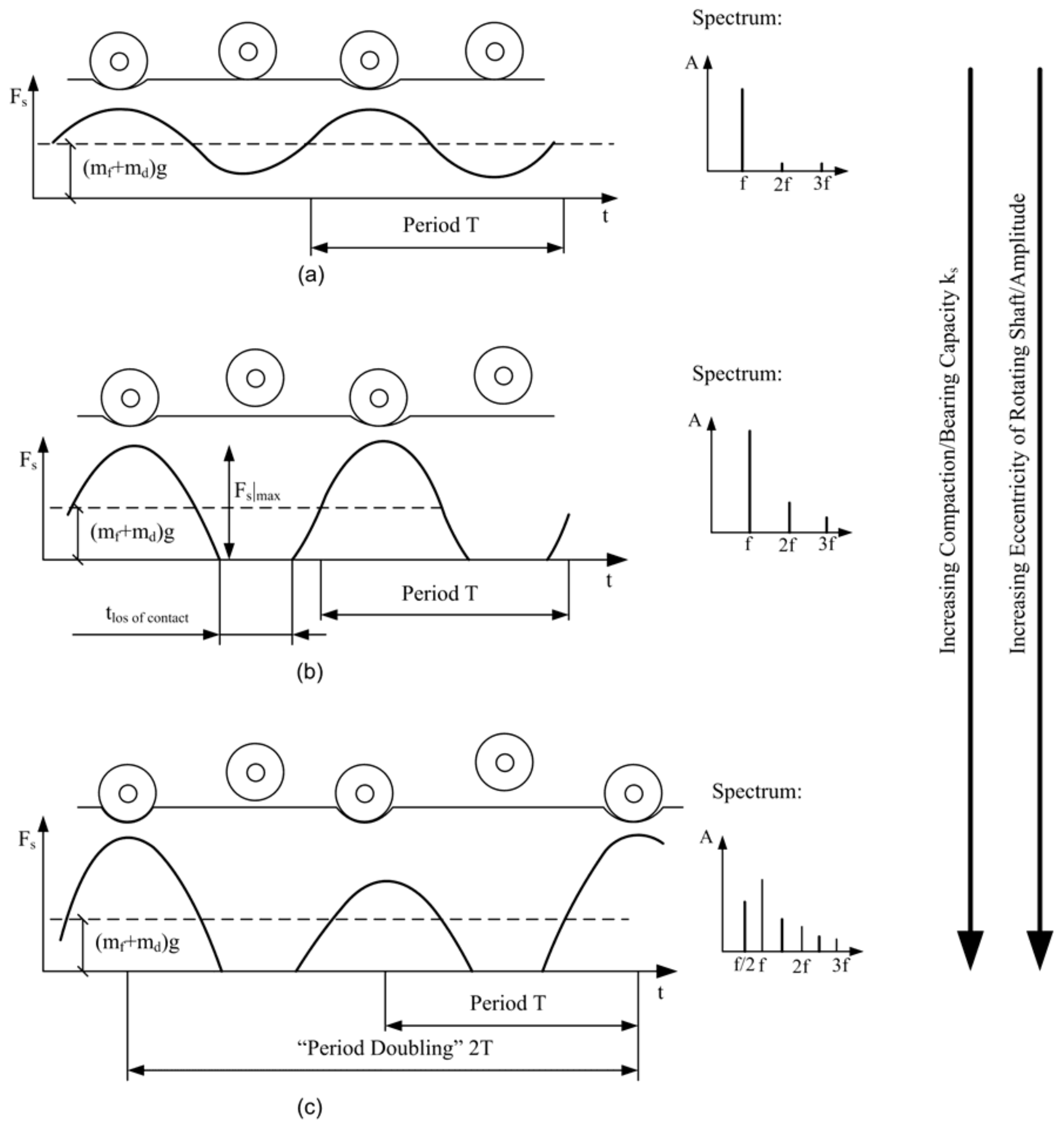

Figure 2.11 **Three basic types of behavior of vibrating drum: (a) contact (every time) (b) periodic loss of contact (c) bouncing or rocking (modified after Andregg and Kaufmann 2004)**

By summing Equations 2.7 and 2.8, while considering only the static frame mass and neglecting the dynamic forces imposed by the elastic frame, Equation 2.12 can be obtained (Andregg and Kaufmann 2004):

$$F_s = (m_d + m_f)g + m_0 r_0 \omega^2 \cos(\omega t) - m_d \ddot{z}_d \tag{2.12}$$

The resulting F_s vs. z_d response is graphically illustrated in Figure 2.12 for continuous contact and partial uplift behavior (after Mooney and Adam 2007). The Ammann k_s is the ratio of F_s to z_d and is computed when the drum is at the bottom of its trajectory and z_d is at its maximum (see Fig. 2.12). This k_s represents a composite static stiffness (spring constant) for the soil and is only valid to the degree which the Kelvin-Voigt model is a reasonable approximation for the soil behavior. The spring-dashpot model has been shown to be effective in representing roller-soil system behavior (e.g., Yoo and Selig 1979, Adam 1996, Mooney and Rinehart 2007).

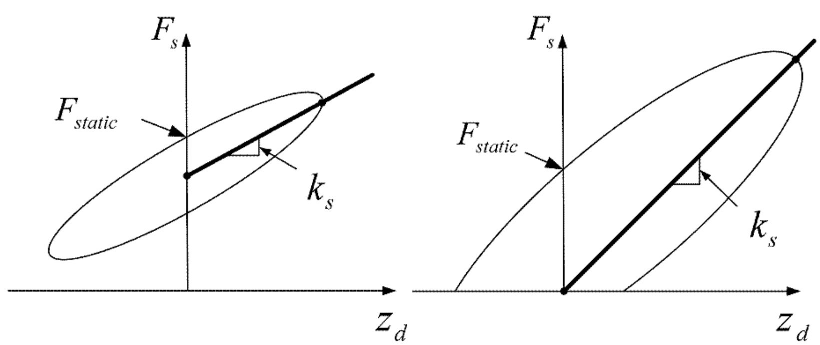

Figure 2.12 Illustration of k_s during contact (left) and partial loss of contact behavior (right) (modified after Mooney and Adam 2007)

Assuming linear elastic soil behavior and nonlinear vibration of the roller, the measured vibration amplitude "A", and the measured phase angle "ϕ" can be used to determine the corresponding value of k_s (Andregg Kaufmann 2004):

$$k_s = \frac{F_s\,|_{\dot{x}=0} - (m_f + m_d).g}{A} \tag{2.13}$$

where, $A = |z_d|$ if $\dot{z}_d = 0$, and if $\ddot{z}_d < 0$ no bouncing or rocking ($A_{1/2}$=0)

In the case of linear vibration without a loss of contact between the drum and soil, k_s can be calculated using the following equation:

$$k_s = 4\pi^2.f^2.\left[m_d + \frac{m_0 r_0.\cos(\phi)}{A}\right] \tag{2.14}$$

Subject to the condition of:

$F_s\,|_{\max} \leq 2\cdot(m_f + m_d).g$

where,

$$F_s\,|_{\max} = (m_f + m_d).g.\pi.\frac{1+\cos(\frac{t_{l.o.c}}{T}.\pi)}{(1-\frac{t_{l.o.c}}{T}).\pi.\cos(\frac{t_{l.o.c}}{T}.\pi) + \sin(\frac{t_{l.o.c}}{T}.\pi)} \tag{2.15}$$

$F_s\,|_{\max}$ is the maximum of the soil-drum interaction force during one period T, and $t_{l.o.c}$ is the time where there is a loss of contact between the drum and soil during one period T (Anderegg and Kaufmann 2004).

2.8.5 Vibratory Modulus (E_{vib})

Using stiffness (k_s) as an indicator for compaction improvement has some disadvantages. The stiffness k_s increases with the drum width and the drum diameter. Furthermore, it depends on the vibrating mass, the mass of the frame structure and the installed unbalanced mass. Generally, it can be observed that, in contrast to the formerly common indirect characteristic quantities (e.g. OMEGA value), the stiffness (k_s) is a physically verifiable characteristic magnitude; unfortunately however, its measured values cannot be directly transferred from one type of roller to another. Consequently, a variety of approaches that use modulus have been developed to address this limitation (Kröber et al. 2001).

Bomag has more recently utilized a lumped parameter vibration model developed using elastic half-space theory to calculate an additional compaction control value called vibratory modulus (E_{vib}) (Kröber et al., 2001). The same assumptions and definitions used for calculating the stiffness value are used in this derivation (see Figure 2.9). The stiffness is extracted from the loading portion of the drum-force deflection curves (Fig. 2.13) to come up with a vibration modulus value (E_{vib}) (Mooney and Adam, 2007).

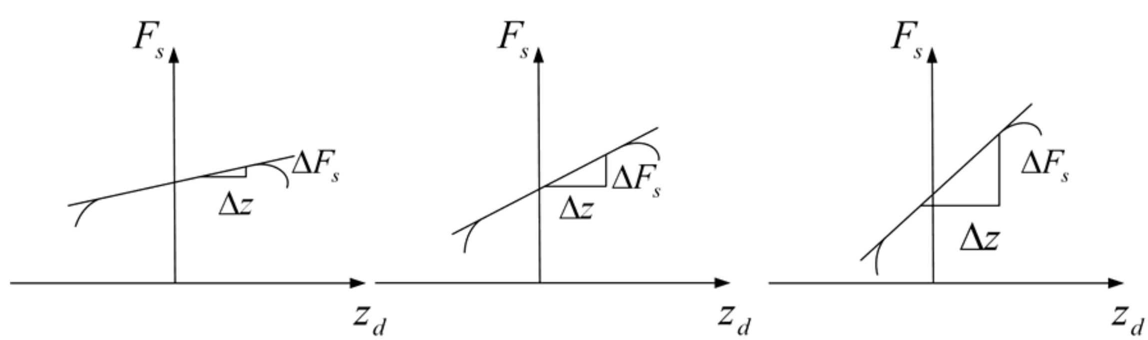

Figure 2.13 Increasing stiffness values in a higher gradient of the force-path characteristic curve (modified after Kröber et al. 2001)

The ratio of ΔF_s to Δz_d represents a characteristics quantity for the evaluation of the soil stiffness (Kröber et al. 2001):

$$k = \frac{\Delta F_s}{\Delta z_d} \tag{2.16}$$

A similar but more simple mechanistic load-response process takes place during a field plate load test (PLT). In a PLT, a circular plate is gradually loaded and unloaded to determine the deformation modulus, as follows:

$$k = \frac{\Delta F_s}{\Delta z_d} = \frac{4 \cdot G \cdot r}{1 - \nu} \tag{2.17}$$

where, G = Shearing modulus, r = Radius of plate, and ν = Poisson ratio.

Equation 2.17 is derived using a closed-form solution for the linear, elastic, isotropic half volume and can be interpreted using the following approach: Based on a measured force-displacement interrelationship (ΔF, Δz_d) and in the presence of a certain geometry (r), the following equations can be applied (Kröber et al., 2001):

$$G = \frac{E}{2(1 + \nu)} \tag{2.18}$$

$$\Delta F = \Delta\sigma \cdot \pi \cdot r^2 \tag{2.19}$$

Combining equation 2.15 to 2.17, we have:

$$E = \frac{\pi \cdot (1 - \nu^2)}{2} \cdot r \cdot \frac{\Delta\sigma}{\Delta z} \tag{2.20}$$

As noted previously, true soil behavior cannot be captured using a linear, elastic, and isotropic material model. If it would fulfill these conditions, the deformation modulus would be the same as the E-modulus. In contrast to a PLT, where the loaded area is defined by the precisely circular load plate, the shape of the contact area for a vibratory roller can be modeled as a cylinder that is lying on its side. The contact width (b), which controls the overall area of roller contact and the corresponding applied static and dynamic pressures, can be determined from the depth of the depression that the drum makes in the soil using Lundberg's formulas (Kröber et al. 2001):

$$b = \sqrt{\frac{16}{\pi} \cdot \frac{R(1-\nu^2)}{E} \cdot \frac{F_B}{L}} \tag{2.21}$$

$$z_d = \frac{1-\nu^2}{E} \cdot \frac{F_B}{L} \cdot \frac{2}{\pi} \cdot (1.8864 + \ln \frac{L}{b}) \tag{2.22}$$

where, b = Contact width, R = Radius of drum, ν = Poisson's ratio, E = Modulus, F_s = Ground contact force, L = Width of drum, and z_d = Depth of depression. These formulas are derived based on a parabolic load area acting across the contact width, where the contact width is always smaller than the width of the drum and the cylindrical roller body is supposed to have a slightly spherical shape (Kröber et al. 2001).

During the PLT, the load curve is used for evaluation. As an analogy to this, the compression part of the indicator diagram is used for calculating the soil modulus, which is called E_{vib}. The relationship between k_s and E_{vib} is shown in Figure 2.14 (Mooney and Adam 2007).

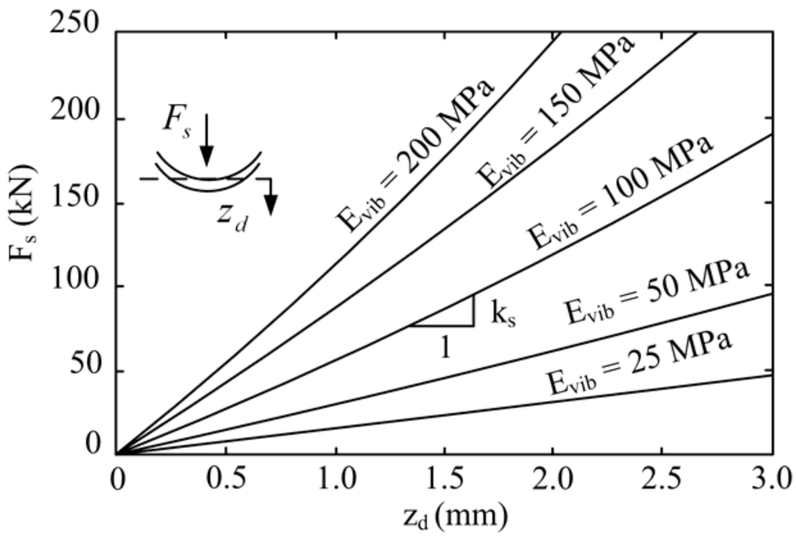

Figure 2.14 Relationship between contact force and drum displacement for a cylinder on an elastic half-space (modified after Mooney and Adam 2007)

By treating the roller like the plate in a PLT, and the underlying soil as the elastic half space, a similar relationship can be derived between the measured stiffness (k_s) and the vibratory modulus (E_{vib}) of the compacted material based on Lundberg's theory (Anderegg and Kaufmann 2004):

$$k_s = \frac{E_{vib} \cdot L \cdot \pi}{2 \cdot (1-\nu^2) \cdot \left(2.14 + \frac{1}{2} \cdot \ln\left[\frac{\pi \cdot L^3 \cdot E_{vib}}{(1-\nu^2) \cdot 16 \cdot (m_f + m_d) \cdot R \cdot g}\right]\right)} \tag{2.23}$$

As a result of these calculations, a compaction indicator value can be derived which is not dimensionless, and which can be transferred to different machines using a special calibration process. This allows the vibration modulus of the ground to be determined with different machines and machine types. Although this approach has been developed for vertical vibration, it is also promising for oscillatory rollers, provided that the direction of oscillation deviates more than 12-15 degrees from the horizontal plane (Kröber et al. 2001). In summary, the benefits of the compaction indicator value E_{vib} are as follows:

- It allows direct determination of soil stiffness in the form of the vibration modulus E_{vib}, which has units of MPa (tsf) during the compaction process
- E_{vib} is directly related to E_{v1} and E_{v2}, which are the first and second loading modulus values obtained from two cycle plate load tests.
- E_{vib} is relatively independent from the amplitude, frequency, and working speed of the roller.

2.8.6 Evaluation of Vibratory Measurement Values

A number of independent studies have been performed to investigate dynamic roller measurement values. Adam and Kopf (2004) numerically simulated roller-soil behavior using finite element analysis of a roller vibrating on an elastic half-space to explore the influence of the soil's Young's modulus (E-modulus in Figure 2.15) on the roller measurement values. The y-axis in Figure 2.15 depicts the relative drum vibration amplitude, i.e., the ratio of z_d to the theoretical maximum $z_{d(max)}$ given by Equation 2.24. The theoretical maximum drum displacement $z_{d(max)}$ is determined by measuring the drum vibration in air (e.g. frame propped up on jack stands); $z_{d(max)}$ is a term often cited in the soil compaction community (Mooney and Adam 2007).

$$z_{d(\max)} = \frac{m_0 e_0}{m_d} \tag{2.24}$$

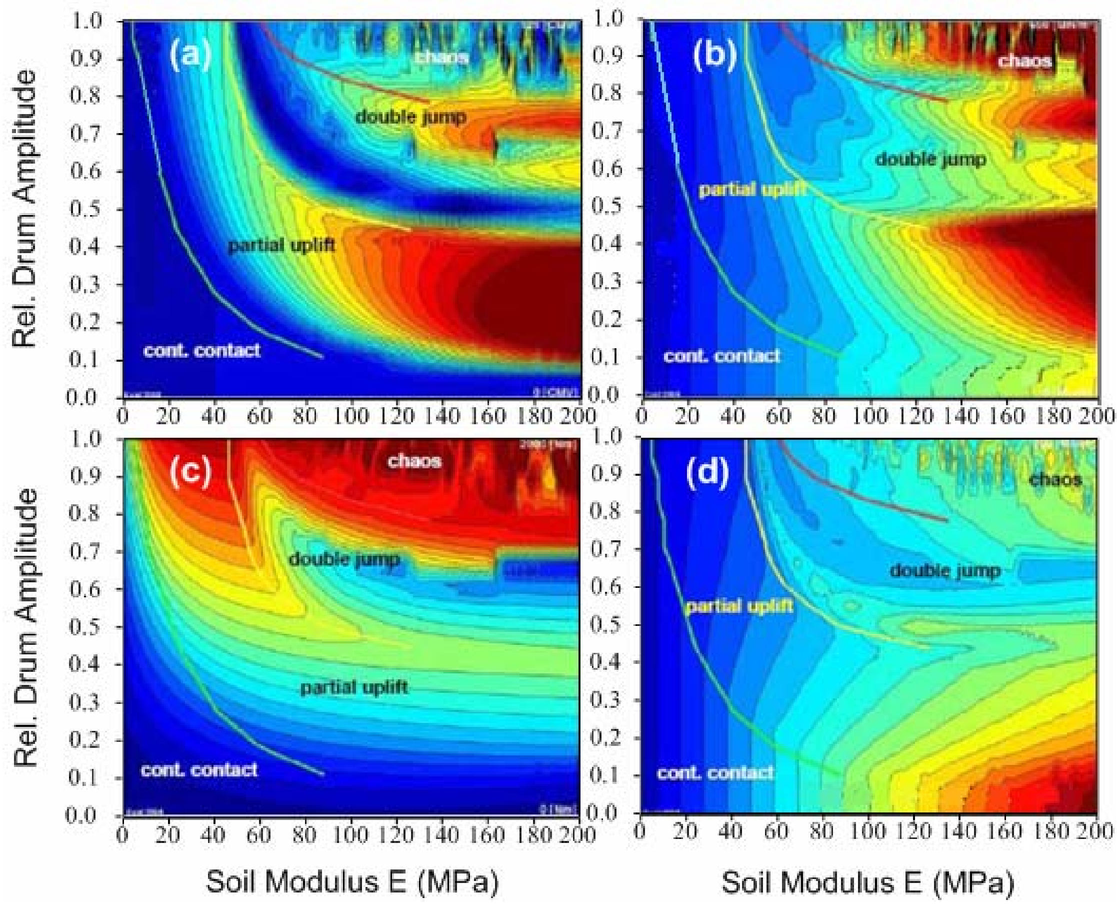

Figure 2.15 Variation of roller measurement value with soil modulus and relative drum vibration amplitude - results of numerical simulations; a) CMV, b) E_{vib}, c) OMEGA, and d) k_s (modified after Mooney and Adam 2007)

Figure 2.14 shows the relative location of various contact modes, their presence as a function of relative drum displacement, amplitude, and soil modulus, and how they are influenced by relative amplitude and soil modulus. Since double jump, rocking, and chaos are now typically avoided via feedback control of the roller, it is most interesting to focus on the behavior of the system during continuous contact and partial uplift modes. As illustrated in Figure 2.14, values of *CMV* are very low and constant when the drum is operating in a continuous contact mode, regardless of the soil modulus. Given that the soil is modeled here as linear elastic, only the curved drum/soil interaction nonlinearity is contributing to the *CMV* during the continuous contact mode. This figure also illustrates how *CMV* values respond to soil stiffness during partial uplift; *CMV* increases as the soil modulus E increases. However, *CMV* at a constant soil modulus is amplitude dependent; therefore, a higher eccentric force will yield a greater *CMV* for the same soil. The amplitude dependency of *CMV* is more pronounced for softer soils than for stiffer soils (Mooney and Adam 2007).

E_{vib} is sensitive to changes in soil modulus during continuous contact and partial uplift modes; an increase in soil modulus leads to an increase in E_{vib}. E_{vib} exhibits little or no amplitude dependency in continuous contact mode but increases with increasing amplitude during partial uplift. This amplitude dependency is more pronounced for stiffer soil. Similar to E_{vib}, k_s increases with soil modulus and is amplitude dependent during partial uplift. However, k_s decreases with increasing amplitude during partial uplift, particularly for stiffer soil. The amplitude-dependency of soil stiffness was also demonstrated in field testing by Mooney and Rinehart (2007). Finally, the OMEGA value was found to be much less sensitive to underlying soil stiffness for constant amplitudes of input vibration. *CMV*, E_{vib}, and k_s each exhibit amplitude dependency at a constant soil modulus. Ideally, one would like the measurement value to be independent of eccentric force and amplitude, particularly for variable amplitude control compaction (Mooney and Adam 2007).

Figure 2.16 presents the numerically derived measurement values as a function of soil modulus for a given relative amplitude. OMEGA, E_{vib} and k_s are linearly dependent on soil modulus during continuous contact mode and *CMV* is fairly constant. During partial uplift, *CMV* is the most sensitive and OMEGA is the least sensitive to changes in soil modulus. Again, the performance of each measurement value during double jump is not so relevant given today's roller technologies (Mooney and Adam 2007).

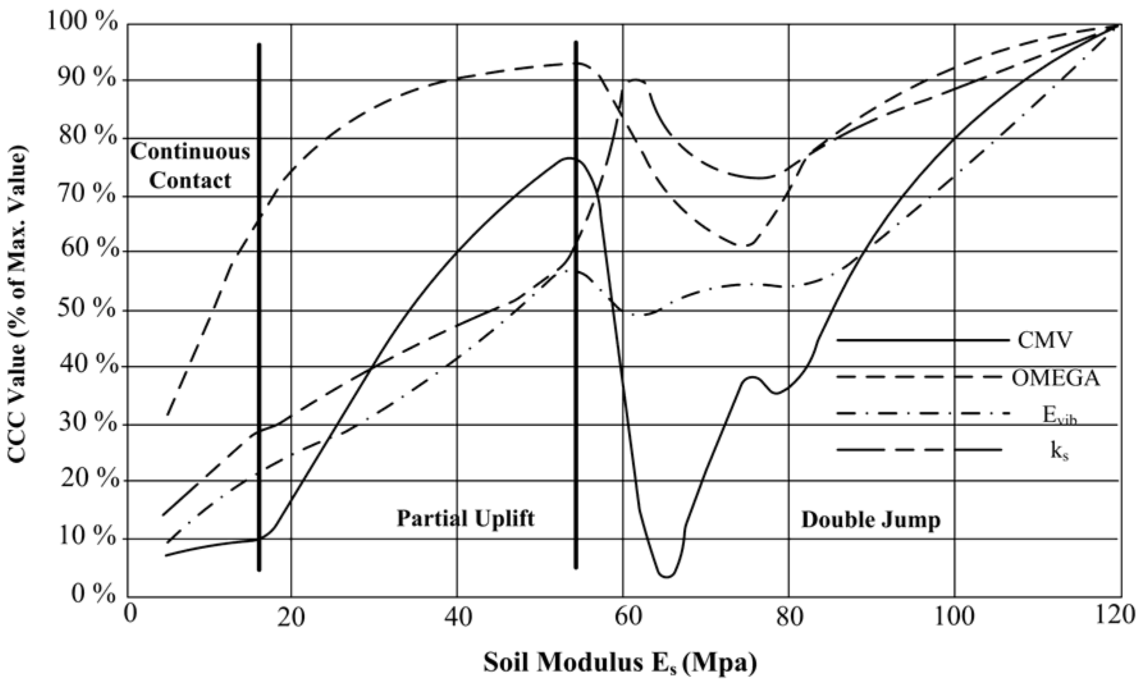

Figure 2.16 Relative roller measurement values (CCC values) as a function of soil modulus as determined from numerical simulations (modified after Adam and Kopf 2004, Mooney and Adam 2007)

2.8.7 Machine Drive Power (MDP)

As noted previously, early development of CCC systems focused on technologies that could be used in conjunction with vibratory compaction equipment. As discussed in Section 2.3, the use of CCC systems with vibratory rollers is more effective for compaction of coarse-grained materials, while fine-grained soils such as clayey soils needs static and kneading compaction where vibratory-based CCC systems may not be applicable. In addition to the challenges that are present for compaction of fine-grained soils, CCC systems also have some difficulty dealing with compaction control on inclined surfaces (Adam and Kopf 1998).

To broaden the useful domain of CCC systems into cohesive and fine-grained soils and to address potential problems with compaction control for inclined surfaces, Caterpillar has introduced a new compaction monitoring system that uses machine drive power (*MDP*) with either static or vibratory rollers (White et al. 2005). Caterpillar's *MDP* system provides a semi-empirical measure of the compaction energy delivered to the soil by measuring the energy necessary to overcome the roller's resistance to motion. The theory behind the operation of this system is that the energy required to move the roller drum is strongly affected by the sinkage of the roller drum into the soil that is being compacted (and the associated resistance to rolling), which in turn is related to the stiffness and modulus of the soil. The technology that is used in this MDP system is comprised of sensors that monitor hydraulic pressure and flow at the roller's torque converters. The resulting product of these machine parameters can be used to calculate the net power (P_n or *MDP*) that propels the roller (Thompson and White 2008). The operating principles behind this type of CCC system are explained in more detail in the following paragraphs.

In 1966, Schuring developed workable formulas identifying motion resistance and the associated energy loss in soil (White et al. 2005). Equation 2.25 presents a simplified two-dimensional relationship relating the energy loss in a soil (E_s) to the torque (M) applied to the roller (Figure 2.17), the radius of the roller (r), the drawbar pulling force (R), the horizontal distance traveled by the roller (l) and the wheel slippage (i) (White et al. 2005).

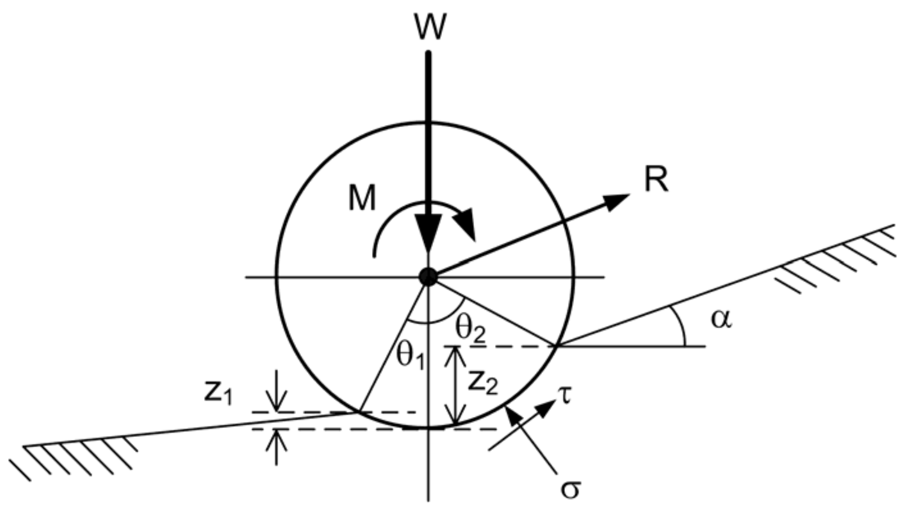

Figure 2.17 Simplified two-dimensional free-body diagram of stresses acting on rigid compaction drum (modified after White et al. 2005)

$$E_s = \frac{l}{1-i}\left[R(i-1) + \frac{M}{r}\right] \tag{2.25}$$

By substituting simplifying relationships for R and M, Equation 2.24 can be rewritten in terms of the resultant horizontal and vertical stresses acting on the roller (σ_h and σ_v) and the circumference of contact between the roller and soil:

$$E_s = \frac{l}{1-i} rb\left[i\int_{\theta_1}^{\theta_2} \sigma_h d\theta + \int_{\theta_1}^{\theta_2} \sigma_v \theta d\theta\right] \tag{2.26}$$

The interface contact angle (Equation 2.27) is further related to the sinkage depth (z), which varies with the shear strength and compressibility of the compacting soil (Equation 2.28).

$$\theta_i = \cos^{-1}\left(\frac{r - z_i}{r}\right) \tag{2.27}$$

$$z_i = \left[\frac{3W}{(3-n)(k_c + k_\varphi)\sqrt{D}}\right]^{\frac{2}{2n+1}} \tag{2.28}$$

Equation 27 shows that sinkage depends on the diameter (D) and weight of the roller (W), the roller width (b), the cohesion and friction moduli of deformation (k_c and k_ϕ) of the soil, and the exponent of soil sinkage (n). These three parameters empirically define the stress-strain relationship of the soil and require PLT tests of multiple sizes for extrapolation to be determined (White et al. 2005). Moduli k_c and k_ϕ depend on soil shear strength parameters, and n is highly sensitive to changes in soil density. Thus, sinkage is directly related to soil compaction. Unfortunately, accurate values of sinkage are nearly impossible to predict because of the inherent variability in soil and unknown sources of error in machine-soil interaction. Thus, using theory as a guide, a more reliable estimate of energy loss as a function of compaction has been developed through semi-empiricism (White et al. 2005).

Using this semi-empirical approach, the gross power (P_g) (energy/time) required to move the compactor drum through an uncompacted layer of fill can be determined using Equation 2.29. Here, P_s represents that portion of the power needed to overcome resistance from moving through the soil and P_{sa} is the additional machine power that is associated with overcoming a sloping grade or compensating for machine accelerations. P_{ml} is the internal machine power loss.

$$P_g = P_{ml} + P_s + P_{sa} \tag{2.29}$$

Equation 2.29 can be rewritten in terms of the energy lost to the soil by rearranging terms and multiplying by a unit time (t) to obtain:

$$E_s = P_g t - P_{ml} t - WV\left(\sin\alpha + \frac{a}{g}\right)t \tag{2.30}$$

where, a = Acceleration of the machine, g = Acceleration of gravity, α = Slope angle (positive for uphill and negative for downhill), t = Time, and V = Velocity of the roller (White et al. 2005).

Considering the various mathematical models introduced by Bekker (1969) for terrain-vehicle interaction, Equation 2.30 can be rewritten to determine the net power (P_n) required to propel the compactor through an uncompacted layer of fill (White et al. 2006):

$$P_n = P_g - WV\left(\sin\alpha + \frac{a}{g}\right) - (mV + b) \tag{2.31}$$

where, m and b are machine internal loss coefficients specific to a particular machine. As mentioned previously, P_g represents the gross power needed to move the machine. A portion of the gross power is the power lost or gained by working on a sloping grade, and this factor, as well as machine accelerations and internal machine losses, must be accounted for so that P_n only represents the machine power (*MDP*) associated with changes in soil physical parameters (i.e. density, strength, and stiffness) (White et al. 2006).

A summary of commonly used CCC values, their descriptions, and the associated compaction equipment manufacturers are presented in Table 2.2.

Table 2.2 Established CCC systems, CCC values, and the associated equipment manufacturers

CCC System	CCC Value	Definition of CCC Value	Manufacturer
Compactometer	CMV (unitless)	acceleration amplitude ratio (first harmonic div. by excitation frequency amplitude) - frequency domain	Geodynamik, Sweden
Terrameter	OMEGA (N.m)	energy transferred to soil (considering soil contact force displacement relationship of 2 excitation cycles) - time domain	Bomag, Germany
Continuous Compaction Value	CCV (unitless)	acceleration amplitude ratio - frequency domain	Sakai, Japan
Terrameter	E_{vib} (MPa)	dynamic elasticity modulus of soil beneath drum (inclination of soil contact force displacement relationship during loading) - time domain	Bomag, Germany
ACE	k_a (MN/m)	spring stiffness of soil beneath drum (derived from soil contact force displacement relationship at maximum drum deflection) - time domain	Ammann, Switzerland
Machine Drive Power	MDP (kW)	net power to propel the roller	Caterpillar, USA

2.9 In-situ test approaches that can be used for compaction QA/QC

An important step in the assessment of CCC and IC systems is establishing a reliable approach for validation of these technologies. Historically, a number of in-situ test methods have been used for QA/QC of the compaction process, falling into two general categories: density-based tests and strength-based tests. Details about these different in-situ testing techniques are provided in the following sections.

2.9.1 Density-based tests

The conventional approach that is used for controlling the quality of compaction is to measure the dry unit weight and moisture content of a compacted soil at random locations throughout a compacted area. The measured values and then compared with acceptable ranges of dry unit weight and moisture content for that specific material. There are two methods to specify a target range for the dry unit weight and moisture content.

The first method is the 5-pt Proctor test, in which five (or sometimes more) specimens are compacted in a uniform, controlled fashion at five different moisture contents. After performing the compaction tests, the dry unit weights and moisture contents of the compacted specimens are measured and plotted, and a compaction curve is drawn that shows the relationship between the measured dry unit weight (y-axis) and the water content (x-axis). From this curve, a maximum dry unit weight can be determined, and this value and the corresponding "optimum" moisture content for compaction are recorded. In general, there are two types of 5-point Proctor tests are commonly used; the standard Proctor test (ASTM D 698) and the modified Proctor test (ASTM D 1557).

The second method is the 1-pt Proctor test (AASHTO T 272) in which only one compaction test is performed and the resulting dry unit weight and moisture content are used with a "family" of compaction curves to determine the optimum moisture content and maximum dry unit weight. The family of curves that are used for a given soil are developed from over time, based on long-term experience with 5-point Proctor tests for a given borrow material. Consequently, it is necessary to have a separate family of curves for each material type that is placed.

Values of dry unit weight obtained from in situ measurements on a compacted lift are then divided by the maximum dry unit weight that is achieved from one of the above methods (1-pt Proctor or 5-pt Proctor), providing the relative compaction (RC), also commonly referred to as the degree of compaction. The measured field moisture content (ω) is also compared with the optimum moisture content (ω_{opt}) obtained from one of the above methods (1-pt Proctor or 5-pt Proctor). Both the relative compaction and moisture content must meet the corresponding acceptance criteria (e.g. RC $\geq$ 95% and $\omega_{opt} - 2\% \leq \omega_{field} \leq \omega_{opt} + 2\%$ (DelDOT 2001), otherwise compaction of the lift that was placed in the field must be repeated.

As noted above, the most commonly used methods for compaction control use measurements of in situ soil density and moisture content to assess the effectiveness of the compaction process. The most common in situ tests that are utilized with this approach are the nuclear density gauge test and sand cone equivalent test.

2.9.1.1 Nuclear Density Gauge (NDG)

The Nuclear Density Gauge (NDG), shown in Figure 2.18, is a quick and fairly accurate way to determine the in situ density and moisture content of a compacted soil.

Figure 2.18 Nuclear density gauge

The NDG uses a radioactive isotope source (Cesium 137) at the soil surface (a backscatter technique) or from a probe placed into the soil (a direct transmission technique). The isotope source gives off photons (usually Gamma and Beta rays), which radiate back to the gauge's detectors on the bottom of the unit. The wet density (ASTM D 2922–05) and water content of the soil (ASTM D 3017–05) are calculated based on the calibrated gauge readings.

2.9.1.2 Sand Cone Equivalent

The Sand Cone Apparatus (Fig. 2.19) is used to determine the in-situ density of any soil that can be excavated to a stable condition with hand tools (test procedure described in ASTM D 1556). According to ASTM D 1556, this method is generally limited to materials with a maximum particle size of 5.1 cm (2 in).

Figure 2.19 Sand cone apparatus

To perform a sand cone replacement test, a hole is excavated in the area where the soil has been compacted, and the dry weight of the soil is obtained by determining the weight of the moist soil that is excavated and its moisture content.

The volume for the hole that has been excavated is determined by placing a uniform, standard sand into the hole, using a controlled "cone" placement procedure. The in situ dry unit weight of the soil is then calculated by dividing the dry weight of the soil by the volume of the hole.

2.9.2 Strength-based tests

Strength-based test approaches provide an estimate of the modulus and/or stiffness of a soil layer, by applying a load to the soil and then measuring the resulting displacement response. While such devices can be used to estimate a value for the elastic modulus of the soil layer, which is in theory an independent soil parameter, factors such as stress variability, moisture content, and unknown spatial effects influence the measurement. The effects of stress are primarily due to differences in the applied mean and deviator stress levels, the applied strain level, and the applied strain rate. These factors vary from device to device and they greatly affect the estimation of soil modulus (Briaud and Seo 2003). This complicates comparative analysis of field devices and characterization of subgrade spatial variability (Camargo et al. 2006). Common strength-based tests include the Plate Load Test (PLT), Light Weight Deflectometer (LWD) test, Falling Weight Deflectometer (FWD) test, Dynamic Cone Penetrometer (DCP) test, and the Soil Stiffness Gauge (GeoGauge) test.

2.9.2.1 Plate Load Test (PLT)

The static plate load test (PLT) is a commonly used approach for testing the performance of pavement and foundation layers in both rigid and flexible pavements. The test involves loading a circular plate resting on the layer to be tested, and measuring the associated deflection of the layer under varying load increments. Different sizes of load plate can be used for this test; however, for roadway testing, the plates are typically 30.5 cm (12 in) in diameter (ASTM D 1196-93). Typically, load is applied to the plate by a hydraulic jack. The plate must be loaded continuously until all measured settlement has subsided so that the actual deflection for each load increment is obtained. The amount of time required for the preliminary settlement to take place is determined by plotting a time-deformation curve during the test. At the point when the curve becomes horizontal, or when the rate of deformation nears 0.0025-cm/min, the next load increment is applied. According to the ASTM D 1196-93 testing method, the test should continue until a peak load is reached or until the ratio of load increment to settlement increment reaches a minimum, steady magnitude. Usually, a PLT is run for two cycles of loading (Figure 2.20), which results in two modulus values, E_1 and E_2. Normally, E_2 is two to three times greater than E_1 (Forssblad 1980).

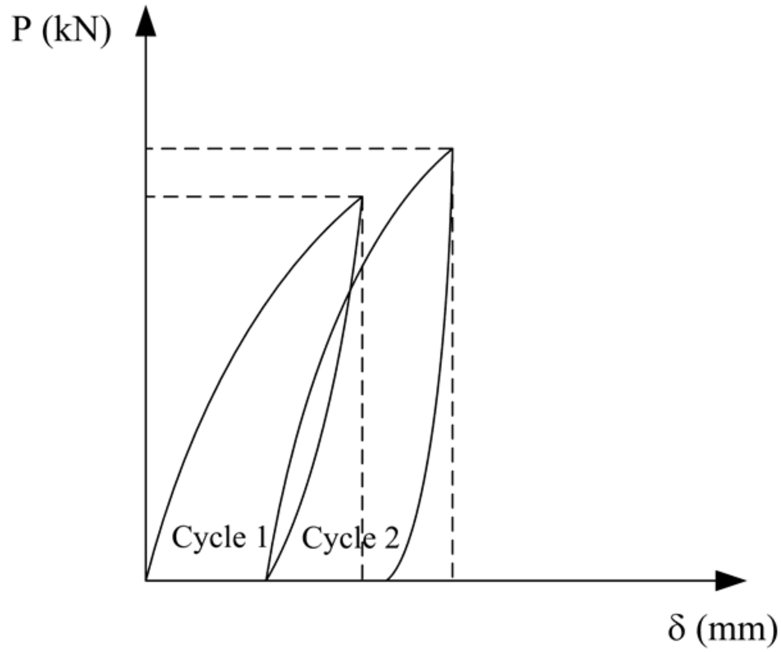

Figure 2.20 Typical loading cycles for PLT test

The elastic modulus of the soil layer that is tested is calculated using Equation 2.32 (Alshibli et al. 2005).

$$E_{PLT} = \frac{k \cdot P \cdot (1 - \nu^2)}{r \cdot \delta} \tag{2.32}$$

where, E_{PLT} = Secant modulus for each cycle of loading (MPa), $k = \pi/2$ and 2 for rigid and flexible plate, P = Applied load (kN), r = Plate radius (m), δ = Deflection of the plate (mm). According to ASTM D 1196, a "rigid plate" is defined as a plate with deflection of less than 0.0025 mm (0.0001 in) from the center to the edge of plate, when the maximum load is applied.

2.9.2.2 Light Weight Deflectometer (LWD)

The light weight deflectometer (Figure 2.21) induces a soil response by dropping a weight onto a plate resting on the test layer (ASTM E 2583–07). A load cell within the instrument measures the time history of the load pulse and a geophone in contact with the test layer measures the time history of the soil's velocity. The velocity is then integrated to determine the displacement. The time history files are automatically exported to a data acquisition system, where the peak load and displacement values are used to calculate modulus values. Time history files can also be analyzed using a fast Fourier transform for a more accurate modulus calculation (Hoffmann et al 2003, Camargo et al. 2006).

The elastic modulus of the subgrade soil is calculated from the surface deflection using the following Boussinesq equation (Rahman et al. 2007):

$$E_{LWD} = \frac{k \cdot \left(1 - \nu^2\right) \cdot \sigma_0 \cdot r}{z_{ave}} \tag{2.33}$$

where, E_{LWD} = LWD modulus (MPa); k = $\pi/2$ and 2 for rigid and flexible plate, respectively (criteria used to determine plate rigidity are the same as for the PLT discussed above); z_{ave} = Average of three measured deflection at center of the plate (μm); σ_0 = Applied stress (kPa); ν = Poisson's Ratio; and r = Plate radius (mm).

Figure 2.21 Light weight deflectometer (300 mm and 200 mm plate)

Generally, there is a good correlation between PLT modulus and LWD modulus (Adam and Kopf 2004). With cohesive soils, a linear relationship is often valid for the entire range of test results. For cohesionless soils, a bi-linear relationship or a logarithmic function shows stronger correlative agreement (Adam and Kopf 2004).

2.9.2.3 Falling Weight Deflectometer (FWD)

The falling weight deflectometer (FWD), shown in Figure 2.22, is a test device which imparts a load pulse to the soil surface to simulate the load produced by a rolling vehicle wheel (ASTM D 4694). The load is produced by dropping a large weight, and the impact energy from this falling weight is transmitted to the pavement through a circular load plate (typically 300 mm (12 in) diameter). A load cell mounted on top of the load plate measures the load imparted to the pavement surface. Deflection sensors, usually consisting of geophones or force-balance seismometers that are mounted radially off the center of the load plate, measure the deformation of the pavement in response to the load. Some typical deflection sensor offsets are 0 mm, 200 mm (8 in), 300 mm (12 in), 450 mm (18 in), 600 mm (24 in), 900 mm (36 in), 1200 mm (480 in), and 1500 mm (60 in). The measured deflections at different stations are then used to back-calculate the modulus of the subgrade soil using Boussinesq's equations (Rahman et al. 2007).

Figure 2.22 Falling weight deflectometer

2.9.2.4 Dynamic Cone Penetrometer (DCP)

The dynamic cone penetrometer (DCP), shown in Figure 2.23, is a test device that provides measurements of penetration resistance over depth, which are indicative of the stability characteristics of pavement layers (ASTM D 5169). The DCP uses the impact force generated by a falling mass to drive a shaft with a conical point into a compacted material. The conical point is sloped at 60°, the falling mass is 8 kg (17.64 lbs), and the drop height is 575 mm (22.64 in) (Camargo et al. 2006).

Figure 2.23 Dynamic cone penetrometer

The shaft's penetration into the soil is measured following every blow, and the resulting measurements of penetration per blow are used to determine the penetration index (DCPI) (Camargo et al. 2006). Penetration index (DCPI), which typically has units of mm per blow, is inversely related to penetration resistance (i.e. soil strength). Equations 2.34 and 2.35 introduce two typical methods to calculate “average” and “weighted mean” DCPI from the soil surface to a depth (*z*) (White et al. 2007).

$$DCPI_{A-z} = \frac{Penetration_z}{\sum Blows} \tag{2.34}$$

$$DCPI_{M-z} = \frac{\sum_{i=1}^{i=n} DCPI_i \cdot z_i}{\sum_{i=1}^{i=n} z_i} \tag{2.35}$$

DCPI can be correlated to other soil or pavement performance indicator values such as California Bearing Ratio (CBR) (Equation 2.36) (Hossain et al. 2006) or elastic modulus (Equation 2.37) (DeBeer 1991).

$$\log CBR = 220 - 0.71(\log DCPI)^{1.5} \tag{2.36}$$

$$\log E_{DCP} = 3.04785 - 1.06166(\log DCPI) \tag{2.37}$$

where, E_{DCP} is the effective elastic modulus.

The California bearing ratio test (CBR) (ASTM D 1883), discussed in the previous paragraph, measures the static penetration resistance of a soil as a function of penetration of a cylinder prior to reaching the ultimate shearing value of the soil. The CBR is defined as a percentage determined by the ratio of the resistance in kPa at 2.5 mm (0.1 in) penetration of the soil being tested to the resistance of a standard, well graded, crushed stone at the same penetration (2.5 mm) (percentage usually expressed as out of 100%). The standard penetration stress for well-graded crushed stone is usually taken to be 6,895 kPa (1,000 psi) (Rahman et al. 2007).

2.9.2.5 Soil Stiffness Gauge (GeoGauge)

The soil stiffness gauge, commonly referred to as the GeoGauge (see Figure 2.24), may be the least destructive device for obtaining the in-situ deformation characteristics of soil.

Figure 2.24 Soil Stiffness Gauge (GeoGauge)

This device has a height of 250 mm (0.8 ft), rests on a 280 mm (0.9 ft) diameter base, and weighs about 10 kg (22 lbs). The base is a rigid ring-shaped foot on the soil surface (with a radius of 57.15 mm (2.25 in) (ASTM D 6758). The GeoGauge works by applying a vibrating force via the underneath rigid ring to the underlying soil. A mechanical shaker, which is attached to the base, vibrates the GeoGauge from 100 to 196 Hz in 4 Hz increments. It produces 25 different frequencies generating a quasi static force of ~ 9 N and a small deflection (Alshibli et. al. 2005). The applied force and the displacement-time history are measured by two velocity sensors. The in-situ soil stiffness is measured at each frequency and finally, the average value is recorded. It measures the stiffness up to 220 to 310 mm (0.7 to 1 ft) of depth from the contact surface (Humboldt Mfg. Co. 2000, White et al. 2007). The corresponding soil modulus can also be calculated from the measured stiffness values (Equation 2.38) if the Poisson's ratio of the soil is available (Humboldt Mfg. Co. 2000, White et al. 2007):

$$E_{SSG} = \frac{F}{\delta} \cdot \frac{1-\nu^2}{1.77R} \tag{2.38}$$

where, E_{SSG} = GeoGauge modulus (MPa), F = Dynamic force caused by the vibrating device (N), δ = Deflection measured with a geophone (mm), ν = Poisson's ratio, and R = Radius of the annular ring (mm).

2.10 Current CCC/IC Construction Specifications

The first specifications for Intelligent Compaction of soils and aggregate were established in the early 1990's in Europe. The following is a timeline of specification development for CCC/IC of soils and aggregates.

- Earthworks (Austria) - 1990 (revised in 1993 and 1999)
- Research Society for Road and Traffic (Germany) - 1994 (updated in 1997)
- Vägverket (Sweden) - 1994 (current specification is 2005)
- ISSMGE (International Society for Soil Mechanics and Geotechnical Engineering) - 2005
- Mn/DOT - 2006 TH 64 (Minnesota DOT) - Pilot Specification in 2006

In this section, a brief review of current specifications that are currently being used for compaction control in conjunction with CCC/IC equipment are presented (White et al. 2007).

2.10.1 Earthworks (Austria)

2.10.1.1 Equipment Specifications

Vibrating roller compactors with rubber wheels and smooth drums that can also be propelled are preferred, but other configurations are acceptable in certain circumstances. The vibration behavior of the drum must be reproducible.

2.10.1.2 Location Specifications (including size, depth, and track overlap)

Sizes of measuring fields and tracks should correspond to those of the test field, usually 100 m (300 ft) long and the width of the site. Test section should be characteristic of the entire site. Track overlap should be less than 10% of the roller drum width. These factors should be attended to: evenness, inhomogeneities of materials or water content, loose surface, and location correspondence of the measurement locations (between the roller and the plate load test).

2.10.1.3 Compaction Process and Specifications

On a compacted test field, a forward measuring pass and then a reverse static pass must occur twice on each track. If the result on a track differs widely from the average of the others, further passes must be performed to attempt additional compaction. Measuring passes for construction should continue until the mean of a pass is no more than 5% higher than the mean of the preceding pass.

Calibration involves the correlation of dynamic measuring values with the modulus of the static 30 cm (12 in) load-bearing plate test (E_{v1}). In the test field, E_{v1} values should be measured immediately after the measurement run in locations with low, medium, and high dynamic measurement values (9 runs in places where no jump mode occurred). A linear regression must show a correlation coefficient greater than 0.7. The minimum value must be greater than 95% of the required E_{v1} value, and the mean must be more than 105% (or greater than 100% during jump operation). No more than 90% of the track should be below the specified minimum for each measuring pass. The measured minimum must be greater than 80% of the specified minimum. The percent standard deviation (relative to the median) must be less than 20% within a measuring pass. The measured maximum within a run cannot exceed the set maximum (i.e., 150% of the determined minimum).

2.10.1.4 Miscellaneous Specifications (moisture, speed, frequency, etc.)

The excitation frequency should be kept constant (within a tolerance of ± 2 Hz). Forward travel velocity should be constant at 2–6 km/h, ± 0.2 km/h (1.2-3.7 mph ± 0.1 mph). When the fraction of fine particles smaller than 0.06 mm (0.002 in) is larger than 15%, special emphasis is laid on water compliance.

2.10.1.5 Documentation Requirements

Measurements must be linked to location coordinates, clearly displayed to the driver, and available for future review. Surface and track plots must be printable. The following should be recorded during calibration: compaction run plan, sequence of compaction and measurement runs, change in amplitude and/or speed (with explanation), and inter-comparison (location and allocation for every measurement run). For measurement runs, the system should automatically document the minimum, maximum, median, and deviation of dynamic measuring values, amplitude, frequency, speed, and jump mode.

2.10.2 Research Society for Road and Traffic (Germany)

2.10.2.1 Equipment Specifications

Self-propelled rollers with rubber tire drive are preferred; towed vibratory rollers with an associated towing vehicle are suitable. The acceleration transducer must be correctly fitted at the drum of the roller. The Operator must be able to read the measuring value, travel speed, and frequency on a display or recording unit.

2.10.2.2 Location Specifications (including size, depth, and track overlap)

Surface must be level and free of puddles. Conditions of the calibration area must be almost identical to that of the testing area in regards to soil type, water content, layer thickness, bearing capacity of the support ground, type of compaction equipment and measuring roller, measuring system, and rest time after compaction. Track overlap should not exceed 10% of the machine width.

2.10.2.2 Compaction Process and Specifications

The calibration field is compacted over the full width, outside strips first. Each calibration area must cover at least 3 partial fields approximately 20 m (66 ft) in length and have areas of light, medium, and high (full) compaction. Testing drives should occur in the same direction as calibration drives, must cover entire area to be evaluated, and cannot be performed during or immediately after heavy rain. Values detected during jump operation cannot be used if not auto-corrected by the system.

Calibration available from a similar construction site may be used with customer agreement.

Calibration is based on either (1) the correlation of the dynamic measuring value and the static modulus of deformation E_{v2} or (2) the degree of compaction. The correlation coefficient resulting from a regression analysis must be greater than 0.7 for the calibration to be valid. Individual area units (the width of the roller drum) must have a dynamic measuring value within 10% of adjacent area units to be suitable for calibration measurements. After the test, poorly compacted spots must be subsequently compacted and re-tested. If widespread, the calibration may no longer be valid. Further examination of soil characteristics may be required.

2.10.2.4 Miscellaneous Specifications (moisture, speed, frequency, etc.)

Frequency and travel speed of the roller should be kept constant.

2.10.2.5 Documentation Requirements

Data must be recorded in a contractually agreed form and must be associated with the exact location of the testing lot, including the measuring value, speed, frequency, jump operation, amplitude, travel distance, time of measurement, roller type, soil type, water content, and layer thickness. Test report also includes purpose of test drive; date, time, file name, or registration number; weather conditions; position of test tracks and rolling direction in test lot; application position or absolute height; local conditions and embankments in marginal areas; machine parameters; and any perceived deviations that occurred in the test drive. Graphical presentations of measuring data should be provided.

2.10.3 Vägverket (Sweden)

2.10.3.1 Equipment Specifications

Roadbases shall be compacted using a vibratory or oscillating single-drum roller exerting a linear load of at least 15–30 kN/m (0.5-1.0 tnf/ft).

2.10.3.2 Location Specifications (including size, depth, and track overlap)

Compaction shall be performed on homogenous layers of non-frozen material. Thickness of the largest layer is typically 0.2-0.6 m (0.6-2.0 ft). The allowable deviation of surface levelness depends on layer type. An accepted layer must be inspected again if (1) an intervening frost season occurs before placement of the next layer, (2) surface has been used by traffic, or (3) adjustment is performed after the inspection. Protective layers less than 0.5 m (1.6 ft) may be compacted with the sub-base.

2.10.3.3 Compaction Process and Specifications

Gravel wearing courses shall be compacted by two passes of a roller exerting a static linear load greater than 15 kN/m (0.5 tnf/ft). For unbound roadbases of surfaced roads in evenness classes 1-2 and for gravel roads, the roller shall make at least 4 passes if a compaction meter with documentation system is used. Areas exhibiting bearing capacity growth shall be compacted further.

Requirements for bearing capacity or degree of compaction should be met for the following objects: protective layers > 0.5 m (1.6 ft) thick and ≤ 6000 m^2 (1.5 acre), sub-bases ≤ 6000 m^2(1.5 acre), and roadbases ≤ 4500 m^2 (1.1 acre). When a roller-mounted compaction meter is employed during compaction of unbound pavements, the bearing capacity or degree of compaction should be measured at two points in the inspection object, at the weakest sections, as indicated by the compaction meter.

Requirements for compaction and for the bearing capacity ratio (Ev_2:Ev_1) of the static plate loading test are dependent upon layer type. The mean of the two bearing capacity ratio values must be greater than 40 for individually compacted protective layers, greater than 110 for sub-bases under roadbases less than 100 mm (4 in) in thickness, greater than 95 for sub-bases under roadbases thickness more than 100 mm (4 in), and greater than 130 for roadbases. The mean of the two degree of compaction values should be greater than 89% for protective layers greater than 0.5 m (1.6 ft) thick and for any sub-base under a roadbase, and the mean should be greater than 90% for roadbases. Other formulas are also in effect for determining the acceptability of measured Ev_2:Ev_1 values and ratios.

2.10.3.4 Miscellaneous Specifications (moisture, speed, frequency, etc.)

Best compaction is achieved if moisture content is close to optimal (as determined by separate procedure). Compactor must move at a constant speed of 2.5-4.0 km/h (1.5-2.5 mph), and low amplitude should be used during compaction. Dry density may be measured via isotope meter (e.g. NDG).

2.10.3.5 Documentation Requirements

None specified.

2.10.4 ISSMGE (International Society for Soil Mechanics and Geotechnical Engineering)

2.10.4.1 Equipment Specifications

The CCC/IC measuring system must enable a clear presentation of the required values, and these values must be displayed directly to the roller operator. The roller should be chosen by experience, considering parameters of the specific construction site.

2.10.4.2 Location Specifications (including size, depth, and track overlap)

The surface of the compacted soil should be homogenous and even, allowing the roller drum to have full ground contact. The Contractor and Controller should jointly determine the measuring field. The sizes of the measuring fields and tracks should correspond to those of the test field. Usually, a section 100 m (300 ft) long by the width of the road (or embankment) is selected as a test field within the construction section. Overlap of roller tracks should not exceed 10% of the roller drum width.

2.10.4.3 Compaction Process and Acceptance Specifications

On a compacted test field, a forward measuring pass and then a reverse static pass must occur at least twice on each track. If any track differs widely from the average of the others, further passes must be performed to attempt additional compaction. Measuring passes for construction should be continued until the mean of a pass is no more than 5% higher than the mean of the preceding pass. Immediately after the test compaction passes, nine measurements of the E_{v1} value must be performed at areas with low, medium, and high measuring values, where no double jump occurred. The "tester" selects measurement points.

The common calibration procedure involves the correlation of dynamic measuring values with the modulus of the static load plate test (E_{v1}); other tests are also allowed. A linear regression between this data must show a correlation coefficient more than 0.7. The minimum must be greater than 95% of the required E_{v1} value, and the mean must be greater than 105% (or more than 100% during jump operation).

No more than 90% of the track should be below the specified minimum for each measuring pass. The measured minimum must be greater than 80% of the specified minimum. The percent standard deviation (relative to the mean) must be less than 20% within a measuring pass.

2.10.4.4 Miscellaneous Specifications (moisture, speed, frequency, etc.)

Rollers must be operated at a constant travel speed of 2-6 km/h, ± 0.2 km/h (1.2-3.7 mph ± 0.1 mph). The excitation frequency must be kept constant during each measuring pass (within a tolerance range of ± 2 Hz). If the fine grained portion of smaller than 0.06 mm (0.002 in) exceeds 15%, special attention must be given to the water content.

2.10.4.5 Documentation Requirements

Calibration must document the following: rolling pattern, sequence of compaction and measuring passes, change of amplitude and/or travel speed (with associated reasons), and comparative tests (locations, allocation to the specific measuring pass). Prior to each measuring pass, a track plot of the dynamic measuring values must be recorded (and must be printable). The minimum, maximum, mean, deviation, and other values must also be automatically documented for the following:

dynamic measuring values, theoretical amplitude, frequency, travel speed, and jump operation. The area plot must be printed. Values must have assigned coordinates, must be stored for future review, and be guaranteed to be free of manipulation.

2.10.5 Mn/DOT - 2006 TH 64 (Minnesota DOT)

2.10.5.1 Equipment Specifications

A smooth drum or padfoot vibratory roller weighing at least 11,300 kg (25,000 lbs) is recommended. The roller must be equipped with an onboard GPS system to allow continuous recording of roller location and corresponding compaction output (e.g., number of roller passes and CCC/IC measurements). The Contractor shall provide at least one roller equipped with a Continuous Compaction Control (CCC) or Intelligent Compaction (IC) system during earthwork construction. The CCC/IC roller must be the final roller used to obtain compaction on the proof layers.

2.10.5.2 Location Specifications (including size, depth, and track overlap)

Each control (calibration) strip must be at least 100 m x 10 m (300 ft x 32 ft) at its base (or another size as approved by the Engineer). The control strip thickness should equal that of the planned granular treatment thickness that will be constructed (up to a maximum of 1.2 m (4.0 ft). It is recommended to construct one control strip for each different type/source of grading material that will be used on the construction site.

2.10.5.3 Compaction Process and Acceptance Specifications

The Contractor and Engineer should save material samples from each of the control strips for comparison with the embankment materials that will be placed.

Compaction and mixing shall be uniform from bottom to top and for the entire length and width of the embankment. Optimum compaction is reached when the engineer determines that additional compaction passes do not result in a significant increase in stiffness. Intelligent Compaction Target Values (IC-TV) for all proof layers shall be the values obtained on the 1.2 m (4.0 ft) layer of each control strip unless the layer thickness is less than 0.75 m (2.5 ft). In that case, IC-TV is the value obtained on the 0.6 m (2.0 ft) layer of the strip. All segments shall be compacted so at least 90% of the IC stiffness measurements are at least 90% of the IC-TV prior to placing the next lift. If localized areas have IC stiffness of less than 80% of the IC-TV, the areas shall be re-compacted. If a significant portion of the grade is more than 30% in excess of the selected IC-TV, the engineer shall re-evaluate the IC-TV.

2.10.5.4 Miscellaneous Specifications (moisture, speed, frequency, etc.)

Water content should be within 65% to 100% of the optimum moisture content, as determined by the standard Proctor density method (ASTM- D 698). The Contractor shall add water, and/or perform blending as needed to meet the moisture requirements. Control strips constructed at each moisture content extreme can be used to determine a linear IC-TV correction trendline. The Engineer may order the Contractor to provide a light weight deflectometer and/or electronic moisture meter or other moisture testing device. The Engineer grants final approval, based on observation of final compaction/stiffness recording pass, approval of weekly QC reports, moisture tests, and test rolling requirements.

2.10.5.5 Documentation Requirements

Weekly QC report must document all compaction results, IC stiffness measurements, moisture testing results, QC activities, and corrective construction actions taken in order to meet specs. Roller output must be immediate to allow for real-time corrections, must be available for review on demand, and must include a plan-view, color-coded plot of roller stiffness and/or pass number measurements (or other approved data format).

2.11 Other New Methods for Compaction Control

Automated compaction control can also be achieved by the spectral analysis surface wave method (SASW) or the continuous surface wave technique (CSW) (Brandl and Adam 2004). Both compaction control methods are non-intrusive and applicable for soils and other granular materials of all types. In contrast to the CCC methods discussed earlier in this chapter, SASW and CSW techniques require separate external testing equipment that has to be placed on a level ground surface, often consisting of an electromagnetic vibrator to generate surface waves and a row of geophones to detect these waves. Consequently, real-time continuous compaction optimization is not possible, and trying to use a continuous compaction control technique with this approach may require extensive calibration. However, a significant advantage of the CWS technique is its deep-reaching capacity which enhances the post-evaluation process of the compaction quality for the entire soil structure (Brandl and Adam 2004).

Continuous density control of a compacted layer has been studied as well using a nuclear-based approach. The first American attempt at continuous density readings was performed in 1984 and was called Density on the Run (DOR) (Minchin and Thomas 2005). This system utilizes gamma photons in the same manner as the nuclear density gauge does, and was mounted on the compactor at a fixed distance from the asphalt surface. It also uses the same air-gap ratio method as the one that is used by stationary NDGs, and involves mounting a radioactive source and a gamma detector below the axle shaft. The detector converts the data to density and percent compaction (Minchin and Thomas 2005). Recently, a new recording system has been developed for making density measurements in pavement construction, called the Onboard Density Measuring System (ODMS). The approach used by this system is patented by Penn State University (patent no. 6,122,601), and offers density measurements in real time at a rate of one per second during the compaction process, thereby providing the constructor with the opportunity to recognize and correct compaction problems immediately while maintaining a permanent record of the entire compaction process. The basis of this method is to establish a relationship between a compactor's vibratory response and the density of the asphalt mat being compacted (Minchin and Thomas 2005).

Chapter 3

FIELD STUDY

3.1 Introduction

An experimental study was performed at Burrice Borrow Pit (Figure 3.1) in Odessa, Delaware in July of 2008 to independently investigate the use of continuous compaction control (CCC) systems under real field conditions and to evaluate the effectiveness and reliability of this technology as a new quality control technique.

Figure 3.1 The designated area for the field study at Burrice Borrow Pit, Odessa, Delaware

In pursuit of this goal, a number of state-of-the-art in-situ tests were performed in areas that had been compacted by a CCC equipped roller, to allow for comparisons between in situ test results (more conventional methods) and CCC measurements. This chapter describes in detail the field study that was conducted.

3.2 Constructing the Embankment

A 61 m long by 6 m wide (200 ft by 20 ft) embankment was built out of poorly-graded sand with silt (SP-SM) and silty sand (SM) (the former was predominant) (ASTM D 2487), a commonly used borrow material for the Delaware Department of Transportation, which conforms to DelDOT class G borrow specifications, Grades V and VI (Figure 3.2).

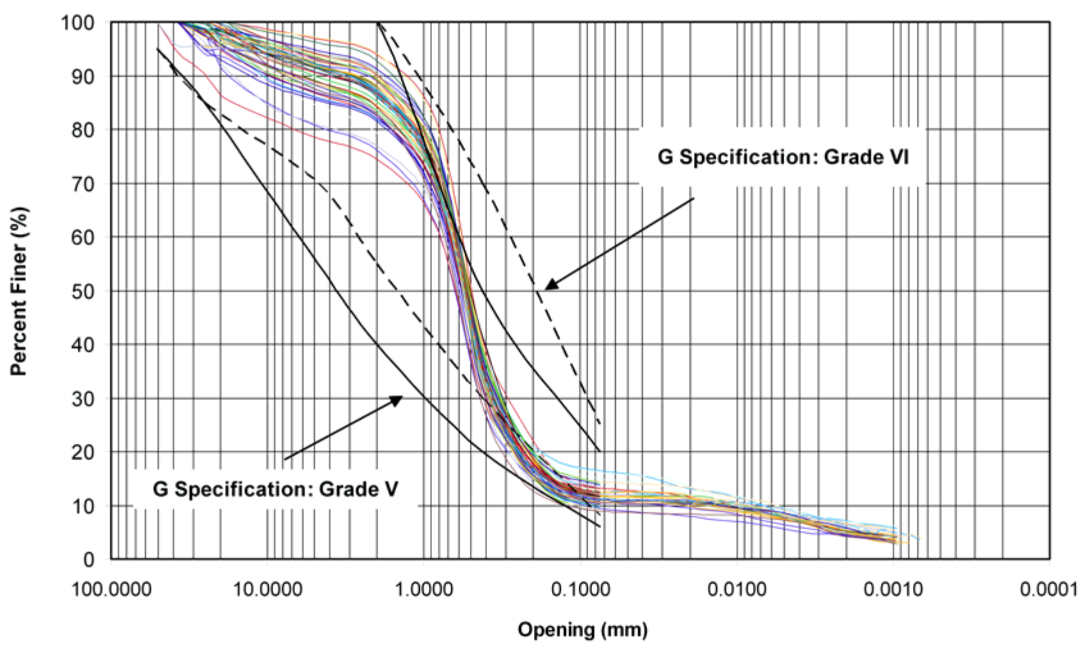

Figure 3.2 Gradation results for field samples taken from in situ test locations

Table 3.1 provides overall gradation information for the compacted soil, as determined from the 53 samples that were analyzed from the field site. In the "Unified Classification" row, the numbers in parentheses refer to the number of samples of each type that were observed: 36 were classified as SP-SM and 17 were classified as SM. However, as shown in Figure 3.2, there was relatively uniform consistency for the soil types that were tested, despite the differing classifications that were observed. A few Atterberg limit tests (ASTM D 4318-05) conducted on the fine portion of the soils indicated that the finer portion of the soils examined in this study were nonplastic (NP) in nature.

Table 3.1 General information of the classification results

Sieve Results	Min	Max	Mean	Std. Dev.	CV (%)
> No. 4 (%)	3.11	21.73	10.01	3.86	38.50
< No. 200 (%)	8.89	16.41	11.67	1.65	14.12
< 2μm (%)	4.23	7.10	5.46	2.81	51.52
C_u	21.71	128.07	66.84	38.52	57.64
C_c	6.78	30.93	16.77	9.45	56.33
Unified Classification.	SM (17)	SP-SM (36)	SP-SM	NA	NA

The embankment was constructed to an approximate total final height of 0.9 m (3.0 ft), by compacting five 20.3 cm (8 in.) loose lift layers, in accordance with Delaware general specifications for road sub-base construction (DelDOT 2001).

Before beginning construction, the designated area was marked by installing grade stakes at approximately 3.0 m (10 ft) intervals on either sides of the construction pad. Elevation readings for independent control of the construction process were taken using a surveyor's level and level rod (Figure 3.3). These tools were also used to align the boundary of the proposed pad and to direct the installation of grade stakes in a relatively straight line. GPS survey was later used to confirm the location of the 26 grade stakes that were installed, as shown in Figure 3.4.

Figure 3.3 Installing the grade stakes; (a) level shooting, (b) driving the grade stakes

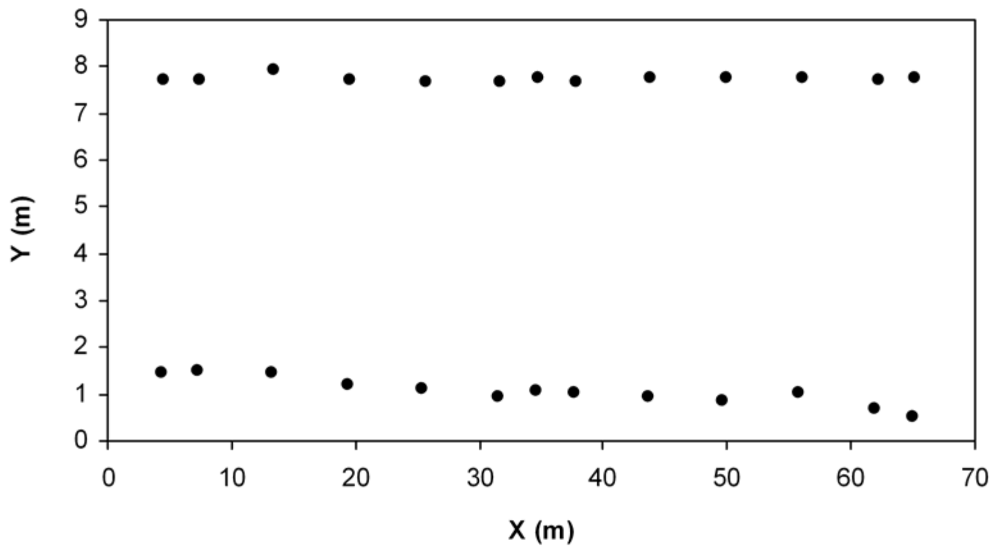

Figure 3.4 Location of grade stakes on the construction area

A GPS base station was also set up before starting construction in the fill area, as shown in Figure 3.5. As described in Chapter 2, all GPS measurements were conducted relative to the defined base station location, which was constant and located in a safe place away from the on-site construction traffic.

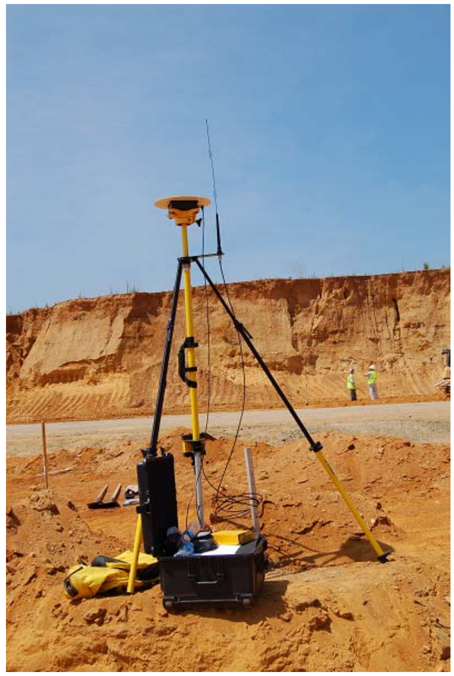

Figure 3.5 Local GPS station

To construct each lift, a Caterpillar 980H bucket loader was used to place fill for spreading by the on-site bulldozer, as shown in Figure 3.6. The material was supplied from a nearby borrow area and deposited in rows at various locations along the test pad for easy and efficient spreading with a bulldozer. The 980H bucket loader did not traffic on the test pad area itself during the construction process.

Figure 3.6 Placing the fill material for spreading

A Caterpillar D6K dozer was then utilized for spreading the material to an approximate loose-lift thickness of 20.3 cm (8 in), as shown in Figure 3.7. The D6K dozer was equipped with a GPS system, which proved beneficial in establishing a more uniform loose-lift thickness.

Figure 3.7 Spreading the fill material using a GPS-equipped bulldozer

Two methods were used to verify the expected loose-lift thickness of each lift; during fill placement the dozer operator checked lift thickness via the GPS control system mounted on the dozer blade, after lift completion the thickness was confirmed by spot-checking elevations throughout the test pad area using a GPS rover unit (Figure 3.8).

Figure 3.8 Spot-checking the loose lift thickness using a GPS rover unit

After spreading each lift, a water truck was driven through the test area as needed to adjust the moisture content of the fill material to achieve optimum compaction (Figure 3.9).

Figure 3.9 Adjusting the moisture content to optimize field compaction

Upon completion of loose-lift soil placement and moisture conditioning, each soil lift was compacted using a Caterpillar CS56 vibratory smooth drum roller (Figure 3.10).

Figure 3.10 Caterpillar CS56 compactor; (a) side view, (b) front view, and (c) back view, preparing to compact on the test pad

This prototype compaction equipment has been specially modified by Caterpillar research engineers to measure both MDP and CMV values simultaneously (refer to Chapter 2 for a detailed discussion of these properties), while also using an on-board GPS system to accurately establish the location of the compactor as it makes in-situ measurements. The roller drum was 2.1 m (7 ft) wide, and had an operating weight of 11414 kg (25164 lbs). Compaction was performed using both low and high amplitude vibration (0.85 and 1.87 mm, 0.033 and 0.074 in), at a vibratory frequency of about 31.9 Hz (1,914 vibrations per minute). Typically, to speed up the compaction process, high amplitude compaction was performed on the loose materials in the first pass for each layer, and the following passes were performed using low amplitude compaction. This approach was used to prevent overcompaction and to generate CMV values that were more representative of the layer that was being compacted (this was necessary because higher amplitude compaction was assumed to cause the measured CMV values to be more affected by the stiffness of underlying soil layers). In addition, it was assumed that using high amplitude compaction for all passes increased the probability to enter into the mode of double jump, which was not desirable. MDP and CMV values were collected approximately every 30 cm (1 ft) along the length of the test sections. The working speed of the roller was about 3.2 km/h (2 mph).

Using the modified Caterpillar CS56 compactor, each lift was compacted in a series of passes using three side-by-side lanes (the roller width was 2.1 m (7 ft), the test pad width was 6 m (20 ft), which left approximately 15 cm (6 in) of overlap at the edges of each compacted soil "lane"). For each lift, between 6 and 9 compactor passes were performed to achieve the desired level of compaction (target dry unit weights $\geq$ 95% of the maximum dry unit weight obtained from a 1-pt Standard Proctor test, used with a "family of curves" compaction approach). Figure 3.11 shows the direction of the roller movement during the compaction of each lift. The numbers that are shown ranging between 1 and 3 give the sequence of lane compaction for each lift.

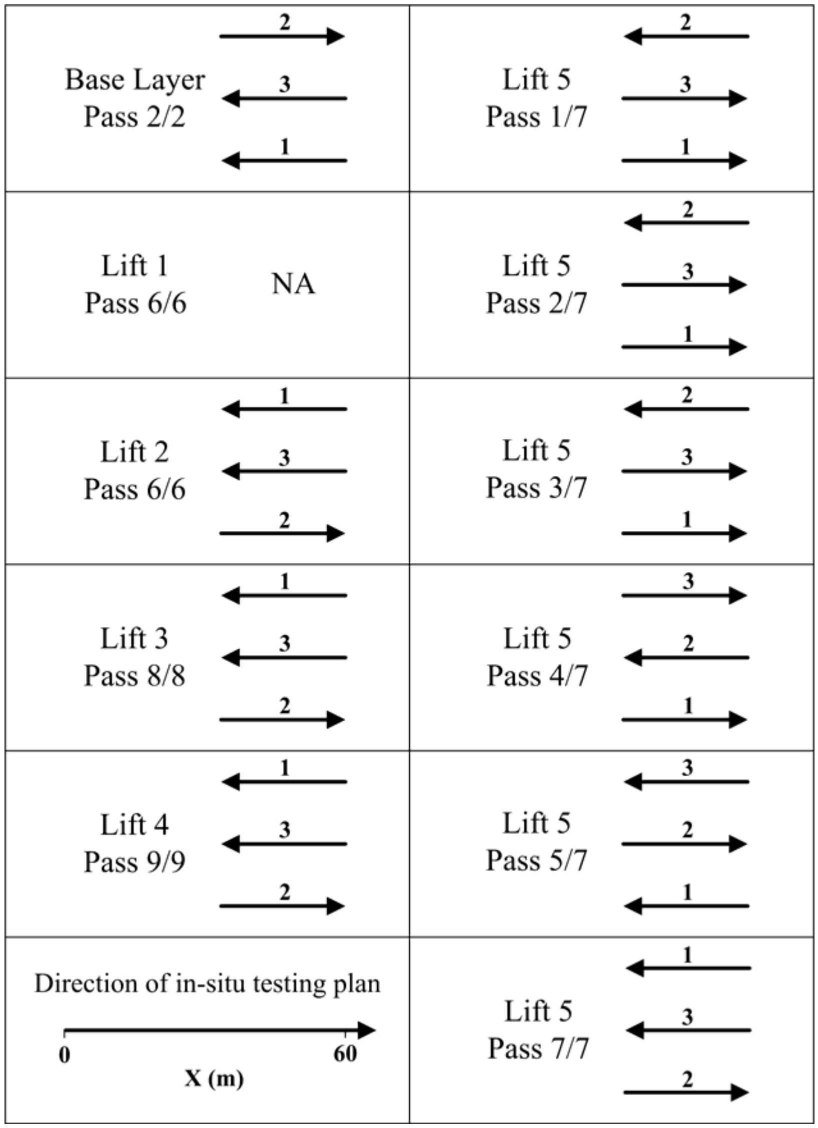

Figure 3.11 Direction of compaction and in-situ testing plan on each lift and pass

During compaction, a computer screen in the cab displayed real-time MDP and CMV measurements to the roller operator using a color-coded map (Figure 3.12).

Figure 3.12   Color-coded map inside the roller cab

Once relatively little change in MDP value was observed by the operator, compaction for a given lift was stopped. The number of compactor passes that were performed to achieve compaction in this study are consistent with the level of compactive effort that is typically required to meet the current DelDOT dry-density specifications, based on technician experience with this borrow soil at other field construction projects (DelDOT representative, personal communication).

Table 3.2 shows the number of passes and time of construction for each compacted lift, and those passes for which CCC and in situ data was recorded for comparison purposes.

Table 3.2 General information of the lift and passes

Lift	Number of Passes Performed	Passes #'s where Data was Recorded	Date	Start of Compaction for this Pass	End of Compaction for this Pass
Base Layer	2	2	7/21/2008	14:18	14:29
Lift 1	6	NA	7/22/2008	NA	NA
Lift 2	6	6	7/22/2008	18:16	18:22
Lift 3	8	8	7/23/2008	11:30	11:36
Lift 4	9	9	7/23/2008	16:22	16:28
Lift 5	7	1	7/24/2008	11:08	11:18
		2	7/24/2008	12:14	12:20
		3	7/24/2008	13:14	13:22
		4	7/24/2008	14:51	14:57
		5	7/24/2008	15:07	15:13
		7	7/24/2008	16:22	16:28

As shown in Table 3.1, the CCC data that was recorded for Lift 1 was lost because of an on-site technical issue related to data storage and download from the CCC equipment. For the sake of time, Lift 5 was the only lift for which successive passes were recorded by the roller operator for comparison with in situ test results; for the other lifts, CCC data were only collected for the final passes for each lift.

3.3 In-situ Testing

During this study, additional in-situ testing was performed for the base materials underlying the test pad and at the completion of the final compactor pass for each lift. In addition, for the 5th lift, in-situ tests were performed after the 1st, 2nd, 3rd, 5th and 7th passes (out of 7 passes total for this lift). For each lift, 19 test stations were established at ≈ 3 m (10 ft) intervals along the centerline. For the 1st, 2nd, 3rd, and 5th passes of lift 5, a reduced in-situ testing plan was followed, to speed the rate of in-situ testing, so the compactor could return to the lift quickly before a significant change in water content could occur. For each in-situ testing series, confirmation of in-situ test locations was performed using the GPS rover unit.

Six types of in-situ tests were performed at various test locations during this study, including the: light weight deflectometer (LWD), GeoGauge, nuclear density gauge (NDG), electronic density gauge (EDG), dynamic cone penetrometer (DCP), and sand cone testing. Each test series was accompanied by disturbed soil sampling, for later determination of the moisture content, particle size characteristics, and Proctor compaction curve. The order of in-situ tests was adopted based on the effect that soil disturbance could have on the in-situ test results. In general, the in-situ tests noted above are listed in the order in which they were performed at each location. Figure 3.13 shows the sequence of in-situ tests being performed on the compacted pad. On the last day, thanks to support provided by the Maryland Department of Transportation, a falling weight deflectometer (FWD) was also added to the in-situ testing methods that were used.

Figure 3.13   Sequence of in-situ tests being performed

In order to effectively accomplish each test series, a slight test location offset was performed with respect to previous test locations. This offset was performed in an attempt to minimize the influence of prior soil sampling for underlying layers on the in-situ test results for the soil layer that is being tested.

3.3 Factors that May Have Influenced the Measured Data

Some significant natural factors had the potential to influence the in-situ test results and associated CCC measurements during the field study. Weather conditions were the first contributing factor, which caused variabilities over time with respect to the in situ moisture content of the soil. Daytime temperatures were in the range of 90 ˚F during the study, which had the tendency to dry the soil over time. In addition, in the evening of 07/22/2008, overnight heavy rains increased the in situ water content of the soil prior to the beginning of the next day's compaction (Figure 3.14).

Figure 3.14 Heavy rain fall affected the water content of the compacted material (07/23/2008, 7:48 AM)

Another factor which had the potential to impact the measured values was the existence of some cobbles in the fill material that could be a potential source of variation in the recorded data (Figure 3.15). Manual "rock-picking was performed periodically in the fill area to try to remove these cobbles when they were encountered (which was not all that frequently). However, the potential presence of these types of rocks in the fill material should be noted, as they can influence the measured test results.

Figure 3.15   Existence of occasional large rocks and cobbles in the fill material

More details on the daily activities that were conducted in this field study can be found in Appendix A, in the form of a daily report of site construction activities.

Chapter 4

IN-SITU MEASUREMENTS

4.1 Introduction

As described in Chapter 3, several in-situ testing techniques were employed in the field study to evaluate the effectiveness of the continuous compaction control system. Prior to any statistical analysis of the recorded CCC data, it is beneficial to see the variation of the recorded in situ test values along the compacted area. This data is presented to provide a brief insight into the nature and quality of the compaction process, prior to further discussion and analysis of the measured CCC results (Chapter 5). This chapter provides an overview of the results from the in situ tests that were performed.

4.2 In-situ Measured Values over the Compacted Area

As discussed in detail in Chapter 2, the goal of compaction is to improve the mechanical and physical properties of the soil. The conventional method that is used to control the quality of the compaction process is to perform a number of random spot tests on the compacted area and to compare the results with standardized laboratory control tests (DelDOT 2001, ASTM D 698, ASTM D 1921, ASTM D 2216). In this study, the types of in situ quality control tests that were performed can be grouped into two general categories: density-based and modulus-based test methods. The nuclear density gauge (NDG) was used for density-based testing. The following devices were used to conduct modulus-based tests: a light weight deflectometer (LWD) with plate diameter of 200 mm (LWD 200), a falling mass of 10 kg (22 lbs), and a drop height of 540 mm (21.3 in); a LWD with a plate diameter of 300 mm (LWD 300), a falling mass of 10 kg (22.0 lb), and a drop height of 730 mm (28.7 in); a dynamic cone penetrometer (DCP) with falling mass of 8 kg (17.6 lbs), a drop height of 575 mm (22.6 in), and an overall penetration depth of 152.4 mm (6 in); and a GeoGauge. The basic operating principles behind each of these tests are described in more detail in Chapter 2. Although other in situ tests were performed periodically during the field study (as described in Chapter 3), these in-situ tests were the most frequently utilized, and consequently their results are the most useful for understanding how compaction progressed for each lift.

All of the data presented in this chapter correspond to in situ tests that were conducted along the middle lane of compaction (in general, along the centerline of the test pad area, with only minor location offsets). Data recorded correspond to in situ tests conducted after the final passes of each lift and for sequential compactor passes on Lift 5. Figures 4.1a and 4.1b show the values of dry unit weight that were measured using the NDG test.

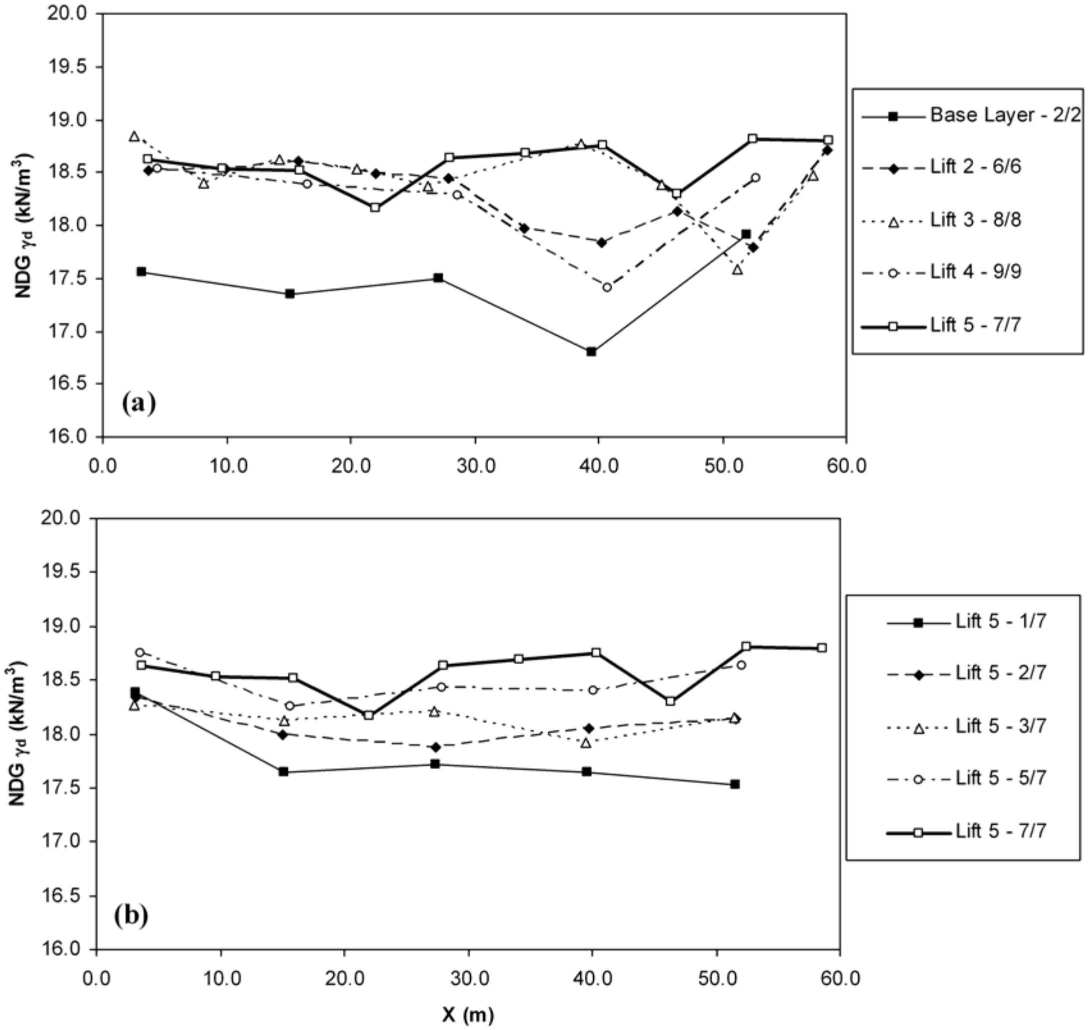

Figure 4.1 Variation of NDG measured dry unit weight along the centerline; a) all final passes b) successive passes on Lift 5

As shown in Figure 4.1, the dry unit weight measured by the NDG varied in the range of 16.5 kN/m^3 to 19.0 kN/m^3. Among the compacted lifts, the base layer had the lowest final dry unit weight and Lift 5 exhibited the largest values overall (note however that the values for Lift 5 were generally consistent with those measured for other lifts at various points along the centerline). The gradual improvement of the soil with successive compaction passes is also apparent in Figure 4.1b.

Figures 4.2a and 4.2b show the degree of compaction or relative compaction (RC) along the centerline. Commonly used for performing compaction control in the State of Delaware, a given value of relative compaction is calculated by dividing the dry unit weight of the soil by the maximum dry unit weight determined using a “family of curves” approach along with data from a 1-pt standard Proctor test (ASHTO T 272). To present the results in percent, the calculated relative compaction value is multiplied by 100.

The Delaware DOT earthwork construction specifications dictate an acceptance criteria of ≥ 95% for the relative compaction; for comparison purposes, this criteria is also shown in Figures 4.2a and 4.2b (DelDOT 2001). As shown in Figure 4.2a, with the exception of the base layer (which was only proof-rolled), the degree of compaction for the final passes of each lift generally met the DelDOT relative compaction criteria (only 3 of the points would have failed by this criteria). Unfortunately, values of relative compaction could not be determined for the successive passes of Lift 5, as 1-pt Proctor tests could not be run at the same location for each pass without extensive soil sampling in the zone of interest, which would have affected the overall test results from the field study. Consequently, corresponding “per pass” values were not available for presentation in Figure 4.2b.

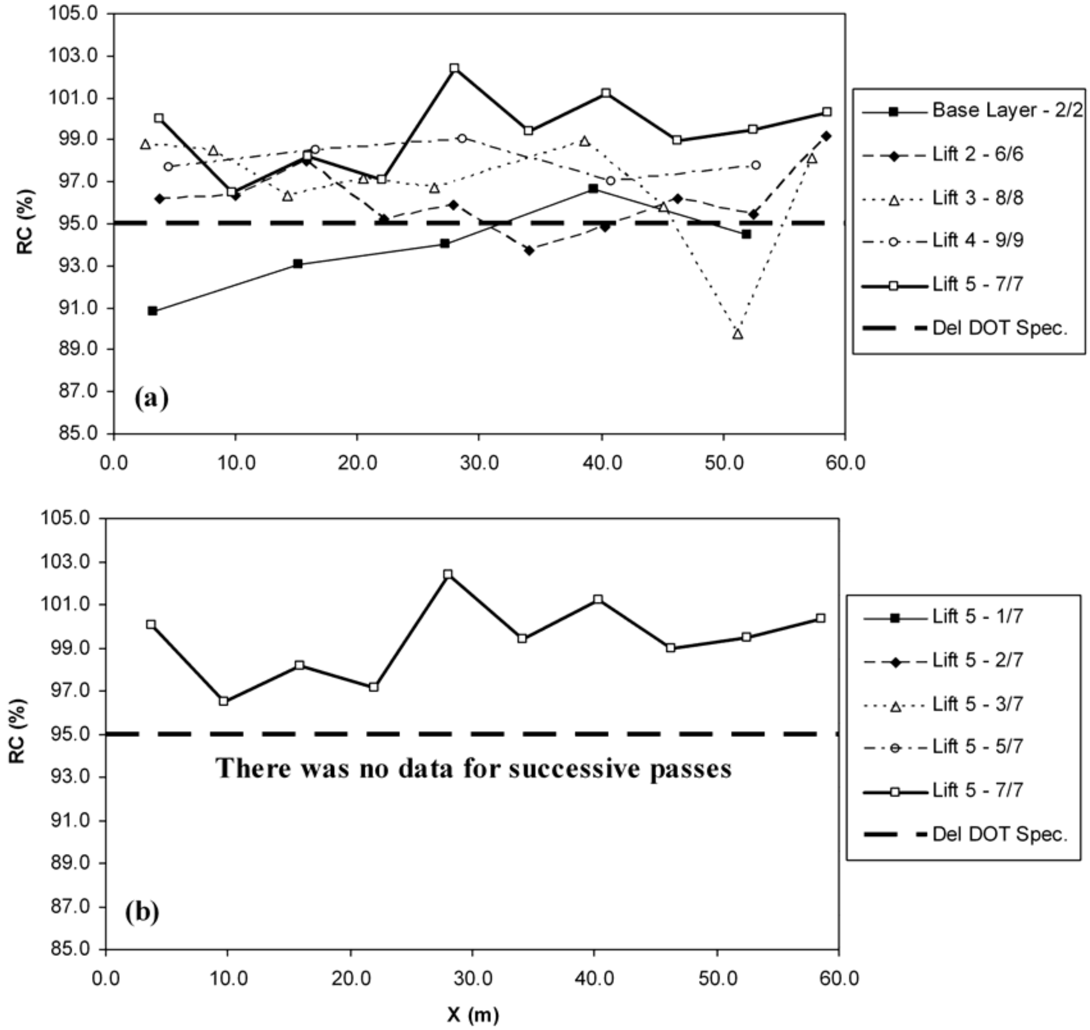

Figure 4.2 Variation of relative compaction values along the centerline; a) all final passes b) successive passes on Lift 5

Figures 4.3a and 4.3b display the variation of NDG measured water contents for the compacted lifts. According to DelDOT specifications, the moisture content of the select borrow base course material at the time of compaction shall be within 2% of the optimum moisture content, which is also provided for each point (from the 1-pt Proctor tests) on the relevant figures. It should be noted that the average of the optimum moisture contents for the compacted material was 11.7%, as determined using the 1-pt Proctor method with the associated family of curves for this borrow material.

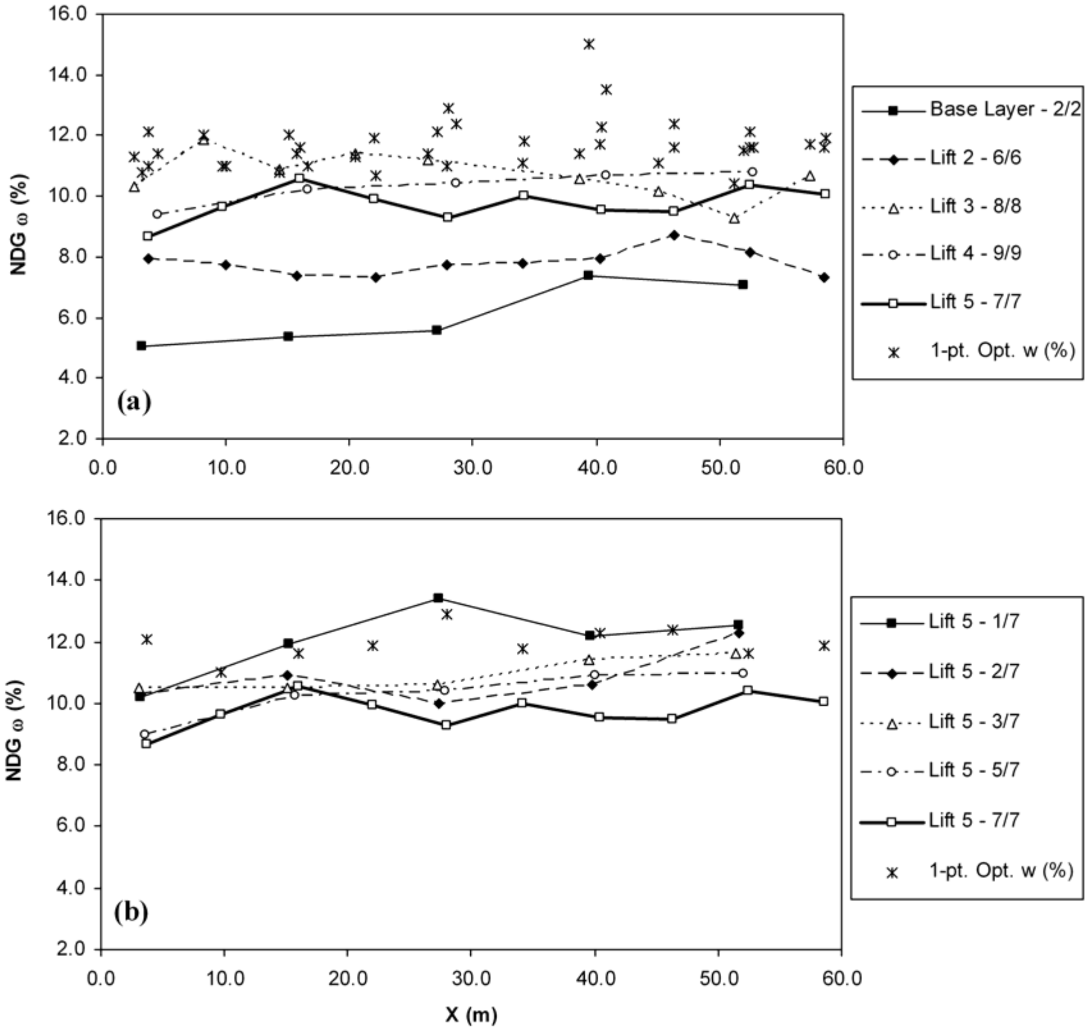

Figure 4.3 Variation of NDG measured water content along the centerline; a) all final passes b) successive passes on Lift 5

The water content of the compacted soil was also measured by performing oven-dried laboratory water content measurements (ASTM D 2216) on specimens taken from the specified stations, as shown in Figure 4.4. For comparison purposes, the associated water content criteria ranges provided in Figure 4.3 are also shown in this figure.

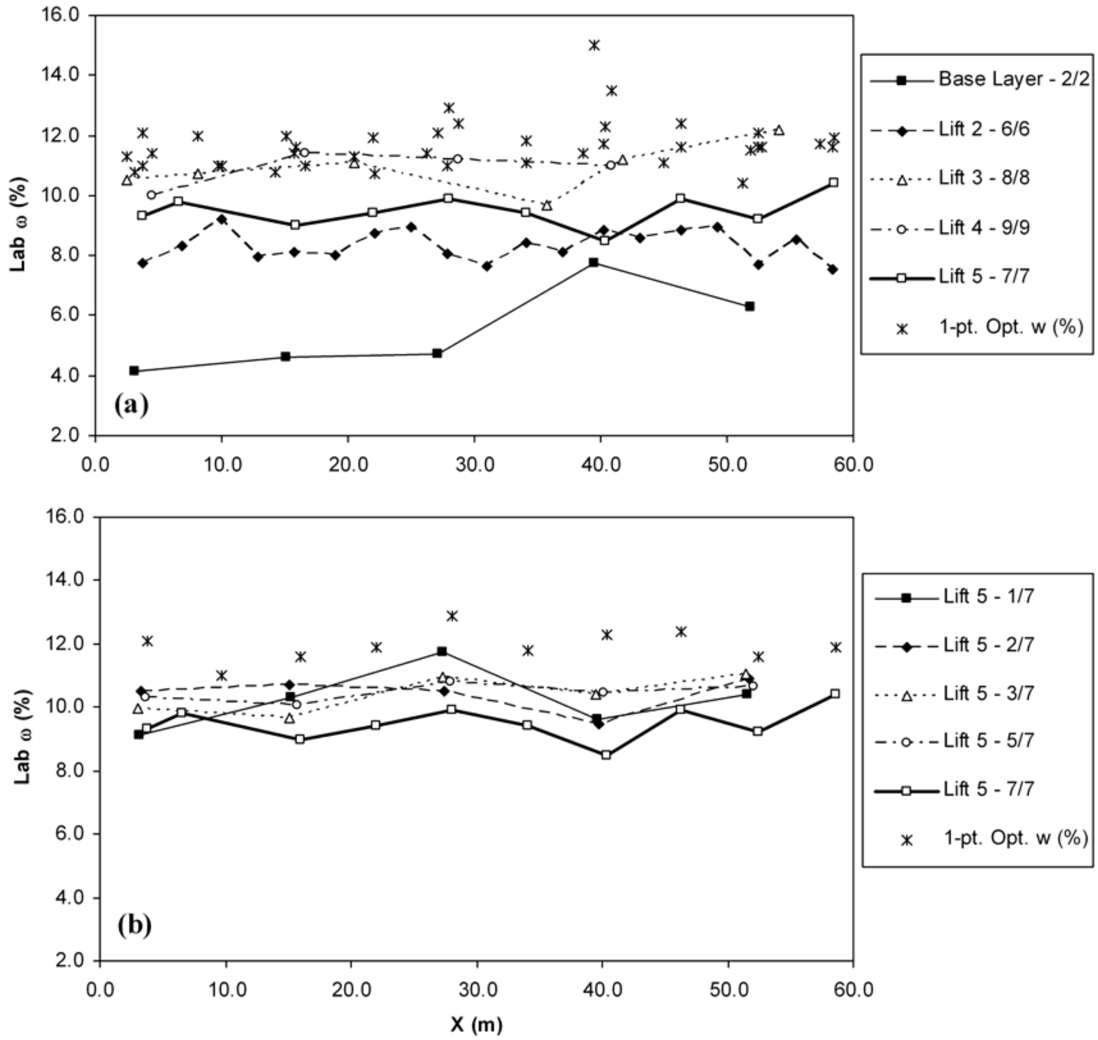

Figure 4.4 Variation of laboratory measured water content along the centerline; a) all final passes b) successive passes on Lift 5

Figure 4.3 and Figure 4.4 both indicate that the base layer was compacted at a significantly lower moisture content than the other lifts (this is not surprising, as moisture conditioning was not performed for the base layer, which was only proof-rolled), and that the successive passes of Lift 5 were compacted at approximately the same water content, within the range of acceptable water content values. In general, compaction of the soil at this project site was performed on the dry side of optimum with respect to the standard Proctor curve for this soil. Figures 4.5 and 4.6 provide a comparison between the measured NDG water contents and the associated Lab water contents, respectively, with their corresponding allowable ranges of water content around the optimum (based on data from 1-pt Proctor tests conducted on the final passes). The measured water contents are presented with solid lines while the corresponding $\omega_{opt} - 2\%$ and $\omega_{opt} + 2\%$ values are specified with dashed lines.

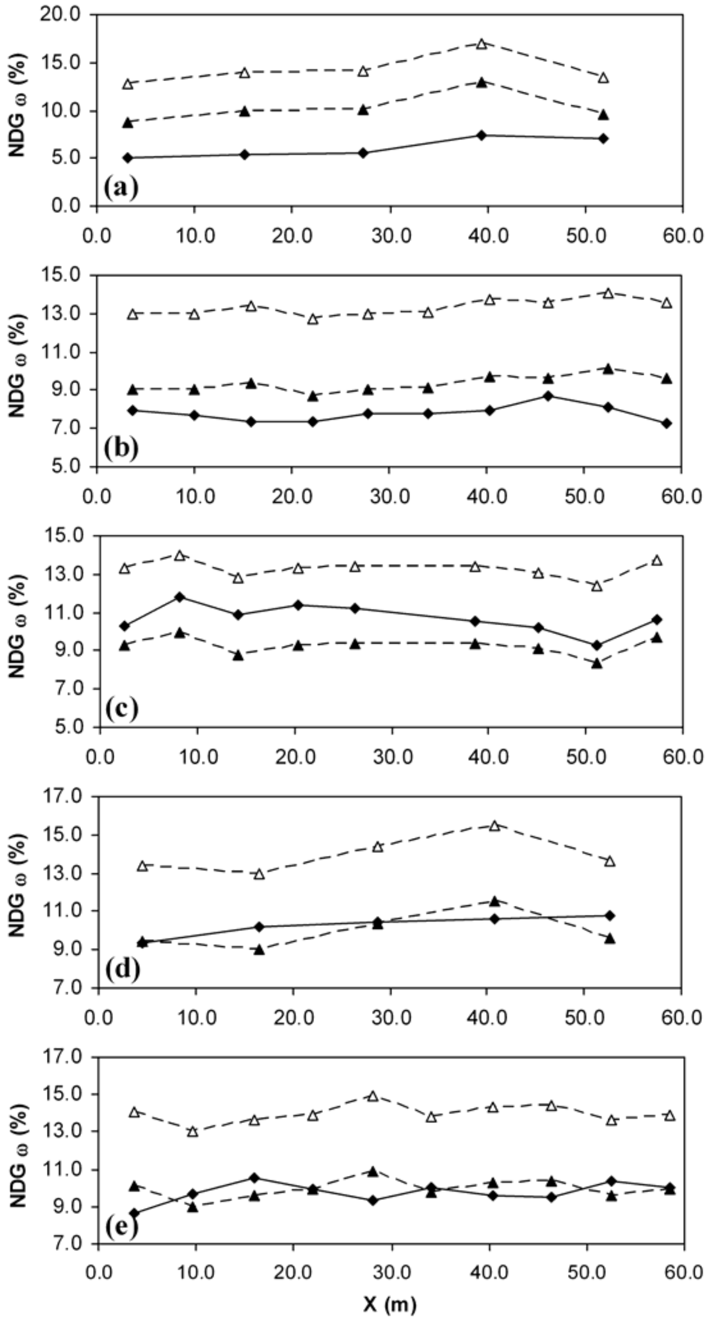

Figure 4.5 Comparing the NDG water contents with the corresponding criteria range around the optimum water contents for the final passes of: a) the base layer, b) Lift 2, c) Lift 3, d) Lift 4, and e) Lift 5

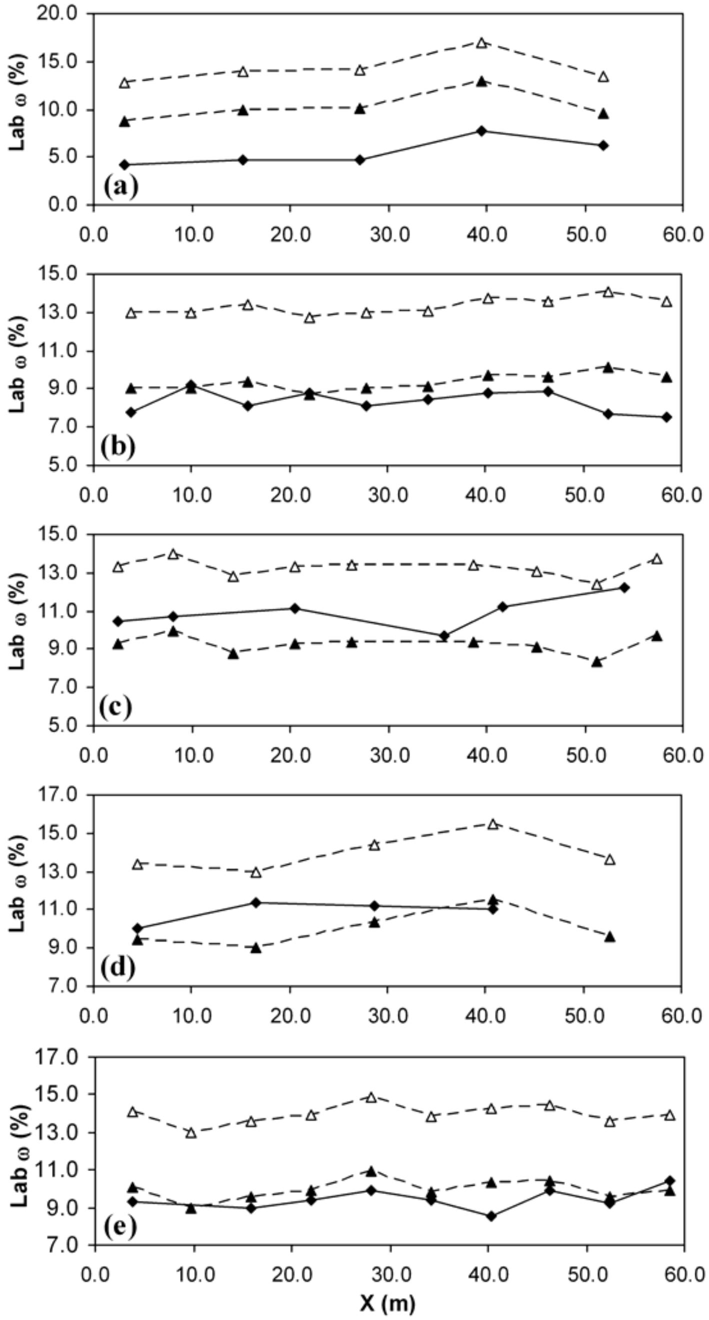

Figure 4.6 Comparing the Lab water contents with the corresponding criteria range around the optimum water contents for the final passes of: a) the base layer, b) Lift 2, c) Lift 3, d) Lift 4, and e) Lift 5

By examining Figures 4.5 and 4.6, it can be seen that the base layer and Lift 2 were compacted below the range of acceptable water content. The same issue holds for half of the measurements for the final pass of Lift 5 and small portion of Lift 4. Lift 3 was the only lift which completely passed the acceptance criteria for moisture content. However, Lifts 4 and 5 were extremely borderline cases, and probably would be considered acceptable by a field engineer, provided that the relative compaction specification was being met in a robust fashion.

Figures 4.7 through 4.11 show the results of modulus-based in-situ tests conducted at the same locations along the compacted lane. In the following figures the modulus is denoted by E.

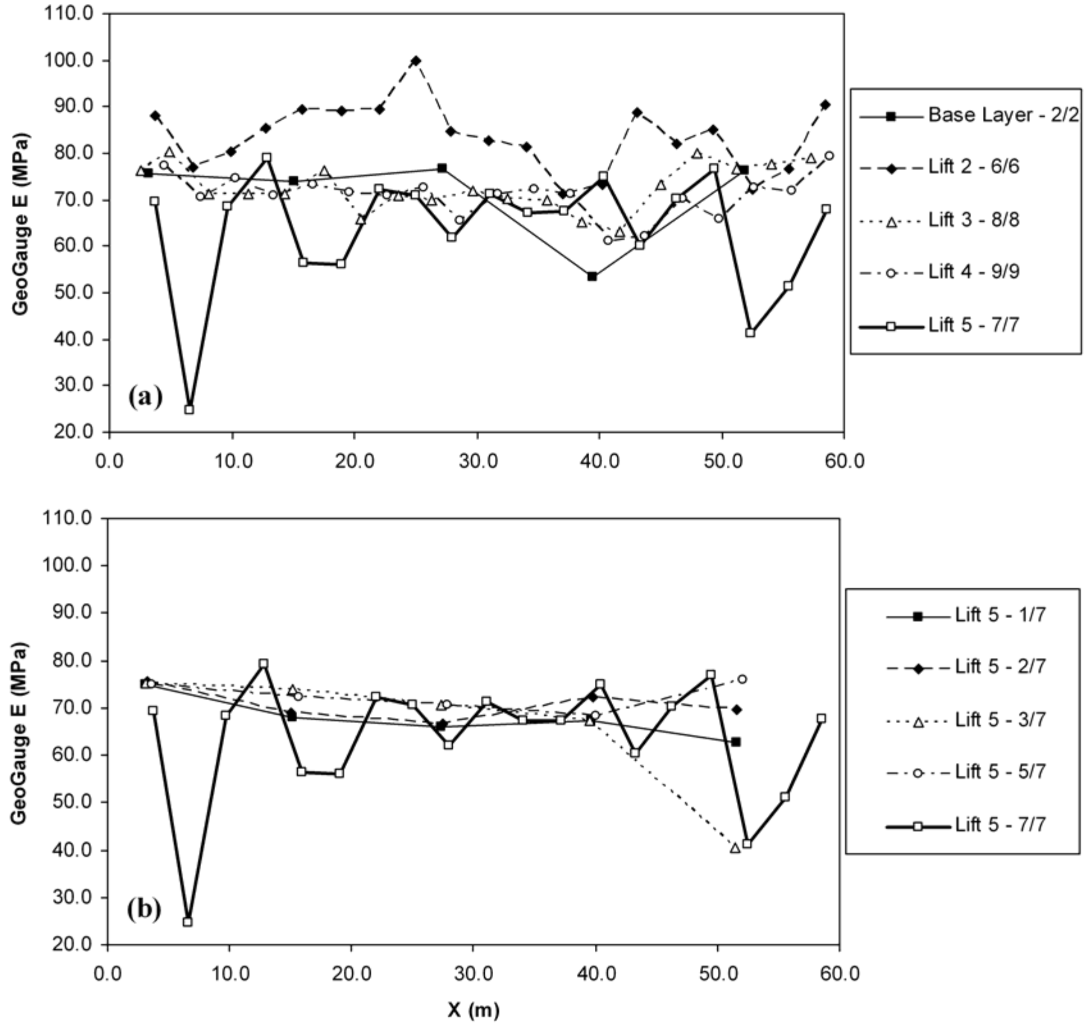

Figure 4.7 Variation of GeoGauge measured modulus along the centerline; a) all final passes b) successive passes on Lift 5

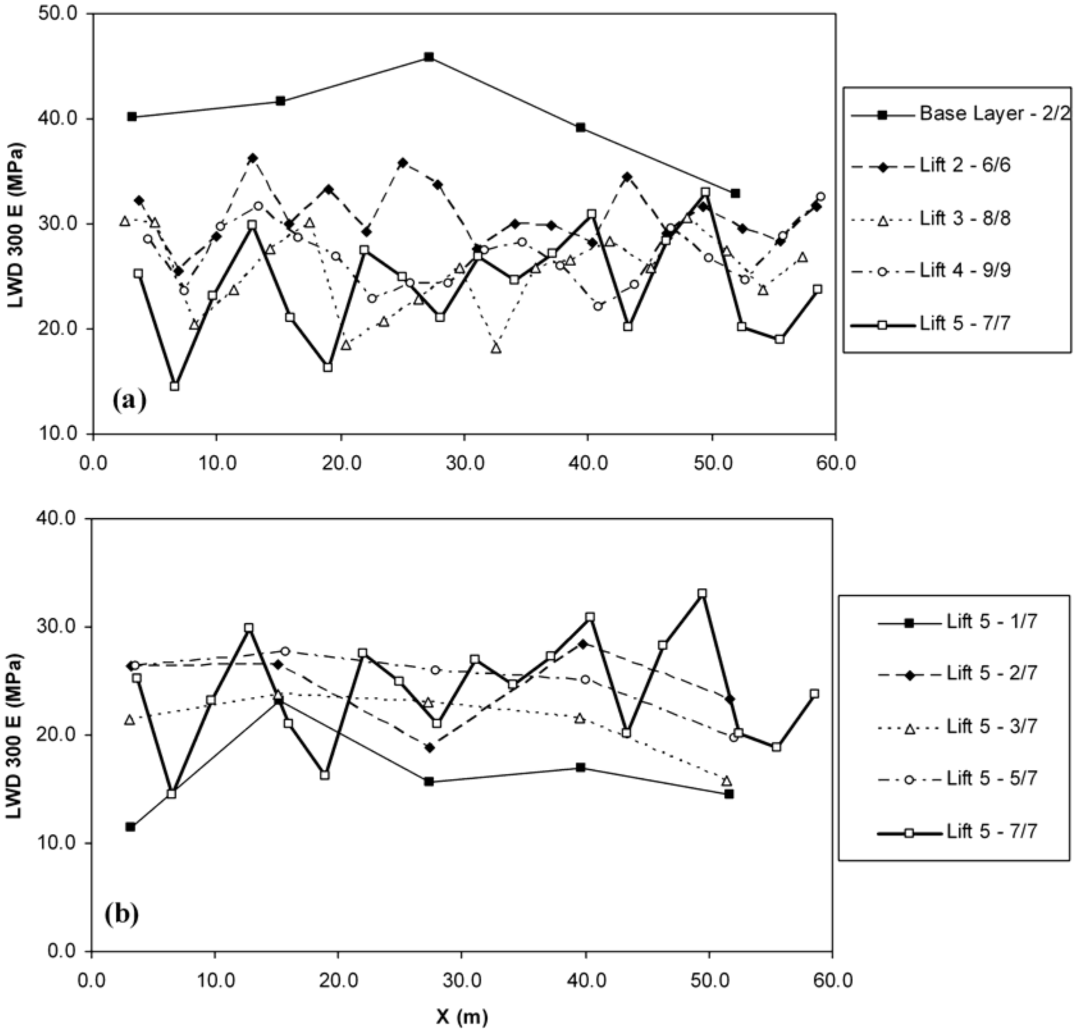

Figure 4.8 Variation of LWD 300 measured modulus along the centerline; a) all final passes b) successive passes on Lift 5

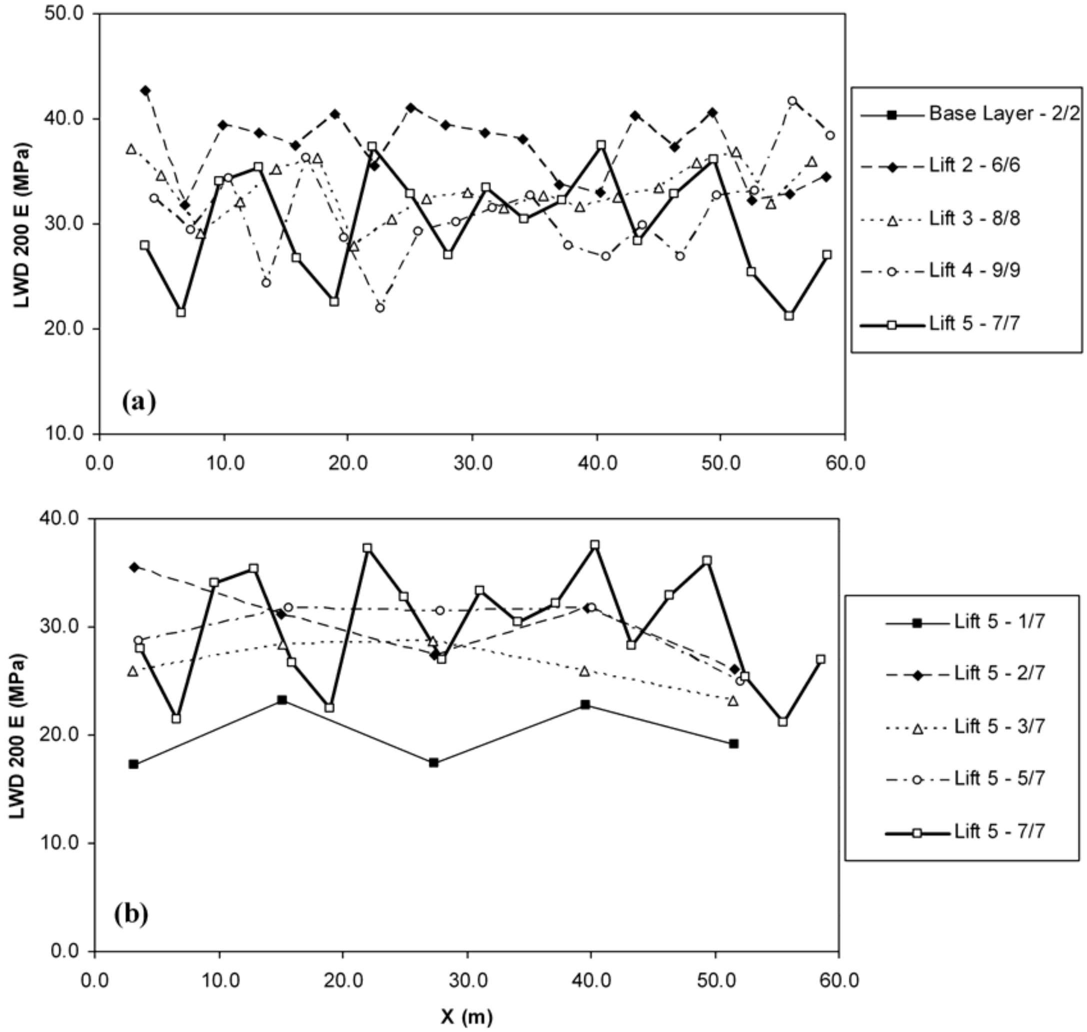

Figure 4.9 **Variation of LWD 200 measured modulus along the centerline; a) all final passes b) successive passes on Lift 5**

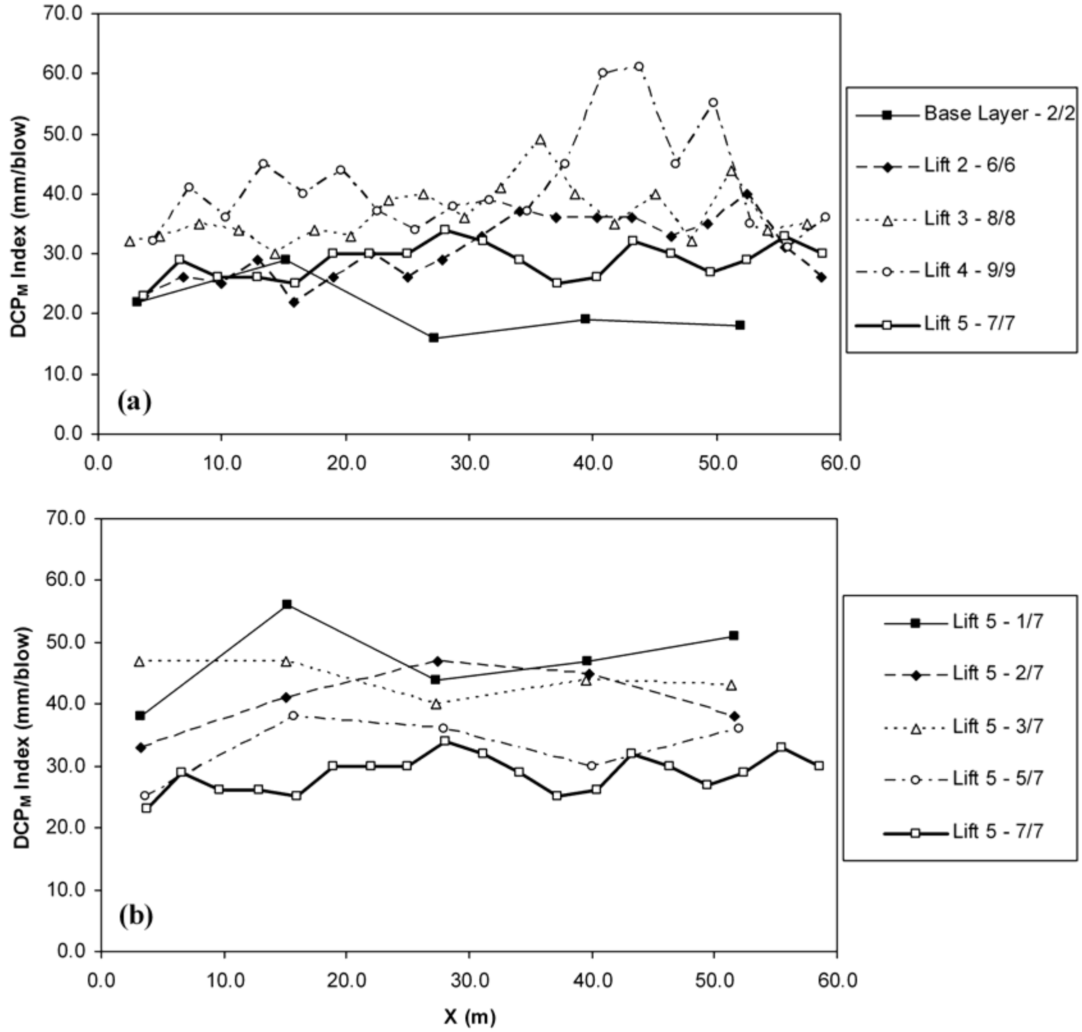

Figure 4.10 Variation of DCP_M index along the centerline; a) all final passes b) successive passes on Lift 5

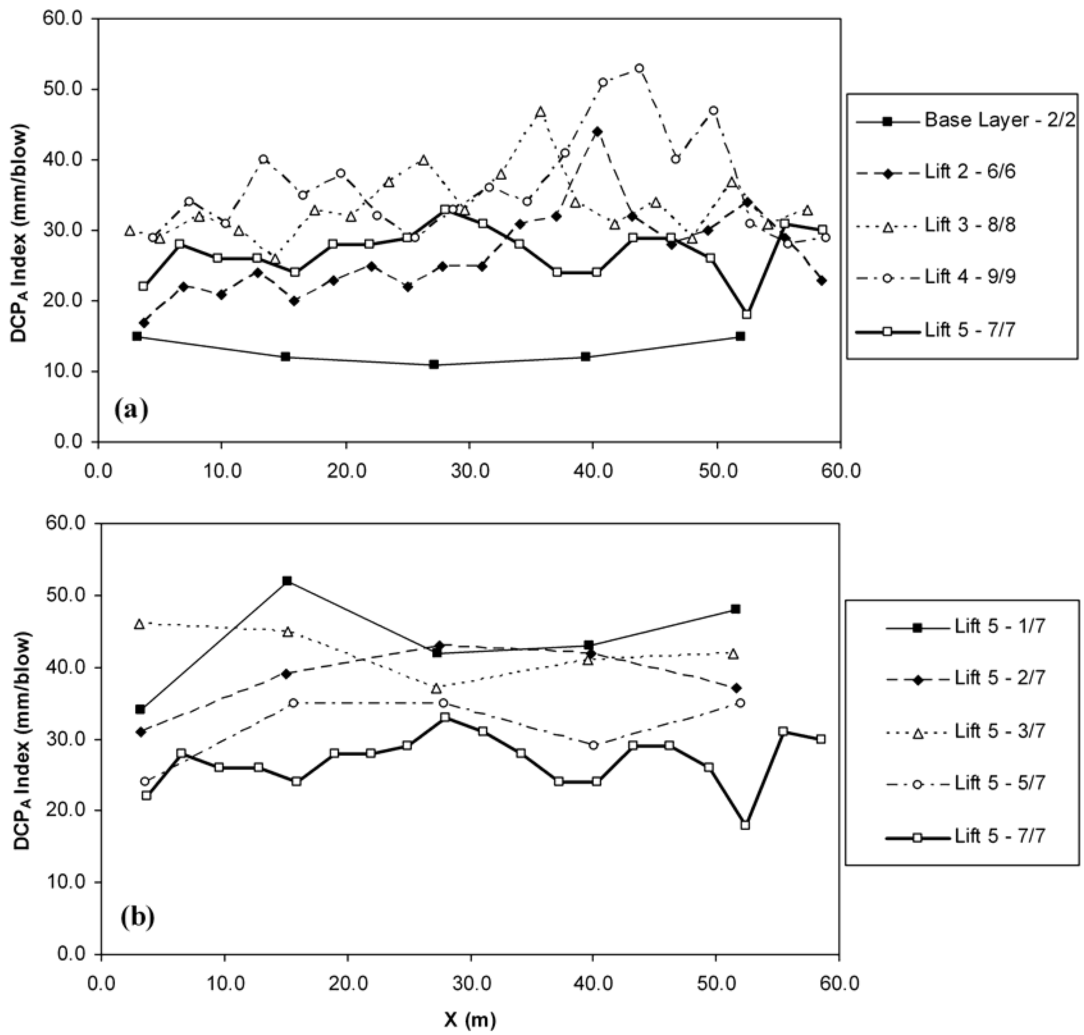

Figure 4.11 Variation of DCP_A index along the centerline; a) all final passes b) successive passes on Lift 5

In general, there are significant differences between the results of the modulus-based in-situ testing methods that were utilized, and it is difficult to compare the variation of the results based solely on the figures that are presented. Variations in the measured values that are presented could be caused by variations in their respective methods of modulus measurement, their different influence depths, or their degree of sensitivity to the site conditions (such as water content) and operator expertise. To provide a better understanding of the measured values, the mean and the coefficient of variation (CV) (Equation 4.1) of the recorded data are presented in Tables 4.1 through 4.4.

$$CV = \frac{\sigma}{\mu} \tag{4.1}$$

where, σ = Standard deviation, and μ = Mean or average.

In the last row of each table, the average of the above values for each lift and pass is provided accordingly.

Table 4.1 Mean values recorded in the density-based tests

Lift - Pass	NDG γ (kN/m^3)	NDG ω (%)	RC (%)	Lab ω (%)
Base - 2/2	17.42	6.07	93.80	5.50
Lift 2 - 6/6	18.30	7.80	96.10	8.33
Lift 3 - 8/8	18.49	10.70	97.00	10.90
Lift 4 - 9/9	18.21	10.29	97.99	10.90
Lift 5 - 1/7	17.78	12.05	NA	10.23
Lift 5 - 2/7	18.08	10.83	NA	10.42
Lift 5 - 3/7	18.13	10.92	NA	10.41
Lift 5 - 5/7	18.50	10.30	NA	10.45
Lift 5 - 7/7	18.58	9.75	99.37	9.48
Average	18.17	9.86	96.85	9.62

As mentioned previously, the optimum moisture content of the compacted material was in the range of 10.4% to 15.0%, with an average value of 11.7%. By examining the water content data shown in Table 4.1, Figure 4.5, and Figure 4.6, it appears that the minimum water content criteria was not met for compaction of the Base Layer or Lift 2, but that this criteria was reasonably satisfied for the remainder of the lifts. Clearly, compaction occurred on the dry side of optimum for nearly the entire project.

Table 4.2 Mean values recorded in the modulus-based tests

Lift - Pass	GeoGauge (MPa)	LWD 300 (MPa)	LWD 200 (MPa)	DCP_M (mm/blow)	DCP_A (mm/blow)
Base - 2/2	71.18	39.88	NA	20.80	13.00
Lift 2 - 6/6	83.52	30.81	37.24	30.47	26.68
Lift 3 - 8/8	72.64	25.46	33.18	36.63	33.47
Lift 4 - 9/9	70.78	26.89	30.97	41.63	36.37
Lift 5 - 1/7	67.70	16.36	19.94	47.20	43.80
Lift 5 - 2/7	70.62	24.70	30.38	40.80	38.40
Lift 5 - 3/7	65.57	21.12	26.44	44.20	42.20
Lift 5 - 5/7	72.48	24.98	29.70	33.00	31.60
Lift 5 - 7/7	63.56	24.06	29.98	28.74	27.05
Average	70.89	26.03	29.73	35.94	32.51

By examining the data shown in Tables 4.1 and 4.2, the following conclusions can be drawn:

- The NDG test was the only in situ test method that showed a consistent increase in measured index values with successive compactor passes. The DCP also appeared to work well in this regard, only with the measured index values decreasing with successive compactor passes (an inverse relationship). The other tests that were conducted seemed to show more sensitivity in the test results to various test factors such as variations in their influence depths or their degree of sensitivity to site conditions (such as water content) or operator expertise.

- The water content values measured by the NDG were different from the water contents measured in the laboratory.
- The average water content of the material placed in the upper three lifts was generally within -2% of the optimum moisture content, which conforms to current DelDOT specifications (DelDOT 2001). The Base Layer and Lift 2 did not satisfy this criteria, although the associated density criteria were satisfied.
- The GeoGauge yielded larger measured values of moduli, as compared to the LWD 300 and LWD 200.
- The measured values of modulus from the LWD 300 were slightly lower than those from the LWD 200.
- The DCP_M index values were larger than the corresponding DCP_A index values. This observation is consistent with the nature of their formulation.

Tables 4.3 and 4.4 summarize the coefficient of variation of the measured values for each of the in-situ tests that were conducted:

Table 4.3 Coefficient of variation of values recorded in the density-based tests

Lift - Pass	NDG γ_d	NDG ω	RC	Lab ω
Base - 2/2	2.33	17.50	2.26	26.86
Lift 2 - 6/6	1.86	5.53	1.60	6.07
Lift 3 - 8/8	2.02	7.01	2.92	7.63
Lift 4 - 9/9	2.52	5.41	0.80	5.70
Lift 5 - 1/7	1.94	9.85	NA	9.65
Lift 5 - 2/7	0.95	8.24	NA	5.35
Lift 5 - 3/7	0.76	4.93	NA	5.89
Lift 5 - 5/7	1.05	7.86	NA	2.90
Lift 5 - 7/7	1.15	5.63	1.80	5.69
Average	1.62	8.00	1.88	8.42

Table 4.4 Coefficient of variation of values recorded in the modulus-based tests

Lift - Pass	GeoGauge	LWD 300	LWD 200	DCP_M	DCP_A
Base - 2/2	13.94	11.81	NA	24.37	14.39
Lift 2 - 6/6	8.76	9.38	9.04	17.31	23.44
Lift 3 - 8/8	6.80	15.40	7.82	13.00	14.24
Lift 4 - 9/9	6.42	10.97	15.28	20.94	20.38
Lift 5 - 1/7	6.74	26.44	14.51	14.48	15.52
Lift 5 - 2/7	4.89	15.19	12.30	13.69	12.43
Lift 5 - 3/7	21.79	14.85	8.44	6.67	8.44
Lift 5 - 5/7	4.28	12.40	9.81	16.32	15.76
Lift 5 - 7/7	20.87	20.54	17.37	10.43	13.18
Average	10.50	15.22	11.82	15.25	15.31

By examining the data shown in Tables 4.3 and 4.4, the following conclusions can be drawn:

- NDG measurements of dry density had the smallest amount of overall variation of all of the in situ test results that were analyzed, based on the average CV of the results.
- The average CV of the water contents measured using the NDG and the oven-based lab procedure were almost the same.
- The GeoGauge test results exhibited the lowest relative variation out of the modulus-based in situ tests that were performed.
- The LWD 300 measurements had a greater CV than the LWD 200 values.
- DCP_M and DCP_A indices had almost the same CV.

4.3 Summary and Conclusion

In this chapter, the results from a series of in-situ tests were presented, to provide insight into the nature and quality of the compaction process, prior to further discussion and analysis of the measured CCC results in the following chapter (Chapter 5). In order to illustrate the behavior of the recorded data, the values of each in-situ test were plotted versus the location along the centerline for each of the test points (distance X, in meters).

According to the NDG measurements, the compaction that was performed generally met the DelDOT density criteria for fill acceptance (RC $\geq$ 95%). The optimum moisture content for the compacted soil was in the range of 10.4%-15.0%, with an average of 11.7%, and the measured water content for most of the engineered lifts and final passes was generally within or very close to the acceptable range around the corresponding optimum moisture contents. The Base layer did not meet the relative compaction and water content specifications. Lift 2 was also placed too dry of optimum, although the relative compaction specifications were still satisfied for this lift.

In general, the density-based in-situ testing measurements exhibited less variability, as compared to the modulus-based in-situ test results. Among the modulus-based in-situ test techniques, the Geogauge test results exhibited less variation than the other modulus-based tests, as indicated by the tests' average CV values. The LWD 300 and LWD 200 showed a general consistency in the measured test results. However, the measured modulus of the LWD 300 and its associated CV were greater than those of the LWD 200. The average DCP_M index values were generally greater than DCP_A index values, while their CV's were the same.

Chapter 5

EVALUATION OF CCC ROLLER MEASUREMENTS

5.1 Introduction

This chapter is dedicated to analyzing the overall CCC roller measurements and to evaluating the respective behavior of these CCC measurements for different lifts and passes. The essential values that are recorded by the CCC system that was used in this study are MDP, CMV, RMV, and the speed of the roller. A detailed discussion of how these values are determined from the raw measured roller data is provided in Chapter 2.

The prototype CS56 roller that was used in this study recorded roller-specific machine drive power values, which are commonly referred to as MDP_2 values (Tehrani and Meehan 2009) or MDP^* values (White et al. 2009). In order to compare the machine drive power values measured in this study with data collected by other researchers (e.g. White et al. 2007), it is useful to calculate standardized MDP values that are not machine-specific (also referred to as MDP_1 values, as noted in Tehrani and Meehan 2009). For the roller used in this study, these values were back-calculated from the machine output data (MDP_2) using Equation (5.1), which is a Caterpillar proprietary relationship (Tehrani and Meehan 2009).

$$MDP = \left(-\frac{54.23\,kW}{150}\right)(MDP_2 - 150) \tag{5.1}$$

By combining the resulting MDP and CMV values with their corresponding point-specific coordinates determined using the onboard GPS system, a spatial map of CCC measurements can be built, and these roller-measured values can be used to provide additional quality control over the compaction process.

In order to develop a basic understanding of what typical CCC data values look like for compacted Delaware soils, it was necessary to perform basic statistical analysis of the measured roller data. This step was essential for obtaining a more thorough understanding about the data that was generated during the field study. In the following sections, the most critical recorded roller data (MDP and CMV values) will be presented in the form of histograms, and the shape of the histograms will be assessed.

5.2 Basic Statistics of the Roller Data

During the CCC process, the recorded roller measurements consist of four main measured values: Machine Drive Power (MDP), Compaction Meter Value (CMV), Resonant Measured Value (RMV), and the speed of the roller. As described in Chapter 2, MDP and CMV are the roller-soil properties that indicate the quality of compaction. All of the recorded MDP and CMV values for each Lift, Pass, and Lane of compaction are provided in Appendix B. In general, as shown in Appendix B and as presented comparatively in Figure 5.1, the spatial distribution of the recorded MDP and CMV values over the compacted area is quite uneven and highly variable from point to point. Note that only the data relevant to the middle lane of compaction for Lift 5 are presented in Figure 5.1; this is to make the shape of the measured traces clearer, and to avoid cluttering the resulting data plot. The solid lines shown in these figures reflect the average of the measured data along each transect. The change in these average values from Pass 2 to Pass 7 (with increasing compactive effort) is quite apparent. However, the point to point variability in recorded MDP and CMV values is quite large in all cases, which makes point-specific comparisons with in-situ test results quite difficult. These comparisons will be discussed further in later chapters.

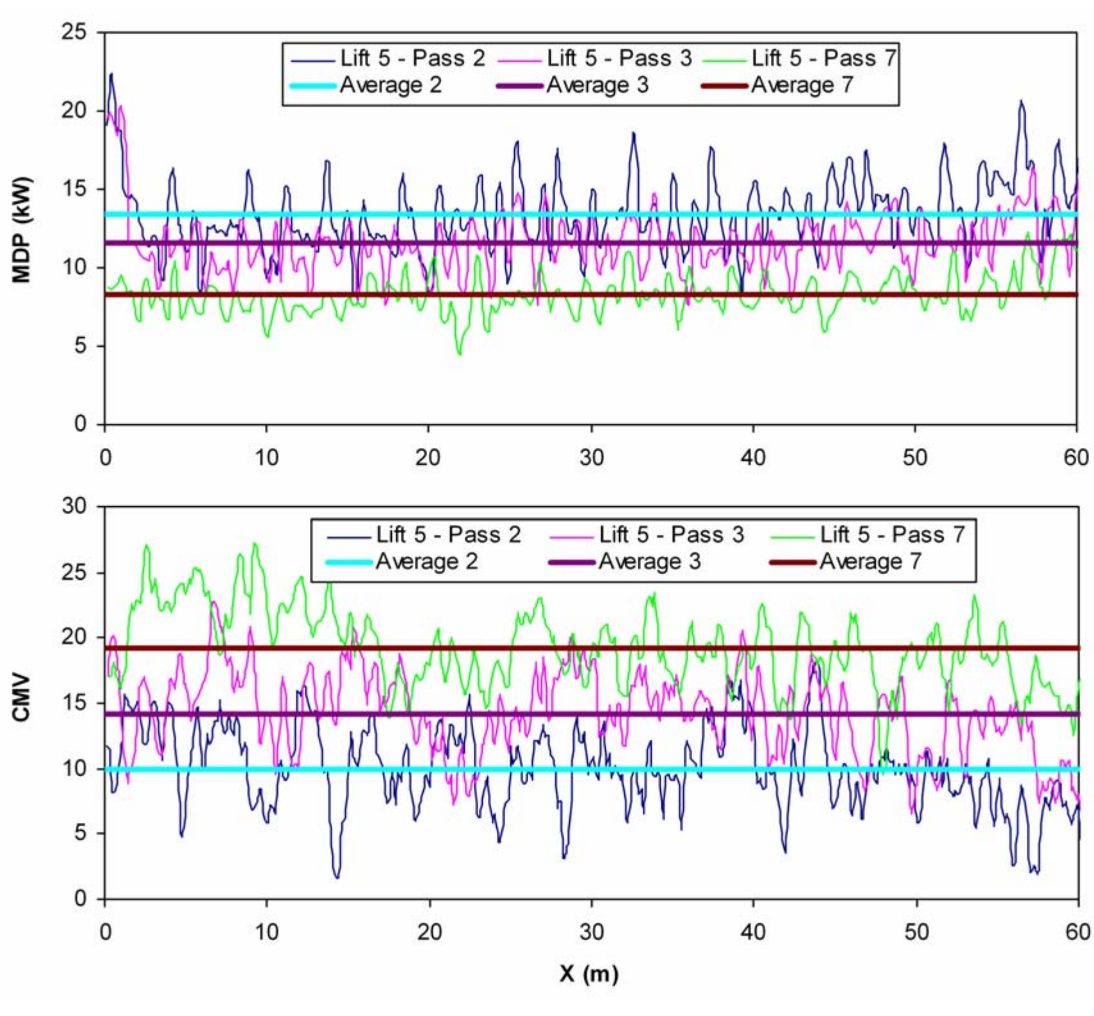

Figure 5.1 Variation of MDP and CMV Values along the Middle Transect of Lift 5

There are a number of possible reasons for the "noisy" MDP and CMV behavior shown in Appendix B and Figure 5.1. Most likely, the primary cause of this variability is the fact that the soil under compaction is not homogeneous and the grain size, grain shape, and in-situ void ratio (and density) of the compacted material can vary significantly along the roller path. Soil-water characteristics can also play a significant role. As noted in Chapter 4, the moisture content of the soil is not constant throughout the compacted area. In addition, it was verified that moisture content had a significant influence on the mechanical properties of compacted soil, particularly strength or modulus based soil measurements (see Chapter 7 and Chapter 8). Other unknown measurement factors also likely have some effect, but are believed to have only a second-order contribution, including: electrical noise in the data acquisition system, variable response of the monitoring instruments, or possible instrumentation errors. Despite the irregular shape of the CCC data over the study area, a clear trend in the average of the data (as can be seen by looking at the solid lines) shows that for increasing compactor passes, the overall CMV values increase and MDP measurements decrease. This behavior is consistent with the relative definitions of these CCC values (Chapter 2).

To develop a greater understanding of the roller measured values, statistical properties for the CCC data sets for each lift were calculated. Table 5.1 and Table 5.2 summarize the essential statistical properties of the MDP and CMV values for different lifts and passes, respectively. It should be noted that the statistical properties shown are for the complete data set for each lift. To further clarify, this means that they are for the total data set that was gathered over all three parallel lane widths for each lift/pass; for comparison purposes, raw data and some basic statistical properties recorded for each lane are provided separately in Appendix B.

Table 5.1 Statistical properties of the MDP values

Lift / Pass	Base	2/6	3/8	4/9	5/1	5/2	5/3	5/4	5/5	5/7
Min (kW)	1.77	0.10	4.70	5.30	0.60	8.10	7.30	3.80	5.20	4.40
1st Qu. (kW)	8.82	5.50	10.00	11.00	16.18	12.80	10.90	9.80	8.70	7.60
Mean (kW)	10.31	6.61	11.29	12.98	18.00	14.48	12.02	10.65	9.62	8.48
Median (kW)	10.45	6.50	11.20	12.50	17.70	14.30	11.90	10.50	9.50	8.40
3rd Qu. (kW)	11.89	7.60	12.30	14.70	19.60	15.80	13.00	11.40	10.30	9.20
Max (kW)	17.32	20.00	24.10	33.90	32.60	26.90	20.40	20.90	20.90	16.80
Total N	996	993	986	884	1056	1079	1083	1053	1038	1095
Variance (kW^2)	5.43	3.39	3.86	9.85	8.58	6.23	3.25	2.92	2.24	1.99
Std Dev. (kW)	2.33	1.84	1.96	3.14	2.93	2.50	1.80	1.71	1.50	1.41
CV (%)	22.61	27.87	17.39	24.17	16.28	17.23	14.99	16.06	15.57	16.62

Table 5.2 Statistical properties of the CMV values (all values shown in the table are unitless)

Lift / Pass	Base	2/6	3/8	4/9	5/1	5/2	5/3	5/4	5/5	5/7
Min	3.40	6.80	3.00	1.70	1.30	1.60	1.40	2.90	4.80	5.60
1st Qu.	10.80	15.10	10.20	8.60	9.40	6.50	9.00	11.40	12.50	13.40
Mean	14.82	18.20	12.72	10.97	11.92	8.69	11.68	14.10	15.38	15.82
Median	13.90	17.90	12.60	10.70	11.70	8.60	11.50	14.00	15.30	15.50
3rd Qu.	17.70	20.80	15.10	13.30	14.70	10.70	14.30	16.60	18.10	18.20
Max	36.30	31.10	22.40	23.20	21.60	18.40	22.80	44.90	27.30	27.30
Total N	996	993	986	884	1056	1079	1083	1053	1038	1095
Variance	31.67	17.85	12.50	12.19	13.87	9.43	13.92	18.18	14.82	13.33
Std Dev.	5.63	4.22	3.54	3.49	3.72	3.07	3.73	4.26	3.85	3.65
CV (%)	37.97	23.21	27.79	31.83	31.26	35.34	31.94	30.24	25.03	23.07

Figures 5.2a and 5.2b present the variation of the mean values of MDP and CMV for final passes and the successive passes of Lift 5, respectively.

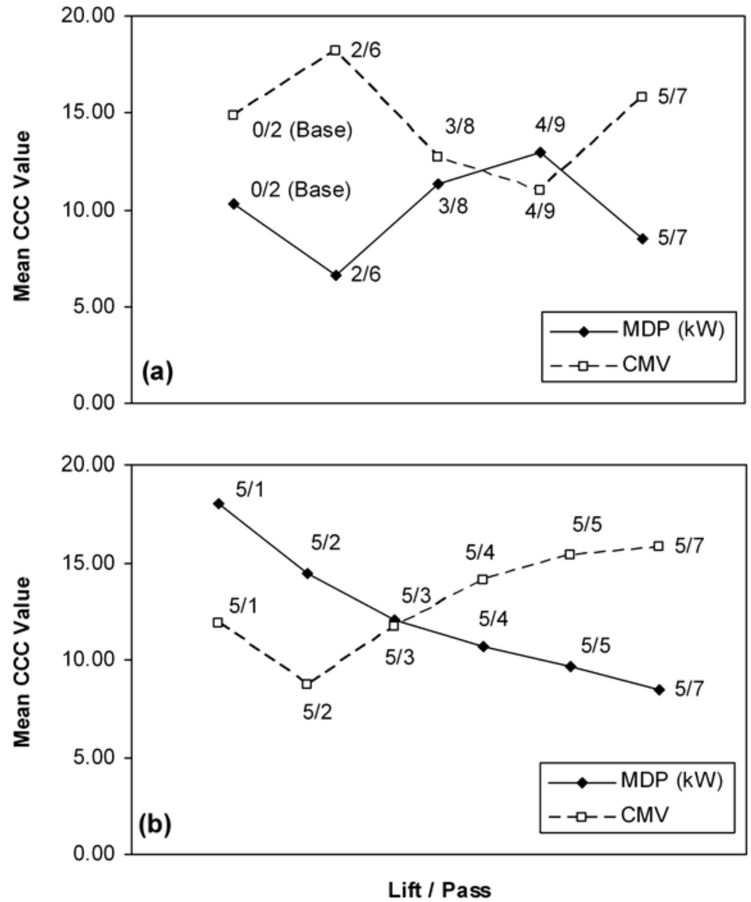

Figure 5.2 Mean Value of the Roller Measurements: a) final passes, and b) successive passes of Lift 5

As shown in Figure 5.2, average values of CMV tend to vary inversely when compared with the corresponding average values of MDP. In addition, by examining the sequential passes for Lift 5 (Figure 5.2b), it is clear that the values of MDP reflect the effect of progressive compactor passes. The same general trend exists for CMV as well, provided that the average data from Pass 1 is disregarded. The reason for the inconsistency between Pass 1 and the other passes for Lift 5 arises from the difference in applied vibratory compaction amplitude for these passes. As indicated in Chapter 3, the first pass of each lift was compacted using high-amplitude vibration (1.87 mm) and the other passes were compacted using low-amplitude vibration (0.85 mm). As discussed in Chapter 2, the amplitude of the first harmonic of the acceleration response signal ($\hat{a}(2\omega_0)$) is used to determine the CMV values (Equation 2.3). However, the magnitude of the acceleration response signal is affected by the amplitude of the input vibration ($\hat{a}(\omega_0)$), which means that the measured CMV values shown in Figure 5.2 are also a function of the amplitude of the input vibration. This observed effect of compaction amplitude on recorded CMV values is consistent with what has been observed by other researchers (Mooney and Adam 2007). As a result of this relationship, care must always be taken when interpreting CMV data, making sure to only compare passes that are compacted using similar amplitudes of vibratory compaction.

Another statistical property that provides useful information about the characteristics of the CCC measurements is the variance of the data. Figures 5.3a and 5.3b present the variance of the MDP and CMV values for the final passes of each lift and the sequential passes of Lift 5, respectively.

As shown in Figure 5.3, CMV values exhibit more variation around the mean than do MDP values. Figure 5.3b confirms this observation and reveals that the variation of MDP measurements typically decreases with further compaction of the soil. Since MDP generally corresponds to the surficial properties of the compacted soil, the reduction in the measured variances with each pass of the compactor supports the conclusion that more uniform surficial compaction is achieved by increasing the number of passes. The trend in variance for CMV values is not as clear. This is not surprising, as CMV values are significantly affected by the stiffness of underlying layers, and consequently more sophisticated analyses are likely warranted to develop a more complete understanding of the observed behavior.

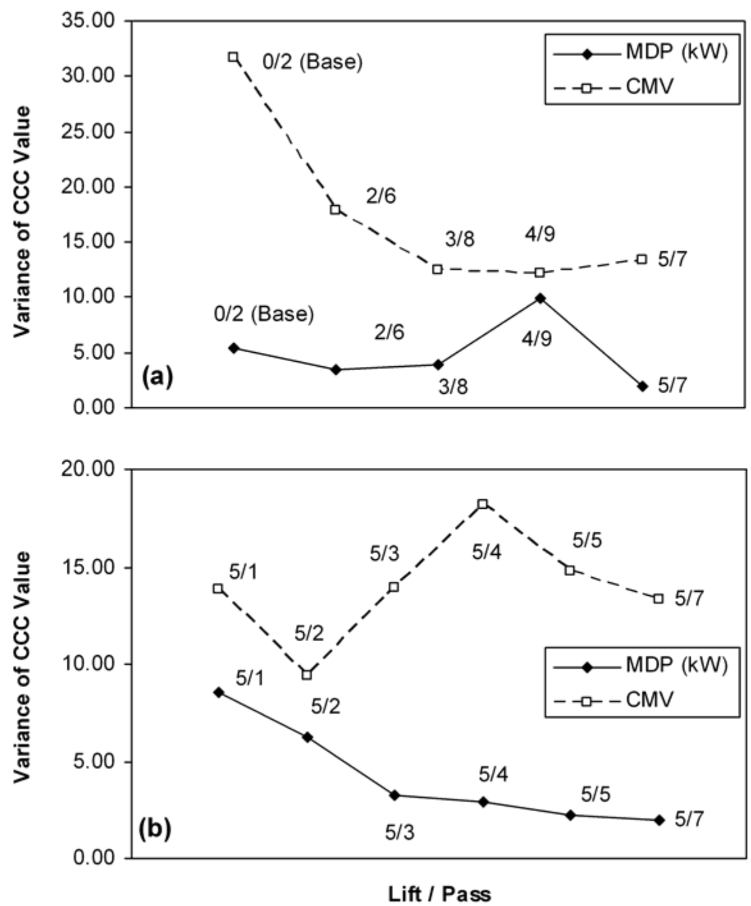

Figure 5.3 Variance of the Roller Measurements: a) final passes, and b) successive passes of Lift 5

The coefficient of variation (CV (%)) is a useful normalized, unitless statistical value that can be used to compare data sets of differing units. Coefficients of variation were useful for visualizing the relative uncertainty of different in-situ tests in Chapter 4, and similarly provide a useful technique for performing relative comparisons of the CCC values. Figure 5.4 shows the varying CV values that were recorded for MDP and CMV for the final passes of each lift and for successive passes on Lift 5.

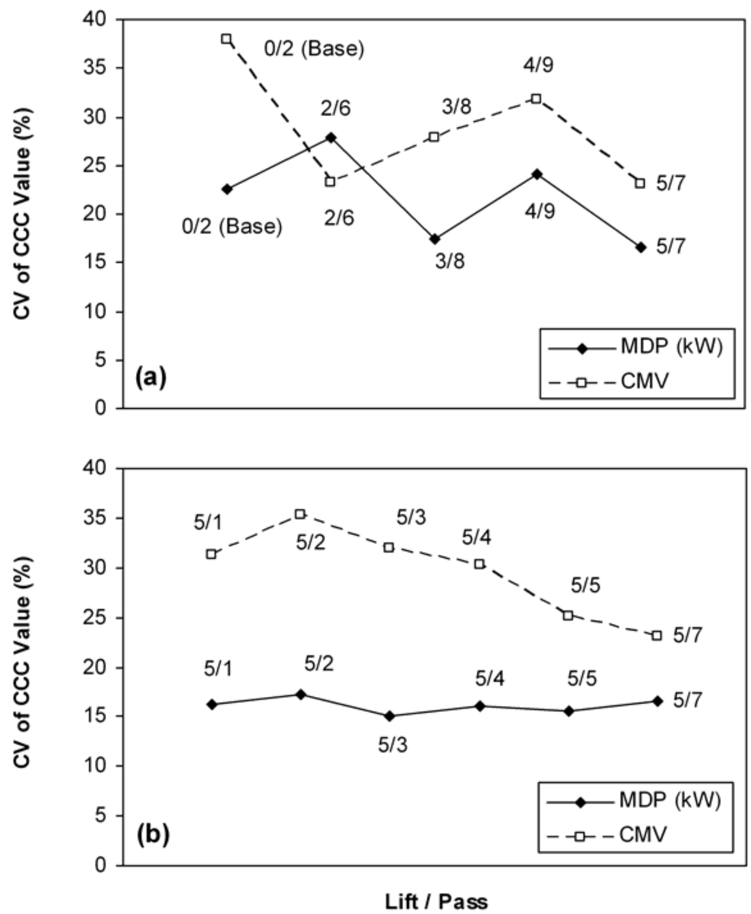

Figure 5.4 Coefficient of variation of the Roller Measurements: a) final passes, and b) successive passes of Lift 5

Examination of Figure 5.4a reveals that, with the exception of Lift 2, CMV and MDP behaved similarly in the final passes with respect to their CV values. Figure 5.4b shows that the recorded MDP values had almost the same CV for successive passes on Lift 5, while the coefficient of variation of CMV values decreased as the number of passes increased (disregarding Pass 1, as differing compaction amplitude was applied for this pass). In general, recorded CMV values had a greater CV than the corresponding MDP values.

As mentioned in the introduction to this chapter, there are two other values of interest that were recorded by the CCC system during the compaction process: RMV and the speed of the roller. As discussed in Chapter 2, the RMV value equals zero for compaction in a "continuous contact" mode of operation, which is usually only observed during compaction of very soft soils. RMV values typically become non-zero as the roller leaves the "continuous contact" mode of compaction, going sequentially into partial uplift and then into double-jump modes of operation (double-jump is undesirable, as it greatly reduces the reliability of CMV measurements, as discussed in detail in Chapter 2). In this project, the RMV values ranged between 0 and 5, which indicated the compaction that was performed was primarily in the partial uplift mode (Nick Oetken, personal communication). Figure 5.5 shows the mean and variance of RMV values for the final passes for each lift and for successive passes of Lift 5.

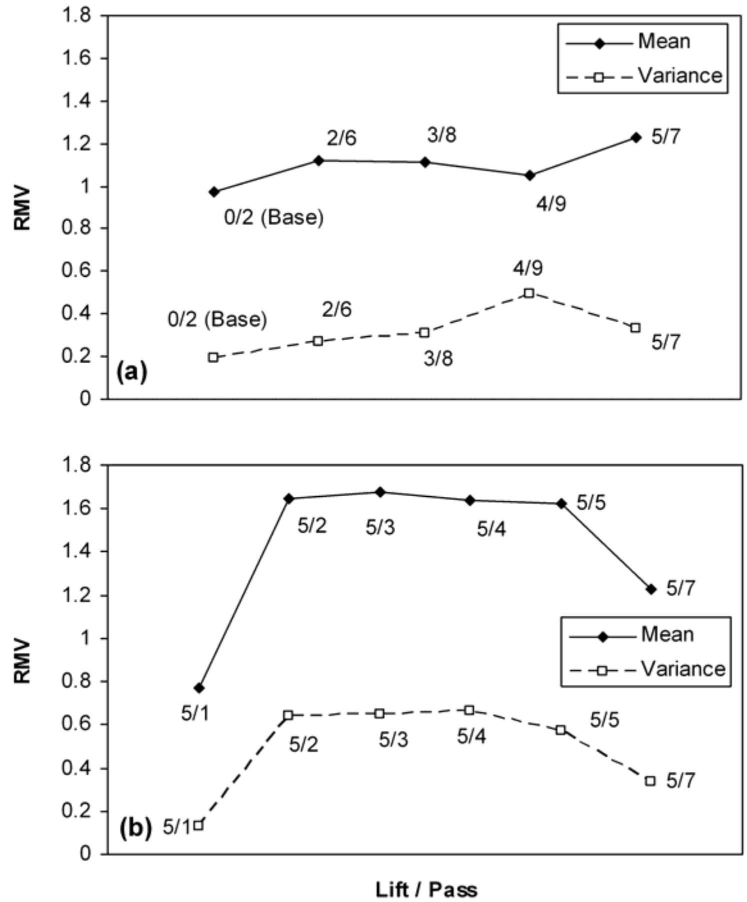

Figure 5.5 Mean and Variance of RMV values; a) final passes, b) successive passes on Lift 5

As shown in Figure 5.5, recorded RMV values generally fluctuated in the range of 0 to 1.8. The low average RMV values recorded for the first pass of Lift 5 are caused by the low degree of compaction of the freshly placed soil. For this pass, when the soil was compacted, it exhibited more continuous contact (less partial uplift) between the drum of the roller and the underlying soil. Considering the range of RMV values shown in Figure 5.5 and comparing it with the range of RMV values that are commonly observed for the partial uplift mode of vibration (Nick Oetken, personal communication), it is concluded that compaction was performed in the partial uplift mode.

The variation of mean and variance of the roller speed is shown in Figures 5.6a and 5.6b.

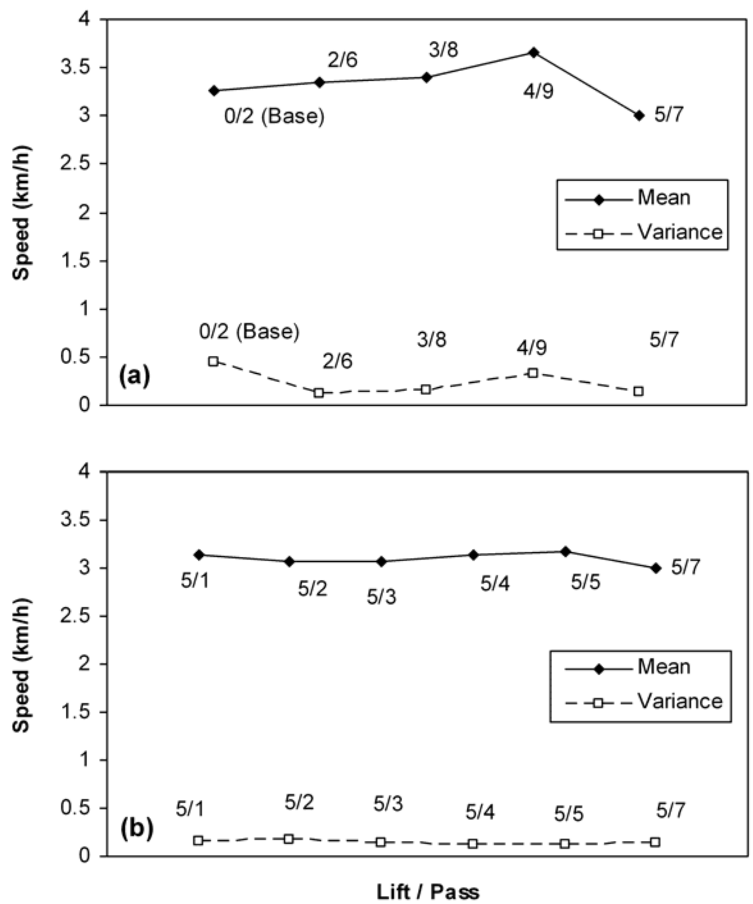

Figure 5.6 Mean and Variance of Roller Speed; a) final passes, b) successive passes on Lift 5

As shown in Figures 5.6a and 5.6b, the roller speed varied slightly around 3.2 km/h (2.0 mph). Slight variations in roller speed in this range do not affect the MDP or CMV measurements significantly (Forssblad 1980).

5.3 Histograms of the CCC Data

Another useful approach for presenting and analyzing the roller measured values is to present the measured data for each lift and pass in the form of histograms. Figures 5.7 and 5.8 show the histograms of the recorded MDP and CMV values for each lift and pass that was recorded. Note that the mid point of the histograms approximately corresponds to the mean value of the data and its width is indicative of the variance of the depicted data; for comparison purposes, the mean and variance of each data set are included on their respective histograms.

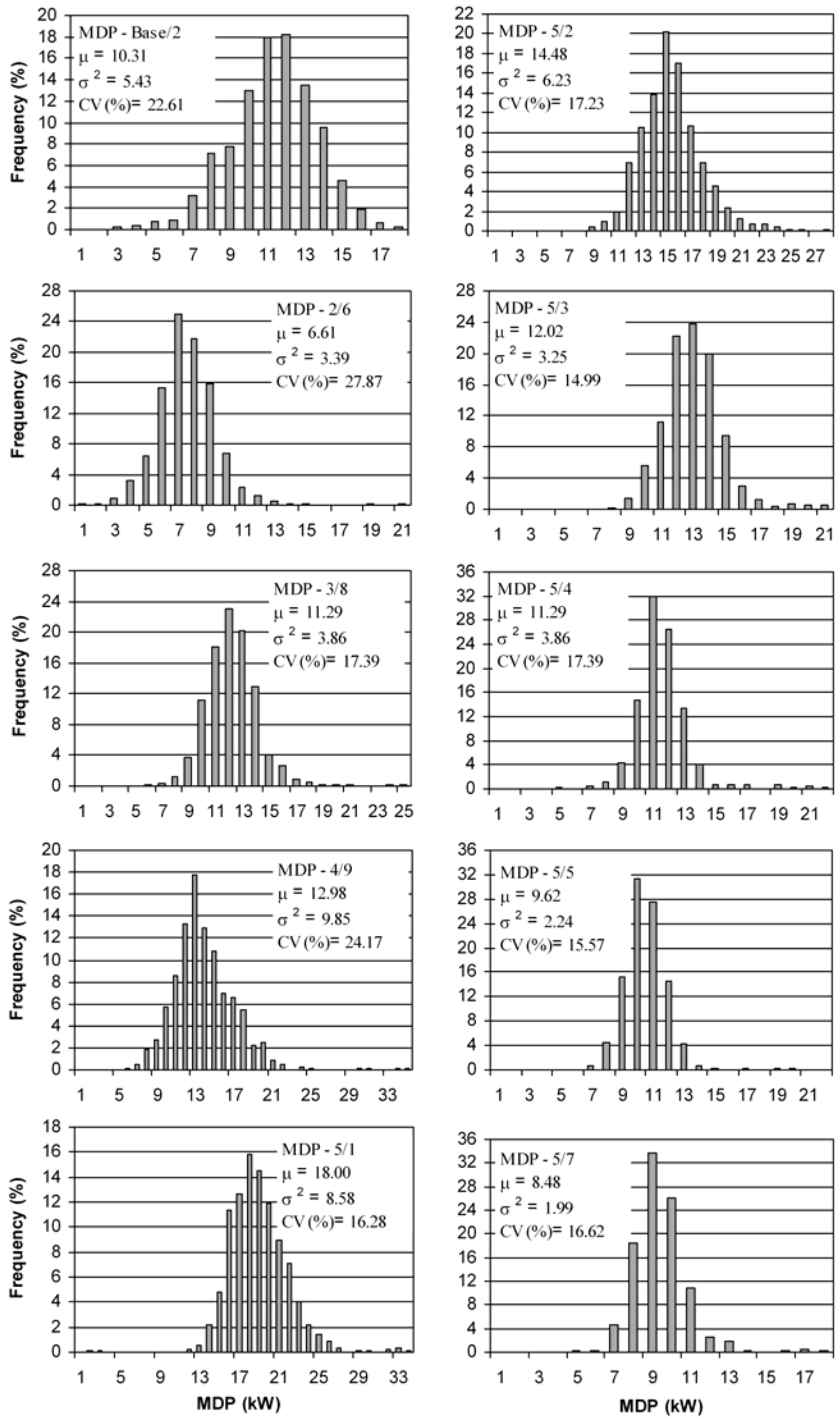

Figure 5.7 Histograms of measured MDP values

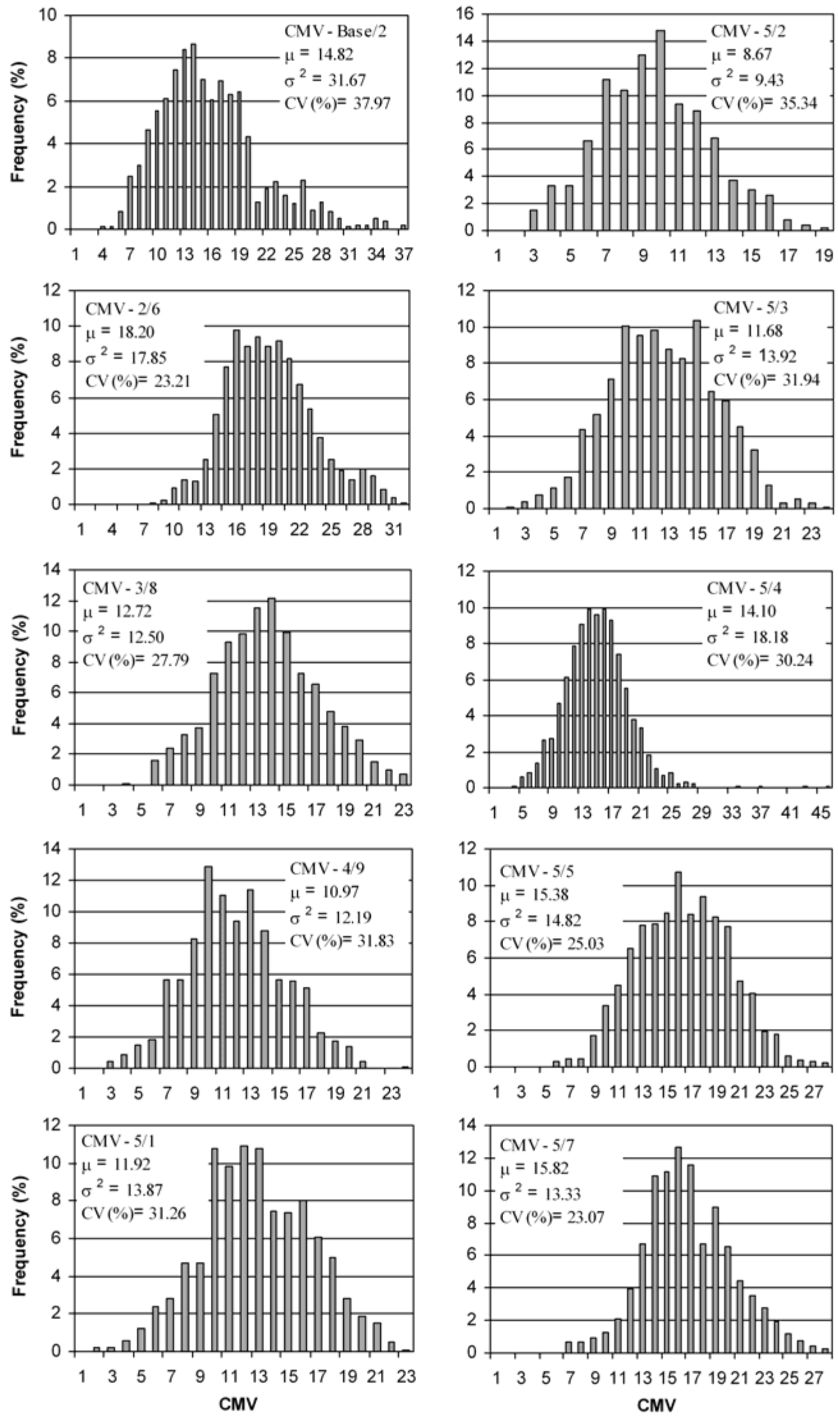

Figure 5.8 Histograms of measured CMV values

In order to compare the respective shape of the histograms presented in Figure 5.7 and Figure 5.8, the data points corresponding to the midpoint of each histogram bar in a given histogram were connected to create an outline or “trace” of the histogram. By drawing this sort of trace for each histogram series, the relative shape of the histograms can be presented in the same plot. Figure 5.9 and Figure 5.10 show a comparison of the resulting histogram shapes for the recorded MDP and CMV data sets, respectively.

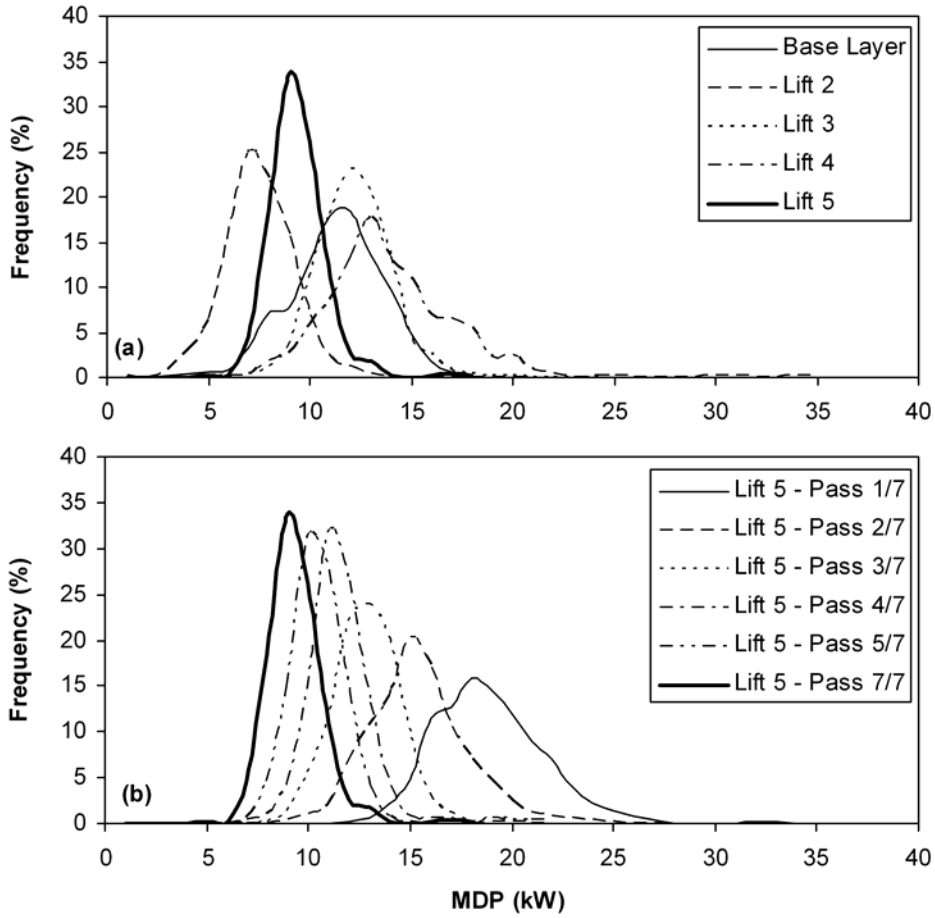

Figure 5.9 Histogram of the MDP values; a) final passes, b) successive passes for Lift 5

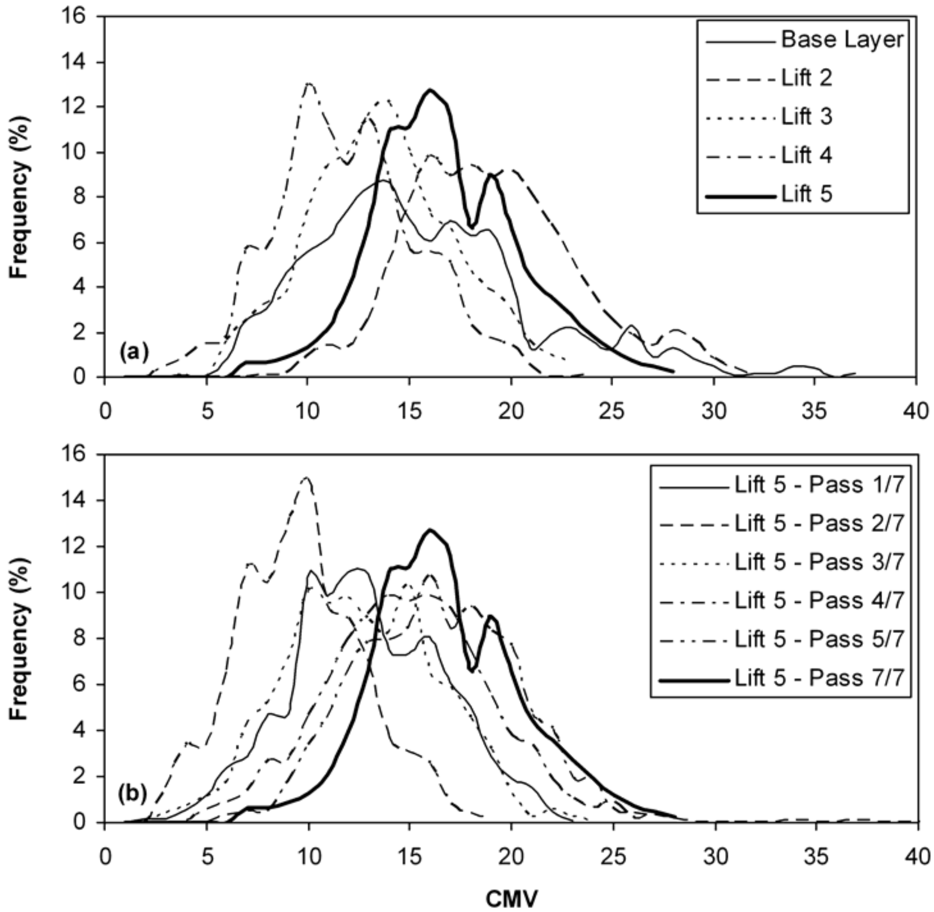

Figure 5.10 Histogram of the CMV values; a) final passes, b) successive passes for Lift 5

By examining Figures 5.7 through 5.10, it can be observed that the recorded MDP values resulted in relatively well-shaped histograms, as compared with the recorded CMV values. This is not surprising, as recorded CMV values are affected by the characteristics of underlying soil layers, which makes them more variable and which can cause the histrogram data sets to have secondary peaks around the mean.

As shown in Figures 5.9 and 5.10, analysis of sequential passes on a given lift is quite instructive about the general behavior of the roller measured values with increasing compactive effort. As shown in Figure 5.9, the relative location of the MDP histograms shifts to the left and become narrower and taller as the number of passes increases. This result is in complete agreement with the observations made in Section 5.2 with respect to the mean and variance of the MDP values with sequential passes. Consequently, interpretation of MDP values may be more direct and straightforward than interpretation of CMV values, as the results do not appear to be strongly affected by the behavior of underlying layers.

As shown in Figure 5.10, the CMV histograms shift to the right as the number of passes increases, which is consistent with the statistical nature of the mean behavior noted for CMV values in Section 5.2. However, the general shape of the CMV histograms is not as clear as what was observed for MDP values, which is likely caused by the influence of underlying layers on the recorded data. This effect is also supported by the observation that the value of CMV variance does not decrease with additional compactive effort for sequential compactor passes (Figure 5.3). This means that interpretation of CMV data (at least with respect to their histograms) for a given lift and pass may be more difficult than interpretation of MDP data. Additionally, this can make a CMV-based construction specification difficult to apply uniformly to all projects, where the nature of underlying layers may have variable effects on the measured data for a newly-constructed lift. This is of particular concern for field cases where underlying layers may not have been placed by the Contractor (e.g. proof-rolled base layers), and which therefore were out of his or her control.

To minimize the dependence of binning on the histogram traces presented in Figures 5.9 and 5.10, the measured data can also be presented by comparing the cumulative distributions of the data sets. Figure 5.11 and Figure 5.12 show a comparison of the resulting cumulative frequency distribution (CFD) shapes for the recorded MDP and CMV data sets, respectively.

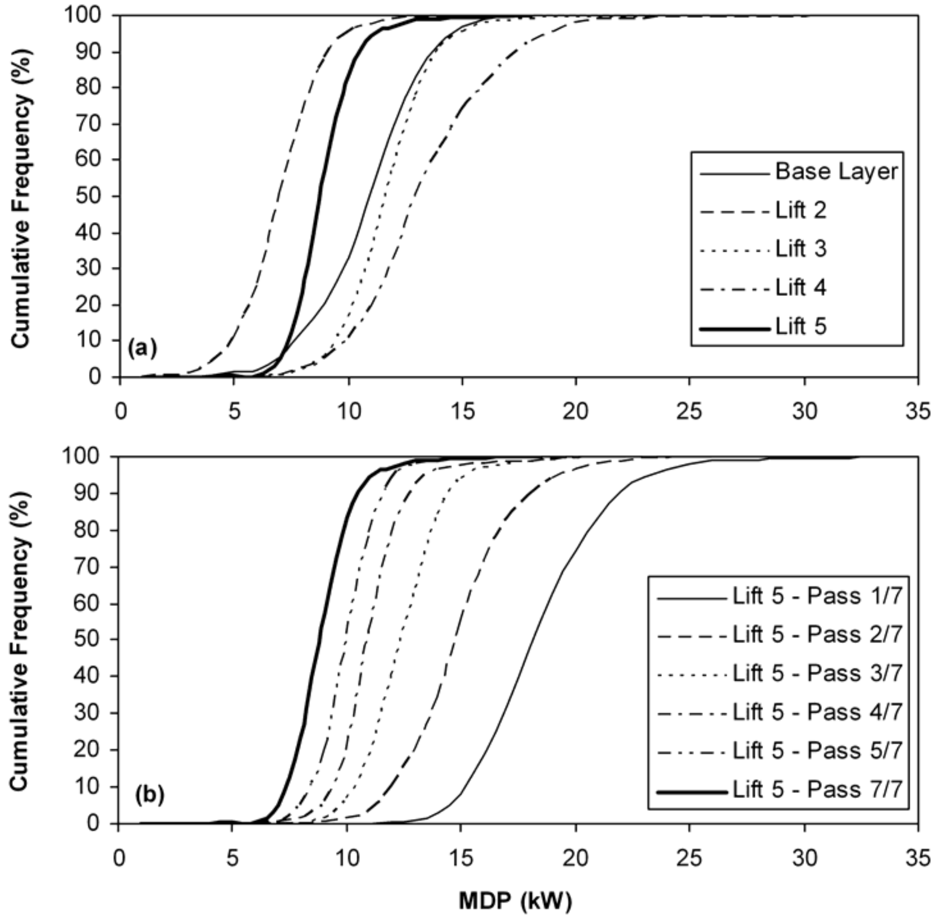

Figure 5.11 Cumulative distribution of the MDP values: a) final passes, and b) successive passes for Lift 5

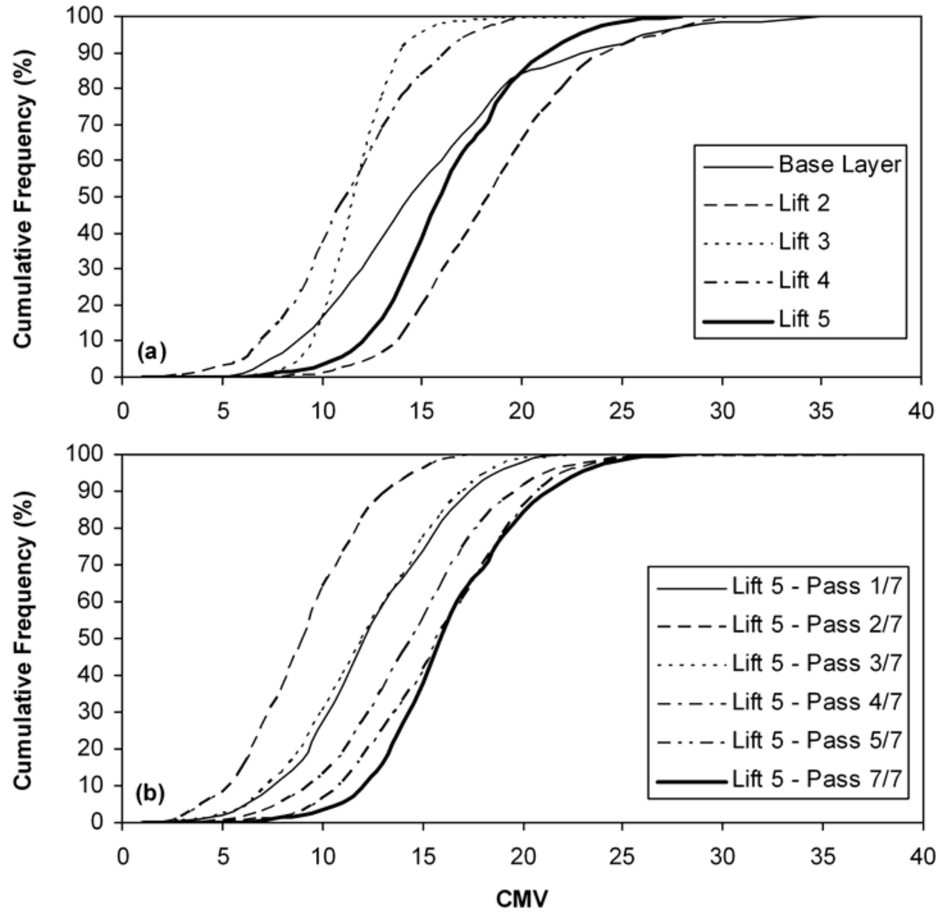

Figure 5.12 Cumulative distribution of the CMV values: a) final passes, and b) successive passes for Lift 5

It should be noted that the mid point of a given cumulative distribution curve represents its mean value, and the slope of the resulting curve illustrates the standard deviation of the data set. As the standard deviation increases, the slope of the curve decreases.

5.4 Summary and conclusions

The roller-measured values were statistically analyzed in this chapter. The analyses that were performed indicated that in general MDP reflects the quality of surficial compaction with less variation than CMV does, while CMV has the tendency to capture the behavior of underlying layers. All in all, MDP demonstrated a descending trend in values with increasing compactive effort, and CMV showed an ascending trend. It should also be noted that the amplitude of the excitation frequency must always be taken into account in interpretation of CMV data, as measured results indicated that there is a significant difference in CMV values between high amplitude and low amplitude compaction. Additionally, it was realized that either the variance or coefficient of variation values could be used to describe the variable results that were observed for a given lift during the compaction process, with each statistical measure having its own relative advantages and disadvantages for interpretation of the CCC roller data sets.

The CCC systems also recorded additional measurements such as RMV and roller speed that were useful for data interpretation. The evaluation of RMV values showed that the CCC roller operated predominantly in a "partial uplift" mode of vibration. The average RMV values ranged between 0 and 1.8 in this study. The speed of the roller is another parameter that can influence the final results if it varies excessively; in this study, the roller speed was approximately constant around 3.2 km/h (2.0 mph), which effectively minimized the effect of variation in roller speed on the measured MDP and CMV values.

Chapter 6

ORDINARY KRIGING METHOD FOR ROLLER MEASUREMENTS

Since the introduction of continuous compaction control systems (CCC) and intelligent compaction technology (IC), the primary approach that has been used to evaluate the reliability of CMV and MDP-type roller measurements has been to compare them with the results of common in-situ testing techniques (e.g. Thurner and Sandström 1980, Adam 1997). To accurately perform these types of comparisons, the first step is to obtain the roller measurements at the same locations as where the in-situ tests have been conducted. Existing CMV and MDP-based compactor systems commonly use on-board GPS systems to establish field data point locations. In the event that field-recorded CCV or MDP data points are recorded at the exact location as in-situ test data points, then comparisons between roller-measured and in situ test-measured data is direct and relatively straightforward. However, for projects of this type, it is much more common that the array of data points measured with the CCC equipment does not exactly correspond to the in-situ test data point locations. Historically, sophisticated kriging methods have been used to interpolate between roller measured points for comparison with in-situ test results in an attempt to address this issue (e.g. Brandl and Adam 2004, Thompson and White 2007, Petersen et. al. 2007). However, even within commonly accepted statistical analysis methodology, a variety of approaches can be used for kriging-based applications, and clear consensus in the engineering literature about how to best interpret this type of spatially varying data for CCC applications is not apparent. In general, to our knowledge, a detailed discussion of how best to perform these types of analyses for reliable interpretation of CCC data (a specific process that could be followed) could not be found in other geotechnical engineering literature.

6.1 Spatial Continuity

Spatial continuity exists in most geotechnical field studies. The underlying assumption in spatial continuity analysis is that two data points measured close to each other are more likely to have similar values than two data points measured that are far apart. The first step in finding the spatial continuity of a set of data is to show all possible pairs of data – values whose locations are separated by a certain distance (Isaak and Srivastava 1989). Therefore, a one to one plot, commonly called an h-scatter plot, is provided whose abscissa is the data value (V_i) at location *i* and whose ordinate is the data value (V_{i+h}) at location *i+h*, where *h* is the distance between the two locations that is independent of the direction between the points (Figure 6.1).

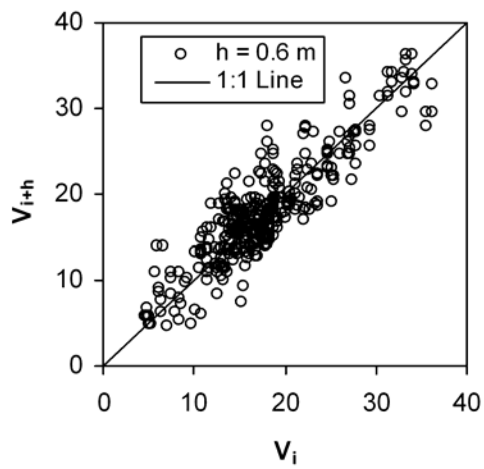

Figure 6.1 Example h-scatter plot of CMV values. Base layer for h = 0.6 m

From this point onwards, *h* will be referred to as the separation distance or lag distance between points. Using the approach shown above, h-scatter plots can be built for all possible lags. The statistical nature of the scatter plots can then be characterized using various approaches such as the correlation coefficient (Equation 6.1), the covariance (Equation 6.3), or the moment of inertia (Equation 6.4).

$$\rho(h) = \frac{\frac{1}{N(h)} \sum_{i=1}^{i=N(h)} [V_i - \mu(i)][V_{i+h} - \mu(i+h)]}{\sigma(i)\sigma(i+h)} \tag{6.1}$$

where,

$$\sigma(i) = \sqrt{\frac{\sum_{i=1}^{i=n} \left[V_i - \mu(i)\right]^2}{n}} \tag{6.2}$$

$$C(h) = \frac{1}{N(h)} \sum_{i=1}^{i=N(h)} [V_i - \mu(i)][V_{i+h} - \mu(i+h)] \tag{6.3}$$

$$\gamma(h) = \frac{\sum_{i=1}^{i=N(h)} \left[V_i - V_{i+h}\right]^2}{2N(h)} \tag{6.4}$$

where, *N(h)* is the number of pairs of data whose locations are separated by *h*, *n* is the number of data points in each set of data, $\mu(i)$ is the mean or average of data whose locations are denoted by *i*'s, $\mu(i+h)$ is the mean of data which are located a distance *h* away from the *i* data set, and $\sigma(i)$ and $\sigma(i+h)$ are the standard deviations of their respective data sets (Equation 6.2).

The correlation coefficient ρ ranges between -1 and +1. A correlation coefficient ρ = +1 means that two variables vary together exactly. A correlation coefficient ρ = −1 means that two variables vary exactly inversely. A correlation coefficient ρ = 0 means that the two variables are unrelated to one another (Baecher and Christian 2003). By looking closely at Equations 6.1 and 6.3, it becomes apparent that the covariance is the numerator of the fraction that defines the correlation coefficient, or in the other words, the correlation coefficient is the covariance normalized by the standard deviations.

The variation of correlation coefficient, covariance and moment of inertia at different lags is called autocorrelation, autocovariance, and semivariogram respectively (Isaak and Srivastava 1989). However, in some literature (e.g. Baecher and Christian 2003), these names have been used for the corresponding single functions as well (i.e. correlation coefficient, covariance and moment of inertia).

In general, as the separation distance (lag) is increased, the correlation coefficient and covariance of a pair of data decreases and the semivariogram increases. This implies a descending trend for the autocorrelation and the autocovariance and an ascending one for the semivariogram. An example of this relationship for typical CCC data measured for the base layer (Lift 0, Pass 2/2) is provided in Figure 6.2. These clear trends reveal that the consistency between the primary variables diminishes as h increases, and that there is no significant correlation between the data beyond a certain value of h.

It should be noted that the shape of the autocorrelation and autocovariance functions is not strictly identical since the standard deviations of V_i and V_{i+h} change from one h-scatter plot to the next (Cressie 1993).

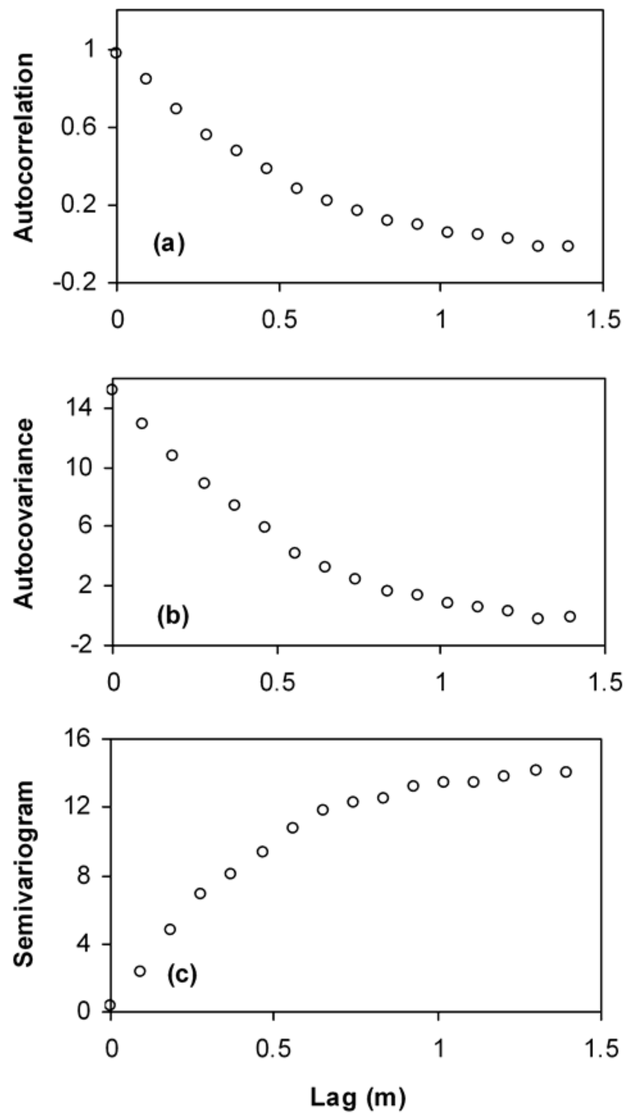

Figure 6.2 Spatial continuity description of CMV data for base layer: (a) autocorrelation, (b) autocovariance, and (c) semivariogram

6.2 Ordinary Kriging

One of the most commonly used spatial continuity analysis techniques is ordinary kriging, which provides a reliable approach for spatial interpolation of data for many data sets (Isaak and Srivastava 1989). This technique, which is most commonly referred to simply as kriging, is often associated with the acronym B.L.U.E for "best linear unbiased estimator". Ordinary kriging is "linear" because its estimates are weighted linear combinations of the available data; it is "unbiased" since it tries to have μ_R, the mean residual or error, equal to 0; it is "best" because it aims at minimizing σ^2_R, the variance of the errors. However, the distinguishing feature of ordinary kriging is its aim of minimizing the error variance (Isaak and Srivastava 1989).

The most commonly used application of kriging, like other spatial interpolation methods, is for predicting the unknown value of a variable at a certain location whose nearby sample values are known. Using this approach, the unknown value at a point is estimated using a weighted linear combination of the available samples (Equation 6.5).

$$\widehat{V} = \sum_{i=1}^{i=n} w_i V_i \tag{6.5}$$

where, $\widehat{V}$ is the estimated value, w_i is the weight given to a known value at a nearby location, and V_i is the known value at a nearby location.

As implied by Equation 6.5, the weight assigned to nearby variables is essential for determining their respective contribution to the final value predicted at the point of interest. In order to estimate the unknown value, it is therefore necessary to first find the respective weighting factors that will be used for points around the chosen location. For convenience, we denote the proposed location with unknown value by *0* and assign the label of *1* to *n* to the nearby points having known values. This leads to the following relationship:

$$\begin{bmatrix} \widetilde{C}_{11} & \dots & \widetilde{C}_{1n} & 1 \\ \vdots & \ddots & & \vdots \\ \widetilde{C}_{n1} & \dots & \widetilde{C}_{nn} & 1 \\ 1 & \dots & 1 & 0 \end{bmatrix}_{(n+1)\times(n+1)} \cdot \begin{bmatrix} w_1 \\ \vdots \\ w_n \\ \lambda \end{bmatrix}_{(n+1)\times 1} = \begin{bmatrix} \widetilde{C}_{10} \\ \vdots \\ \widetilde{C}_{n0} \\ 1 \end{bmatrix}_{(n+1)\times 1} \tag{6.6}$$

where, $\widetilde{C}_{ij}$ is the value of the autocovariance function between i^{th} and j^{th} neighbors with respect to the distance between them, $\widetilde{C}_{i0}$ is the value of the autocovariance function between the i^{th} neighbor and the point of interest having an unknown value, and λ is the unknown Lagrange multiplier which is introduced to the equation to convert a constrained minimization problem into an unconstrained one. Equation 6.6 can be rewritten in the form of matrix notation as:

$$\mathbf{C} \cdot \mathbf{w} = \mathbf{D} \tag{6.7}$$

To obtain the necessary weighting values, both sides of Equation 6.7 are multiplied by $\mathbf{C}^{-1}$**,** which is the inverse of the autocovariance matrix shown on the left-hand side above:

$$\mathbf{C}^{-1} \cdot \mathbf{C} \cdot \mathbf{w} = \mathbf{C}^{-1} \cdot \mathbf{D}$$

$$\mathbf{I} \cdot \mathbf{w} = \mathbf{C}^{-1} \cdot \mathbf{D} \tag{6.8}$$

$$\mathbf{w} = \mathbf{C}^{-1} \cdot \mathbf{D}$$

By plugging the weighting factors (w_i values) derived using the above approach into Equation 6.5, the unknown value at the point of interest can be predicted. The autocovariance function that is used with this approach is a mathematical expression of a "best fit" curve that is passed through the sample autocovariance of the spatial data shown in Figure 6.2b.

To find the value of the weights (the w_i values), it is also common to use the semivariogram function instead of the autocovariance function, which means that $\widetilde{C}_{ij}$ and $\widetilde{C}_{i0}$ in Equation 6.6 are replaced by γ_{ij} and γ_{i0}, respectively. If semivariograms are used, the matrix forms **C** and **D** presented in Equation 6.7 are replaced by Γ and Λ, respectively.

6.3 Analytical Assumptions Made in our Analyses

The following assumptions were made in our analyses:

- The data we are dealing with have second-order stationarity which means that the mean μ and variance σ^2 is constant for each pair of data and $cov(V_i\,, V_{i+h})$ is a function of only h.
- The data in the field are distributed in a two-dimensional fashion. This assumption means that omni directional analysis will be performed on the data. In the analyses presented herein, only the magnitude of the distance between two values is taken into account, and the direction of the distance vector between two points is assumed not to affect their spatial continuity.
- The data set has a normal (Gaussian) distribution.

6.4 Spatial Continuity of CCC Roller Data

As noted in Chapter 3, two types of CCC indicator values of soil-roller interaction were measured during the field study: compaction meter value (CMV) and machine drive power (MDP). The methodology and approach used to calculate these values, as well as the numerous associated details of the CCC field study that was performed are provided in Chapter 2 and Chapter 3.

To evaluate the spatial continuity of the MDP and CMV values, semivariograms of the final pass for each lift and individual passes for the fifth lift (passes 1, 2, 3, 4, 5, and 7) are taken into account in the analysis. A computer program written using the MATLAB™ platform was developed to generate the autocorrelation, autocovariance, and semivariogram functions for each of the roller data sets. Representative semivariogram shapes for MDP and CMV data sets over the entire range of possible lag values are shown in Figure 6.3; the final compaction pass performed on Lift 5 (Pass 7) is shown, and is typical of the type of semivariogram shapes that were observed.

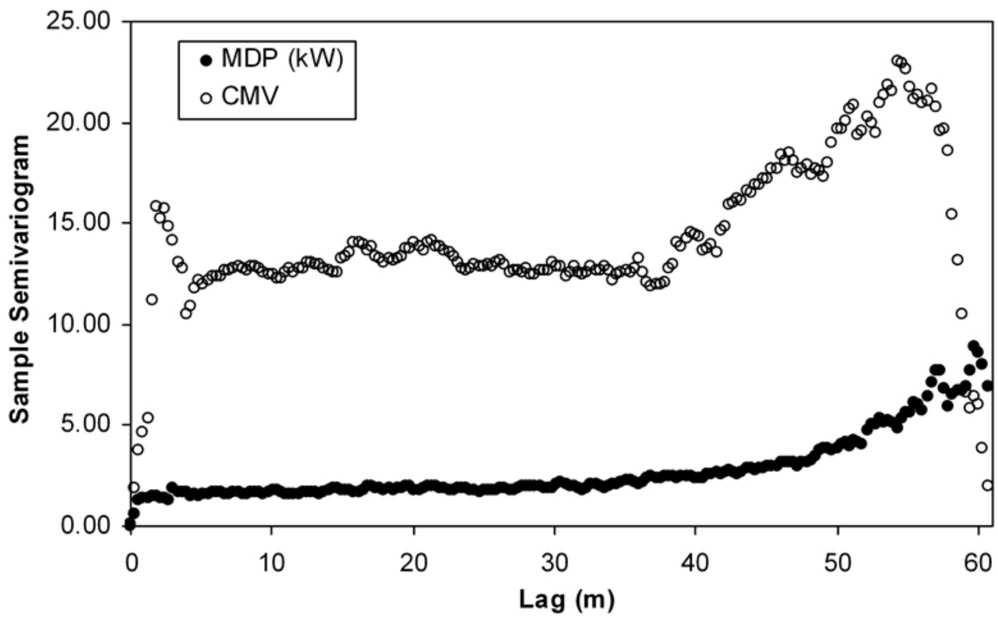

Figure 6.3 Sample semivariogram for MDP and CMV for Lift 5, Pass 7

As shown in Figure 6.3, over the entire range of possible lag values, the sample semivariograms for the base layer show approximately an asymptotic behavior for both MDP and CMV values. This type of behavior is also seen in the other lifts and passes which are presented in Appendix C.

Figure 6.4 shows the sample autocovariance for the same data sets, which can be compared with the semivariogram shapes.

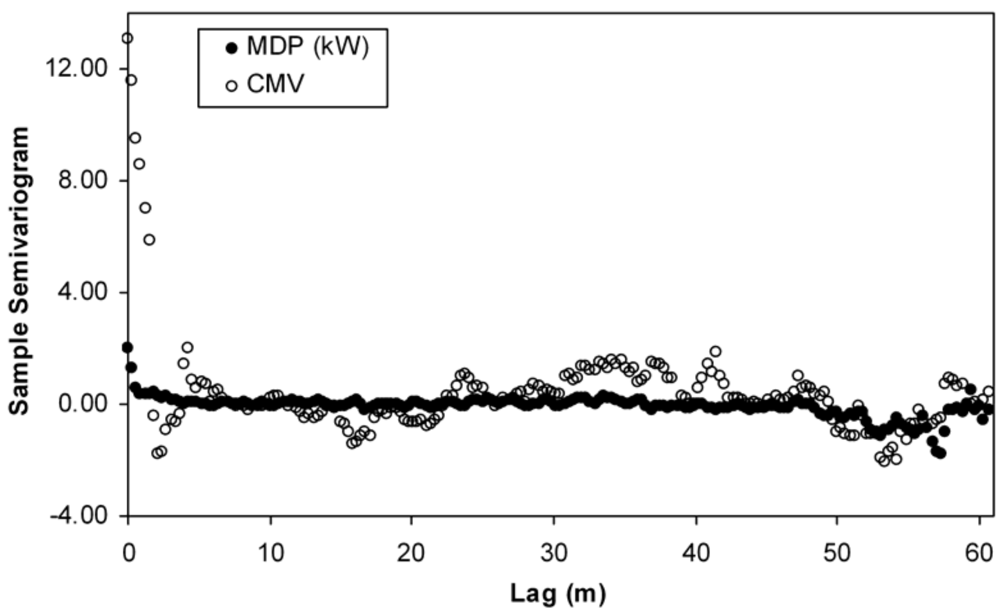

Figure 6.4 Sample autocovariance for MDP and CMV for Lift 5, Pass 7

6.5 Semivariogram and Autocovariance Models

Although a set of sample semivariograms and autocovariances provide a good descriptive summary of the spatial continuity of the data, a mathematical model is needed for use with kriging which can be used to estimate the values at unknown points (Isaak and Srivastava 1989). It is unwise to choose an arbitrary mathematical function to define this relationship, even if the model fit through the sample variogram (or autocovariance) appears reasonable; certain conditions must be followed in selecting the mathematical fitting functions (Cressie 1993).

As noted earlier, the resultant semivariogram and autocovariance functions can be used in kriging techniques such as ordinary kriging. It is desirable to have one (and only one) stable solution for kriging. To satisfy this criteria, the **C** or **Γ** matrix in Equation 6.7 must satisfy the positive definiteness condition. A necessary condition that guarantees the positive definiteness of the **Γ** (or **C**) matrix is given by

$$\mathbf{w}^{\mathbf{t}}\,\boldsymbol{\Gamma}\,\mathbf{w} > 0 \qquad (6.9)$$

where, **w** is any vector of weights presented in Equation 6.6 which has at least one of its arrays as non-zero. Table 6.1 summarizes the most popular models that meet the positive definiteness condition (Cressie 1993, Isaak and Srivastava 1989).

Table 6.1 Mathematical models for semivariogram

Model	Mathematical Equation	θ
Linear	$\gamma(h;\theta)=\begin{cases}0 & , \quad h=0\\ c_0+b_l h & , \quad h\neq 0\end{cases}$	$c_0 \geq 0$ $b_l \geq 0$
Spherical	$\gamma(h;\theta)=\begin{cases}0 & , \quad h=0\\ c_0+c_s\left\{\frac{3}{2}(\frac{h}{a_s})-\frac{1}{2}(\frac{h}{a_s})^3\right\} & , \quad 0<h<a_s\\ c_0+c_s & , \quad h\geq a_s\end{cases}$	$c_0 \geq 0$ $c_s \geq 0$ $a_s \geq 0$
Exponential	$\gamma(h;\theta)=\begin{cases}0 & , \quad h=0\\ c_0+c_e\left\{1-e^{-\frac{3h}{a_e}}\right\} & , \quad h\neq 0\end{cases}$	$c_0 \geq 0$ $c_e \geq 0$ $a_e \geq 0$
Gaussian	$\gamma(h;\theta)=\begin{cases}0 & , \quad h=0\\ c_0+c_g\left\{1-e^{-\frac{3h^2}{a_g^2}}\right\} & , \quad h\neq 0\end{cases}$	$c_0 \geq 0$ $c_g \geq 0$ $a_g \geq 1$
Rational Quadratic	$\gamma(h;\theta)=\begin{cases}0 & , \quad h=0\\ c_0+c_r\dfrac{h^2}{1+\dfrac{h^2}{a_r}} & , \quad h\neq 0\end{cases}$	$c_0 \geq 0$ $c_r \geq 0$ $a_r \geq 0$
Wave	$\gamma(h;\theta)=\begin{cases}0 & , \quad h=0\\ c_0+c_w\left\{1-\frac{a_w}{h}\sin(\frac{h}{a_w})\right\} & , \quad h\neq 0\end{cases}$	$c_0 \geq 0$ $c_w \geq 0$ $a_w \geq 0$

Figure 6.5 provides a graphical demonstration of the models introduced in Table 6.5. The same models can also be used for autocovariance functions with respect to Equation 6.10.

$$\gamma(h)=C(0)-C(h) \qquad (6.10)$$

where, C(0) is the variance of the set of data σ^2.

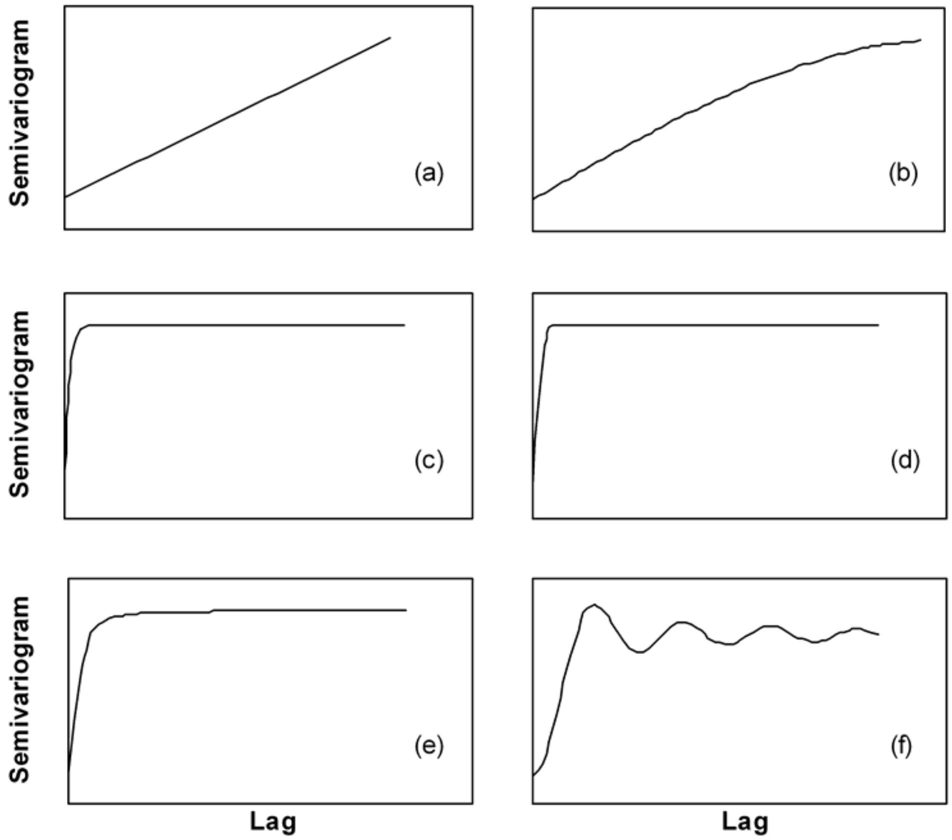

Figure 6.5 Semivariogram models: (a) Linear, (b) Spherical, (c) Exponential, (d) Gaussian, (e) Rational Quadratic, and (f) Wave

The semivariogram functions introduced above are commonly considered to be the basic semivariogram model functions (Cressie 1993). These models can be divided generally into two major categories: the ones which reach a plateau at greater separation distances and those that do not (Isaak and Srivastava 1989). The models in the first category are commonly referred to as transition models; in the list shown above, the transition models are the Exponential, Rational Quadratic, Spherical, and Gaussian models. The plateau they reach is called the *sill* and the lag over which this plateau is reached is called the *range* (Figure 6.6). Practically speaking, the range is the distance beyond which there is only a very small amount of spatial continuity remaining between data points. The second category of semivariogram model does not behave asymptotically as the separation lag is increased; the models mentioned above in this category include the Linear model and Wave model.

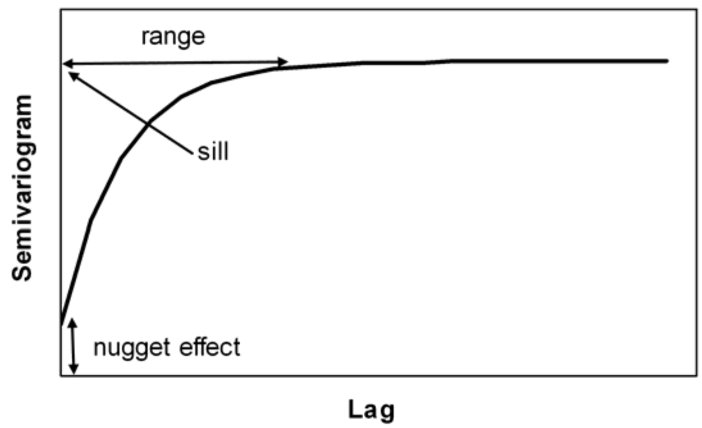

Figure 6.6 The properties of a transition semivariogram

For a theoretical semivariogram (Equation 6.4), it is expected that $\gamma(h)$ approaches zero at $h = 0$. In reality however, it is common that micro scale variation causes a discontinuity at the origin that leads to $\gamma(0) = c_0 > 0$ (Cressie 1993). The value $c_0 > 0$ is commonly referred to as the *nugget effect*. The possible reasons for $c_0 > 0$ are measurement errors (Cressie 1993) and also the effect of errors caused by the "binning" process (which is described in detail in section 6.6), where spatial distances between a pair of data points are rounded slightly to the nearest lag distance that was used to create the semivariogram.

6.6 Curve fitting process used to obtain the semivariogram functions

As noted in Section 6.4, the sample semivariograms and autocovariances of all existing CCC roller measurements were obtained using a MATLAB code that utilized Equations 6.1 to 6.4; the resulting plots are provided in Appendix C. Separation distance multiples of $h = 0.3048\ m$ (1 ft) were used in the code, and varied using ~ 0.3 m (1 ft) multiples from a minimum h of zero to a maximum h corresponding to the longest distance between two points that was recorded for the lifts and passes that were analyzed. In order to achieve a well-structured sample semivariogram and autocovariance, the measured distance between each pair of points having coordinates of x and y was rounded to the nearest multiple of 0.3 m (1 ft).

The next step that was performed was to utilize the mathematical models introduced in Table 6.1 to obtain the appropriate semivariogram functions over different lag distances. This is a critical step, because the choice of lag distance over which the model fit is performed can significantly affect the shape of the resulting model. This concept is illustrated in Figure 6.7.

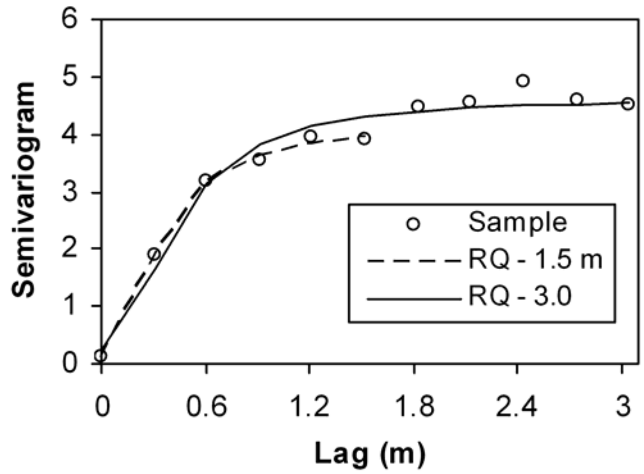

Figure 6.7 Effect of lag selection on the resulting semivariogram function (results from fitting an RQ model to the Base layer data set)

Examining Figure 6.7 shows the importance of choosing the maximum lag on the resulted semivariogram function.

For these analyses, the wave model was disregarded, because the roller data did not show periodic behavior over short separation distances. Lag distances of ~ 1.5 m (5 ft), ~ 3 m (10 ft), ~ 6 m (20 ft), and ~ 15 m (50 ft) were employed for the curve fitting operation. The reason for examining a variety of separation lags was to identify both the optimal lag and set of semivariogram functions for the kriging process, in order to minimize the kriging model prediction errors (Isaak and Srivastava 1989).

The method of linear-least squares was applied for curve fitting using the curve fitting toolbox in MATLAB™. The quality of model fit was evaluated by using residual analysis and the associated R-squared value that is shown in Equation 6.11.

$$R^2 = 1 - \frac{SS_{err}}{SS_{tot}} \tag{6.11}$$

where, SS_{err} is the sum of square differences of the actual and estimated data (Equation 6.12) and SS_{tot} is the sum of the square differences between the actual data and the mean (Equation 6.13).

$$SS_{err} = \sum_{i=1}^{i=n} w_i (\hat{y}_i - y_i)^2 \tag{6.12}$$

$$SS_{tot} = \sum_{i=1}^{i=n} w_i (y_i - \bar{y})^2 \tag{6.13}$$

where, n is the number of data points in each set of data, w_i is an assigned weighting value (in this case assumed to be equal to one – no weighting factors were used), $\hat{y}_i$ is the estimated value (from the fitted curve), y_i is the measured data that was recorded at a given point, and $\bar{y}$ is the mean of the measured data. Using residual analysis, the resulting R-squared values can vary between 0 and 1, with a value closer to 1 indicating a better fit.

In order to perform the residual analyses, the differences between the fitted models and the sample semivariograms at available points were plotted against the separation lag. A randomly distributed scatter plot around a value of zero on the abscissa (which in this case is the lag) indicates an appropriately fitted curve, while a patterned scatter plot means that a better fit may exist. Figures 6.8a and 6.8b illustrate this concept.

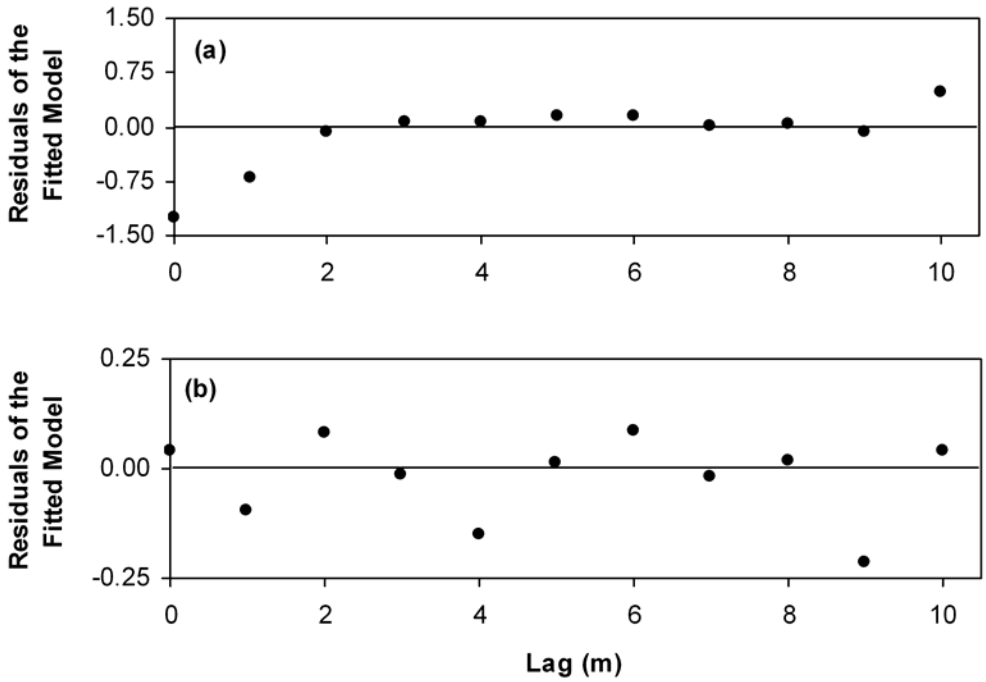

Figure 6.8 Residual analysis of the fitted curve: a) poor fit and b) good fit.

The resultant R-squared values for each model curve that was fit to the sample semivariograms for MDP and CMV are presented in Table 6.2 and Table 6.3 respectively. For the sake of space, data corresponding only to maximum lags of 1.5 m (5 ft) and 3.0 m (10 ft) are presented here; more detailed information and data from additional lag spacings is provided in Appendix C.

Table 6.2 R-squared values for "best-fit" semivariogram functions for MDP for maximum lag of 1.5 m and 3.0 m

Lift/Pass	Exponential		Gaussian		RQ		Spherical		Linear	
	1.5 m	3.0 m	1.5 m	3.0 m	1.5 m	3.0 m	1.5 m	3.0 m	1.5 m	3.0 m
Base	0.99	0.98	0.99	0.93	1.00	0.97	0.94	0.85	0.82	0.72
2	0.98	0.96	1.00	0.98	0.99	0.96	0.89	0.53	0.75	0.39
3	0.98	0.95	1.00	0.96	0.99	0.96	0.88	0.63	0.75	0.48
4	0.89	0.87	0.94	0.88	0.89	0.88	0.67	0.68	0.49	0.59
5/1	0.98	0.89	0.94	0.92	0.95	0.90	0.98	0.80	0.98	0.64
5/2	0.98	0.96	0.99	0.92	0.99	0.96	0.94	0.84	0.84	0.74
5/3	0.98	0.98	1.00	0.99	0.99	0.99	0.91	0.66	0.78	0.53
5/4	0.98	0.78	0.96	0.82	0.97	0.79	0.98	0.51	0.98	0.35
5/5	0.98	0.89	0.93	0.90	0.95	0.90	0.97	0.68	0.97	0.51
5/7	0.98	0.91	1.00	0.92	0.99	0.92	0.93	0.67	0.81	0.58

Table 6.3 R-squared values for "best-fit" semivariogram functions for CMV for maximum lag of 1.5 m and 3.0 m

Lift/Pass	Exponential		Gaussian		RQ		Spherical		Linear	
	1.5 m	3.0 m	1.5 m	3.0 m	1.5 m	3.0 m	1.5 m	3.0 m	1.5 m	3.0 m
Base	1.00	0.90	0.99	0.94	1.00	0.93	1.00	0.90	0.98	0.90
2	0.96	0.95	0.95	0.98	0.95	0.97	0.96	0.97	0.96	0.90
3	0.99	0.97	0.97	0.98	0.98	0.98	0.99	0.98	0.99	0.90
4	1.00	0.92	0.99	0.93	1.00	0.93	1.00	0.92	0.95	0.92
5/1	0.86	0.88	0.98	0.93	0.98	0.92	0.86	0.88	0.86	0.88
5/2	0.99	1.00	0.98	0.97	0.99	0.99	0.99	0.92	0.94	0.80
5/3	0.97	0.96	0.94	0.95	0.96	0.95	0.96	0.96	0.95	0.88
5/4	0.99	0.98	0.99	0.96	1.00	0.97	1.00	0.98	0.95	0.91
5/5	0.98	0.88	0.95	0.89	0.97	0.88	0.98	0.86	0.97	0.75
5/7	0.88	0.88	0.92	0.94	0.92	0.92	0.88	0.91	0.88	0.85

6.7 Evaluation of Ordinary Kriging Models for Prediction of CCC Data

To evaluate the use of ordinary kriging for estimation of CCC data, kriging was applied to the recorded MDP and CMV data sets using the five models shown in Tables 6.2 and 6.3. Using this approach, the five kriging models were used to estimate MDP and CMV values at each of the locations in the data set where point values were already known. Comparison between the values predicted by the kriging model and the values that were actually recorded at each point provided insight into the reliability of the kriging method for each of the models that were examined.

According to Table 6.2 and Table 6.3, some models appeared to have a better mathematical fit than others, as indicated by the relative magnitude of the R-squared values. However, care must be taken when assessing the reliability of a given kriging method to not use only the semivariogram R-squared values as the model selection criterion. The data sets examined in this study indicate that other criteria should also be considered when selecting the "best" model for point-estimation of CCC values at unknown locations. These criteria are discussed in more detail in the following sections.

6.7.1 Singularity

One of the most common problems encountered when solving a matrix equation such as Equation 6.7, $\mathbf{\Gamma w} = \mathbf{\Lambda}$, is the appearance of singularities in the multiples matrix $\mathbf{\Gamma}$ (in the left hand side of the equation) that lead to a zero value for the associated matrix determinant. Matrix singularity occurs when there are some rows or columns in the matrix that are dependent on each other. More specifically, singularities occur when one row (or column) is the linear combination of one or more other rows (or columns). Singularities also occur when there is a row or column in the matrix that has the same values repeated throughout. Another problem that is sometimes encountered is when the matrix $\mathbf{\Gamma}$ is "poorly structured", which means that the determinant of the matrix is close to zero. In this case, solving the matrix equation leads to abnormally large values in the **w** matrix, which is undesirable.

In general, there are two ways for dealing with these types of mathematical problems: the first is to disregard the solution of the matrix equation altogether, and the second is to make adjustments to the matrix to resolve or remove the associated singularities. For this project, the second approach was utilized, and associated singularities were removed by omitting the rows and columns that created the dependence in the matrix. This method is satisfactory if the omission of the dependent matrix values does not significantly influence the accuracy of the kriged point values. Since the size of the square matrices used in these data analyses was usually large, deleting a few rows and columns in many cases does not significantly change the end results. However, the results from kriging using these types of modified Γ matrices should be examined carefully and treated with caution. Although this method is a simple method, it generally worked well for the data sets that were recorded in our field study.

In this study, as a first step in the kriging process, five different models were used to fit the associated semivariogram functions: Exponential, Gaussian, Rational Quadratic (RQ), Spherical, and Linear. Semivariogram fit functions were developed for each of these five models by fitting the models over four different lag ranges; ~ 1.5 m (5.0 ft), ~ 3.0 m (10 ft), ~ 6.0 m (20 ft), and ~ 15.0 m (50 ft). This approach allowed for independent examination of the effect of both the nature of the semivariogram fit function (model type) and the lag range over which each model was fit (lag range for model fit).

The resulting number of singularities encountered for each model run are presented in Appendix C. Of the five models that were examined, the Gaussian model and the RQ model tended to have the most problems with matrix singularity or poorly-structured Γ matrices. The Gaussian model in particular exhibited numerous singularities for many of the MDP and CMV data sets, while the RQ model seemed to only have these problems with the CMV data sets. Therefore, given the significant amount of matrix singularities that were encountered, results from the Gaussian kriging model were disregarded for both the MDP and CMV data sets, and results from the RQ kriging model were disregarded for the CMV data sets.

6.7.2 Relative Error of the Predicted Values

A second criteria that was found to be useful for selecting the best model for kriging was the relative error between kriging-predicted values at known data points and the actual recorded values themselves (Equation 6.14).

$$RE = \frac{\left|V_i - \hat{V}_i\right|}{V_i} \times 100(\%) \tag{6.14}$$

where, V_i is the actual recorded value at a given point and $\hat{V}_i$ is the value predicted by a given kriging model at the same point.

To gain a better insight into the distribution of the relative errors for the different kriging models that were examined, the normalized cumulative frequency of each of the relative errors was plotted versus the associated relative error for each lift-pass and model. Figures 6.9.a to 6.9.d compare the relative error distributions for each of the model types and lag ranges for the kriging models that were found to be of the most interest (fewest errors, better results, etc.). The raw results from these runs, as well as a variety of results from additional model runs (other lag spacings, model types that exhibited more significant singularity errors, etc.) are presented in Appendix C.

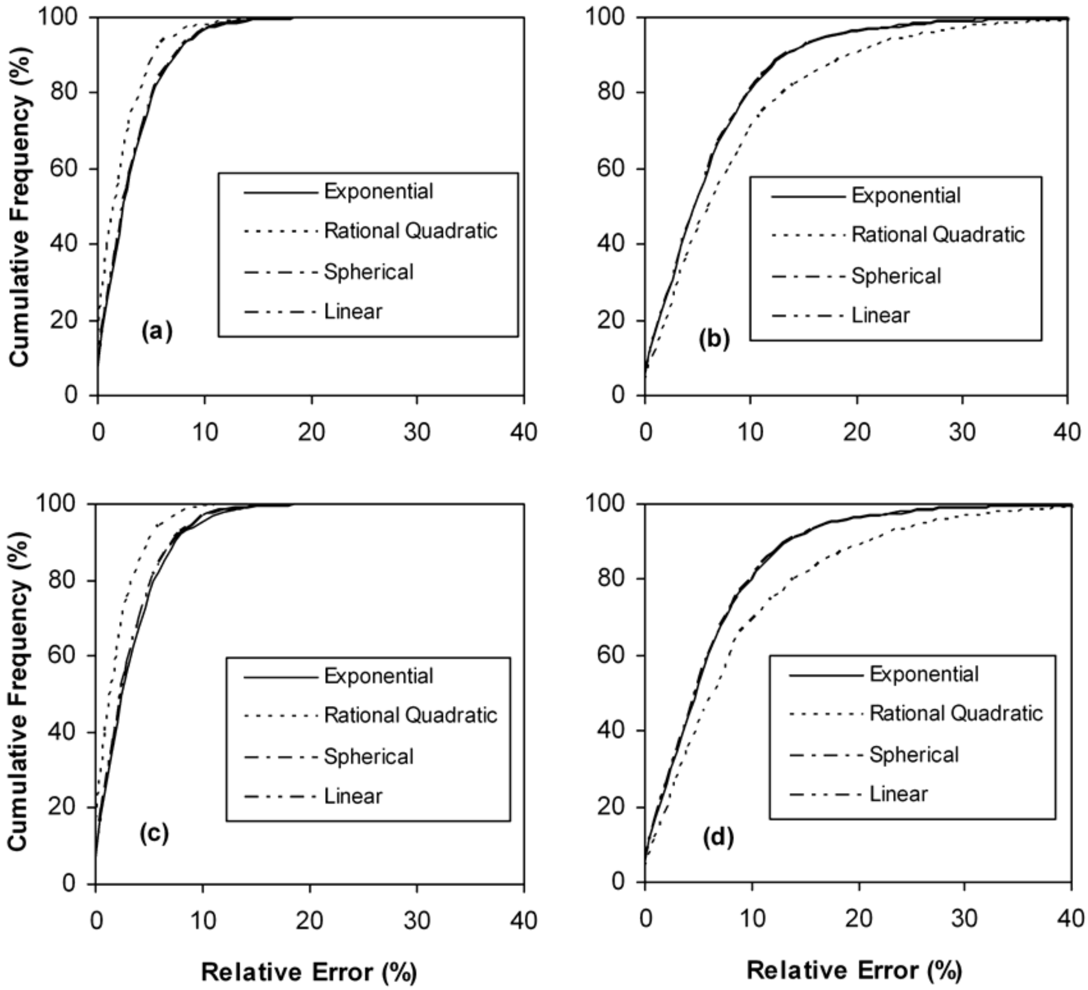

Figure 6.9 Cumulative frequency of relative error vs. relative error for Lift 5, Pass 5: a) MDP, 1.5 m, b) CMV, 1.5 m, c) MDP, 3.0 m, and d) CMV, 3.0 m

The same trends shown in Figure 6.9 were also observed for all other lifts and passes where values were predicted using kriging models fitted with a maximum lag of ~ 1.5 m (5 ft) and ~ 3.0 m (10 ft). As shown in this figure, the RQ kriging model resulted in the least amount of relative error when examining the MDP data, while the Exponential, Spherical, and Linear models showed the least amount of error (with relative errors all in good agreement) for the CMV data. From these results, the RQ model was selected as the most accurate model for kriging of the MDP data and the Exponential, Spherical and Linear models were selected for kriging of the CMV data.

Table 6.4 to Table 6.7 show the resulting correlation coefficients between the actual and predicted values for each data set, as well as the average relative and absolute errors (Equation 6.15) between the actual and predicted values using the kriging models that were selected for the MDP and CMV data sets. The last two rows of each table present the average of the associated data for the final passes of each lift and the successive passes of Lift 5, respectively. More detailed information is provided in Appendix C.

$$AE = \frac{V_i - \hat{V}_i}{V_i} \times 100(\%) \tag{6.15}$$

Table 6.4 Summary statistics of the kriging method using RQ model for MDP values

Lift / Pass	Max lag = 1.5 m			Max lag = 3.0 m		
	$\rho(h)$	μ_{RE} (%)	μ_{AE} (%)	$\rho(h)$	μ_{RE} (%)	μ_{AE} (%)
Base	0.9545	5.3280	-0.6031	0.9547	5.2635	-0.4329
Lift 2	0.9337	10.3786	-3.9781	0.9285	11.6579	-5.1155
Lift 3	0.9542	4.0402	-0.3241	0.9534	4.0686	-0.2819
Lift 4	0.9360	6.8405	-1.1179	0.9491	5.9686	-0.6887
Lift 5 - Pass 1	0.9320	3.5845	0.1692	0.9846	2.2736	-0.2044
Lift 5 - Pass 2	0.9698	3.0985	-0.1317	0.9670	3.2481	-0.0677
Lift 5 - Pass 3	0.9558	3.3438	-0.1680	0.9558	3.3654	-0.1707
Lift 5 - Pass 4	0.9493	3.5707	-0.0233	0.9761	2.5689	-0.0947
Lift 5 - Pass 5	0.9710	2.7344	-0.0586	0.9775	2.4850	-0.0748
Lift 5 - Pass 7	0.9759	2.7455	-0.1446	0.9756	2.7547	-0.1524
Final Passes	0.9509	5.8666	-1.2336	0.9523	5.9426	-1.3343
Lift 5	0.9590	3.1796	-0.0595	0.9728	2.7826	-0.1274

Table 6.5 Summary statistics of the kriging method using Exponential model for CMV values

Lift / Pass	Max lag = 1.5 m			Max lag = 3.0 m		
	$\rho(h)$	μ_{RE} (%)	μ_{AE} (%)	$\rho(h)$	μ_{RE} (%)	μ_{AE} (%)
Base	0.9885	5.1696	-0.6153	0.9884	5.1705	-0.5985
Lift 2	0.9786	4.0437	-0.3564	0.9785	4.0473	-0.3789
Lift 3	0.9728	5.6696	-0.7515	0.9728	5.6967	-0.8474
Lift 4	0.9637	6.9934	-1.1250	0.9635	6.9851	-1.0712
Lift 5 - Pass 1	0.9853	4.8911	-0.5645	0.9852	4.8942	-0.5699
Lift 5 - Pass 2	0.9076	14.4923	-3.9723	0.9076	14.5800	-4.1564
Lift 5 - Pass 3	0.9386	10.5288	-2.0842	0.9385	10.5598	-2.1641
Lift 5 - Pass 4	0.9561	8.0045	-1.2512	0.9559	8.0033	-1.3016
Lift 5 - Pass 5	0.9500	6.7169	-0.8475	0.9500	6.7309	-0.9006
Lift 5 - Pass 7	0.9652	5.1888	-0.5517	0.9653	5.1833	-0.5687
Final Passes	0.9737	5.4130	-0.6800	0.9737	5.4166	-0.6930
Lift 5	0.9504	8.3037	-1.5453	0.9504	8.3252	-1.6102

Table 6.6 Summary statistics of the kriging method using Spherical model for CMV values

Lift / Pass	Max lag = 1.5 m			Max lag = 3.0 m		
	$\rho(h)$	μ_{RE} (%)	μ_{AE} (%)	$\rho(h)$	μ_{RE} (%)	μ_{AE} (%)
Base	0.9886	5.1427	-0.5684	0.9884	5.1705	-0.5985
Lift 2	0.9786	4.0437	-0.3564	0.9786	4.0401	-0.3677
Lift 3	0.9728	5.6695	-0.7514	0.9729	5.6809	-0.8270
Lift 4	0.9639	6.9319	-0.9991	0.9635	6.9821	-1.0782
Lift 5 - Pass 1	0.9853	4.8911	-0.5645	0.9852	4.8942	-0.5820
Lift 5 - Pass 2	0.9081	14.3301	-3.7014	0.9078	14.4186	-3.8178
Lift 5 - Pass 3	0.9386	10.4934	-1.9919	0.9358	10.5524	-2.0445
Lift 5 - Pass 4	0.9561	7.9988	-1.1826	0.9563	7.9874	-1.2646
Lift 5 - Pass 5	0.9500	6.7139	-0.8115	0.9499	6.7150	-0.8390
Lift 5 - Pass 7	0.9652	5.1888	-0.5517	0.9654	5.1837	-0.5959
Final Passes	0.9738	5.3953	-0.6454	0.9737	5.4115	-0.6935
Lift 5	0.9505	8.2693	-1.4673	0.9500	8.2919	-1.5240

Table 6.7 Summary statistics of the kriging method using Linear model for CMV values

Lift / Pass	Max lag = 1.5 m			Max lag = 3.0 m		
	$\rho(h)$	μ_{RE} (%)	μ_{AE} (%)	$\rho(h)$	μ_{RE} (%)	μ_{AE} (%)
Base	0.9886	5.1533	-0.5972	0.9884	5.1705	-0.5985
Lift 2	0.9786	4.0437	-0.3564	0.9785	4.0450	-0.3570
Lift 3	0.9728	5.6696	-0.7515	0.9728	5.6795	-0.7609
Lift 4	0.9639	6.9110	-1.0173	0.9635	6.9850	-1.0697
Lift 5 - Pass 1	0.9853	4.8911	-0.5645	0.9852	4.8942	-0.5698
Lift 5 - Pass 2	0.9077	14.4074	-3.7931	0.9076	14.4084	-3.7952
Lift 5 - Pass 3	0.9385	10.5117	-2.0396	0.9385	10.5259	-2.0469
Lift 5 - Pass 4	0.9565	7.9874	-1.2078	0.9562	7.9881	-1.2300
Lift 5 - Pass 5	0.9500	6.7114	-0.8286	0.9500	6.7130	-0.8223
Lift 5 - Pass 7	0.9652	5.1888	-0.5517	0.9653	5.1784	-0.5346
Final Passes	0.9738	5.3933	-0.6548	0.9737	5.4117	-0.6642
Lift 5	0.9505	8.2830	-1.4975	0.9505	8.2847	-1.4998

Some interesting conclusions can be drawn by examining the resulting statistical data in the above tables. The correlation coefficients for each of the data sets for all of the models that were examined are quite high (ranging from 0.91 to 0.99). This is consistent with the "best linear unbiased estimator" (b.l.u.e) approach that is employed by ordinary kriging, as all of the models that were used minimized the errors of the predicted values, resulting in generally high correlation coefficients. This means that the correlation coefficient between predicted and existing values can reasonably be used for "first pass" kriging model assessment; if the resulting correlation coefficients for kriging of a given CCC data set are less than 0.9, the semivariogram model should probably be discarded in favor of a more accurate model.

Another interesting observation is that the relatively high correlation coefficients that were observed in Tables 6.4 through 6.7 occurred despite the much lower R-squared values that were often observed (in some cases in the range of 0.4 to 0.7, as shown in Tables 6.2 and 6.3) for each of the semivariogram fitting functions. Broadly speaking, this means that the semivariogram R-squared values are not necessarily reliable indicators about the relative accuracy of a given kriging model.

Unfortunately, the subtle variations that were observed in the correlation coefficient values did not provide enough information to allow for final model selection between each of the three "short-listed" models that were used for analysis of the CMV data (Exponential, Spherical, Linear) or for selection of the ideal lag length for model fit in the kriging analysis. Consequently, it is concluded that although the correlation coefficient is a useful tool for "first pass" kriging model assessment, it is not by itself a robust enough indicator for selecting the best semivariogram model or lag spacing.

As indicated by the average absolute error values shown in Tables 6.4 through Table 6.7, the average absolute error of the kriging results is always negative, which means that, on average, the kriging methods that were used tended to overpredict the estimated values for our data set.

The average relative errors of the final passes for both MDP and CMV are almost the same but for the successive passes of Lift 5 they are quite different, as the corresponding differences in average relative error for MDP is relatively small (~ 3.2%) and that of CMV is relatively high (~ 8.3%). One possible reason could be the nature of the models that were selected as the best ones for MDP and CMV. The other reason is the inherent difference between MDP and CMV values and their characteristics, which were discussed in detail in Chapter 5.

Another significant finding indicated by the data in Table 6.5 to Table 6.7 is that the average relative error for predicted CMV values decreases as the number of passes increases from 2 to 7 (also shown clearly in Figures 6.10 and 6.11). Pass 1 of Lift 5 was intentionally ignored for this comparison, because different amplitude compaction was used for this pass; the significance of this is discussed in Chapter 5. This observation indicates that, as the soil becomes more compacted, the relative error of the predicted values decreases. In addition, it is clear that Pass 1 of Lift 5, which was compacted using a higher vibratory amplitude, generated the least average relative error compared to the other passes. This deviation might be caused by the fact that a higher compaction amplitude was applied for this pass relative to the other passes.

These above-mentioned trends in behavior were not as clear for MDP, as the MDP data was much more tightly grouped when compared pass by pass, as shown in Figures 6.10 and 6.11.

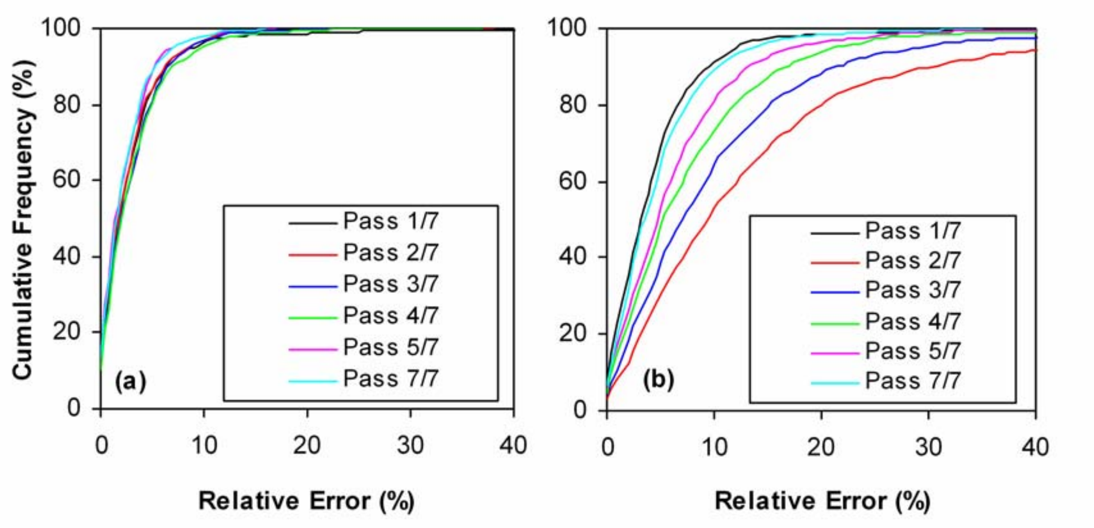

Figure 6.10: The improvement of the relative error in Lift 5 for a maximum lag of 1.5 m: a) MDP, RQ model, b) CMV, Exponential model

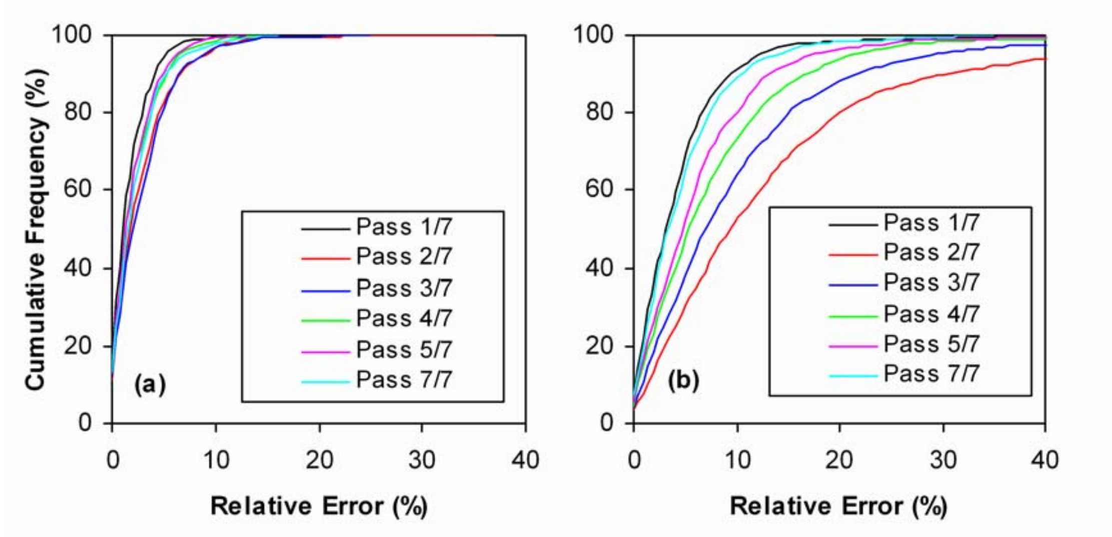

Figure 6.11: The improvement of the relative error in Lift 5 for a maximum lag of 3.0 m: a) MDP, RQ model, b) CMV, Exponential model

In order to conclude the current discussion on relative error, and to make final comparisons between different models, it is useful to compare the frequency of the predicted values existing within specific ranges of relative error for each model that was analyzed. Tables 6.8 to Table 6.11 provide the frequency of occurrence of relative error values for the predicted data sets for MDP and CMV. As the relative error for final passes is technically different from the sequential passes, these data sets are presented separately.

Table 6.8 Frequency of the Relative Error for Final Passes (%) – Maximum Lag = 1.5 m

Range (%)	MDP	CMV		
	RQ	Exponential	Spherical	Linear
< 5	67.1	63.3	63.3	63.4
5 - 10	20.8	24.6	24.7	24.5
10 - 20	9.3	10.3	10.3	10.3
20 - 40	2.3	1.5	1.5	1.5
40 - 60	0.3	0.1	0.1	0.1
> 60	0.2	0.1	0.1	0.1

Table 6.9 Frequency of the Relative Error for Final Passes (%) - Maximum Lag = 3.0 m

Range (%)	MDP	CMV		
	RQ	Exponential	Spherical	Linear
< 5	68.2	63.6	63.4	63.7
5 - 10	20.0	24.4	24.5	24.2
10 - 20	9.1	10.2	10.3	10.3
20 - 40	2.2	1.6	1.5	1.6
40 - 60	0.4	0.1	0.1	0.1
> 60	0.2	0.1	0.1	0.1

Table 6.10 Frequency of the Relative Error for Lift 5 (%) - Maximum Lag = 1.5 m

Range (%)	MDP	CMV		
	RQ	Exponential	Spherical	Linear
< 5	84.3	50.6	50.3	50.5
5 - 10	12.6	24.7	25.1	24.8
10 - 20	2.7	17.2	17.1	17.3
20 - 40	0.3	5.8	5.9	5.8
40 - 60	0.0	1.0	1.0	1.0
> 60	0.0	0.6	0.6	0.6

Table 6.11 Frequency of the Relative Error for Lift 5 (%) - Maximum Lag = 3.0 m

Range (%)	MDP	CMV		
	RQ	Exponential	Spherical	Linear
< 5	87.7	50.6	50.6	50.6
5 - 10	10.5	26.6	26.7	26.8
10 - 20	1.7	17.2	17.3	17.2
20 - 40	0.1	5.8	5.8	5.8
40 - 60	0.0	1.1	5.8	1.0
> 60	0.0	0.6	0.6	0.6

By examining the figures presented earlier in the chapter, and looking closely at Tables 6.8 through 6.11, it can be observed that a high percentage of the predicted data have a low relative error. This observation demonstrates the reliability of the ordinary kriging method for each of the semivariogram models that were used for both the MDP and the CMV data sets. In all cases, it is clear that the frequency of the predicted data having relative errors greater than 20% is trivial, which gives confidence to our use of the ordinary kriging method for point-estimation with CCC data sets.

6.7.3 Selecting the Kriging Neighborhood

One of the most essential issues in kriging is selecting an appropriate maximum separation lag or "kriging neighborhood". There are various opinions about how to select the proper neighborhood in the literature. In some cases the reliable maximum lag is defined as the range of the semivariogram function (e.g. Petersen et al. 2007). Although this recommendation seems practically reasonable, it has some limitations. The primary disadvantage of this method is that it is only applicable for transition semivariogram models (e.g. Exponential, RQ), and is not valid for other model types of interest in this study (e.g. Linear). There is another potential drawback for this type of “range” approach to kriging: The most commonly used procedure for choosing a model for kriging is to first estimate a maximum lag and to then fit a series of semivariogram models through the data over the selected lag distance (Isaak and Srivastava 1989). However, by employing this approach for kriging, each model that is fit is not separately optimized for the data set that it is being fit to. That is, separate ranges are not calculated for each of the models, and the effect of model sensitivity to the selection of lag distance is not explored in detail.

An alternative method proposed by Rivoirard (1987) suggests that a reliable kriging neighborhood can be determined by selecting the lag that minimizes the Lagrange multiplier in the matrix equation of kriging. Cressi (1993) recommendeds that the kriging domain be increased until the Lagrange multiplier becomes as small as possible (even negative). Although these suggestions may theoretically be correct, they do not consider practical kriging issues for large data sets, such as the run time of the kriging program (which can be quite large if the lag distance is increased significantly) or the nature of the material properties for which the kriging is applied. Additionally, for this study, these recommendations to increase the maximum lag did not yield reliable minimum (or negative) Lagrange values.

As noted above, kriging of CCC data sets is a computationally intensive process that can have a long run time using conventional computing systems. As a result of this observation, it was decided to run the kriging code in a few cases for maximum separation lags of ~ 6.0 m (20 ft) and ~ 15 m (50 ft), which took approximately 1 hr and 10 hrs, respectively. The results from analyses conducted using these larger separation lags were compared to results from 1.5 m and 3.0 m separation lag analyses, and it was concluded that there was not a significant difference between the point-estimated kriging values or the corresponding relative errors. Figure 6.12 clearly confirms this observation.

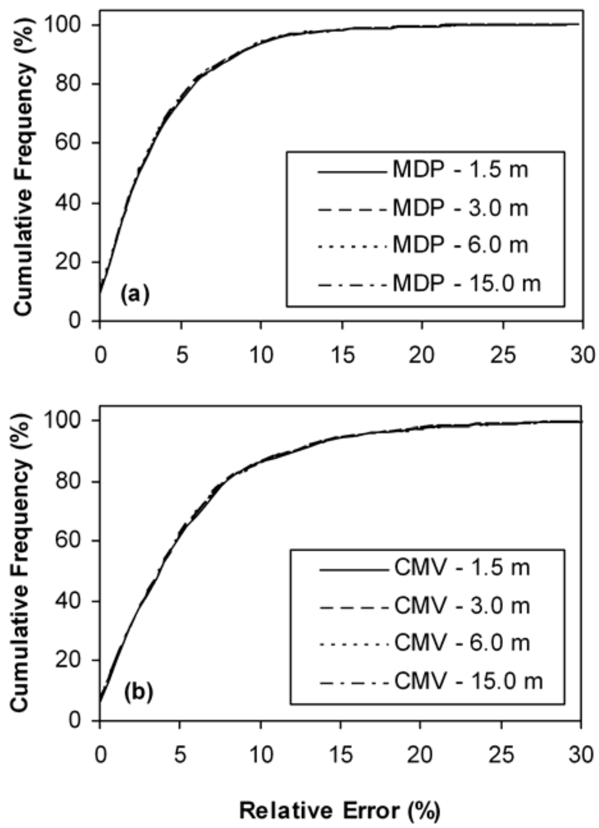

Figure 6.12 A comparison between the relative errors of different kriging neighborhoods for Lift 3, using the selected models: a) RQ model for MDP and b) Exponential model for CMV.

It should be noted that for the sake of space Exponential model was selected as a representative model for CMV. The same results was also obtained for Linear and Spherical models.

Although the recommendations made by others make more mathematical and statistical “sense”, it was concluded that practical considerations impose an equally important criteria, which must be satisfied when selecting the kriging neighborhood. The density of the distributed data in the area of interest was found to play a remarkable role in choosing the maximum lag for the kriging models. The run time of the kriging code exhibited a practically significant obstacle at larger separation lags, especially when there was a large amount of data that needed to be analyzed. Based on these factors, it is desirable to minimize the kriging neighborhood as much as possible, while taking into account the relative data population size in the neighborhood of the point of interest. In the other words, if the density of the overall population is not large, it is acceptable to increase the maximum lag, but if the density of the scattered data around the point of interest is high, then having a relatively small kriging neighborhood may be reasonable.

As discussed in the initial portion of this chapter, one of the parameters that can reveal the spatial continuity of the data is the correlation coefficient. As mentioned earlier, a correlation coefficient of zero means that there is no spatial relation between corresponding data sets. This fact was used to provide confidence in our selection of a relatively small kriging neighborhood for analysis of our CCC data set: 1.5 m and/or 3.0 m were the final values that were recommended as appropriate. Both of these lags gave relatively accurate results with very quick run times in the model. The model results for these two lags were also consistent with each other, and did not improve with selection of larger lag distances. To provide insight in this area, Table 6.12 presents the distances at which the autocorrelation or coefficient of correlation of the CCC data became close to zero for each of the final passes that were analyzed in the data set.

Table 6.12 The separation distance (lag) at which the correlation coefficient approaches zero

Lift / Pass	Lag (m)		Lift / Pass	Lag (m)	
	MDP	CMV		MDP	CMV
Base / 2	4.0	6.4	5 / 2	2.1	2.1
2 / 6	3.4	9.4	5 / 3	5.2	1.8
3 / 8	1.8	7.9	5 / 4	3.7	3.7
4 / 9	4.0	2.4	5 / 5	2.4	4.3
5 / 1	4.0	1.8	5 / 7	5.8	1.8

Based on Table 6.12 it can be stated that the minimum distance that correlation coefficient approaches zero is 1.8 m which is greater than our selected minimum kriging neighborhood of 1.5 m. This implies that our selected neighborhood distance was conservative enough.

6.8 Conclusions and recommendations

This chapter presented the use of the ordinary kriging method as a robust tool for assessing the spatial continuity of CCC roller data and for performing point estimation of unknown values in CCC and IC field studies.

A number of basic semivariogram models were examined for use with the ordinary kriging method, and eventually the Rational Quadratic model was selected as the most reliable semivariogram model for analyzing MDP data, and the Exponential, Spherical, and Linear semivariogram models were selected as the most reliable approaches for analyzing the CMV data. The main criteria that was used for model selection, in order of importance, was as follows: 1- The most useful models are the ones that have little or no singularities and well-structured Γ matrices. 2- The models that generate lthe least amount of relative error over the entire area of data sampling are the most desirable. Based on the analyses that were performed, it was concluded that the R-squared value of the model-fit sample semivariograms is not necessarily a reliable indicator of the quality of the point-estimated values that are later determined via kriging. Additionally, as the kriging method itself inherently minimizes the error of the predicted values, the correlation coefficient between actual and predicted values is not generally a robust tool for selecting a better model, as all the resulting correlation coefficients tend to be quite high.

Additional examination of the resulting kriged data points indicated that, in general, the relative error of the predicted MDP values was less than the predicted CMV values. This is consistent with the nature of these respective data sets, which is discussed in detail in Chapter 5. Another interesting observation about the calculated relative error is that there is a direct relationship between the degree of compaction of the soil and the associated accuracy of the kriging method. As the soil becomes denser and stiffer, the values predicted using kriging become closer to the actual values.

For selecting the kriging neighborhood or maximum separation lag, it is recommended to take practical conditions into account since there are not any significant changes in the kriging results as the separation lag is increased beyond 1.5 m (5.0 ft). This means that the runtime of the kriging computer program and the density of the scattered data around the proposed kriging point are playing essential role in selecting the kriging neighborhood.

Chapter 7

UNIVARIATE REGRESSION ANALYSIS

7.1 Introduction

As noted in Chapter 2, one of the primary objectives of continuous compaction control and intelligent compaction systems is to develop a reliable method for quality control of the compaction process, which minimizes dependence on conventional quality control methods. To achieve this objective, it is first necessary to establish a reliable correlation between CCC roller measurements and conventional in-situ testing measurements that are used as part of the compaction QA/QC process. These types of correlations allow new CCC methods for compaction control to be verified against existing in-situ test methods, where a large amount of historical experience with successful project construction exists. On a given project, calibration of the CCC roller data with the in-situ test methods that are currently being utilized can be performed by constructing a test pad, or by performing the calibration process in the early stages of the construction process itself. Once a reasonable relationship between roller measured values and the associated in-situ tests has been developed, this relationship can be used throughout the remainder of the project, potentially allowing for significant minimization of the in-situ testing program over time.

A statistical tool that is commonly used to establish correlations between different types of data is regression analysis. In statistics, regression analysis refers to techniques for analyzing and modeling numerical data consisting of values of a dependent variable and an independent variable (univariate or simple regression analysis) or a dependent variable with more than one independent variable (multivariate or multiple regression analysis) (Draper and Smith 1998).

As presented in Chapters 4 and 5, there was a significant amount of variation in both the in-situ test measured values and the CCC data itself. Even though significant amounts of scatter were observed in both the in-situ test and CCC values over the compacted area, it is hoped that there is still a reasonably strong relationship that exists between the current in-situ test methods and the measured CCC data. Without this type of relationship, CCC data cannot reasonably be used for QA/QC of the compaction process in the same ways that we currently use in-situ tests for applying end-result compaction specifications.

If a strong correlation exists between CCC results and the associated in-situ test data points, both in-situ test methods and CCC results will show consistent trends of improvement with additional soil compaction, and should be able to identify those zones of soil where insufficient compaction has been applied. The current chapter will use univariate regression analysis to explore the relationships between CCC roller measured values (i.e. MDP and CMV) and the results from commonly performed in-situ tests that are used for QA/QC of the soil compaction process (i.e. soil modulus, dry unit weight, and water content). The effect of water content on the mechanical properties of the compacted soil will also be studied separately using univariate regression analyses.

In order to establish a relationship between CCC data and the corresponding in-situ test measurements, there is a need to predict the CCC values at the same location as each in-situ test that was performed using a spatial interpolation method. As discussed in Chapter 6, a universally accepted geostatitistical method for spatial interpolation of the CCC data is the ordinary kriging method. The results of extensive kriging analyses performed in Chapter 6 indicated that the RQ model was the most accurate for interpolation of MDP values and the Exponential, Spherical, and Linear models were the most accurate for interpolation of CMV values, with approximately the same amount of relative errors being observed for each of these models. In addition, it was discovered that maximum lags of 1.5 m (5 ft) and 3.0 m (10 ft) gave relatively accurate and consistent kriging results for the selected kriging models mentioned above, and proved to be computationally efficient choices for the kriging neighborhood. As a result of these analyses, the RQ model and Exponential model were selected for kriging the MDP and CMV data sets, respectively, with a maximum lag of 1.5 m (5 ft) being used for the kriging neighborhood over which each of these models were fit. The results from these kriging analyses are what is presented for comparison purposes with the in-situ test results in the univariate analyses described in this chapter and the multivariate analyses described in Chapter 8

7.2 Univariate Regression Analysis

The simplest univariate model involves only one independent variable and states that the true mean of the dependent variable changes at a constant rate as the value of the independent variable increases or decreases (Draper and Smith 1998). Thus, the function relationship between the true mean of Y_i, denoted by $E(Y_i)$, and X_i is the equation of a straight line as follows:

$$E(Y_i) = \beta_0 + \beta_1 X_i \tag{7.1}$$

where, β_0 is the y-intercept of the line, and β_1 is the slope of the line, or the rate of change in $E(Y_i)$ per unit change in X.

Using this model, observations of the dependent variable Y_i are assumed to be randomly performed on populations of randomly occurring variables that have a mean of each population that is given by $E(Y_i)$. The deviation of an observation Y_i from its population mean $E(Y_i)$ is taken into account by adding a random error ε_i to yield the statistical model shown in Equation 7.2.

$$Y_i = \beta_0 + \beta_1 X_i + \varepsilon_i \tag{7.2}$$

The subscript i indicates the particular observational unit, $i = 1, 2, \ldots, n$. The X_i values correspond to the n observations that are made on the independent variable, and they are assumed to be measured without error. The random error ε_i's have zero mean and are assumed to have common variance σ^2 and to be pairwise independent. Since the only random element in the model is ε_i, these assumptions imply that the Y_i's also have a common variance σ^2 and are pairwise independent.

The method of least squares is then used with the above model to predict the parameters that correspond to the "best fit". The least squares estimation procedure uses the criterion that the solution must give the smallest possible sum of the squared deviations of the observed Y_i from the estimates of their true means that are provided by the solution (Draper and Smith 1998). By letting $\hat{\beta}_0$ and $\hat{\beta}_1$ be numerical estimates of the parameters β_0 and β_1, respectively, we have:

$$\hat{Y}_i = \hat{\beta}_0 + \hat{\beta}_1 X_i \tag{7.3}$$

Equation 7.4 can then be used to calculate the sum of the squares of the residuals, denoted by SSR.

$$SSR = \sum_{i=1}^{n} (Y_i - \hat{Y}_i)^2 = \sum e_i^{\,2} \tag{7.4}$$

where, $e_i = (Y_i - \hat{Y}_i)$ is the observed residual for the ith observation.

The least squares principle then chooses $\hat{\beta}_0$ and $\hat{\beta}_1$ such that the *SSR* is minimized (Equations 7.5 and 7.6).

$$\hat{\beta}_0 = \overline{Y} - \hat{\beta}_1 \overline{X} \tag{7.5}$$

$$\hat{\beta}_1 = \frac{\sum X_i Y_i - \frac{(\sum X_i)(\sum Y_i)}{n}}{\sum X_i^{\,2} - \frac{(\sum X_i)^2}{n}} \tag{7.6}$$

where, $\overline{Y}$ and $\overline{X}$ are the corresponding sample means.

Among the various methods that are commonly used to evaluate the resulting fit function, the R-squared value is probably the most common term that is used to assess the quality of the resulting model fit (this parameter is discussed in detail in Chapter 6). The correlation coefficient between the real and predicted values can also be used for final model evaluation (see Chapter 6).

There are other univariate regression models, such as polynomial and trigonometric models, which use the same general approach and concepts as the simple model, but which use higher order polynomial expressions or other more sophisticated mathematical expressions in the right hand side of Equations 7.1 and 7.2.

7.3 Univariate Regression Analysis of the Field Data

7.3.1 Correlation Coefficient Analysis

As discussed in Chapter 6, one way to identify a linear correlation between a set of actual values and set of corresponding predicted values is to calculate and analyze the relevant correlation coefficient. In this section, the correlation coefficients between in-situ test results and the “best-guess” (kriged) CCC roller values at each of the corresponding in-situ test locations are calculated. By examining these correlation coefficient values, it is hoped that an initial understanding of possible relationships between CCC results and in-situ test results can be developed. Table 7.1 presents the resulting correlation coefficients between the kriged MDP values at each in-situ test point and the corresponding values measured in each of the in-situ tests. For comparison purposes, the correlation coefficient between the kriged MDP values and the associated kriged CMV values is also presented.

Table 7.1 Correlation Coefficients between MDP Measurements and Corresponding In-situ Test Results

Lift - Pass	CMV	GeoGauge (MPa)	LWD 300 (MPa)	LWD 200 (MPa)	$DCPI_{M-152.4}$ (mm/blow)	$DCPI_{A-152.4}$ (mm/blow)	Lab ω (%)	NDG γ_d (kN/m^3)	NDG ω (%)
Base – 2/2	-0.27	-0.47	-0.40	NA	0.71	0.27	0.27	-0.40	0.16
Lift 2 – 6/6	-0.16	-0.44	-0.43	-0.44	0.21	0.14	-0.39	-0.51	0.32
Lift 3 – 8/8	-0.21	-0.21	0.25	0.02	-0.13	-0.21	-0.21	0.16	0.10
Lift 4 – 9/9	0.02	-0.17	0.02	0.10	0.31	0.31	0.21	0.10	-0.02
Lift 5 – 1/7	-0.73	-0.51	-0.10	-0.56	0.08	0.20	0.86	-0.30	0.62
Lift 5 – 2/7	-0.33	-0.57	-0.55	-0.93	0.37	0.45	0.19	-0.39	0.60
Lift 5 – 3/7	0.12	-0.46	-0.20	0.13	-0.72	-0.65	0.64	0.17	0.14
Lift 5 – 5/7	0.24	-0.93	0.23	0.65	-0.10	-0.08	0.05	-0.53	0.48
Lift 5 – 7/7	-0.33	-0.25	-0.10	-0.35	0.17	-0.12	0.50	0.84	0.38
All	-0.53	-0.37	-0.37	-0.60	0.61	0.54	0.39	-0.45	0.58
Averag e	-0.57	-0.48	-0.78	-0.82	0.90	0.91	0.63	-0.80	0.91

In the table above, the term "All" corresponds to the correlation coefficient that was calculated by examining the entire data set at once, instead of pass by pass. The term "Average" corresponds to the correlation coefficient that was calculated by looking at the relationship between the average of the kriged CCC values for each lift and pass as compared to the average of the in-situ values for each lift and pass. In order to use this approach, kriging is first performed on the CCC data set to determine the CCC test values for comparison with each in-situ test point. The resulting kriged values for each lift and pass are then averaged to come up with a single representative value for each lift and pass. The in-situ test results are also averaged for each lift and pass. The averaged in-situ values are then compared with the averaged kriged CCC values, using the correlation coefficient. This approach to looking at the average of the kriged values for each lift and pass is consistent with what has been performed by others (e.g. White et al. 2005).

By examining Table 7.1, it is apparent that there is generally not a strong correlation between MDP and the other measurements if individual lifts and passes are considered. However, the average of the measured in-situ data show more promising relationships when compared with average MDP values. The nature of these relationships will be explored in more detail in the following sections.

Table 7.2 presents the resulting correlation coefficients between the kriged CMV values at each in-situ test point and the corresponding values measured in each of the in-situ tests. For comparison purposes, the correlation coefficient between the kriged CMV values and the associated kriged MDP values is also presented.

Table 7.2 Correlation Coefficients between CMV Measurements and Corresponding In-situ Test Results

Lift - Pass	MDP (kW)	GeoGauge (MPa)	LWD 300 (MPa)	LWD 200 (MPa)	$DCPI_{M-152.4}$ (mm/blow)	$DCPI_{A-152.4}$ (mm/blow)	Lab ω (%)	NDG γ_d (kN/m^3)	NDG ω (%)
Base – 2/2	-0.27	-0.65	0.05	NA	-0.77	-0.20	0.63	-0.50	0.55
Lift 2 – 6/6	-0.16	0.07	0.19	0.64	-0.10	-0.16	-0.07	-0.07	0.31
Lift 3 – 8/8	-0.21	-0.17	-0.02	-0.10	0.11	0.05	-0.10	0.22	-0.06
Lift 4 – 9/9	0.02	0.04	-0.08	0.21	-0.22	-0.18	0.49	0.14	0.71
Lift 5 – 1/7	-0.73	0.06	0.73	0.95	0.51	0.42	-0.36	-0.26	-0.10
Lift 5 – 2/7	-0.33	0.82	0.35	0.62	-0.35	-0.44	-0.54	0.67	-0.37
Lift 5 – 3/7	0.12	0.53	0.77	0.76	-0.01	-0.22	-0.37	-0.50	-0.29
Lift 5 – 5/7	0.24	-0.42	0.94	0.75	-0.48	-0.56	-0.48	-0.20	-0.68
Lift 5 – 7/7	-0.33	0.09	0.20	0.30	-0.40	-0.24	-0.47	-0.09	-0.45
All	-0.53	0.07	0.12	0.27	-0.45	-0.37	-0.23	0.17	-0.21
Average	-0.57	0.17	0.07	0.08	-0.61	-0.59	-0.68	0.38	-0.47

As shown in Table 7.2, for some lifts and passes relatively high correlation coefficients were observed. However, these trends were generally not consistent for the other lifts and passes, and in general no robust trend could be determined. In addition, taking the averages of the kriged values into account, as was done for the MDP analysis, did not appear to yield as successful results.

7.3.2 In-situ Testing Measurements versus Kriged CCC Values

In order to explore the nature of the relationships between CCC data and in-situ testing measurements further, a series of univariate regression analyses were performed to determine correlation functions between data sets. Univariate regression analysis were performed using linear regression (denoted by L and a solid line) and second-degree polynomial regression (denoted by P and a dashed line) to generate the trend lines shown in the following figures.

To illustrate the overall scatter in the measured data, a series of plots are used to compare the in-situ test measurements with the kriged CCC data points at each in-situ test location (Figure 7.1 to Figure 7.3). These figures present comparisons between in-situ test and CCC measured values for the entire data set – that is, that the data are not broken down by lift and pass. The only data omitted in this analysis (and from all of the regression analyses from here on out) is the CMV values that were recorded for Pass 1 of Lift 5. The detailed reasoning for not including these values in the regression analysis is provided in Chapter 5, and has to do with the relative effect of the differing degree of vibratory compaction amplitude that was applied for this lift and pass (the compaction for Pass 1 of Lift 5 was high amplitude, while for all other lifts and passes low amplitude compaction was used). In all the presented figures, if the R-squared value is greater than 0.7, the mathematical function of the fitted curve will be presented in the corresponding figure.

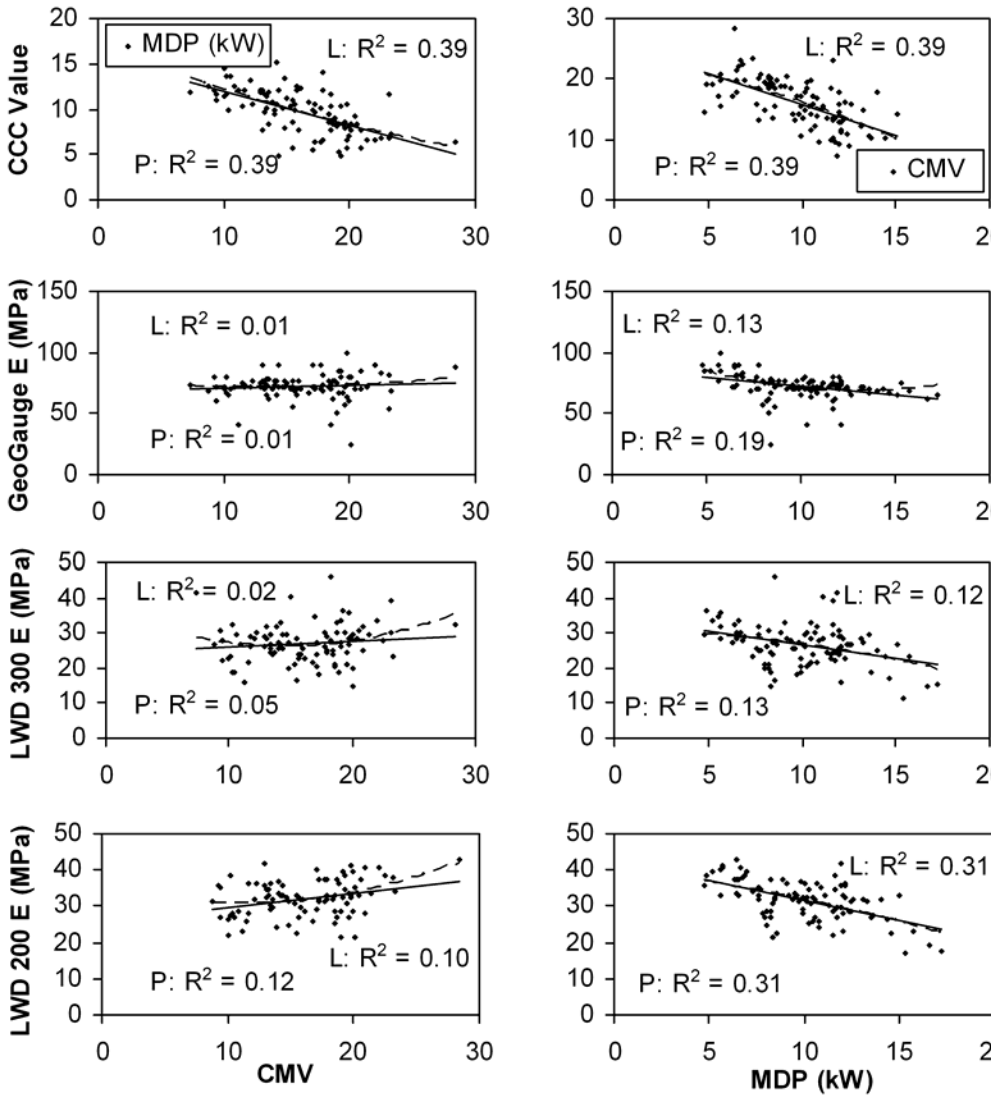

Figure 7.1 **Univariate regression analyses of CCC, GeoGauge, and LWD measured values, vs. kriged CMV and MDP measurements for each of the in-situ test locations**

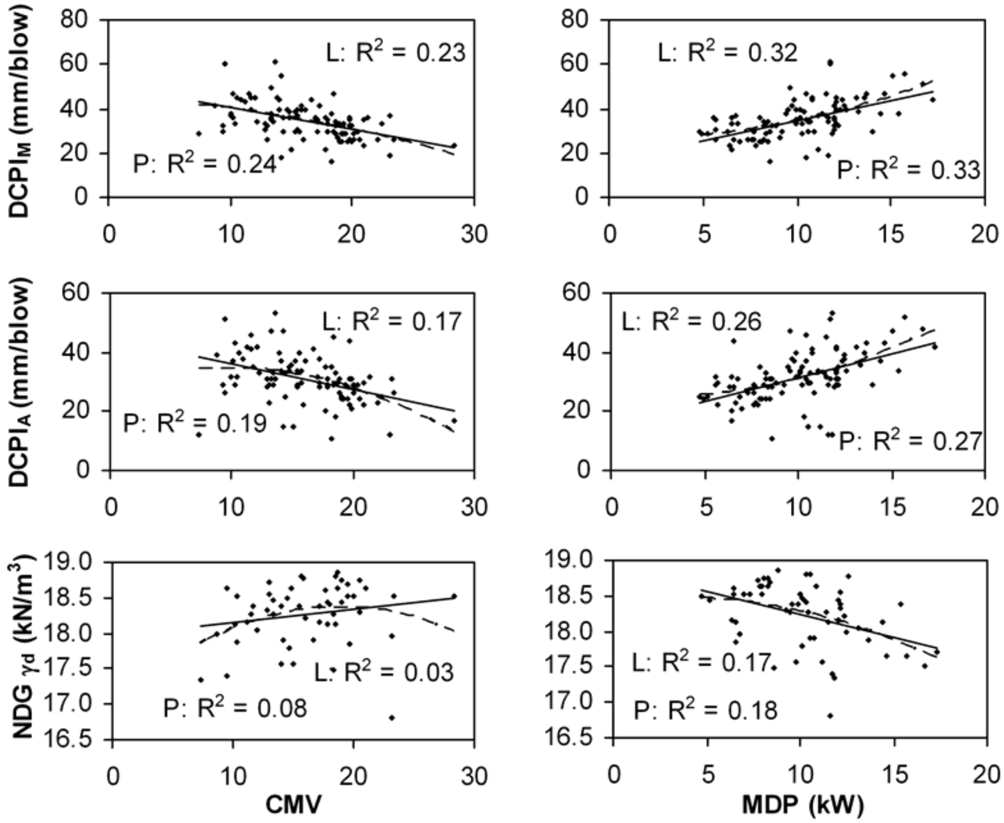

Figure 7.2 Univariate regression analyses of DCP and NDG measured values, vs. kriged CMV and MDP measurements for each of the in-situ test locations

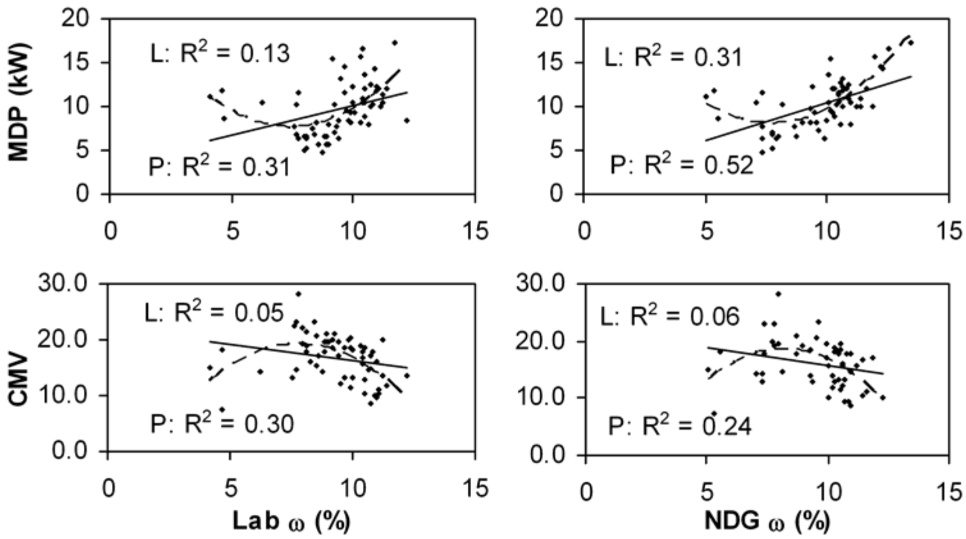

Figure 7.3 Univariate regression analyses of Lab and NDG water contents, vs. kriged CMV and MDP measurements for each of the in-situ test locations.

As shown in Figures 7.1 through 7.3, there is not a strong linear or quadratic relationship between the measured in-situ test results and the corresponding kriged CCC values at each of the in-situ test locations. This conclusion is in agreement with the preliminary findings shown by the correlation coefficients presented in Tables 7.1 and 7.2.

In an attempt to see whether or not the data from the final passes of each lift was obscuring the univariate regression results, it was useful to perform separate univariate regression analyses on only the kriged results from Lift 5, Passes 1 through 7, to see if a consistent trend emerged that could be used for CCC data calibration. As noted earlier (in the previous section and in Chapter 5), the CMV values that were recorded for Pass 1 of Lift 5 were omitted from this analysis, as the vibratory compaction amplitude that was applied for this pass was high amplitude, while the other passes were subjected to low amplitude compaction. The results from these univariate regression analyses are provided in Figures 7.4 through 7.6.

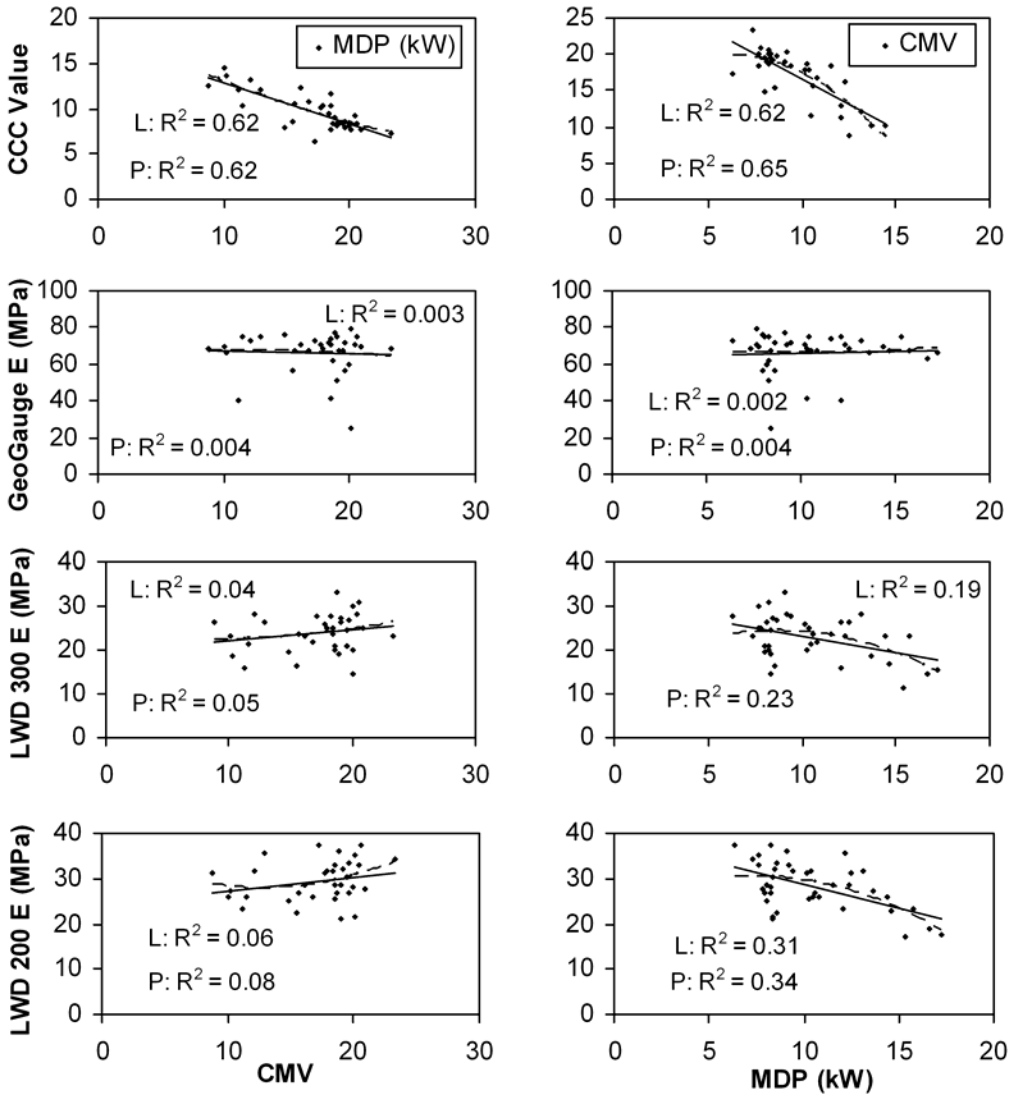

Figure 7.4 Univariate regression analyses of CCC, GeoGauge, and LWD measured values, vs. kriged CMV and MDP measurements for the Lift 5 in-situ test results

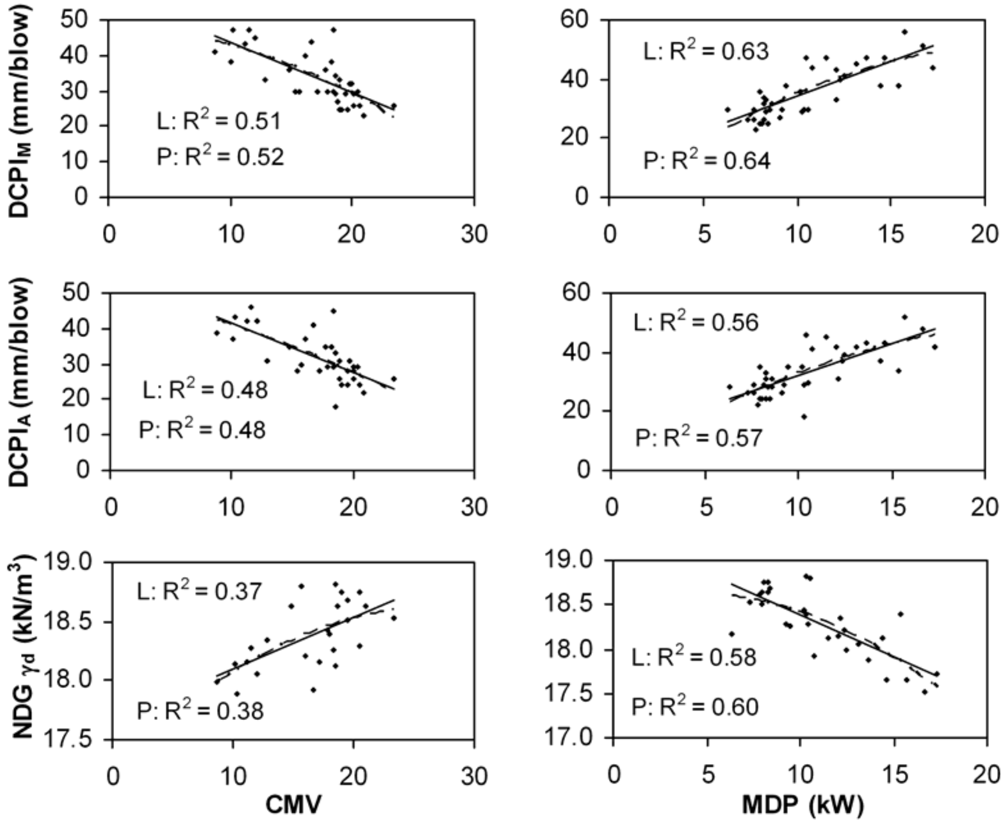

Figure 7.5 **Univariate regression analyses of DCP and NDG measured values, vs. kriged CMV and MDP measurements for the Lift 5 in-situ test results**

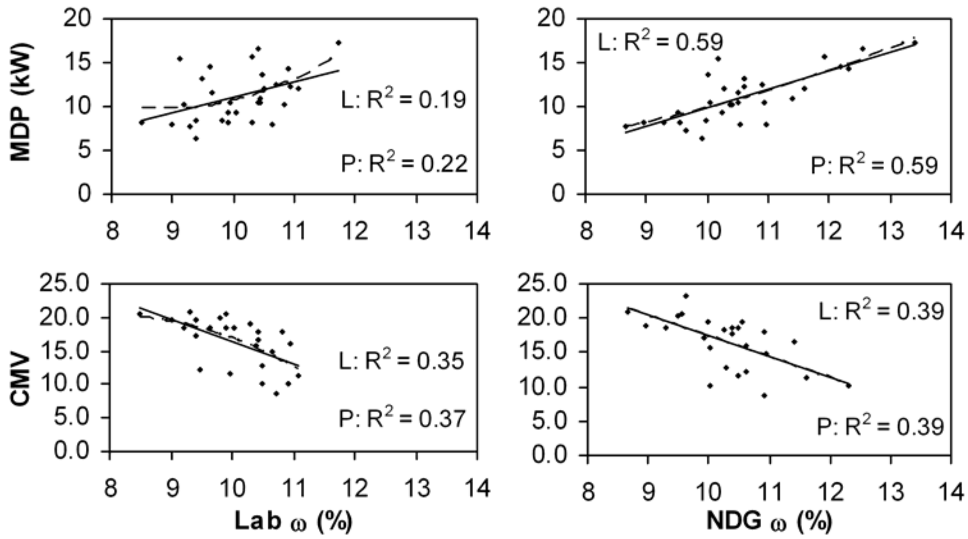

Figure 7.6 Univariate regression analyses of Lab and NDG water contents, vs. kriged CMV and MDP measurements for the Lift 5 in-situ test results

As shown in Figures 7.4 through 7.6, there is not a strong linear or quadratic relationship between the measured in-situ test results and the corresponding kriged CCC values that could be developed by analyzing only the Lift 5 data, even though a significant amount of pass-by-pass data exists for this lift.

Further univariate regression analyses were also performed between in-situ test data points and kriged CCC values on a lift-by-lift, pass-by-pass basis. The R-squared values resulting from these analyses are presented in Tables 7.3 and 7.4. Consistent with the previous section, in all of the analyses that were performed, the associated CCC values (MDP and CMV) were the independent variables (with the exception of the NDG and Lab water content results shown in Table 7.4, which used the corresponding water contents as the independent variables; this is consistent with the earlier univariate analyses that are shown in this chapter). The associated values of MDP are presented in gray. To highlight strong correlations that may be of interest, R-squared values greater than or equal to 0.7 are presented in boldface text in the tables.

Table 7.3 Summary of univariate regression analysis between CCC values and modulus-based tests for single lifts and passes

Lift / Pass	CMV											
	MDP (kW)											
	CCC		GeoGauge E (MPa)		LWD 300 E (MPa)		LWD 200 E (MPa)		$DCPI_M$ (mm/blow)		$DCPI_A$ (mm/blow)	
	L	P	L	P	L	P	L	P	L	P	L	P
Base - 2/2	0.07	0.07	0.42	**0.91**	0.00	0.03	NA	NA	0.60	**0.86**	0.04	0.39
	0.07	0.44	0.22	0.29	0.16	**0.81**	NA	NA	0.51	0.62	0.07	**0.93**
Lift 2 - 6/6	0.03	0.20	0.01	0.02	0.04	0.04	0.41	0.41	0.01	0.08	0.03	0.13
	0.03	0.10	0.19	0.20	0.18	0.27	0.20	0.22	0.04	0.15	0.02	0.05
Lift 3 - 8/8	0.05	0.05	0.03	0.03	0.00	0.14	0.01	0.04	0.001	0.40	0.00	0.38
	0.05	0.07	0.04	0.05	0.06	0.08	1E-04	0.01	0.02	0.02	0.04	0.05
Lift 4 - 9/9	0.001	0.04	0.002	0.002	0.01	0.10	0.04	0.07	0.05	0.05	0.03	0.03
	0.001	0.03	0.02	0.08	0.01	0.02	0.01	0.04	0.08	0.14	0.09	0.14
Lift 5 - 1/7	0.54	0.54	0.00	0.68	0.53	0.62	**0.90**	**0.93**	0.26	0.39	0.18	0.38
	0.54	0.77	0.26	0.32	0.01	0.04	0.32	0.32	0.06	0.11	0.04	0.11
Lift 5 - 2/7	0.11	0.12	0.68	**0.88**	0.12	0.45	0.38	**0.96**	0.13	0.42	0.19	0.51
	0.11	**0.90**	0.32	0.50	0.30	0.31	**0.87**	**0.88**	0.13	**0.98**	0.20	**0.96**
Lift 5 - 3/7	0.01	0.34	0.28	0.30	0.59	0.61	0.58	0.60	7E-05	0.53	0.05	0.66
	0.01	0.02	0.21	0.22	0.04	0.05	0.02	0.02	0.52	**0.70**	0.43	0.53
Lift 5 - 5/7	0.12	0.23	0.18	**0.88**	**0.89**	**0.93**	0.56	**0.98**	0.23	0.52	0.32	0.63
	0.12	**0.98**	**0.95**	**0.96**	0.22	0.53	**0.73**	**0.85**	0.06	0.29	0.06	0.18
Lift 5 - 7/7	0.11	0.24	0.01	0.01	0.04	0.08	0.09	0.09	0.16	0.18	0.06	0.06
	0.11	0.11	0.06	0.07	0.01	0.02	0.12	0.16	0.03	0.03	0.02	0.04

Table 7.4 Summary of univariate regression analysis between CCC values and modulus-based tests for single lifts and passes

Lift / Pass	CMV / MDP (kW)					
	NDG γ_d (kN/m^3)		NDG ω (%)		Lab ω (%)	
	L	P	L	P	L	P
Base - 2/2	0.25	**0.92**	0.30	0.37	0.39	0.54
	0.16	0.58	0.02	0.45	0.07	0.22
Lift 2 - 6/6	0.003	0.12	0.06	0.37	0.01	0.01
	0.18	0.22	0.07	0.11	0.15	0.30
Lift 3 - 8/8	0.01	0.33	0.004	0.02	0.16	0.01
	0.06	0.24	0.01	0.07	0.08	0.42
Lift 4 - 9/9	0.44	**0.87**	0.04	0.27	0.08	0.35
	0.18	**0.77**	0.21	0.30	0.20	0.60
Lift 5 - 1/7	0.07	**0.73**	0.01	0.62	0.13	0.44
	0.04	0.11	0.39	0.66	**0.74**	**0.74**
Lift 5 - 2/7	0.45	0.62	0.14	0.15	0.29	0.36
	0.15	**0.73**	0.36	0.69	0.03	0.38
Lift 5 - 3/7	0.25	0.27	0.09	0.41	0.14	0.14
	0.03	0.43	0.02	0.02	0.41	**0.84**
Lift 5 - 5/7	0.04	0.67	0.46	0.56	0.24	0.25
	0.59	**0.88**	0.17	0.41	0.02	0.13
Lift 5 - 7/7	0.01	0.01	0.15	0.15	0.27	0.34
	0.39	0.46	0.08	0.08	0.15	0.32

As shown in Tables 7.3 and 7.4, in some cases there is a strong univariate regression relationship between CCC values and their corresponding in-situ measurements. Unfortunately, these trends only appear for correlations developed using only a few points for specific lifts and passes, and are not consistent for different lifts and passes. Consequently, upon careful examination of Figures 7.1 through 7.6 and Tables 7.3 and 7.4, it appears that in general there is not a significant linear or quadratic univariate relationship between the roller and in-situ testing data that can be found by making point-to-point comparisons of the kriged CCC values with the in-situ test results. This observation is consistent with what has been observed by other researchers that have studied the use of CCC technology (e.g. White and Thompson 2008, Kröber et. al. 2001).

In an attempt to resolve this issue, another approach is needed to develop better correlations between the measured in-situ test results and the corresponding kriged CCC values at each of the in-situ test locations. In order to smooth the data and minimize the point-specific inaccuracies that are characteristic of both the CCC and in-situ test data sets, *average* in-situ test value were calculated for each lift and pass, and compared to the *average* of the kriged CCC data points for each lift and pass. Regression analysis was then performed on the resulting data set of *average* CCC and in-situ test values. The results from these univariate regression analyses are provided in Figures 7.7 through Figure 7.9.

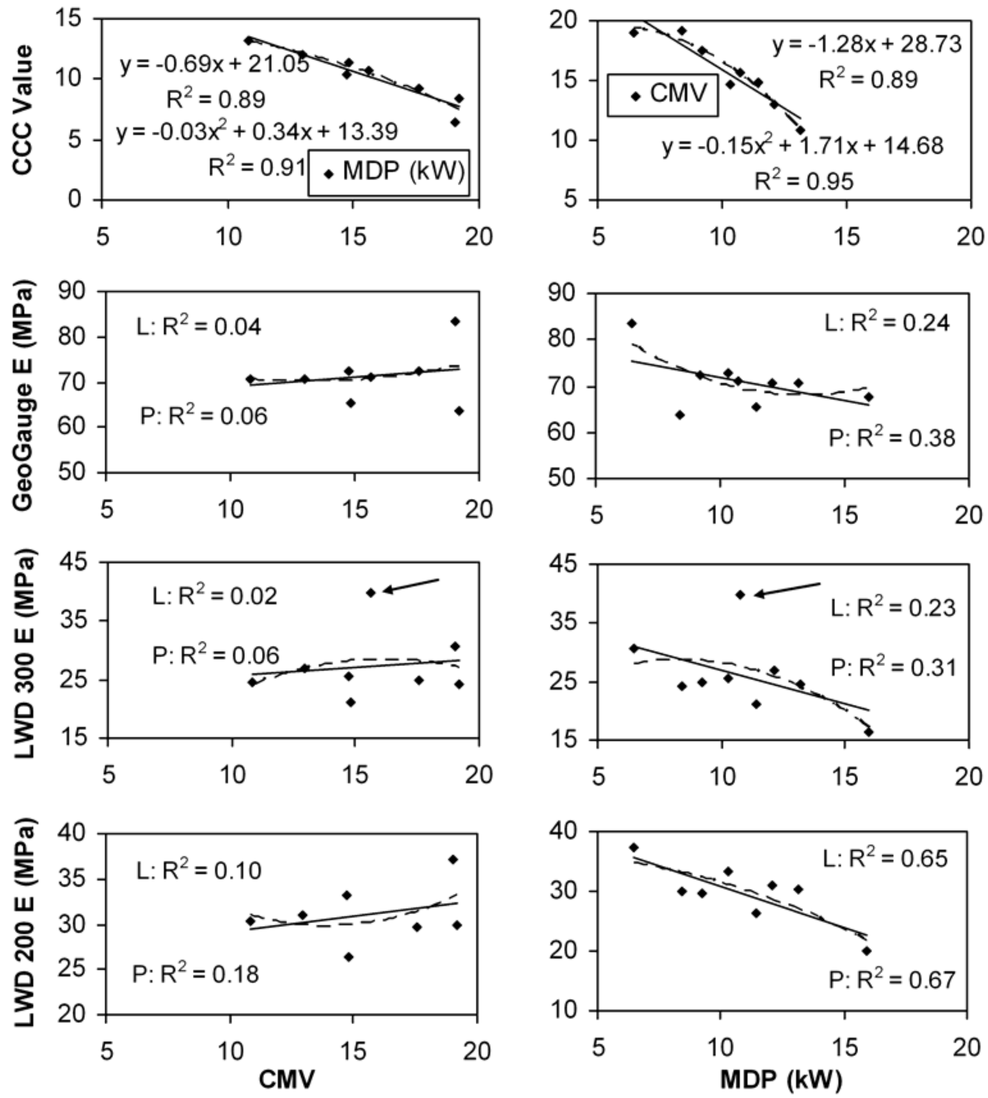

Figure 7.7 **Univariate regression analyses of average in-situ testing values vs. average CCC data for all lift and passes**

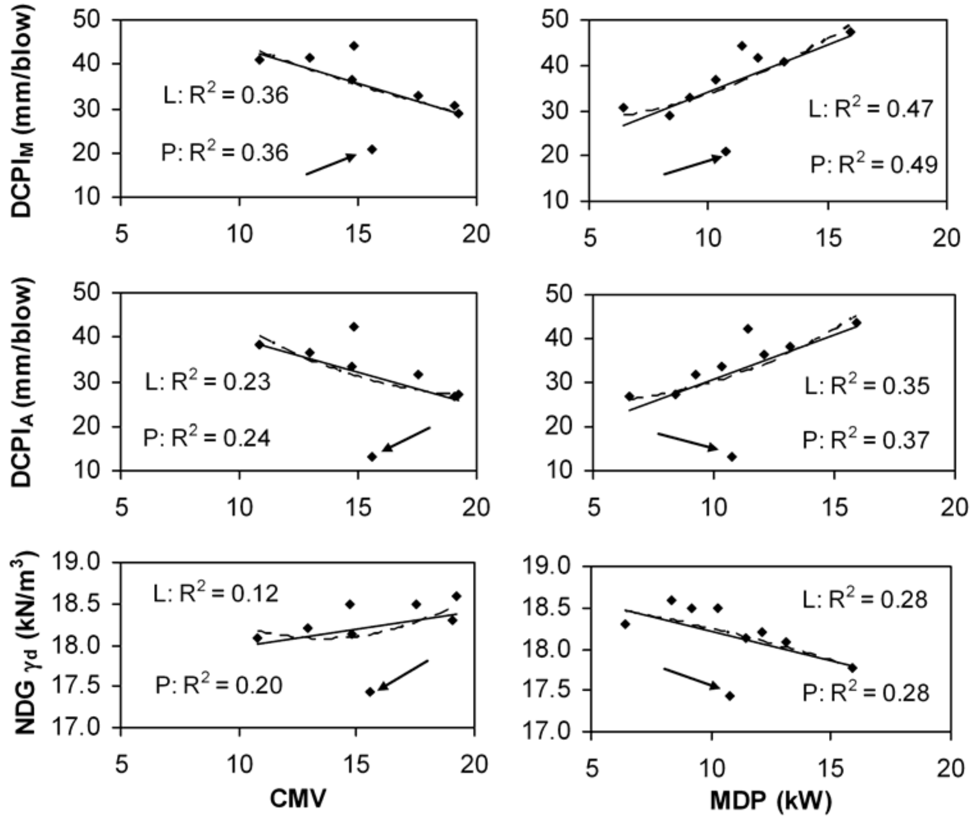

Figure 7.8 **Univariate regression analyses of average in-situ testing values vs. average CCC data for all lift and passes**

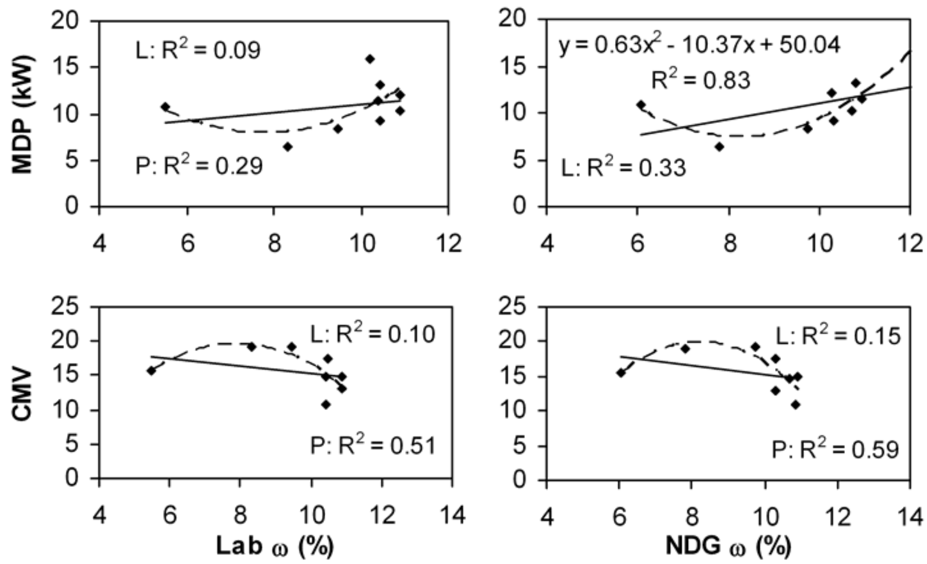

Figure 7.9 Univariate regression analyses of average in-situ testing values vs. average CCC data for all lift and passes

As shown in Figures 7.7 through 7.9, the corresponding R^2 values for both the linear and quadratic regression analyses are significantly higher than the values that were calculated when regression analyses were performed on individual data points (Figures 7.1 through 7.6). This means that linear regression analysis of the *average* values for each lift and pass is a technique that shows significant promise for interpretation and calibration of CCC test results. These findings are consistent with what has been observed by other researchers that have analyzed CCC data sets (Thompson and White 2008).

By examining Figures 7.7 through 7.9, it can also be observed that there was a significant data outlier in many of the plots. This outlier value, which is noted by an arrow in a number of the presented regression plots, belongs to the average values that were recorded for the base layer. As the base layer is itself not an engineered lift (it was not mixed like the other layers, sampled to confirm uniformity with the other soil types, moisture conditioned, or sufficiently compacted), it is reasonable to exclude this data point from consideration for purposes of regression analysis. Consequently, it was decided to repeat the univariate regression analyses using the average lift/pass approach and excluding the base layer data point from each of the plots; the results from these analyses are provided in Figures 7.10 through Figure 7.12.

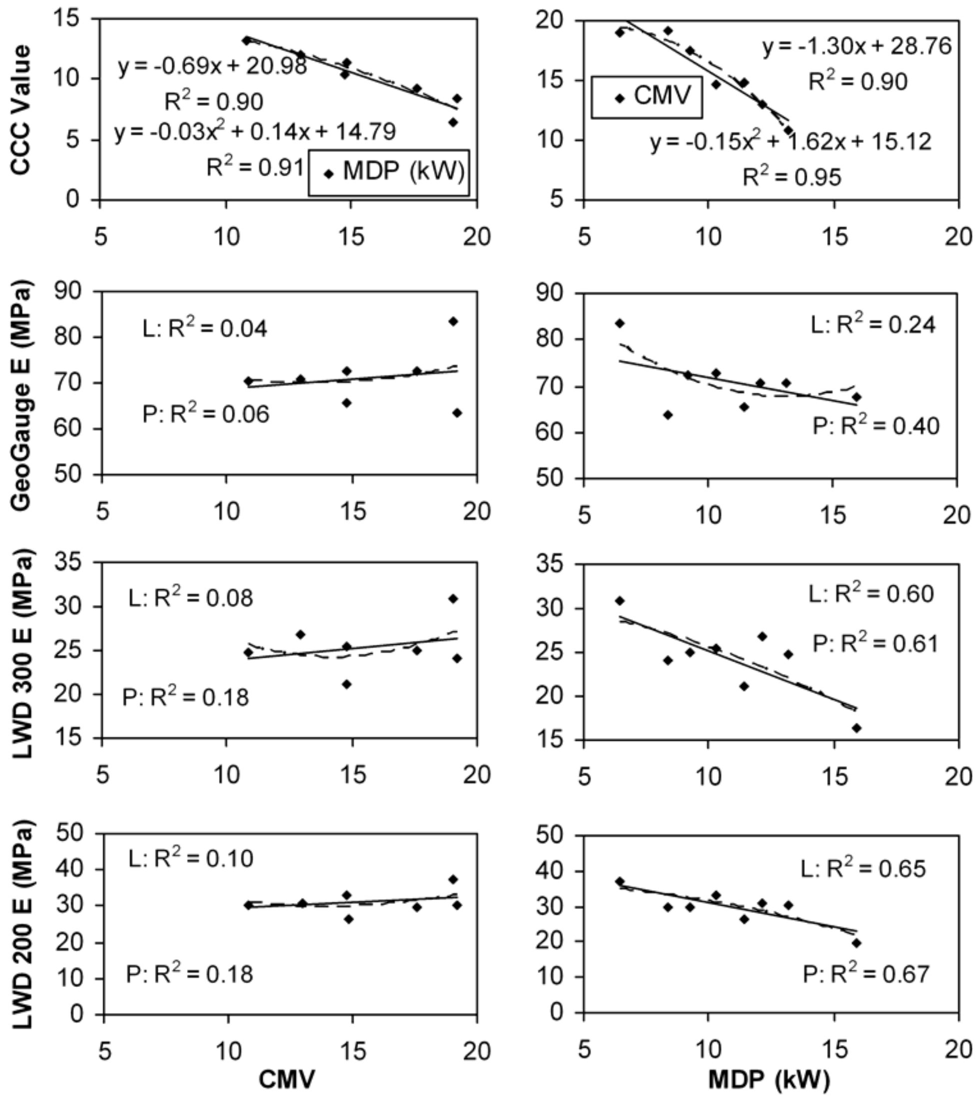

Figure 7.10 Univariate regression analyses of average in-situ testing values vs. average CCC data for all lifts and passes, excluding the base layer

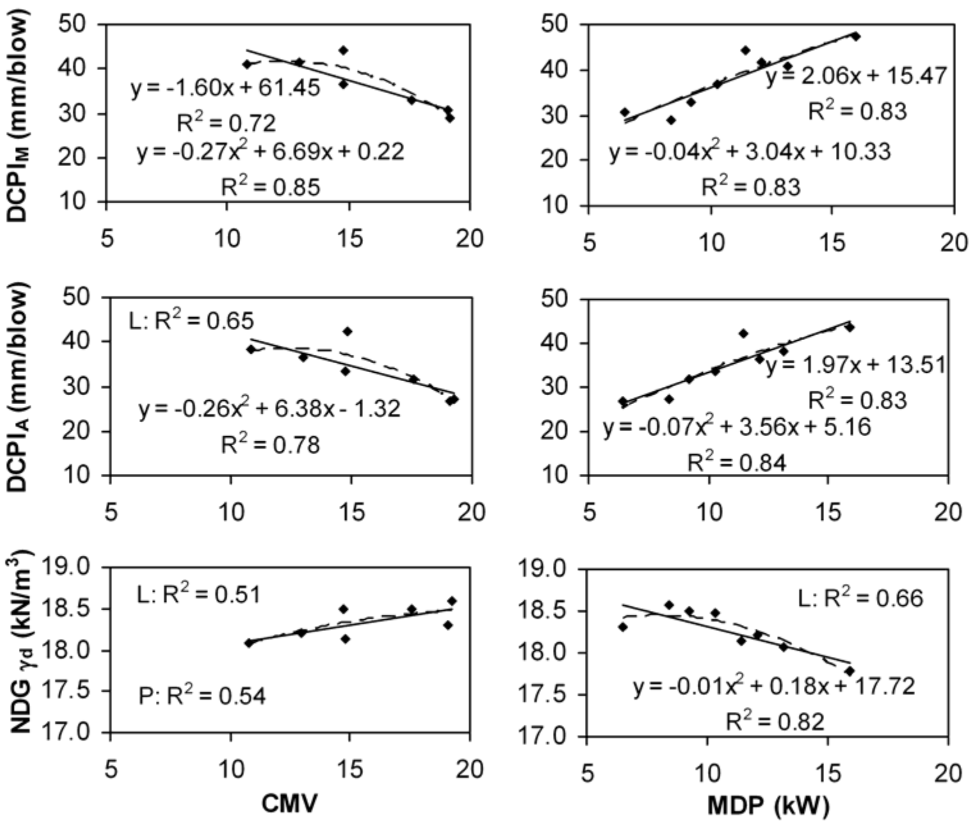

Figure 7.11 Univariate regression analyses of average in-situ testing values vs. average CCC data for all lifts and passes, excluding the base layer

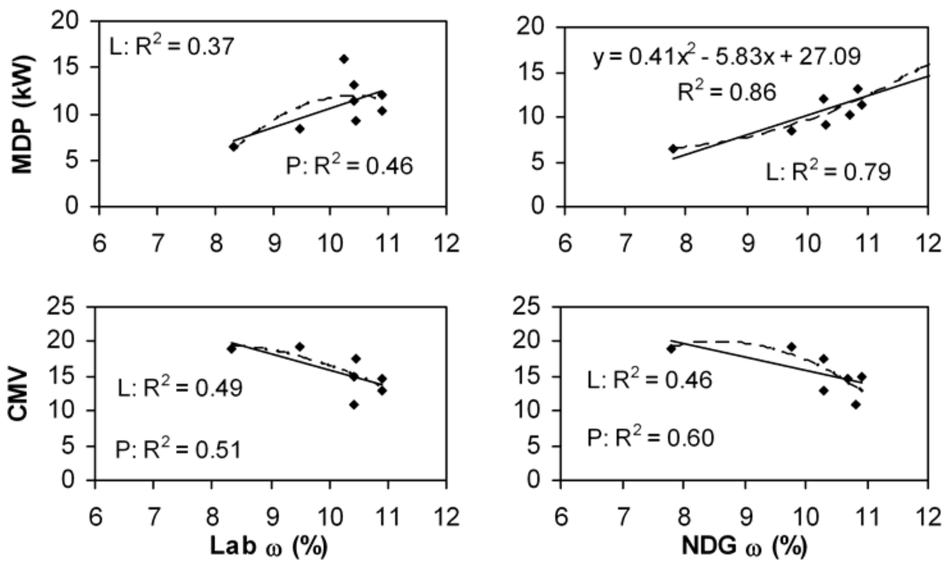

Figure 7.12 Univariate regression analyses of average CCC values vs. average Lab and NDG water contents for all lift and passes, excluding the base layer

By examining Figures 7.10 through 7.12, it can be observed that removing the base layer data point from the regression analyses leads to improved R-squared values in a number of the cases, most notably the LWD 300 modulus, the LWD 200 modulus, DCP indices, and the NDG dry unit weight. One possible reason for such improvement in the resulting analyses is that the base layer was not an engineered lift, which means that it may exhibit significantly different behavior than the other compacted lifts (as discussed previously). Another possible reason for this point being such a significant outlier is the fact that it had a significantly lower water content than what was observed for the other layers that were placed in a more controlled fashion (see Chapter 4). The influence of water content on the test results can be examined more effectively using multiple regression analysis, which is discussed in detail in the next chapter.

In order to develop an understanding of the type of calibrations that could be developed from analysis of a single lift only, univariate regression analyses were also performed looking only at the results from the various passes of Lift 5. The results from these univariate regression analyses are provided in Figures 7.13 through Figure 7.15.

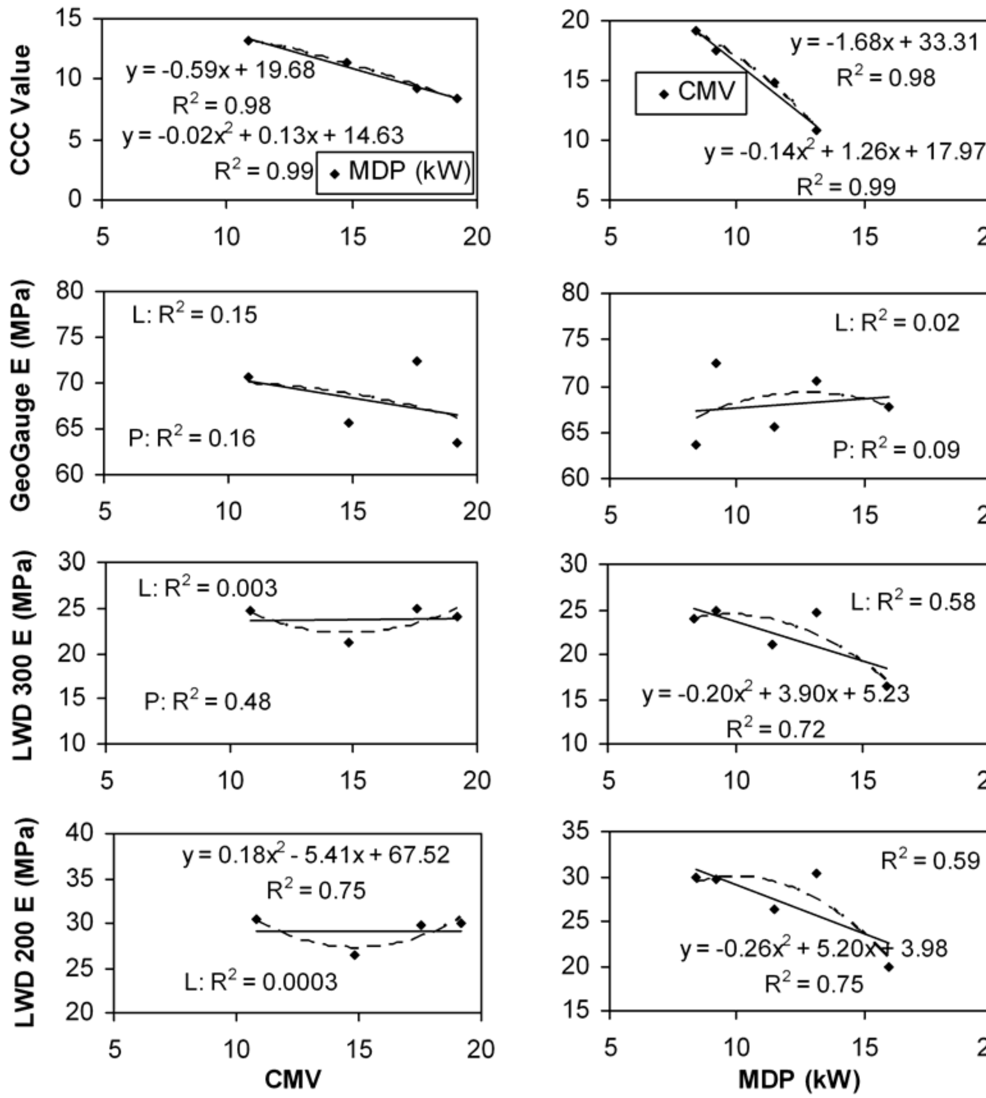

Figure 7.13 Univariate regression analyses of average in-situ testing values vs. average CCC data for Lift 5

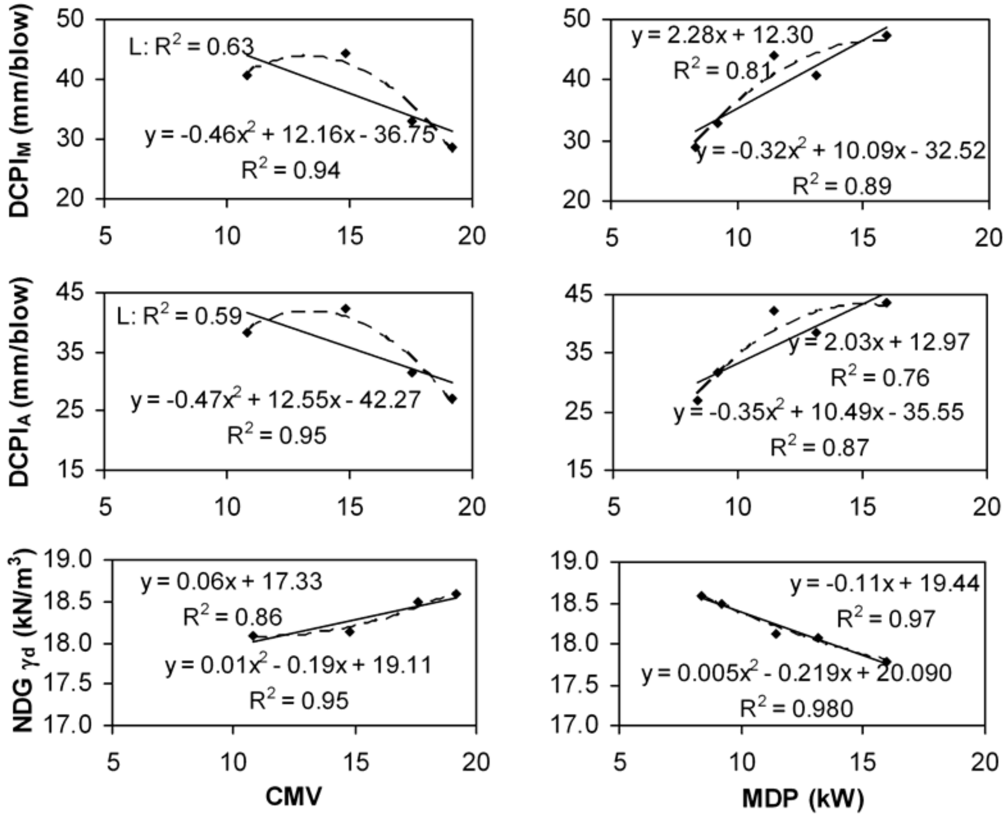

Figure 7.14 Univariate regression analyses of average in-situ testing values vs. average CCC data for Lift 5

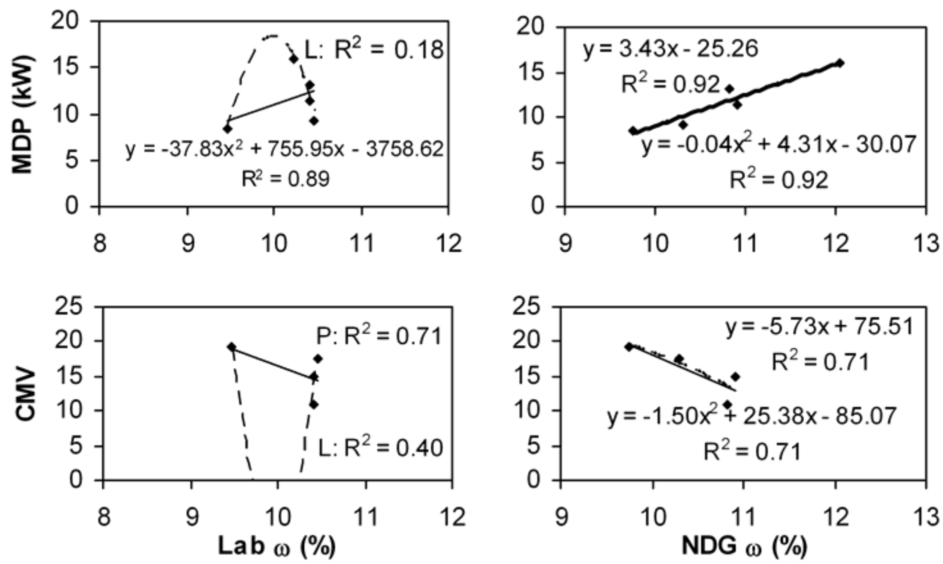

Figure 7.15 Univariate regression analyses of average CCC values vs. average Lab and NDG water contents for Lift 5

By comparing the univariate regression results of analyses performed only on the averaged data from Lift 5 with regression results from analyses performed on the averaged data from all lifts and passes, it can be observed that the quality of the fit (as indicated by the R^2 values) generally improves for most of the cases. In most of these cases, it is likely that the quality of the fit improves due to a reduction in the number of sample data points, with the points being omitted generally being redundant intermediate values that exhibited some significant scatter.

Table 7.5 presents a summary of the R-squared values that are shown in Figures 7.1 through 7.15. In the following table, L and P reflect respectively the linear and polynomial models for each complete data set, while L_{ave} and P_{ave} are related to the linear and polynomial models for the averaged values of each lift and pass. L^*_{ave} and P^*_{ave} describe the linear and second-degree polynomial models for the average values of all lift and passes, excluding the base layer results. To highlight strong correlations that may be of interest, R-squared values greater than 0.7 are presented in boldface text in the table.

Table 7.5 R-square values between roller measurements and in-situ testing data

RMV	Model	MDP (kW)	CMV	GeoGauge (MPa)	LWD 300 (MPa)	LWD 200 (MPa)	$DCPI_M$ (mm/blow)	$DCPI_A$ (mm/blow)	NDG γ_d (kN/m^3)
CMV (all)	L	0.39	1.00	0.01	0.02	0.10	0.23	0.17	0.03
	L_{ave}	**0.89**	1.00	0.04	0.15	0.10	0.36	0.23	0.12
	L^*_{ave}	**0.90**	1.00	0.04	0.08	0.10	**0.72**	0.65	0.51
	P	0.39	1.00	0.01	0.05	0.12	0.24	0.19	0.08
	P_{ave}	**0.91**	1.00	0.06	0.55	0.18	0.36	0.24	0.20
	P^*_{ave}	**0.91**	1.00	0.06	0.18	0.18	**0.85**	**0.78**	0.54
CMV (Lift 5)	L	0.62	1.00	0.003	0.04	0.06	0.51	0.48	0.37
	L_{ave}	**0.98**	1.00	0.15	0.003	0.0003	0.63	0.59	**0.86**
	P	0.62	1.00	0.004	0.050	0.08	0.52	0.48	0.38
	P_{ave}	**0.99**	1.00	0.16	0.48	**0.75**	**0.94**	**0.95**	**0.95**
MDP (all)	L	1.00	0.39	0.13	0.12	0.31	0.32	0.26	0.17
	L_{ave}	1.00	**0.89**	0.24	0.23	0.65	0.47	0.35	0.28
	L^*_{ave}	1.00	**0.90**	0.24	0.60	0.65	**0.83**	**0.83**	0.66
	P	1.00	0.39	0.19	0.13	0.31	0.33	0.27	0.18
	P_{ave}	1.00	**0.95**	0.38	0.31	0.67	0.49	0.37	0.28
	P^*_{ave}	1.00	**0.95**	0.4	0.61	0.67	**0.83**	**0.84**	**0.82**
MDP (Lift 5)	L	1.00	0.62	0.002	0.19	0.31	0.63	0.56	0.58
	L_{ave}	1.00	**0.98**	0.02	0.58	0.59	**0.81**	**0.76**	**0.97**
	P	1.00	0.65	0.004	0.23	0.34	0.64	0.57	0.60
	P_{ave}	1.00	**0.99**	0.09	**0.72**	**0.75**	**0.89**	**0.87**	**0.98**

Analysis of the data presented in Table 7.5 and Figures 7.1 to 7.15 leads to the following general conclusions:

- In a number of the cases (e.g. DCP indices, NDG dry unit weight, and NDG and Lab measured water content, the use of second-degree polynomial regression models resulted in significantly higher R-squared values than the use of a linear regression models.

- In general, point-by-point comparisons between kriged CCC data and individual in-situ test results yield poor-quality correlations.
- Comparisons between *average* kriged CCC data points and *average* in-situ test results for each lift and pass yield relatively high-quality correlations.
- Exclusion of the base layer average values from the associated regression analyses yields improved R-squared values, and reveals that there is a relatively strong relationship between CCC data and some of the in-situ testing measurements.
- In general, MDP values tend to correlate more strongly with in-situ test results than the CMV values do. This observation is likely linked to the fact that the influence depth of MDP is closer to the influence depths of the various in-situ testing methods that were utilized in this study (~ 20 to 60 cm (0.6 ft to 2 ft)). This is in contrast with the deeper influence depths that are commonly cited for CMV data (e.g 0.8 m – 1.5 m (2.6 ft – 4.9 ft), as noted by White and Thompson 2008).
- Average NDG measured dry unit weight and DCP indices showed the strongest correlation with average CCC values, as compared to those values measured in the other in-situ tests.
- LWD 200 test results showed better correlation with the measured CCC data than the LWD 300 test results did.

- Of the in-situ testing methods that were utilized, the Geogauge tended to show the poorest correlation with the recorded CCC data.

7.3.3 Effect of Water Content on the Mechanical Properties of Compacted Soil

Water content has widely been referred to as one of the most significant factors that can influence the mechanical properties of a compacted soil (see Adam 1997, White et. al. 2007). To investigate the influence of water content on the recorded CCC data and the in-situ test results for this project, univariate regression analyses were performed on the available data from the final passes of each lift. The justification for selecting only the final passes was to remove a primary source of variability in the results, the degree of compaction, from the analysis (although it should be noted here that there is also some variability in the relative compaction values after the final passes for each lift, as shown in Figure 4.2.

As discussed earlier in this chapter, it was difficult to discern a clear trend between the single measured values for each lift or pass. Therefore, the average values of each lift and pass are the only ones analyzed in this section. The same process as the previous section was adopted to explore possible relationships between the water content of the soil and the corresponding measured mechanical properties. It is worth mentioning that the water content of the compacted soil was measured by two methods; first by conducting in-situ measurements using a Nuclear Density Gauge (NDG) (ASTM D 3017) and then by taking in-situ samples and using an oven-based laboratory determination procedure (ASTM D 2216). For simplicity, and to differentiate these water contents with respect to those measured by the NDG, this type of water content was called the laboratory water content, or Lab ω.

Figure 7.16 and Figure 7.17 show the effect of water content on the physical and mechanical properties of the compacted soil.

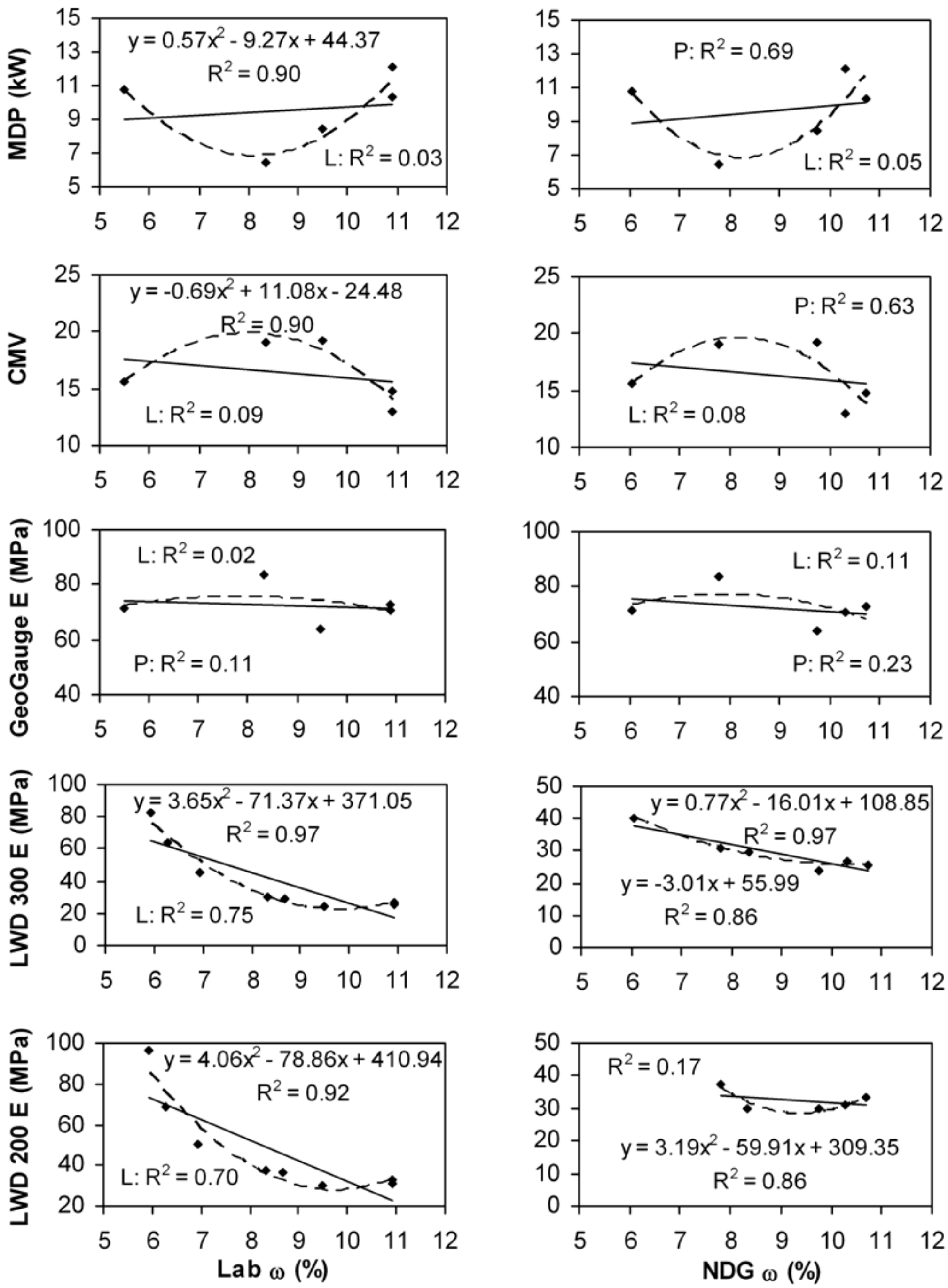

Figure 7.16 Univariate regression analysis of average CCC data and in-situ testing values vs. average measured water contents (final passes)

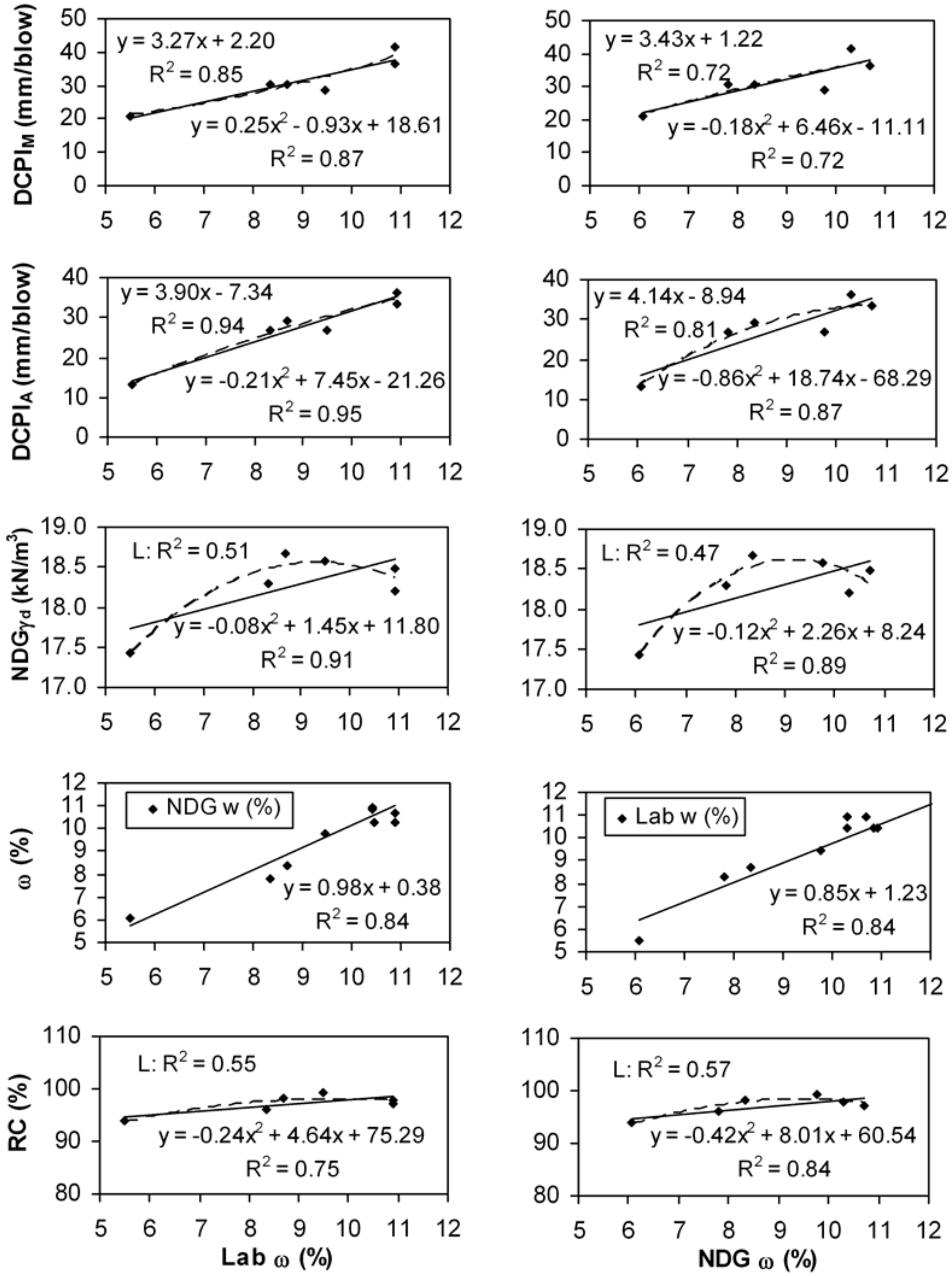

Figure 7.17 Univariate regression analysis of average in-situ testing values vs. average measured water contents (final passes)

As shown in Figure 7.16 and Figure 7.17, there is often excellent agreement between the water content of the soil and other CCC roller data or in-situ test measured values, provided that the data sets are examined for relatively similar amounts of compactive effort. As demonstrated in Figure 7.16 and Figure 7.17, many of the data sets that were examined exhibited a strong polynomial relationship between the average measured properties of the soil and the corresponding average water content. This trend is consistent with the characteristics of a standard Proctor compaction curve, where γ_d values are shown to have a maximum value at an optimum water content for a constant amount of applied compactive effort. Interestingly, this strong quadratic trend was not observed for either the GeoGauge or the DCP measured results, which indicates that the results from these tests may not be as strongly influenced by water content.

For those data sets shown in Figures 7.16 and 7.17 that exhibited high-quality second-order polynomial relationships, it is interesting to find the corresponding optimum moisture content and optimum CCC or in-situ test value. The resulting "measured point" (MP) optimum values are presented in Table 7.6.

Table 7.6 Optimum values for each of the measured CCC and in-situ test data sets, and the corresponding optimum water content

Data Set Analyzed	Lab ω_{opt} (%)	MP_{opt}	NDG ω_{opt} (%)	MP_{opt}
MDP (kW)	8.1	6.7	NA	NA
CMV	8.0	20.0	NA	NA
LWD 300 E (MPa)	9.8	22.2	10.4	25.6
LWD 200 E (MPa)	9.7	28.0	9.4	28.1
NDG γ_d (kN/m3)	9.1	18.4	9.4	18.9
RC (%)	9.7	97.7	9.5	98.7

The “optimum” values presented in Table 7.4 should be treated with caution, as only some of the optimum values correspond to maximum recorded data values (CMV, NDG dry unit weight, and relative compaction), while others correspond to minimum data values (MDP, LWD 300, and LWD 200).

As noted in Chapter 4, the average optimum water content for the compacted material was 11.7%. In addition, the average of the maximum dry unit weights resulting from the series of 1-pt standard Proctor tests (and the assocated family of curves approach) was 18.8 kN/m^3. The average measured modulus from the LWD 300 and LWD 200 tests for the final passes were 27.6 MPa and 32.8 MPa, respectively. As shown in Table 7.4, the optimum moisture content calculated from polynomial regression analysis of the measured CCC values was about 8.0%. The optimum moisture contents back-calculated from regression analysis of the in-situ test values yield results ranging from 9.1% to 9.8%. These back-calculated optimum values are lower than the average optimum water contents resulted from the 1-pt standard Proctor test (11.7%), as described in Chapter 4.

7.4 Summary and conclusions

In this chapter, potential relationships between the CCC data and the in-situ testing methods were examined using univariate regression analysis. Linear and second-degree polynomial models were employed in the univariate regression analyses.

At the beginning of this chapter, the relationship between individual CCC data points and a variety of in-situ test measurements was explored. Examination of the entire data set for regression analysis indicated that there were not any strong correlations between these measured values. As a result, regression analyses of average values from each lift and pass were performed. Overall, regression analysis results from this chapter showed that:

- In some cases, the use of second-order polynomial regression models significantly improved the quality of the model fit, as compared with the relationships developed from the linear regression analyses that were performed.
- Point-by-point comparisons between kriged CCC data and individual in-situ test results yield poor-quality correlations.
- Comparisons between *average* kriged CCC data points and *average* in-situ test results for each lift and pass yield relatively high-quality univariate regression correlations.
- Exclusion of the base layer average values from the associated regression analyses yields improved R-squared values, and reveals that there is a relatively strong relationship between CCC data and some of the in-situ testing measurements.
- In general, MDP values tend to correlate more strongly with in-situ test results than the CMV values do. This observation is likely linked to the fact that the influence depth of MDP is closer to the influence depths of the various in-situ testing methods that were utilized in this study. This is in contrast with the deeper influence depths that are commonly cited for CMV data.
- Average NDG measured dry unit weight and DCP indices showed the strongest correlation with average CCC values, as compared to those values measured in the other in-situ tests.

- LWD 200 test results showed better correlation with the measured CCC data than the LWD 300 test results did.
- Of the in-situ testing methods that were utilized, the Geogauge tended to show the poorest correlation with the recorded CCC data
- The water content had a significant influence on roller and in-situ testing measurements.
- The optimum water content for the recorded average CCC values was ~8.0%, as back-calculated from univariate regression analyses.
- In addition, it was realized that the resulted LWD moduli for this value of water content were greater than the average LWD's measured moduli.

In the next chapter (Chapter 8), the effect of water content on the mechanical and physical properties of the compacted soil will be discussed, using the results from a series of multivariate regression analyses.

Chapter 8

MULTIPLE REGRESSION ANALYSIS

8.1 Introduction

In Chapter 7, univariate regression analysis was applied to the measured field data and in some cases, significant relationships were observed between the CCC and in-situ testing data sets. In order for these strong correlations to be identified, it was necessary to perform univariate regression analysis of the *average* values that were recorded for each lift and pass, for each data set. In addition, it was realized that the corresponding average measured values of the base layer produced an outlier in most of the regression analyses. This observation is consistent with the fact that the base layer was not an engineered lift, which means that it had significantly more variability in potential soil characteristics (as the soil was not mixed, spread, and compacted like the other lifts). Additionally, its measured water contents were lower than the other lifts that were placed. The effect of water content on the measured mechanical properties of the compacted soil was also evaluated and the analyses showed a significant influence of water content on both the measurements from the CCC roller and the in-situ tests that were performed. As a result of the water content based regression analyses that were performed in Chapter 7, it seems reasonable to include the effect of water content in regression analysis to discover the relationship between the CCC values, the measured water contents, and the associated in-situ testing measurements. This approach has been recommended by other researchers doing work in this area (e.g. White and Thompson 2008; White et al. 2005).

The objective of the current chapter is to use multiple regression analysis techniques to develop correlations between the CCC roller data and in-situ testing measurements, which include the associated water content as one of the independent variables.

8.2 Multiple Regression Analysis

As mentioned in 7.1, multiple regression techniques use more than one independent variable in the regression analysis. Multiple regression analyses using a linear additive model are considered here, as described in Rawlings et al. (1998).

Equation 8.1 illustrates the general form of a linear additive model that can be used to relate a dependent variable to p independent variables.

$$Y_i = \beta_0 + \beta_1 X_{i1} + \beta_2 X_{i2} + \cdots + \beta_p X_{ip} + \varepsilon_i \tag{8.1}$$

where, β_0 is the intercept, and the β_i's are the rate of change in Y_i (the dependent variables) per unit change in X_i's (the independent variables). The ε_i's are the random errors associated with each independent variable.

Equation 8.1 can be extended into a matrix form, as follows:

$$\begin{bmatrix} Y_1 \\ Y_2 \\ \vdots \\ Y_n \end{bmatrix}_{n\times 1} = \begin{bmatrix} 1 & X_{11} & \cdots & X_{1p} \\ 1 & X_{21} & \cdots & X_{2p} \\ \vdots & \vdots & \ddots & \vdots \\ 1 & X_{n1} & \cdots & X_{np} \end{bmatrix}_{n\times p} \begin{bmatrix} \beta_0 \\ \beta_1 \\ \vdots \\ \beta_p \end{bmatrix}_{p\times 1} + \begin{bmatrix} \varepsilon_0 \\ \varepsilon_1 \\ \vdots \\ \varepsilon_p \end{bmatrix}_{n\times 1} \tag{8.2}$$

or, more briefly, as:

$$\mathbf{Y} = \mathbf{X}\boldsymbol{\beta} + \boldsymbol{\varepsilon} \tag{8.3}$$

The predicted values for the dependent variable are obtained by solving Equation 8.3. It should be noted that the X_i's themselves can be a function of other variables.

The quality of the resulting model fit can be evaluated using R-squared values as described in Chapter 6. There are some other criteria for evaluation of the regression results which were followed in this study, as will be explained in the following sections.

8.3 Multiple Regression Analysis of CCC Data Sets

8.3.1 Regression models employed

To include the effect of water content in the regression analysis, two types of regression models were utilized. In the first model, a combination of roller-recorded values (*RRV*) and water contents (ω(%)) were used as the independent variables to predict the value of each in-situ testing measurement (*ITM*), the dependent variable. The general form of the equation that was used is shown in Equation 8.4.

$$ITM_i = A + B(RRV_i)^b + C(\omega_i)^c \tag{8.4}$$

where, A is the intercept at the origin, B and C are the multiple regression coefficients for each term, and b and c are the exponents of the independent variables.

In the second model, a term consisted of the product of *RRV* and ω was added to the previous model, as shown in Equation 8.5.

$$ITM_i = A + B(RRV_i)^b + C(\omega_i)^c + D(RRVi.\omega_i)^d \tag{8.5}$$

where, B, C, and D are the coefficients and b, c, and d are the exponents of the independent variables.

Measured modulus values from the GeoGauge, LWD 300, and LWD 200, as well as the DCP_M index, the DCP_A index, and the NDG dry unit weights were used separately as the dependent variables. The individual MDP and CMV values predicted by the kriging method were utilized as the roller-recorded independent variables. The laboratory measured water contents (not the NDG measured water contents) were used as the other independent variable in the multiple regression models shown above.

As laboratory water contents were not available for all of the test locations for which data was recorded, there are some differences in the overall data sets for the regression analyses presented in this chapter, as compared with the data sets that were used for the univariate regression analyses performed in Chapter 7.

To perform the multiple regression analyses, a computer program was developed using MATLAB™. The code consisted of two loops for the first model and three loops for the second model. In each loop, an iterative process was performed for the corresponding exponent (b, c, or d), assigning consecutive values of 0.1 to 4.0 with a step interval of 0.1, in an attempt to obtain the highest quality model fit results, as determined by the resulting R-squared values.

Some criteria were used in evaluating the fitted models. The first criterion was the R-squared value, which was calculated according to Equation 6.10. In the analyses that were performed, an R-squared value greater than 0.70 was assumed to be an acceptable value.

The second criterion for model evaluation was minimization of the overall variance of errors between the predicted and actual values (Draper and Smith 1998) (Equations 8.6 and 8.7).

$$AD_i = P_i - A_i \qquad (8.6)$$

where, AD_i = Absolute difference for each pair of predicted and actual values, P_i = Predicted value, A_i = Actual value

$$\sigma^2{}_{AD} = \frac{(AD_i - \mu(AD_i))^2}{n - n'} \qquad (8.7)$$

where, $\sigma^2{}_{AD}$ = Error variance, $\mu\ (AD_i)$ = Mean of absolute differences, n = Number of predicted values or number of *RRV* data, n' = Number of missing data. More information on n and n' is provided in the following section (8.3.2). With respect to model selection criterion, a low magnitude of error variance indicates a higher quality of model fit.

Another criterion that was used to make a decision on the quality of the model fit was the p-values that were generated as a result of the model analysis. In statistics, the p-value (or significance probability) refers to the probability that an effect at least as extreme as the current observation has occurred by chance (Schervish 1996). P-values of less than 0.05 are universally accepted as an acceptance limit for different types of regression models (Schervish 1996). In some cases, a p-value less than 0.01 is also used as the acceptance limit (Schervish 1996); however, it is felt that this criteria is too restrictive for analysis of the current data set.

8.3.2 Multiple regression analysis of individual in-situ test values

As a first attempt at multiple regression, analyses of each of the entire data sets were performed, comparing each of the in-situ test values of interest vs. each of the CCC recorded values and the corresponding water content. The results of these analyses are presented in Figure 8.1 and Figure 8.2. $R^2{}_1$ and $R^2{}_2$ are the resulting R-squared values for the first model (Equation 8.4 – solid line) and the second model

(Equation 8.5 – dashed line), respectively. The number of independent variables in each set is denoted by *n*. In some locations, the in-situ testing measured values were not available at the locations where laboratory measured water contents were measured (e.g. NDG γ_d and LWD 200 E). The number of points excluded from the analysis because of missing in-situ testing values is shown by *n´* in the following figures. As noted earlier in Chapters 5 and 7, values of CMV for Pass 1 of Lift 5 were eliminated from these analyses, due to the differing amplitude of vibratory compaction that was applied for this pass. This omission is consistent with the univariate regression analyses that were performed in Chapter 7.

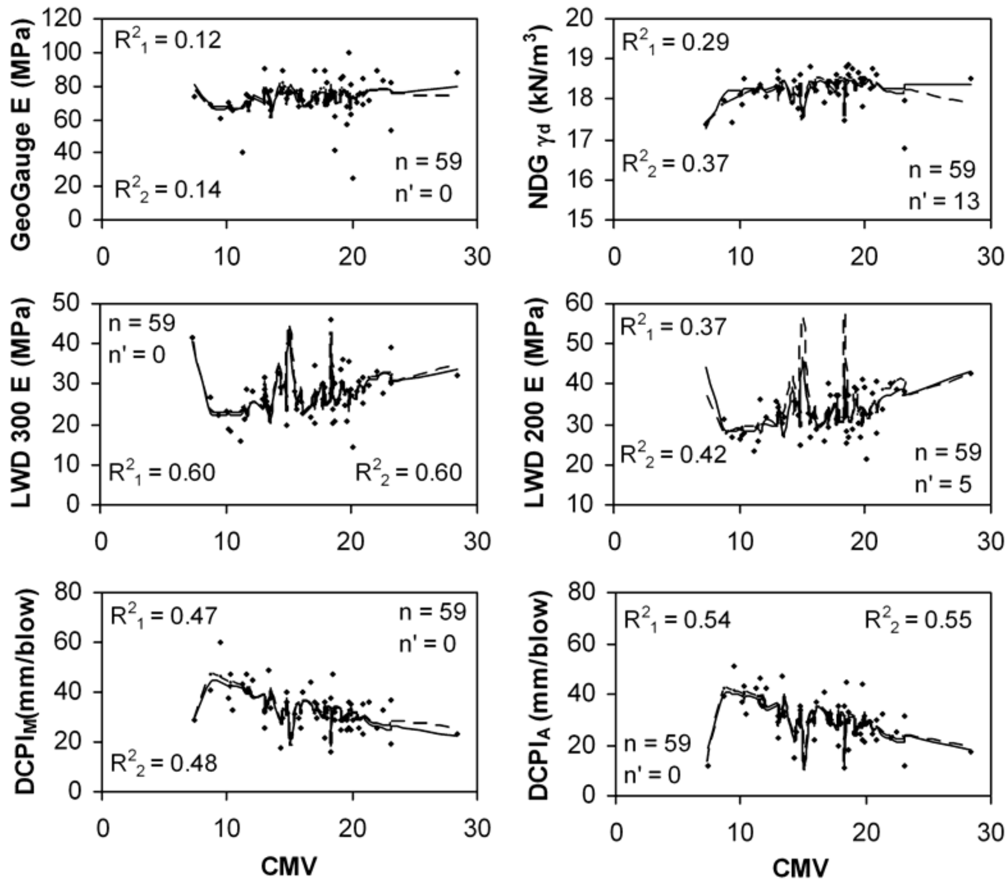

Figure 8.1 Multiple regression analysis of in-situ testing measurements vs. kriged CMV data points, using the entire data set

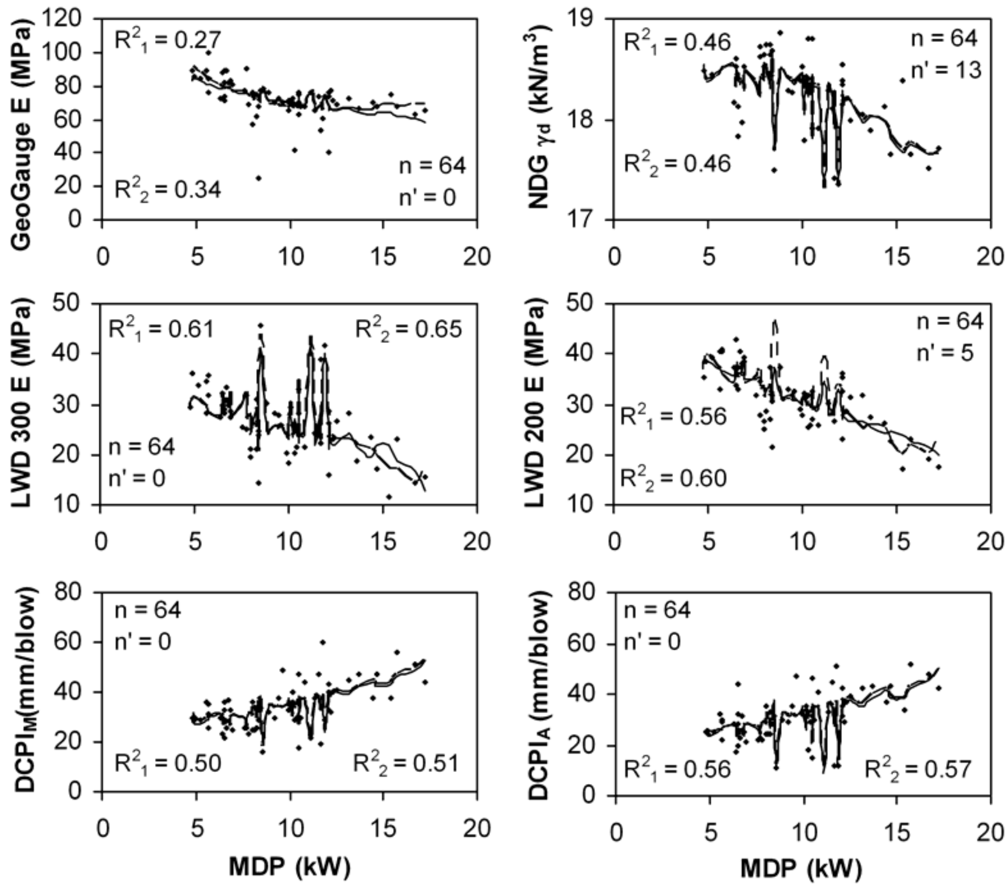

Figure 8.2 Multiple regression analysis of in-situ testing measurements vs. kriged MDP data points, using the entire data set

As shown in Figures 8.1 and 8.2, there is a significant improvement in the resulting R-squared values over the univariate regression analysis results presented in Chapter 7. However, similar to what was concluded for the entire data set univariate regression analyses, the resulting R-squared values are still quite low, which indicates that there is not a strong correlation between the measured data sets.

As univariate regression analyses in Chapter 7 indicated that the base layer data points were significant outliers, it was desirable to repeat the point-by-point multivariate regression analyses while excluding these values from the data set. Figures 8.3 and 8.4 show the results of these multivariate regression analyses.

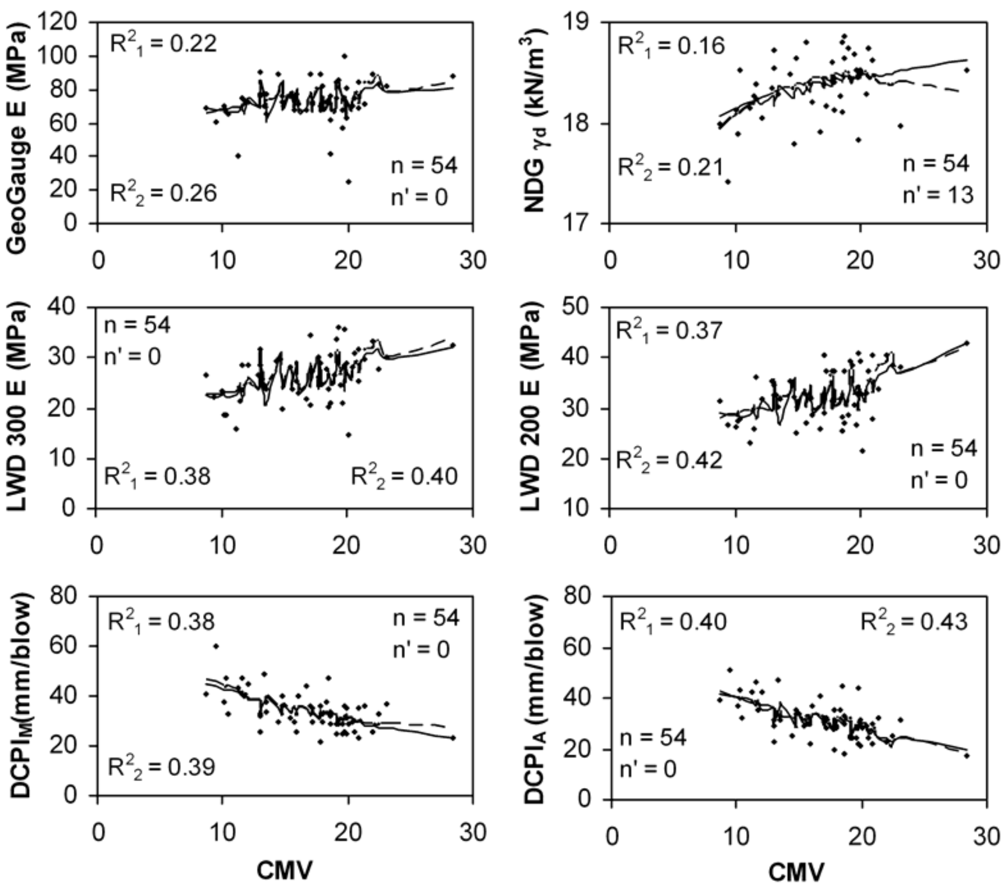

Figure 8.3 Multiple regression analysis of in-situ testing measurements vs. kriged CMV data points, using the entire data set and excluding the base layer

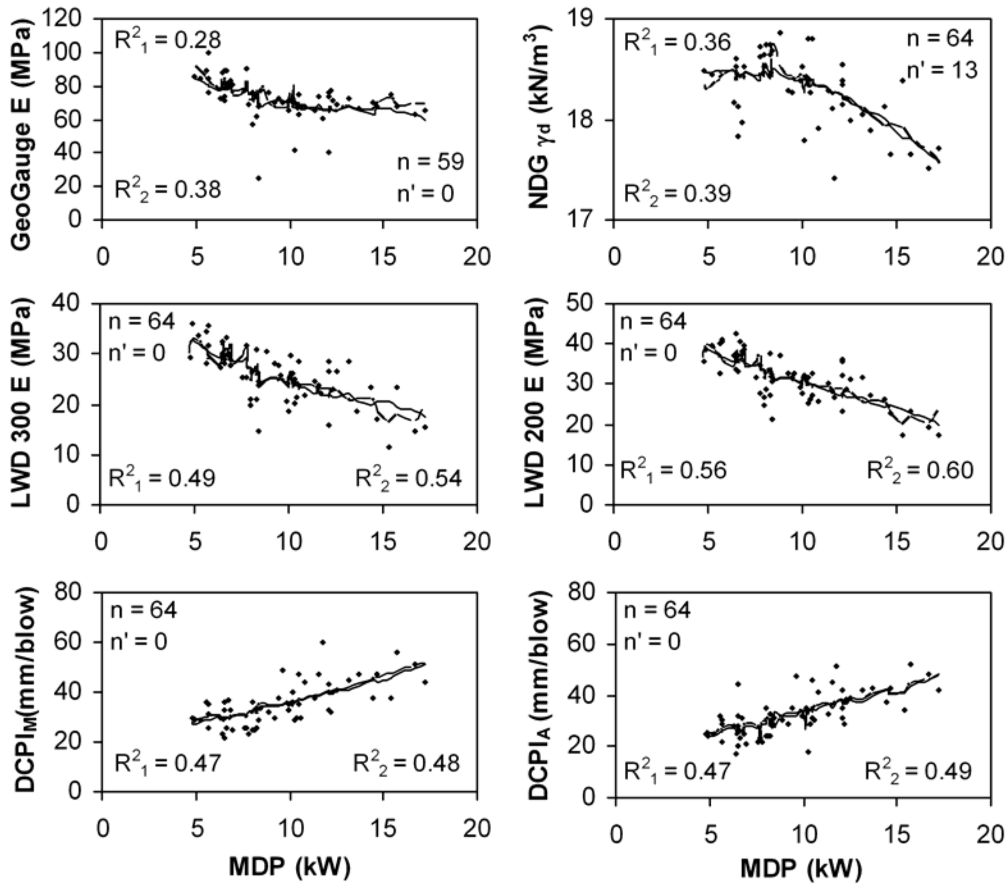

Figure 8.4 Multiple regression analysis of in-situ testing measurements vs. kriged MDP data points, using the entire data set and excluding the base layer

For comparative purposes, similar multivariate regression analyses were performed looking only at the final passes for each of the compacted lifts. Figures 8.5 and 8.6 show the results of these multivariate regression analyses.

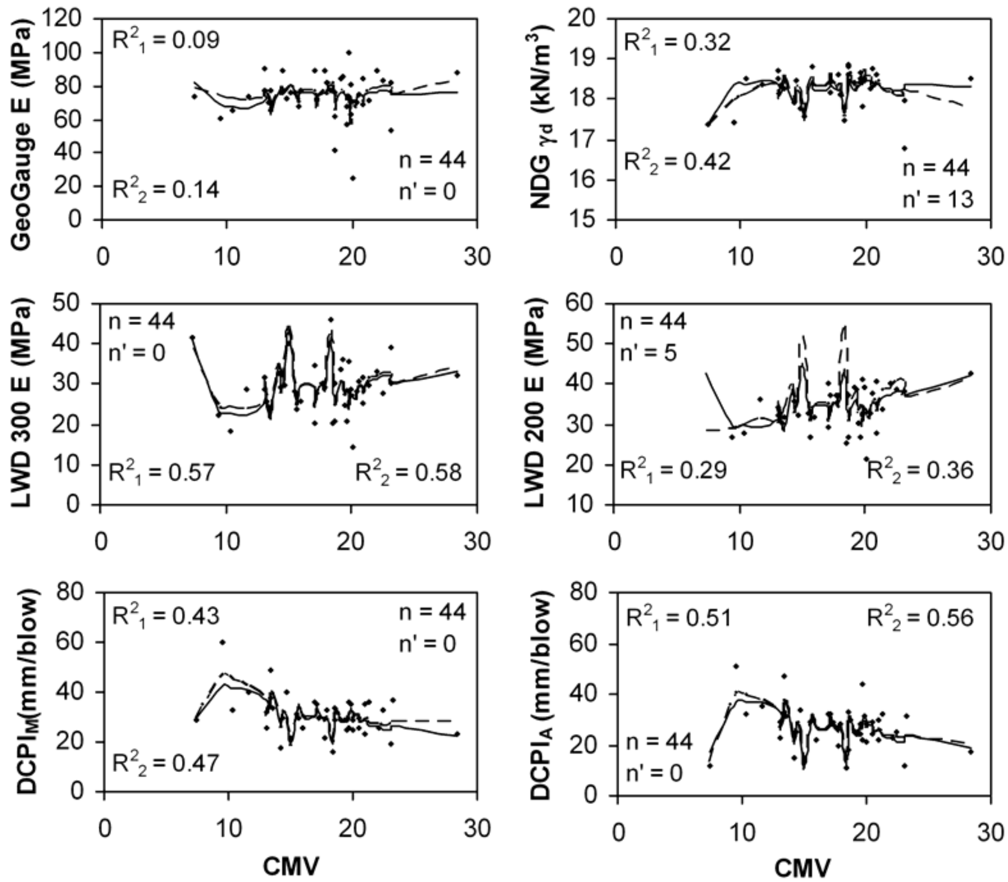

Figure 8.5 Multiple regression analysis of in-situ testing measurements vs. kriged CMV data points, using only the data for the final passes of each lift

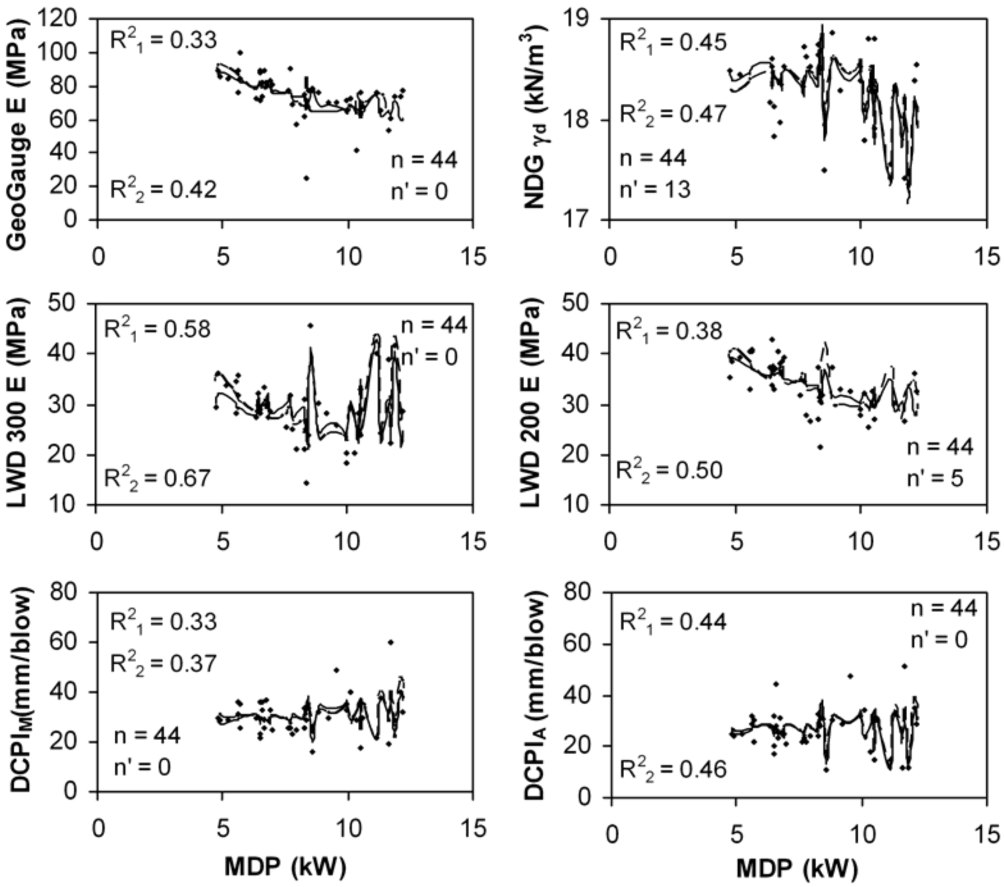

Figure 8.6 Multiple regression analysis of in-situ testing measurements vs. kriged MDP data points, using only the data for the final passes of each lift

To examine the sensitivity of the measured results to the outlying base layer data points, the same regression analyses on the final passes of each lift were repeated while disregarding the base layer points. The results from these analyses are presented in Figures 8.7 and 8.8.

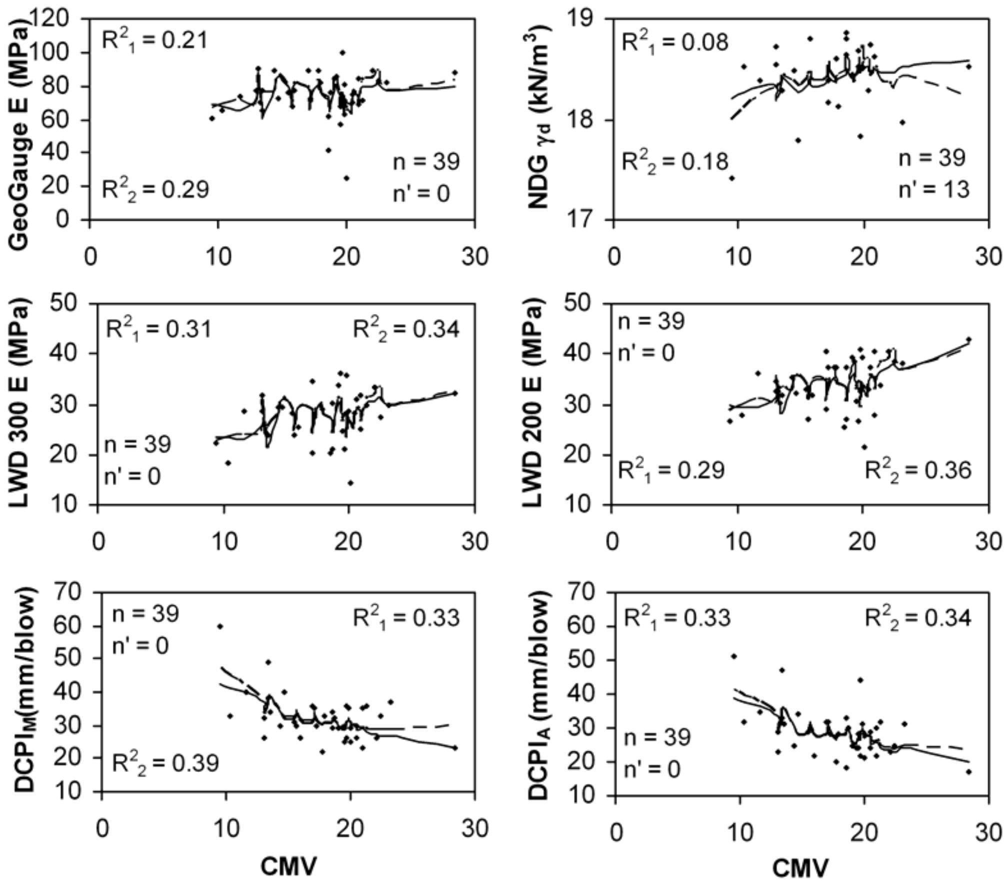

Figure 8.7 Multiple regression analysis of in-situ testing measurements vs. kriged CMV data points, using only the data for the final passes of each lift (with the base layer points excluded)

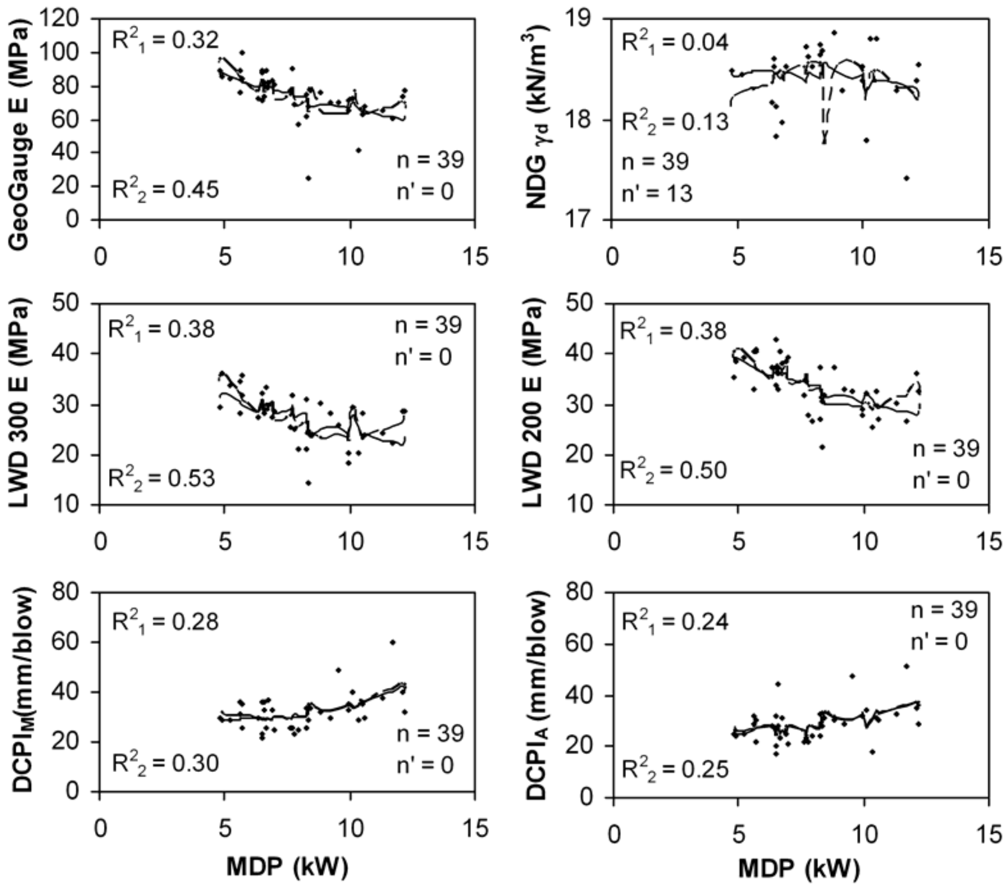

Figure 8.8 Multiple regression analysis of in-situ testing measurements vs. kriged MDP data points, using only the data for the final passes of each lift (with the base layer points excluded)

For comparative purposes, multivariate regression analyses were also performed looking at all of the data points that were recorded for each of the passes for Lift 5. Figures 8.9 and 8.10 show the results of these multivariate regression analyses.

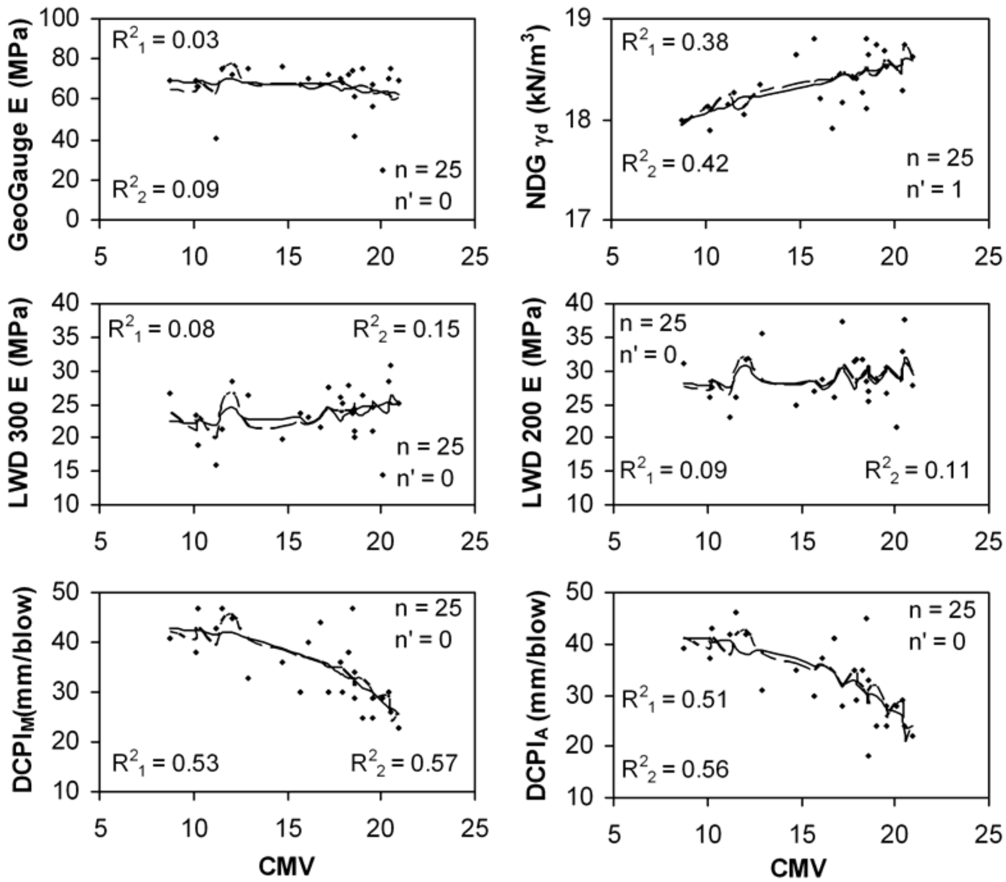

Figure 8.9 Multiple regression analysis of in-situ testing measurements vs. kriged CMV data points, using only the data for Lift 5

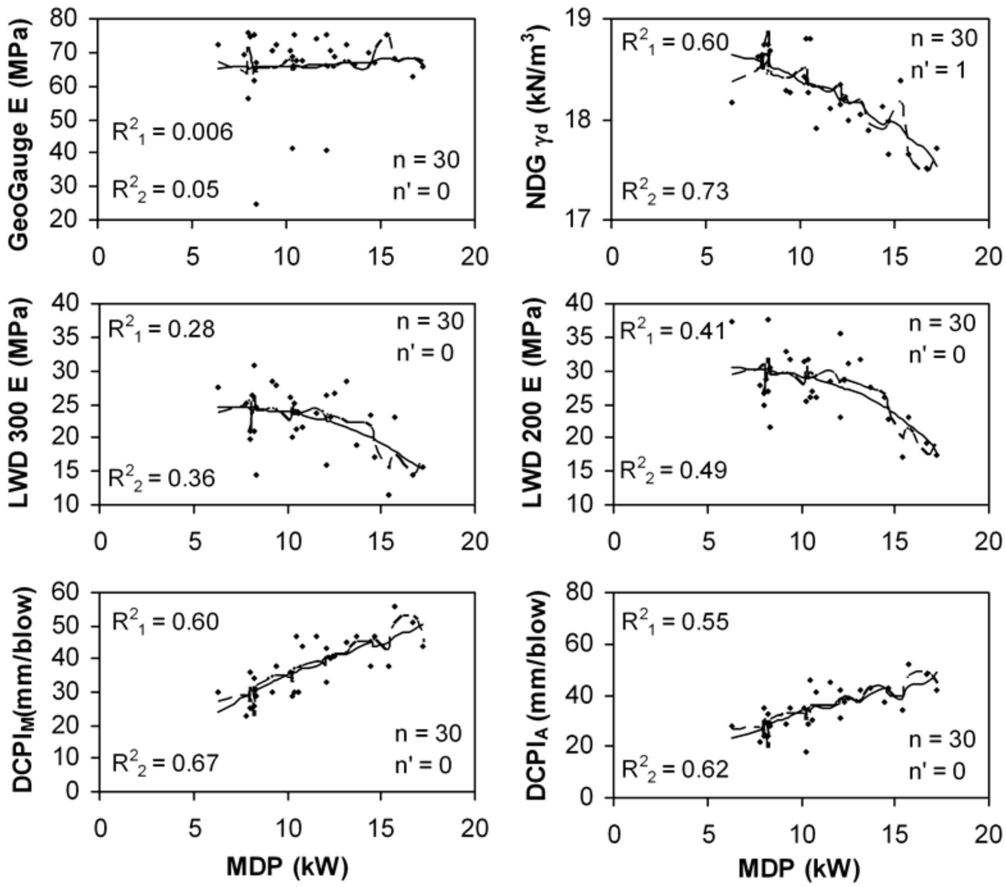

Figure 8.10 Multiple regression analysis of in-situ testing measurements vs. kriged MDP data points, using only the data for Lift 5

As shown in Figures 8.1 through 8.10, numerous multiple regression analyses have been performed, looking at the relationships been the measured in-situ test results (dependent variable) and the kriged CCC data points and corresponding laboratory-measured water contents (independent variables). To compare the results from these analyses, the resulting R-squared values from Figures 8.1 to 8.10 are presented in Table 8.1. Models that have a p-value for model fit greater than 0.05 are specified by an asterisk (*), and the models that have a p-value between 0.01 and 0.05

are marked with a cross (†). As the resulting models did not have high R-squared values, their error variances are not presented here.

Table 8.1 R-squared values from the multivariate regression analyses that were performed on individual data points

In-sit testing	All		All excluding base layer		Finals		Finals excluding base layer		Lift 5	
	R^2_1	R^2_2	R^2_1	R^2_2	R^2_1	R^2_2	R^2_1	R^2_2	R^2_1	R^2_2
Geogauge E (MPa) vs. CMV	0.12†	0.14†	0.22	0.26	0.09*	0.14*	0.21†	0.29	0.03*	0.09*
Geogauge E (MPa) vs. MDP (kW)	0.27	0.34	0.28	0.38	0.33	0.42	0.32	0.45	0.01*	0.05*
NDG γ_d (kN/m^3) vs. CMV	0.29	0.37	0.16†	0.21†	0.32	0.42	0.08*	0.18*	0.38	0.42†
NDG γ_d (kN/m^3) vs. MDP (kW)	0.46	0.46	0.36	0.39	0.45	0.47	0.04*	0.13*	0.60	**0.73**
LWD 300 E (MPa) vs. CMV	0.60	0.60	0.38	0.40	0.57	0.58	0.31	0.34	0.08*	0.15*
LWD 300 E (MPa) vs. MDP (kW)	0.61	0.65	0.49	0.54	0.58	0.67	0.38	0.53	0.28†	0.36
LWD 200 E (MPa) vs. CMV	0.37	0.42	0.37	0.42	0.29	0.36	0.29	0.36	0.09*	0.11*
LWD 200 E (MPa) vs. MDP (kW)	0.56	0.6	0.56	0.60	0.38	0.5	0.38	0.5	0.41	0.49
DCPI$_M$ (mm/blow) vs. CMV	0.47	0.48	0.38	0.39	0.43	0.47	0.33	0.39	0.53	0.57
DCPI$_M$ (mm/blow) vs. MDP (kW)	0.5	0.51	0.47	0.48	0.33	0.37	0.28	0.3	0.6	0.67
DCPI$_A$ (mm/blow) vs. CMV	0.54	0.55	0.4	0.43	0.51	0.56	0.33	0.34	0.51	0.56
DCPI$_A$ (mm/blow) vs. MDP (kW)	0.56	0.57	0.47	0.49	0.44	0.46	0.24	0.25†	0.55	0.62

*: Models that have a p-value greater than 0.05
†: Models that have a p-value between 0.01 and 0.05

As shown in Table 8.1, the strongest measured relationship that could be determined by regression analysis of individual values had an R^2 value of 0.73. This result corresponded to the multivariate relationship between the NDG dry unit weight and the kriged values for MDP (including the effect of the measured water content).

The resulting mathematical form of the regression equation is presented in Equation 8.8.

$$\gamma_d = -130.03 + 219.44\,(MDP)^{0.1} + 0.14\,(\omega)^2 - 56.58\,(MDP.\omega)^{0.2} \tag{8.8}$$

where, the error variance was 0.042 and the p-value was less than 0.01.

In addition, the following conclusions were drawn from the regression results presented in Table 8.1:

- In general, there is not a significant relationship between individual kriged CCC values and their corresponding in-situ test results for any of the data sets that were examined (the corresponding R^2 values were all less than 0.8). This observation is consistent with observations made when performing the univariate regression analyses discussed in the previous chapter.
- In general, kriged MDP data points showed better correlation with in-situ measured values than did kriged CMV data points.
- Adding additional terms to the form of the multivariate regression model (e.g. the second model as compared to the first model) improved the resulting R-squared values, which seems reasonable.
- Of all of the in-situ tests that were used, the GeoGauge showed the weakest relationship with the measured CCC data.
- Excluding the base layer from the analysis of either the entire data set or the final pass data set tended to lower the R-squared values. This trend supports the hypothesis that water content plays a significant role in the correlation between the CCC data and the in-situ testing values. Additionally, it supports the conclusion that

the reason that the base layer points were such significant outliers in the univariate regression analyses had to do with the significantly lower water contents that were present in this layer at the time of testing.

8.3.3 Analysis of averages of data

As a result of the observations that made during univariate analyses in Chapter 7, comparisons between the average in-situ test results and the average kriged CCC values for each lift and pass were considered in the multiple regression analysis. The same general steps as what were performed in section 8.3.2 are followed in this section. Figures 8.11 and 8.12 present the results of multiple regression analysis performed using the entire data set of averaged values.

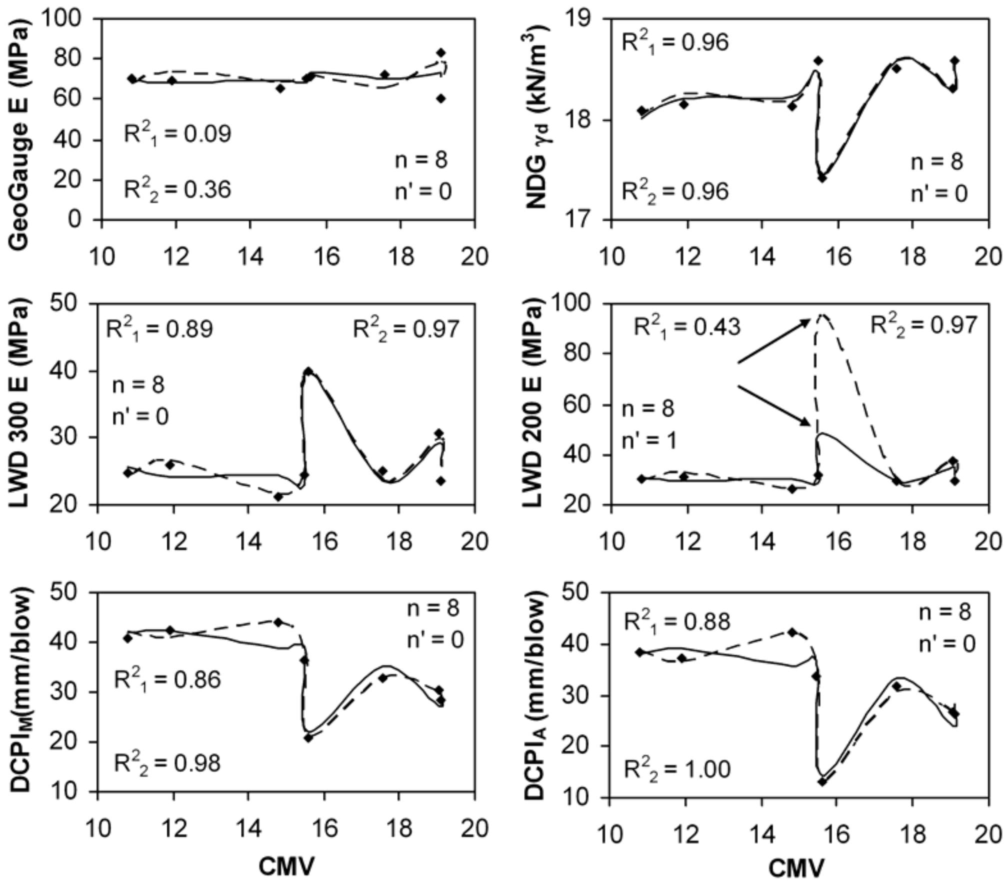

Figure 8.11 Multiple regression analysis using pass-by-pass average in-situ testing measurements vs. average kriged CMV data points, using the entire data set

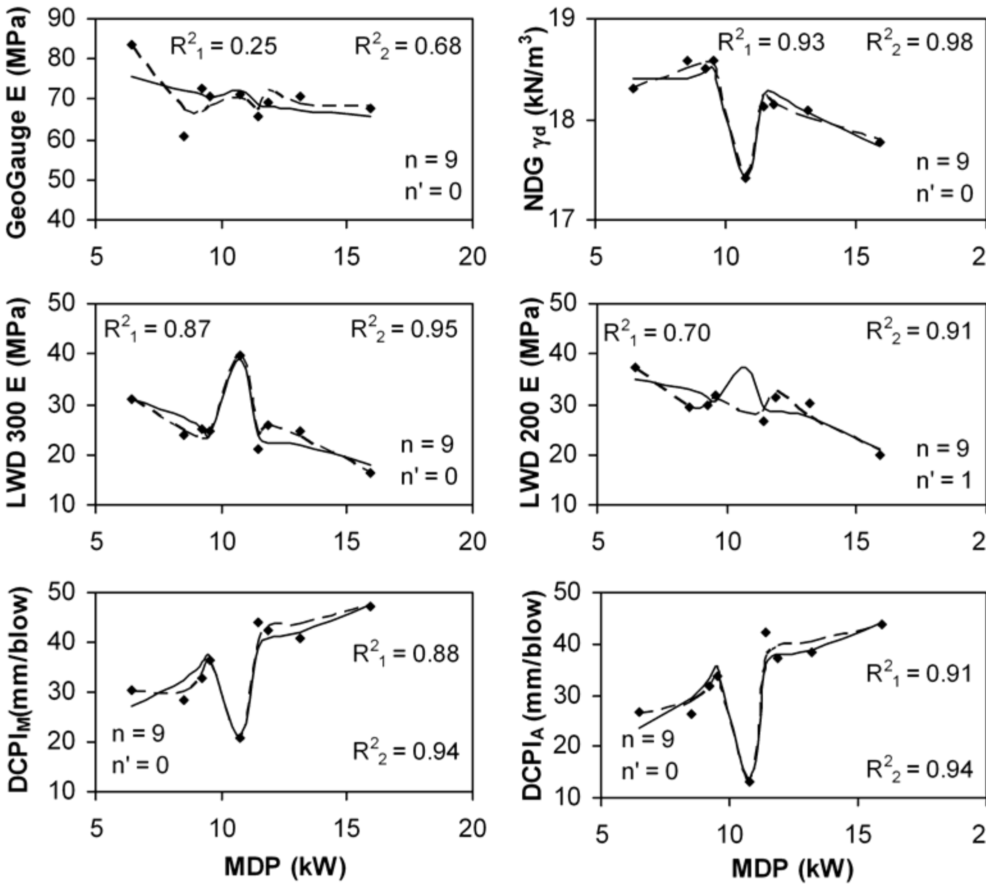

Figure 8.12 Multiple regression analysis using pass-by-pass average in-situ testing measurements vs. average kriged MDP data points, using the entire data set

As shown by a pair of arrows in Figure 8.11, it is clear that the second model significantly mispredicted the missing values for the LWD 200 results. Compared to the corresponding plot for LWD 300 and the corresponding actual and predicted values at the same point, it seems that the first model yielded better predictions of the corresponding missing value of LWD 200 modulus.

Tables 8.2 and 8.3 present the regression coefficients that resulted from the multivariate regression analysis of the CMV and MDP data sets. The coefficients shown correspond to those shown in Equations 8.4 and 8.5. For consistency, results are shown for all of the in-situ testing techniques that were analyzed, even those that exhibited less-than-desirable model fit results. It should be noted that in all of the following tables in this chapter, the corresponding values of MDP are shown in gray cells, the regression coefficients are rounded to the nearest 0.0001, and the R-squared values and error variance are rounded to the nearest 0.01.

Table 8.2 Components of the first fitted model for all averages

In-situ testing	b	c	A	B	C	R^2_1	σ^2_{AD}
Geogauge E (MPa) vs. CMV	4.0	3.8	73.47	9.30E-06	-5.96E-04	0.09*	54.09
Geogauge E (MPa) vs. MDP (kW)	0.1	1.5	175.83	-80.4480	-0.13	0.25*	37.99
NDG γ_d (kN/m^3) vs. CMV	4.0	3.4	16.91	6.92E-06	3.46E-04	**0.96**	0.01
NDG γ_d (kN/m^3) vs. MDP (kW)	1.3	0.1	4.54	-0.04	11.57	**0.93**	0.01
LWD 300 E (MPa) vs. CMV	0.1	0.1	313.57	-27.20	-200.57	**0.89**	5.29
LWD 300 E (MPa) vs. MDP (kW)	4.0	0.1	263.54	-1.29E-04	-187.99	**0.87**	7.57
LWD 200 E (MPa) vs. CMV	4.0	0.1	332.22	-2.08E-05	-237.94	0.43*	9.27
LWD 200 E (MPa) vs. MDP (kW)	4.0	0.1	145.17	-1.82E-04	-88.96	**0.70**†	10.12
$DCPI_M$ (mm/blow) vs. CMV	3.0	0.1	-212.84	-1.58E-03	203.03	**0.86**	12.09
$DCPI_M$ (mm/blow) vs. MDP (kW)	2.3	0.1	-235.86	0.03	210.95	**0.88**	11.51
$DCPI_A$ (mm/blow) vs. CMV	3.6	0.1	-301.88	-1.83E-04	269.53	**0.88**	13.97
$DCPI_A$ (mm/blow) vs. MDP (kW)	2.8	0.1	-314.05	6.30E-03	272.33	**0.91**	10.81

*: Models that have a p-value greater than 0.05
†: Models that have a p-value between 0.01 and 0.05

Table 8.3 Components of the second fitted model for all averages

In-situ testing	b	c	d	A	B	C	D	R^2_2	σ^2_{AD}
Geogauge E (MPa) vs. CMV	2.0	4.0	2.8	15.41	0.25	3.35E-03	-3.11E-05	0.36*	47.30
Geogauge E (MPa) vs. MDP (kW)	0.9	0.1	1.0	2317.29	-36.77	-1758.57	2.54	0.68	19.66
NDG γ_d (kN/m^3) vs. CMV	4.0	3.6	0.2	19.73	1.07E-05	3.02E-04	-1.26	**0.96**	0.01
NDG γ_d (kN/m^3) vs. MDP (kW)	0.7	0.2	0.6	-37.82	2.87	38.34	-1.19	**0.98**	0.01
LWD 300 E (MPa) vs. CMV	1.7	4.0	0.9	36.79	0.65	3.31E-03	-1.27	**0.97**	1.92
LWD 300 E (MPa) vs. MDP (kW)	1.9	0.1	1.4	1094.58	-0.70	-866.41	0.12	**0.95**	3.47
LWD 200 E (MPa) vs. CMV	0.5	3.1	0.1	1955.10	135.85	0.07	-1544.45	**0.97**	0.63
LWD 200 E (MPa) vs. MDP (kW)	2.3	0.1	2.2	674.72	-0.23	-511.05	1.68E-03	**0.91**†	3.97
$DCPI_M$ (mm/blow) vs. CMV	1.0	1.3	0.1	-2330.50	-22.78	-14.02	1816.65	**0.98**	1.83
$DCPI_M$ (mm/blow) vs. MDP (kW)	0.2	0.1	0.2	6526.91	-2128.69	-5242.98	1386.02	**0.94**	6.80
$DCPI_A$ (mm/blow) vs. CMV	2.0	3.6	0.1	-1201.67	-0.39	-0.01	843.41	**1.00**	0.53
$DCPI_A$ (mm/blow) vs. MDP (kW)	0.1	0.1	0.1	9236.52	-7538.97	-7469.32	6114.06	**0.94**	9.02

*: Models that have a p-value greater than 0.05
†: Models that have a p-value between 0.01 and 0.05

From analysis of the data shown in Figures 8.11 and 8.12 and in Tables 8.2 and 8.3, it can be concluded that adding an extra term to the multiple regression model increased the R-squared values and decreased the error variance significantly. For the average values from the in-situ and CCC data sets (with the exception of the GeoGauge), there are strong correlations between all average in-situ testing measurements and average CCC values.

Figures 8.13 and 8.14 present the results of regression analysis on all averages excluding the base layer.

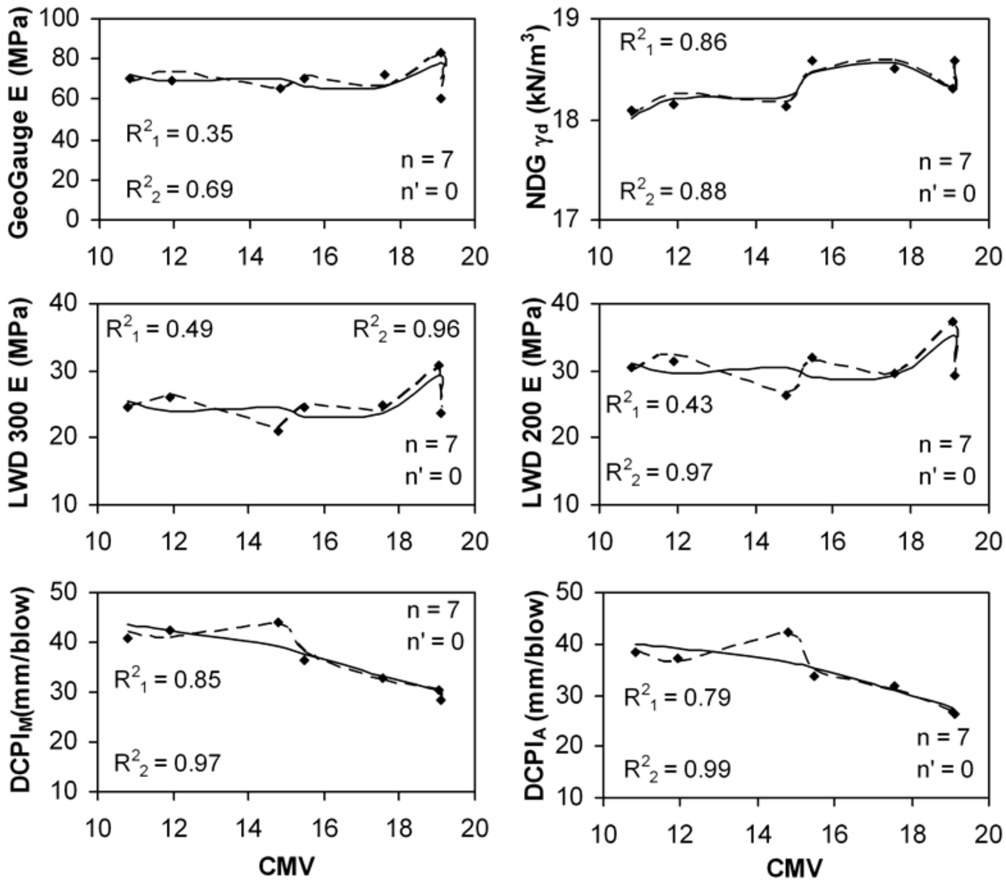

Figure 8.13 Multiple regression analysis using pass-by-pass average in-situ testing measurements vs. average kriged CMV data points, using the entire data set and excluding the base layer

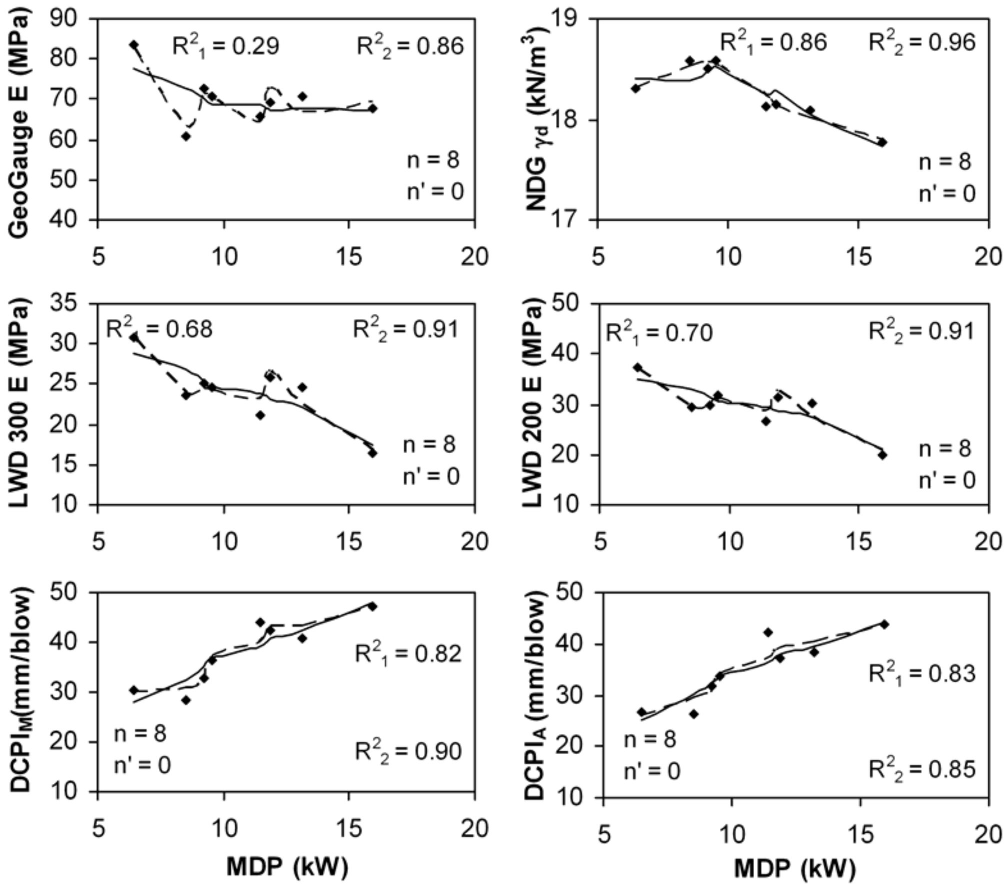

Figure 8.14 Multiple regression analysis using pass-by-pass average in-situ testing measurements vs. average kriged MDP data points, using the entire data set and excluding the base layer

Tables 8.4 and 8.5 present the regression coefficients that resulted from the multivariate regression analysis of the entire CMV and MDP data sets, with the base layer data points excluded.

Table 8.4 Components of the first fitted model for all averages excluding the base layer

In-situ testing	b	c	A	B	C	R^2_1	σ^2_{AD}
Geogauge E (MPa) vs. CMV	4.0	0.1	725.17	-7.06E-05	-515.62	0.35*	48.39
Geogauge E (MPa) vs. MDP (kW)	0.1	0.1	371.83	-49.38	-189.90	0.29*	43.06
NDG γ_d (kN/m^3) vs. CMV	4.0	4.0	17.06	6.77E-06	7.21E-05	**0.86**†	0.01
NDG γ_d (kN/m^3) vs. MDP (kW)	0.9	0.1	1.94	-0.15	13.98	**0.86**	0.02
LWD 300 E (MPa) vs. CMV	0.1	0.1	319.66	-28.19	-204.38	0.49*	6.61
LWD 300 E (MPa) vs. MDP (kW)	4.0	0.1	148.85	-1.42E-04	-96.88	0.68†	7.54
LWD 200 E (MPa) vs. CMV	4.0	0.1	332.22	-2.08E-05	-237.94	0.43*	9.27
LWD 200 E (MPa) vs. MDP (kW)	4.0	0.1	145.17	-1.82E-04	-88.96	**0.70**†	10.12
$DCPI_M$ (mm/blow) vs. CMV	4.0	4.0	48.29	-1.27E-04	-2.47E-04	**0.85**†	8.61
$DCPI_M$ (mm/blow) vs. MDP (kW)	1.4	4.0	19.10	0.50	4.16E-04	**0.82**†	11.86
$DCPI_A$ (mm/blow) vs. CMV	4.0	4.0	42.17	-1.09E-04	-5.87E-05	**0.79**†	11.40
$DCPI_A$ (mm/blow) vs. MDP (kW)	0.8	4.0	7.20	3.69	2.94E-04	**0.83**†	10.33

*: Models that have a p-value greater than 0.05
†: Models that have a p-value between 0.01 and 0.05

Table 8.5 Components of the second fitted model for all averages excluding the base layer

In-situ testing	b	c	d	A	B	C	D	R^2_2	σ^2_{AD}
Geogauge E (MPa) vs. CMV	0.2	2.7	0.1	2429.94	1510.37	0.40	-3129.83	0.69*	30.26
Geogauge E (MPa) vs. MDP (kW)	0.2	1.5	0.3	5995.25	-7989.61	-47.12	2064.13	**0.86†**	10.79
NDG γ_d (kN/m^3) vs. CMV	1.5	2.4	0.1	54.43	0.07	0.01	-26.58	**0.88***	0.01
NDG γ_d (kN/m^3) vs. MDP (kW)	0.1	0.2	0.1	-443.25	742.02	298.26	-596.36	**0.96**	0.01
LWD 300 E (MPa) vs. CMV	0.4	1.9	0.1	2370.14	296.58	2.47	-2073.82	**0.96†**	0.71
LWD 300 E (MPa) vs. MDP (kW)	1.0	3.3	1.0	121.31	-33.85	-0.04	3.20	**0.91†**	2.68
LWD 200 E (MPa) vs. CMV	0.5	3.1	0.1	1955.10	135.85	0.07	-1544.45	**0.97**	0.63
LWD 200 E (MPa) vs. MDP (kW)	2.3	0.1	2.2	674.72	-0.23	-511.05	1.68E-03	**0.91†**	3.97
$DCPI_M$ (mm/blow) vs. CMV	0.9	1.0	0.1	-2472.44	-36.42	-39.42	2017.19	**0.97**	2.32
$DCPI_M$ (mm/blow) vs. MDP (kW)	0.1	2.7	0.2	-4271.39	6082.48	0.50	-1434.16	**0.90†**	8.33
$DCPI_A$ (mm/blow) vs. CMV	2.2	4.0	0.1	-1063.87	-0.19	-0.0048	744.25	**0.99**	0.70
$DCPI_A$ (mm/blow) vs. MDP (kW)	0.1	2.3	0.2	-3391.09	4775.79	1.16	-1122.13	**0.85†**	11.04

*: Models that have a p-value greater than 0.05
†: Models that have a p-value between 0.01 and 0.05

In general, the same findings were achieved for analysis of this data set as were achieved from the data analysis on the entire set of data. The one notable difference is that the GeoGauge correlations do improve somewhat with exclusion of this data point. However the error variance is still relatively high and the corresponding p-value is between 0.01 and 0.05, which means that these results are still less than desirable.

For comparative purposes, and to be consistent with the data sets that were examined and the analyses that were performed earlier in this chapter, similar multivariate regression analyses were performed looking only at the final passes for each of the compacted lifts. Figures 8.15 and 8.16 show the results of these multivariate regression analyses.

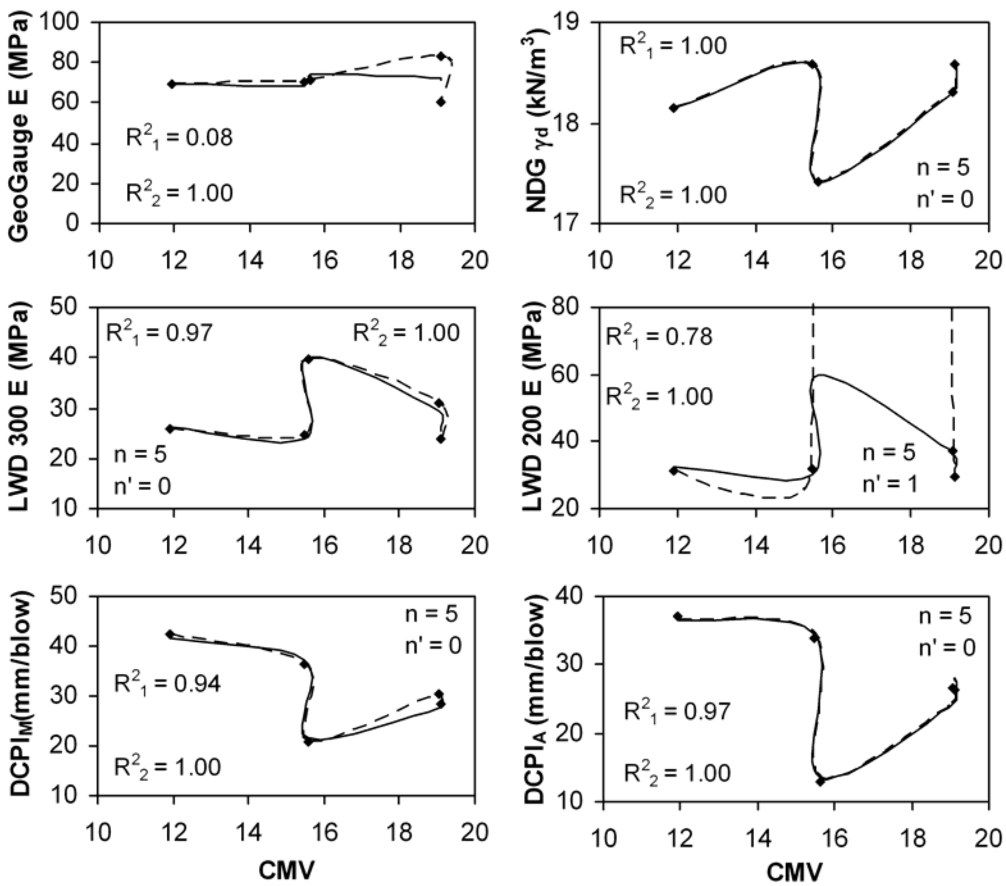

Figure 8.15 Multiple regression analysis using pass-by-pass average in-situ testing measurements vs. average kriged CMV data points, using only the data for the final passes of each lift

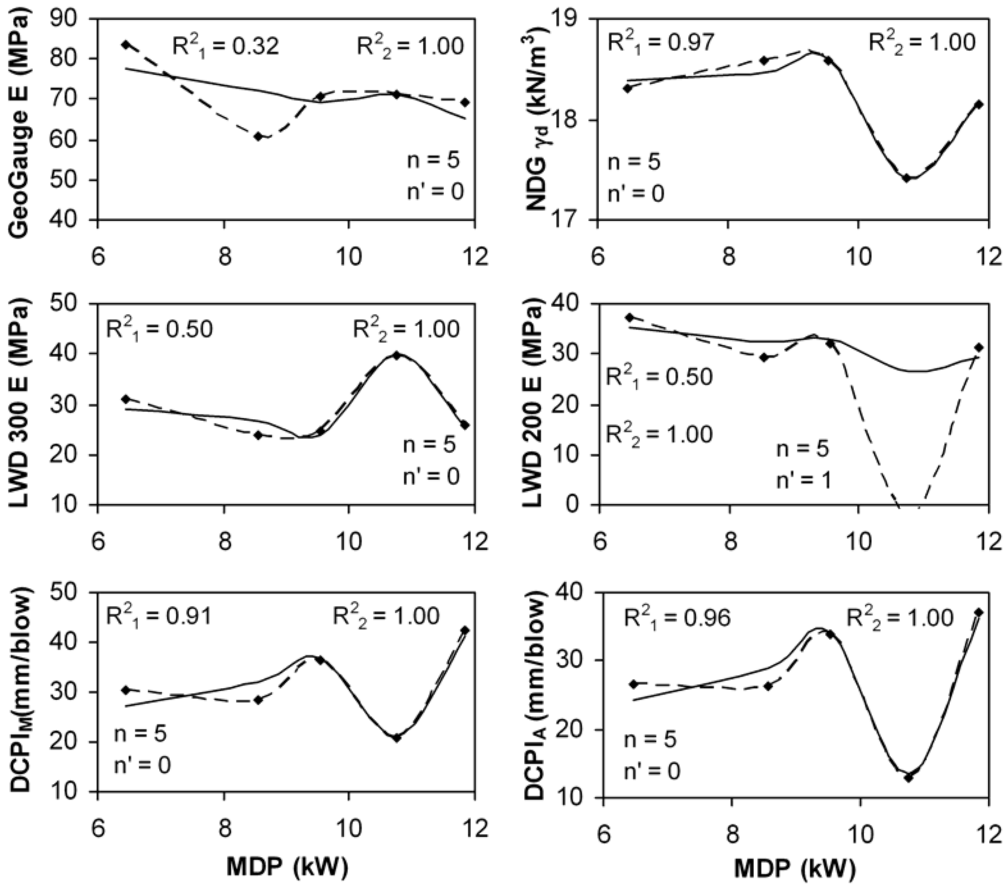

Figure 8.16 Multiple regression analysis using pass-by-pass average in-situ testing measurements vs. average kriged MDP data points, using only the data for the final passes of each lift

Once more, it is clear that the second model mispredicts the missing value of the LWD 200 modulus. In general, the R-squared values of the models significantly improved as compared with the previous case that was analyzed. However, it is suspected that much of this improvement is due to the overall reduction in the number of points that are used for regression, as sophisticated models with only a few data points will usually have relatively high R-squared values. Tables 8.6 and

8.7 present the regression coefficients that resulted from the multivariate regression analysis of the CMV and MDP data sets, using only the data for the final passes of each lift.

Table 8.6 Components of the first fitted model for averages of final passes

In-situ testing	b	c	A	B	C	R^2_1	σ^2_{AD}
Geogauge E (MPa) vs. CMV	0.1	4.0	83.10	-6.45	-4.19E-04	0.08*	122.63
Geogauge E (MPa) vs. MDP (kW)	0.1	0.1	314.95	-146.99	-48.49	0.32*	90.90
NDG γ_d (kN/m^3) vs. CMV	0.5	2.2	13.51	0.91	7.94E-03	1.00	0.00
NDG γ_d (kN/m^3) vs. MDP (kW)	4.0	0.9	16.74	-3.81E-05	0.25	0.97†	0.01
LWD 300 E (MPa) vs. CMV	4.0	3.2	46.31	-6.83E-05	-8.94E-03	0.97†	2.63
LWD 300 E (MPa) vs. MDP (kW)	4.0	0.1	256.51	1.55E-04	-184.31	0.93*	6.15
LWD 200 E (MPa) vs. CMV	4.0	0.1	491.44	-7.38E-05	-360.09	0.78*	7.59
LWD 200 E (MPa) vs. MDP (kW)	0.1	4.0	175.86	-117.95	3.31E-04	0.50*	16.95
$DCPI_M$ (mm/blow) vs. CMV	0.1	0.1	-29.55	-128.74	186.01	0.94*	7.44
$DCPI_M$ (mm/blow) vs. MDP (kW)	4.0	0.1	-229.53	3.95E-04	207.14	0.91*	12.33
$DCPI_A$ (mm/blow) vs. CMV	0.1	0.1	-193.60	-64.38	246.18	0.97†	4.97
$DCPI_A$ (mm/blow) vs. MDP (kW)	4.0	0.1	-293.59	1.78E-04	256.89	0.96†	6.91

*: Models that have a p-value greater than 0.05
†: Models that have a p-value between 0.01 and 0.05

Table 8.7 Components of the second fitted model for averages of final passes

In-situ testing	b	c	d	A	B	C	D	R^2_2	σ^2_{AD}
Geogauge E (MPa) vs. CMV	0.8	3.8	3.3	-261.42	37.33	0.01	-4.77E-06	**1.00**	0.00
Geogauge E (MPa) vs. MDP (kW)	2.8	2.1	0.5	340.31	0.14	1.47	-55.74	**1.00**	0.00
NDG γ_d (kN/m^3) vs. CMV	3.7	3.1	0.7	15.60	-6.30E-06	-3.05E-05	0.09	**1.00**	0.00
NDG γ_d (kN/m^3) vs. MDP (kW)	3.6	1.8	1.3	19.31	-7.52E-04	-0.08	0.02	**1.00**	0.00
LWD 300 E (MPa) vs. CMV	0.3	2.7	1.6	-243.89	132.31	0.06	-0.02	**1.00**	0.00
LWD 300 E (MPa) vs. MDP (kW)	3.5	3.0	1.0	57.15	0.0087	0.04	-0.99	**1.00**	0.00
LWD 200 E (MPa) vs. CMV	0.1	0.1	0.1	1.75E+06	-1.30E+06	-1.38E+06	1.02E+06	**1.00***	0.00
LWD 200 E (MPa) vs. MDP (kW)	0.1	0.1	0.1	1.32E+04	-1.08E+04	-1.04E+04	8.50E+03	**1.00***	0.00
$DCPI_M$ (mm/blow) vs. CMV	2.6	1.6	3.9	-4.37	8.17E-03	1.05	-3.60E-08	**1.00**	0.00
$DCPI_M$ (mm/blow) vs. MDP (kW)	3.7	1.6	0.7	39.04	5.42E-03	2.36	-5.16	**1.00**	0.00
$DCPI_A$ (mm/blow) vs. CMV	2.3	2.9	3.0	-19.47	0.05	0.05	-6.12E-06	**1.00**	0.00
$DCPI_A$ (mm/blow) vs. MDP (kW)	0.3	4.0	3.8	82.51	-34.88	9.81E-04	1.32E-07	**1.00**	0.00

*: Models that have a p-value greater than 0.05
†: Models that have a p-value between 0.01 and 0.05

Tables 8.6 and 8.7 illustrate the limitations of using only R-squared values for assessment of model fit, particularly for cases where there are only a few points that are being analyzed to develop the regression equation. As shown here, R-squared values may sometimes be quite high, while the significance probability values (p-values) are unacceptable (as they are greater than 0.05).

Similar multivariate regression analyses were performed looking only at the final passes for each of the compacted lifts, with the base layer data points excluded. Figures 8.17 and 8.18 show the results of these multivariate regression analyses.

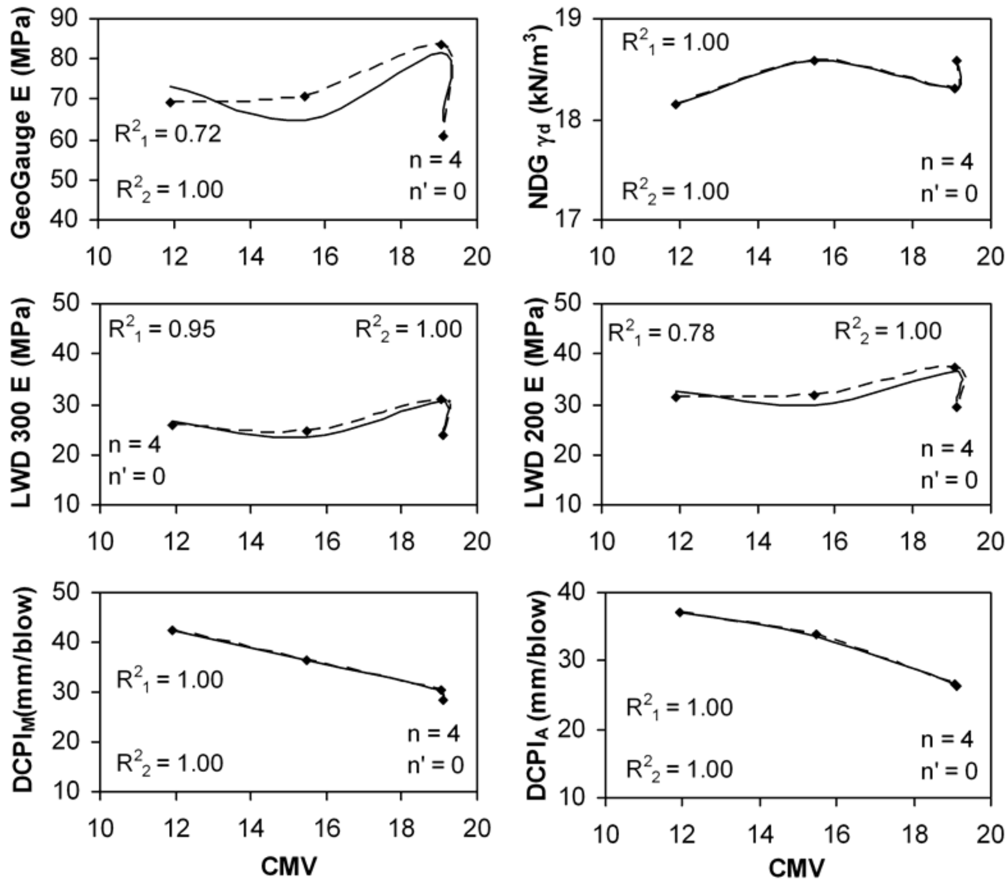

Figure 8.17 Multiple regression analysis using pass-by-pass average in-situ testing measurements vs. average kriged CMV data points, using only the data for the final passes of each lift and excluding the base layer

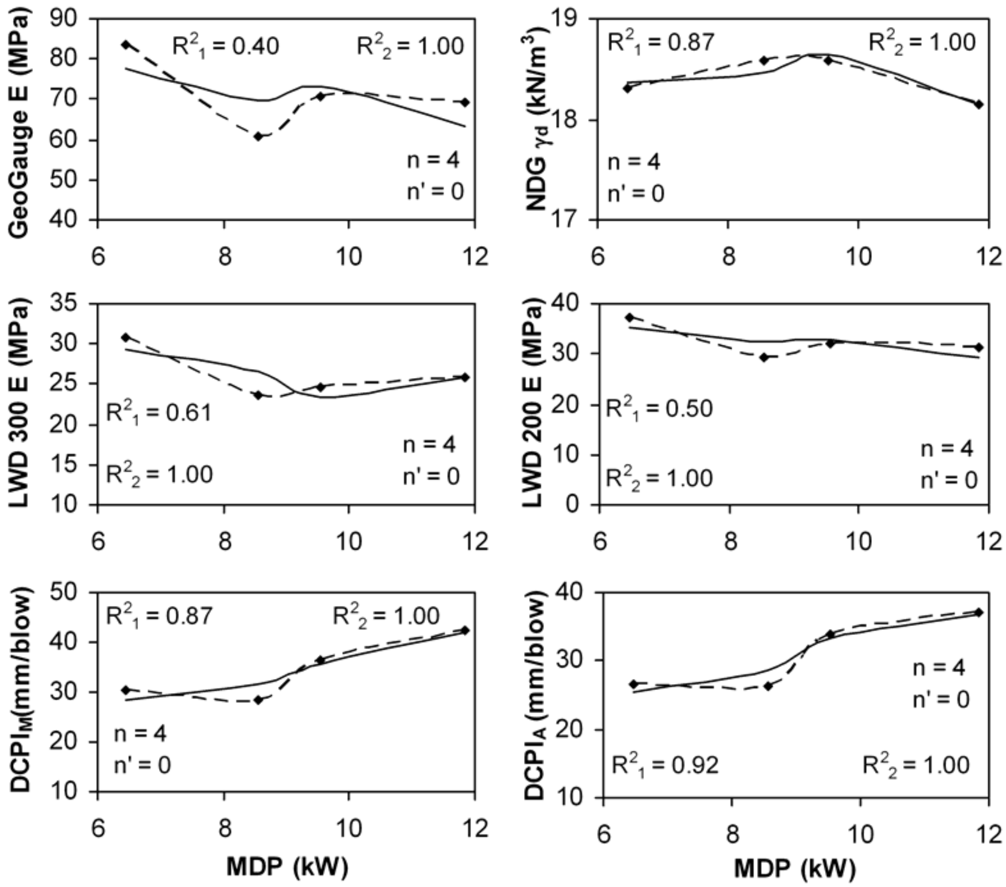

Figure 8.18 Multiple regression analysis using pass-by-pass average in-situ testing measurements vs. average kriged MDP data points, using only the data for the final passes of each lift and excluding the base layer

Tables 8.8 and 8.9 present the regression coefficients that resulted from the multivariate regression analysis of the CMV and MDP data sets, using only the data for the final passes of each lift and excluding the base layer data points.

Table 8.8 Components of the first fitted model for averages of final passes excluding the base layer

In-situ testing	b	c	A	B	C	R^2_1	σ^2_{AD}
Geogauge E (MPa) vs. CMV	4.0	0.1	1368.93	-2.34E-04	-1016.57	**0.72****	74.90
Geogauge E (MPa) vs. MDP (kW)	0.1	4.0	505.58	-360.77	1.40E-03	0.40*	160.34
NDG γ_d (kN/m^3) vs. CMV	1.3	3.6	15.84	0.04	2.26E-04	**1.00**	0.00
NDG γ_d (kN/m^3) vs. MDP (kW)	4.0	0.1	-1.95	-4.23E-05	16.49	**0.87***	0.02
LWD 300 E (MPa) vs. CMV	4.0	0.1	508.40	-0.0001	-378.24	**0.95***	1.66
LWD 300 E (MPa) vs. MDP (kW)	4.0	0.1	304.11	2.22E-04	-222.61	0.61*	11.82
LWD 200 E (MPa) vs. CMV	4.0	0.1	491.44	-7.38E-05	-360.09	**0.78***	7.59
LWD 200 E (MPa) vs. MDP (kW)	0.1	4.0	175.86	-117.95	3.31E-04	0.50*	16.95
$DCPI_M$ (mm/blow) vs. CMV	3.3	2.9	55.70	-1.27E-03	-0.0085	**1.00**	0.00
$DCPI_M$ (mm/blow) vs. MDP (kW)	4.0	4.0	25.64	5.76E-04	3.66E-04	**0.87***	15.02
$DCPI_A$ (mm/blow) vs. CMV	4.0	4.0	38.68	-9.22E-05	1.98E-05	**1.00**†	0.07
$DCPI_A$ (mm/blow) vs. MDP (kW)	4.0	4.0	21.65	3.01E-04	6.51E-04	**0.92***	6.66

*: Models that have a p-value greater than 0.05
†: Models that have a p-value between 0.01 and 0.05

Table 8.9 Components of the second fitted model for averages of final passes excluding the base layer

In-situ testing	b	c	d	A	B	C	D	R^2_2	σ^2_{AD}
Geogauge E (MPa) vs. CMV	0.1	0.1	0.1	5.50E+06	-4.10E+06	-4.33E+06	3.23E+06	**1.00***	0.00
Geogauge E (MPa) vs. MDP (kW)	0.1	0.1	0.1	4.17E+04	-3.42E+04	-3.27E+04	2.69E+04	**1.00***	0.00
NDG γ_d (kN/m^3) vs. CMV	0.1	0.1	0.1	9.43E+03	-7.03E+03	-7.43E+03	5.55E+03	**1.00***	0.00
NDG γ_d (kN/m^3) vs. MDP (kW)	0.1	0.1	0.1	-8.30E+02	6.72E+02	6.84E+02	-5.42E+02	**1.00***	0.00
LWD 300 E (MPa) vs. CMV	0.1	0.1	0.1	1.12E+06	-8.37E+05	-8.85E+05	6.59E+05	**1.00***	0.00
LWD 300 E (MPa) vs. MDP (kW)	0.1	0.1	0.1	1.22E+04	-9.84E+03	-9.65E+03	7.79E+03	**1.00***	0.00
LWD 200 E (MPa) vs. CMV	0.1	0.1	0.1	1.75E+06	-1.30E+06	-1.38E+06	1.02E+06	**1.00***	0.00
LWD 200 E (MPa) vs. MDP (kW)	0.1	0.1	0.1	1.32E+04	-1.08E+04	-1.04E+04	8.50E+03	**1.00***	0.00
$DCPI_M$ (mm/blow) vs. CMV	0.1	0.1	0.1	7.33E+05	-5.46E+05	-5.77E+05	4.30E+05	**1.00***	0.00
$DCPI_M$ (mm/blow) vs. MDP (kW)	0.1	0.1	0.1	1.86E+04	-1.52E+04	-1.48E+04	1.22E+04	**1.00***	0.00
$DCPI_A$ (mm/blow) vs. CMV	0.1	0.1	0.1	7.72E+05	-5.75E+05	-6.08E+05	4.53E+05	**1.00***	0.00
$DCPI_A$ (mm/blow) vs. MDP (kW)	0.1	0.1	0.1	1.26E+04	-1.05E+04	-9.98E+03	8.32E+03	**1.00***	0.00

*: Models that have a p-value greater than 0.05
†: Models that have a p-value between 0.01 and 0.05

As shown in Tables 8.8 and 8.9, with the exception of the relationship between CMV and the NDG dry unit weight and DCP indices for the first model, all of the correlations that are obtained are rejected, because their p-values are all greater than 0.05. Additionally, the corresponding p-value for the relationship between CMV and the DCP_A index is greater than 0.01 and the results from this regression analysis should be treated with caution.

Figures 8.19 and 8.20 show the results of regression analysis on the average values of Lift 5.

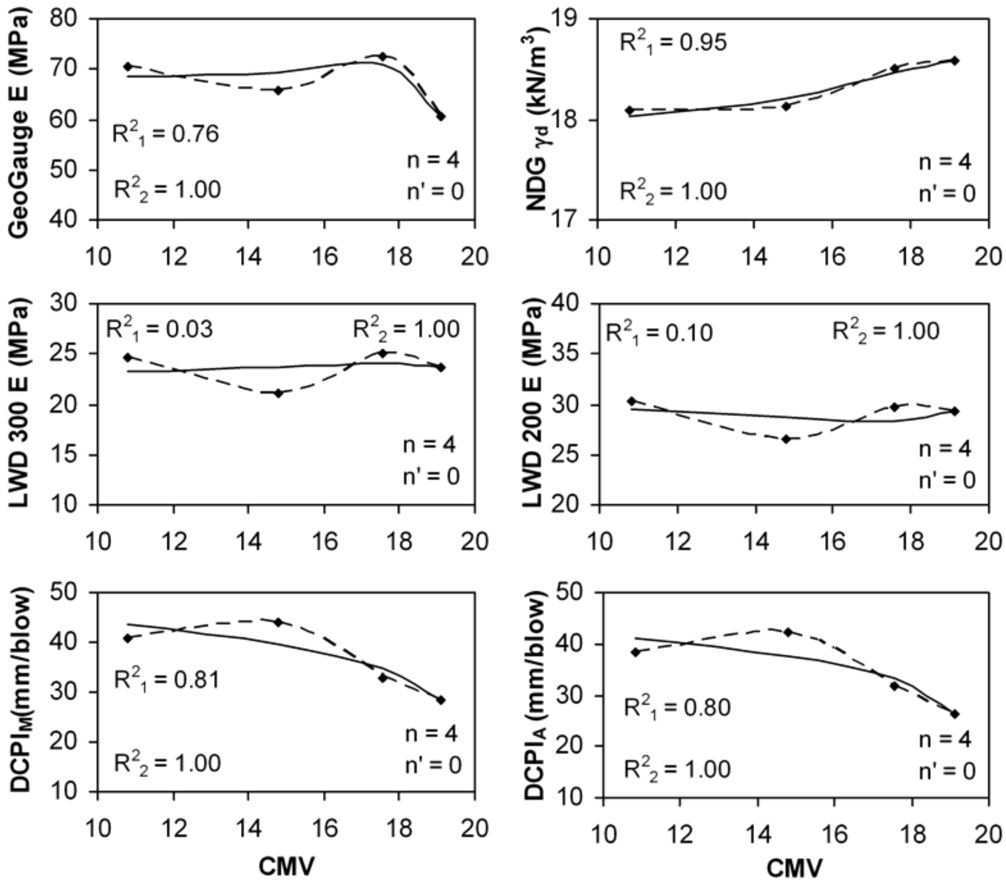

Figure 8.19 Multiple regression analysis using pass-by-pass average in-situ testing measurements vs. average kriged CMV data points, using only the data for Lift 5

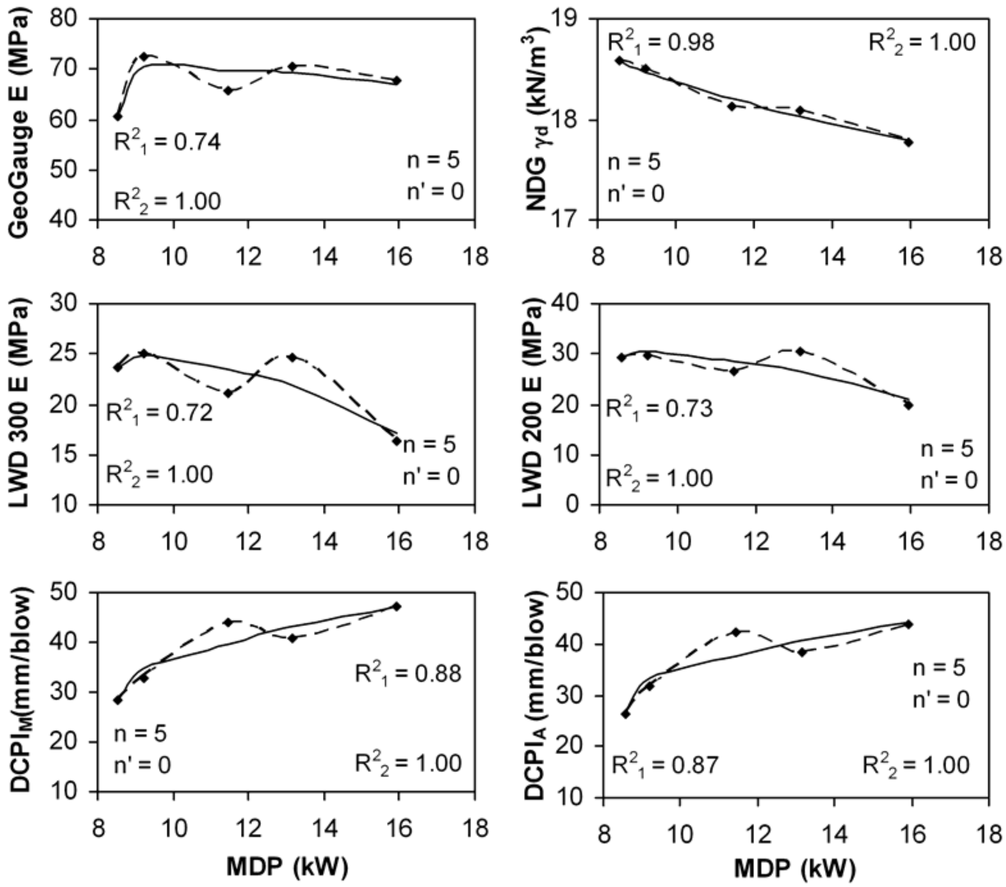

Figure 8.20 Multiple regression analysis using pass-by-pass average in-situ testing measurements vs. average kriged MDP data points, using only the data for Lift 5

Tables 8.10 and 8.11 present the regression coefficients that resulted from the multivariate regression analysis of the CMV and MDP data sets, using only the data from Lift 5.

Table 8.10 Components of the first fitted model for averages of Lift 5

In-situ testing	b	c	A	B	C	R^2_1	σ^2_{AD}
Geogauge E (MPa) vs. CMV	4.0	4.0	32.88	2.63E-05	2.99E-03	**0.76***	20.16
Geogauge E (MPa) vs. MDP (kW)	0.1	0.1	-934.20	-17.95	812.25	**0.74***	11.04
NDG γ_d (kN/m^3) vs. CMV	4.0	4.0	17.71	5.25E-06	2.12E-05	**0.95***	0.01
NDG γ_d (kN/m^3) vs. MDP (kW)	0.1	0.1	32.62	-9.81	-1.50	**0.98†**	0.00
LWD 300 E (MPa) vs. CMV	4.0	4.0	20.79	9.34E-06	1.99E-04	0.03*	8.95
LWD 300 E (MPa) vs. MDP (kW)	4.0	4.0	20.82	-1.29E-04	4.19E-04	**0.72***	7.17
LWD 200 E (MPa) vs. CMV	0.1	0.1	179.67	-19.01	-99.69	0.10*	8.16
LWD 200 E (MPa) vs. MDP (kW)	4.0	4.0	26.91	-1.56E-04	3.79E-04	**0.73***	10.12
$DCPI_M$ (mm/blow) vs. CMV	4.0	0.1	-164.23	-1.08E-04	165.45	**0.81***	29.94
$DCPI_M$ (mm/blow) vs. MDP (kW)	0.1	0.1	-651.74	192.83	352.44	**0.88***	14.30
$DCPI_A$ (mm/blow) vs. CMV	4.0	0.1	-285.02	-9.59E-05	258.98	**0.80***	29.99
$DCPI_A$ (mm/blow) vs. MDP (kW)	0.1	0.1	-727.49	167.64	436.18	**0.87***	14.44

*: Models that have a p-value greater than 0.05

†: Models that have a p-value between 0.01 and 0.05

Table 8.11 Components of the second fitted model for averages of Lift 5

In-situ testing	b	c	d	A	B	C	D	R^2_2	σ^2_{AD}
Geogauge E (MPa) vs. CMV	0.1	0.1	0.1	-1.62E+06	1.20E+06	1.28E+06	-9.51E+05	**1.00***	0.00
Geogauge E (MPa) vs. MDP (kW)	1.4	0.1	1.7	4926.4361	-26.1527	-3736.5165	0.1938	**1.00**	0.00
NDG γ_d (kN/m^3) vs. CMV	0.1	0.1	0.1	-5.85E+04	4.36E+04	4.63E+04	-3.45E+04	**1.00***	0.00
NDG γ_d (kN/m^3) vs. MDP (kW)	1.4	1.3	1.7	34.37	-0.67	-0.57	4.74E-03	**1.00**	0.00
LWD 300 E (MPa) vs. CMV	0.1	0.1	0.1	-1.02E+06	7.62E+05	8.09E+05	-6.03E+05	**1.00***	0.00
LWD 300 E (MPa) vs. MDP (kW)	2.6	2.1	2.9	178.46	-0.50	-0.94	2.41E-04	**1.00**	0.00
LWD 200 E (MPa) vs. CMV	0.1	0.1	0.1	-9.62E+05	7.16E+05	7.61E+05	-5.67E+05	**1.00***	0.00
LWD 200 E (MPa) vs. MDP (kW)	0.9	0.5	1.0	3088.74	-244.88	-883.52	16.66	**1.00**	0.00
$DCPI_M$ (mm/blow) vs. CMV	0.1	0.1	0.1	2.34E+06	-1.74E+06	-1.85E+06	1.38E+06	**1.00***	0.00
$DCPI_M$ (mm/blow) vs. MDP (kW)	3.0	3.3	3.5	-113.48	0.22	0.05	-1.49E-05	**1.00**	0.00
$DCPI_A$ (mm/blow) vs. CMV	0.1	0.1	0.1	2.28E+06	-1.70E+06	-1.80E+06	1.34E+06	**1.00***	0.00
$DCPI_A$ (mm/blow) vs. MDP (kW)	2.2	0.7	2.6	-728.03	2.38	133.14	-1.70E-03	**1.00**	0.00

*: Models that have a p-value greater than 0.05
†: Models that have a p-value between 0.01 and 0.05

The data presented in Tables 8.10 and 8.11 indicates that the models that were utilized were not able to establish reliable correlations between the average kriged CMV values and the corresponding in-situ test results for successive passes of Lift 5. This is not surprising, as the water content values did not vary significantly for additional compaction of Lift 5, and as such, there was not sufficient data in this data set to clearly discern the relative contribution of the second variable in the bivariate regression analyses (water content). Similar to the analyses performed looking at only the final passes for each lift, many of the cases that were examined here were rejected because their p-values were greater than 0.05.

As shown in Table 8.11, there are excellent correlations between MDP and the measured in-situ test values. It should be noted that this outstanding relationship between MDP and other measurements in Lift 5 likely originates from the reduction in the number of data points in this data set (as compared with the other data sets, which were larger), as noted for analysis of the base layer data points. In general, these results conform to the results of the univariate regression analyses presented in Chapter 7.

Similar to Section 8.3.2, a summary of all of the analyses that were performed are presented in Table 8.12.

Table 8.12 R-squared values of the utilized model for the employed data sets

In-sit testing	All		All without base layer		Finals		Finals without base layer		Lift 5	
	R^2_1	R^2_2	R^2_1	R^2_2	R^2_1	R^2_2	R^2_1	R^2_2	R^2_1	R^2_2
Geogauge E (MPa) vs. CMV	0.09*	0.36*	0.35*	0.69*	0.08*	1.00	0.72*	1.00*	0.76*	1.00*
Geogauge E (MPa) vs. MDP (kW)	0.25*	0.68	0.29*	0.86†	0.32*	1.00	0.40*	1.00*	0.74*	1.00
NDG γ_d (kN/m^3) vs. CMV	0.96	0.96	0.86†	0.88*	1.00	1.00	1.00	1.00*	0.95*	1.00*
NDG γ_d (kN/m^3) vs. MDP (kW)	0.93	0.98	0.86	0.96	0.97†	1.00	0.87*	1.00*	0.98†	1.00
LWD 300 E (MPa) vs. CMV	0.89	0.97	0.49*	0.96†	0.97†	1.00	0.95*	1.00*	0.03*	1.00*
LWD 300 E (MPa) vs. MDP (kW)	0.87	0.95	0.68†	0.91†	0.93*	1.00	0.61*	1.00*	0.72*	1.00
LWD 200 E (MPa) vs. CMV	0.43*	0.97	0.43*	0.97	0.78*	1.00*	0.78*	1.00*	0.10*	1.00*
LWD 200 E (MPa) vs. MDP (kW)	0.70†	0.91†	0.70†	0.91†	0.50*	1.00*	0.50*	1.00*	0.73*	1.00
DCPI$_M$ (mm/blow) vs. CMV	0.86	0.98	0.85†	0.97	0.94*	1.00	1.00	1.00*	0.81*	1.00*
DCPI$_M$ (mm/blow) vs. MDP (kW)	0.88	0.94	0.82†	0.90†	0.91*	1.00	0.87*	1.00*	0.88*	1.00
DCPI$_A$ (mm/blow) vs. CMV	0.88	1.00	0.79†	0.99	0.97†	1.00	1.00†	1.00*	0.80*	1.00*
DCPI$_A$ (mm/blow) vs. MDP (kW)	0.91	0.94	0.83†	0.85†	0.96†	1.00	0.92*	1.00*	0.87*	1.00

*: Models that have a p-value greater than 0.05
†: Models that have a p-value between 0.01 and 0.05

By examining Table 8.12, it is possible to make the following observations (Note that in all the conclusions that are presented in the following bullet points, the acceptable criteria for R-squared values is those that are greater than 0.70, and the criteria for p-values corresponds to those that are less than 0.05):

- In most cases, the second multivariate regression model that was used resulted in stronger correlations than the first model that was used. This is not surprising, as the general form of these two equations was the same, with the second equation just having another term that allowed for more accurate model fit results.
- In general, removing the base layer data point from the analyses that were performed did not improve the quality of model fit. As this conclusion is the opposite of what was observed in the univariate regression analysis chapter, it is believed that it is the water content of this layer that causes this point to be so problematic in the univariate regression analyses.
- In general, significant reduction in the number of regression points that are used, decreases the reliability of the fitted models. This decrease in reliability does not show up in the R-squared values, but is rather reflected in the high p-values that are observed. Unfortunately, this is an inherent limitation of only comparing the "average" data sets that are recorded for each compacted layer, rather than individual test points. As a result of this observation, the Author believes that a significant number of layers ought be

compacted in order to build a well-calibrated, reliable regression model for each soil type that is studied.

- As was observed in the univariate regression analyses that are discussed in Chapter 7, excellent correlations can be achieved between averaged in-situ testing measurements for a given lift and pass and average kriged CCC data points.
- The GeoGauge showed strong correlations with CCC values in only 20% of the overall cases (i.e. 4 models for both CMV and MDP).
- The NDG dry unit weight was strongly correlated to the CCC measurements in 65% of the analyses that were performed.
- The LWD 300 measured modulus values showed a significant relationship with CCC values in 50% of the calculations.
- The LWD 200 measured modulus values were well-correlated to the CCC values in 30% of the experiments.
- DCP_M and DCP_A indices showed strong correlation with CMV and MDP values in 60% and 70% of the cases, respectively.
- MDP and CMV make strong correlations with in-situ testing values in 57% and 45% of all cases, respectively.

8.4 Summary and Conclusions

In this chapter, multiple regression analysis techniques were utilized to include the effect of water content in the correlations between the in-situ testing data and CCC roller values. At the beginning of the chapter, the entire set of data was considered in the analysis, on a point-by-point basis. Strong correlations were not achieved using any of the point-by-point analysis approaches that were utilized.

As a next step, the average values of measured data were taken into account. As was observed with the univariate regression analyses, the resulting R-squared values remarkably improved. Results from these analyses also showed that R-squared values are not the only condition that must be reasonably satisfied for model acceptance, particularly for models fitted to only a few data points. The use of a p-value acceptance limit of 0.05 was found to be an additional criteria that was useful for acceptance of model fit results.

The analyses of the average values showed that DCP indices and NDG dry unit weights have the strongest correlation with CCC values, as compared to the other in-situ testing techniques that were used in this study. In particular, the GeoGauge had trouble correlating with the CCC results. The LWD 300 modulus values yielded stronger correlations than the LWD 200 modulus values. In general, MDP showed more robust correlations with the in-situ testing methods than did CMV, which is the same observation as was made from the univariate regression analyses described in Chapter 7.

Chapter 9

CONCLUSIONS AND RECOMMENDATIONS

9.1 Conclusions

The effectiveness of two Continuous Compaction Control systems were evaluated in this research project. A CCC roller equipped with MDP and CMV measurement systems was used for compaction of a five-lift embankment. The compacted soil used in this study was a common borrow material for the Delaware Department of Transportation, which conforms to DelDOT class G borrow specifications, Grades V and VI, and which can be classified as predominantly a poorly-graded sand with silt (SP-SM), according to the unified soil classification system (USCS). A series of in-situ quality control tests were performed along the centerline of the designated pad after compaction for each lift. The primary testing methods consisted of a Light Weight Deflectometer (LWD) with plate diameters of 300 mm (12 in) and 200 mm (8 in), a GeoGauge, a Nuclear Density Gauge (NDG), and a Dynamic Cone Penetrometer (DCP).

The preliminary evaluation of the in-situ testing data indicated that:

- The NDG-measured dry unit weights of the compacted lifts passed DelDOT's acceptance criteria for relative compaction (RC $\geq$ 95 %).

- In most cases, the compaction was conducted on the dry side of the optimum water content, with field measured water contents ranging between 4.2% and 12.9%.
- In general, the GeoGauge showed significant inconsistencies with the range of modulus values measured in the other modulus-based tests.

Statistical analysis of the roller data showed that:

- The MDP measured values decreased as the number of compaction passes increased for a given lift.
- For soils compacted using the same input amplitude of compaction vibration, the measured values of CMV increased as the number of compaction passes increased for a given lift.
- As compaction progressed, the variation of MDP values decreased.
- In general, the variation of CMV values was greater than the variation of MDP values.
- MDP measurements appeared to reflect the surficial properties of a compacted lift, while CMV values appeared to be influenced by both the lift that was being compacted and the relative stiffness of soil layers that were underlying the lift that was being compacted.
- The average RMV values ranged between 0 and 2, indicating that the vibratory compaction was predominantly conducted in the "partial uplift" mode of vibration.

The key findings of the geostatistical analysis of the roller data follows:

- Kriging analyses are essential for spatially interpolating between measured CCC data points, in order for the most accurate comparisons of CCC values with point-specific in-situ tests.
- The R-squared value of a model that is fit to a sample semivariogram is by itself not a useful enough indicator for selecting a semivariogram model for kriging analysis of CCC data.
- Cumulative frequency distributions of relative errors between the values predicted by a given kriging model and the actual value recorded at a specific point were extremely useful for selecting the most reliable semivariogram model for each type of CCC measurement (i.e. MDP and CMV).
- Among the semivariogram models that were examined, the Rational Quadratic model was selected for kriging of the MDP values and the Exponential, Spherical, and Linear models were all recommended as equally reliable models for kriging of the CMV values.
- Additional examination of the resulting kriged data points indicated that, in general, the relative error of the predicted MDP values was less than the predicted CMV values.
- There was a direct relationship between the degree of compaction of the soil and the associated accuracy of the kriging method. As the soil became denser and stiffer, the values predicted using kriging became closer to the actual values.

- Beyond a separation distance (or lag) of 1.5 m (5.0 ft), the resulting accuracy of the kriging models that were chosen was not found to be significantly different. Consequently, the lag that was chosen for kriging was 1.5 m (5.0 ft), based on the fact that this lag had the shortest model run time in the kriging algorithm that was used.

Univariate regression analysis between the kriged CCC data points and the corresponding in-situ testing values showed that:

- In general, there was not a strong relationship between the individual kriged CCC values and the corresponding in-situ measured values.
- Relatively strong correlations were observed between the average in situ measured values for each lift and pass vs. the average of the kriged MDP and CMV values for each lift and pass.
- Excluding the base layer average values from the related univariate regression analysis resulted in a significant improvement in the R-squared values of the fitted curves for a number of the in-situ tests that were analyzed and revealed a number of strong correlations between the CCC data and some of the in-situ testing measurements.
- In general, MDP values were better correlated with the in-situ testing measurements than were the CMV values.

- NDG measured dry unit weights and DCP indices showed the best correlation with CCC values, relative to the other in-situ measurements that were analyzed.
- The LWD 200 showed a better correlation with the measured CCC data than did the LWD 300.
- Among the in-situ testing methods that were utilized, the GeoGauge showed the least amount of correlation with the CCC data.
- Water content was shown to have a significant influence on the roller data and many of the in-situ testing measurements, and there were strong correlations between the average laboratory measured water contents and the average values of roller data and in situ testing methods that were developed.

To include the effect of water content in the correlation between CCC values and in-situ testing measurements, a series of multiple regression analysis were performed. The results from these analyses confirmed that:

- Similar to the univariate regression analysis, there was no strong correlation between individual CCC values and in-situ measured values, considering the data set as a whole.
- It was discovered that R-squared values could not be used as the sole reliable acceptance criterion for fitting a regression model. The use of a p-value criterion of 0.05 was found to be a useful supplemental criterion for model acceptance.

- The results from multivariate regression analyses of average in situ test values vs. average kriged model results showed that the DCP indices and NDG dry unit weights had the strongest correlation with the average of the kriged CCC values. The GeoGauge test results exhibited the least amount of correlation with the average of the kriged CCC values.
- The LWD 300 modulus yielded stronger correlations than the LWD 200 modulus.
- In general, MDP values showed more robust correlations with the in-situ testing methods than did the CMV values.

9.2 Recommendations

For future utilization of CCC technology by the Delaware DOT, the following recommendations are made:

- To evaluate the effectiveness and productivity of CCC systems, extra field studies are needed on a variety of commonly used soils and other construction materials which are utilized by the DOT for road-embankment construction.
- If a CMV-based CCC roller is utilized, it is recommended to apply high amplitude compaction for all lifts and passes in future field studies. This produces a larger numerator in the CMV formula, and will likely yield more rapid compaction and possibly more reliable CCC results.
- Since the CMV values showed a relatively high variation it is recommended to examine other types of vibratory CCC rollers

equipped with direct modulus-stiffness measurement systems in future studies.

- CCC values should be recorded for every compaction pass that is run in a project.

For quality control methods, the followings are recommended:

- It is recommended to use Plate Load Tests (PLT) and Falling Weight Deflectometer tests, which are considered to be better modulus-based in-situ testing methods, for validating CCC measurements.
- To obtain the variation of soil properties along the width of the drum of the CCC roller it is recommended to distribute the test spots in at least three parallel lines which are located in the width of the roller drum.
- The sand cone equivalent test is an old but reliable test, as compared to other density-based tests. Therefore, it is recommended to perform more sand cone tests for the final passes of each constructed lift.
- For DCP tests, it is recommended to penetrate the rod to greater depths to obtain a better understanding about the underlying layers.
- Since the moisture content showed a significant influence on the measurements, more attention should be paid to maintain it in the range of optimum moisture content.

Appendix A

DAILY REPORTS

University of Delaware

Departmenet of Civil and Environmental Engineering

DAILY PROGRESS REPORT (PAGE 1 / 10)

Project Title:	Investigation of CCC Technology		
Date:	Monday 7/21/2008	Site:	Burrice Pit (Odessa)
Start Time:	6:30	End Time:	18:00
Weather:	Sunny	Temp.:	33 C (91 F)

NUMBER OF PERSONNEL

Organization/Contractor/Subcontractor	Hours	Supervisors	Staff Engineers	Technicians	Truck Drivers	Labors	Trainees		
University of Delaware/Geotech. Group	6:30-18:0	1	6						
Del DOT		1		2					
Caterpillar & Ransome Dealership		1	4		1				
Greggo & Ferrara Inc					1				
Kessler Soils Engineering Products, Inc.									
Humboldt				1					

NUMBER OF MAJOR MACHINES AND EQUIPMENTS

Organization/Contractor/Subcontractor	Type & Number
Caterpillar & Ransome Dealership	1 Dozer D56K, 1 Wheel Loader 980H, 1 Roller CS56, 1 GPS Rover, 1 DCP, 1 LWD
Del DOT	2 Nuclear Gauge
Humboldt	1 EDG, 1 GeoGauge
Greggo & Ferrara Inc	1 Wheel Loader 924H, 1 Water Truck
Kessler Soils Engineering Products, Inc.	1 LWD
University of Delaware/Geotech. Group	Sand Cone Supplies, Level, Misc Other Supplies

DESCRIPTION OF WORK & ACTIVITY

Hours		Description
6:30	7:30	Meet on campus, load van and depart UD
8:00	8:15	Arrive on site, unload van
8:15	9:00	Level shooting and put 26 grade stakes in stations (see Figure 3.4) at 10 or 20 ft intervals (Faraz and Farshid)
8:30		Meet with Jim Reynolds (Site Manager) and Al Strauss (Del DOT) by Dr. Meehan
9:00		All parties on site, setup GPS
9:15		Adam (Humboldt), Fan and Baris get donuts, ice and coffee
10:00		1st point set as reference point for local coordinate system in GPS rover (6000',6000',200')
11:10	11:40	DCP and LWD training by Caterpillar team members (Nick & Mario)
11:30		Dozer starts pre-leveling (no working GPS). Variable elevation, lowest pt was 199.55'. Roller set up.
12:15	14:15	Begin compacting the base layer. 2 passes in total. Final Elevation was 200.14'
14:35		Start In-situ tests on the base layer at 5 points (St. 0+10, 0+50, 0+90, 1+30 and 1+70, centerline)

University of Delaware

Departmenet of Civil and Environmental Engineering

DAILY PROGRESS REPORT (PAGE 2 / 10)

Date: Monday 7/21/2008

DESCRIPTION OF WORK CONTINUED

Hours		Description
14:35	14:55	LWD tests by Farshid and Baris at 5 pts on the base layer
14:45	15:04	GeoGauge tests by Yueru and Majid at 5 pts on the base layer
14:52	15:15	Nuclear gauge tests by Tony (Del DOT) at 5 pts on the base layer
14:57	15:22	EDG tests by Adam (Humboldt) at 5 pts on the base layer
15:28	15:43	DCP tests by Faraz and Fan at 5 pts on the base layer
15:33	15:46	1 point Proctor samples at 5 locations (DelDOT). Sampling (w%) at 5 test stations (UD). 1 bucket for 5 point proctor at side of fill area. (See sample list for sample locations).
		GPS Rover shooting for test locations (see attached sheets)
16:30	17:00	GPS Rover shooting post-compaction elevations to determine 1st lift target elevation (see attached)
17:00		Loading van
17:20		Leave site
17:50		Arrive at campus, unload van and schedule for next day

EFFECTS ON WORK (WEATHER, ACCIDENTS, BREAKDOWNS, DELAYS, PERSONNEL, ETC.)

No.	Description
1	First day set up and checking of equipment was time consuming.
2	Problems with on-board GPS on the roller caused delay in compaction progress.
3	Significant loss of roller data due to bad card reader.
4	Was unable to get GPS control for bulldozer blade. Initial elevations cut by eye using operator judgement.

PROJECT VISITORS

Del DOT	Jim Pappas, Hani Fakri
Greggo & Ferrara Inc	Nicky Ferrara, Jim Reynolds, Dave

REMARKS

Staff Names:	
UD Team	Dr. Meehan, Faraz, Majid, Yeuru, Fan, Farshid, Baris
Del DOT	Al Strauss, Tyrone Nelson, Tony Marcozzi
Caterpillar	AJ Lee, Dick Costello, Mario Souraty, Nick Oetken, Brett Barrett
Humboldt	Adam Houghton
Greggo & Ferrara	Dave McQuiry

PREPARED BY: Farshid Vahedifard and Faraz S.Tehrani

University of Delaware

Departmenet of Civil and Environmental Engineering

DAILY PROGRESS REPORT (PAGE 3 / 10)

Project Title:	Investigation of CCC Technology		
Date:	Tuesday 7/22/2008	Site:	Burrice Pit (Odessa)
Start Time:	6:00	End Time:	18:20
Weather:	Sunny	Temp.:	33 C (91 F)

NUMBER OF PERSONNEL

Organization/Contractor/Subcontractor	Hours	Supervisors	Staff Engineers	Technicians	Truck Drivers	Labors	Trainees		
University of Delaware/Geotech. Group	6:00-18:20	1	6						
Del DOT		1		2					
Caterpillar & Ransome Dealership		1	3		1				
Greggo & Ferrara Inc					1				
Kessler Soils Engineering Products, Inc.		1							
Humboldt				1					

NUMBER OF MAJOR MACHINES AND EQUIPMENTS

Organization/Contractor/Subcontractor	Type & Number
Caterpillar & Ransome Dealership	1 Dozer D56K, 1 Wheel Loader 980H, 1 Roller CS56, 1 GPS Rover, 1 DCP, 1 LWD
Del DOT	2 Nuclear Gauge
Humboldt	1 EDG, 1 GeoGauge
Greggo & Ferrara Inc	1 Wheel Loader 924H, 1 Water Truck
Kessler Soils Engineering Products, Inc.	1LWD
University of Delaware/Geotech. Group	Sand Cone Supplies, Level, Misc Other Supplies

DESCRIPTION OF WORK & ACTIVITY

Hours		Description
6:00	6:45	Meet on campus, load van and depart UD, pick up Farshid then Adam
7:15	7:30	Arrive on site, unload van
7:15	7:20	Passes with water truck on base layer (2 passes)
7:00	7:30	Fill stockpiled and mixed from cut face using 980H loader (C & G material)
7:34	9:00	Start spreading first lift in the test pad using D6K bulldozer.
7:30	7:35	One pass with dust control outside of fill area
7:45		Al Strauss (Del DOT) arrives in site
8:05		Ken Kessler arrives in site, immediately begins discussion and training with grad students
8:31		Al Strauss takes field hot plate moisture of soil from stockpile (dug down a bit), w=8.7%
8:25	8:40	Faraz rock picking first lift, one sample from loose lift (samples 59)
8:40		Tony Marcozzi (Del DOT) arrives on site with second Del DOT van, Al Strauss left
9:08	9:15	2 passes water truck
9:00	11:27	Dan Sajedi (MD DOT) on site with colleagues
9:15	10:00	Roller started running on fisrt lift (comp. elv. 200.6)
		1st pass Max. Amplitude (1.8 mm), 3 more passes low amplitude (0.8 mm) (CMV & MDP)
		5th pass proof roll, no vibration (MDP)
		6th pass vibration (CMV)
10:10	12:40	In-situ testing on first lift (on centerline location)
10:10	11:16	LWD small (200mm dia.) and large (300 mm dia.) at 19 pts by Farshid and Baris (St. 0+10, 0+20, ..,1+90)

University of Delaware

Departmenet of Civil and Environmental Engineering

DAILY PROGRESS REPORT (PAGE 4 / 10)

Date: Tuesday 7/22/2008

DESCRIPTION OF WORK CONTINUED

Hours		Description
10:12	11:30	GeoGauge tests by Yueru and Majid at 19 pts on the first layer (St. 0+10, 0+20, ..,1+90)
		Nuclear gauge tests by Tony (DelDOT) at 10 pts on the first layer (St. 0+10, 0+30, …, 1+90)
10:42	11:49	DCP tests by Faraz and Fan at 19 pts on the first layer (St. 0+10, 0+20, ..,1+90)
		EDG tests by Adam (Humboldt) at 9 pts on the first layer (St. 0+10, 0+30, …, 1+70)
		Sand Cone test by Yueru and Majid at 1 point on the first layer (St. 1+00) - check this point
11:20	11:40	GPS Rover shooting for test locations, 1st lift, final pass (see attached)
12:00	12:20	Taking 1 bucket and 1 bag sample (1+00) middle lane and 5 moisture tin samples (0+10,0+50, ...,1+50)
12:43		1 pass water truck
13:00	13:30	Spreading second lift
13:43	13:46	3 passes water truck
13:50	14:36	Roller started running on second lift (loose elv. 201.3)
		1st pass Max. Amplitude (1.8 mm), 3 more passes low amplitude (0.8 mm) (CMV & MDP)
		5th pass proof roll, no vibration (MDP)
		6th pass low amplitude vibration (CMV)
14:50	17:40	In situ testing on second lift (on centerline location)
14:55	16:10	LWD small (200mm dia.) and large (300 mm dia.) in 19 pts by Farshid and Baris (St. 0+12, 0+22, ..,1+92)
15:00		GeoGauge tests by Yueru and Majid in 19 pts on the second layer (St. 0+12, 0+22, ..,1+92)
		Nuclear gauge tests by Tony (Del DOT) in 10 pts on the second layer (St. 0+12, 0+32, ..,1+92)
15:15	16:44	DCP tests by Faraz and Fan in 19 pts on the second layer (St. 0+12, 0+22, ..,1+92)
		EDG tests by Adam (Humboldt) at 10 pts on the second layer (St. 0+12, 0+32, ..,1+92)
		Sand Cone tests by Yueru and Majid in 3 points on the second layer (St. 1+00)
16:30	16:45	GPS Rover shooting for test locations, 2nd lift, final pass (see attached)
17:45		Leave site
18:20		Arrive in campus, unload van and schedule for newt day

EFFECTS ON WORK (WEATHER, ACCIDENTS, BREAKDOWNS, DELAYS, PERSONNEL, ETC.)

No.	Description
1	Again, On-board Roller's GPS had problem couple of times and it caused delay in compaction progress

PROJECT VISITORS

MD DOT	Dan Sajedi, Raj Chavan, Bob Kochen

REMARKS

Staff Names:	
UD Team	Dr. Meehan, Faraz, Majid, Yeuru, Fan, Farshid, Baris
Del DOT	Al Strauss, Tyrone Nelson, Tony Marcozzi
Caterpillar	Aj Lee, Dick Costello, Mario Souraty, Nick Oetken
Humboldt	Adam Houghton
Kessler	Ken Kessler
Greggo & Ferrara	Dave McQuiry

PREPARED BY: Farshid Vahedifard and Faraz S.Tehrani

University of Delaware

Departmenet of Civil and Environmental Engineering

DAILY PROGRESS REPORT (PAGE 5 / 10)

Project Title:	Investigation of CCC Technology		
Date:	Wednesday 7/23/2008	Site:	Burrice Pit (Odessa)
Start Time:	6:00	End Time:	18:50
Weather:	Sunny, some rain in afternoon	Temp.:	29 C (85 F)

NUMBER OF PERSONNEL

Organization/Contractor/Subcontractor	Hours	Supervisors	Staff Engineers	Technicians	Truck Drivers	Labors	Trainees		
University of Delaware/Geotech. Group	6:00-18:50	1	6						
Del DOT		1		2					
Caterpillar & Ransome Dealership		1	3		1				
Greggo & Ferrara Inc					1				
Kessler Soils Engineering Products, Inc.		1							
Humboldt				1					

NUMBER OF MAJOR MACHINES AND EQUIPMENTS

Organization/Contractor/Subcontractor	Type & Number
Caterpillar & Ransome Dealership	1 Dozer D56K, 1 Wheel Loader 980H, 1 Roller CS56, 1 GPS Rover, 1 DCP, 1 LWD
Del DOT	2 Nuclear Gauge
Humboldt	1 EDG, 1 GeoGauge
Greggo & Ferrara Inc	1 Wheel Loader 924H, 1 Water Truck
Kessler Soils Engineering Products, Inc.	2 LWD's plus one DCP
University of Delaware/Geotech. Group	Sand Cone Supplies, Level, Misc Other Supplies

DESCRIPTION OF WORK & ACTIVITY

Hours		Description
6:00	6:54	Meet on campus, load van and depart UD, pick up Farshid then Adam
7:20	7:40	Arrive on site, unload van
8:00	8:20	In situ testing on second lift (on centerline location) (repeated tests runs on this lift after last night rain)
8:00	8:18	LWD small (200mm dia.) and large (300 mm dia.) in 5 pts by Farshid and Baris and Faraz and Adam(St. 0+10, 0+50, ..,1+70)
8:16		GeoGauge tests by Yueru and Majid in 5 pts on the second layer (St. 0+10, 0+50, ..,1+70)
8:20	9:13	Spreading third lift in the test pad
8:43		GPS back on-line
9:15		Dozer grading side slopes of fill area
		(GPS Rover not used to shoot test locations due to equipment problems, CHECK LOCATION WITH DATA SHE
		2 Nuc. test on uncompacted fill from spreading, freshly made stockpile (DD=110.9, WD=120.1, m%+8.2)
		(DD=110.9, WD=120.1, m%+8.2 for 0+50 and DD=110.9, WD=120.1, m%+8.2 for St. 1+50)
10:11	10:15	2 passes water truck
10:21	11:46	Roller started running on third lift (loose elv. 202.4)
10:21		1st pass Max. Amplitude (1.8 mm), 4 more passes low amplitude (0.8 mm)
10:56		6th pass no vibration
11:03		7th pass low vibration
11:32		8th pass, proof roll, low amplitude vibration (CMV)
11:41		9th pass proof roll, no vibration (MDP)
11:45	13:40	In situ testing on third lift (on centerline location)

University of Delaware
Departmenet of Civil and Environmental Engineering
DAILY PROGRESS REPORT (PAGE 6 / 10)

Date: Wednesday 7/23/2008

DESCRIPTION OF WORK CONTINUED

Hours		Description
11:45	13:00	LWD small (200mm dia.) and large (300 mm dia.) in 19 pts by Farshid and Baris (St. 0+8, 0+18, ..,1+88)
12:01	13:15	GeoGauge tests by Yueru and Majid in 19 pts on the third layer (St. 0+8, 0+18, ..,1+88)
		Nuclear gauge tests by Tony (Del DOT) in 10 pts on the third layer (St. 0+8, 0+28, …, 1+88)
12:16	13:17	DCP tests by Faraz and Fan in 19 pts on the third layer (St. 0+8, 0+18, ..,1+88)
		EDG tests by Adam (Humboldt) at 10 pts on the third layer (St. 0+8, 0+28, …, 1+88)
		Sand Cone tests by Yueru and Majid in 3 points on the third layer (St. 1+00) - check data points here
13:36	13:46	GPS Rover shooting for test locations, 3rd lift, final pass (see attached)
14:10		1 pass water truck
14:12	15:13	Spreading fourth lift in the test pad by Dozer
14:42		GPS on dozer down again
15:21		1 pass water truck
15:24	16:28	Roller started running on fourth lift (loose elv. 203.1)
15:24		1st pass Max. Amplitude (1.8 mm), 4 more passes low amplitude (0.8 mm)
15:53		6th pass no vibration
15:59		7th pass low vibration
16:13		8th pass proof roll, no vibration (MDP)
16:22		9th pass, proof roll, low amplitude vibration (CMV)
16:38	18:10	In situ testing on fourth lift (on centerline location)
16:40	17:50	LWD small (200mm dia.) and large (300 mm dia.) in 19 pts by Farshid and Baris (St. 0+14, 0+24, ..,1+94)
16:54		GeoGauge tests by Yueru and Majid in 19 pts on the fourth layer (St. 0+14, 0+24, ..,1+94)
		Nuclear gauge tests by Tony (Del DOT) at 5 pts on the fourth layer (St. 0+14, 0+54, ..,1+74)
17:14	18:04	DCP tests by Faraz and Fan in 19 pts on the fourth layer (St. 0+14, 0+24, ..,1+94)
		EDG tests by Adam (Humboldt) at 5 pts on the fourth layer (St. 0+14, 0+54, ..,1+74)
16:38	16:50	GPS Rover shooting for test locations, 4th lift, final pass (see attached)
18:05		Taking 5 bucket samples for 5-pts proctor tests from St.0+14, 0+54, 0+94,1+34 and 1+74
18:30		Leave site
18:50		Arrive in campus, unload van and schedule for next day

EFFECTS ON WORK (WEATHER, ACCIDENTS, BREAKDOWNS, DELAYS, PERSONNEL, ETC.)

No.	Description
1	Again, On-board Roller's GPS had problem couple of times and it caused delay in compaction progress
2	Some rain in afternoon (15:30)

PROJECT VISITORS

REMARKS

Staff Names:	
UD Team	Dr. Meehan, Faraz, Majid, Yeuru, Fan, Farshid, Baris
Del DOT	Al Strauss, Richard Taylor, Tony Marcozzi
Caterpillar	Aj Lee, Dick Costello, Mario Souraty, Nick Oetken
Humboldt	Adam Houghton
Kessler	Ken Kessler
Greggo & Ferrara	Dave McQuiry

PREPARED BY: Farshid Vahedifard and Faraz S.Tehrani

University of Delaware
Departmenet of Civil and Environmental Engineering
DAILY PROGRESS REPORT (PAGE 7 / 10)

Project Title:	Investigation of CCC Technology		
Date:	Thursday 7/24/2008	Site:	Burrice Pit (Odessa)
Start Time:	6:00	End Time:	20:20
Weather:	Sunny, some cloudy in afternoon	Temp.:	28 C (82 F)

NUMBER OF PERSONNEL

Organization/Contractor/Subcontractor	Hours	Supervisors	Staff Engineers	Technicians	Truck Drivers	Labors	Trainees		
University of Delaware/Geotech. Group	6:00-20:20	1	6						
Del DOT		1		2					
Caterpillar & Ransome Dealership		1	3		1				
Greggo & Ferrara Inc					1				
Kessler Soils Engineering Products, Inc.		1							
Humboldt				1					

NUMBER OF MAJOR MACHINES AND EQUIPMENTS

Organization/Contractor/Subcontractor	Type & Number
Caterpillar & Ransome Dealership	1 Dozer D56K, 1 Wheel Loader 980H, 1 Roller CS56, 1 GPS Rover, 1 DCP, 1 LWD
Del DOT	2 Nuclear Gauge
Humboldt	1 EDG, 1 GeoGauge
Greggo & Ferrara Inc	1 Wheel Loader 924H, 1 Water Truck
Kessler Soils Engineering Products, Inc.	1LWD
University of Delaware/Geotech. Group	Sand Cone Supplies, Level, Misc Other Supplies

DESCRIPTION OF WORK & ACTIVITY

Hours		Description
6:00	6:57	Meet on campus, load van and depart UD, pick up Adam, gas station
7:23	7:40	Arrive on site, unload van
7:25	8:10	Drain ponded water due to last night heavy rain with shovel, taking photo
8:24	9:10	In situ testing on fourth lift (off+2'R) (second run of testing on this lift after last night rain)
8:25		LWD small (200mm dia.) and large (300 mm dia.) in 5 pts by Farshid and Baris (St. 0+14, 0+54, ..,1+74)
8:25	8:50	GeoGauge tests by Yueru and Majid in 5 pts on the fourth layer (St. 0+14, 0+54, ..,1+74)
		Nuclear gauge tests by Tony (Del DOT) in 5 pts on the fourth layer (St. 0+14, 0+34, ..,1+94)
8:45	8:59	DCP tests by Faraz and Fan in 5 pts on the fourth layer (St. 0+14, 0+54, ..,1+74)
		EDG tests by Adam (Humboldt) in 5 pts on the fourth layer (St. 0+14, 0+54, ..,1+74)
		GPS Rover shooting for test locations, 4th lift, final pass after heavy rain (see attached)
8:35		Al Strauss took two fry pan water contents from stockpile (freshly mixed: 10.7, mixed yesterday: 11.9)
8:57		GPS rover used to shoot test points
9:50		Dr Meehan and Baris left job site to buy buckets and water
9:24	10:23	Spreading fifth lift in the test pad by Dozer
10:59	11:07	3 passes water truck
11:09		Roller started running on fifth lift (loose elv. 203.1)
11:09	11:17	1st pass high amplitude (1.8 mm) on fifth layer
		In situ testing on fifth lift, first pass (CL)
11:10	11:37	LWD small (200mm dia.) and large (300 mm dia.) in 5 pts by Farshid and Baris (St. 0+10, 0+50, ..,1+70)
11:26		GeoGauge tests by Yueru and Majid in 5 pts (St. 0+10, 0+50, ..,1+70)
		Nuclear gauge tests by Tony (Del DOT) in 5 pts (St. 0+10, 0+50, ..,1+70)
11:32	11:49	DCP tests by Faraz and Fan in 5 pts (St. 0+10, 0+50, ..,1+70)
		EDG tests by Adam (Humboldt) in 5 pts (St. 0+10, 0+50, ..,1+70)
		GPS Rover shooting for test locations, 5th lift, first pass (see attached)
12:13	12:19	2nd pass low amplitude (0.8 mm) on fifth layer
12:20		In situ testing on fifth lift, second pass (off+2'L)

University of Delaware
Departmenet of Civil and Environmental Engineering
DAILY PROGRESS REPORT (PAGE 8 / 10)

Date: Thursday 7/24/2008

DESCRIPTION OF WORK CONTINUED

Hours		Description
12:20	12:45	LWD small (200mm dia.) and large (300 mm dia.) in 5 pts by Farshid and Baris (St. 0+10, 0+50, ..,1+70)
12:31	12:52	GeoGauge tests by Yueru and Majid in 5 pts (St. 0+10, 0+50, ..,1+70)
		Nuclear gauge tests by Tony (Del DOT) in 5 pts (St. 0+10, 0+50, ..,1+70)
12:40	12:56	DCP tests by Faraz and Fan in 5 pts (St. 0+10, 0+50, ..,1+70)
		EDG tests by Adam (Humboldt) in 5 pts (St. 0+10, 0+50, ..,1+70)
12:00	12:10	GPS Rover shooting for test locations, 5th lift, 2nd pass (see attached)
13:14	13:20	3rd pass of Roller on fifth layer with low amplitude (0.8 mm)
13:38	14:40	In situ testing on fifth lift, third pass (off+2R)
13:40	14:05	LWD small (200mm dia.) and large (300 mm dia.) in 5 pts by Farshid and Baris (St. 0+10, 0+50, ..,1+70)
13:40	14:12	GeoGauge tests by Yueru and Majid in 5 pts (St. 0+10, 0+50, ..,1+70)
		Nuclear gauge tests by Tony (Del DOT) in 5 pts (St. 0+10, 0+50, ..,1+70)
13:56	14:16	DCP tests by Faraz and Fan in 5 pts (St. 0+10, 0+50, ..,1+70)
		EDG tests by Adam (Humboldt) in 5 pts (St. 0+10, 0+50, ..,1+70)
		GPS Rover shooting for test locations, 5th lift, 3rd pass (see attached)
14:45	16:00	OPEN HOUSE
14:50	15:13	4th and 5th passes of Roller on fifth layer with low amplitude (0.8 mm)
15:20	16:10	In situ testing on fifth lift, fifth pass (off+2R, see attached)
15:23	15:45	LWD small (200mm dia.) and large (300 mm dia.) in 5 pts by Farshid and Baris (St. 0+12, 0+52, ..,1+72)
		GeoGauge tests by Yueru and Majid in 5 pts (St. 0+12, 0+52, ..,1+72)
		Nuclear gauge tests by Tony (Del DOT) in 5 pts (St. 0+12, 0+52, ..,1+72)
15:34	15:54	DCP tests by Faraz and Fan in 5 pts (St. 0+12, 0+52, ..,1+72)
		EDG tests by Adam (Humboldt) in 5 pts (St. 0+12, 0+52, ..,1+72)
		GPS Rover shooting for test locations, 5th lift, 5th pass (see attached)
16:16	16:28	6th pass of Roller on fifth layer w/o vibration and 7th pass with low amplitude (0.8 mm)
16:30	19:15	In situ testing on fifth lift, seventh pass (off+2L)
16:50	18:23	LWD small (200mm dia.) and large (300 mm dia.) in 19 pts by Farshid and Baris (St. 0+12, 0+22, ..,1+92)
17:00	18:23	GeoGauge tests by Yueru and Majid in 19 pts (St. 0+12, 0+22, ..,1+92)
		Nuclear gauge tests by Tony (Del DOT) in 10 pts (St. 0+12, 0+32, ..,1+92)
17:16	18:39	DCP tests by Faraz and Fan in 19 pts (St. 0+12, 0+22, ..,1+92)
		EDG tests by Adam (Humboldt) in 10 pts (St. 0+12, 0+32, ..,1+92)
17:00	17:15	GPS Rover shooting for test locations, 5th lift, 7th pass, final pass (see attached)
		Sand Cone test by Yueru and Majid in 1 point (St. 1+00) - check this data later
		Found large rock (photos taken) at St.0+32 test location for final lift
19:10		Taking 5 bucket samples for 5-pts proctor tests from St.0+12, 0+52, 0+92,1+32 and 1+72
19:30		load van and leave site
20:20		Arrive in campus, unload van and schedule for next day

EFFECTS ON WORK (WEATHER, ACCIDENTS, BREAKDOWNS, DELAYS, PERSONNEL, ETC.)

No.	Description
1	On-board Roller's GPS had problem couple of times and it caused delay in compaction progress

PROJECT VISITORS

This day, as announced before, open house was held in afternoon. 15-20 participants from Del DOT, MD DOT, contractors attended talks by Dr. Meehan Aj Lee and Ken Kessler about IC technology, undertaken research plan and goals, in-situ tests, used equipments and machines and etc.

REMARKS

Staff Names:

UD Team	Dr. Meehan, Faraz, Majid, Yeuru, Fan, Farshid, Baris
Del DOT	Al Strauss, Tyrone Nelson, Tony Marcozzi
Caterpillar	Aj Lee, Dick Costello, Mario Souraty, Nick Oetken
Humboldt	Adam Houghton
Kessler	Ken Kessler
Greggo & Ferrara	Dave McQuiry

PREPARED BY: Farshid Vahedifard and Faraz S.Tehrani

University of Delaware
Departmenet of Civil and Environmental Engineering
DAILY PROGRESS REPORT (PAGE 9 / 10)

Project Title:	Investigation of CCC Technology		
Date:	Friday 7/25/2008	Site:	Burrice Pit (Odessa)
Start Time:	6:20	End Time:	14:00
Weather:	Sunny	Temp.:	31 C (87 F)

NUMBER OF PERSONNEL

Organization/Contractor/Subcontractor	Hours	Supervisors	Staff Engineers	Technicians	Truck Drivers	Labors	Trainees		
University of Delaware/Geotech. Group	6:20-14:00	1	1						
Del DOT		1		2					
Caterpillar & Ransome Dealership		1	3		1				
Greggo & Ferrara Inc		1			1				
Kessler Soils Engineering Products, Inc.		1							
Humboldt				1					

NUMBER OF MAJOR MACHINES AND EQUIPMENTS

Organization/Contractor/Subcontractor	Type & Number
Caterpillar & Ransome Dealership	1 Dozer D56K, 1 Wheel Loader 980H, 1 Roller CS56, 1 GPS Rover, 1 DCP, 1 LWD
Del DOT	2 Nuclear Gauge
Humboldt	1 EDG, 1 GeoGauge
Greggo & Ferrara Inc	1 Wheel Loader 924H, 1 Water Truck
Kessler Soils Engineering Products, Inc.	1LWD
University of Delaware/Geotech. Group	Sand Cone Supplies, Level, Misc Other Supplies
MD DOT	FWD

DESCRIPTION OF WORK & ACTIVITY

Hours		Description
6:20	7:12	Meet on campus, load van and depart UD, pick up Adam
7:50	8:00	Arrive on site, unload van
8:34	9:00	FWD testing by Dr Meehan and Faraz in 5pts on fifth layer (St. 0+16, 0+56, 0+96, 1+36, 1+76 CL) on 7/7
9:00	10:12	FWD testing by Dr Meehan and Faraz in 15pts on fifth layer (St. 0+16, 0+56, 0+96, 1+36, 1+76 CL+5'L & 5'R)
		LWD testing by Faraz and Adam
10:27	11:32	Nuclear gauge tests by Tony (Del DOT) in 5 pts on the fifth layer (St. 0+16, 0+56, ..,1+76 CL)
		DCP testing by Faraz and Adam
		EDG tests by Adam (Humboldt) in 5 pts on the fifth layer (St. 0+16, 0+56, ..,1+76 CL)
		GPS Rover shooting for FWD test locations, 5th lift, no additional passes from 7-24-08 (see attached)
11:30		Taking 5 bucket samples at St.0+16, 0+56, …, 1+76 CL and gave to CJ to take to Dan Sajedi for Resilient Modulus tests
11:35		Taking 5 bag samples for sieve and moisture testsat St.0+16, 0+56, …, 1+76 CL
		Back-filed holes and tumped with foot and shovel
11:35		Roller proof, no vibration (MDP) again on fifth lift - 5th lift, 8th pass
		Roller proof, low amplitude vibration (CMV) - 5th lift, 9th pass
12:20		Leave site, Cat packing up their equipment, roller still on site
13:50		Drop off Adam
14:00		Arrive in campus, unload van

University of Delaware

Departmenet of Civil and Environmental Engineering

DAILY PROGRESS REPORT (PAGE 10 / 10)

Date: Friday 7/25/2008

DESCRIPTION OF WORK CONTINUED

Hours		Description

EFFECTS ON WORK (WEATHER, ACCIDENTS, BREAKDOWNS, DELAYS, PERSONNEL, ETC.)

No.	Description

PROJECT VISITORS

MD DOT CJ Swank

REMARKS

Staff Names:

UD Team	Dr. Meehan, Faraz
Del DOT	Al Strauss, Richard Taylor, Tony Marcozzi
Caterpillar	Aj Lee, Jeff Ogborn
Humboldt	Adam Houghton
Greggo & Ferrara	Jim Reynolds, Dave McQuiry

PREPARED BY: Farshid Vahedifard and Faraz S.Tehrani

Test Locations

Station	North (ft)	East (ft)	Elevation (ft)	Lift - Pass	Date	Time	
						Start	End
East1	6006.879	6019.335	201.03	Locations of Grade Stakes			
East2	5997.995	6022.828	201.139				
East3	5980.117	6030.636	201.78				
East4	5960.82	6037.454	201.864				
East5	5942.143	6044.694	201.931				
East6	5923.847	6051.95	201.826				
East7	5914.673	6055.872	201.869				
East8	5905.289	6059.248	201.874				
East9	5886.787	6066.885	202				
East10	5868.228	6074.313	201.643				
East11	5849.535	6081.613	201.958				
East12	5830.926	6088.876	201.429				
East13	5821.7	6092.624	201.851				
West1	6000	6000	201.769				
West2	5991.119	6003.556	201.799				
West3	5972.699	6010.72	201.694				
West4	5953.828	6017.272	201.603				
West5	5935.049	6024.431	201.729				
West6	5916.272	6031.214	201.761				
West7	5907.09	6035.328	201.352				
West8	5897.768	6038.77	201.641				
West9	5879.306	6045.767	201.185				
West10	5860.972	6052.791	201.164				
West11	5842.153	6060.813	201.466				
West12	5813.847	6070.224	201.643				
West13	5823.032	6067.149	201.852				
8	5996.138	6012.826	201.821	2 - 6/6	7/22/2008	16:30	16:45
18	5988.470	6015.011	201.900				
28	5978.539	6018.310	201.858				
38	5968.723	6022.114	201.992				
48	5959.789	6025.649	201.867				
58	5949.616	6029.133	201.975				
68	5940.718	6032.732	201.950				
78	5931.380	6036.593	201.872				
88	5923.014	6039.975	201.853				
98	5912.801	6043.927	201.941				
108	5903.900	6047.509	201.746				
118	5894.148	6051.429	201.878				
128	5885.445	6054.800	201.865				
138	5876.060	6058.748	201.909				
148	5865.836	6062.681	201.894				
158	5857.135	6066.867	201.878				
168	5847.074	6070.051	201.803				
178	5838.358	6073.607	201.840				
188	5828.158	6076.791	201.949				

Station	North (ft)	East (ft)	Elevation (ft)	Lift - Pass	Date	Time	
						Start	End
8	5996.138	6012.826	201.821	3 - 8/8	7/23/2008	13:36	13:46
18	5988.470	6015.011	201.900				
28	5978.539	6018.310	201.858				
38	5968.723	6022.114	201.992				
48	5959.789	6025.649	201.867				
58	5949.616	6029.133	201.975				
68	5940.718	6032.732	201.950				
78	5931.380	6036.593	201.872				
88	5923.014	6039.975	201.853				
98	5912.801	6043.927	201.941				
108	5903.900	6047.509	201.746				
118	5894.148	6051.429	201.878				
128	5885.445	6054.800	201.865				
138	5876.060	6058.748	201.909				
148	5865.836	6062.681	201.894				
158	5857.135	6066.867	201.878				
168	5847.074	6070.051	201.803				
178	5838.358	6073.607	201.840				
188	5828.158	6076.791	201.949				
14	5989.827	6014.218	202.476	4 - 9/9	7/23/2008	16:38	16:50
24	5980.551	6017.080	202.500				
34	5971.771	6021.123	202.489				
44	5962.335	6024.469	202.404				
54	5952.731	6028.622	202.424				
64	5942.894	6031.128	202.536				
74	5933.865	6034.890	202.489				
84	5924.683	6038.638	202.455				
94	5915.294	6041.845	202.457				
104	5906.255	6045.689	202.537				
114	5897.024	6049.084	202.509				
124	5887.838	6052.993	202.504				
134	5878.244	6056.377	202.476				
144	5869.160	6059.732	202.449				
154	5859.983	6063.308	202.501				
164	5850.868	6066.769	202.479				
174	5841.951	6070.456	202.424				
184	5832.493	6073.957	202.459				
194	5823.405	6078.179	202.410				
10	5989.366	6012.290	202.485	4 - 9/9	7/24/2008	-	-
50	5951.641	6026.522	202.460				
90	5914.554	6040.244	202.489				
130	5877.159	6054.205	202.435				
170	5839.408	6069.148	202.441				

Station	North (ft)	East (ft)	Elevation (ft)	Lift - Pass	Date	Time	
						Start	End
10	5994.148	6013.437	203.037	5 - 1/7	7/24/2008	-	-
50	5957.186	6027.309	202.996				
90	5919.944	6041.571	203.024				
130	5882.489	6056.511	202.981				
170	5845.554	6070.002	202.977				
10	5994.356	6014.461	203.047	5 - 2/7	7/24/2008	-	-
50	5958.122	6028.766	203.112				
90	5920.359	6043.398	203.150				
130	5882.675	6058.249	203.071				
170	5846.248	6071.917	203.063				
10	5993.499	6011.004	203.053	5 - 3/7	7/24/2008	-	-
50	5956.737	6025.548	203.027				
90	5919.426	6039.734	203.036				
130	5882.039	6054.335	203.011				
170	5845.428	6067.985	203.015				
12	5991.812	6011.421	202.867	5 - 5/7	7/24/2008	-	-
52	5955.079	6026.361	203.076				
92	5917.333	6040.037	202.961				
132	5880.376	6055.100	202.980				
172	5843.484	6068.615	202.901				
12	5992.753	6014.994	202.893	5 - 7/7	7/24/2008	-	-
22	5983.875	6017.953	204.050				
32	5974.219	6021.290	203.941				
42	5964.703	6025.386	203.999				
52	5955.149	6028.727	203.948				
62	5945.794	6032.322	203.989				
72	5936.577	6036.014	203.896				
82	5927.577	6039.806	204.023				
92	5918.188	6043.372	203.936				
102	5908.865	6047.124	203.975				
112	5899.626	6050.812	203.962				
122	5890.218	6054.279	203.946				
132	5880.428	6057.956	203.957				
142	5871.481	6061.417	203.925				
152	5862.209	6064.768	203.969				
162	5852.645	6068.763	203.950				
172	5843.442	6072.039	203.921				
182	5833.974	6075.598	203.943				
192	5824.759	6079.331	203.991				

Appendix B

MDP AND CMV MEASUREMENTS

This appendix contains figures that demonstrate the variation of MDP and CMV measurements for each lift and pass on three parallel lanes, as referred to in Chapter 5. Note that in the left lane of Lift 4, Pass 9/9 (Figure B.4) the GPS signal was lost for a short period of time and the corresponding MDP and CMV values were not recorded.

The “KP” points shown on the “Middle Lane” roller transects in the following Appendix pages correspond to the kriged MDP and CMV values at each of the corresponding in situ test point locations. These values are the ones that were used and the univariate and multivariate regression analyses discussed in Chapters 7 and 8.

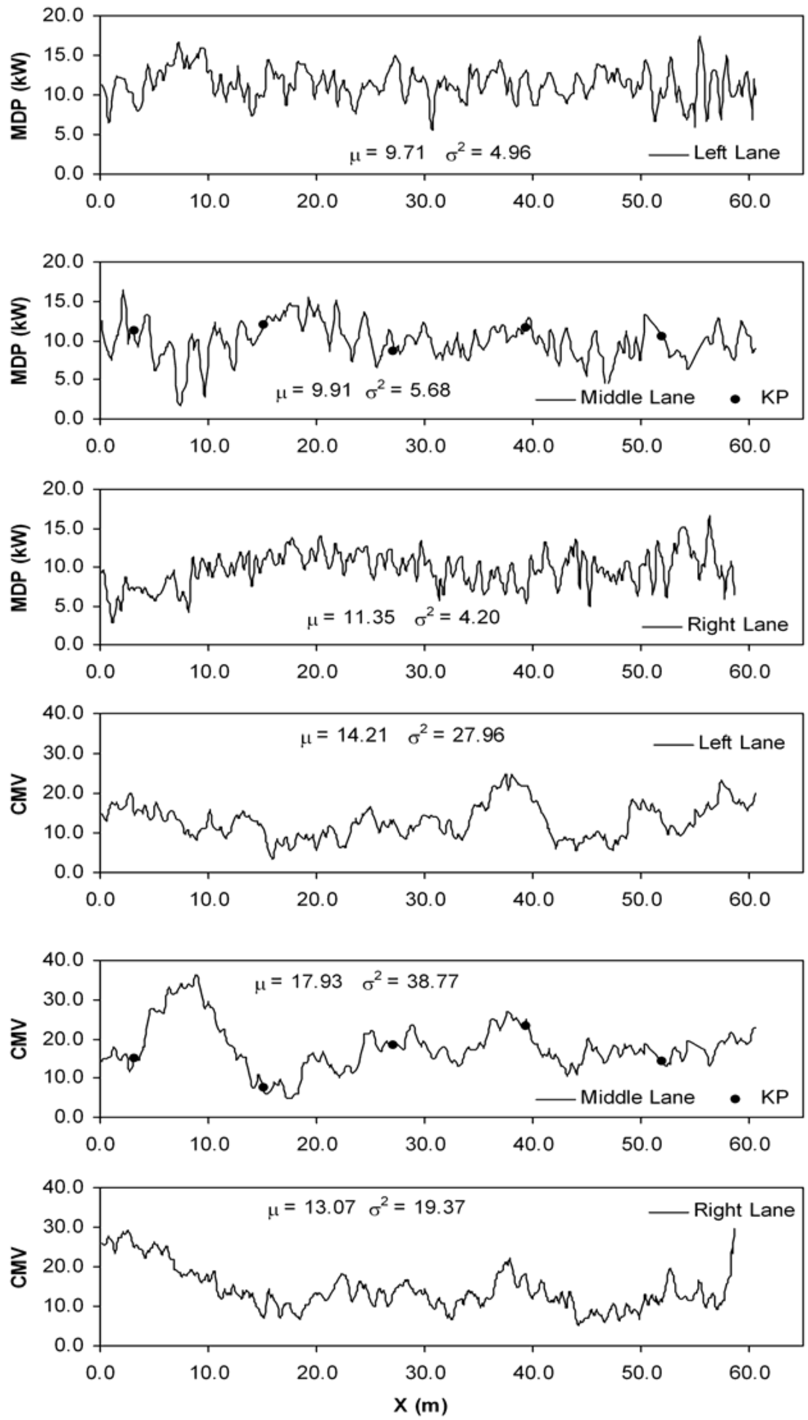

Figure B.1 Variation of CCC values for Base Layer, Pass 2/2

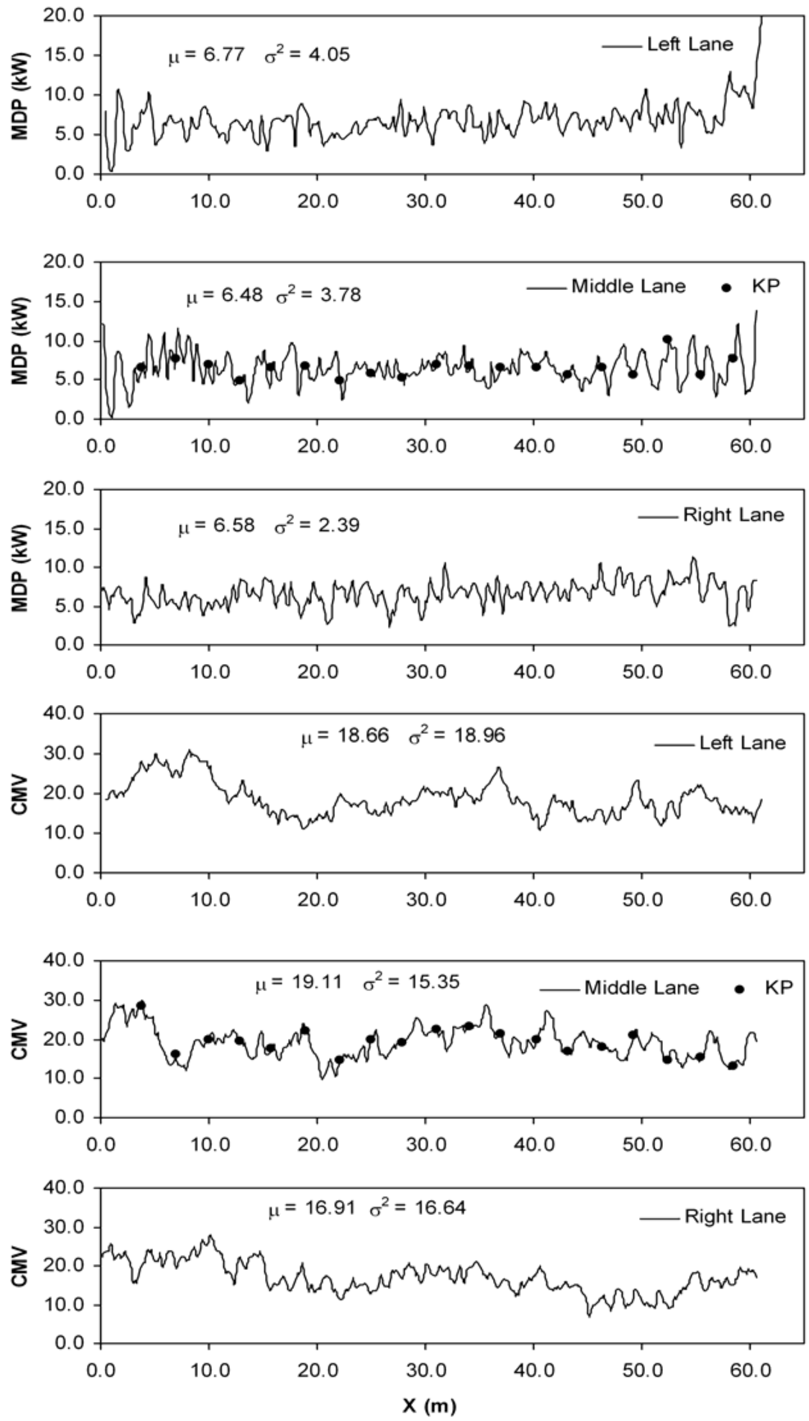

Figure B.2 Variation of CCC values for Lift 2, Pass 6/6

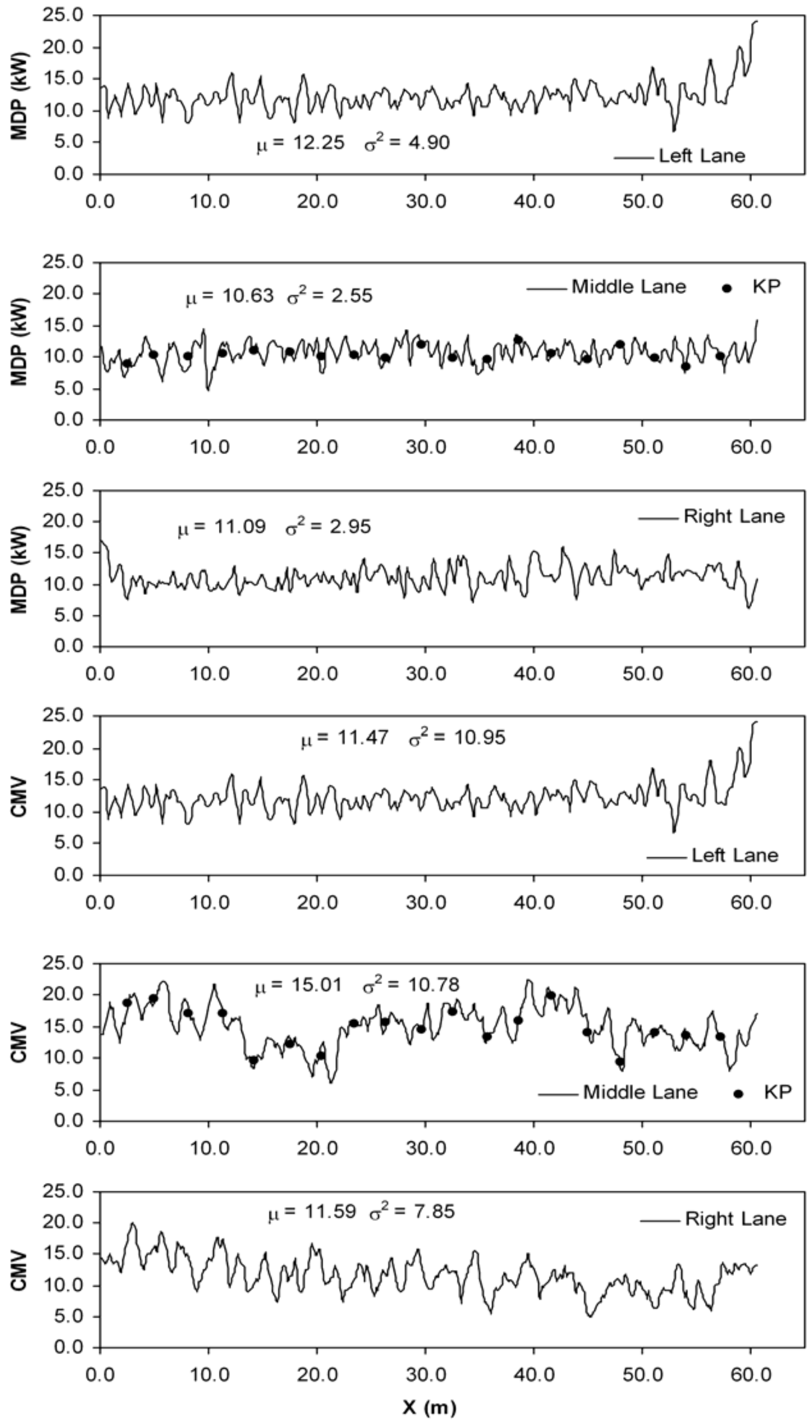

Figure B.3 Variation of CCC values for Lift 3, Pass 8/8

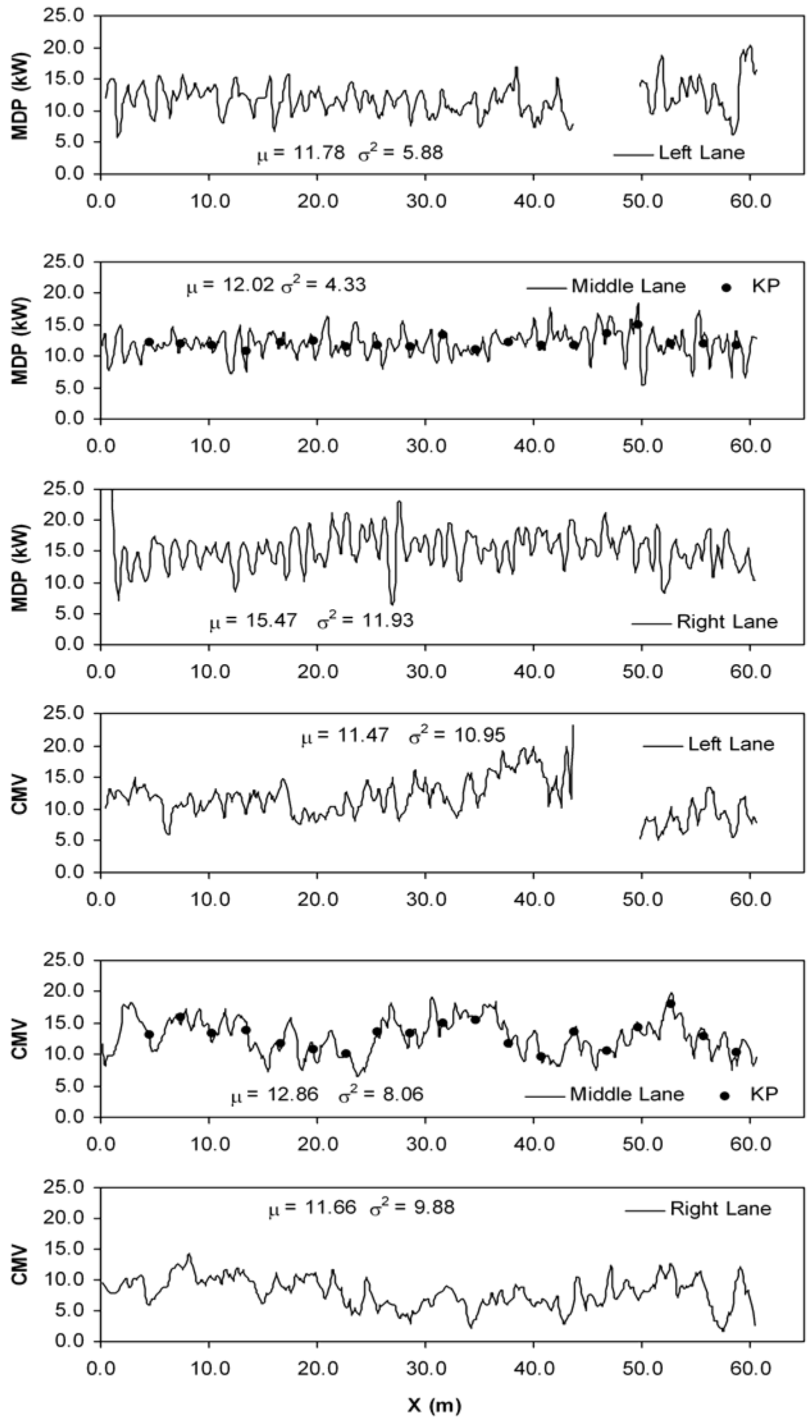

Figure B.4 Variation of CCC values for Lift 4, Pass 9/9

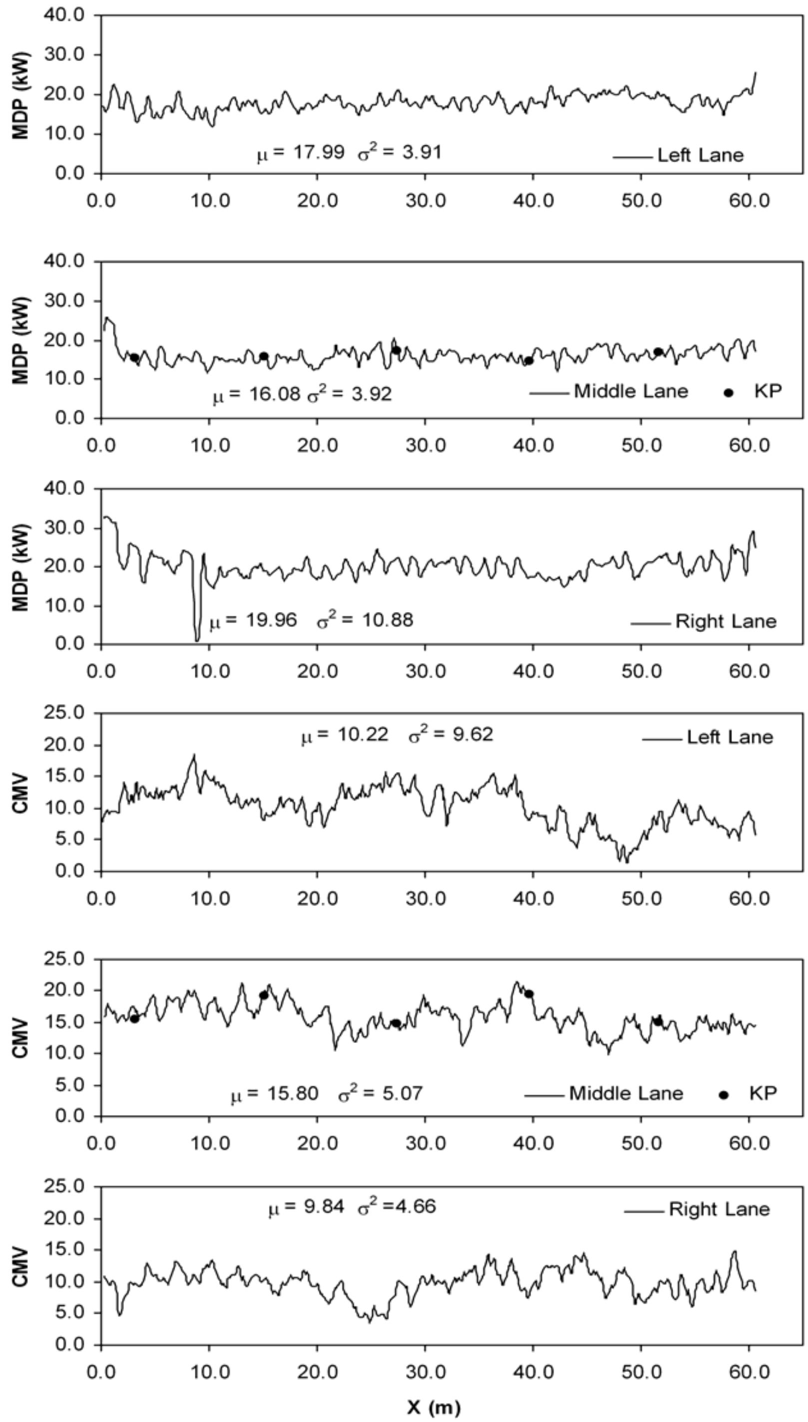

Figure B.5 Variation of CCC values for Lift 5, Pass 1/7

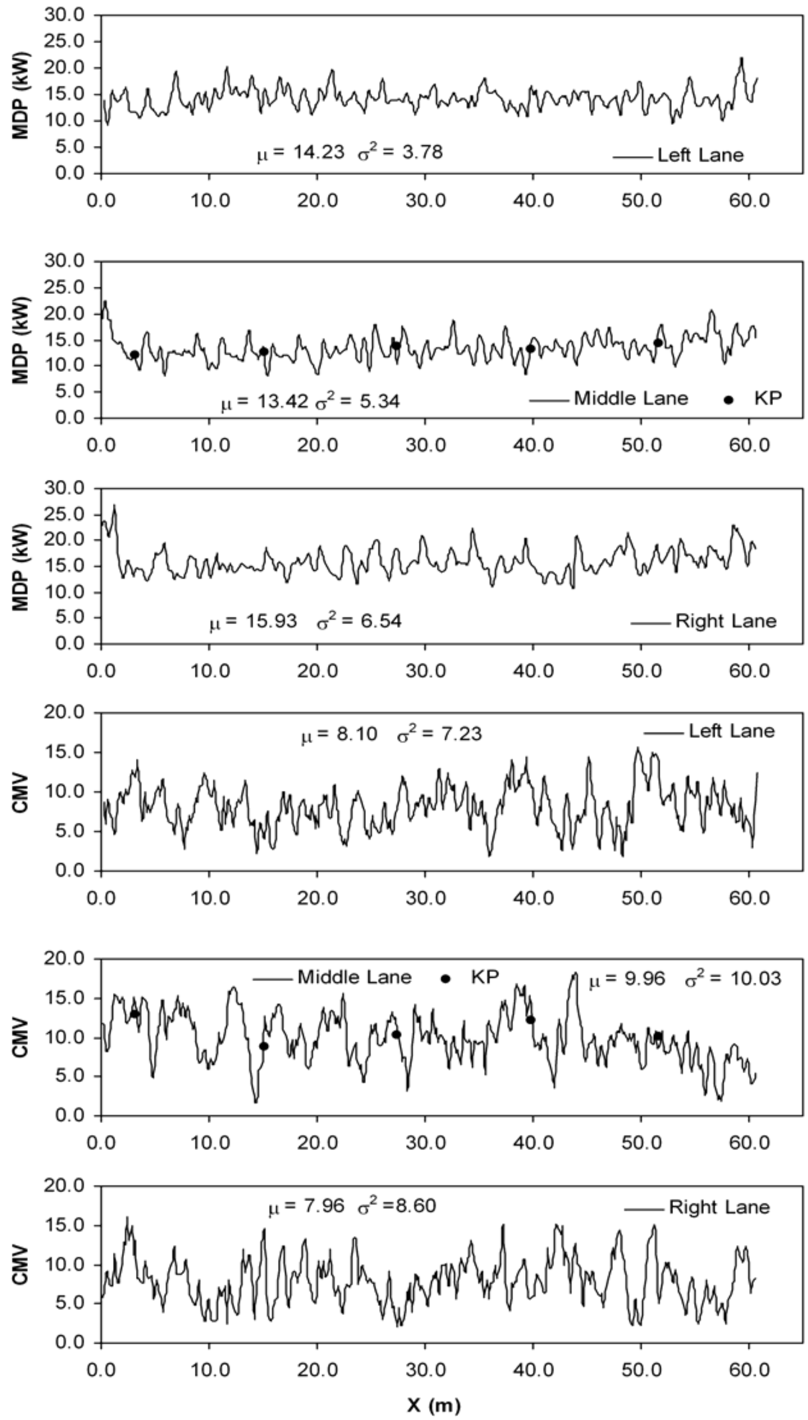

Figure B.6 Variation of CCC values for Lift 5, Pass 2/7

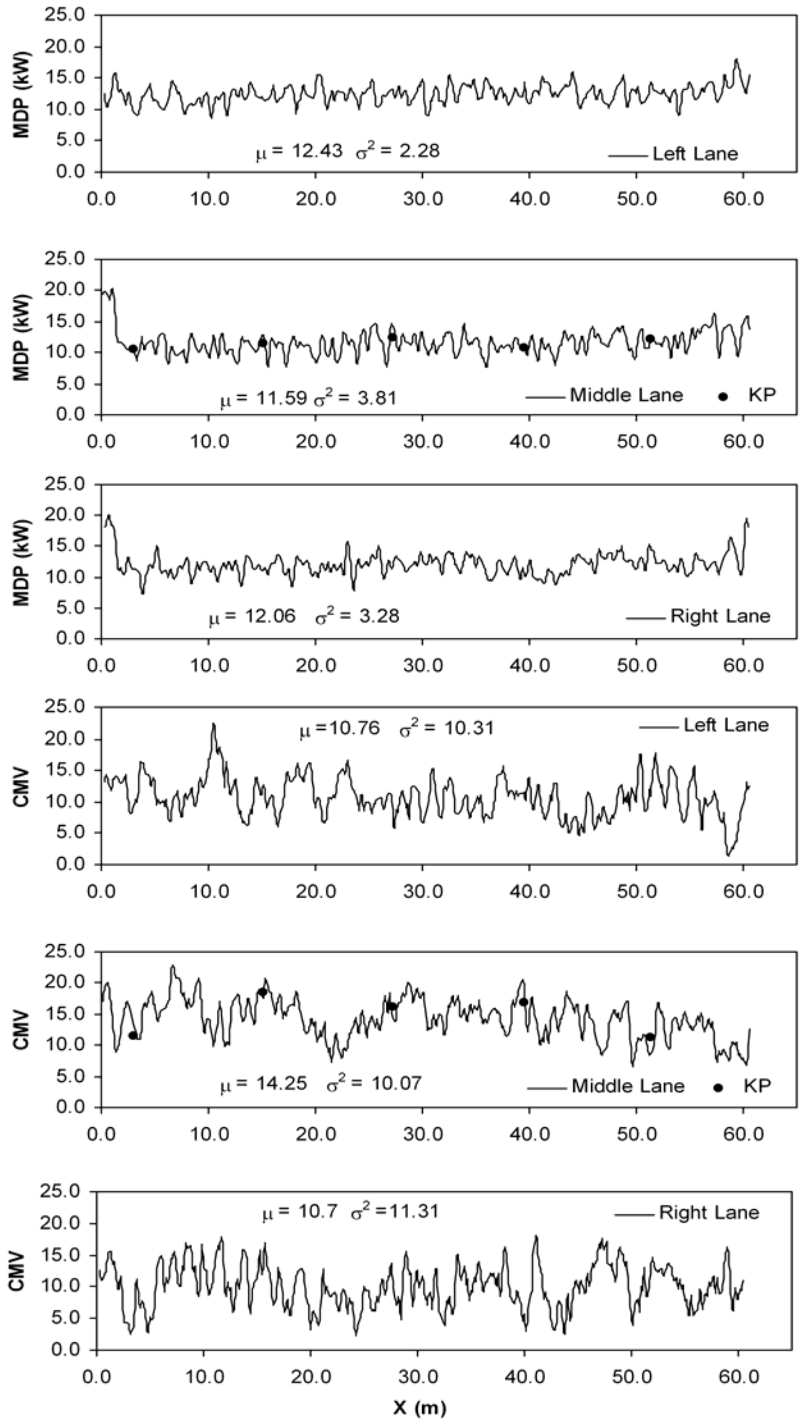

Figure B.7 Variation of CCC values for Lift 5, Pass 3/7

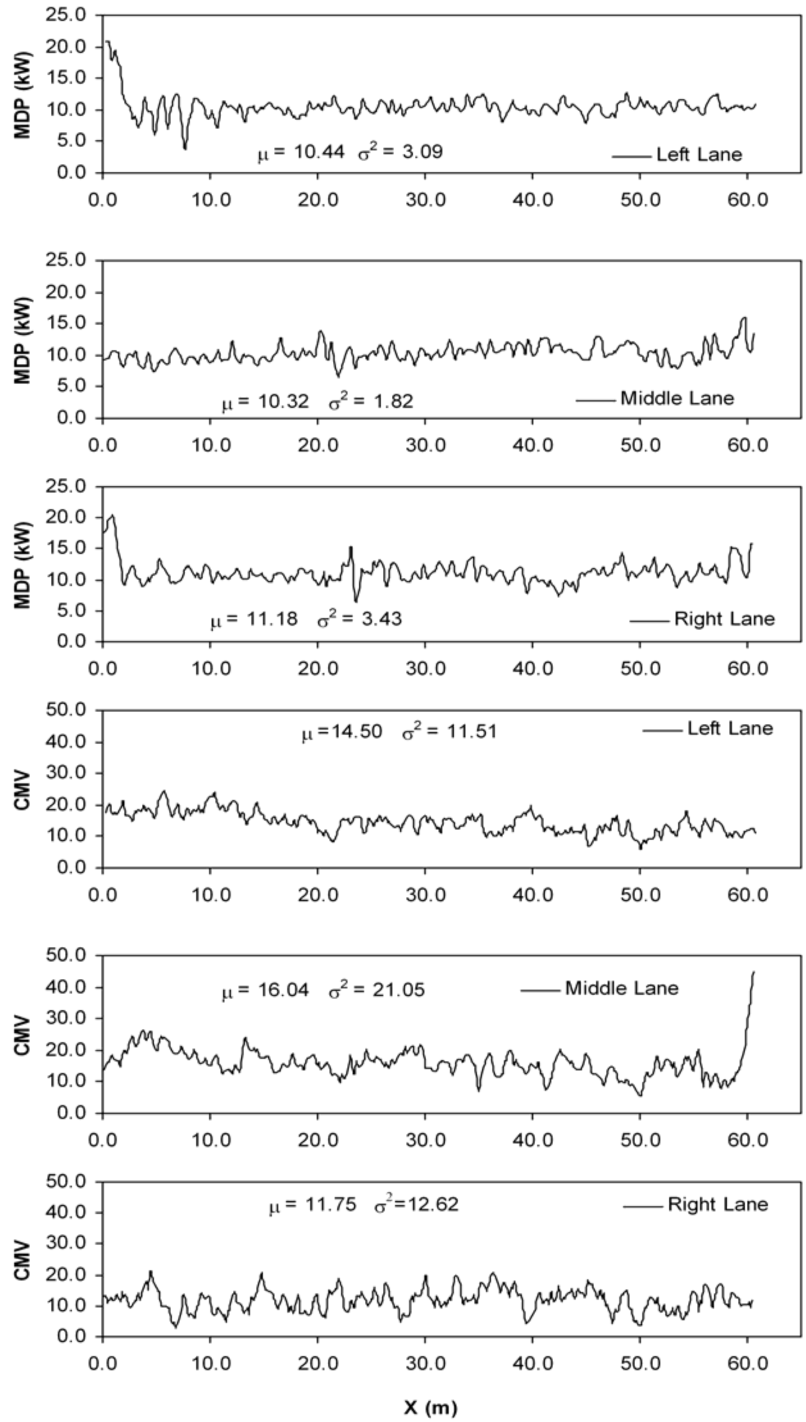

Figure B.8 Variation of CCC values for Lift 5, Pass 4/7

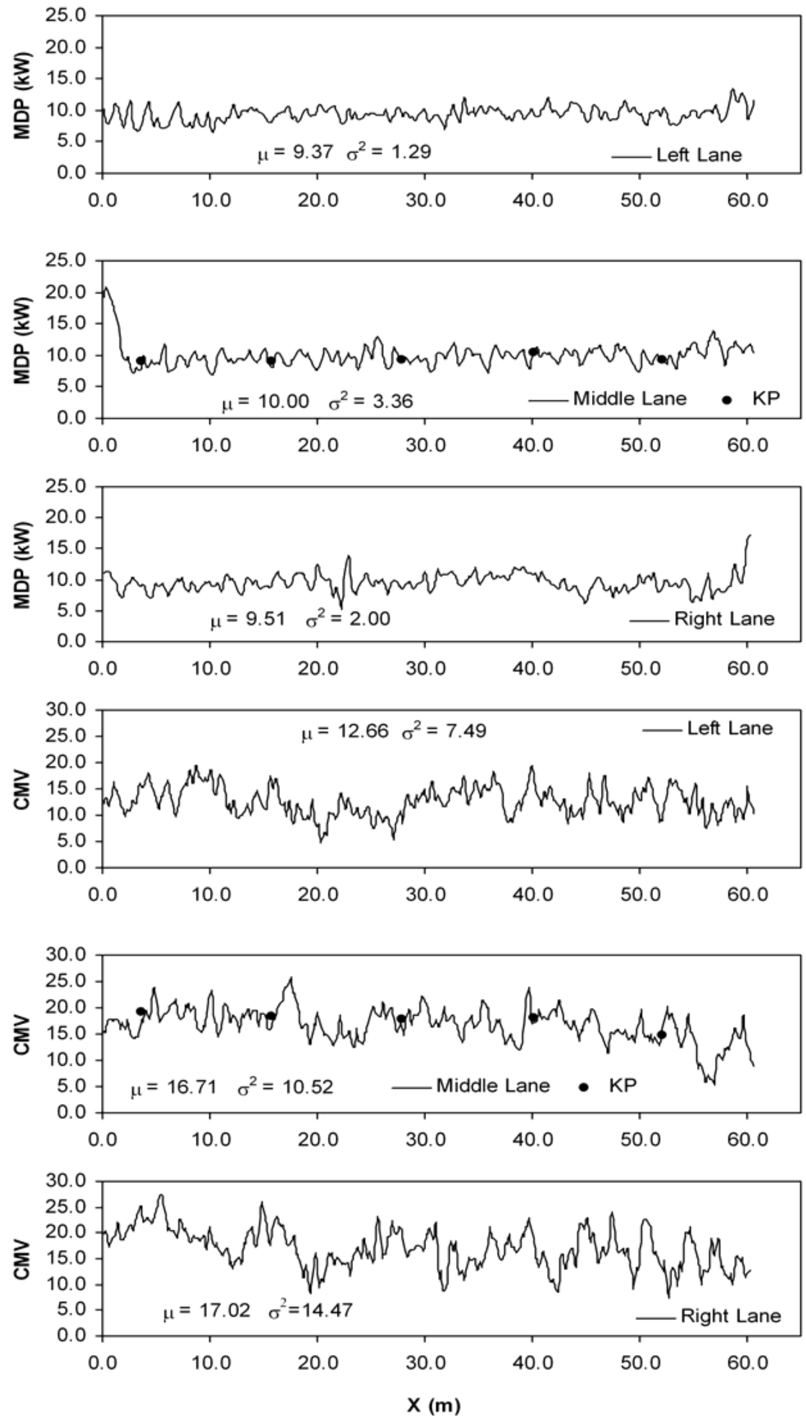

Figure B.9 Variation of CCC values for Lift 5, Pass 5/7

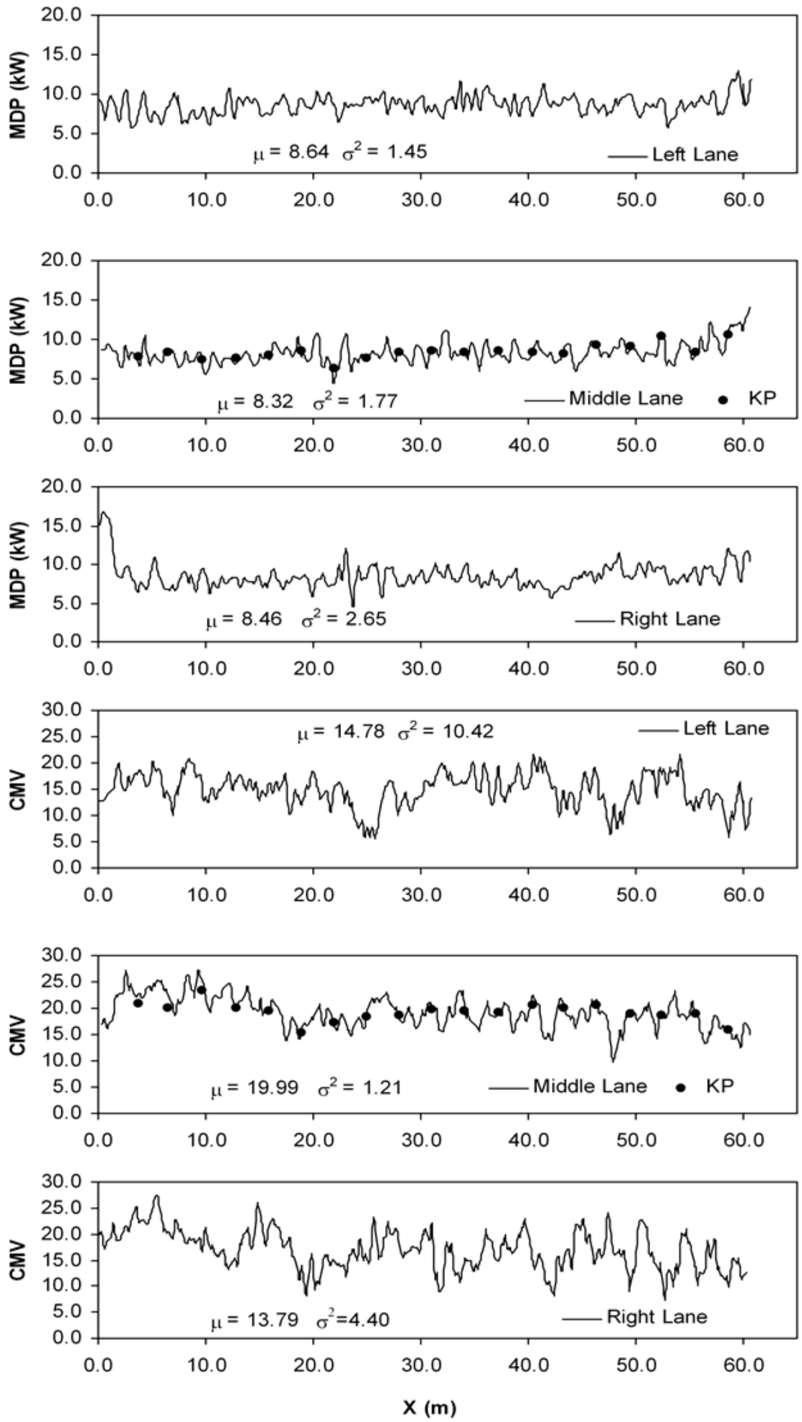

Figure B.10 Variation of CCC values for Lift 5, Pass 7/7

Appendix C

SEMIVARIOGRAM AND KRIGING RESULTS

This appendix contains figures that demonstrate the semivariogram and kriging results. Figures C.1 through C.10 illustrate the sample semivariograms for each lift and pass. Figures C.11 through C.110 present the results of kriging interpolation using Exponential, Gaussian, Rational Quadratic, Spherical and Linear models for maximum lags of 1.5 (5.0 ft) and 3.0 m (10 ft). It should be noted that subscripts R and P denote real (actual) and predicted values, respectively. In addition, the term N_0 denotes the initial number of input data points that were used in the kriging analysis and N_f corresponds to the number of data points that remain after correcting the kriging matrix when singularities occurred. In the cases where N_0 is equal to N_f, then there are no singularities in the kriging matrices.

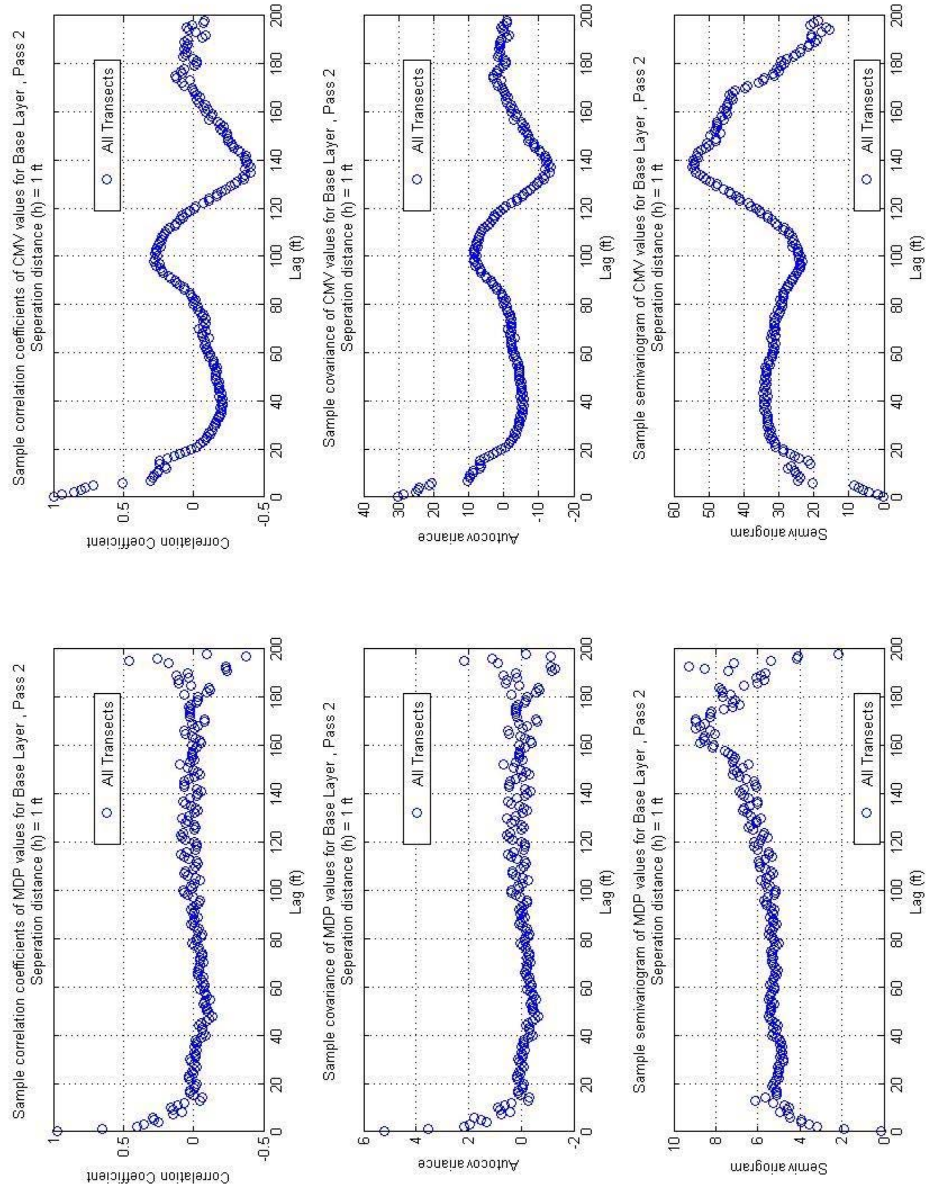

Figure C.1 Spatial continuity of CCC values for Base layer, pass 2/2

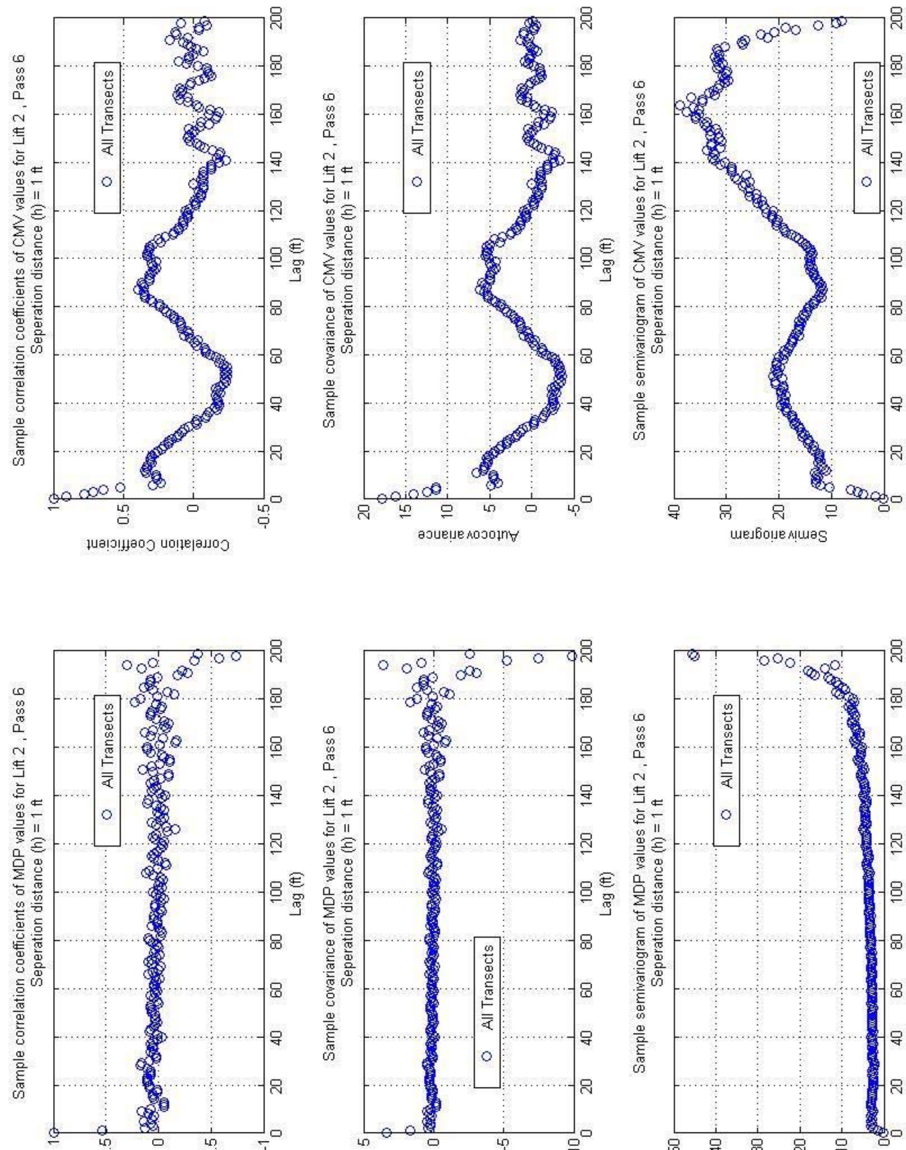

Figure C.2 Spatial continuity of CCC values for Lift 2, pass 6/6

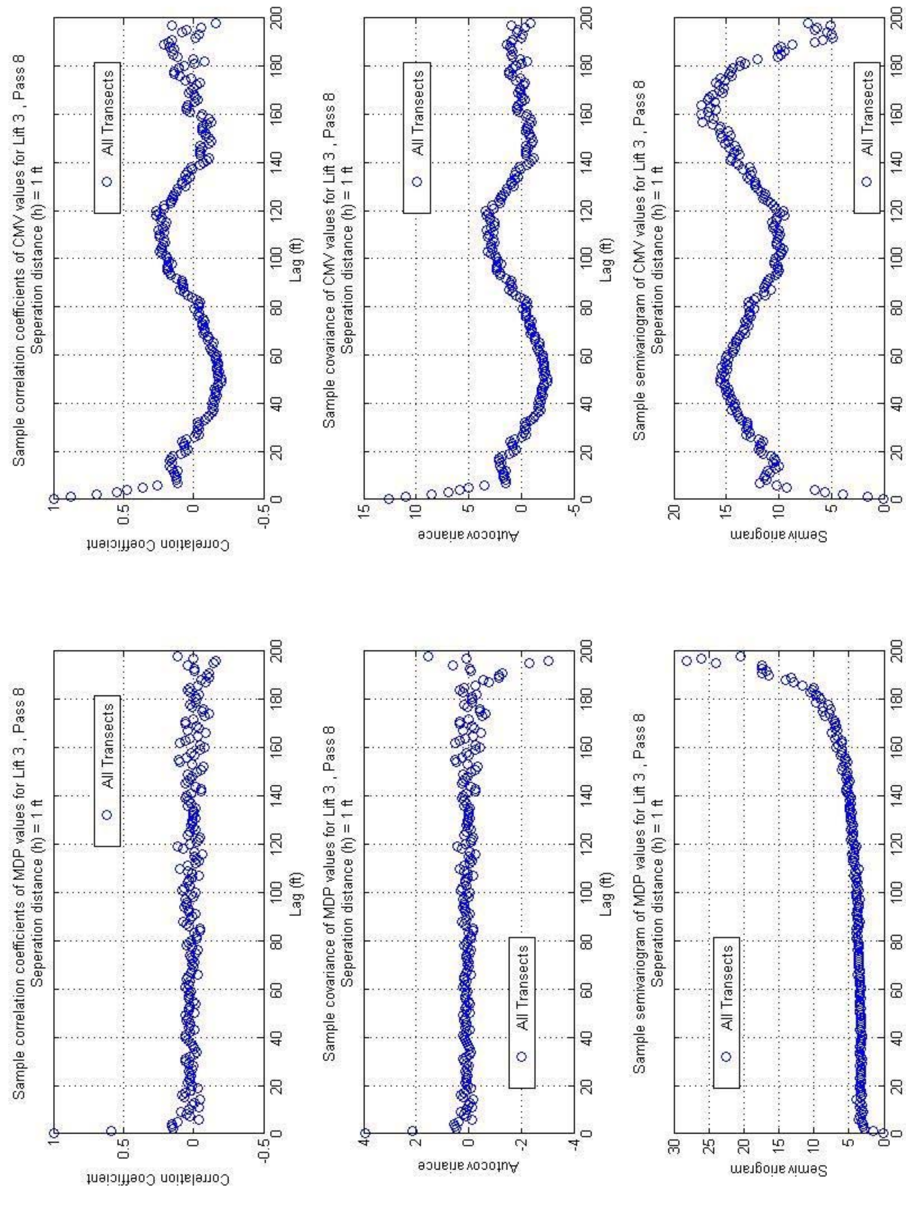

Figure C.3 Spatial continuity of CCC values for Lift 3, pass 8/8

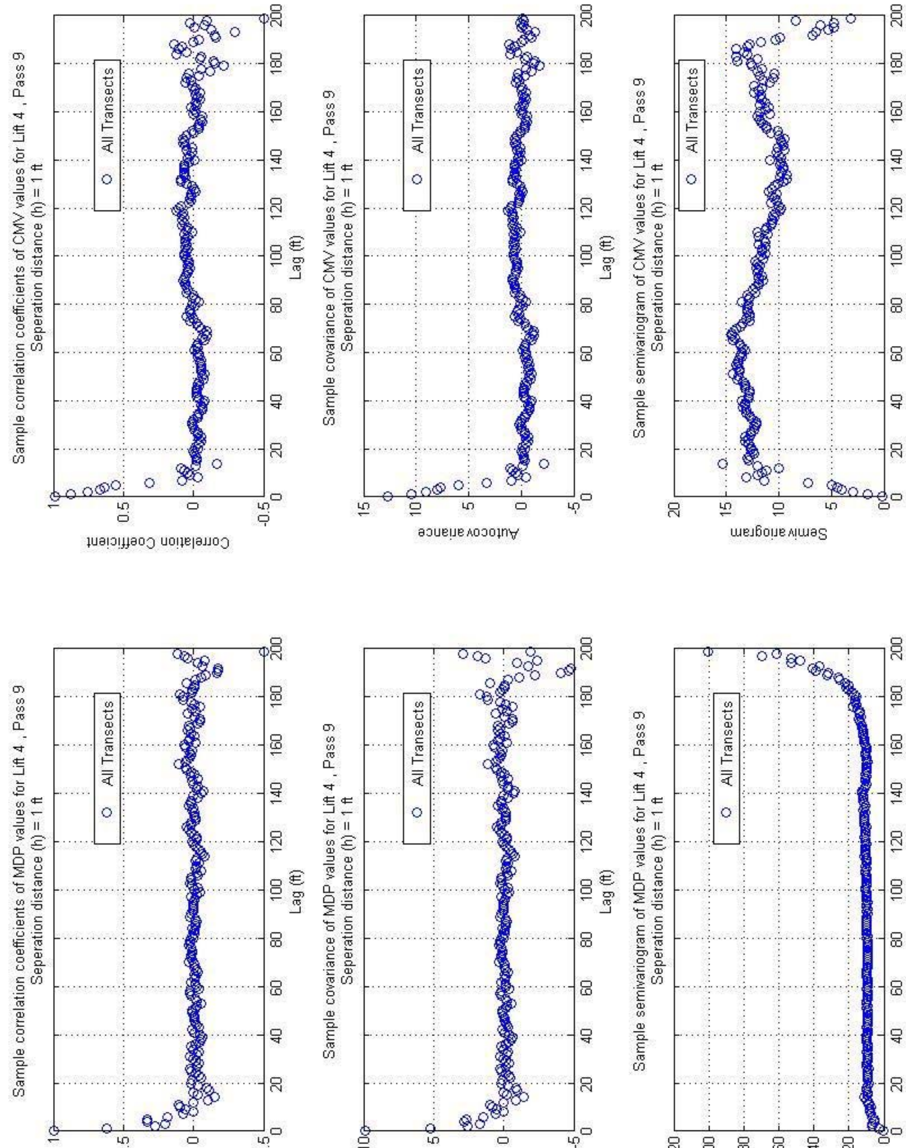

Figure C.4 Spatial continuity of CCC values for Lift 4, pass 9/9

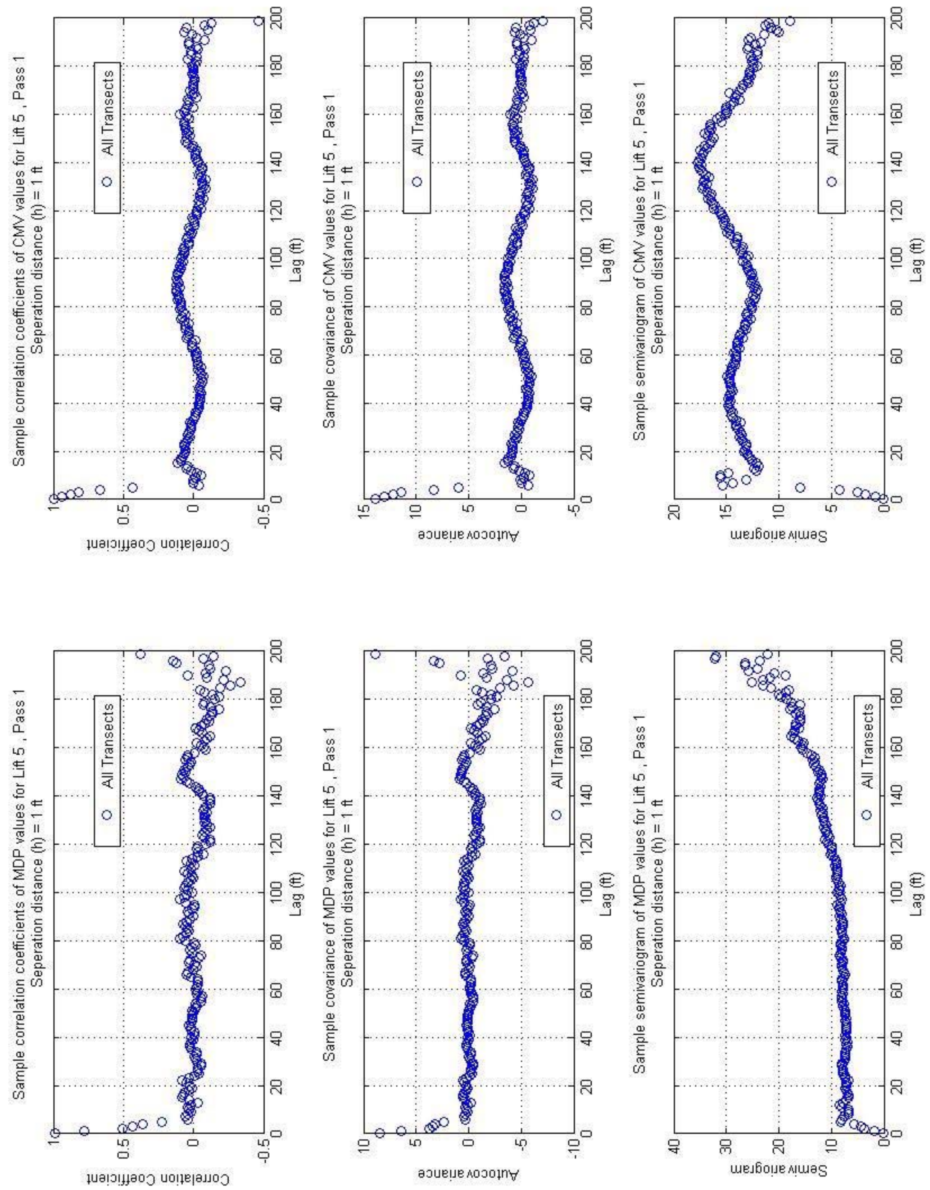

Figure C.5 Spatial continuity of CCC values for Lift 5, pass 1/7

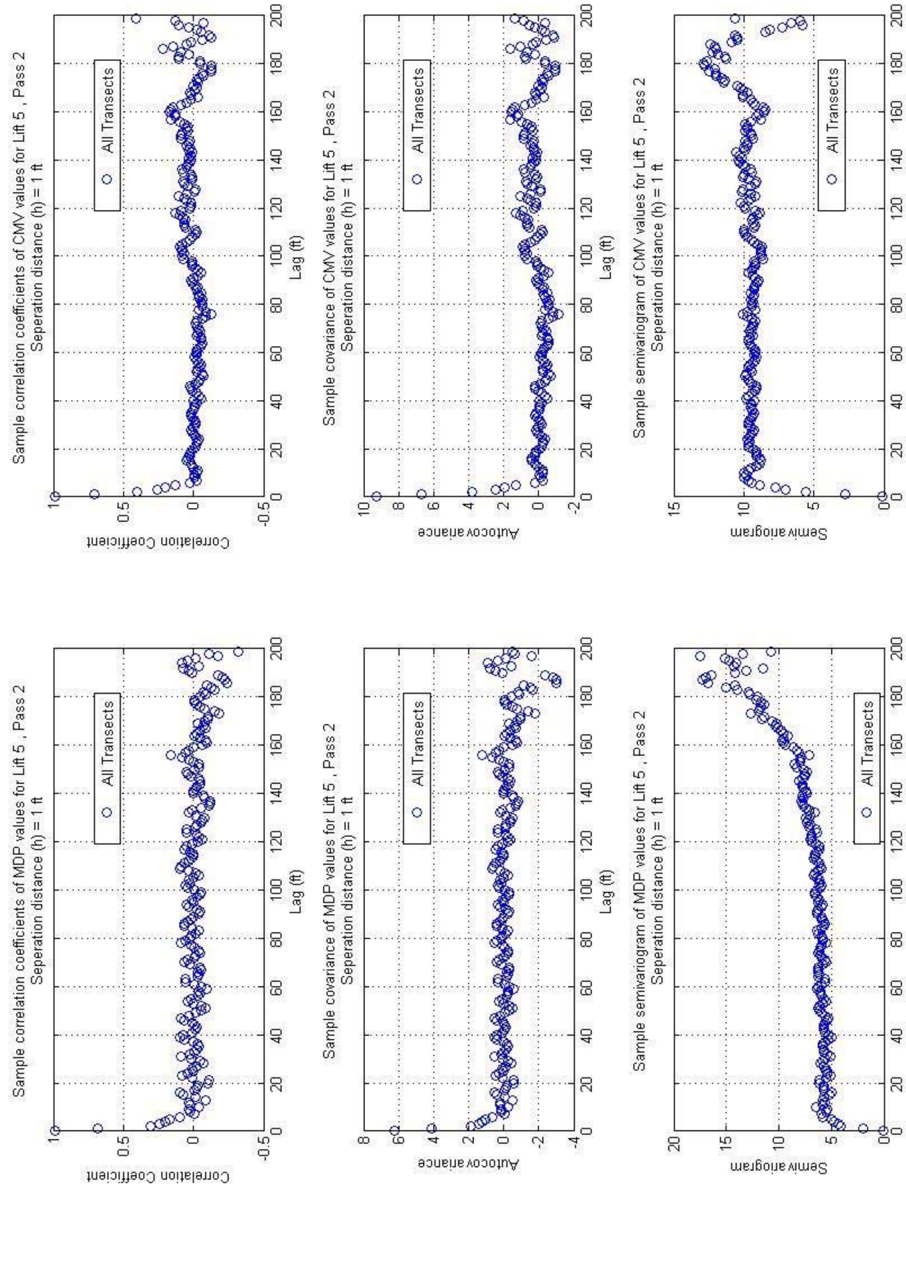

Figure C.6 Spatial continuity of CCC values for Lift 5, pass 2/7

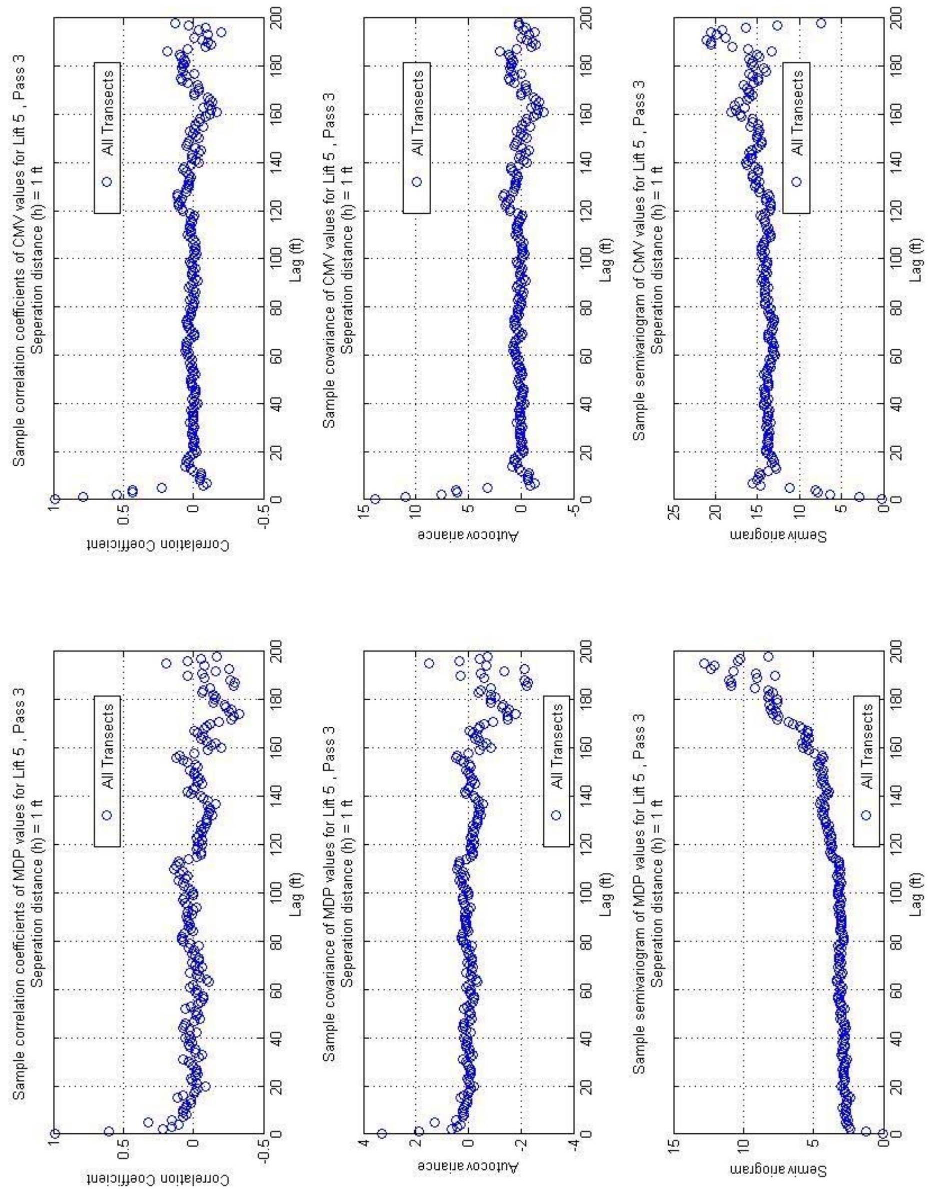

Figure C.7 Spatial continuity of CCC values for Lift 5, pass 3/7

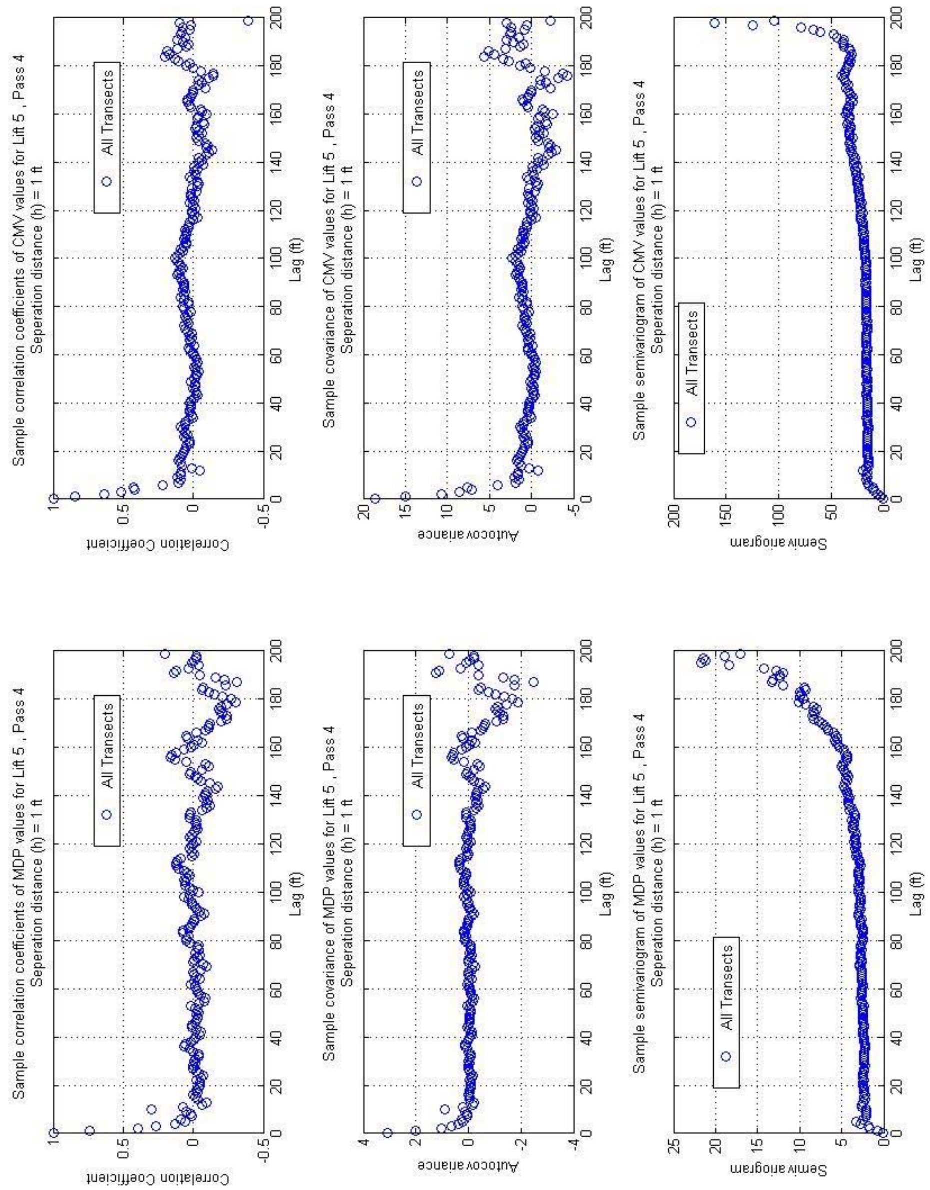

Figure C.8 Spatial continuity of CCC values for Lift 5, pass 4/7

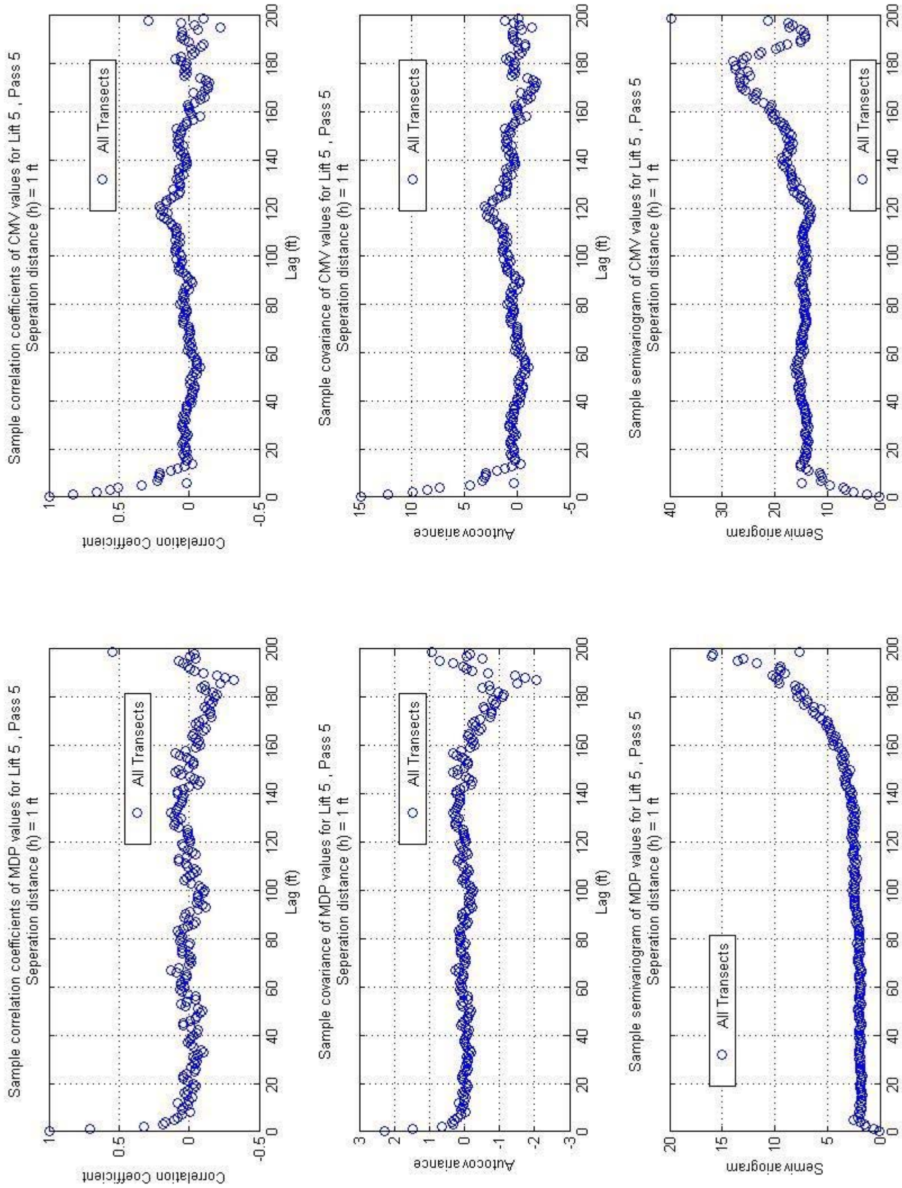

Figure C.9 Spatial continuity of CCC values for Lift 5, pass 5/7

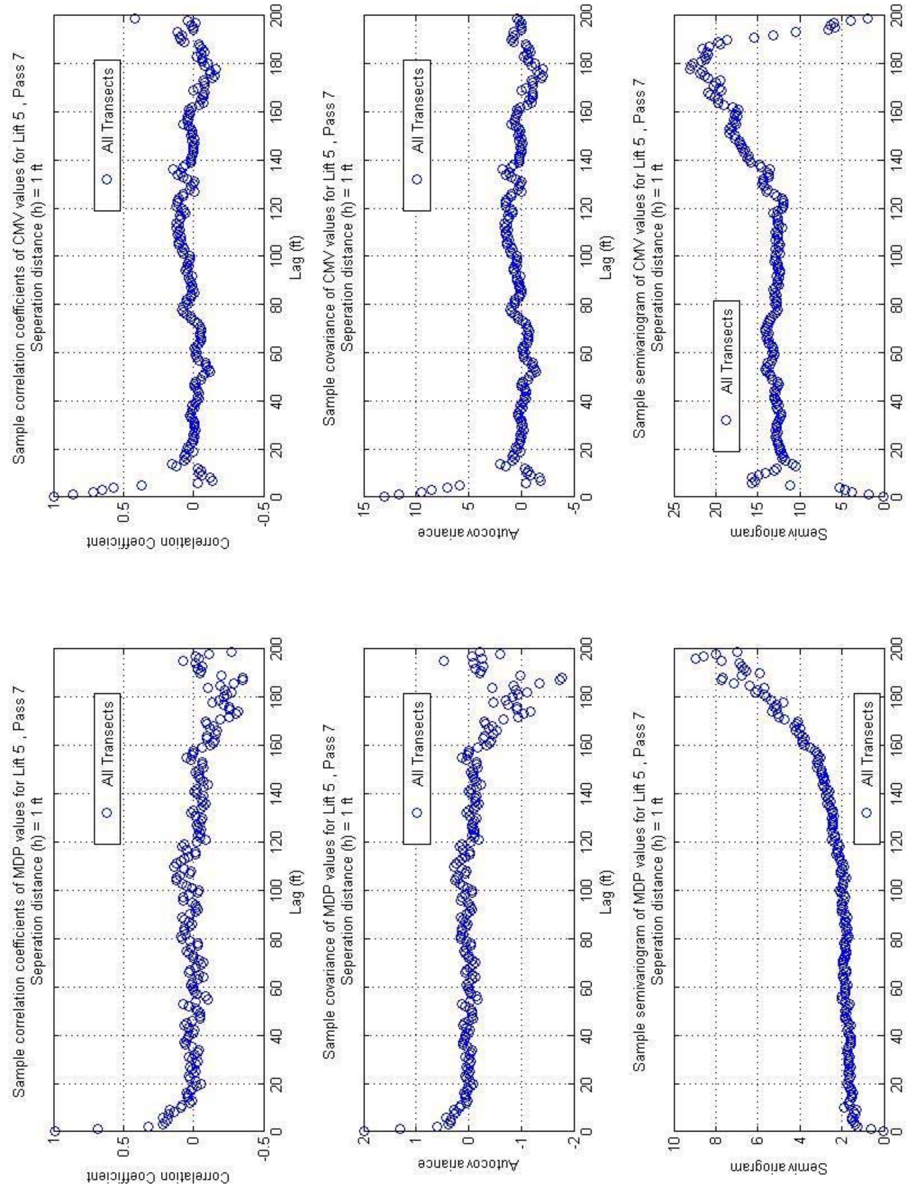

Figure C.10 Spatial continuity of CCC values for Lift 5, pass 7/7

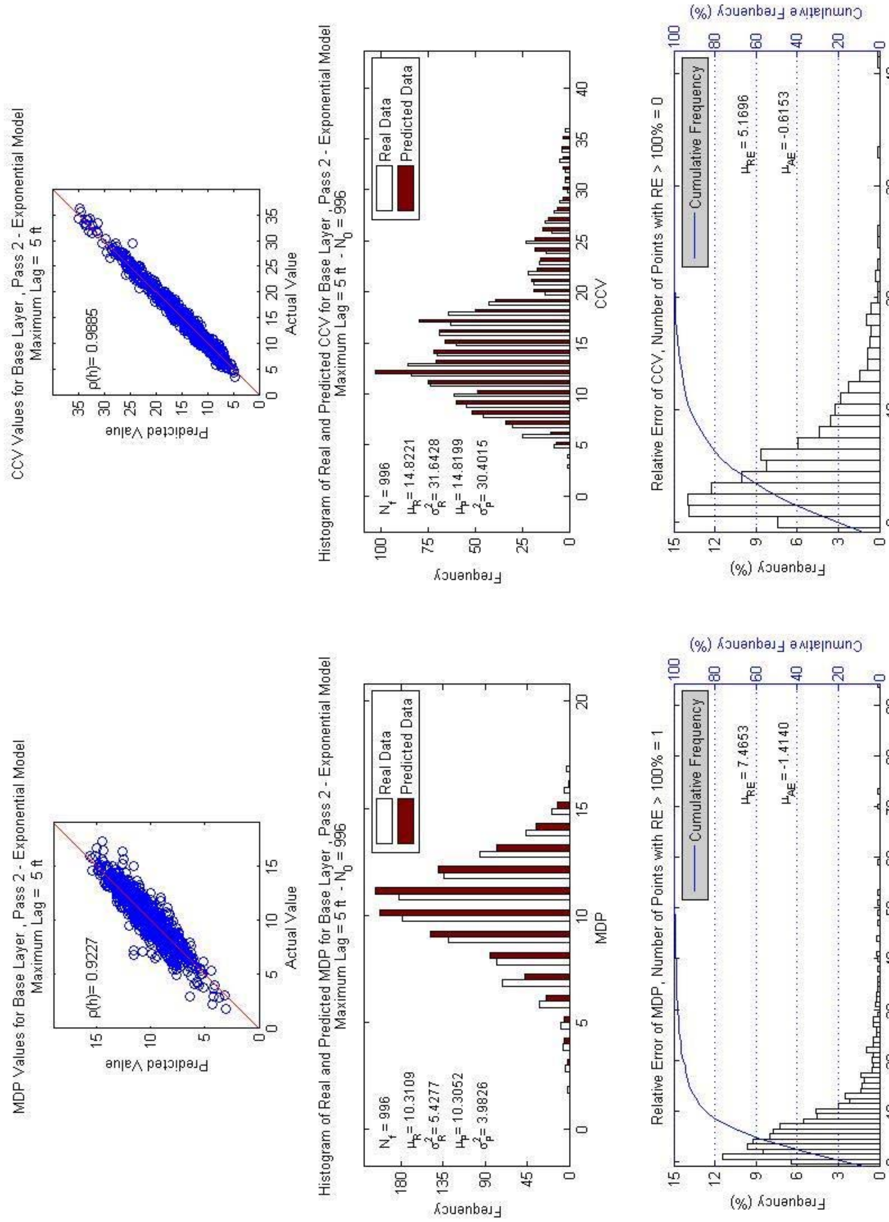

Figure C.11 Kriging results of CCC values for Base layer, Pass 2/2, using Exponential model and maximum lag of 1.5 m (5 ft)

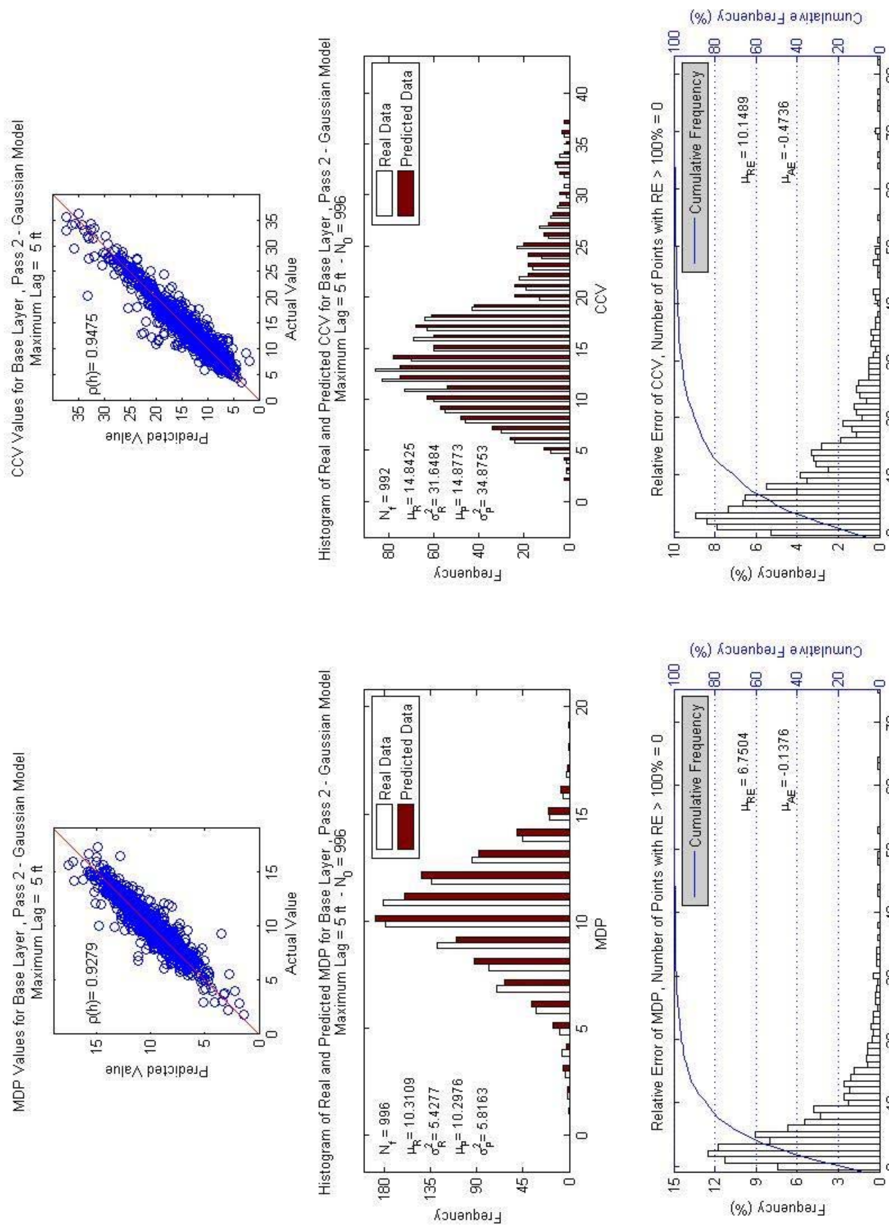

Figure C.12 Kriging results of CCC values for Base layer, Pass 2/2, using Gaussian model and maximum lag of 1.5 m (5 ft)

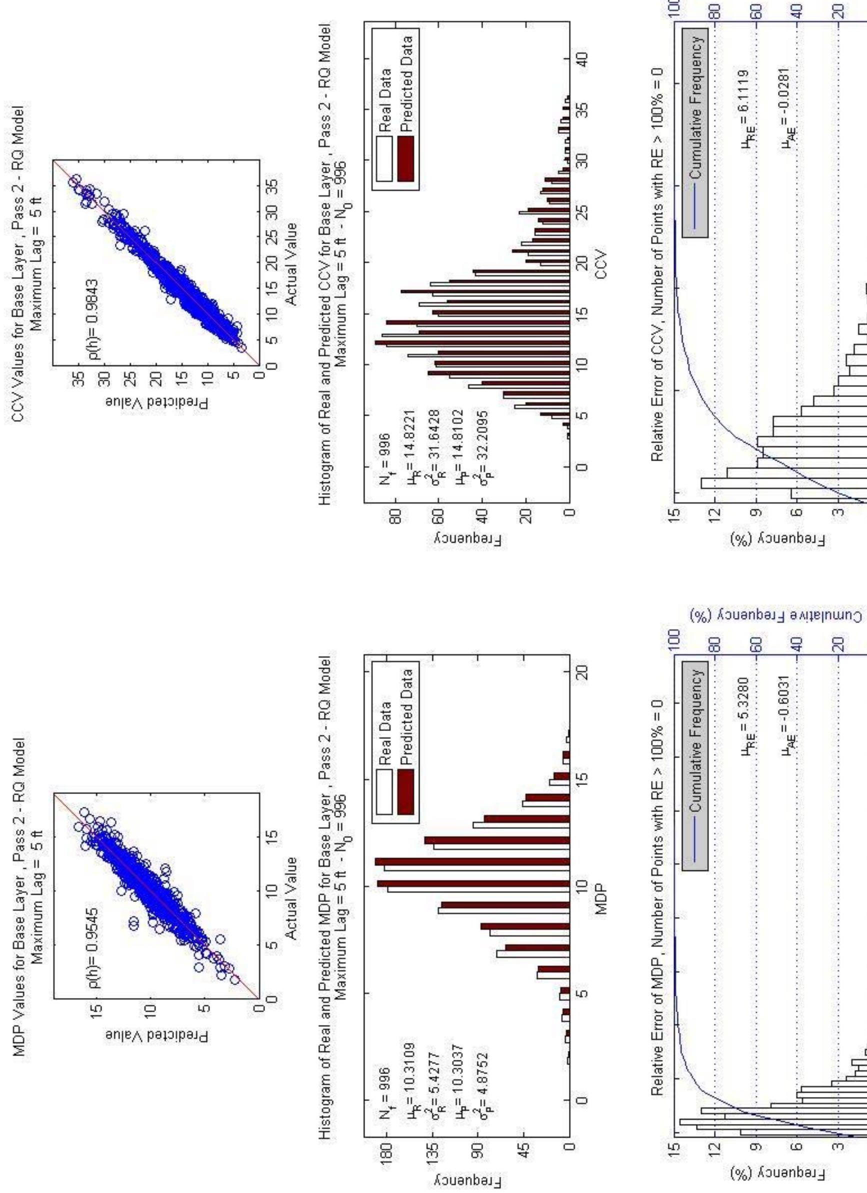

Figure C.13 Kriging results of CCC values for Base layer, Pass 2/2, using Rational Quadratic (RQ) model and maximum lag of 1.5 m (5 ft)

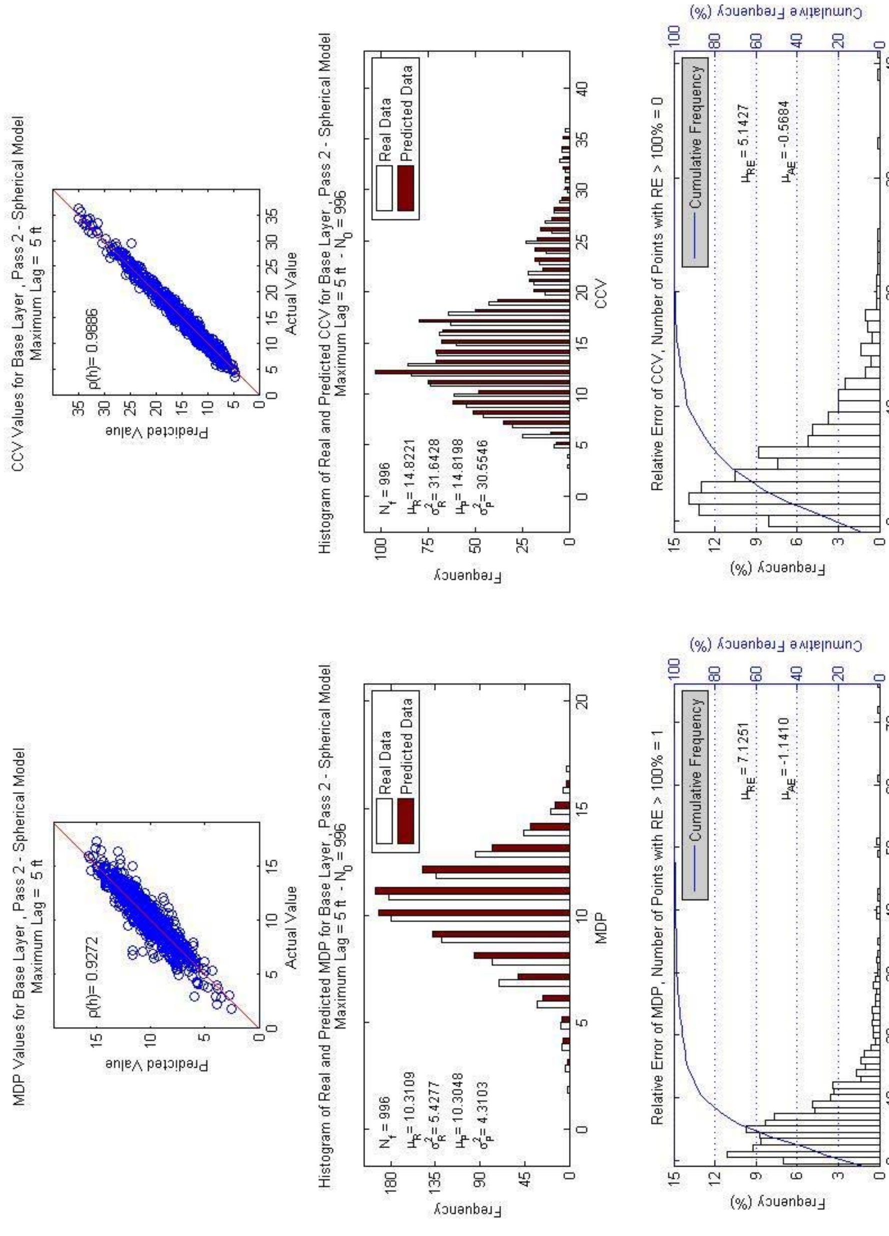

Figure C.14 Kriging results of CCC values for Base layer, Pass 2/2, using Spherical model and maximum lag of 1.5 m (5 ft)

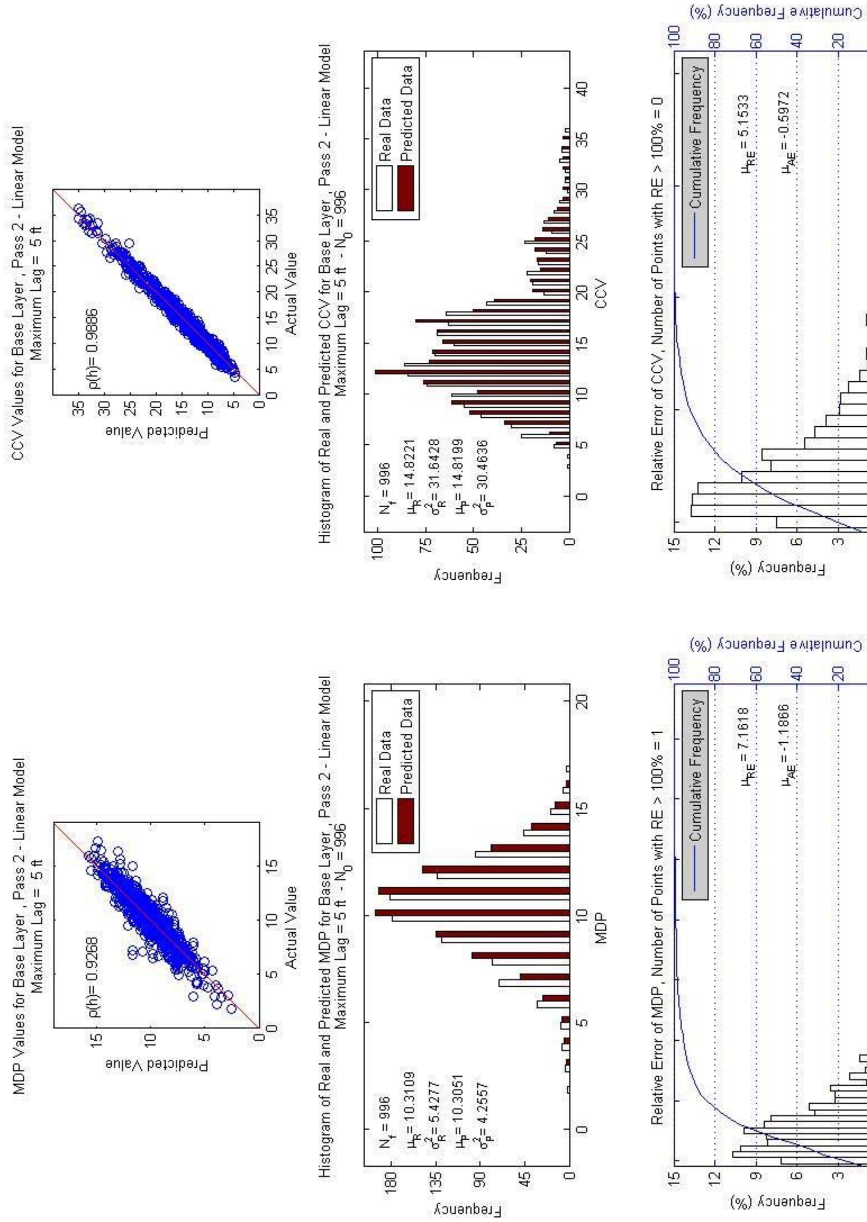

Figure C.15 Kriging results of CCC values for Base layer, Pass 2/2, using Linear model and maximum lag of 1.5 m (5 ft)

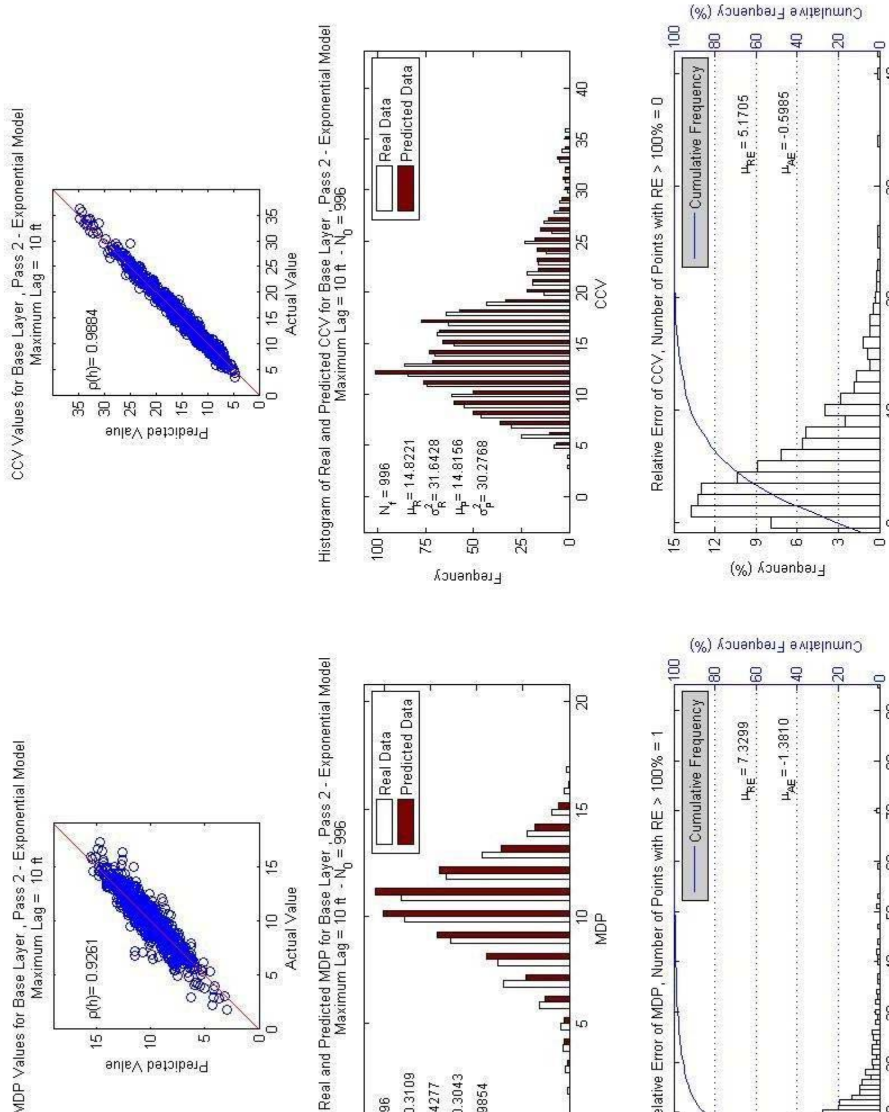

Figure C.16 Kriging results of CCC values for Base layer, Pass 2/2, using Exponential model and maximum lag of 3.0 m (10 ft)

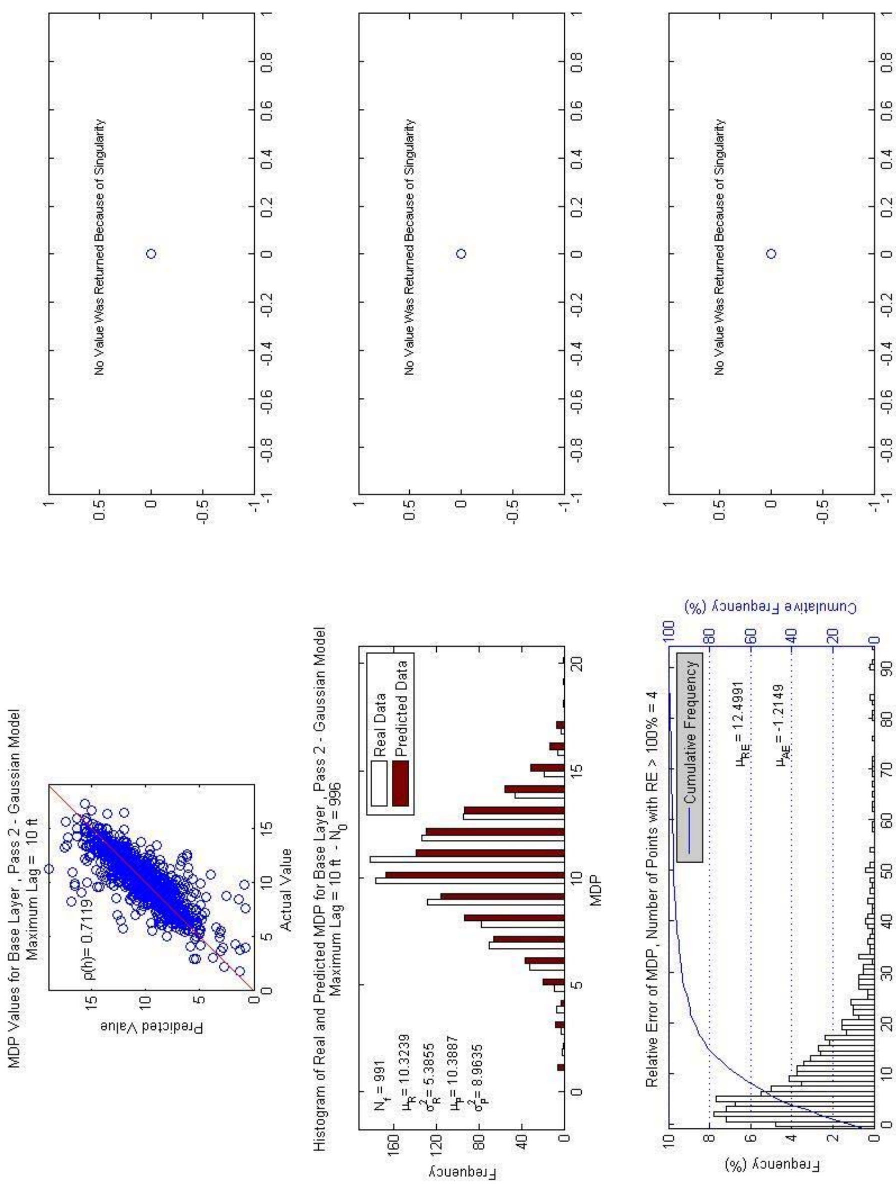

Figure C.17 Kriging results of CCC values for Base layer, Pass 2/2, using Gaussian model and maximum lag of 3.0 m (10 ft)

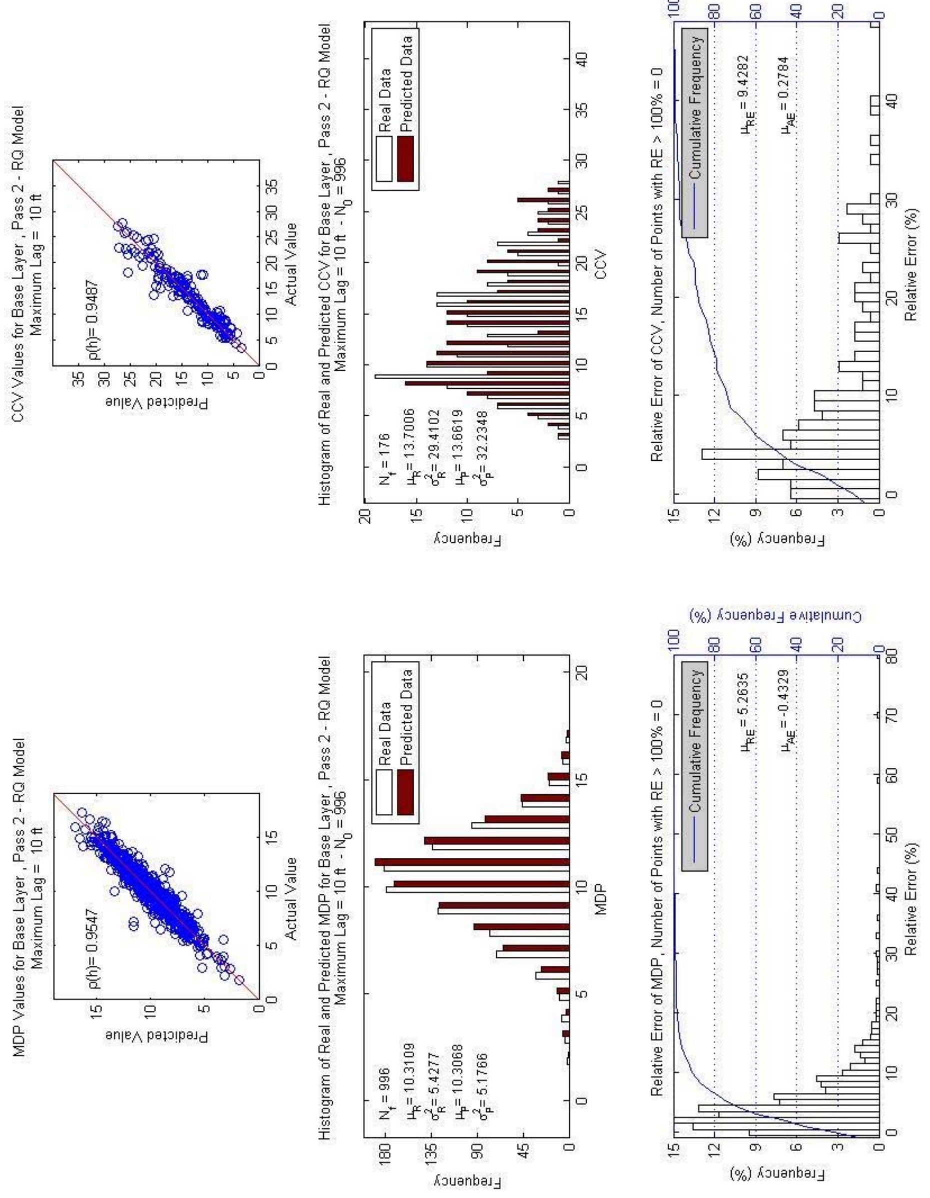

Figure C.18 Kriging results of CCC values for Base layer, Pass 2/2, using Rational Quadratic (RQ) model and maximum lag of 3.0 m (10 ft)

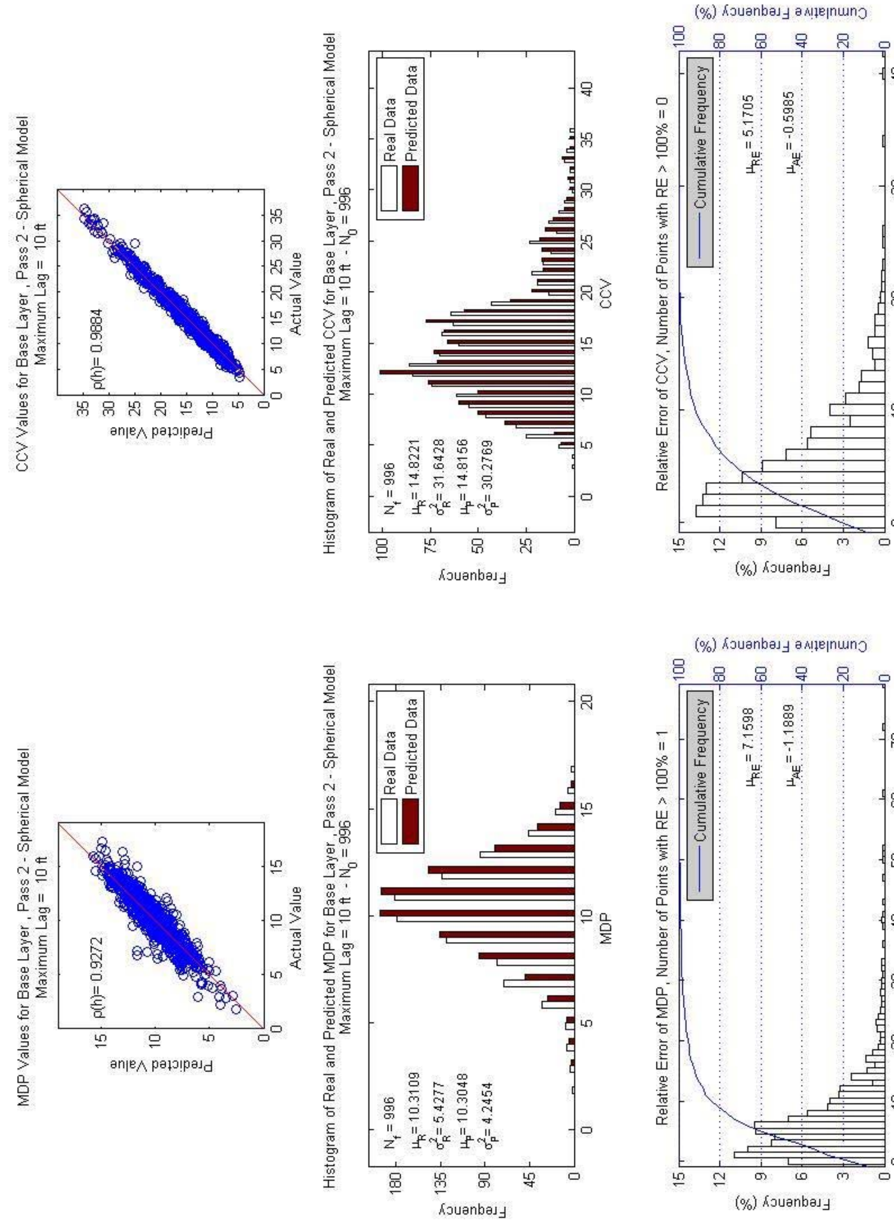

Figure C.19 Kriging results of CCC values for Base layer, Pass 2/2, using Spherical model and maximum lag of 3.0 m (10 ft)

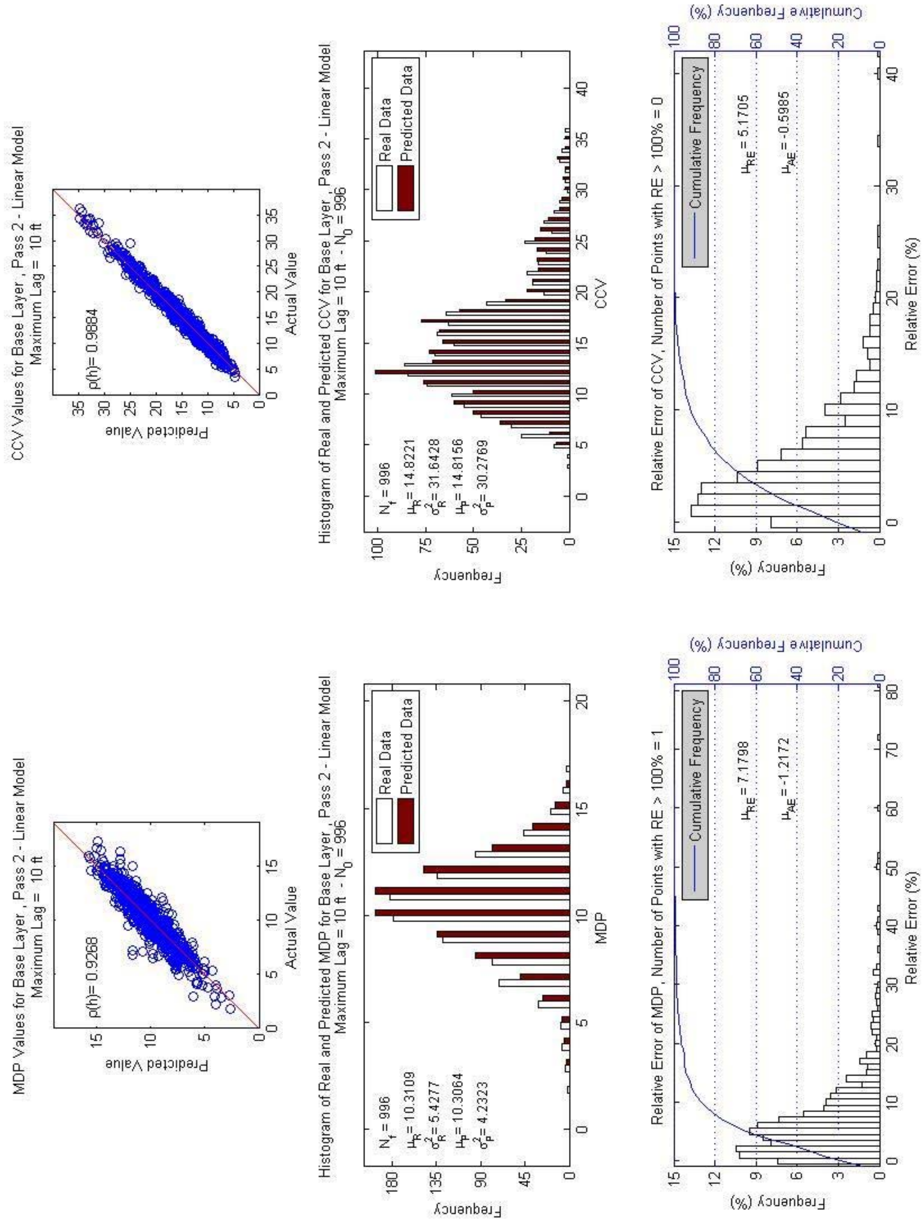

Figure C.20 Kriging results of CCC values for Base layer, Pass 2/2, using Linear model and maximum lag of 3.0 m (10 ft)

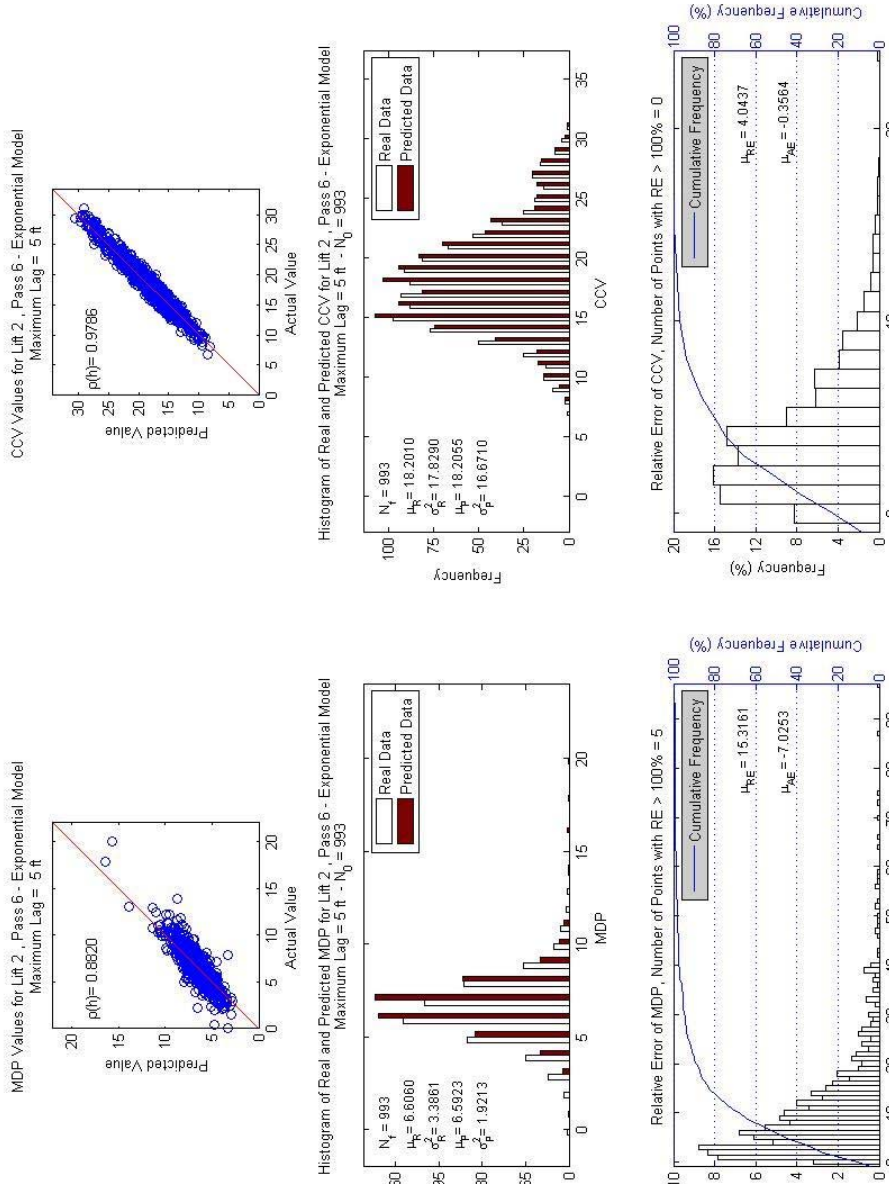

Figure C.21 Kriging results of CCC values for Lift 2, Pass 6/6, using Exponential model and maximum lag of 1.5 m (5 ft)

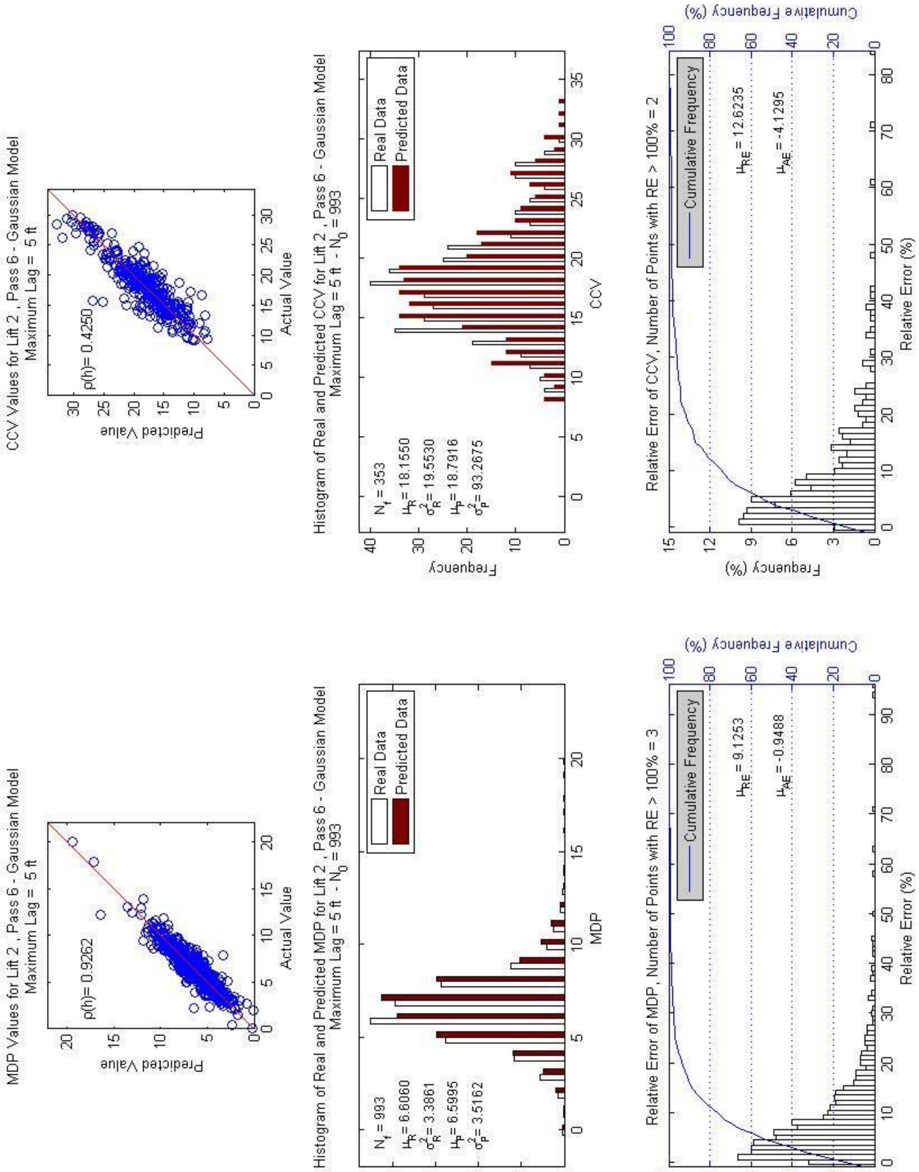

Figure C.22 Kriging results of CCC values for Lift 2, Pass 6/6, using Gaussian model and maximum lag of 1.5 m (5 ft)

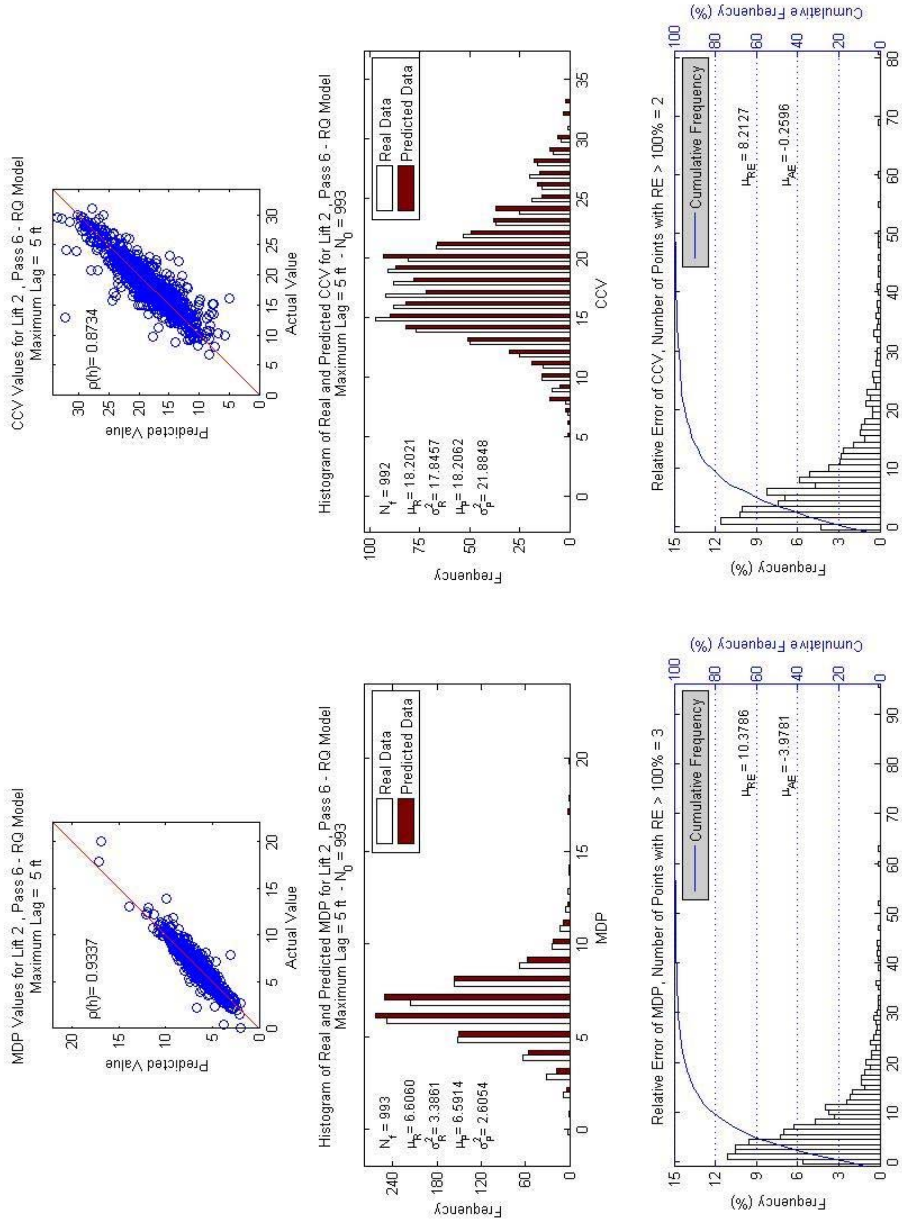

Figure C.23 Kriging results of CCC values for Lift 2, Pass 6/6, using Rational Quadratic (RQ) model and maximum lag of 1.5 m (5 ft)

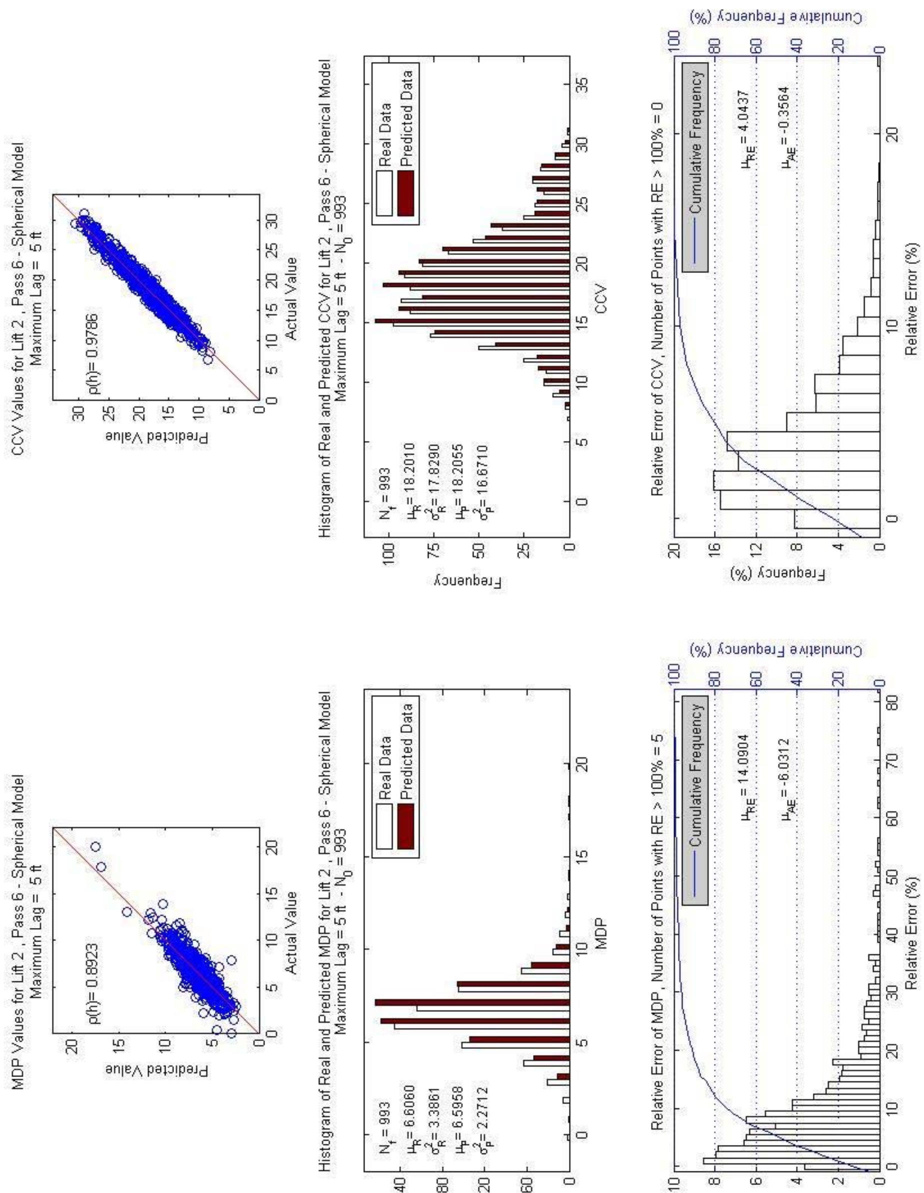

Figure C.24 Kriging results of CCC values for Lift 2, Pass 6/6, using Spherical model and maximum lag of 1.5 m (5 ft)

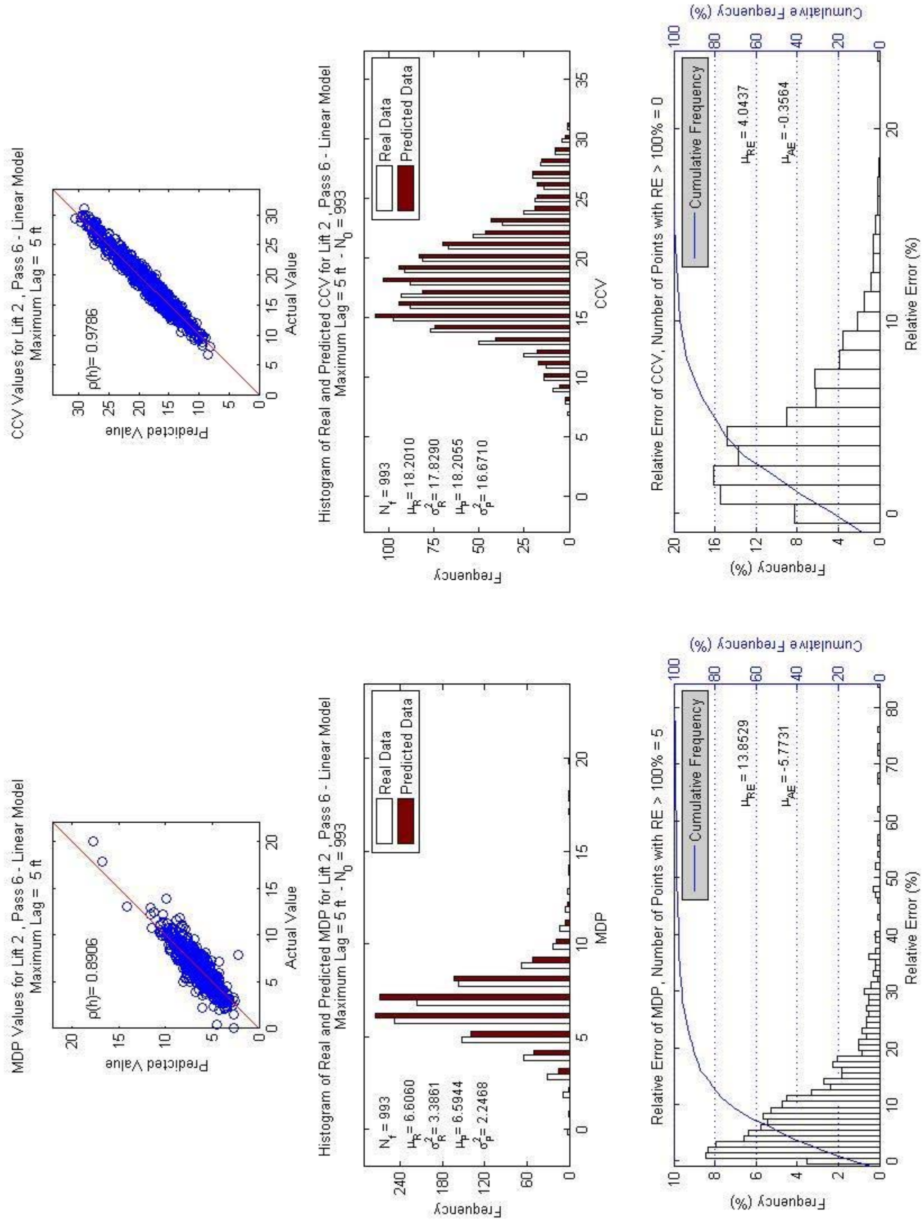

Figure C.25 Kriging results of CCC values for Lift 2, Pass 6/6, using Linear model and maximum lag of 1.5 m (5 ft)

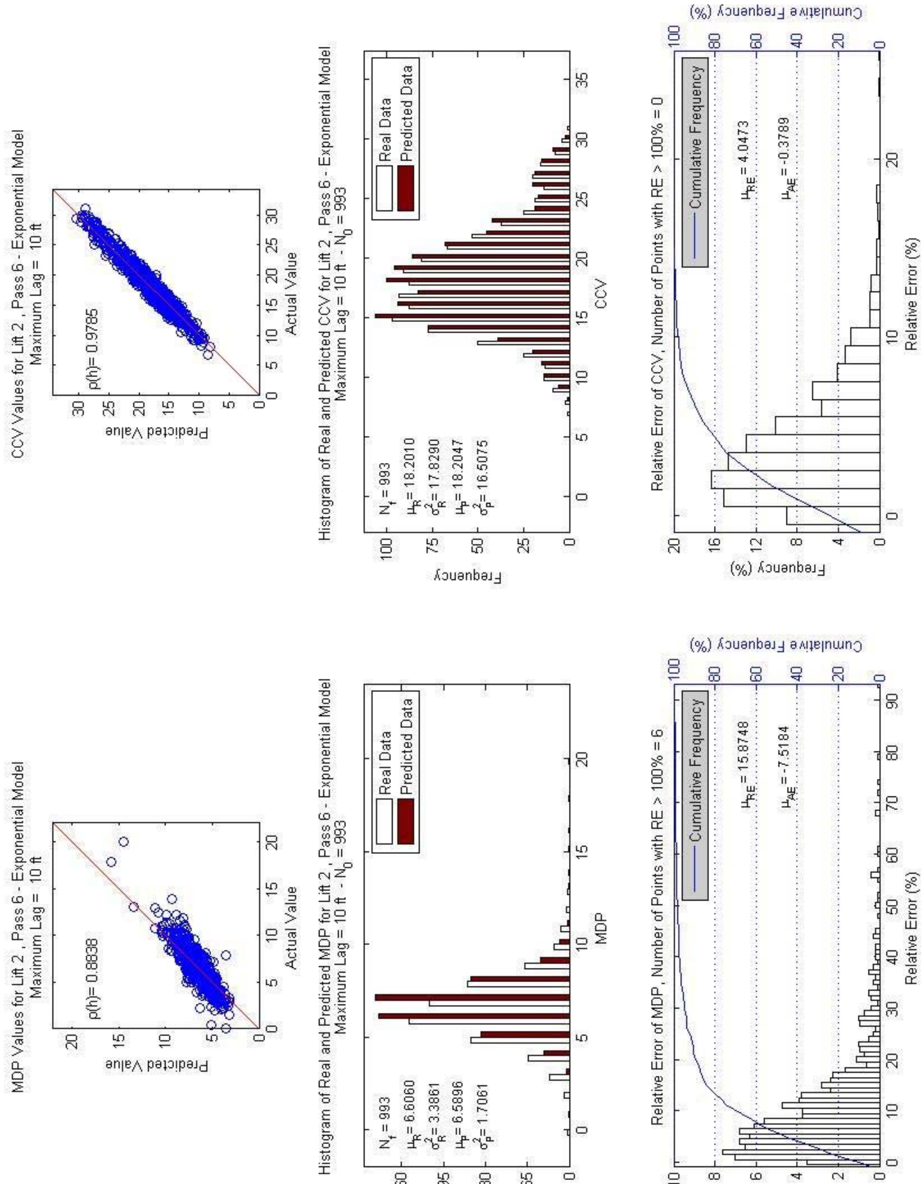

Figure C.26 Kriging results of CCC values for Lift 2, Pass 6/6, using Exponential model and maximum lag of 3.0 m (10 ft)

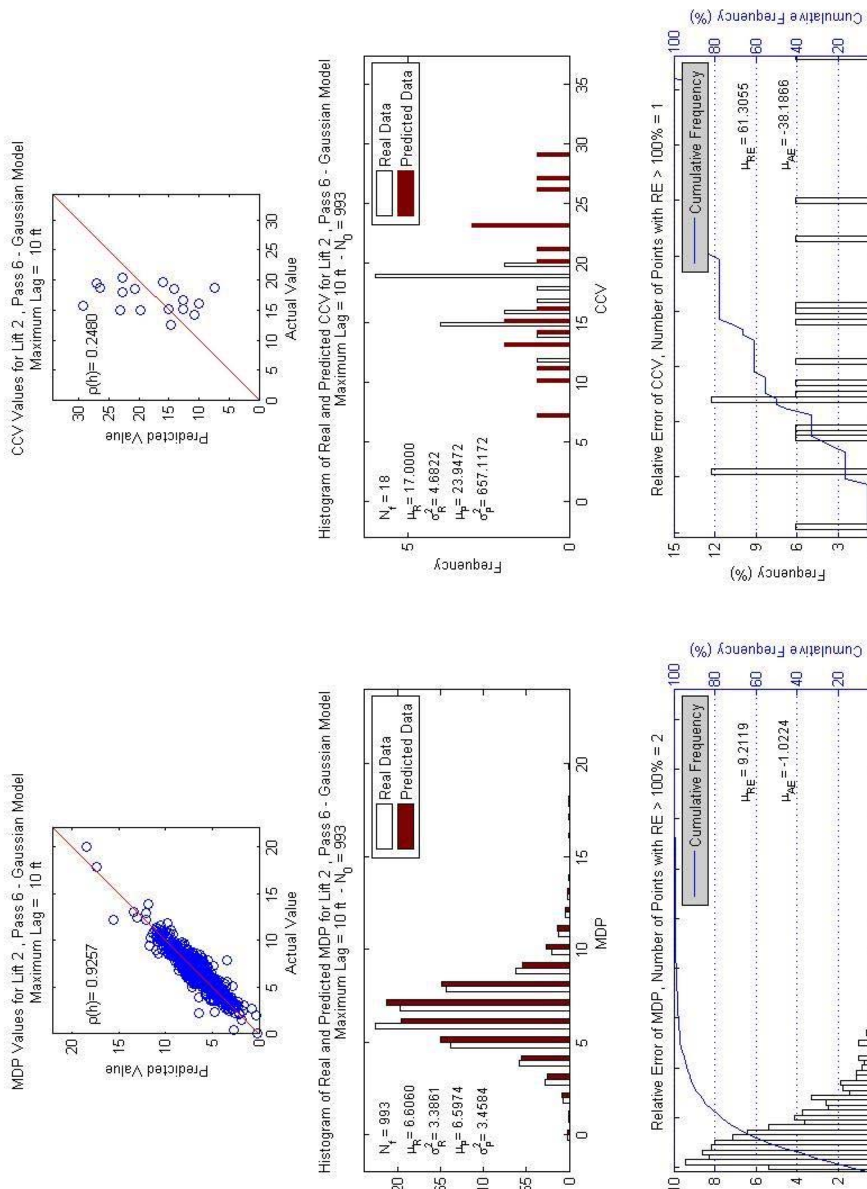

Figure C.27 Kriging results of CCC values for Lift 2, Pass 6/6, using Gaussian model and maximum lag of 3.0 m (10 ft)

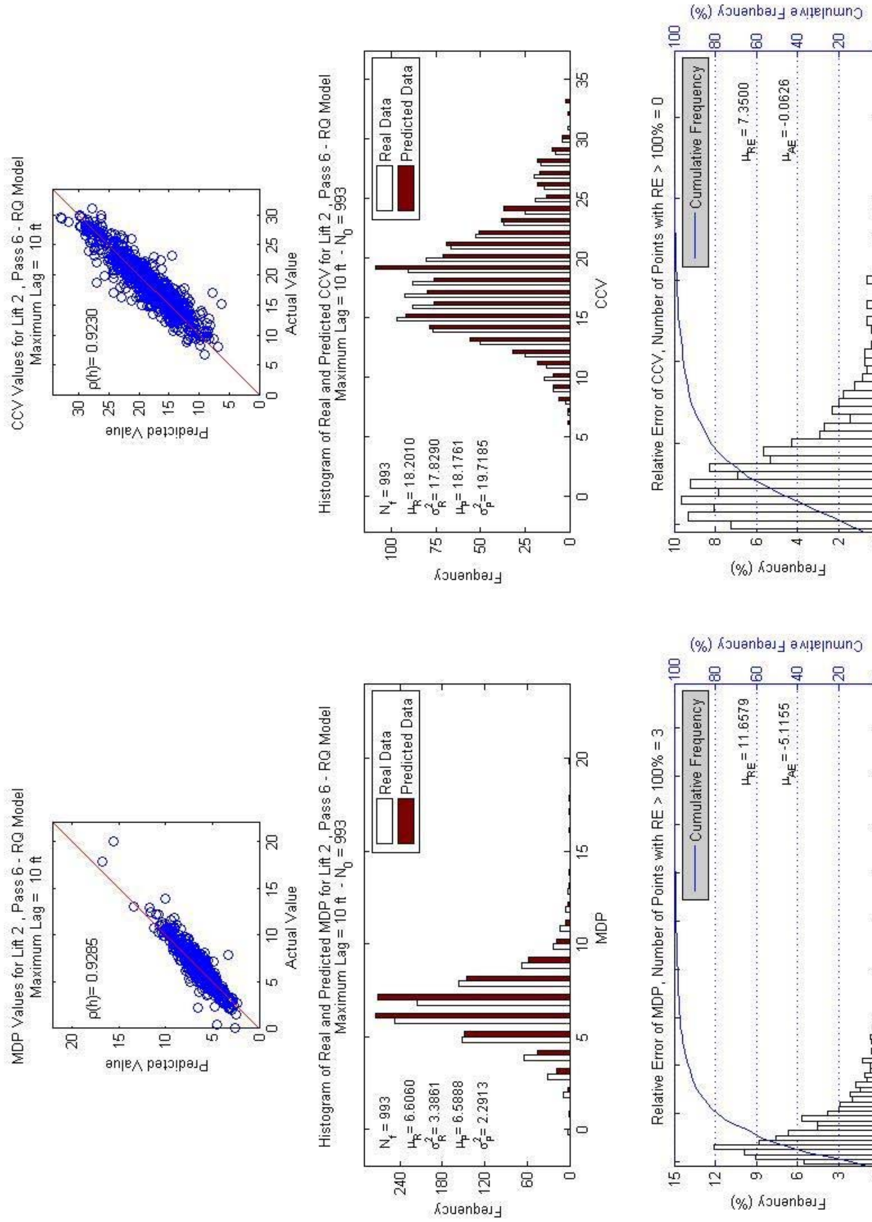

Figure C.28 Kriging results of CCC values for Lift 2, Pass 6/6, using Rational Quadratic (RQ) model and maximum lag of 3.0 m (10 ft)

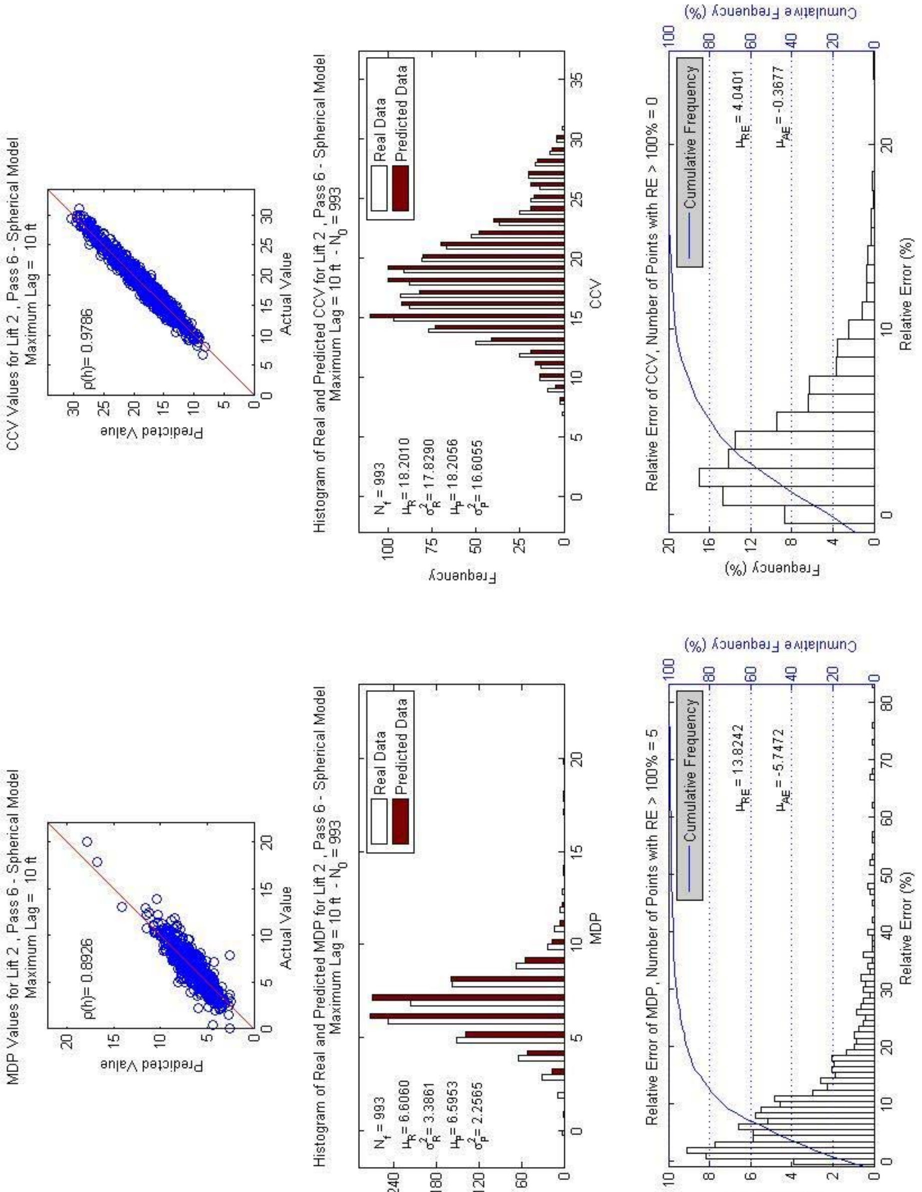

Figure C.29 Kriging results of CCC values for Lift 2, Pass 6/6, using Spherical model and maximum lag of 3.0 m (10 ft)

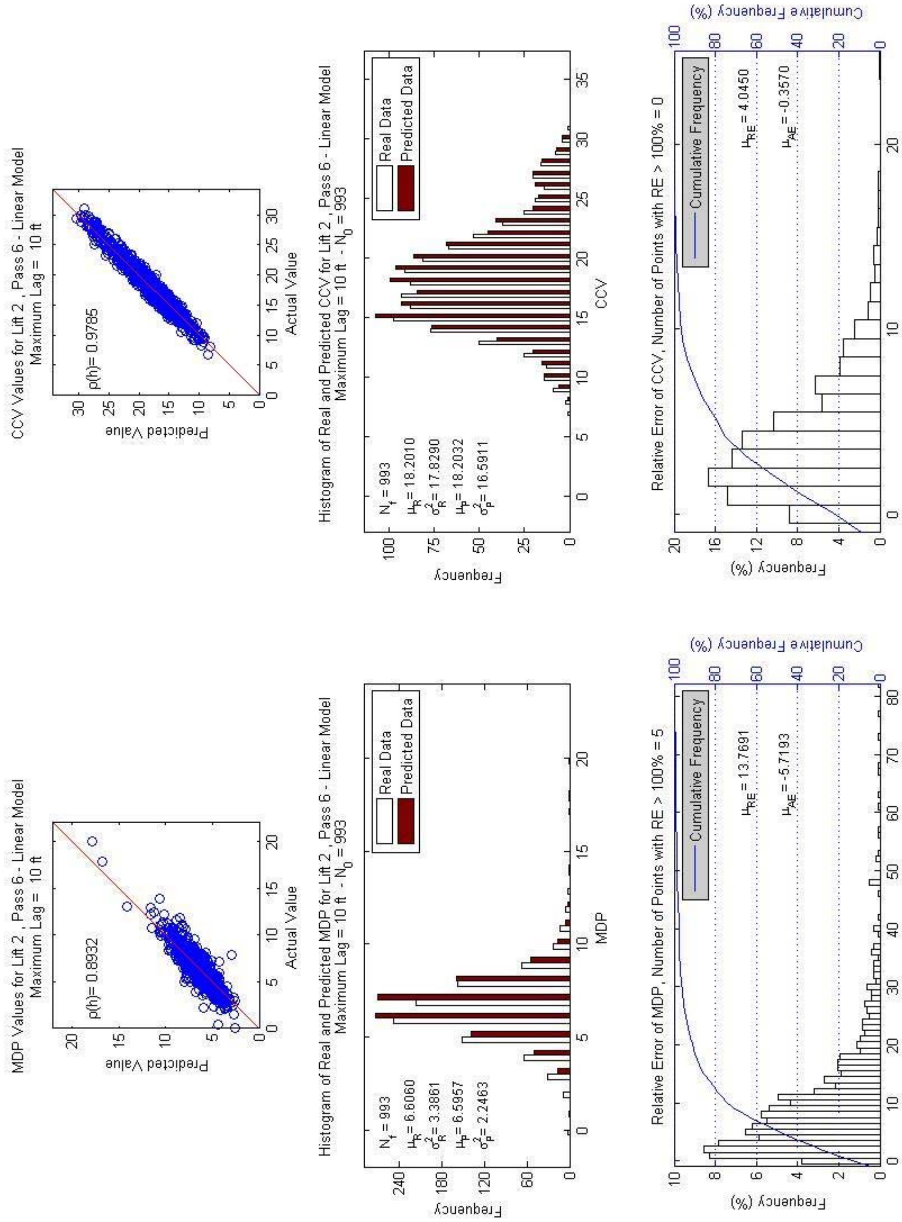

Figure C.30 Kriging results of CCC values for Lift 2, Pass 6/6, using Linear model and maximum lag of 3.0 m (10 ft)

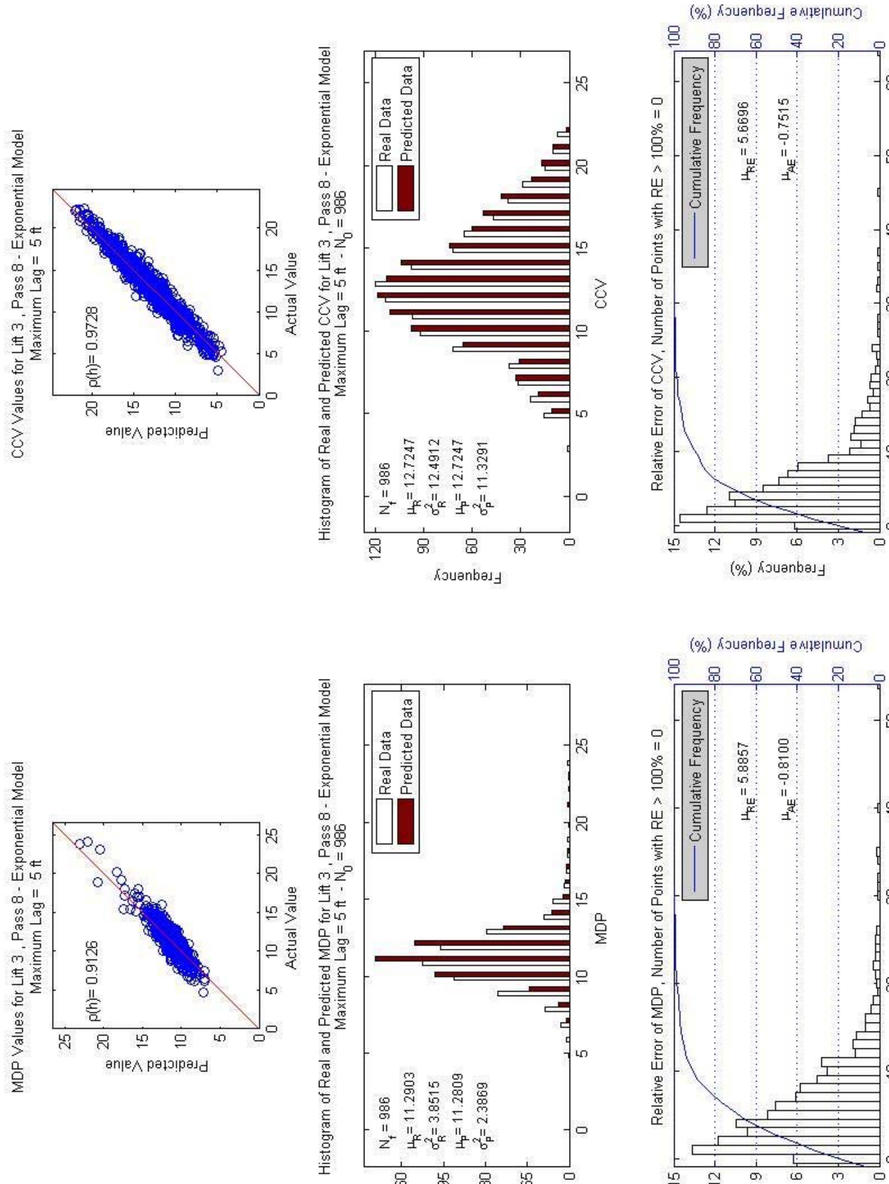

Figure C.31 Kriging results of CCC values for Lift 3, Pass 8/8, using Exponential model and maximum lag of 1.5 m (5 ft)

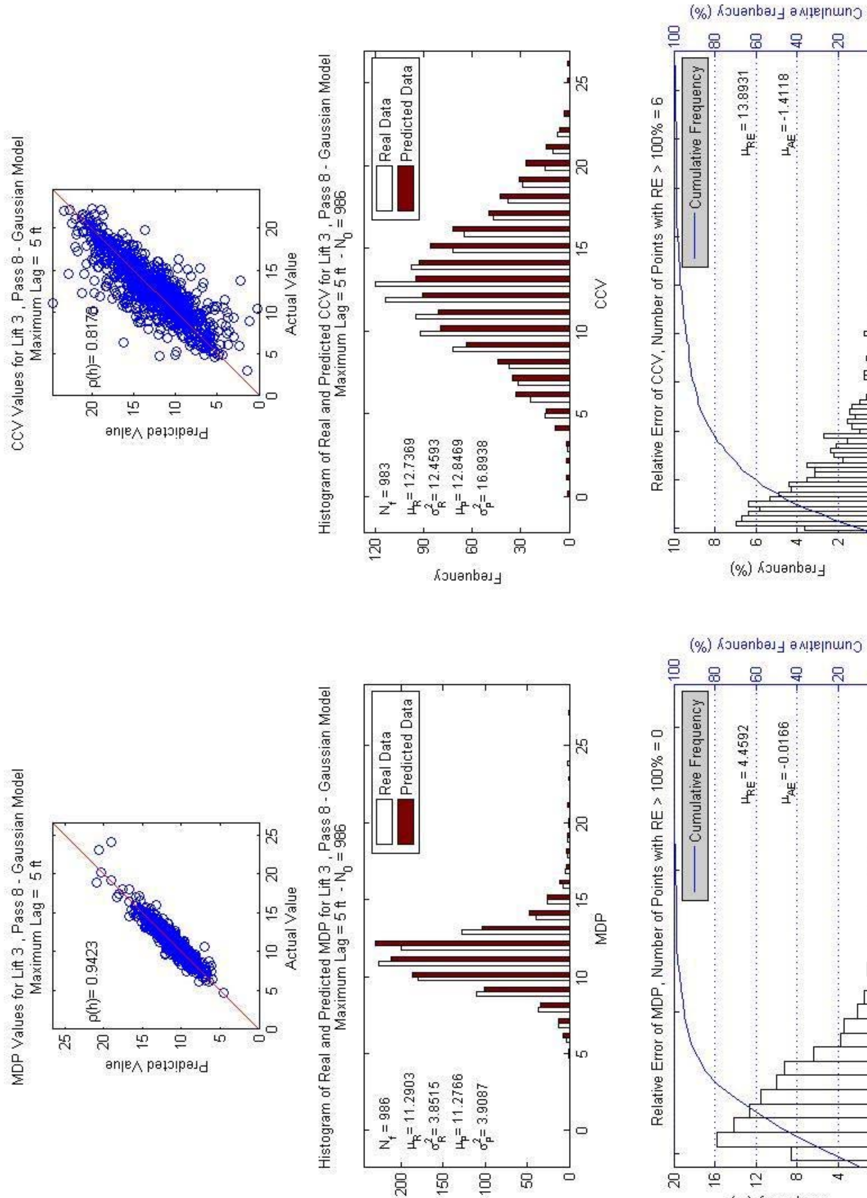

Figure C.32 Kriging results of CCC values for Lift 3, Pass 8/8, using Gaussian model and maximum lag of 1.5 (5 ft)

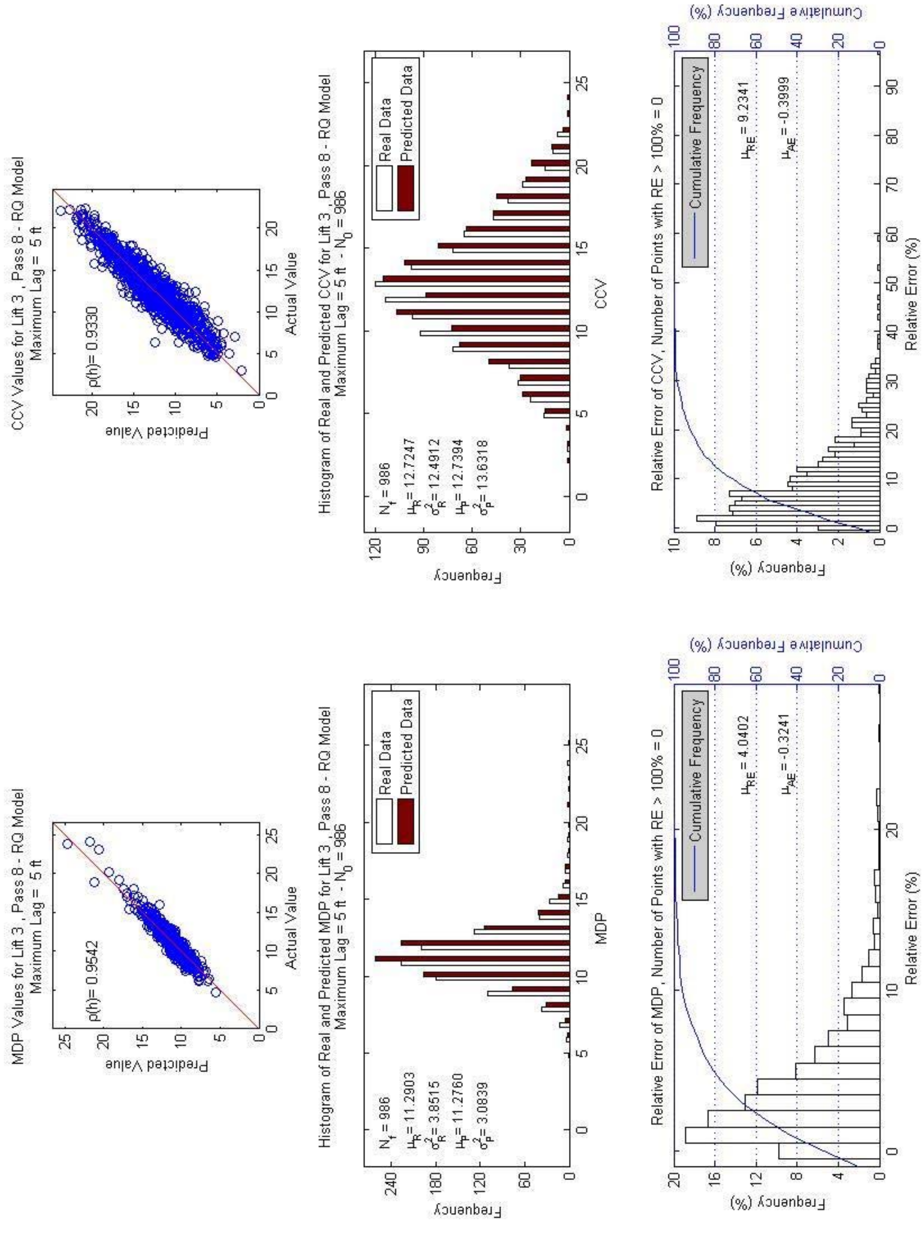

Figure C.33 Kriging results of CCC values for Lift 3, Pass 8/8, using Rational Quadratic (RQ) model and maximum lag of 1.5 m (5 ft)

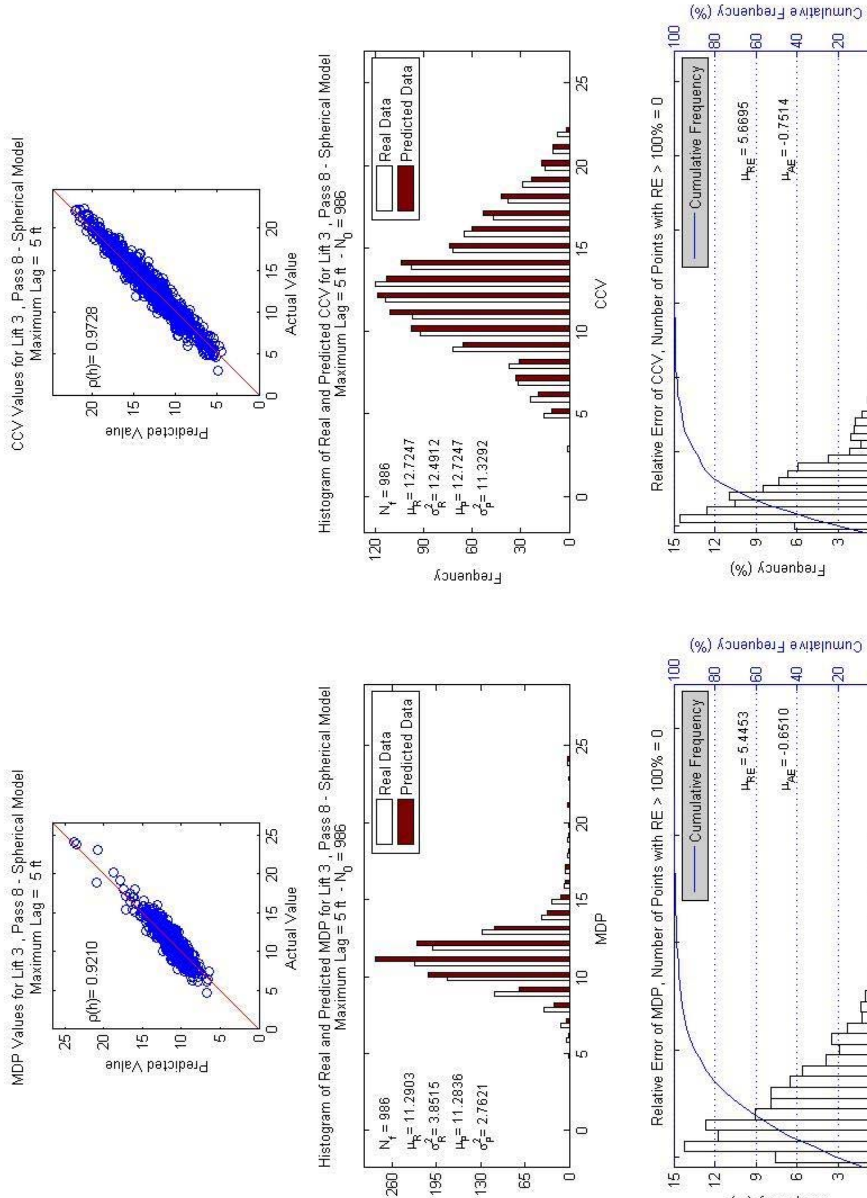

Figure C.34 Kriging results of CCC values for Lift 3, Pass 8/8, using Spherical model and maximum lag of 1.5 m (5 ft)

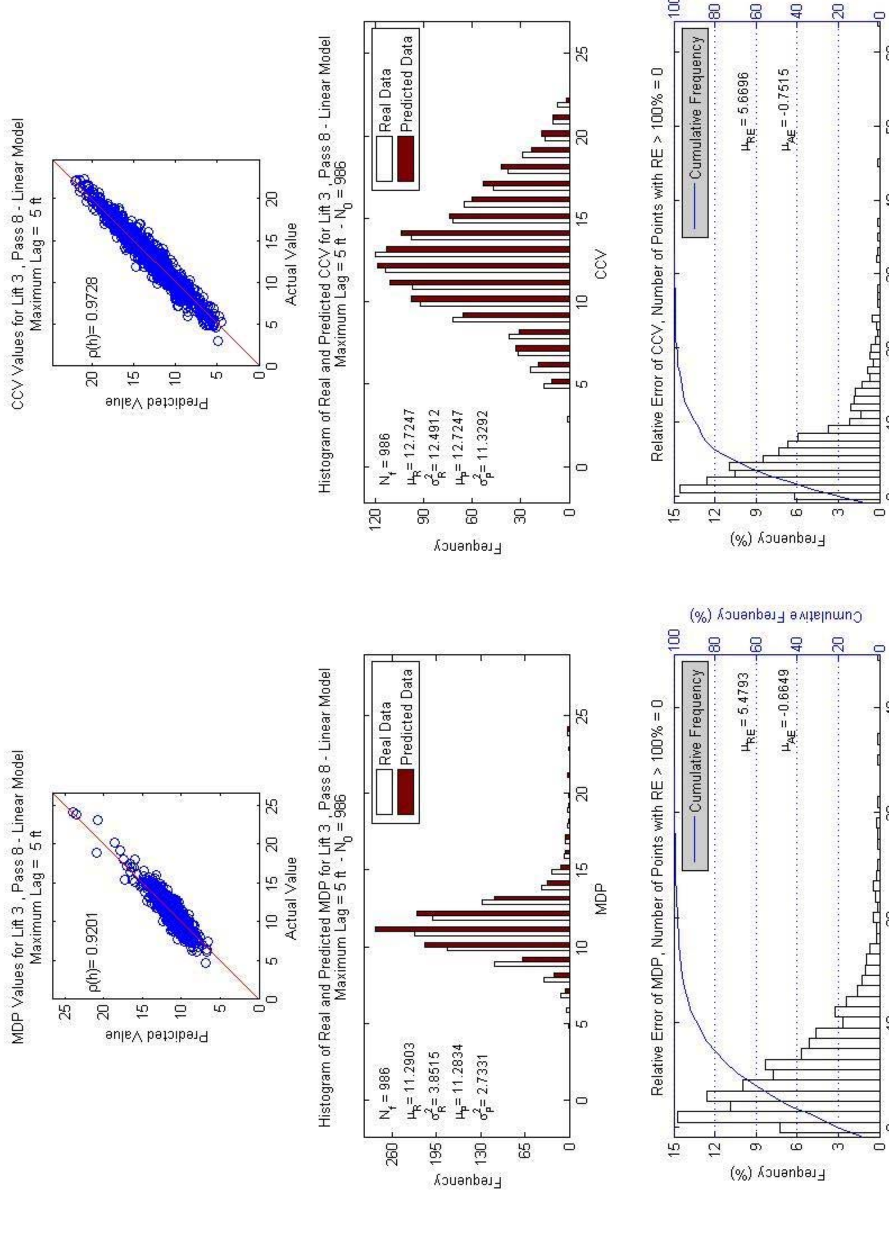

Figure C.35 Kriging results of CCC values for Lift 3, Pass 8/8, using Linear model and maximum lag of 1.5 m (5 ft)

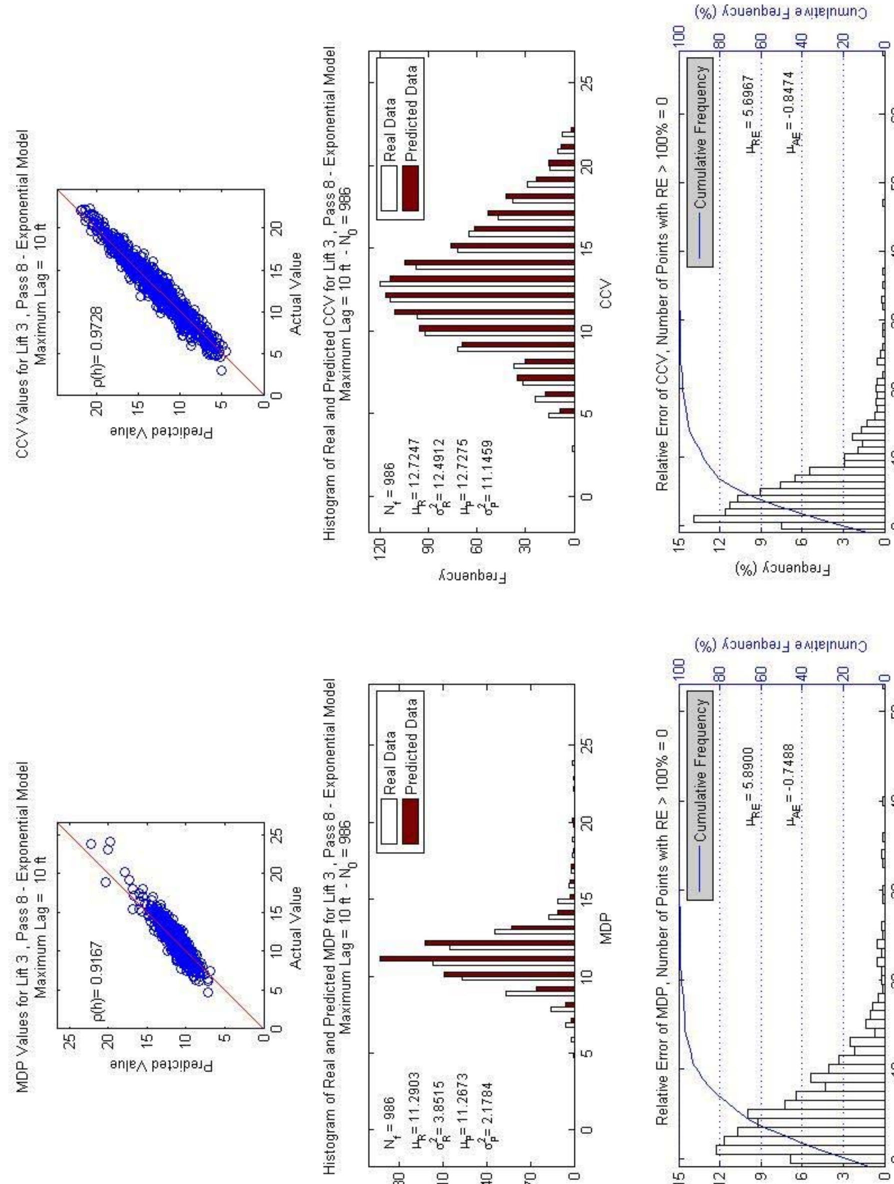

Figure C.36 Kriging results of CCC values for Lift 3, Pass 8/8, using Exponential model and maximum lag of 3.0 (10 ft)

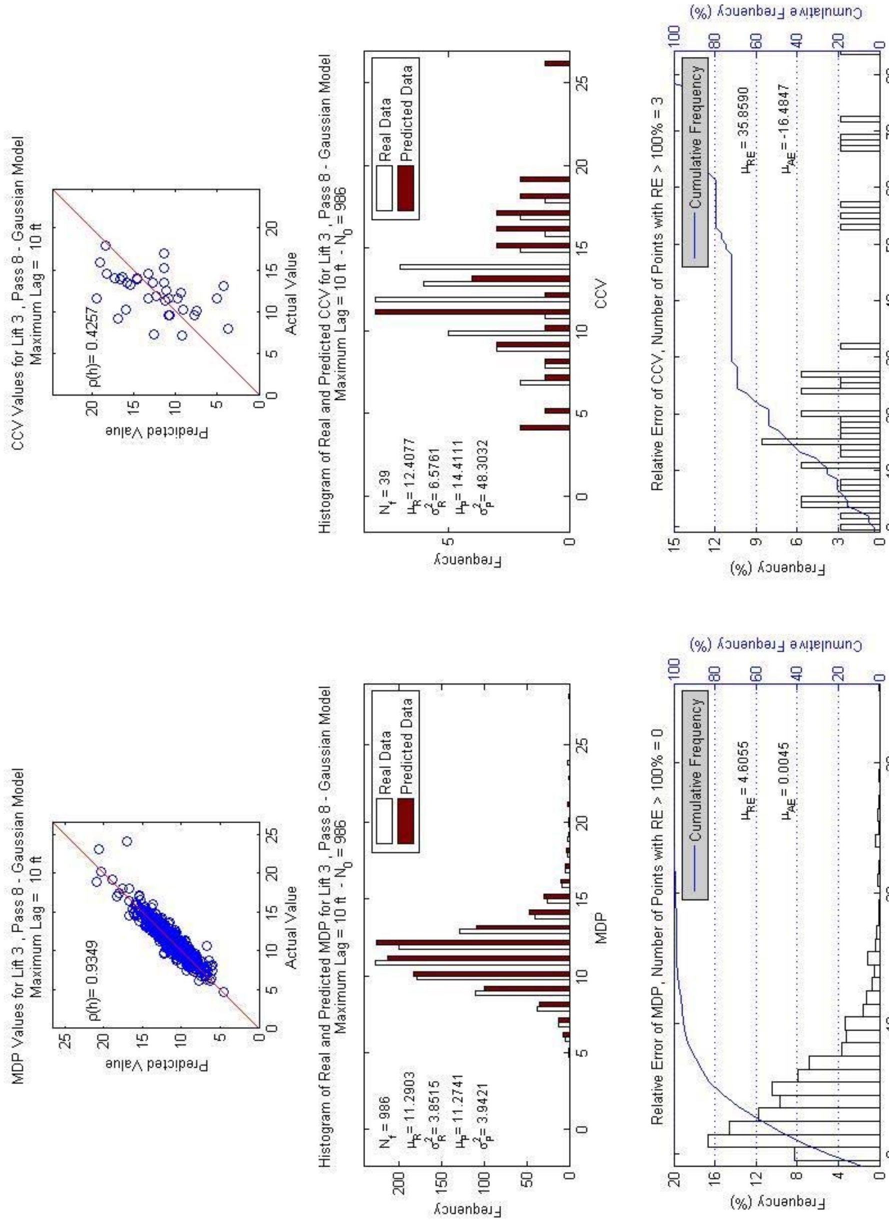

Figure C.37 Kriging results of CCC values for Lift 3, Pass 8/8, using Gaussian model and maximum lag of 3.0 (10 ft)

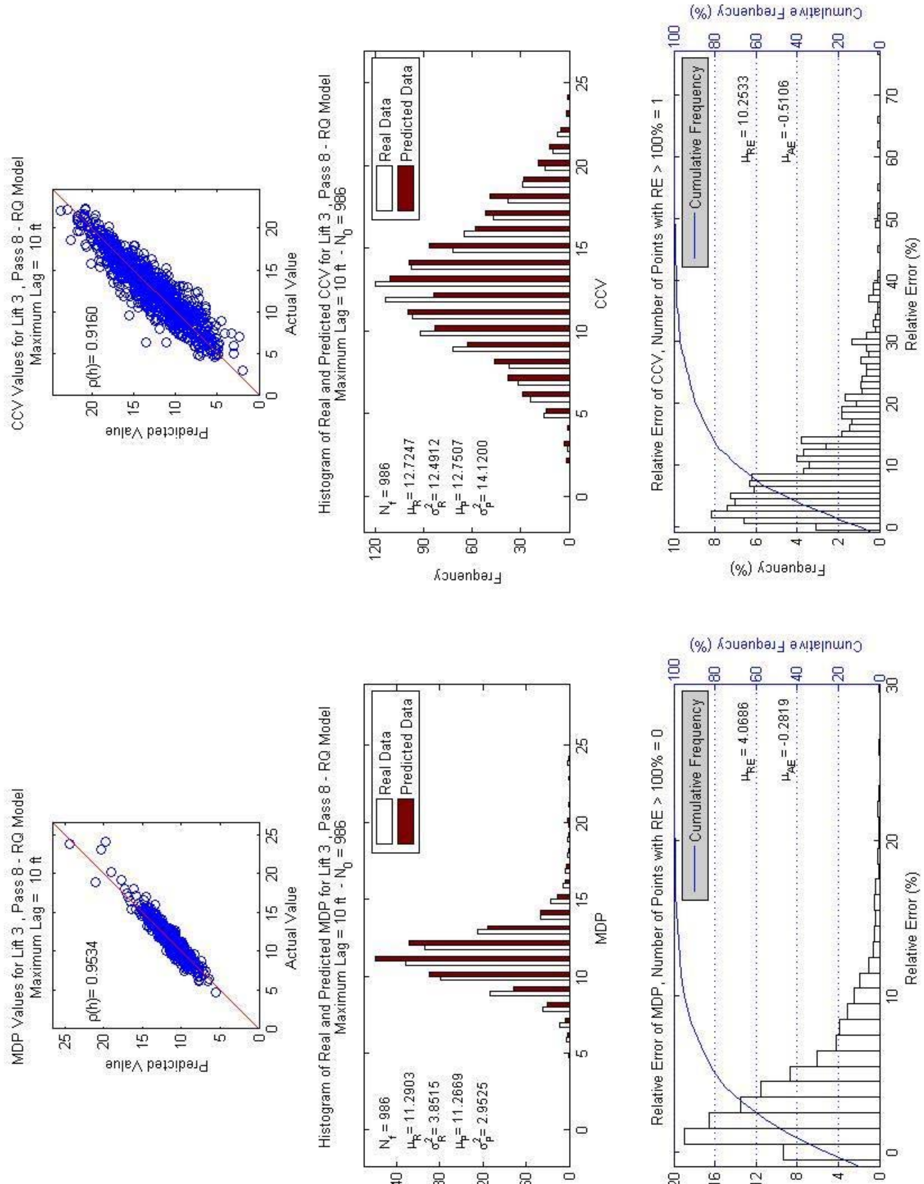

Figure C.38 Kriging results of CCC values for Lift 3, Pass 8/8, using Rational Quadratic (RQ) model and maximum lag of 3.0 (10 ft)

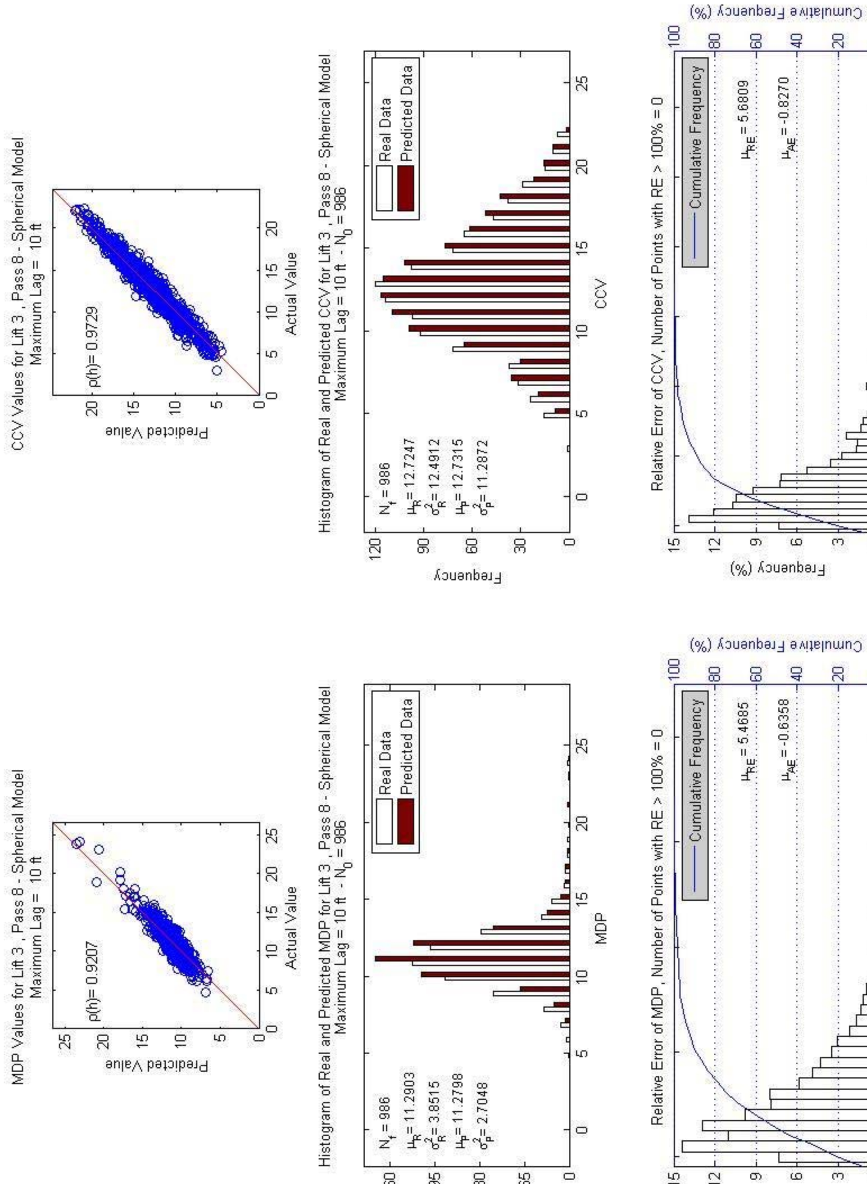

Figure C.39 Kriging results of CCC values for Lift 3, Pass 8/8, using Spherical model and maximum lag of 3.0 (10 ft)

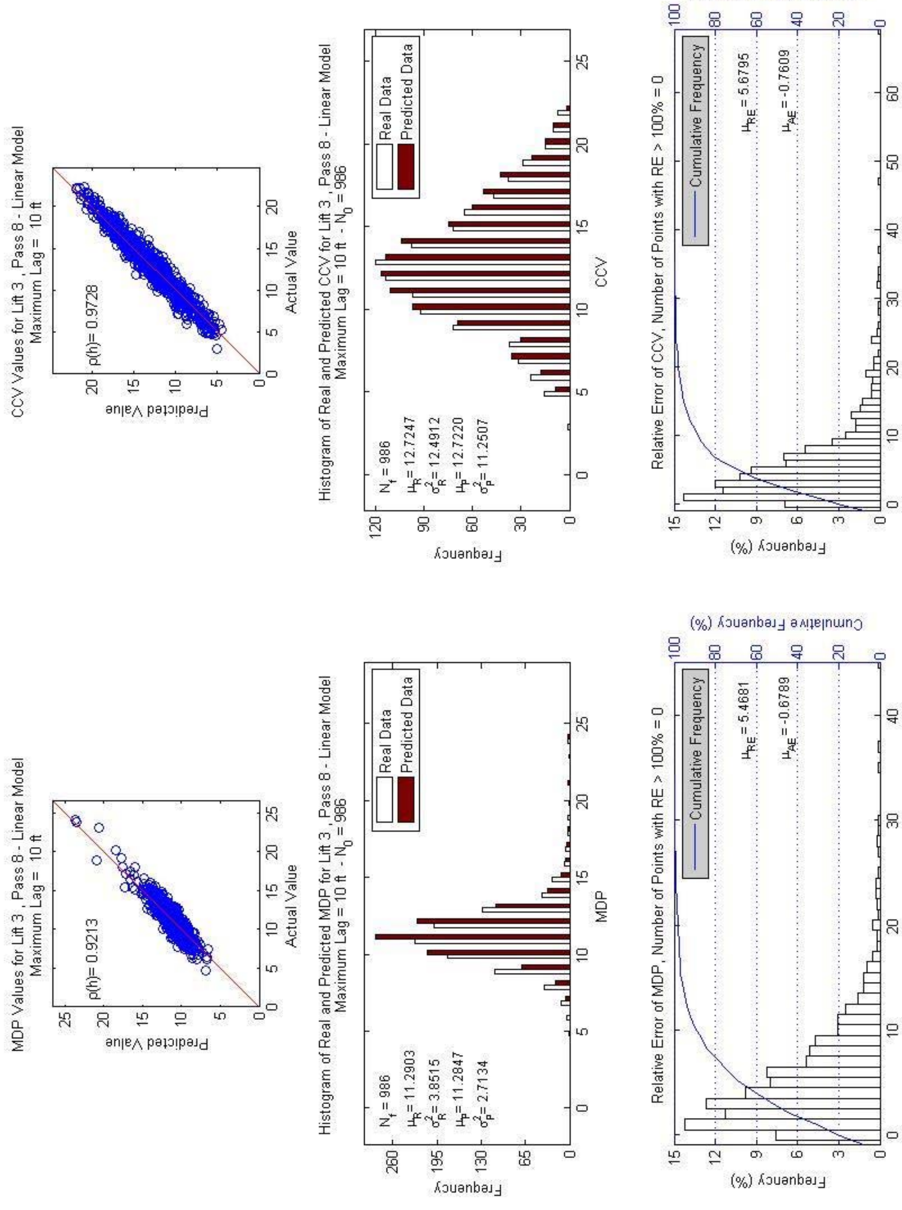

Figure C.40 Kriging results of CCC values for Lift 3, Pass 8/8, using Linear model and maximum lag of 3.0 (10 ft)

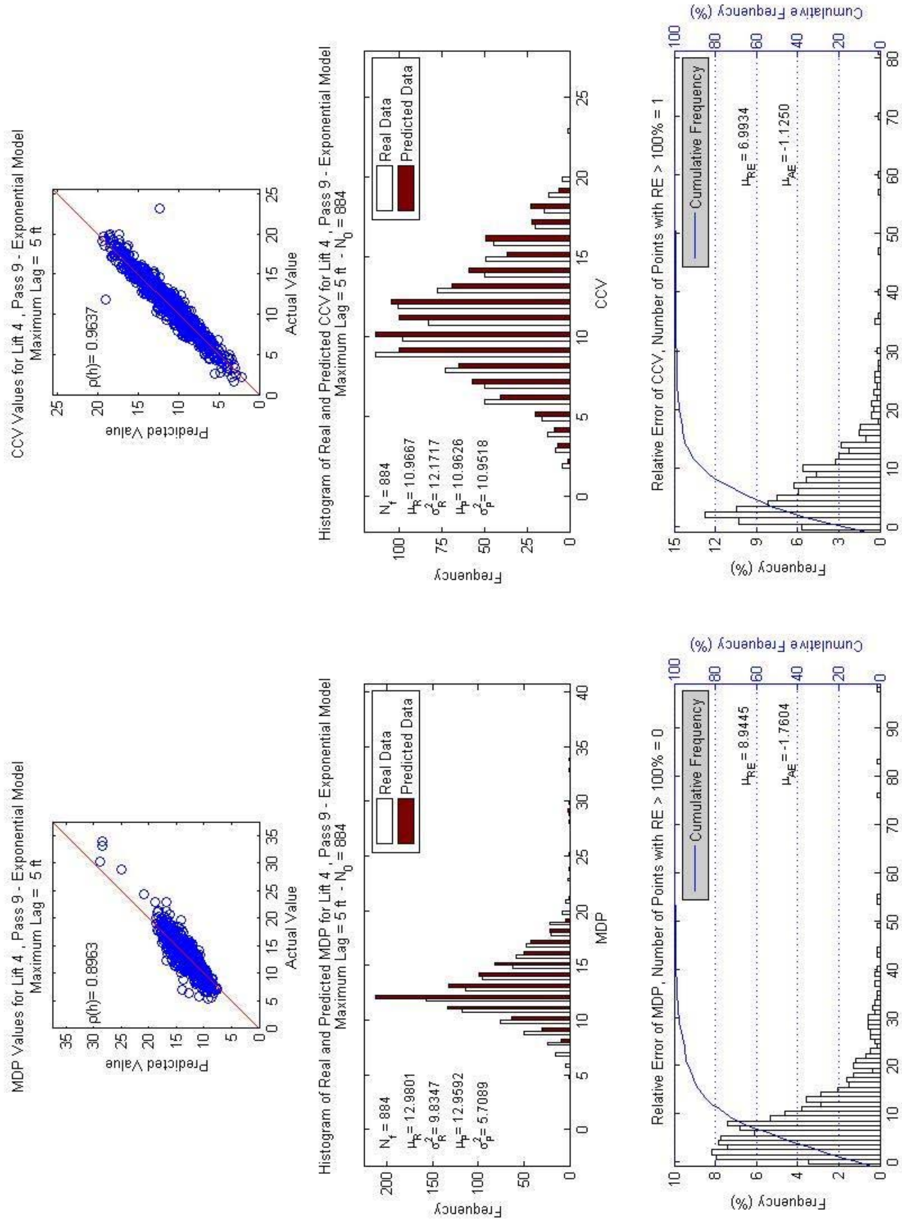

Figure C.41 Kriging results of CCC values for Lift 4, Pass 9/9, using Exponential model and maximum lag of 1.5 (5 ft)

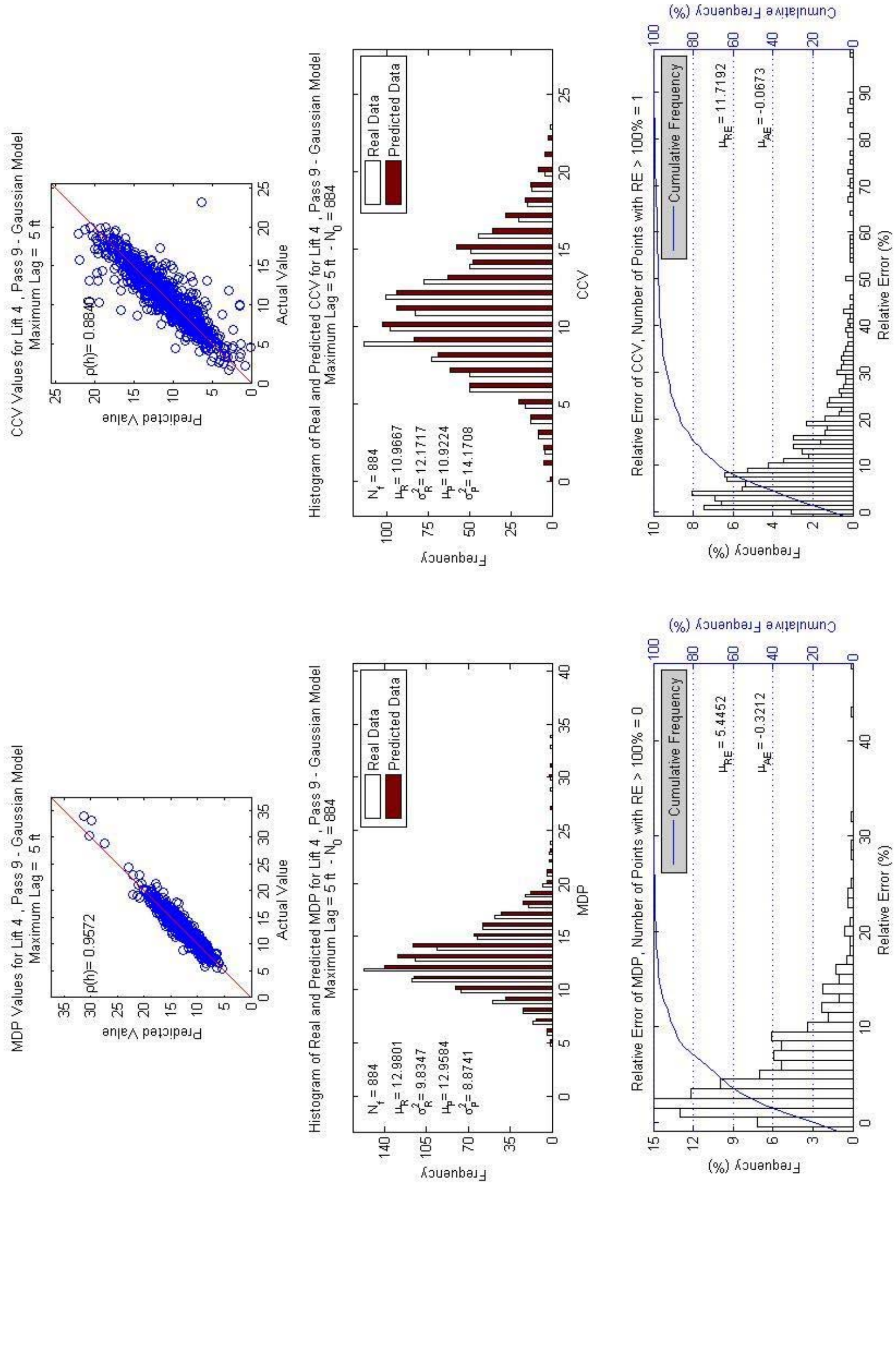

Figure C.42 Kriging results of CCC values for Lift 4, Pass 9/9, using Gaussian model and maximum lag of 1.5 (5 ft)

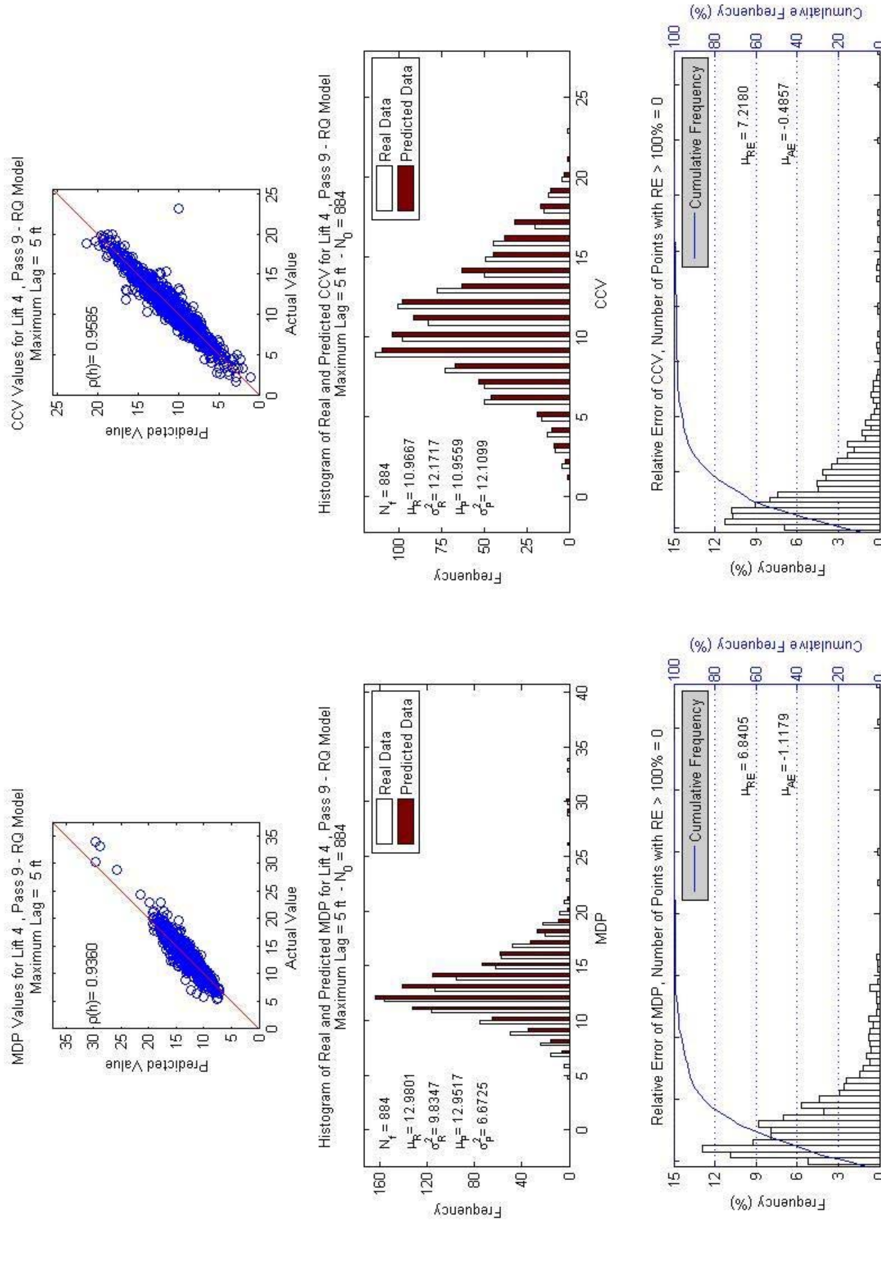

Figure C.43 Kriging results of CCC values for Lift 4, Pass 9/9, using Rational Quadratic (RQ) model and maximum lag of 1.5 (5 ft)

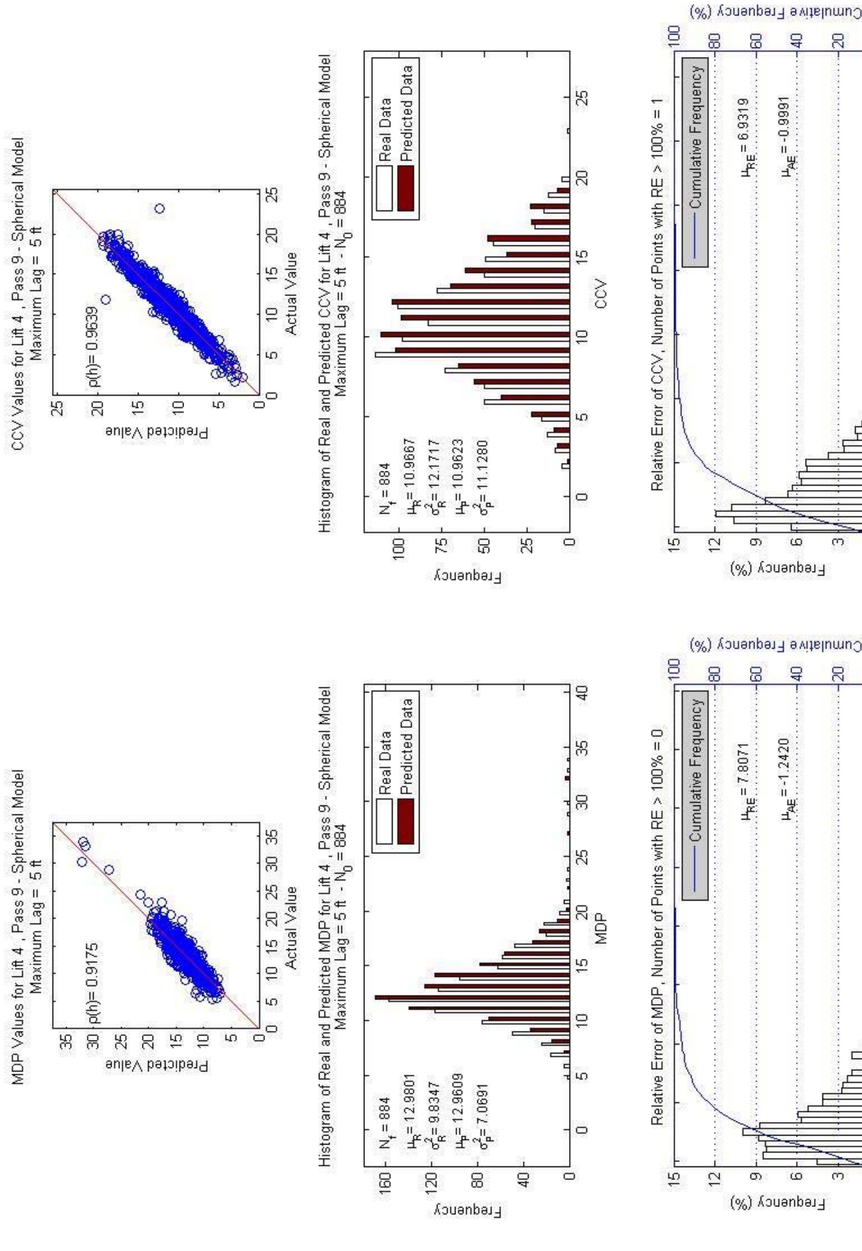

Figure C.44 Kriging results of CCC values for Lift 4, Pass 9/9, using Spherical model and maximum lag of 1.5 (5 ft)

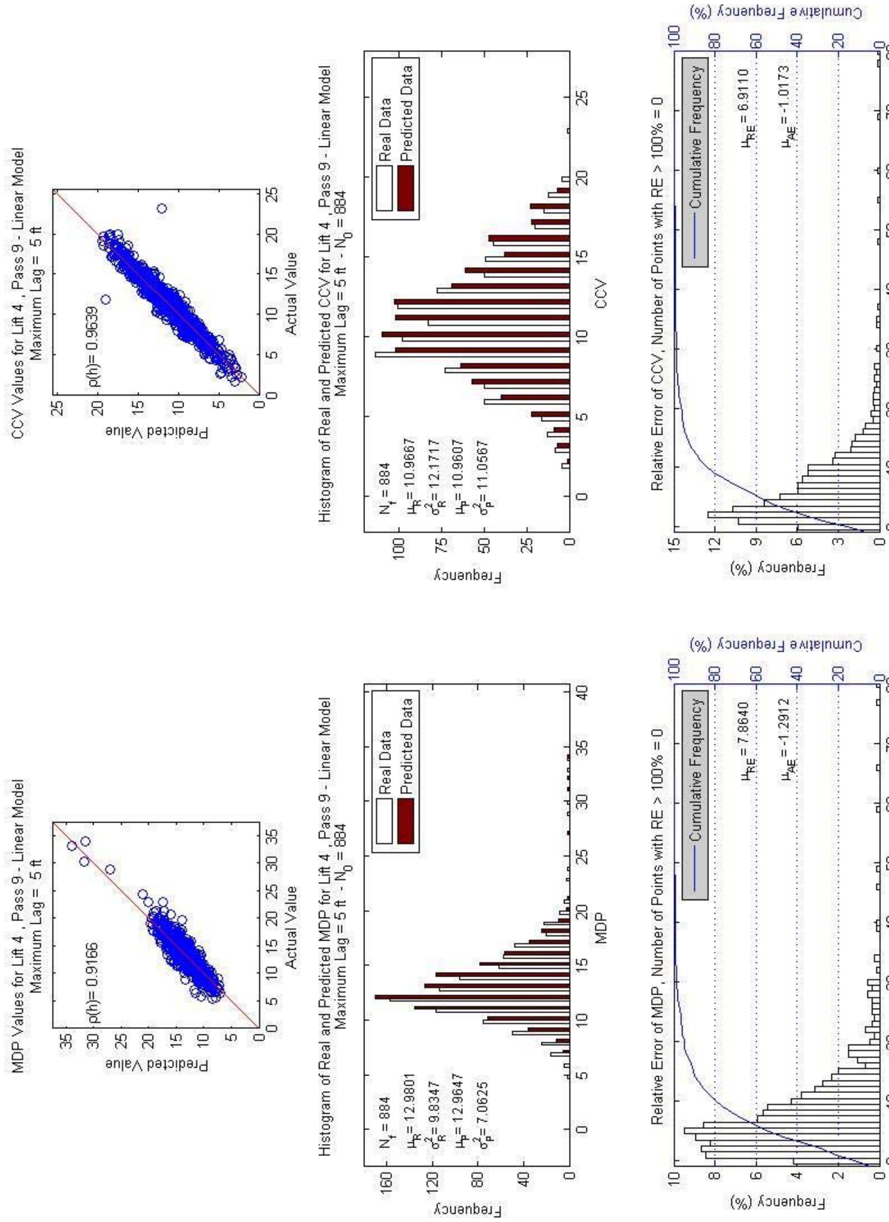

Figure C.45 Kriging results of CCC values for Lift 4, Pass 9/9, using Linear model and maximum lag of 1.5 (5 ft)

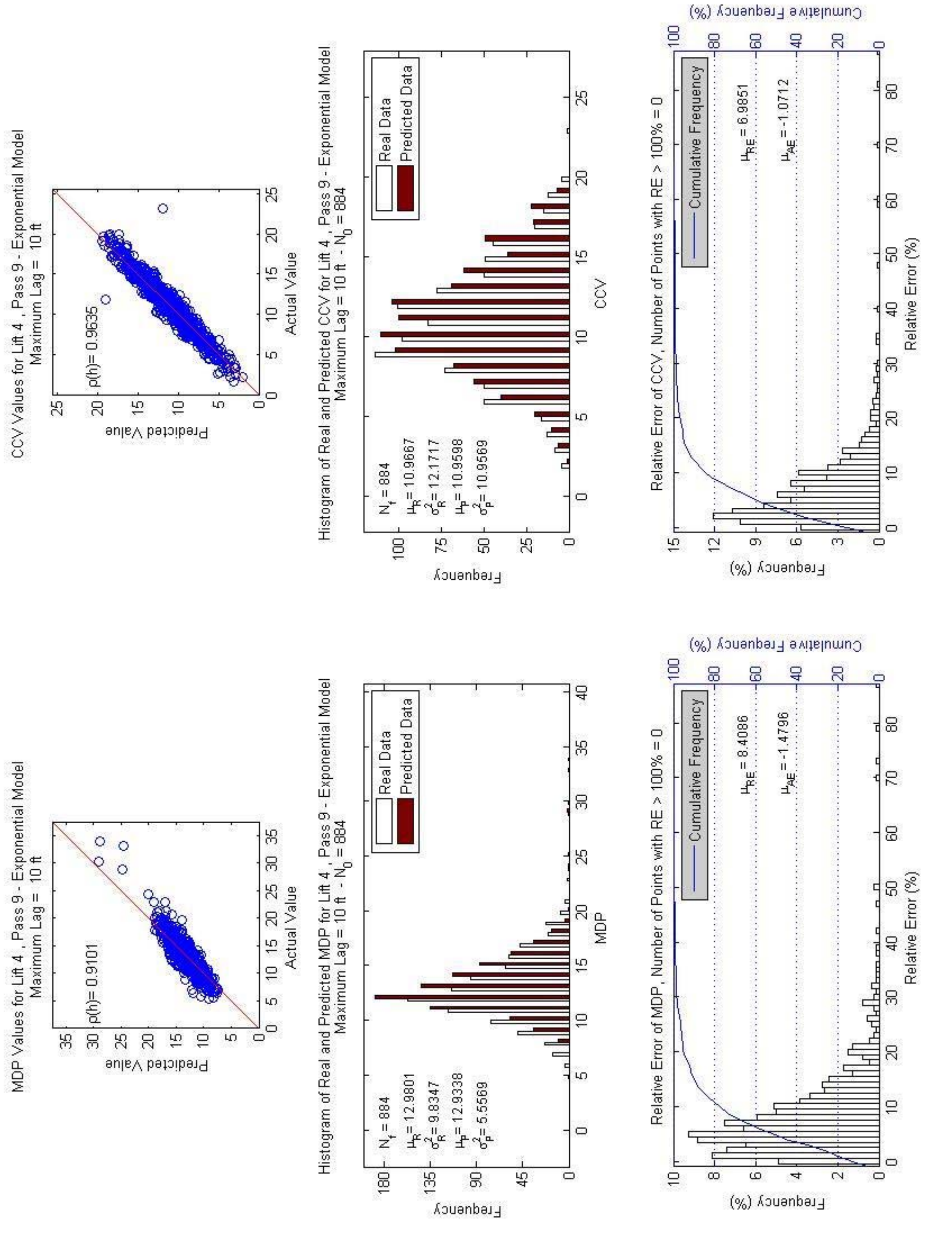

Figure C.46 Kriging results of CCC values for Lift 4, Pass 9/9, using Exponential model and maximum lag of 3.0 (10 ft)

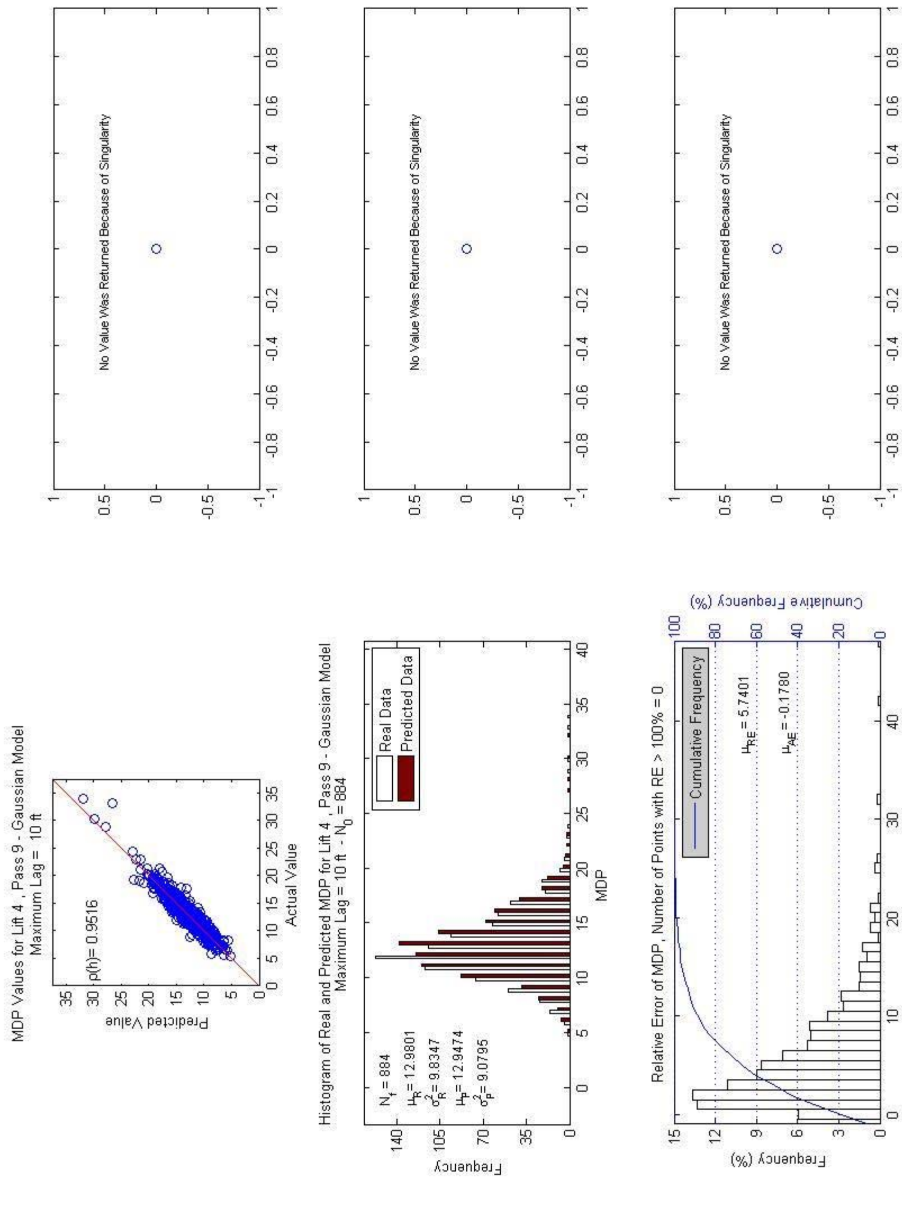

Figure C.47 Kriging results of CCC values for Lift 4, Pass 9/9, using Gaussian model and maximum lag of 3.0 (10 ft)

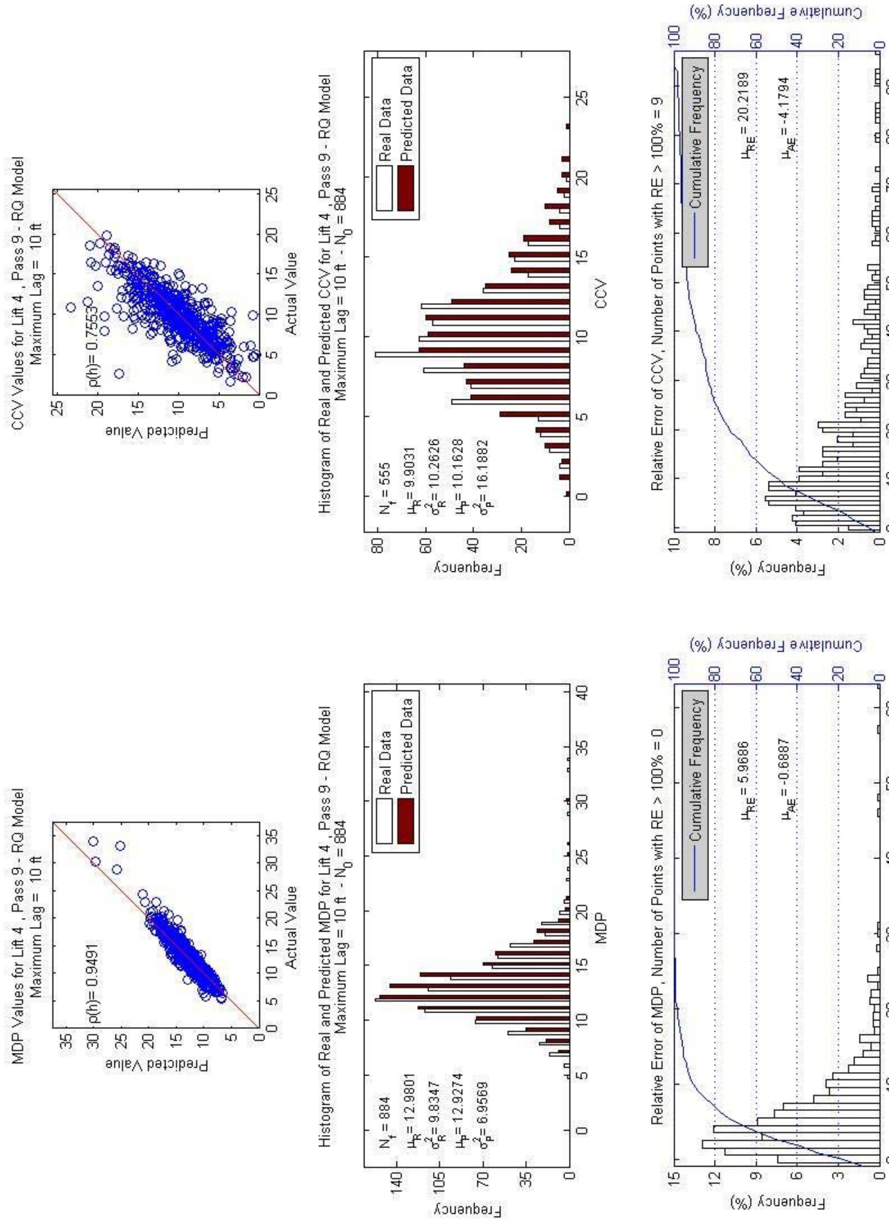

Figure C.48 Kriging results of CCC values for Lift 4, Pass 9/9, using Rational Quadratic (RQ) model and maximum lag of 3.0 (10 ft)

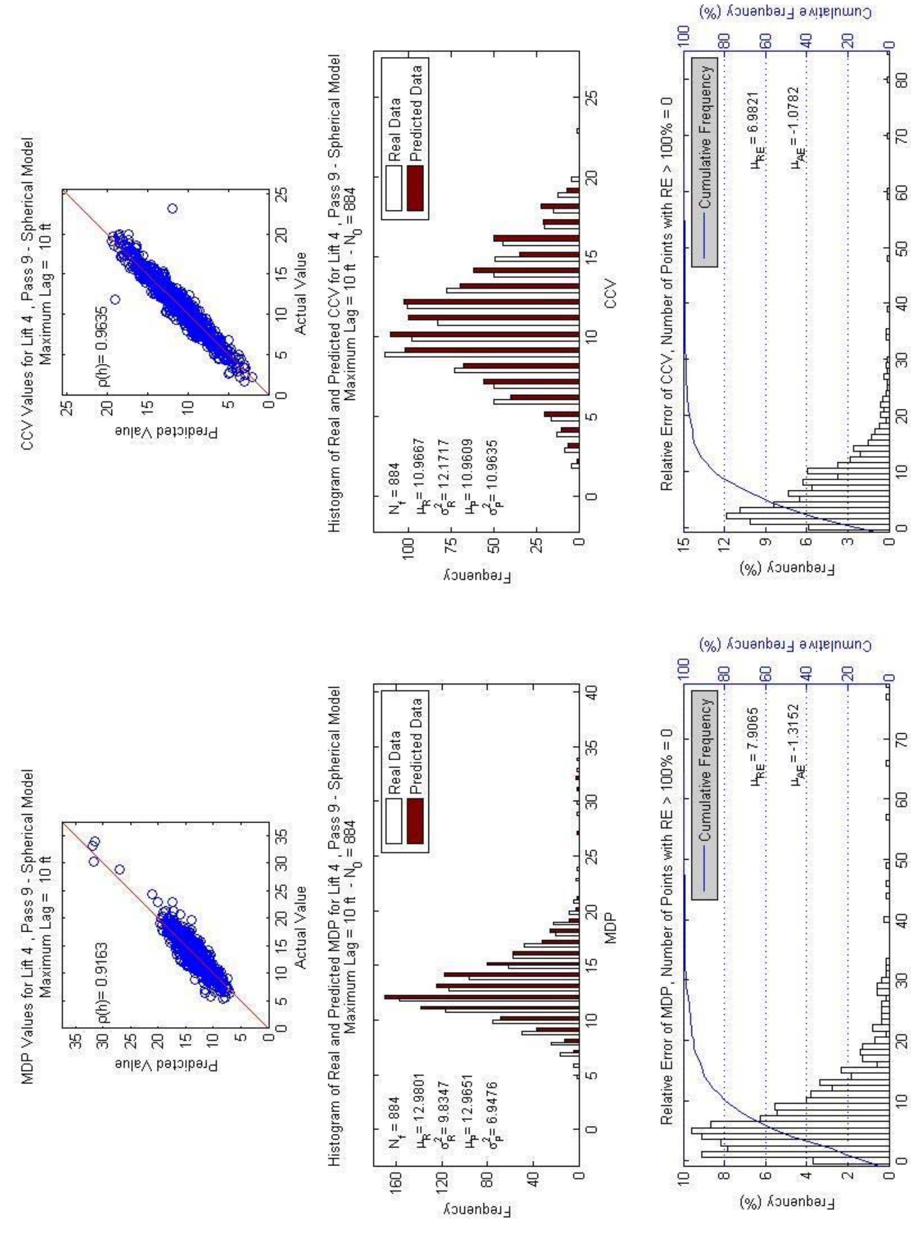

Figure C.49 Kriging results of CCC values for Lift 4, Pass 9/9, using Spherical model and maximum lag of 3.0 (10 ft)

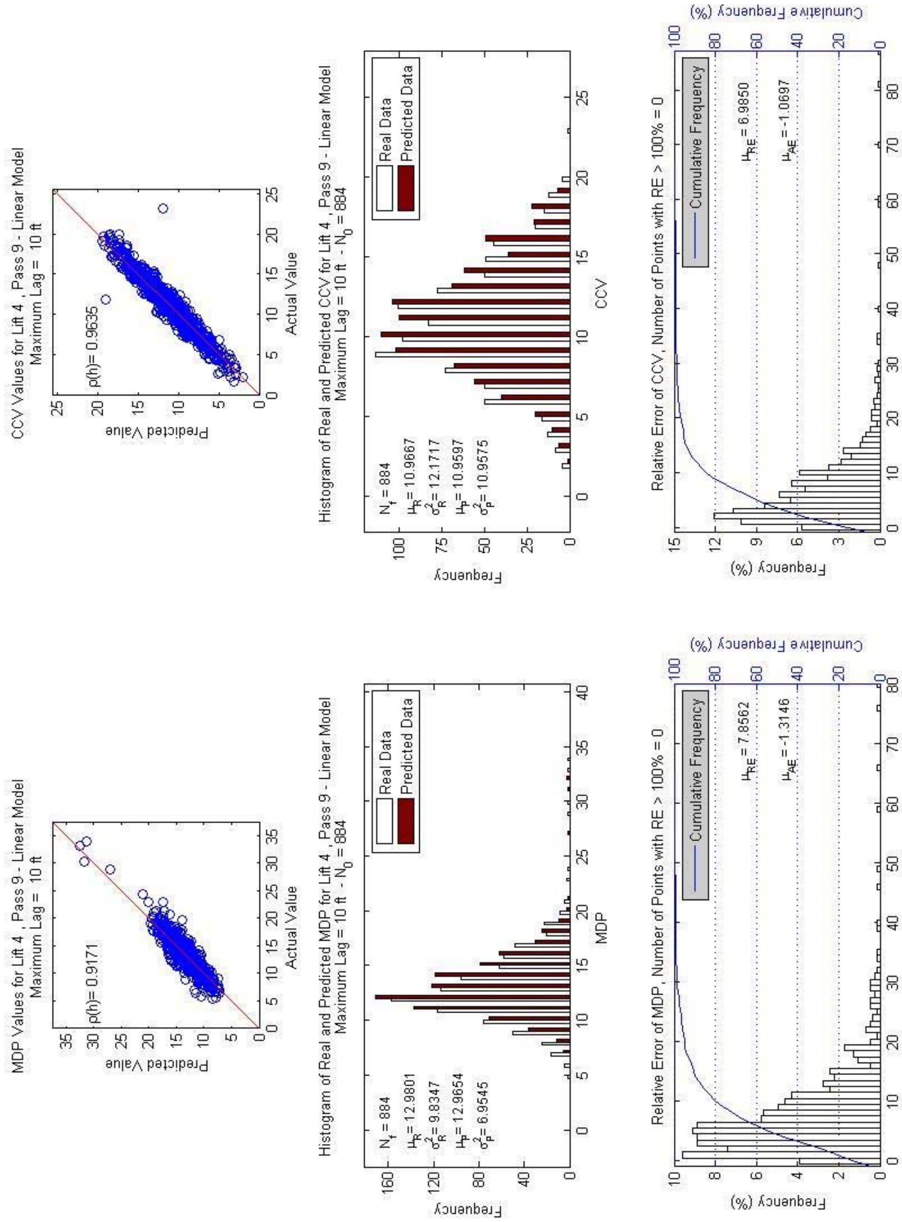

Figure C.50 Kriging results of CCC values for Lift 4, Pass 9/9, using Linear model and maximum lag of 3.0 (10 ft)

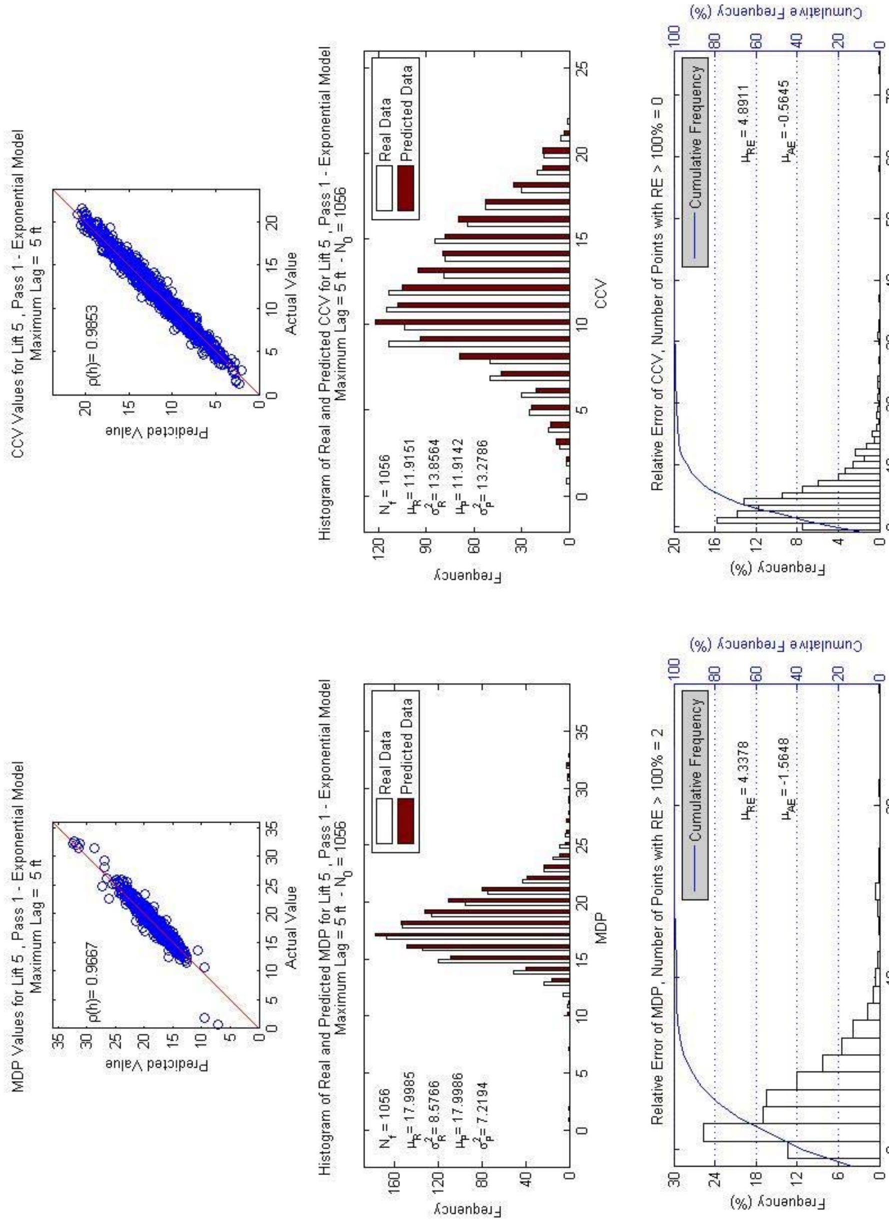

Figure C.51 Kriging results of CCC values for Lift 5, Pass 1/7, using Exponential model and maximum lag of 1.5 (5 ft)

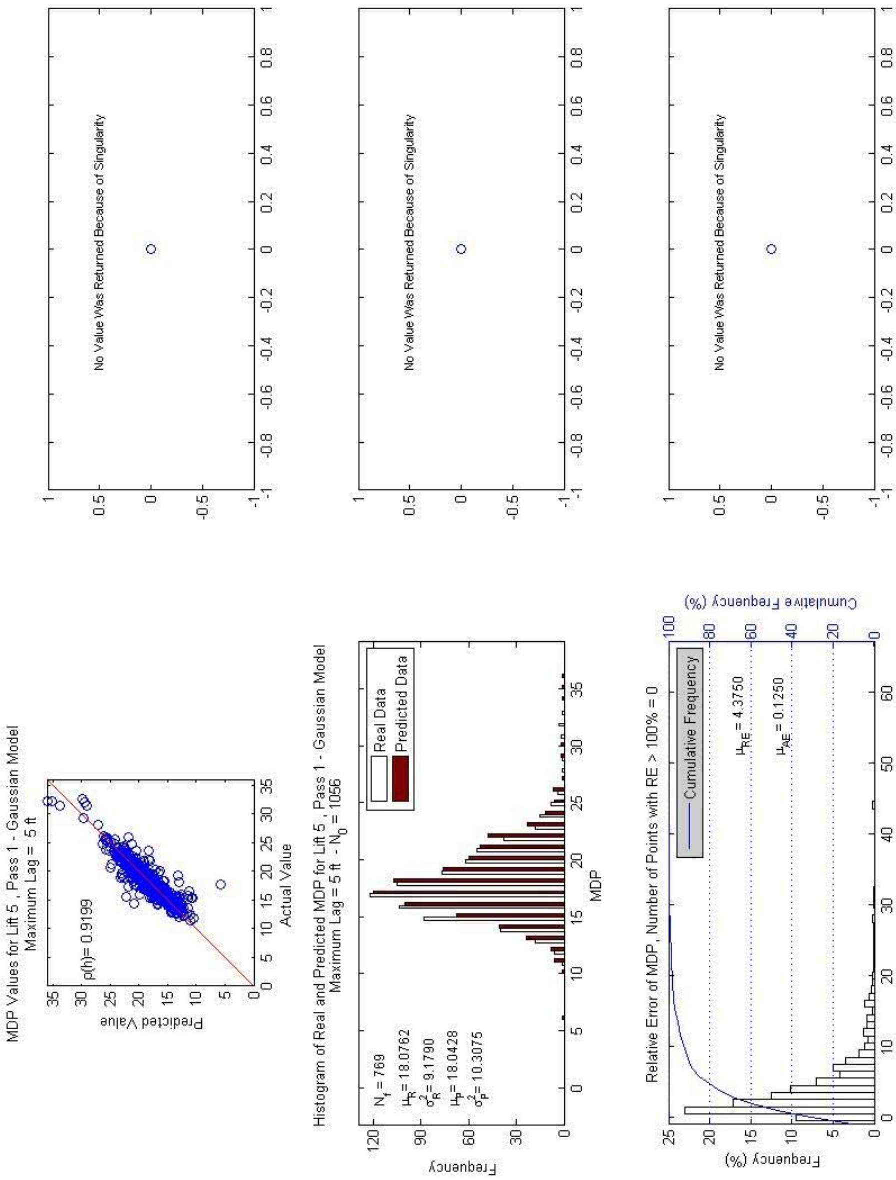

Figure C.52 Kriging results of CCC values for Lift 5, Pass 1/7, using Gaussian model and maximum lag of 1.5 (5 ft)

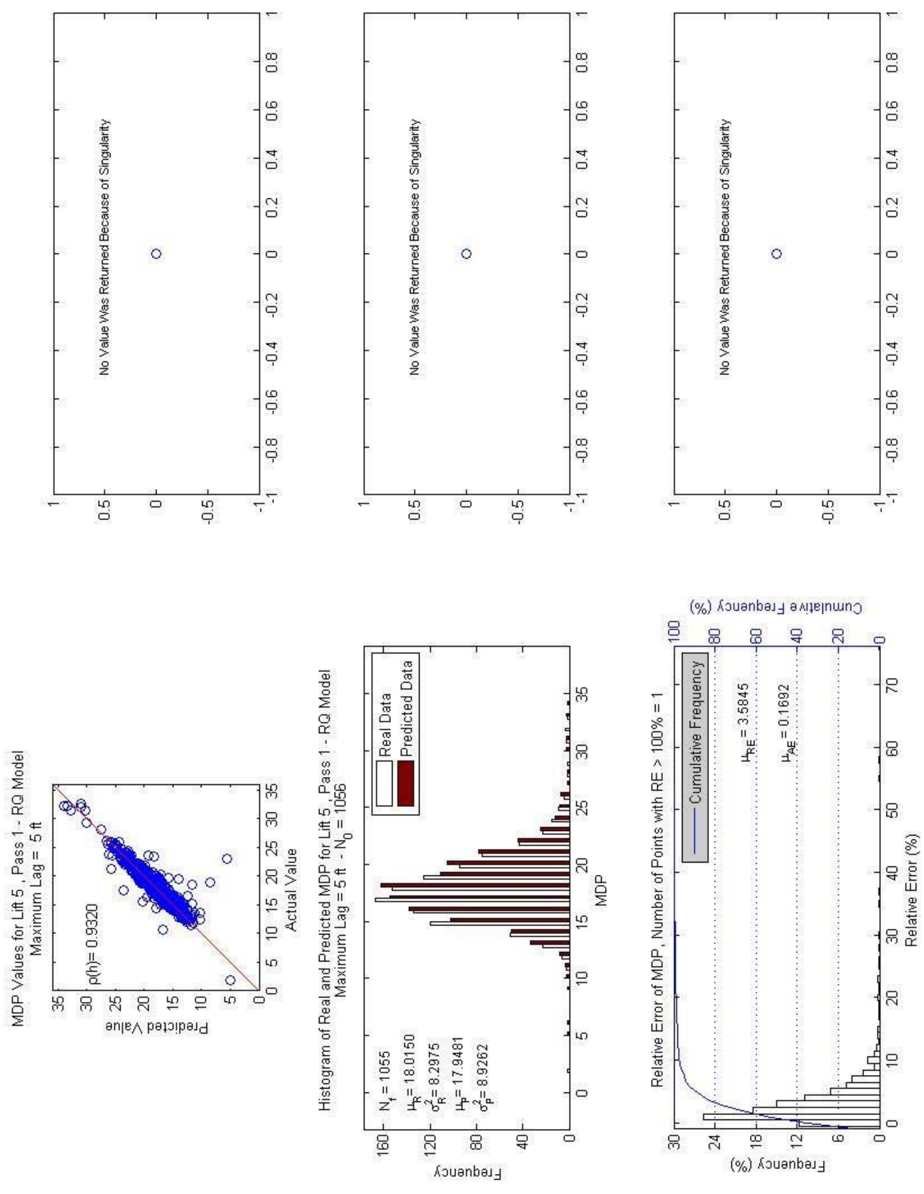

Figure C.53 Kriging results of CCC values for Lift 5, Pass 1/7, using Rational Quadratic (RQ) model and maximum lag of 1.5 (5 ft)

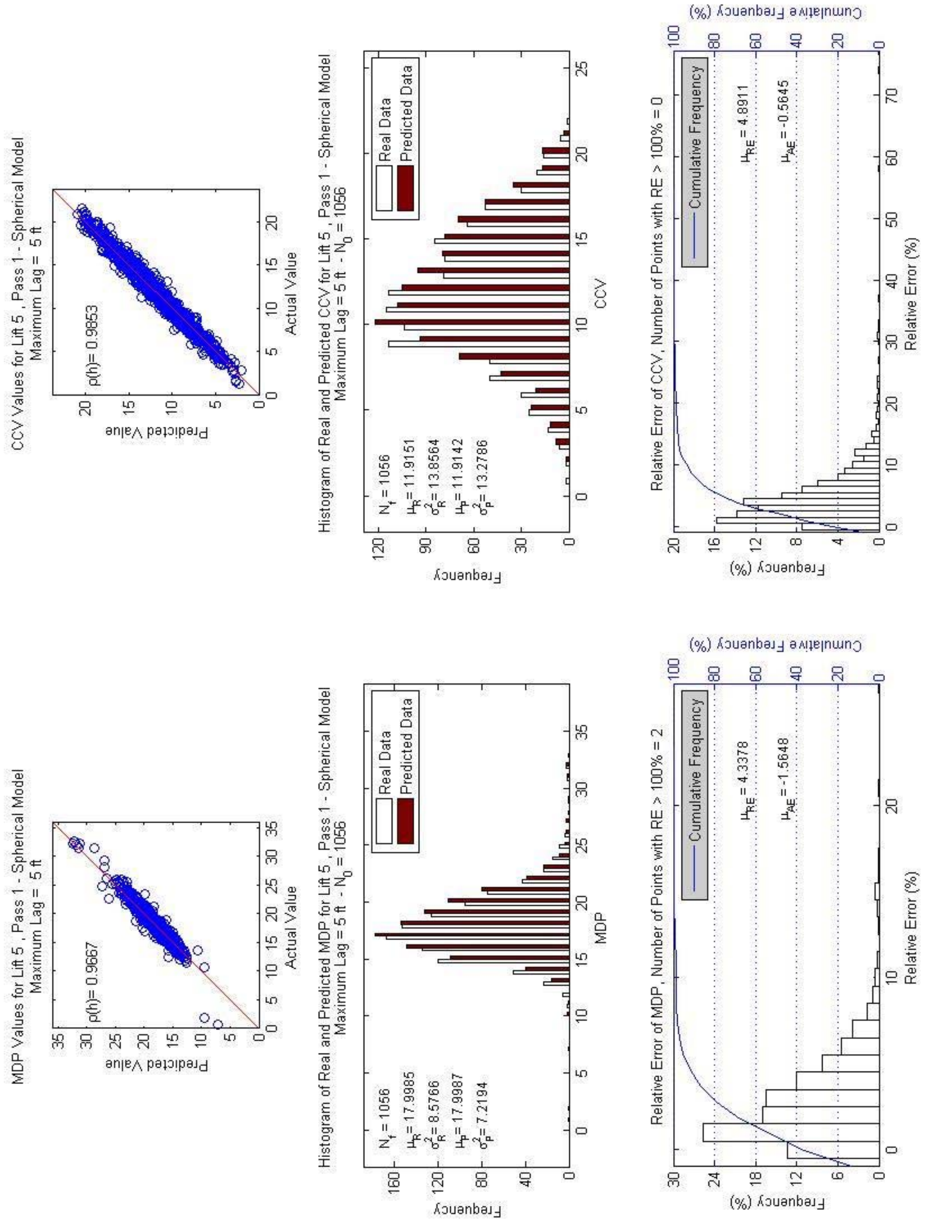

Figure C.54 Kriging results of CCC values for Lift 5, Pass 1/7, using Spherical model and maximum lag of 1.5 (5 ft)

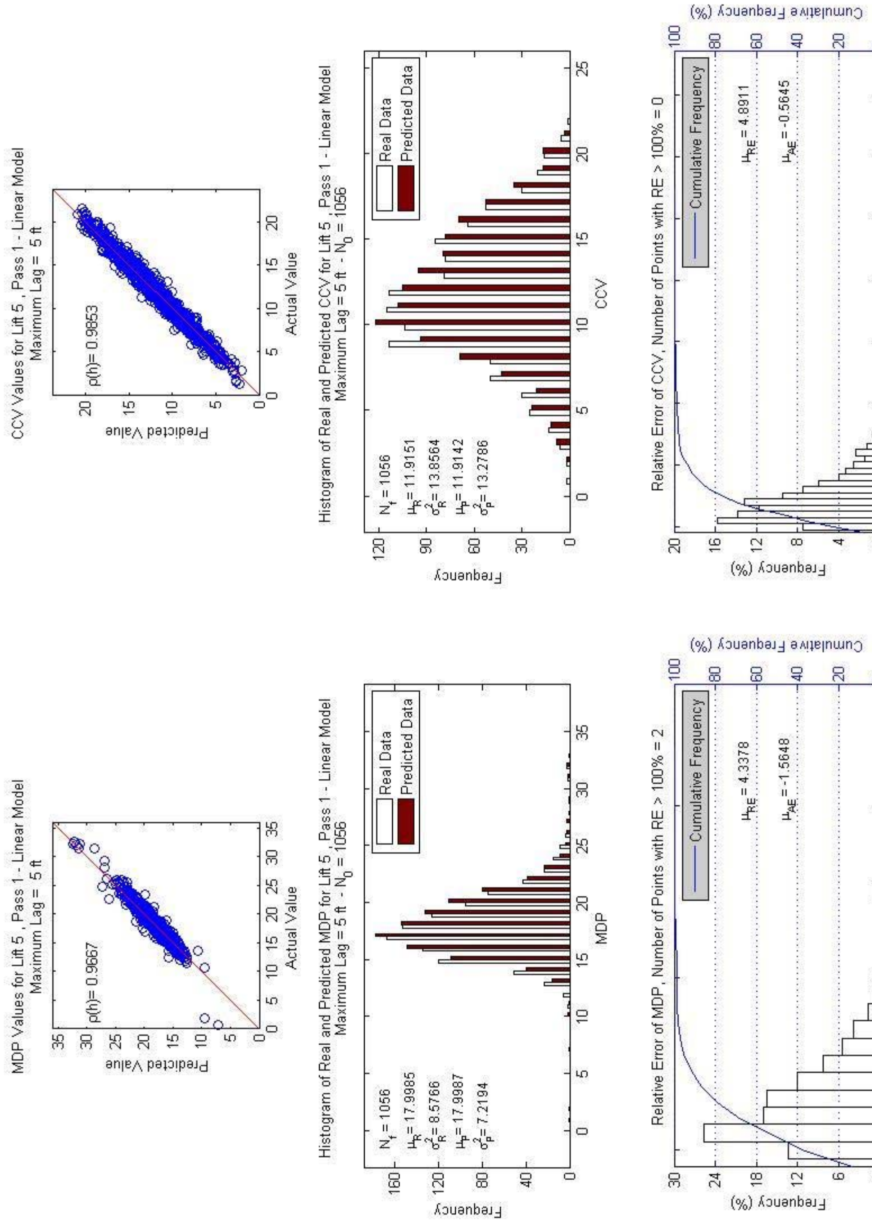

Figure C.55 Kriging results of CCC values for Lift 5, Pass 1/7, using Linear model and maximum lag of 1.5 (5 ft)

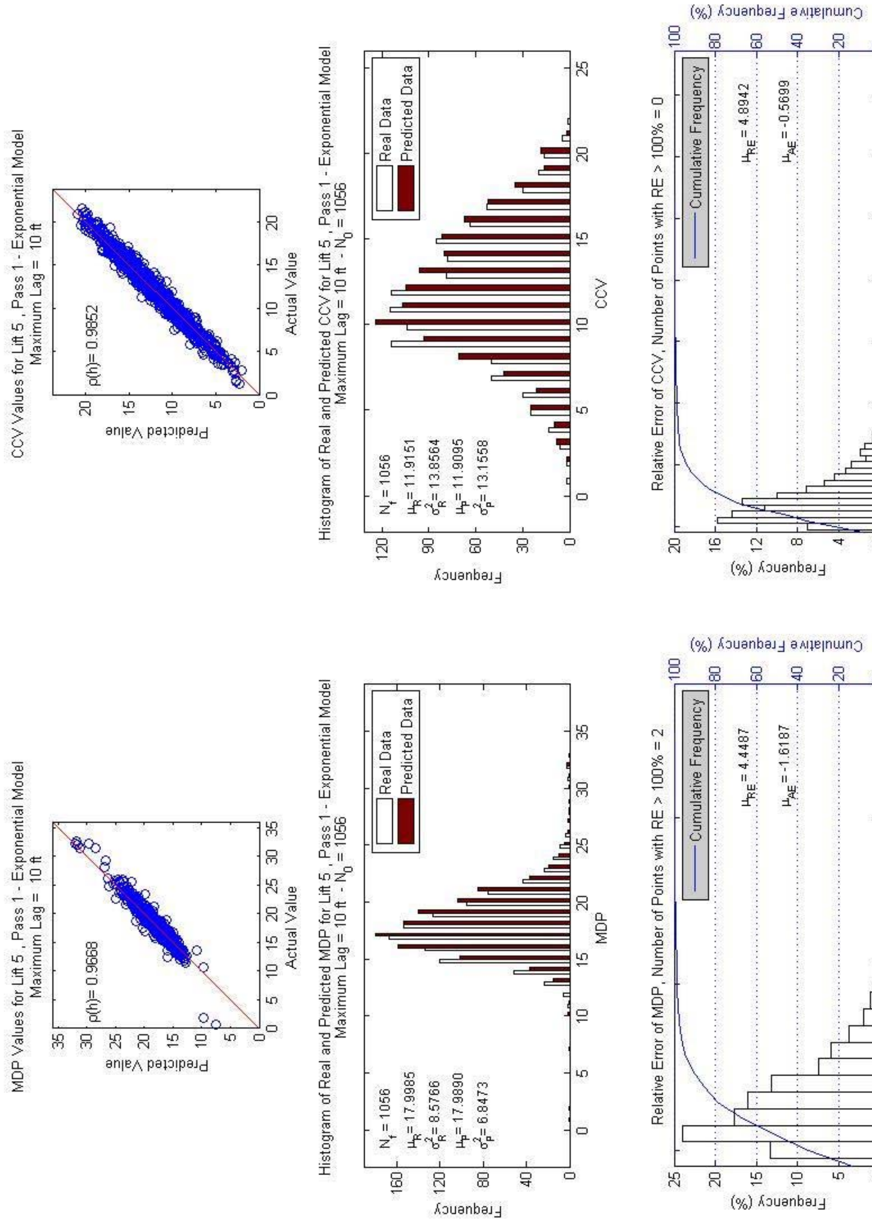

Figure C.56 Kriging results of CCC values for Lift 5, Pass 1/7, using Exponential model and maximum lag of 3.0 (10 ft)

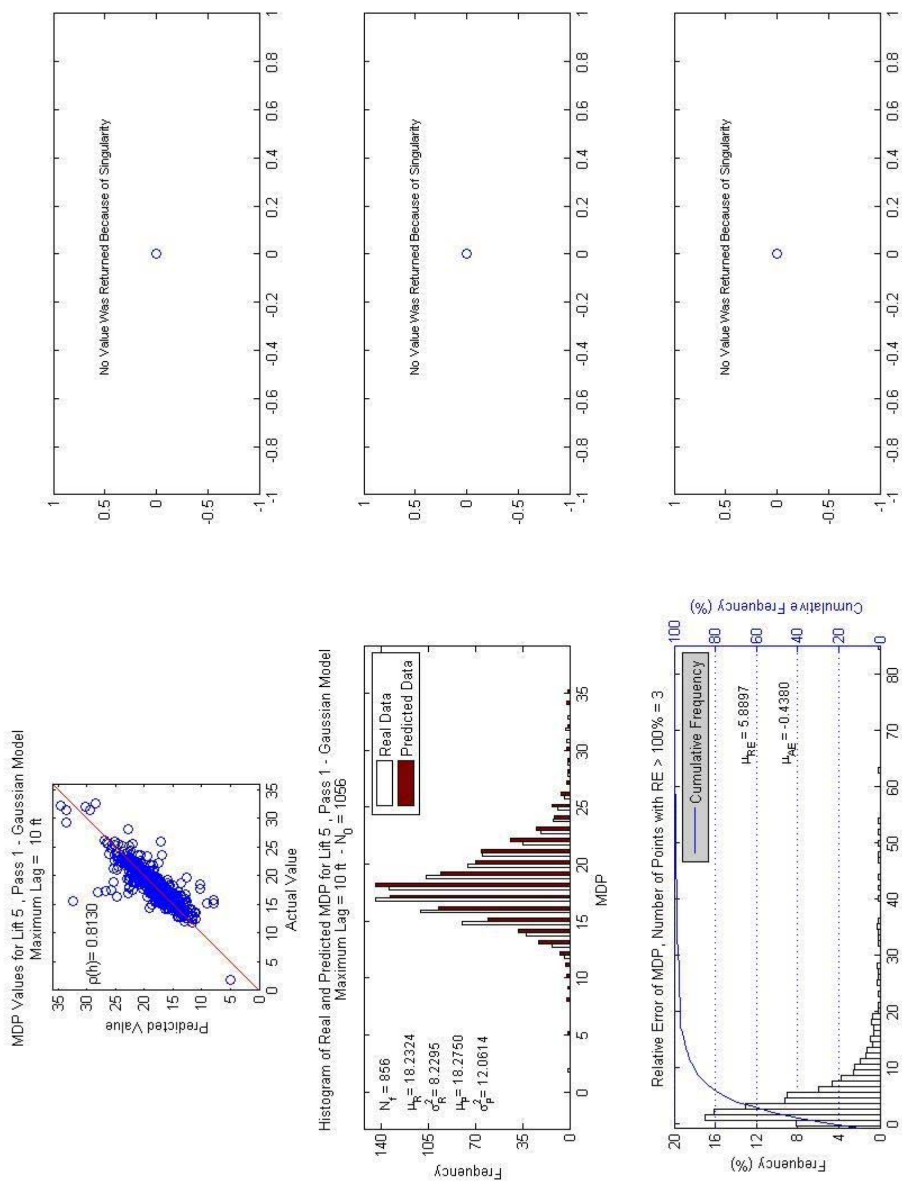

Figure C.57 Kriging results of CCC values for Lift 5, Pass 1/7, using Gaussian model and maximum lag of 3.0 (10 ft)

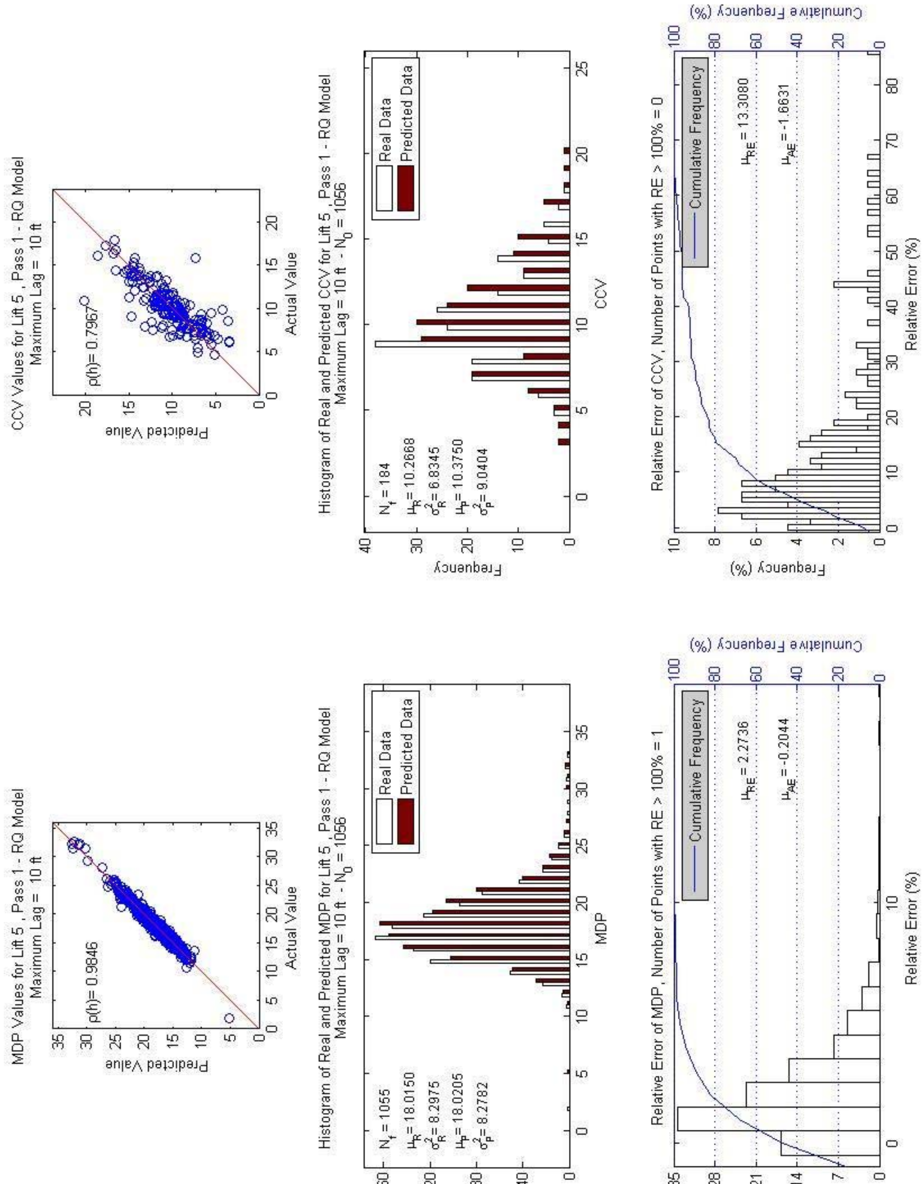

Figure C.58 Kriging results of CCC values for Lift 5, Pass 1/7, using Rational Quadratic (RQ) model and maximum lag of 3.0 (10 ft)

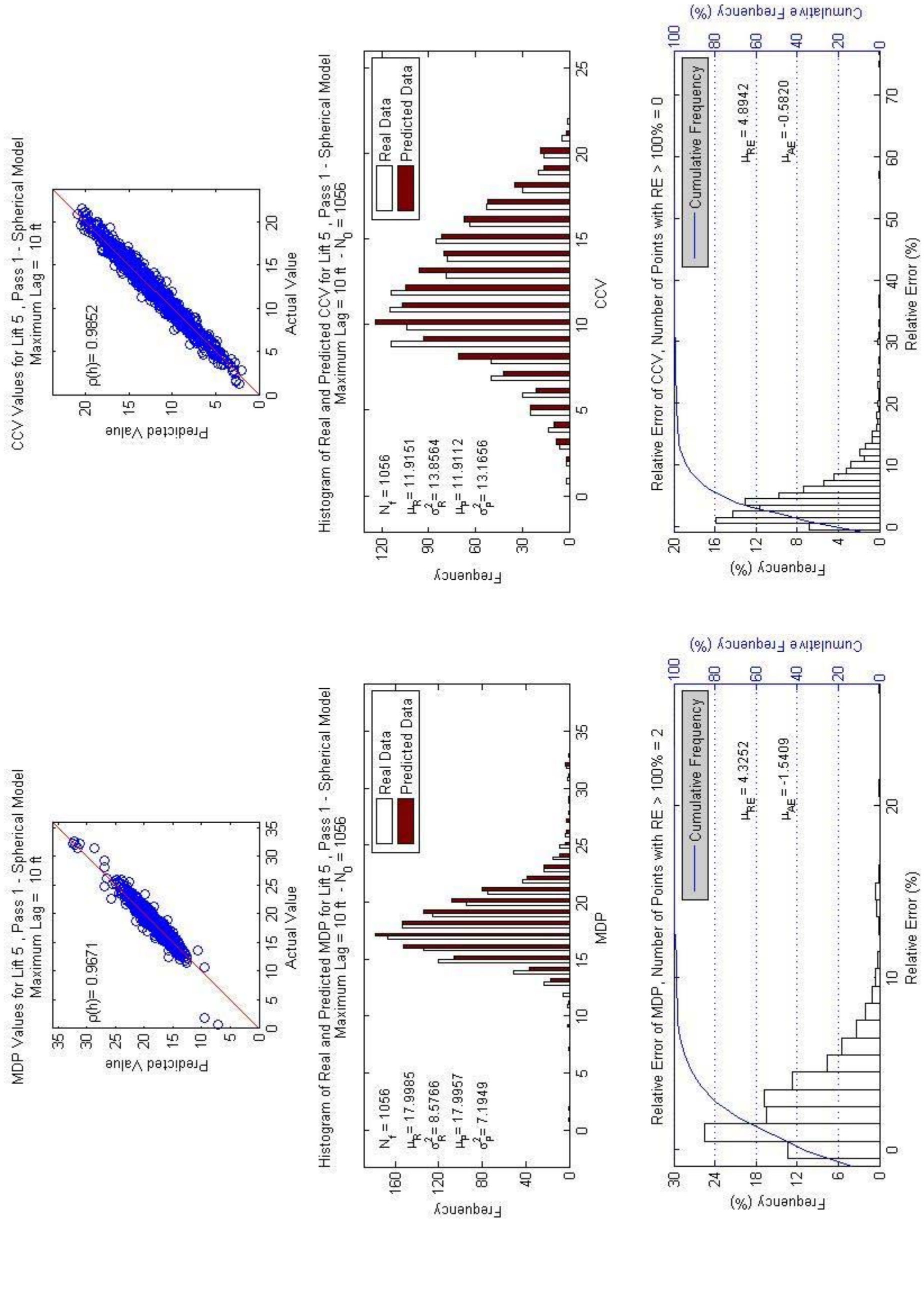

Figure C.59 Kriging results of CCC values for Lift 5, Pass 1/7, using Spherical model and maximum lag of 3.0 (10 ft)

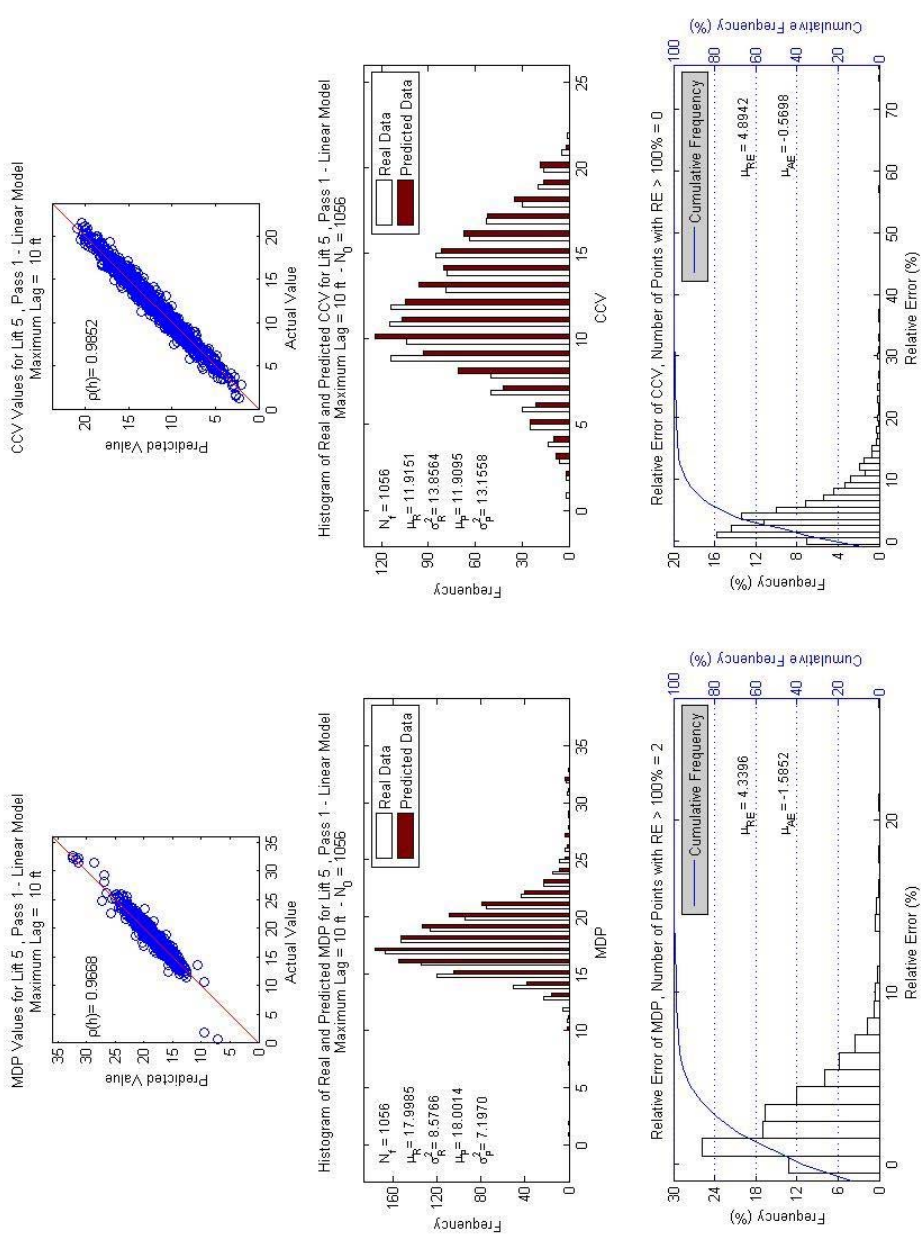

Figure C.60 Kriging results of CCC values for Lift 5, Pass 1/7, using Linear model and maximum lag of 3.0 (10 ft)

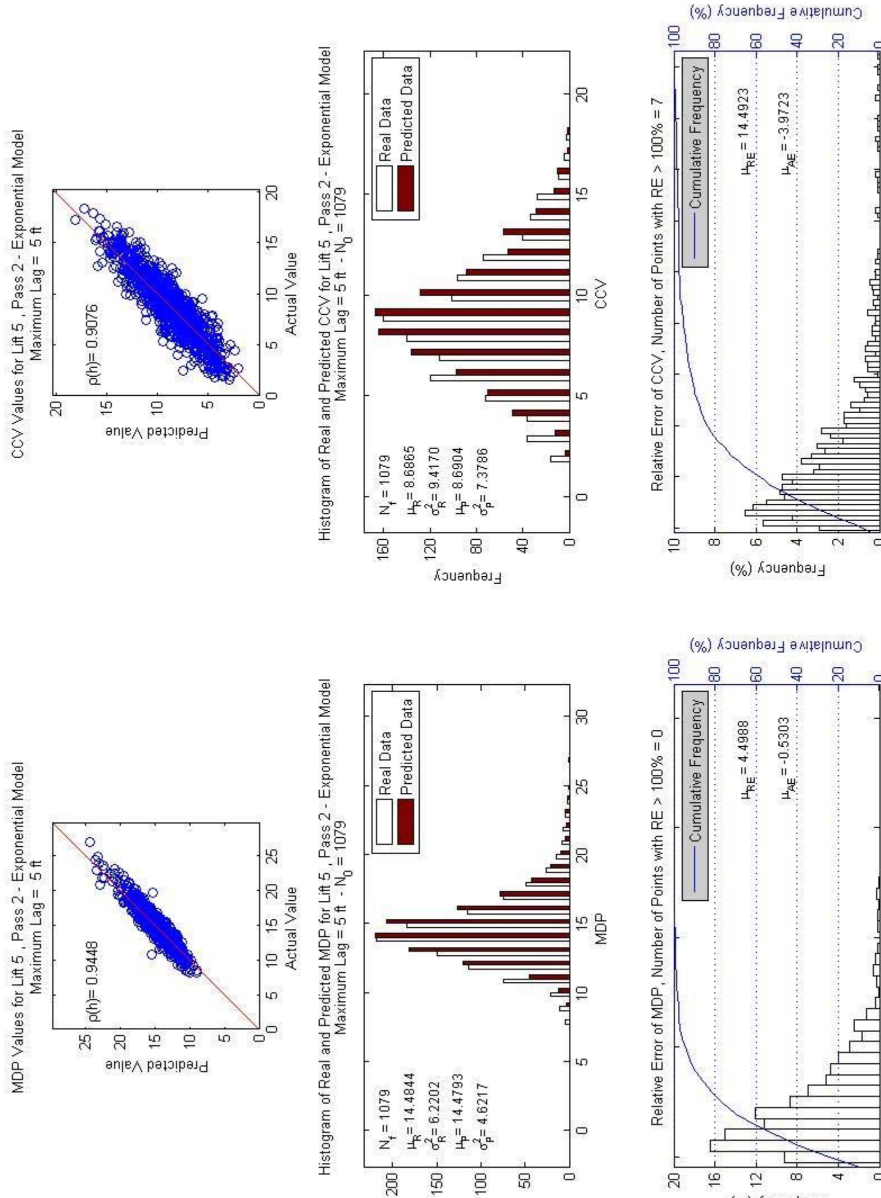

Figure C.61 Kriging results of CCC values for Lift 5, Pass 2/7, using Exponential model and maximum lag of 1.5 (5 ft)

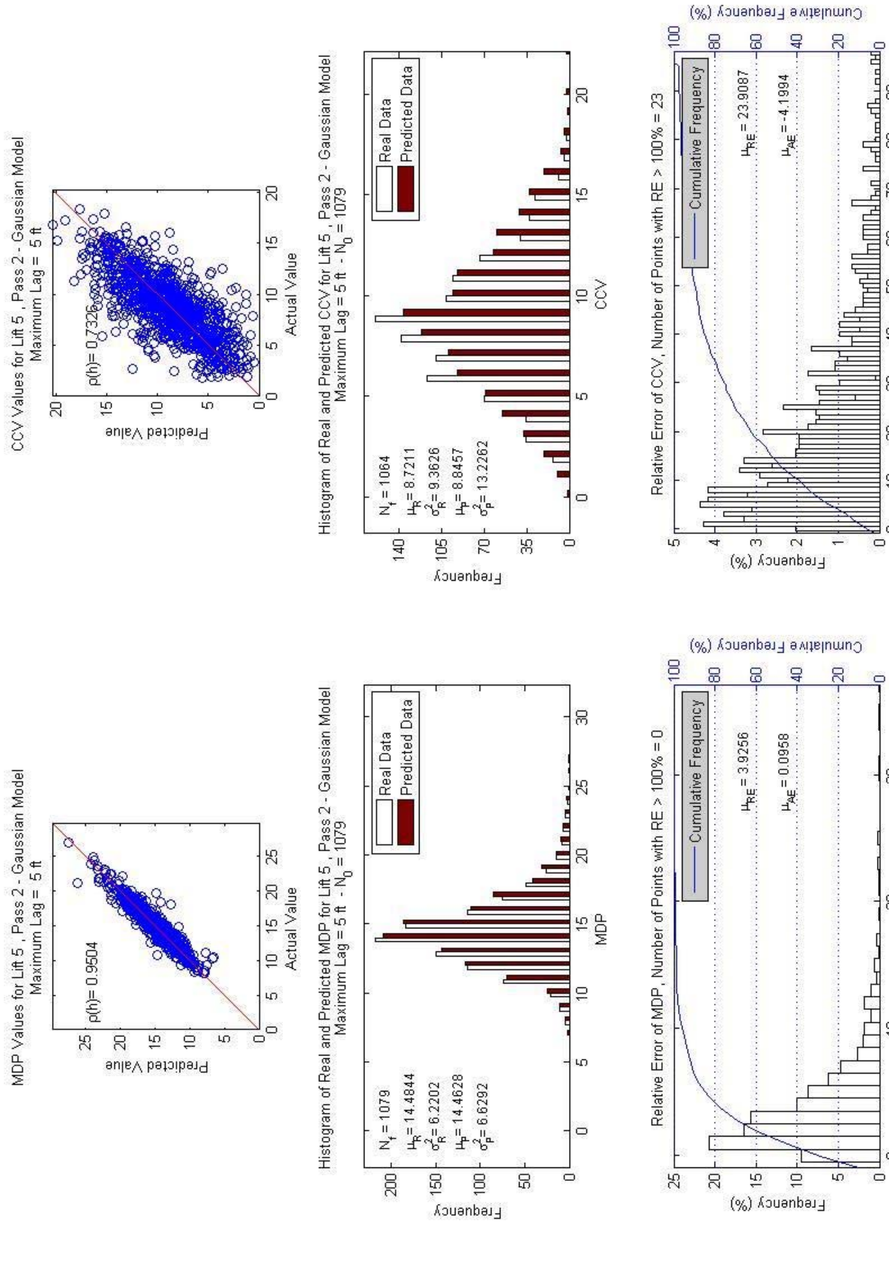

Figure C.62 Kriging results of CCC values for Lift 5, Pass 2/7, using Gaussian model and maximum lag of 1.5 (5 ft)

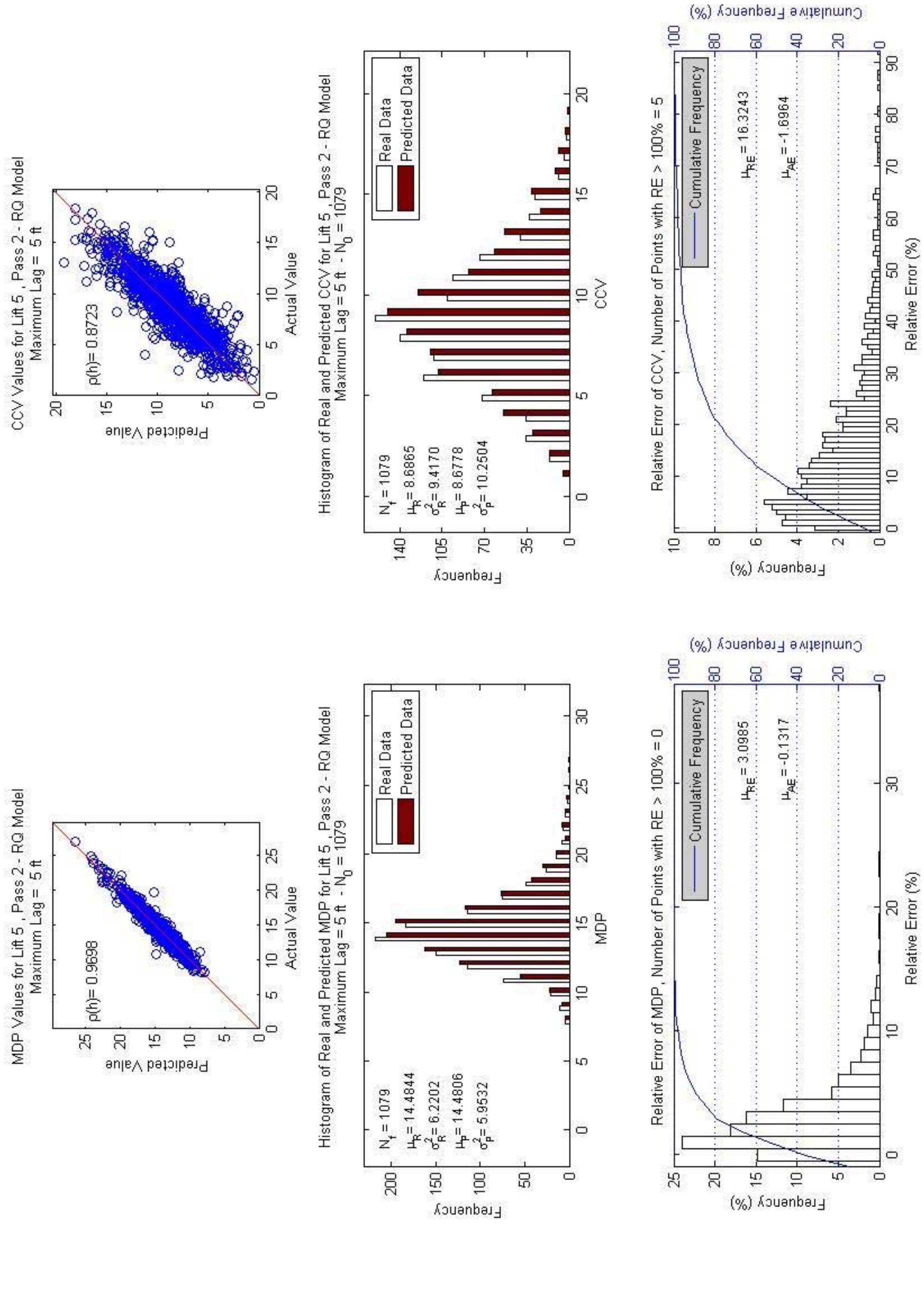

Figure C.63 Kriging results of CCC values for Lift 5, Pass 2/7, using Rational Quadratic (RQ) model and maximum lag of 1.5 (5 ft)

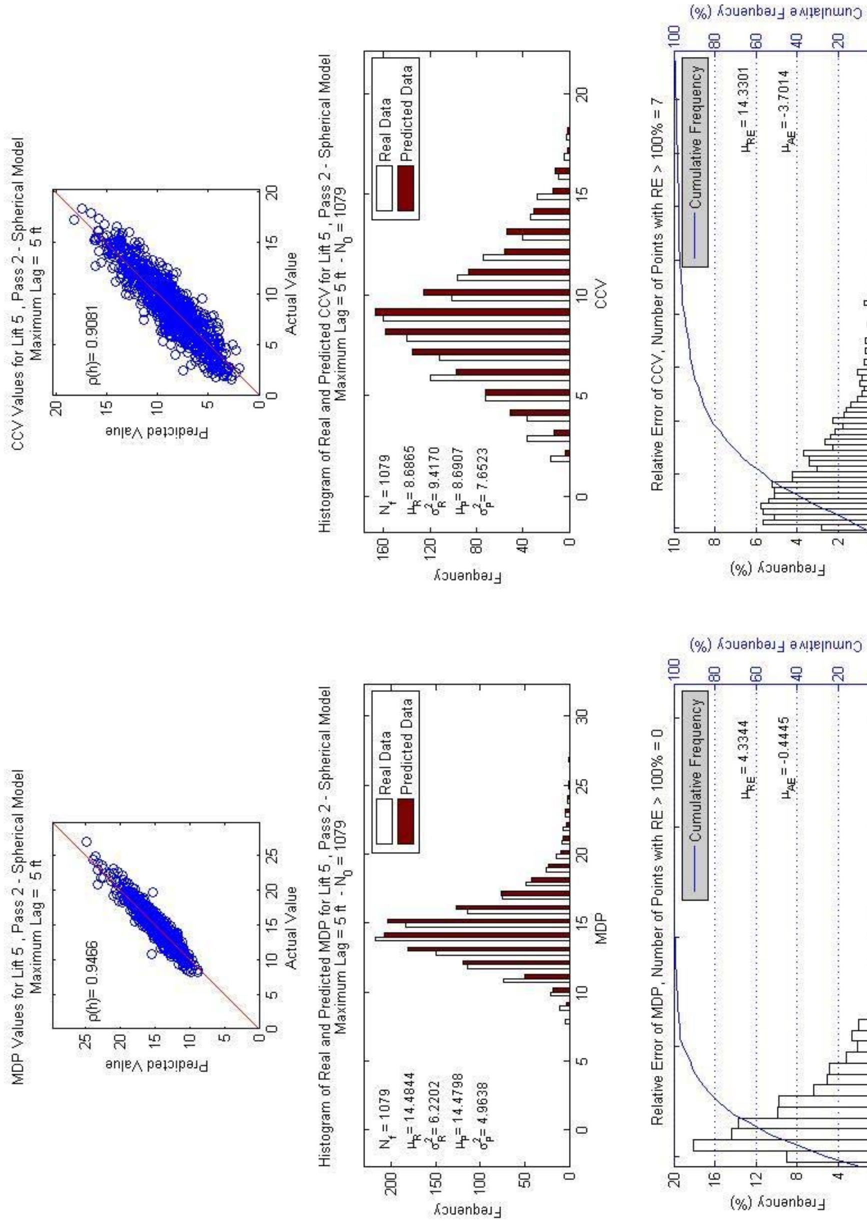

Figure C.64 Kriging results of CCC values for Lift 5, Pass 2/7, using Spherical model and maximum lag of 1.5 (5 ft)

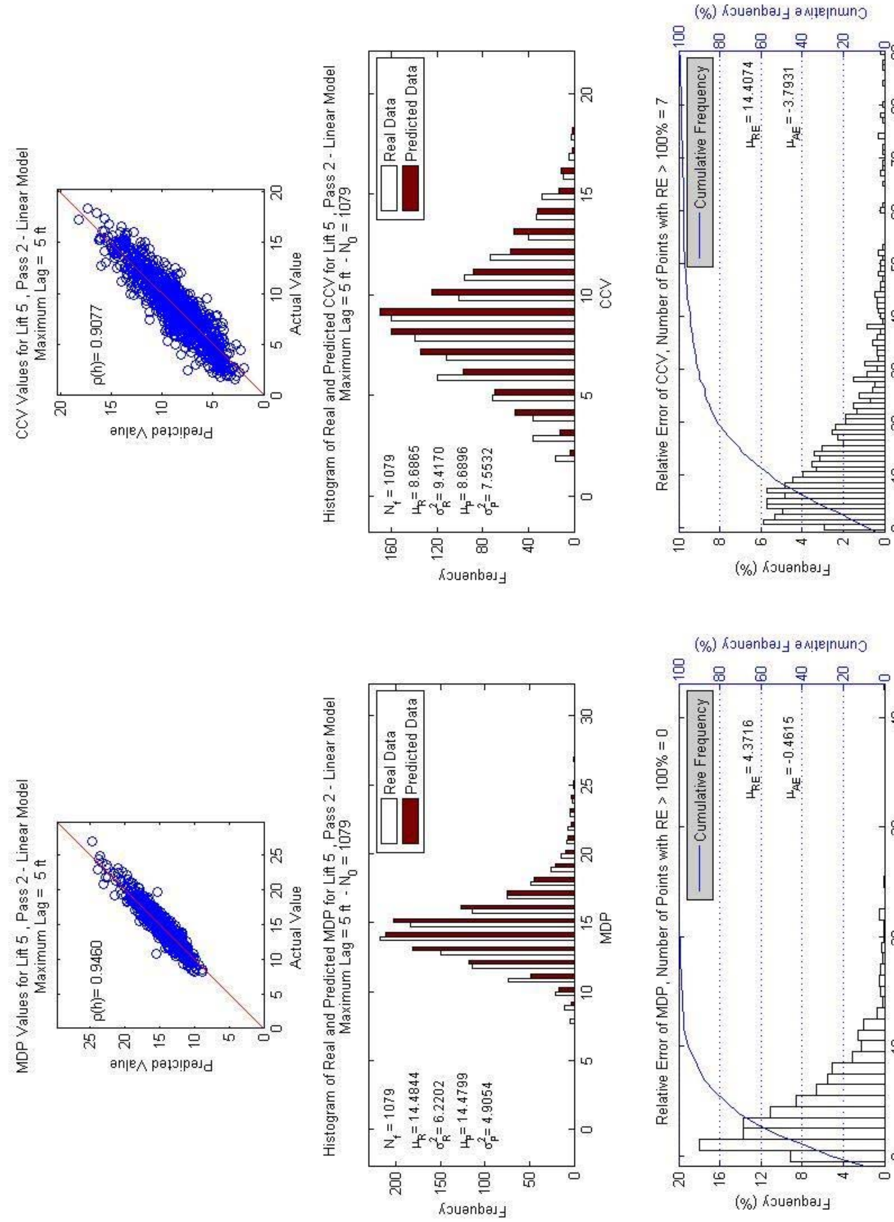

Figure C.65 Kriging results of CCC values for Lift 5, Pass 2/7, using Linear model and maximum lag of 1.5 (5 ft)

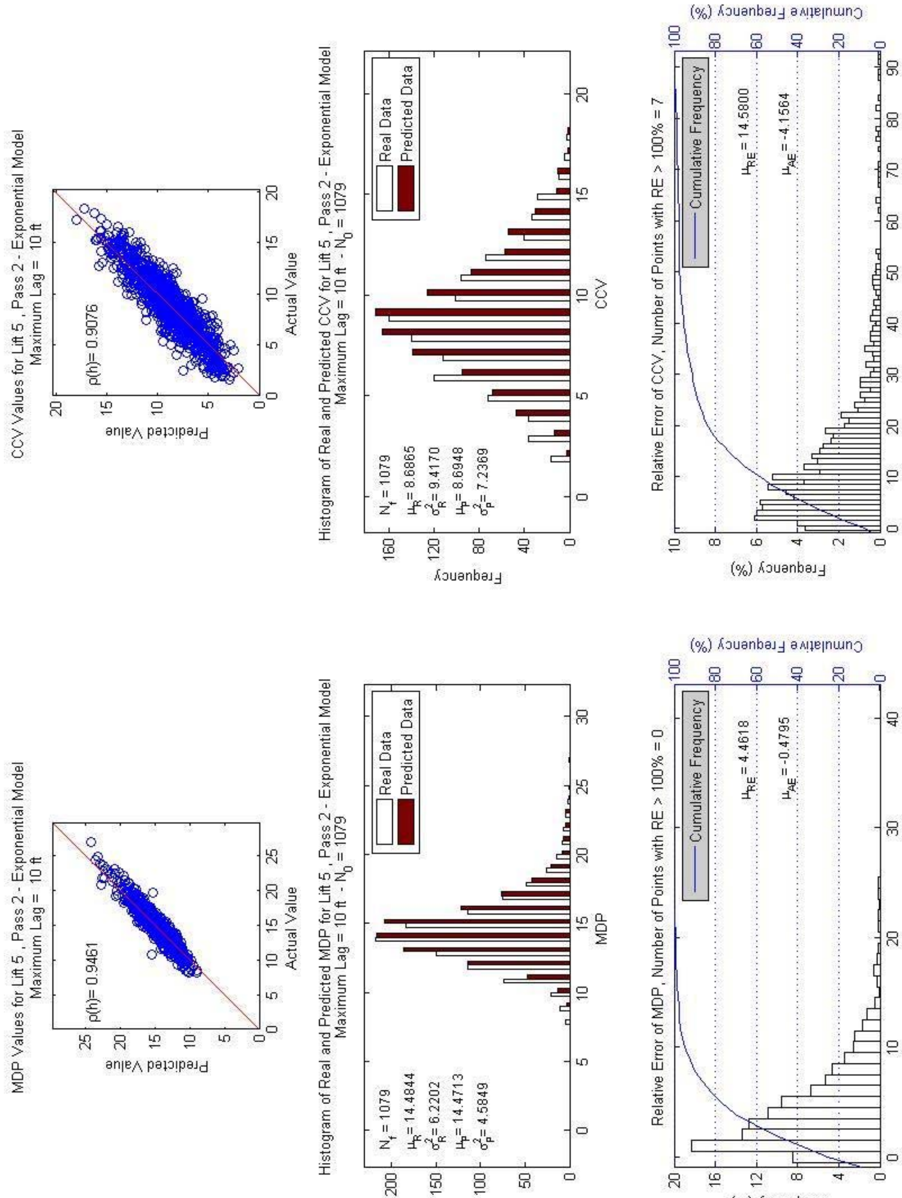

Figure C.66 Kriging results of CCC values for Lift 5, Pass 2/7, using Exponential model and maximum lag of 3.0 (10 ft)

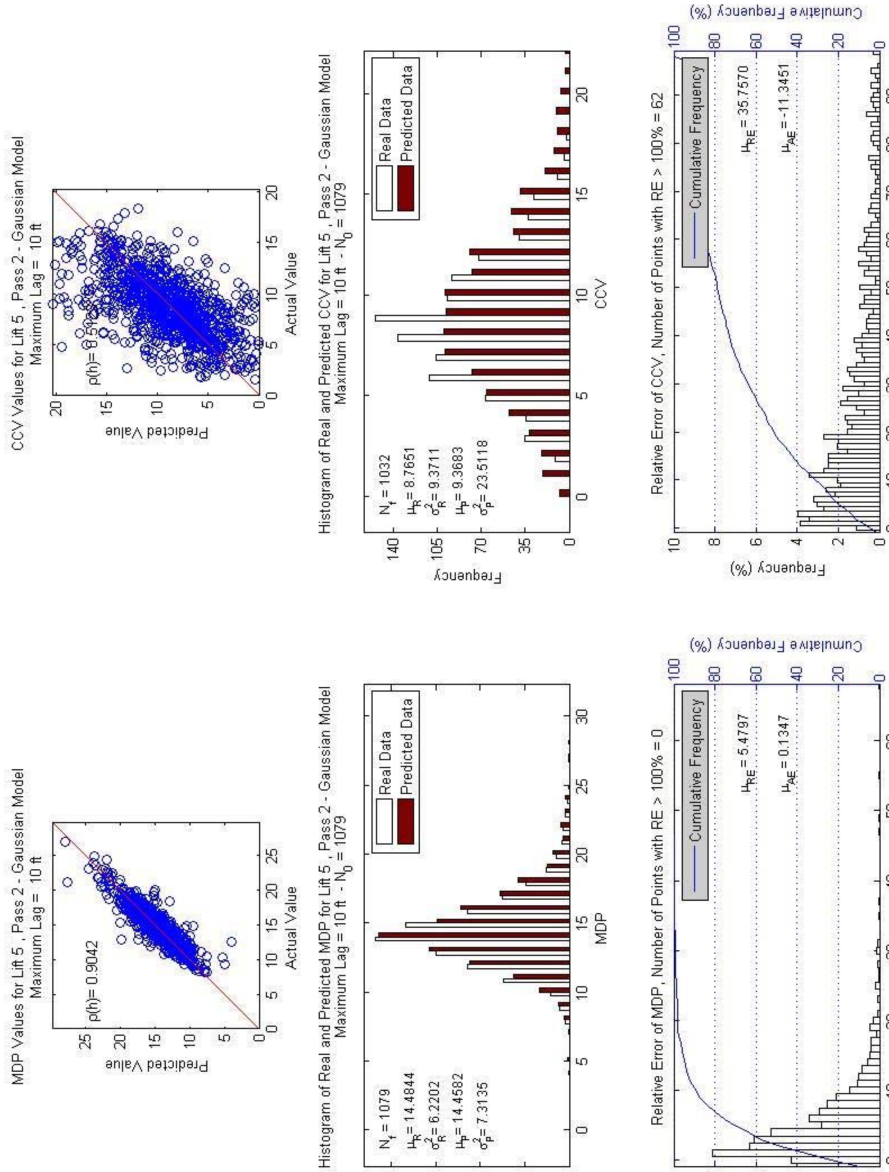

Figure C.67 Kriging results of CCC values for Lift 5, Pass 2/7, using Gaussian model and maximum lag of 3.0 (10 ft)

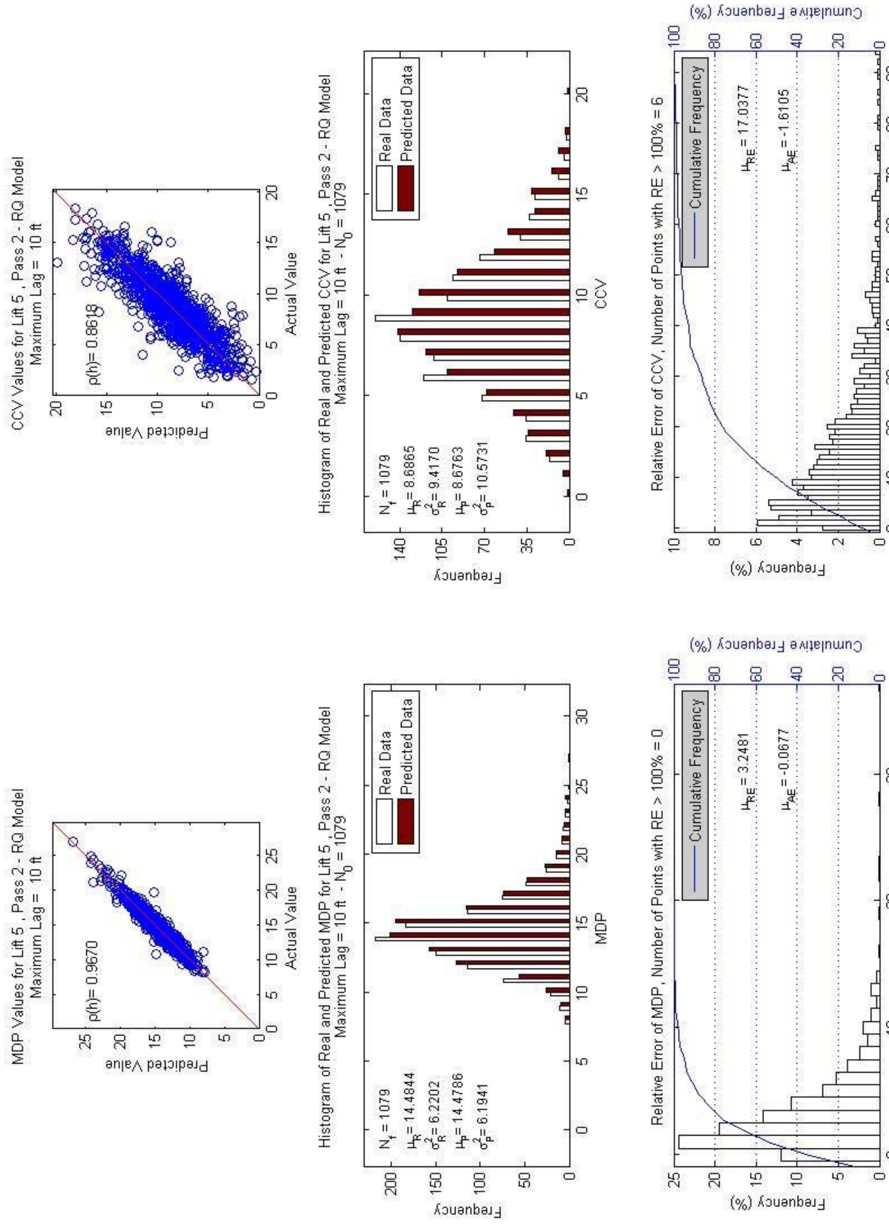

Figure C.68 Kriging results of CCC values for Lift 5, Pass 2/7, using Rational Quadratic (RQ) model and maximum lag of 3.0 (10 ft)

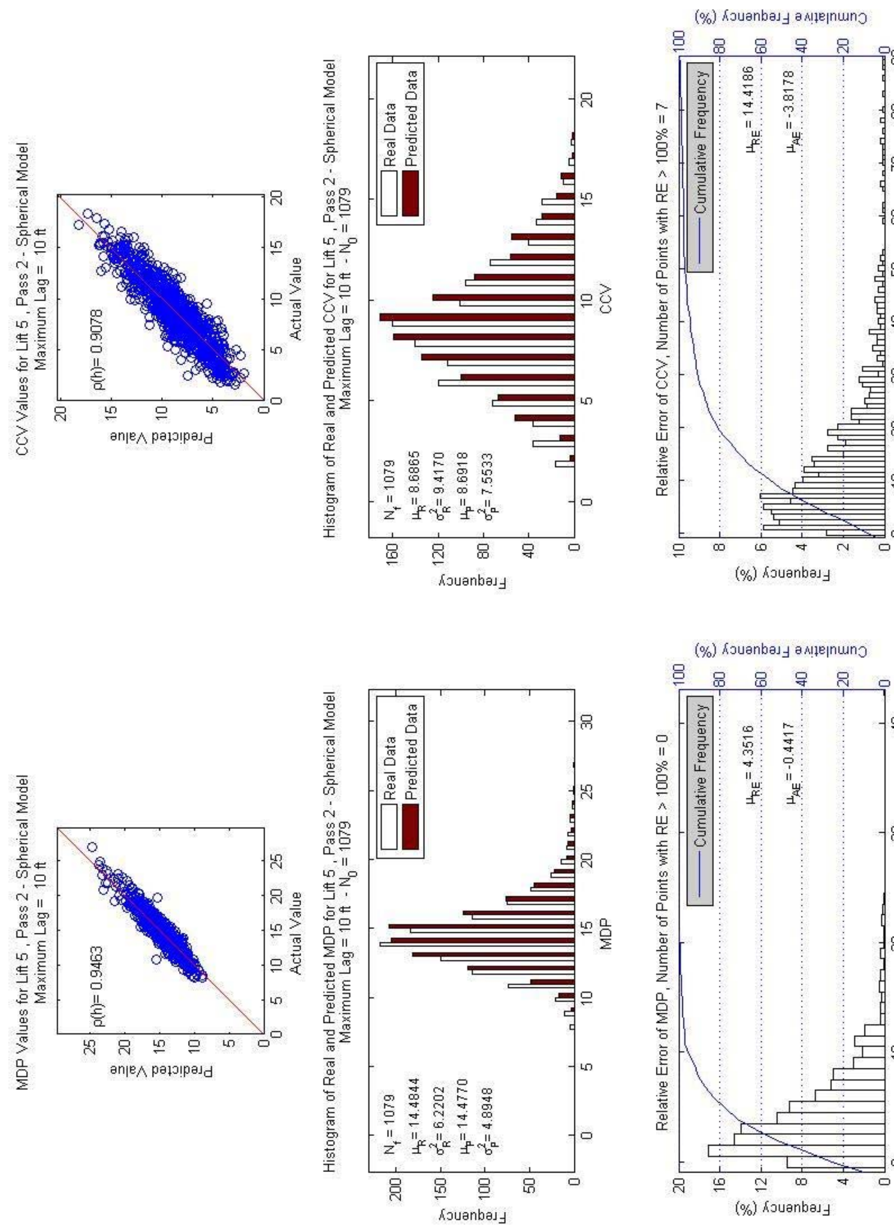

Figure C.69 Kriging results of CCC values for Lift 5, Pass 2/7, using Spherical model and maximum lag of 3.0 (10 ft)

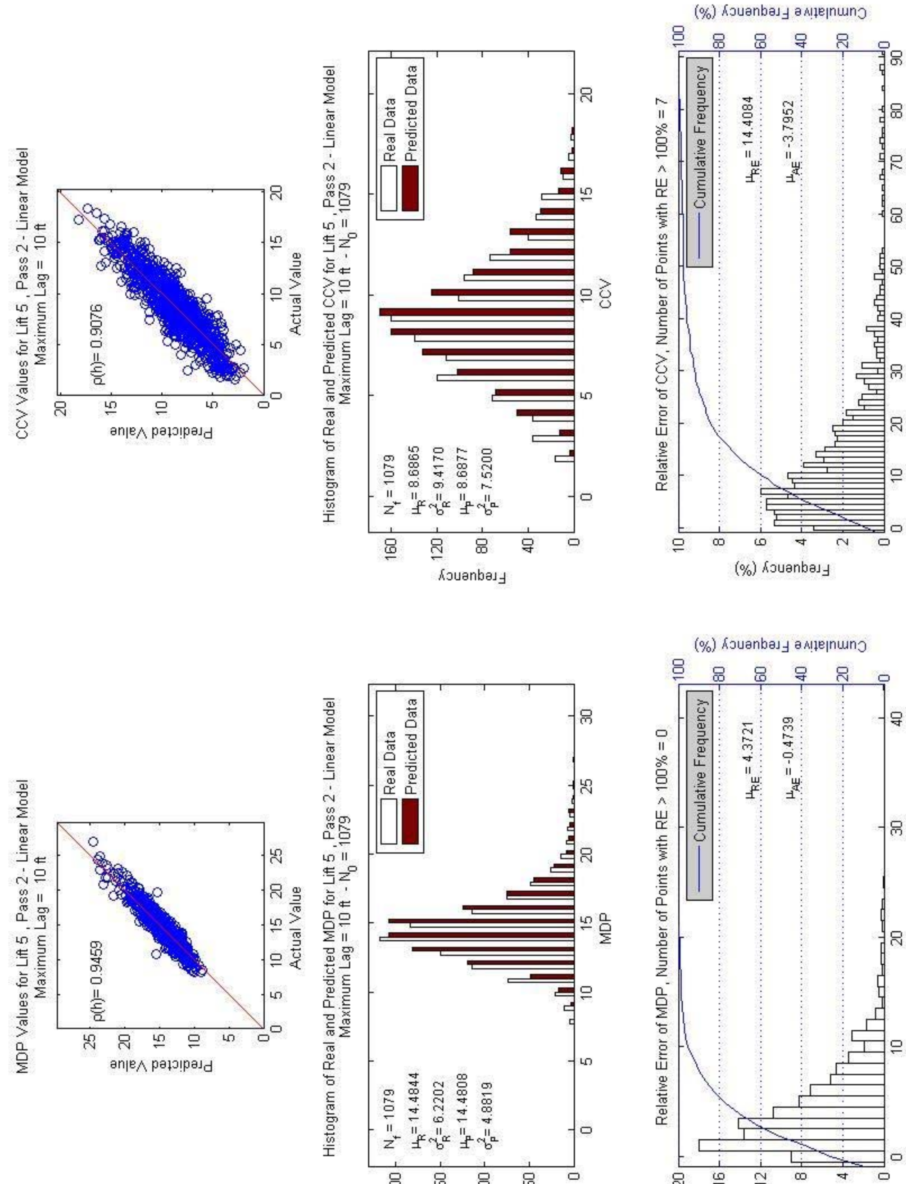

Figure C.70 Kriging results of CCC values for Lift 5, Pass 2/7, using Linear model and maximum lag of 3.0 (10 ft)

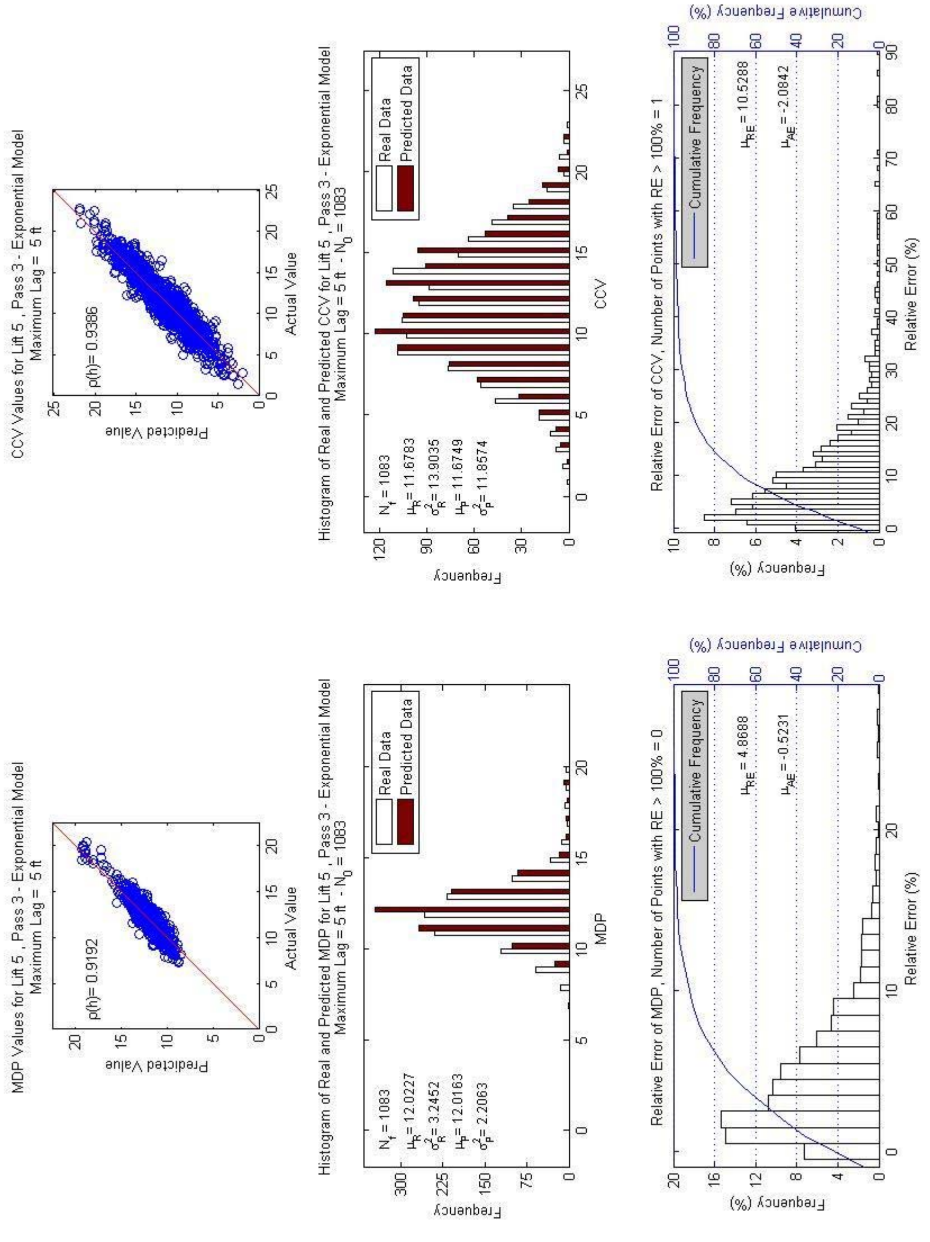

Figure C.71 Kriging results of CCC values for Lift 5, Pass 3/7, using Exponential model and maximum lag of 1.5 (5 ft)

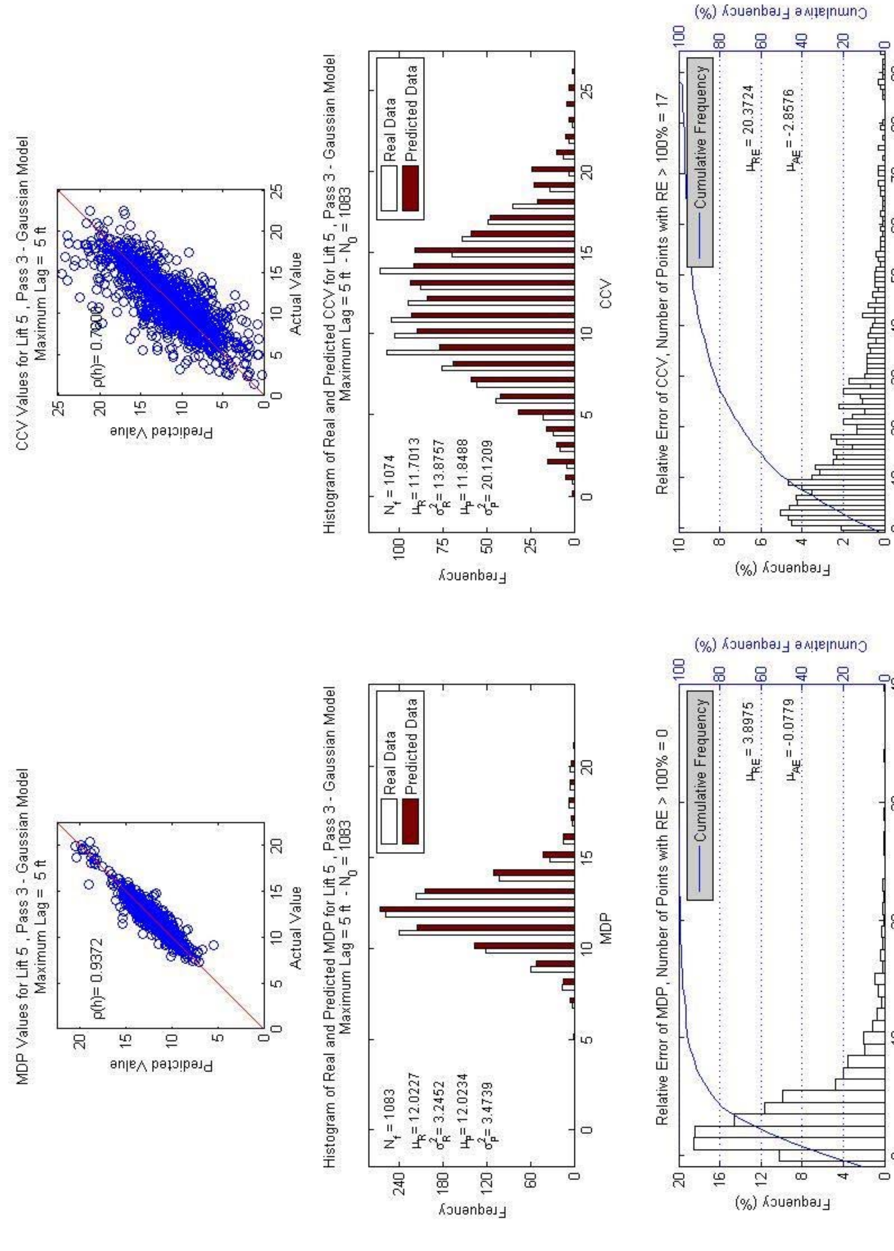

Figure C.72 Kriging results of CCC values for Lift 5, Pass 3/7, using Gaussian model and maximum lag of 1.5 (5 ft)

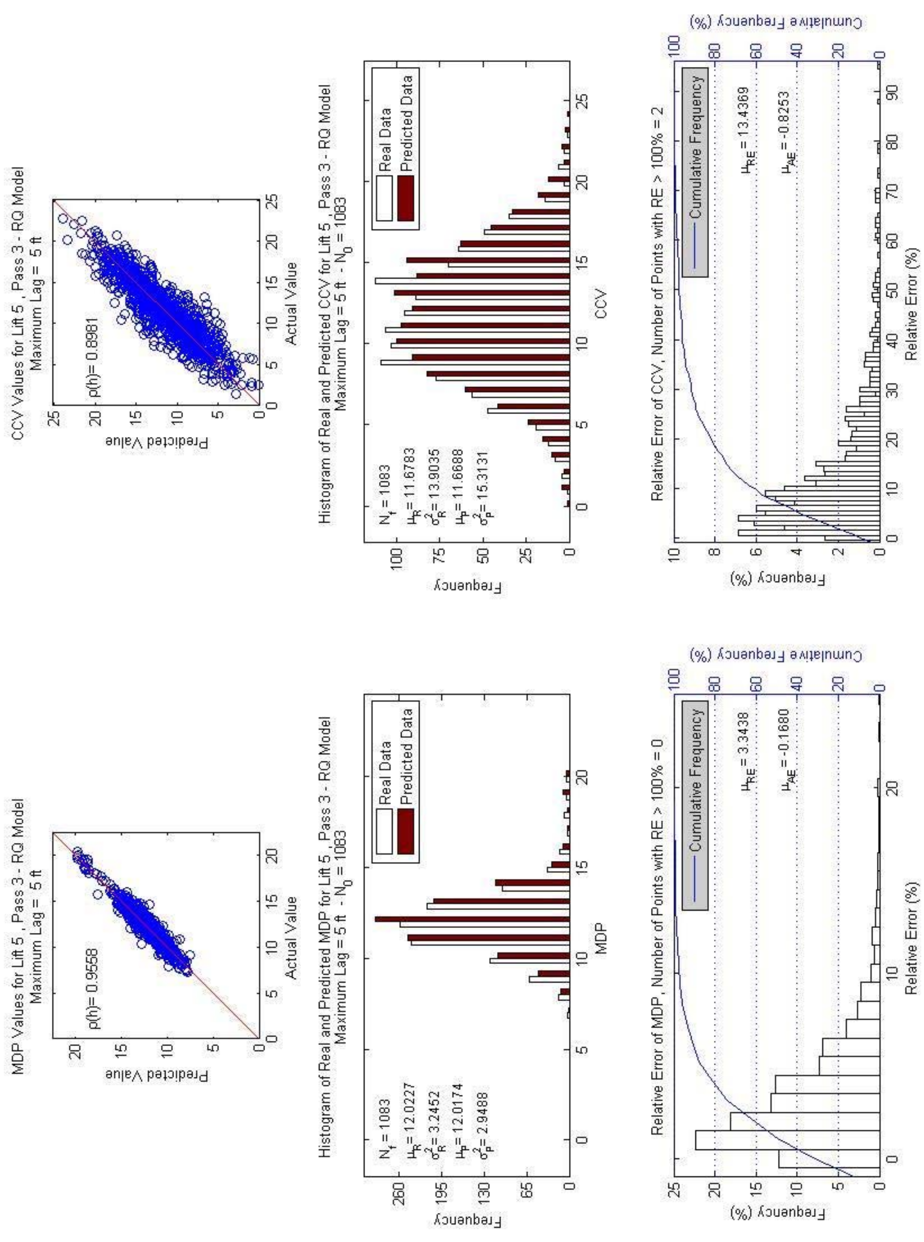

Figure C.73 Kriging results of CCC values for Lift 5, Pass 3/7, using Rational Quadratic (RQ) model and maximum lag of 1.5 (5 ft)

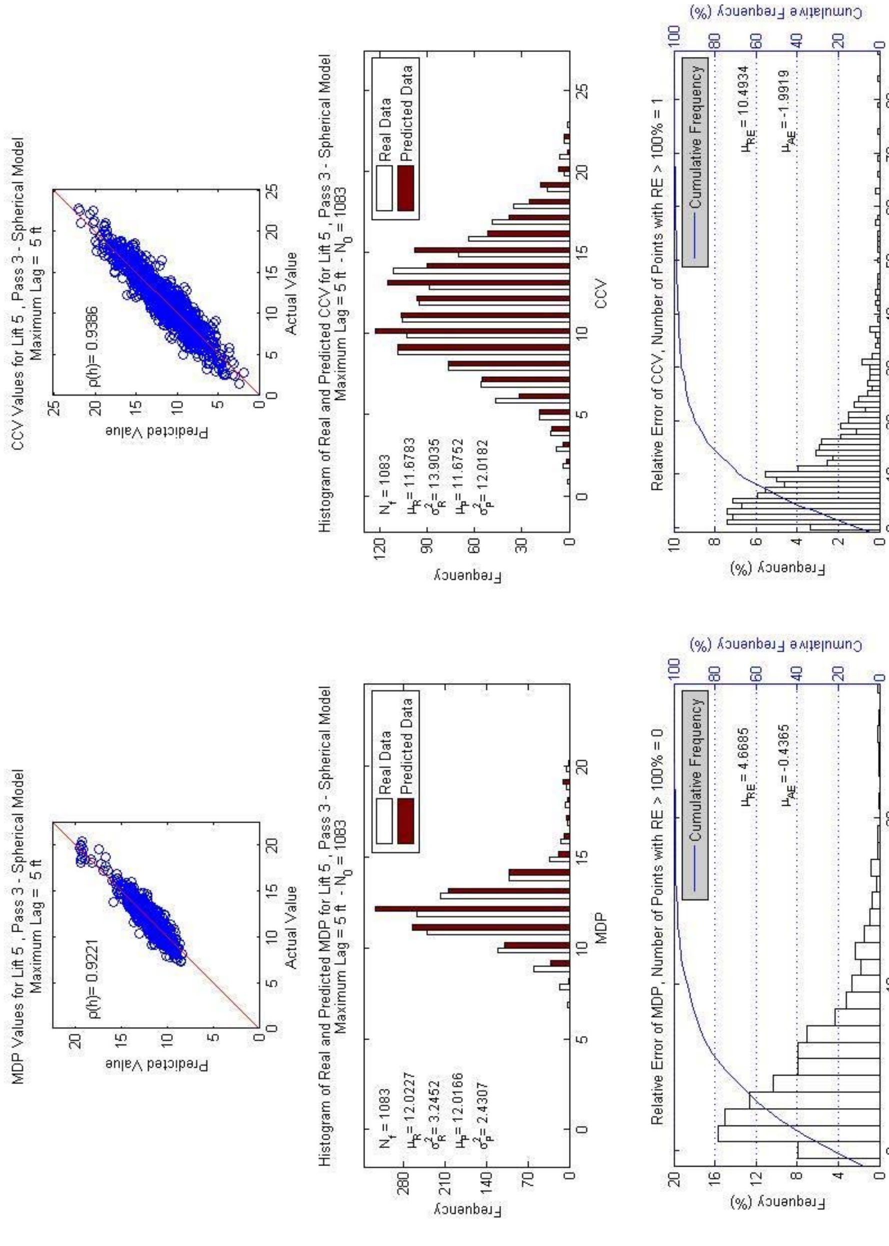

Figure C.74 Kriging results of CCC values for Lift 5, Pass 3/7, using Spherical model and maximum lag of 1.5 (5 ft)

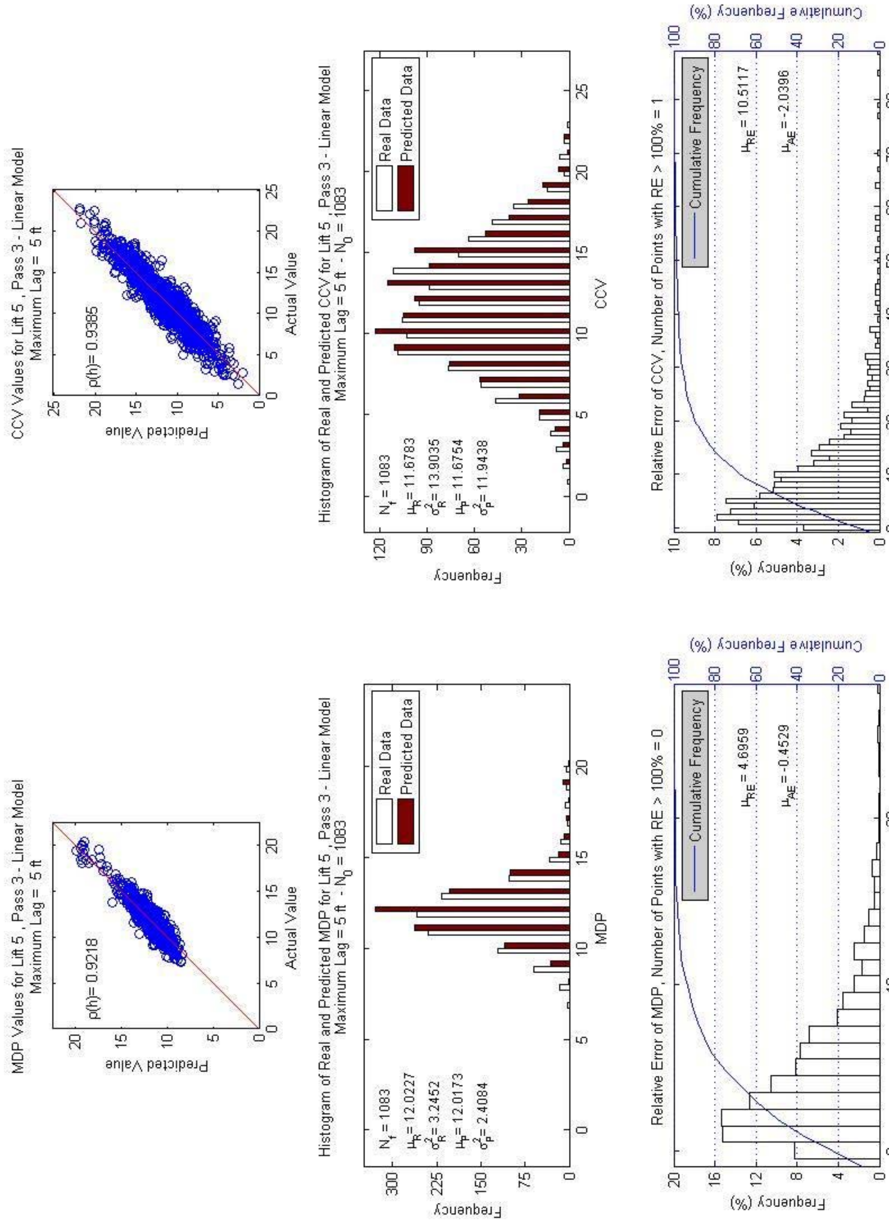

Figure C.75 Kriging results of CCC values for Lift 5, Pass 3/7, using Linear model and maximum lag of 1.5 (5 ft)

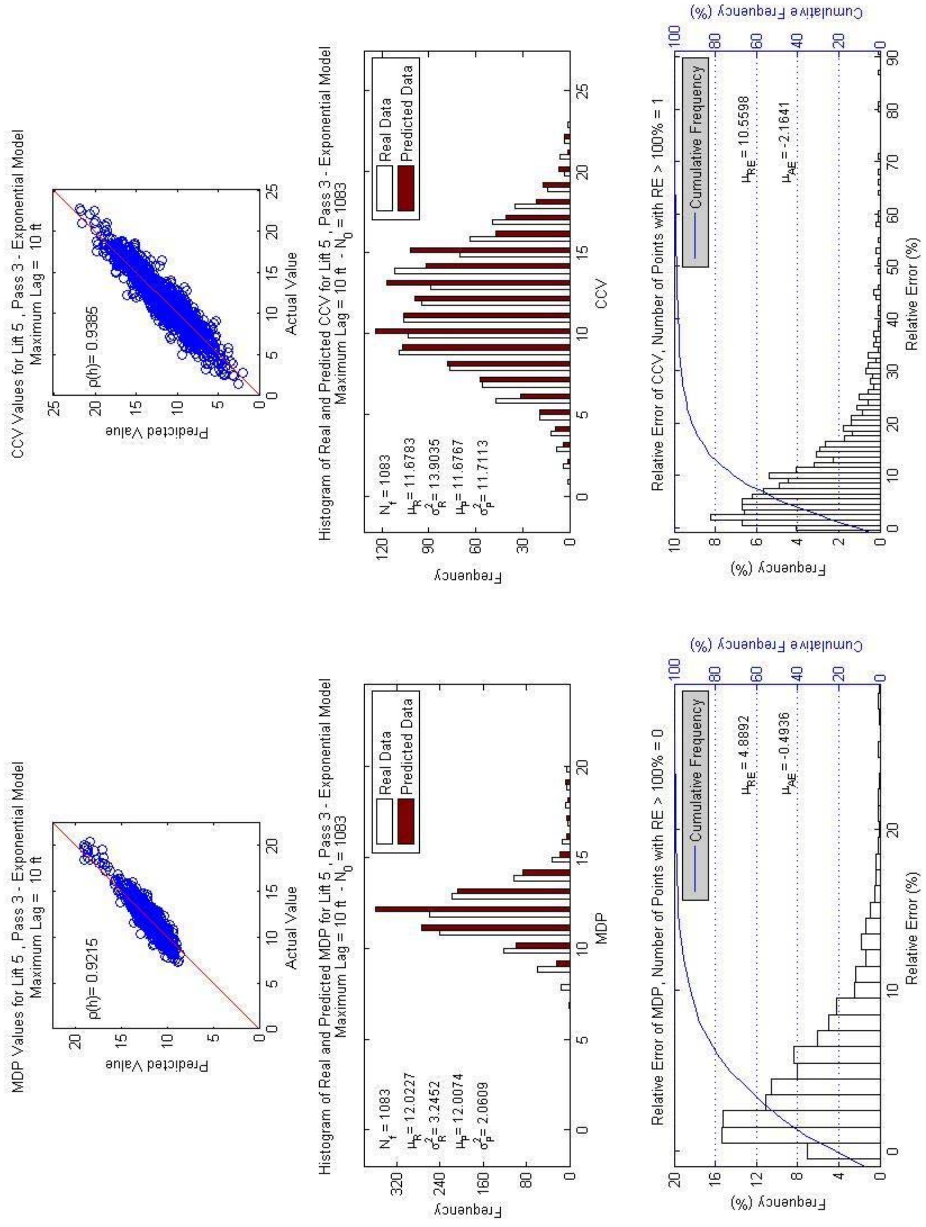

Figure C.76 Kriging results of CCC values for Lift 5, Pass 3/7, using Exponential model and maximum lag of 3.0 (10 ft)

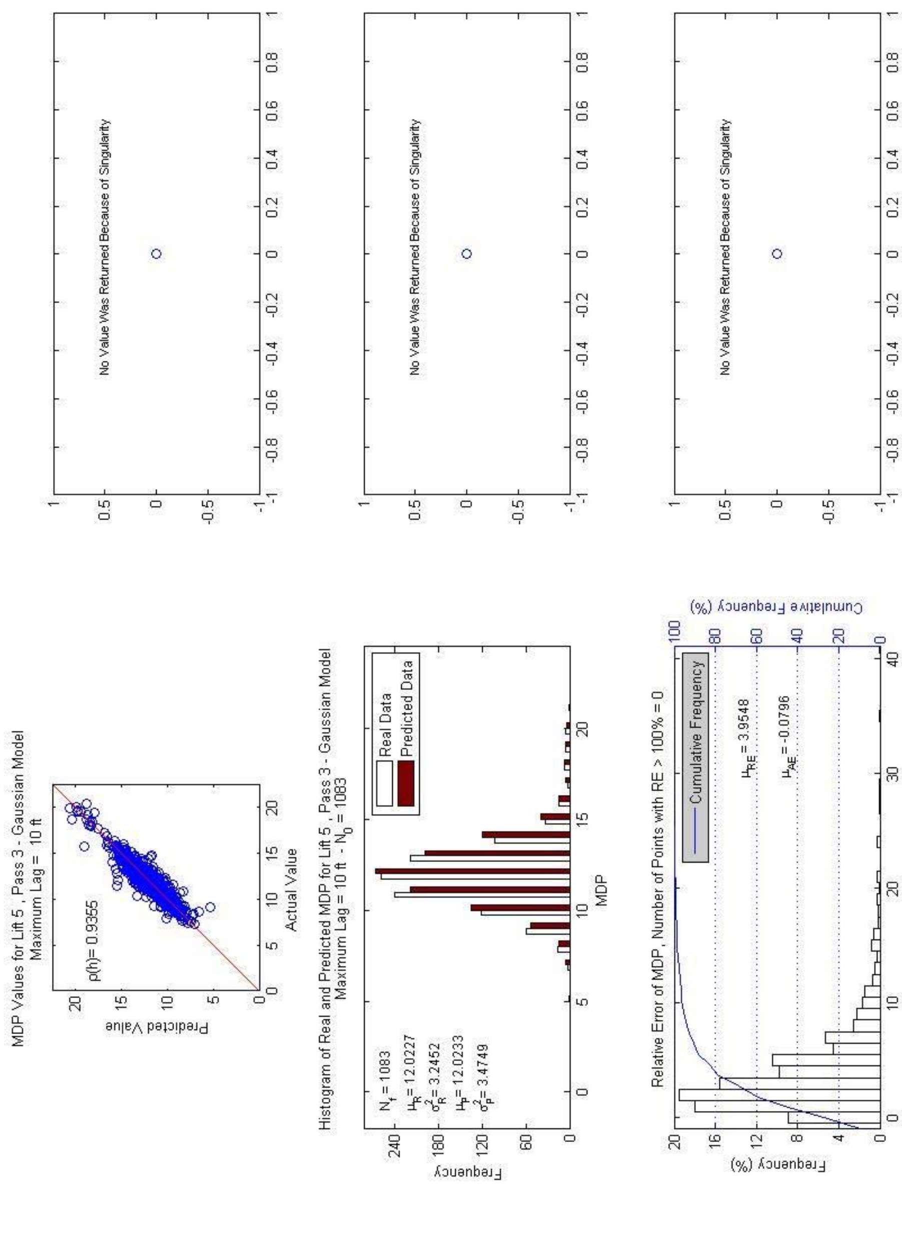

Figure C.77 Kriging results of CCC values for Lift 5, Pass 3/7, using Gaussian model and maximum lag of 3.0 (10 ft)

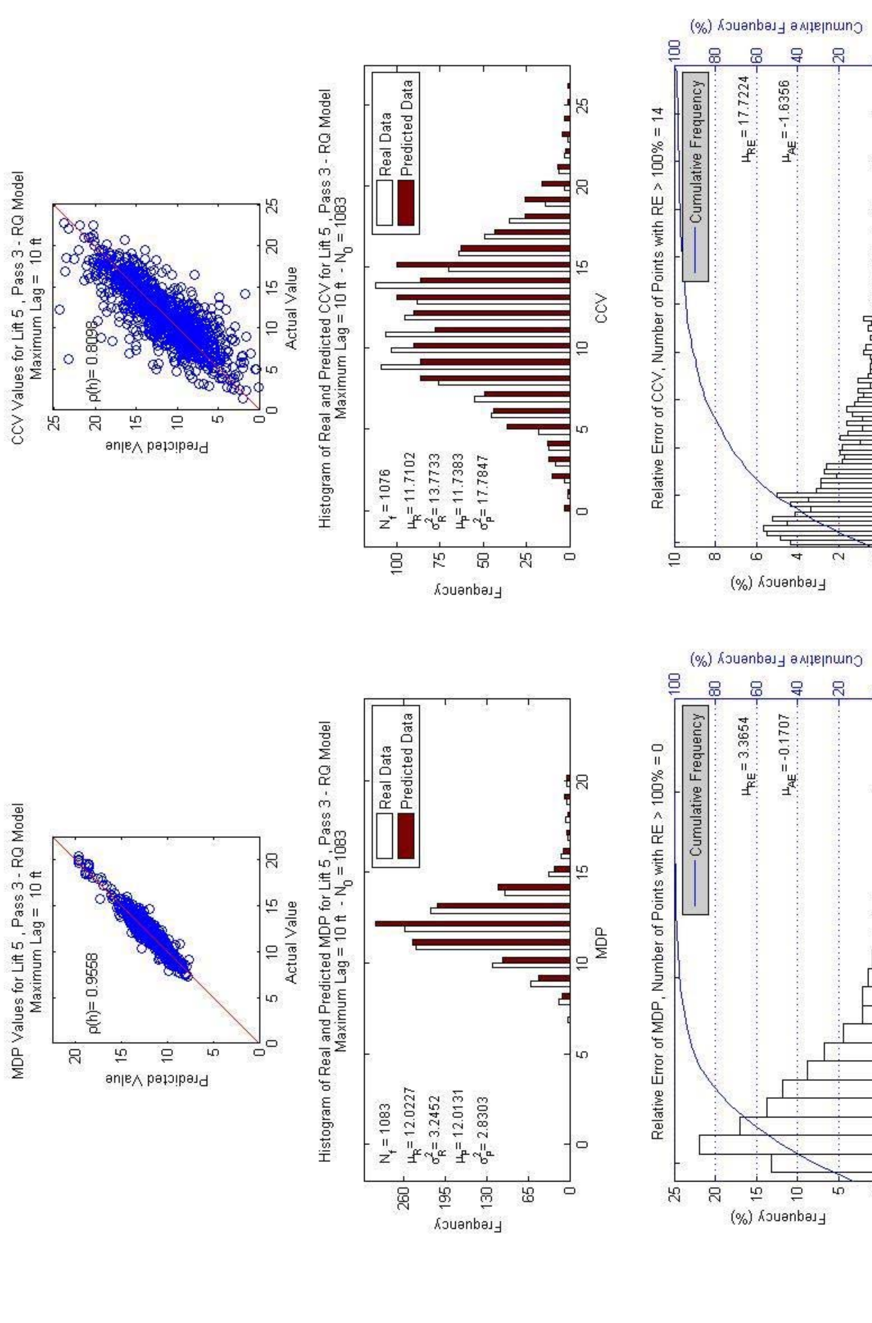

Figure C.78 Kriging results of CCC values for Lift 5, Pass 3/7, using Rational Quadratic (RQ) model and maximum lag of 3.0 (10 ft)

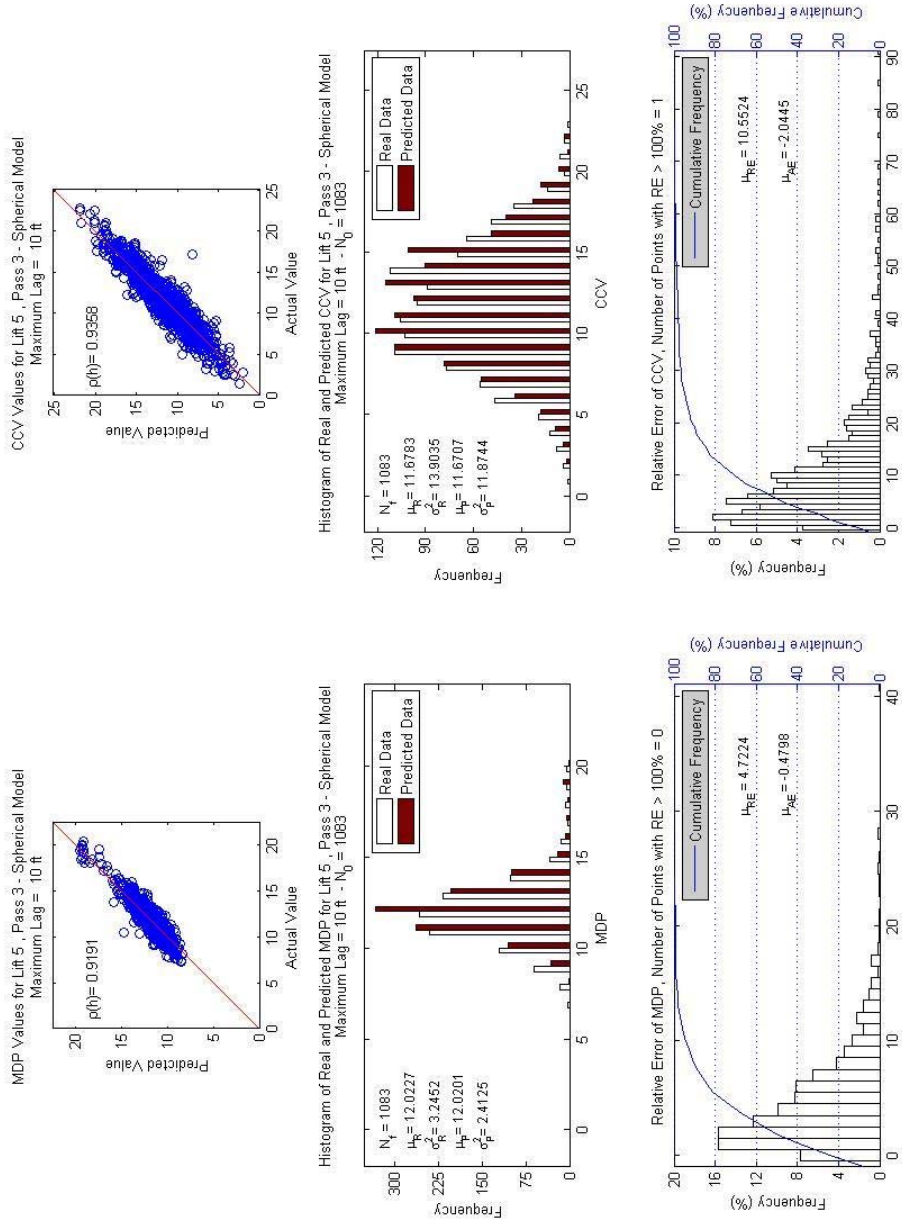

Figure C.79 Kriging results of CCC values for Lift 5, Pass 3/7, using Spherical model and maximum lag of 3.0 (10 ft)

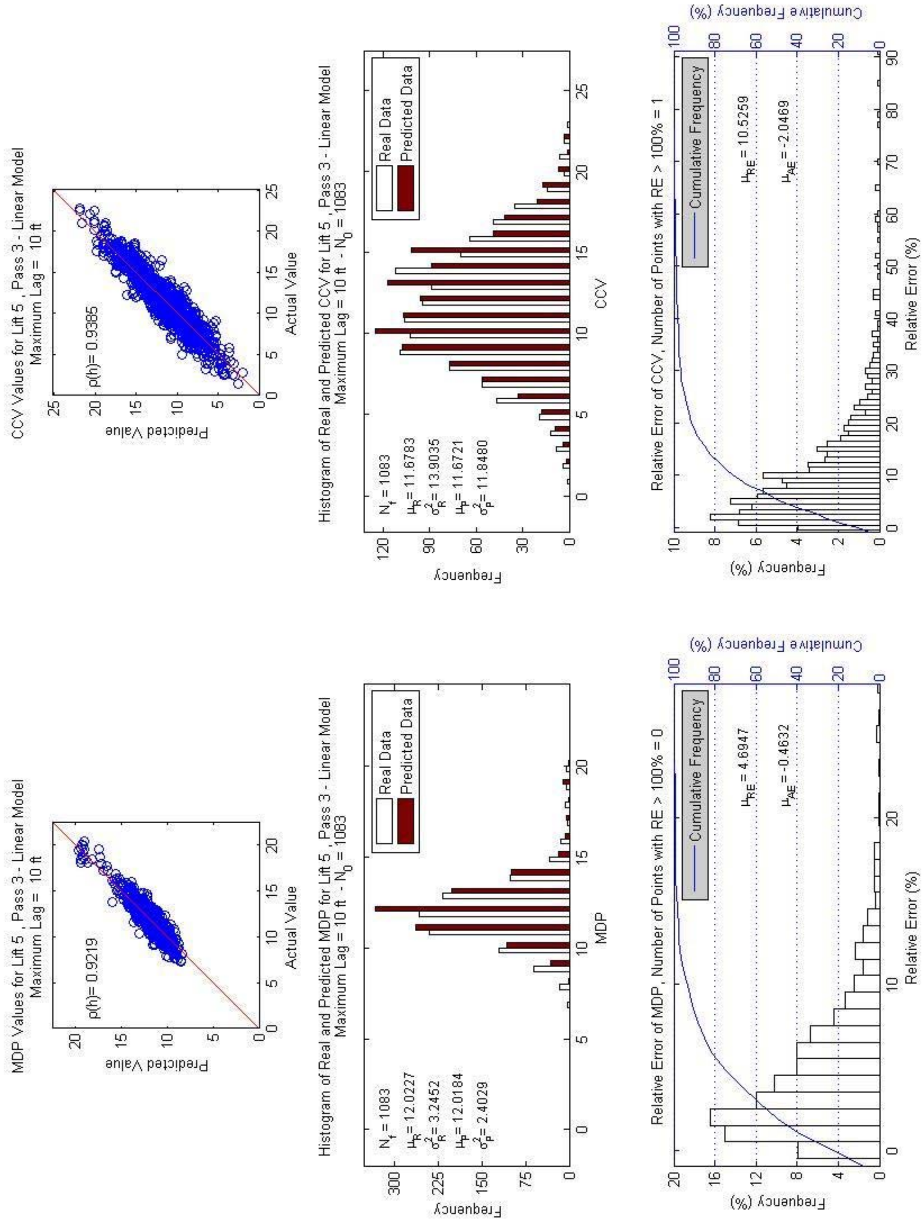

Figure C.80 Kriging results of CCC values for Lift 5, Pass 3/7, using Linear model and maximum lag of 3.0 (10 ft)

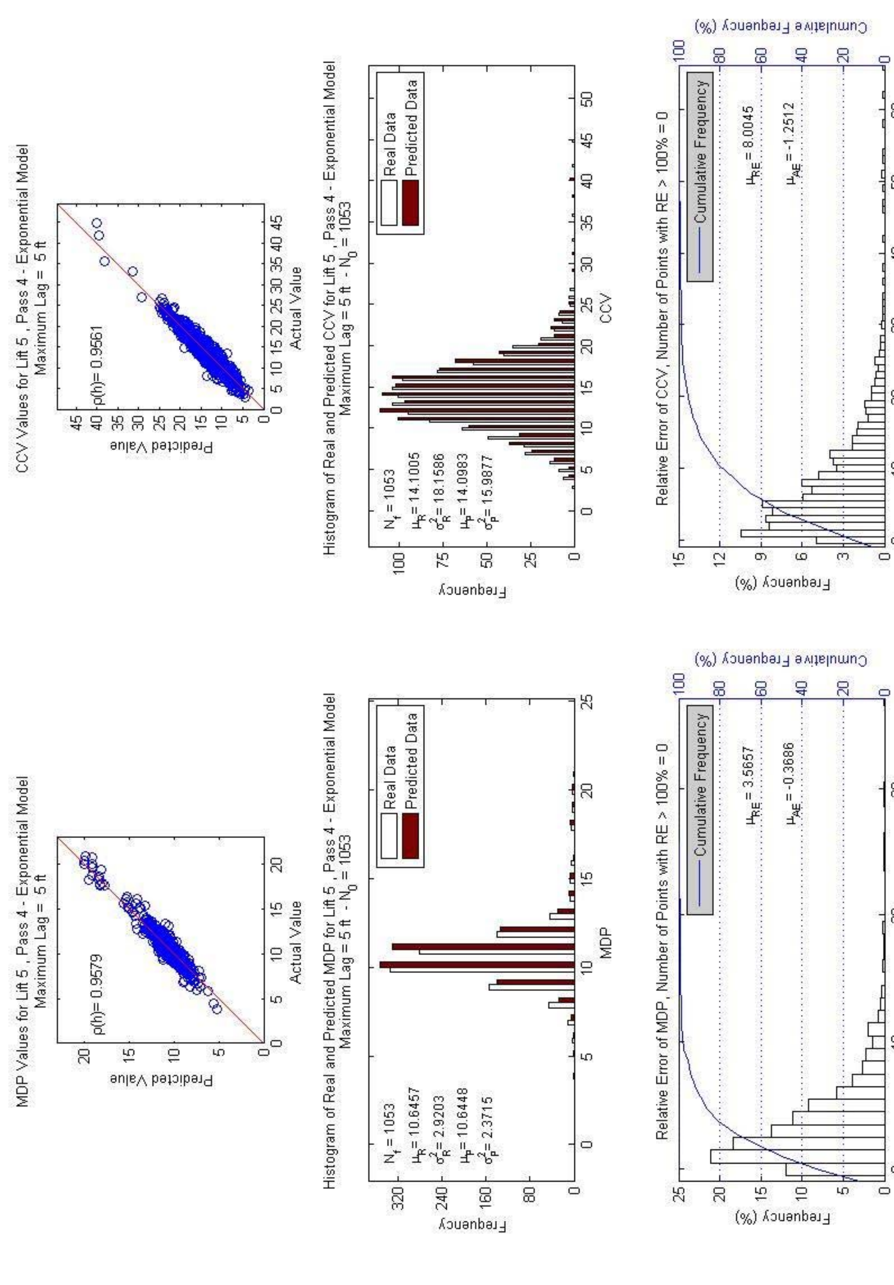

Figure C.81 Kriging results of CCC values for Lift 5, Pass 4/7, using Exponential model and maximum lag of 1.5 (5 ft)

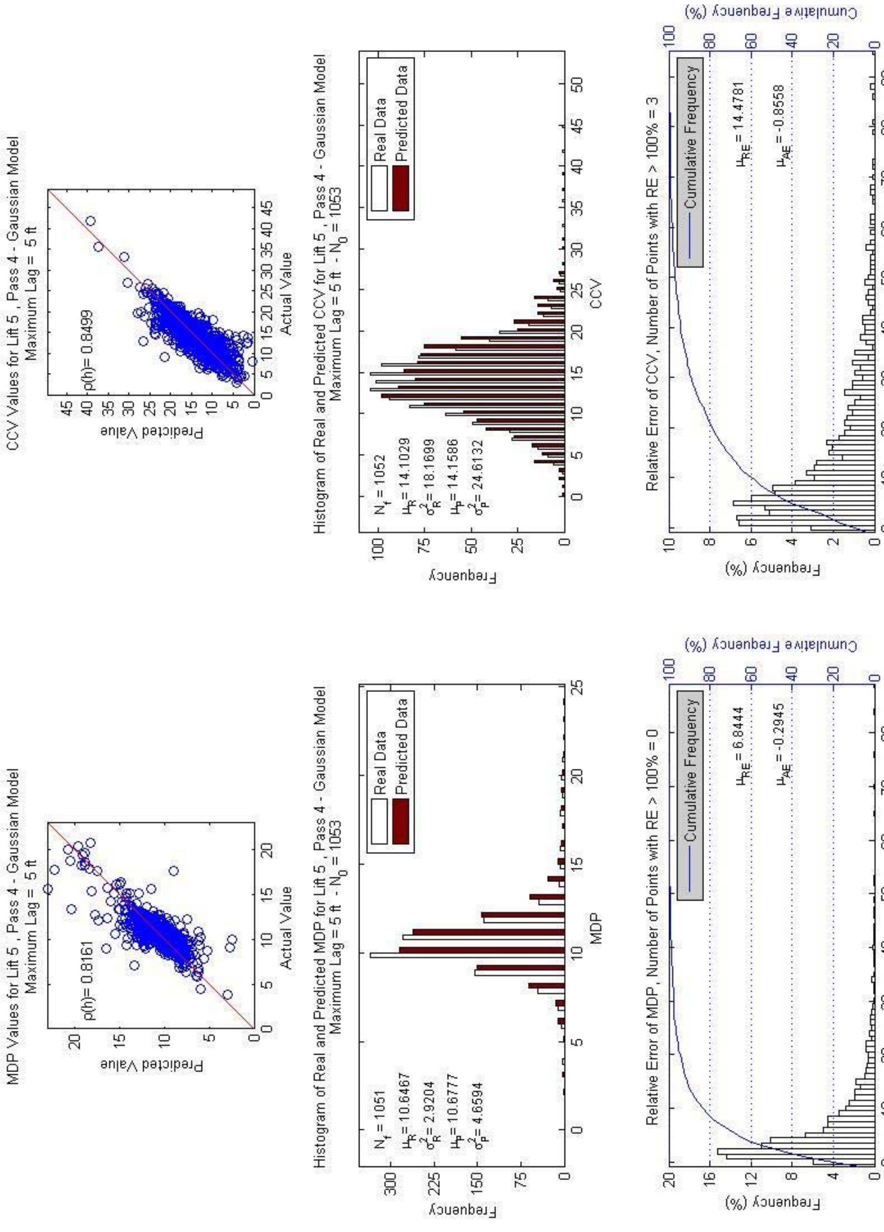

Figure C.82 Kriging results of CCC values for Lift 5, Pass 4/7, using Gaussian model and maximum lag of 1.5 (5 ft)

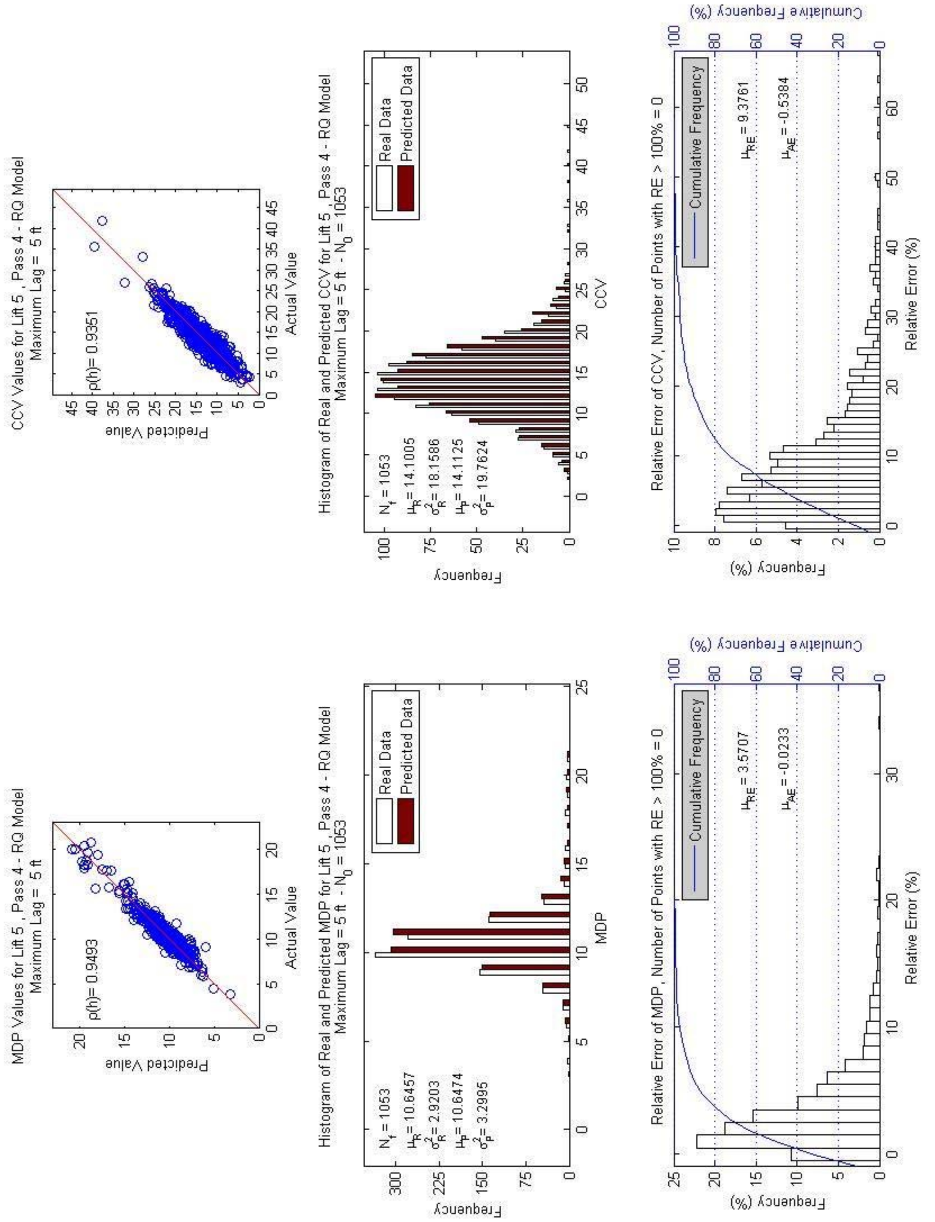

Figure C.83 Kriging results of CCC values for Lift 5, Pass 4/7, using Rational Quadratic (RQ) model and maximum lag of 1.5 (5 ft)

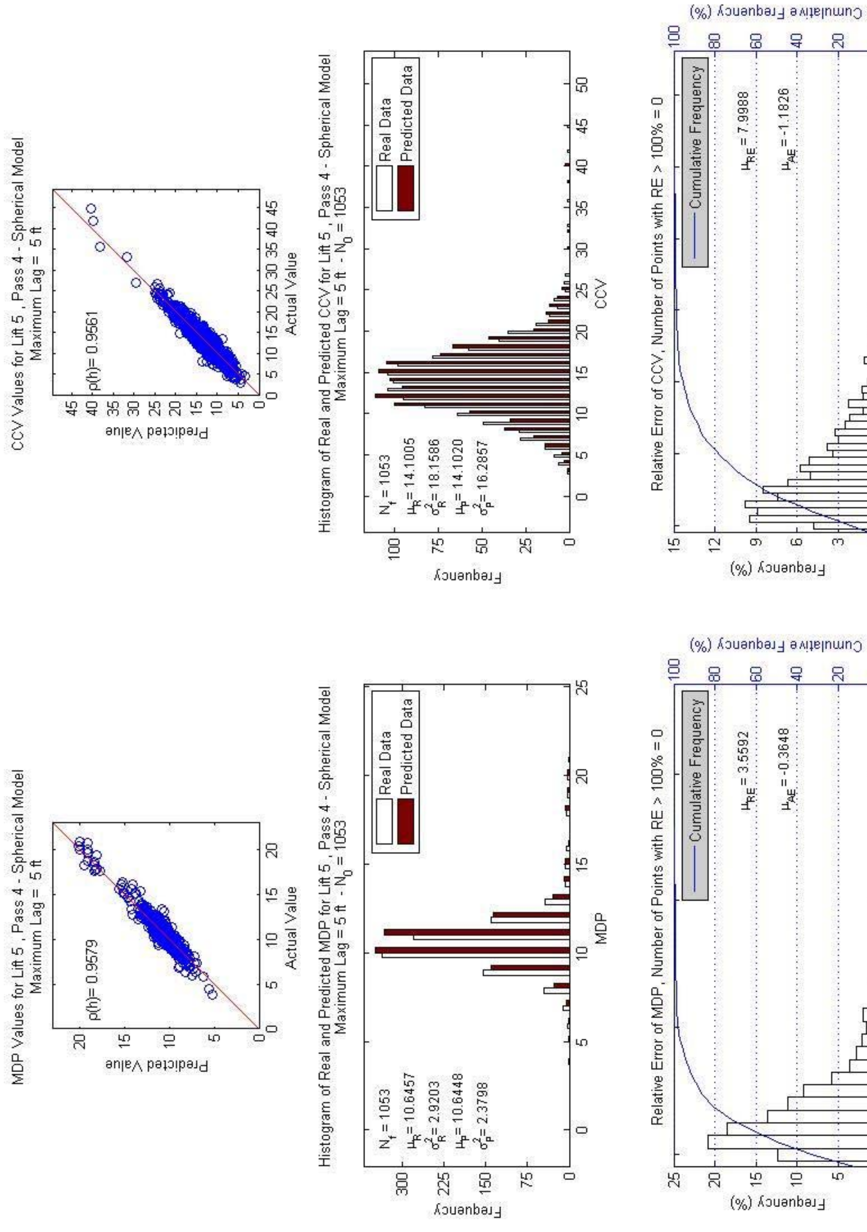

Figure C.84 Kriging results of CCC values for Lift 5, Pass 4/7, using Spherical model and maximum lag of 1.5 (5 ft)

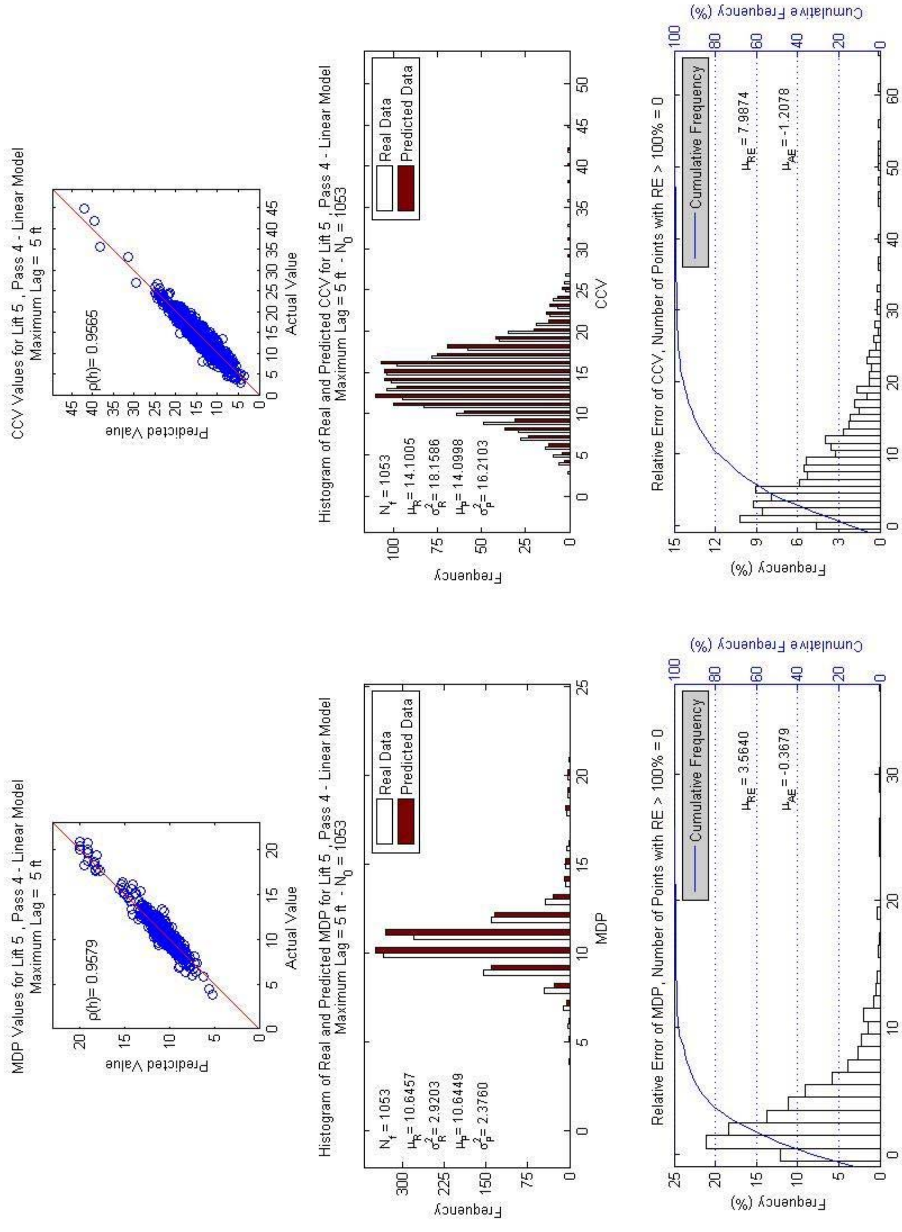

Figure C.85 Kriging results of CCC values for Lift 5, Pass 4/7, using Linear model and maximum lag of 1.5 (5 ft)

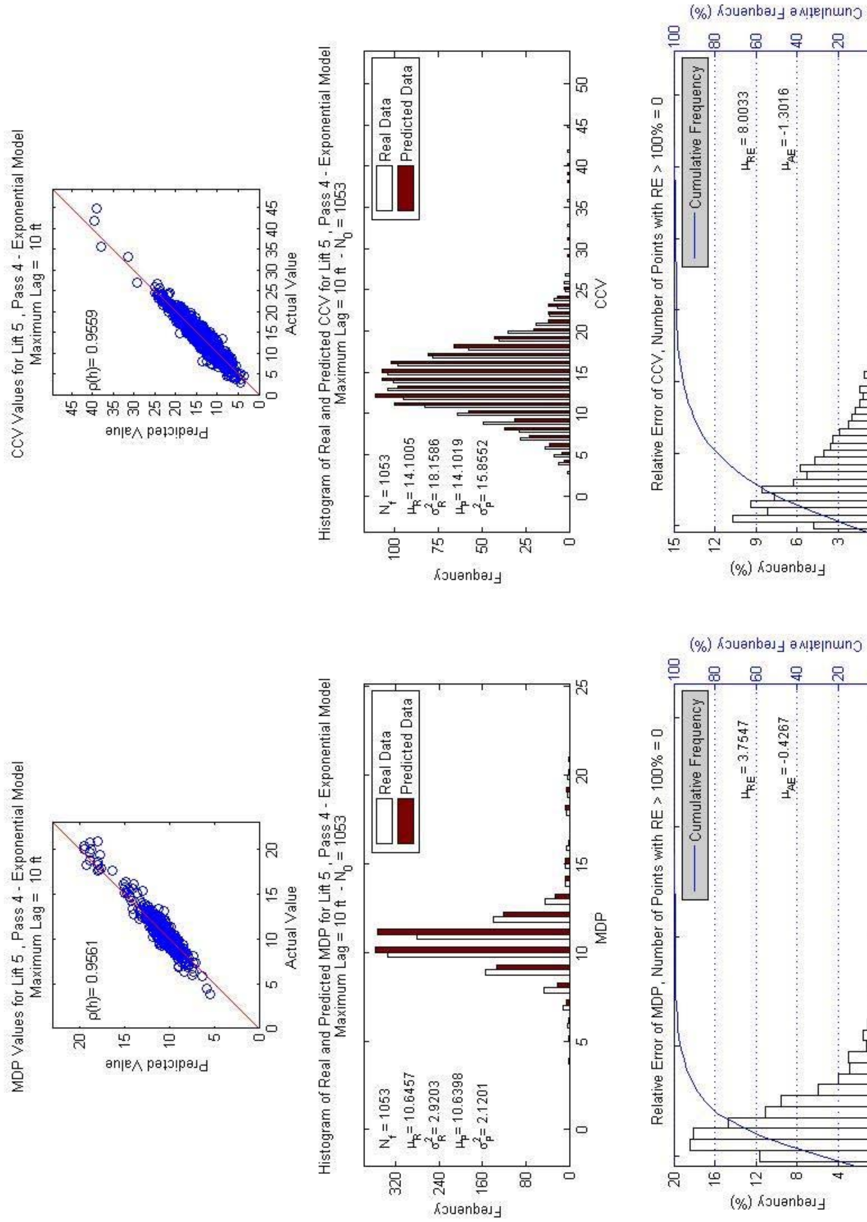

Figure C.86 Kriging results of CCC values for Lift 5, Pass 4/7, using Exponential model and maximum lag of 3.0 (10 ft)

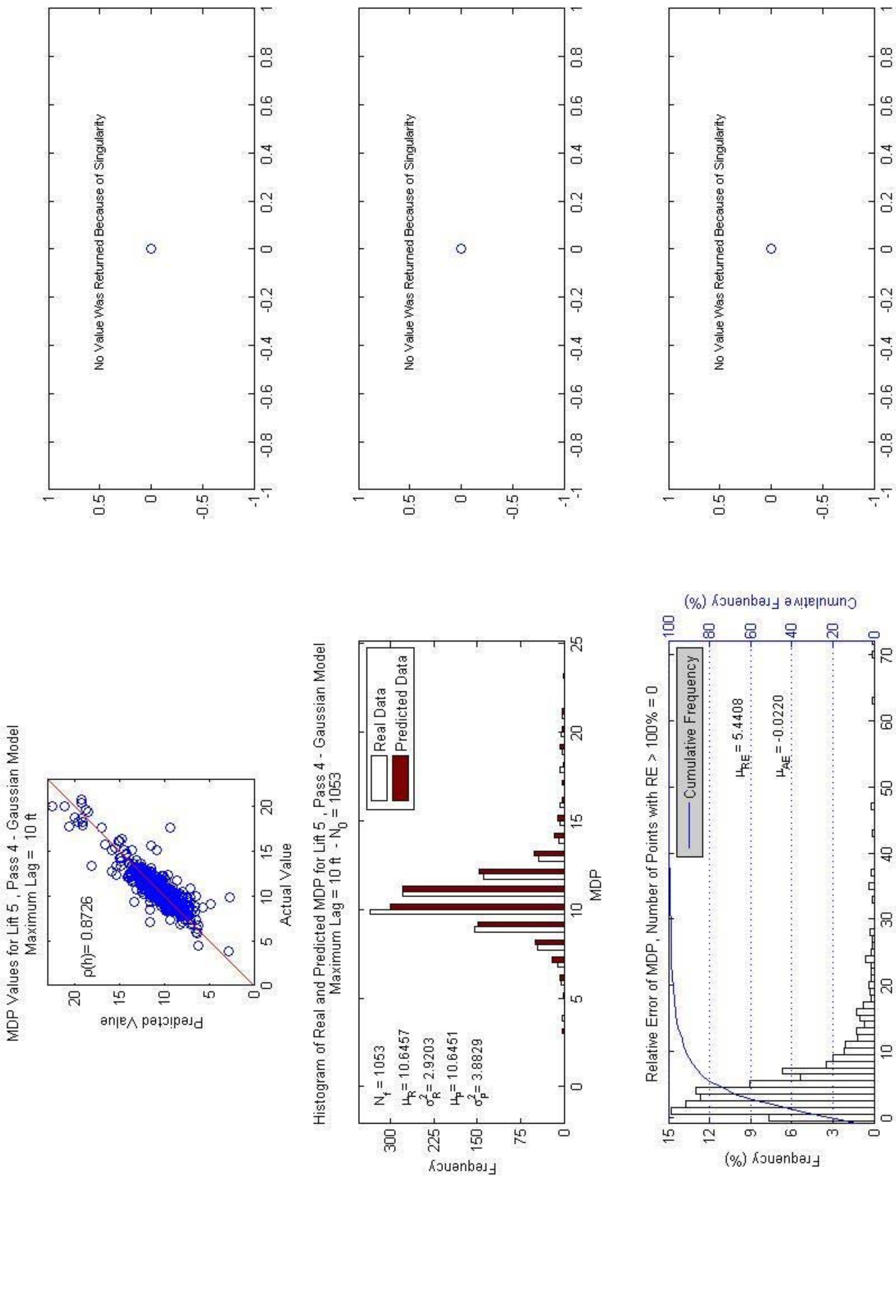

Figure C.87 Kriging results of CCC values for Lift 5, Pass 4/7, using Gaussian model and maximum lag of 3.0 (10 ft)

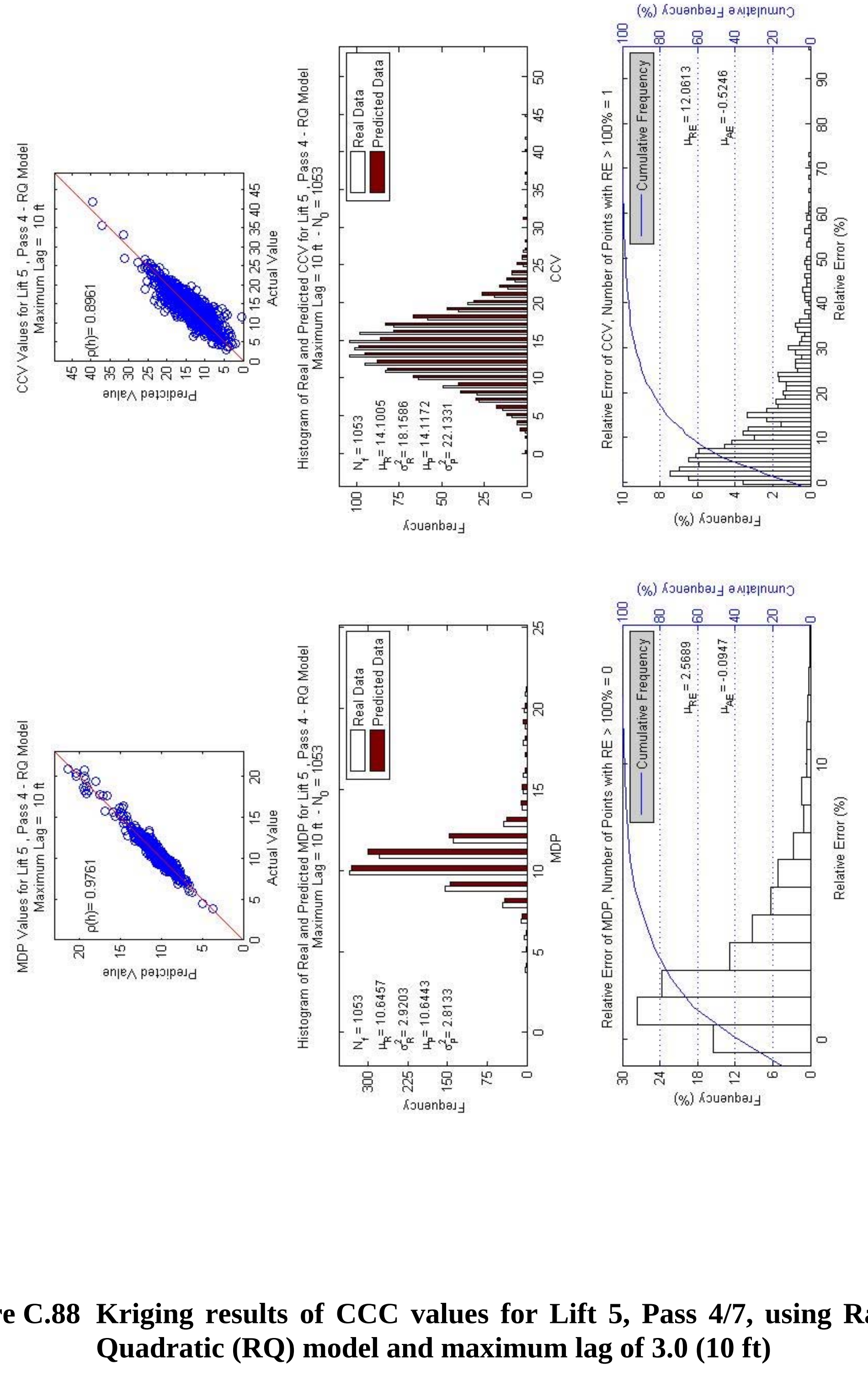

Figure C.88 Kriging results of CCC values for Lift 5, Pass 4/7, using Rational Quadratic (RQ) model and maximum lag of 3.0 (10 ft)

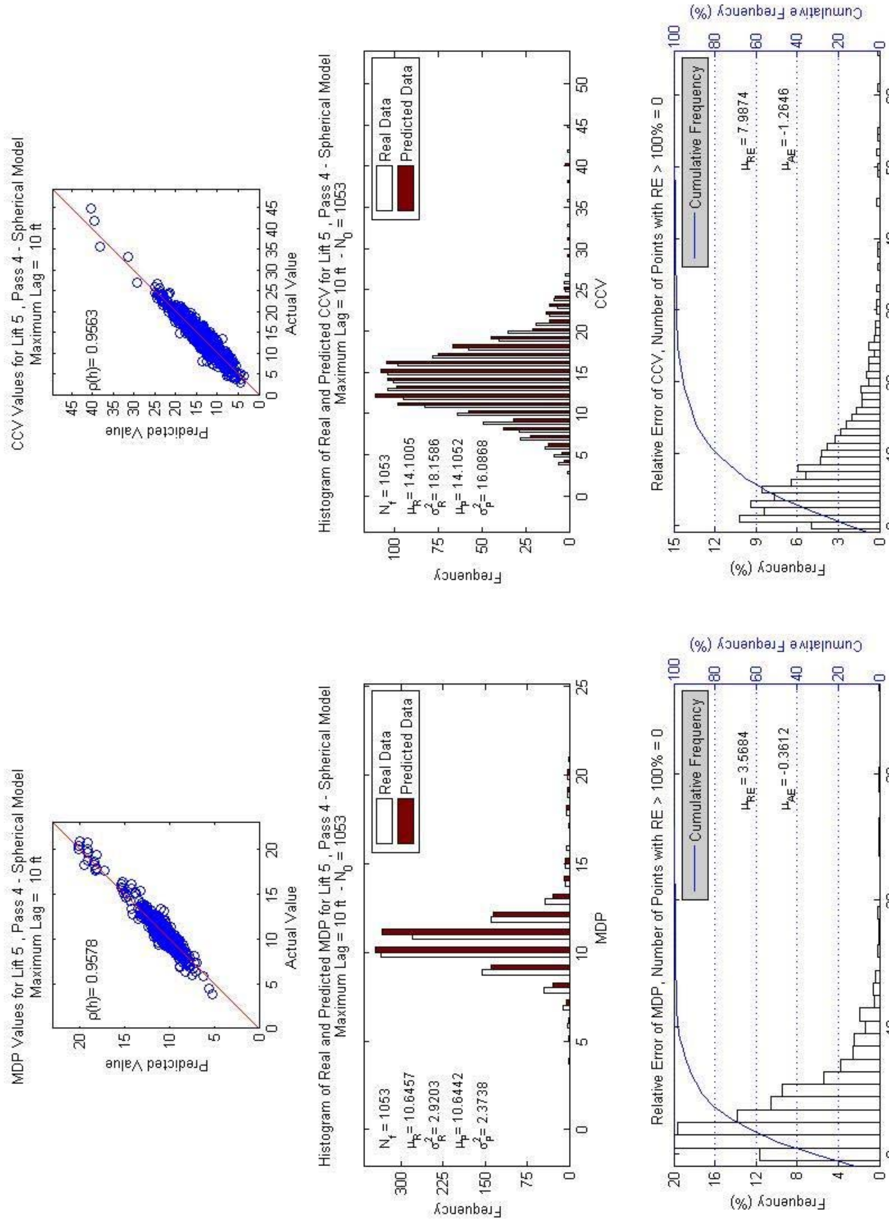

Figure C.89 Kriging results of CCC values for Lift 5, Pass 4/7, using Spherical model and maximum lag of 3.0 (10 ft)

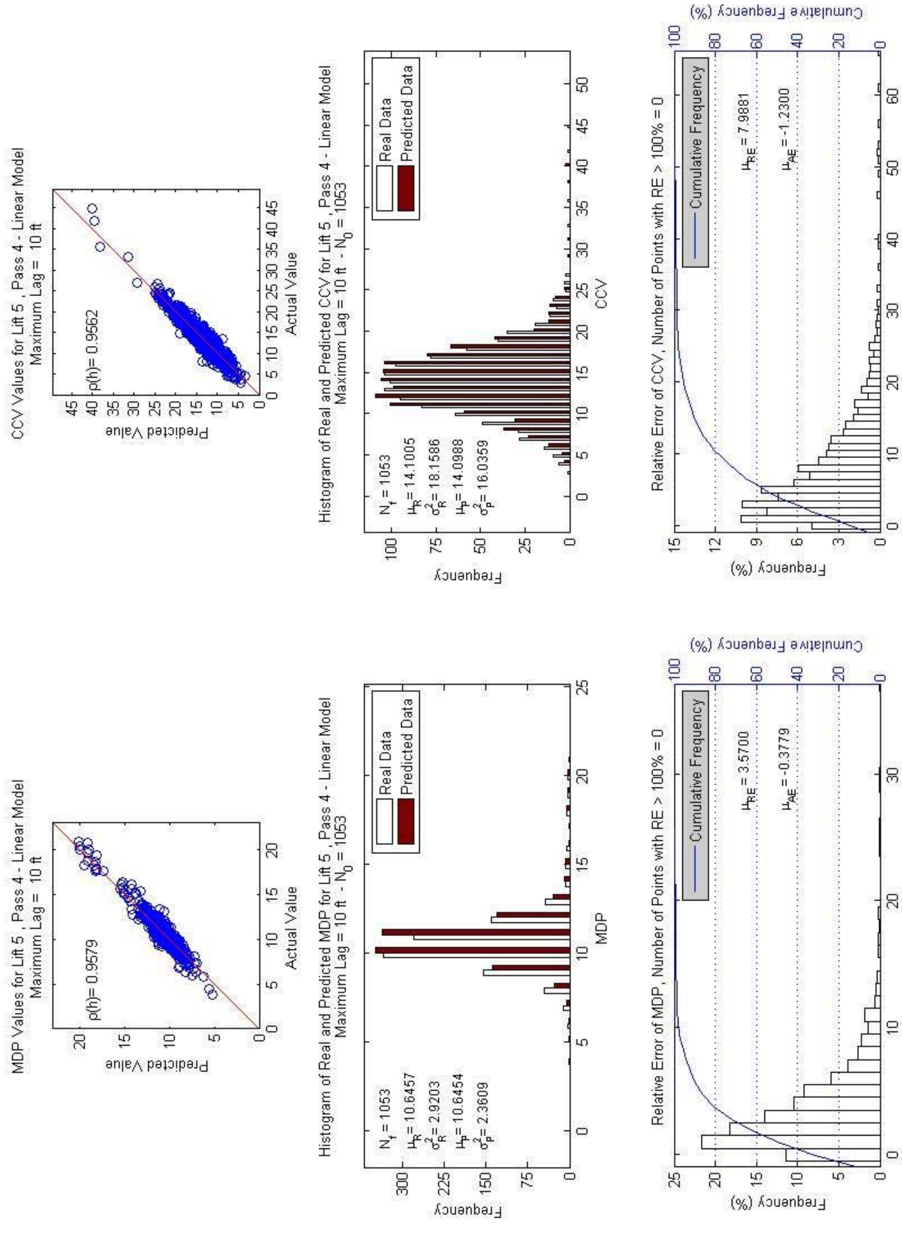

Figure C.90 Kriging results of CCC values for Lift 5, Pass 4/7, using Linear model and maximum lag of 3.0 (10 ft)

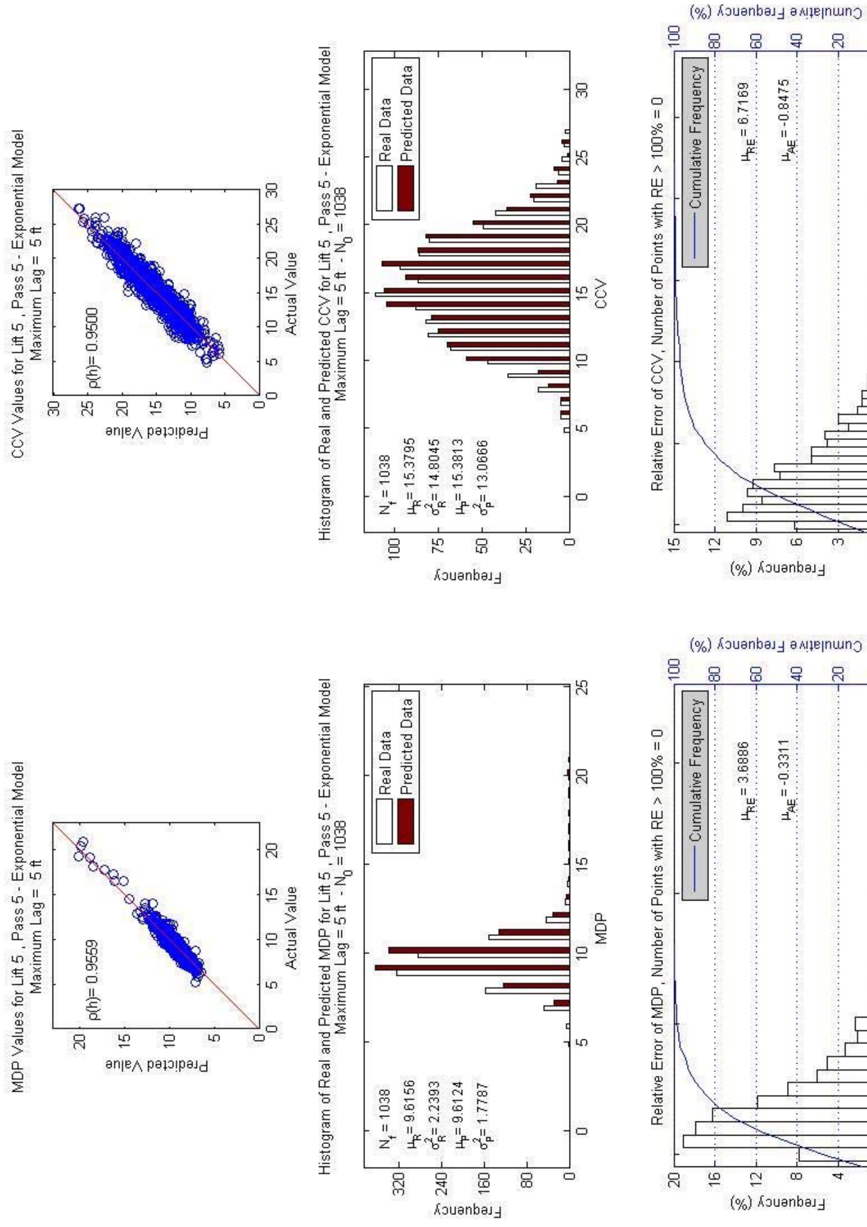

Figure C.91 Kriging results of CCC values for Lift 5, Pass 5/7, using Exponential model and maximum lag of 1.5 (5 ft)

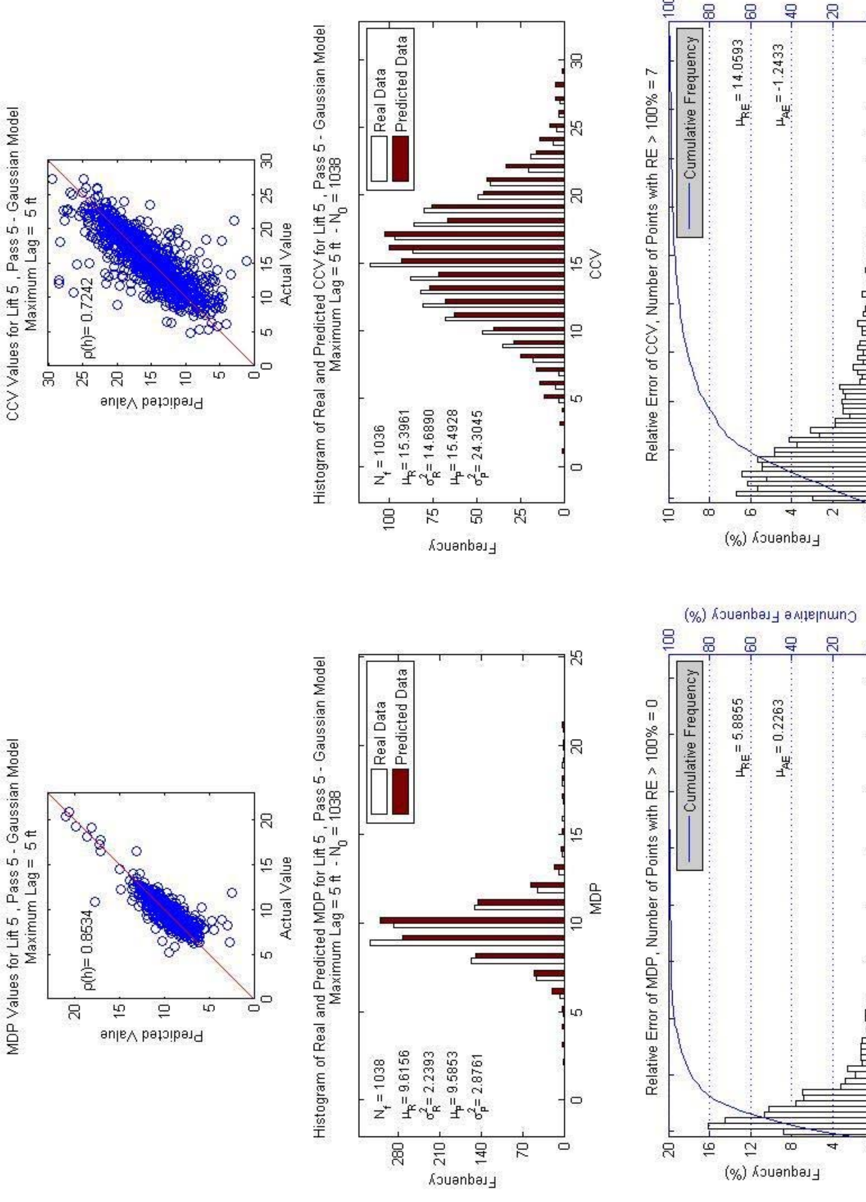

Figure C.92 Kriging results of CCC values for Lift 5, Pass 5/7, using Gaussian model and maximum lag of 1.5 (5 ft)

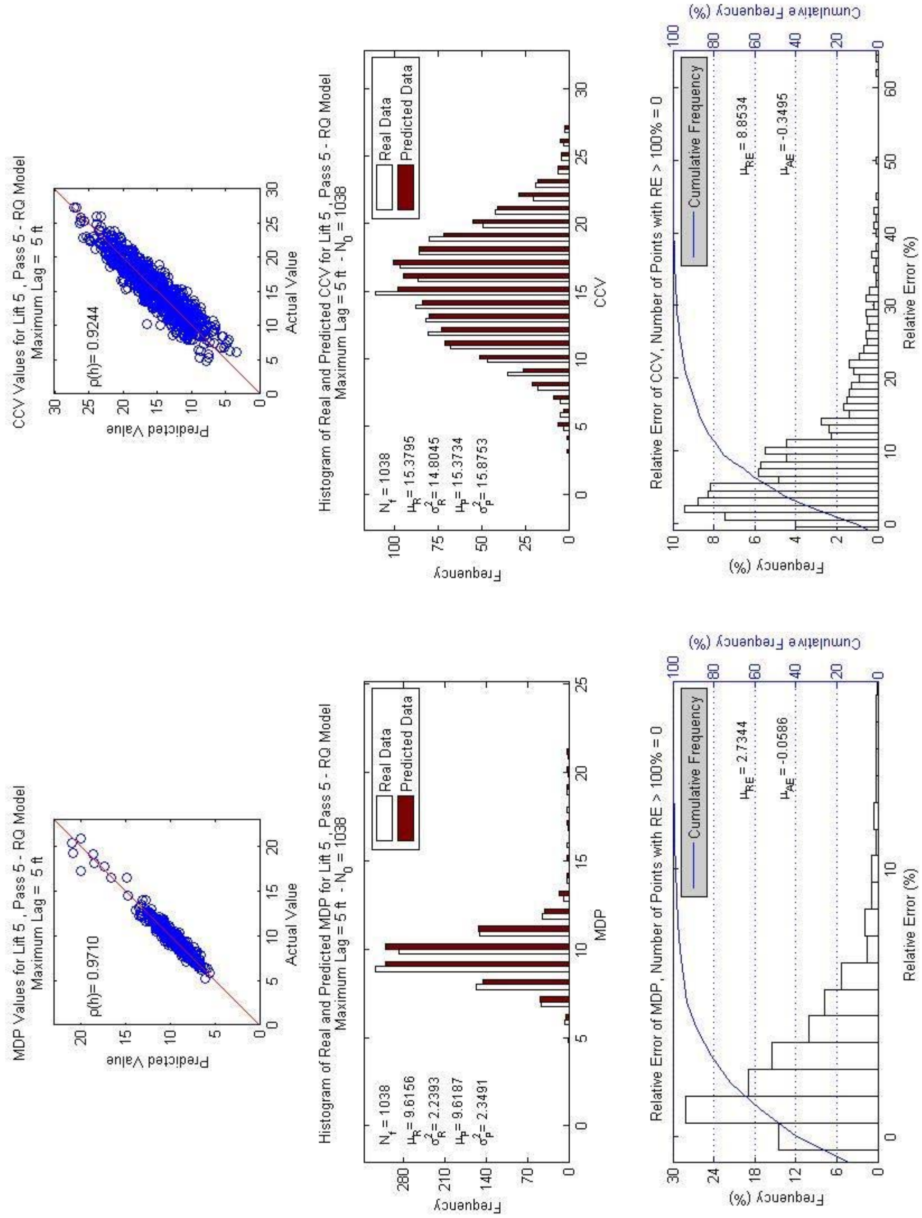

Figure C.93 Kriging results of CCC values for Lift 5, Pass 5/7, using Rational Quadratic (RQ) model and maximum lag of 1.5 (5 ft)

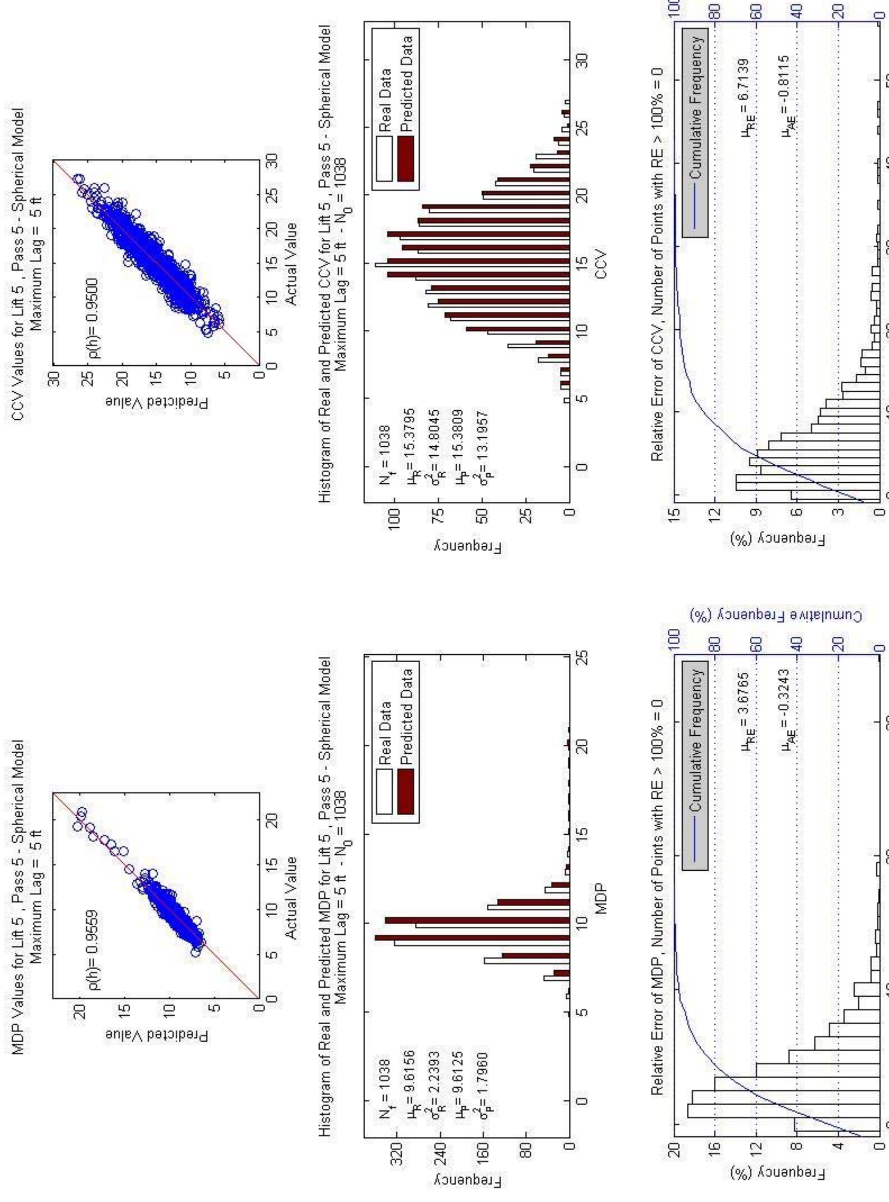

Figure C.94 Kriging results of CCC values for Lift 5, Pass 5/7, using Spherical model and maximum lag of 1.5 (5 ft)

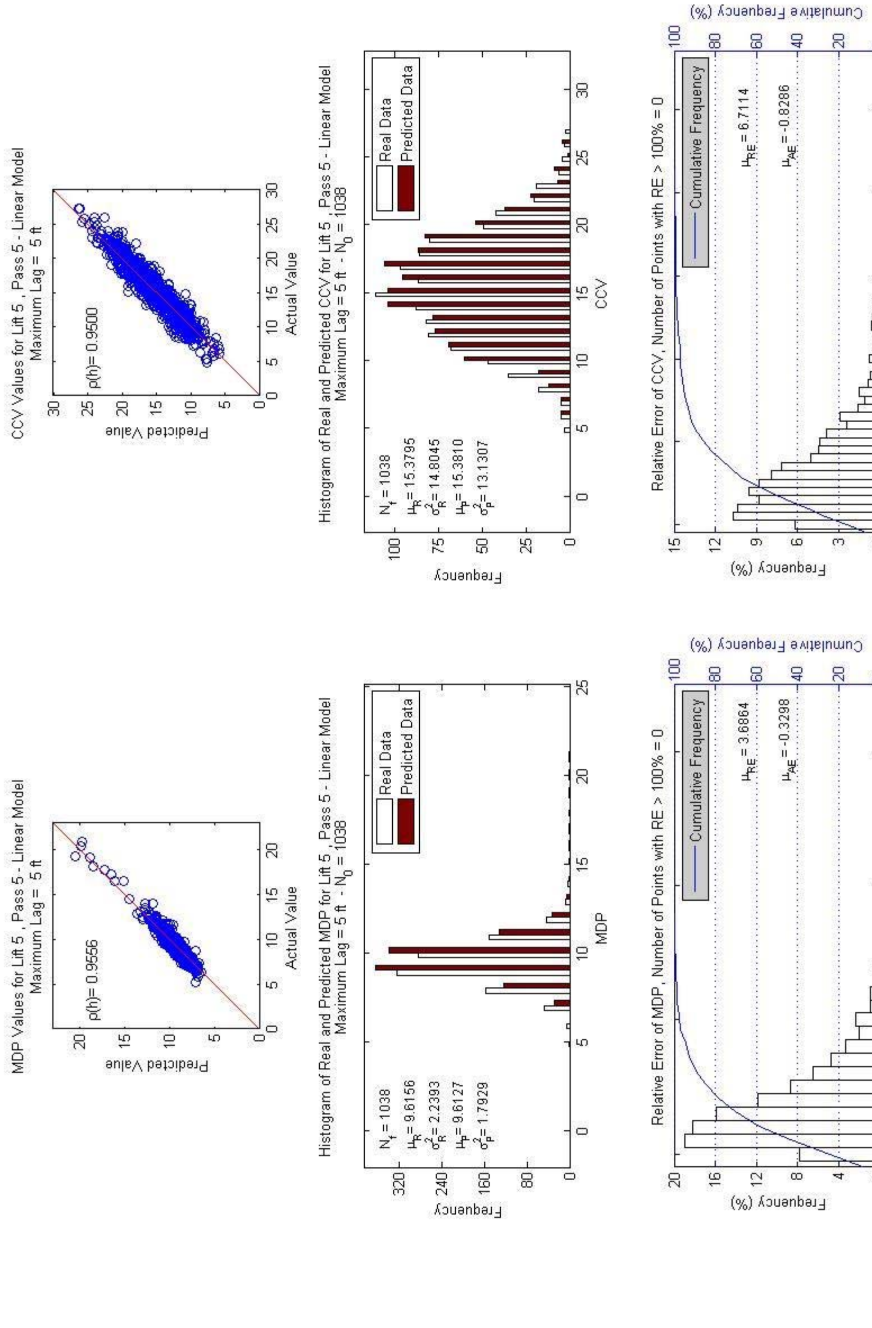

Figure C.95 Kriging results of CCC values for Lift 5, Pass 5/7, using Linear model and maximum lag of 1.5 (5 ft)

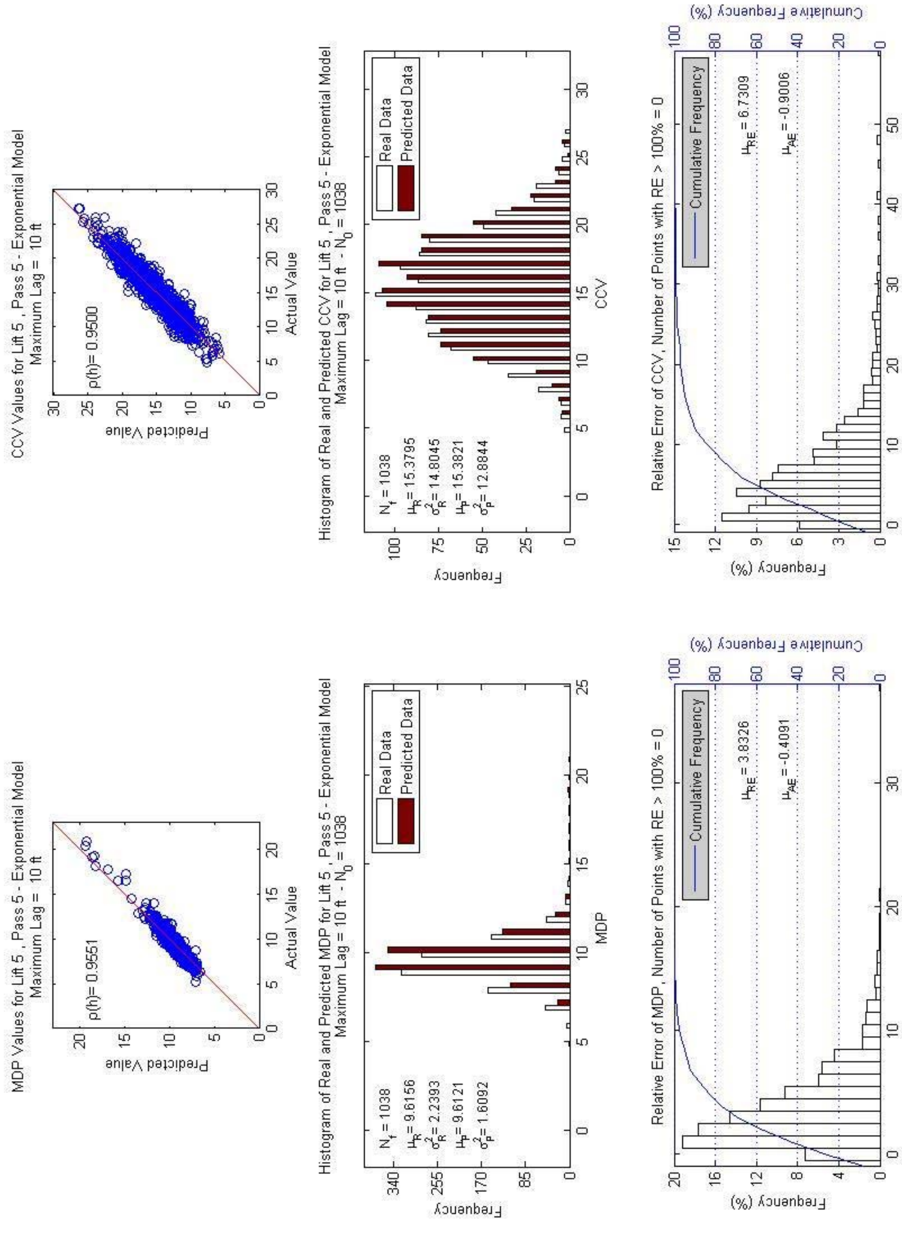

Figure C.96 Kriging results of CCC values for Lift 5, Pass 5/7, using Exponential model and maximum lag of 3.0 (10 ft)

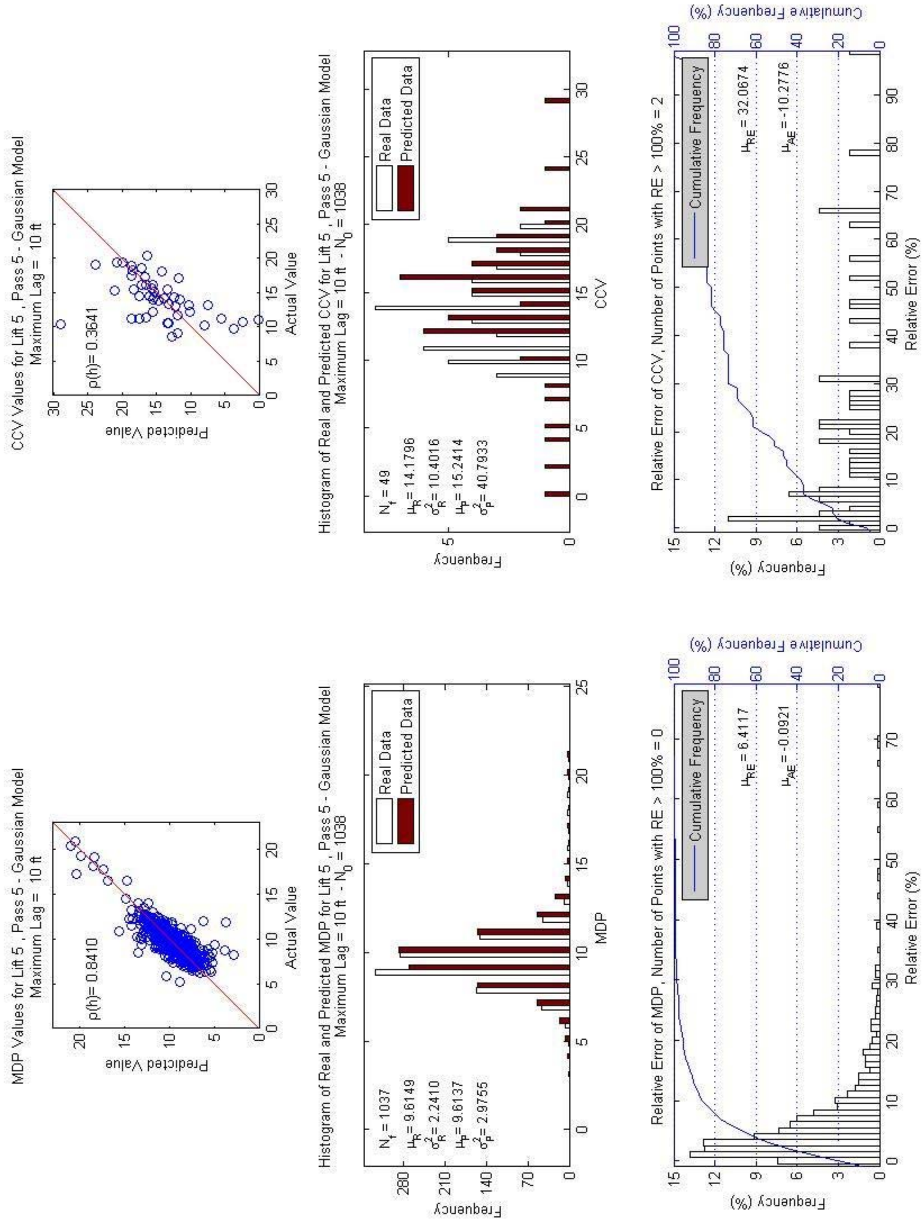

Figure C.97 Kriging results of CCC values for Lift 5, Pass 5/7, using Gaussian model and maximum lag of 3.0 (10 ft)

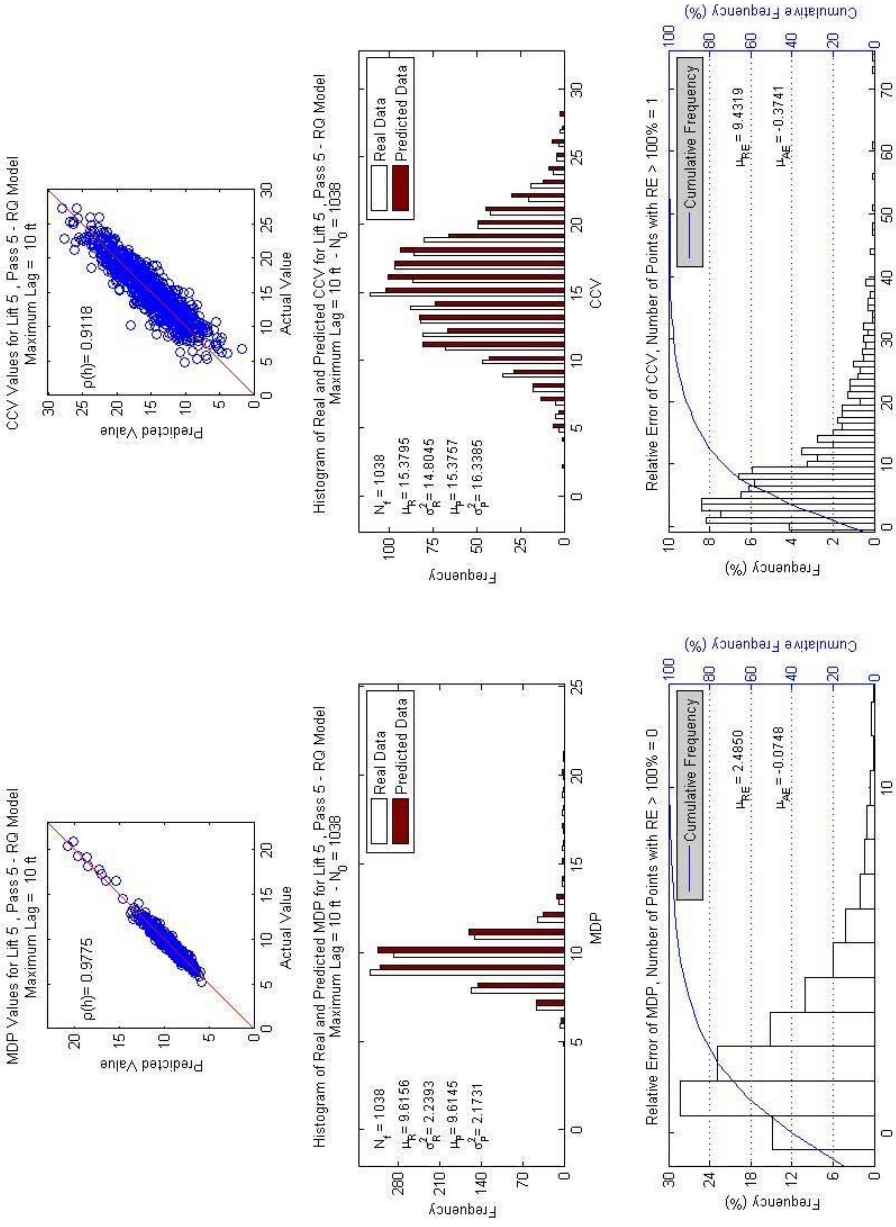

Figure C.98 Kriging results of CCC values for Lift 5, Pass 5/7, using Rational Quadratic (RQ) model and maximum lag of 3.0 (10 ft)

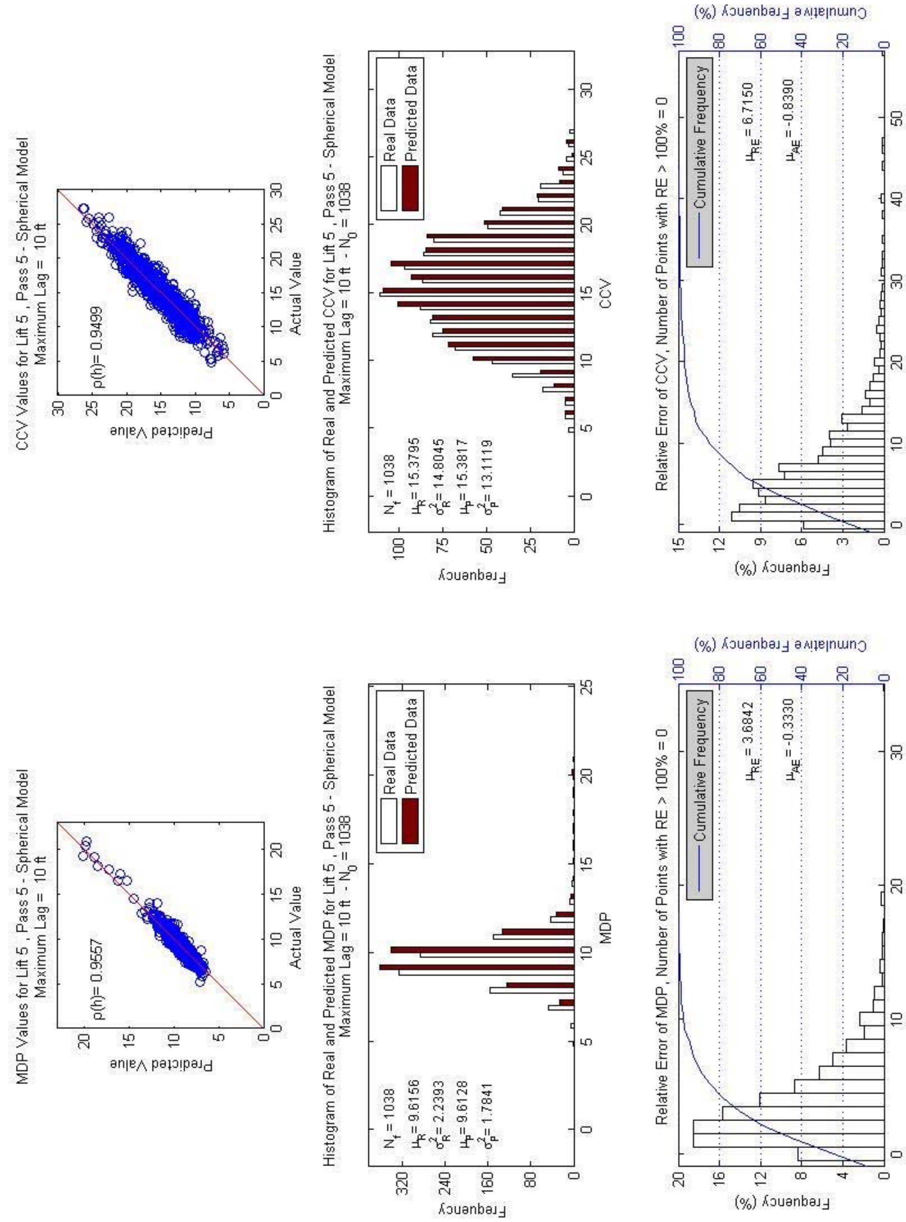

Figure C.99 Kriging results of CCC values for Lift 5, Pass 5/7, using Spherical model and maximum lag of 3.0 (10 ft)

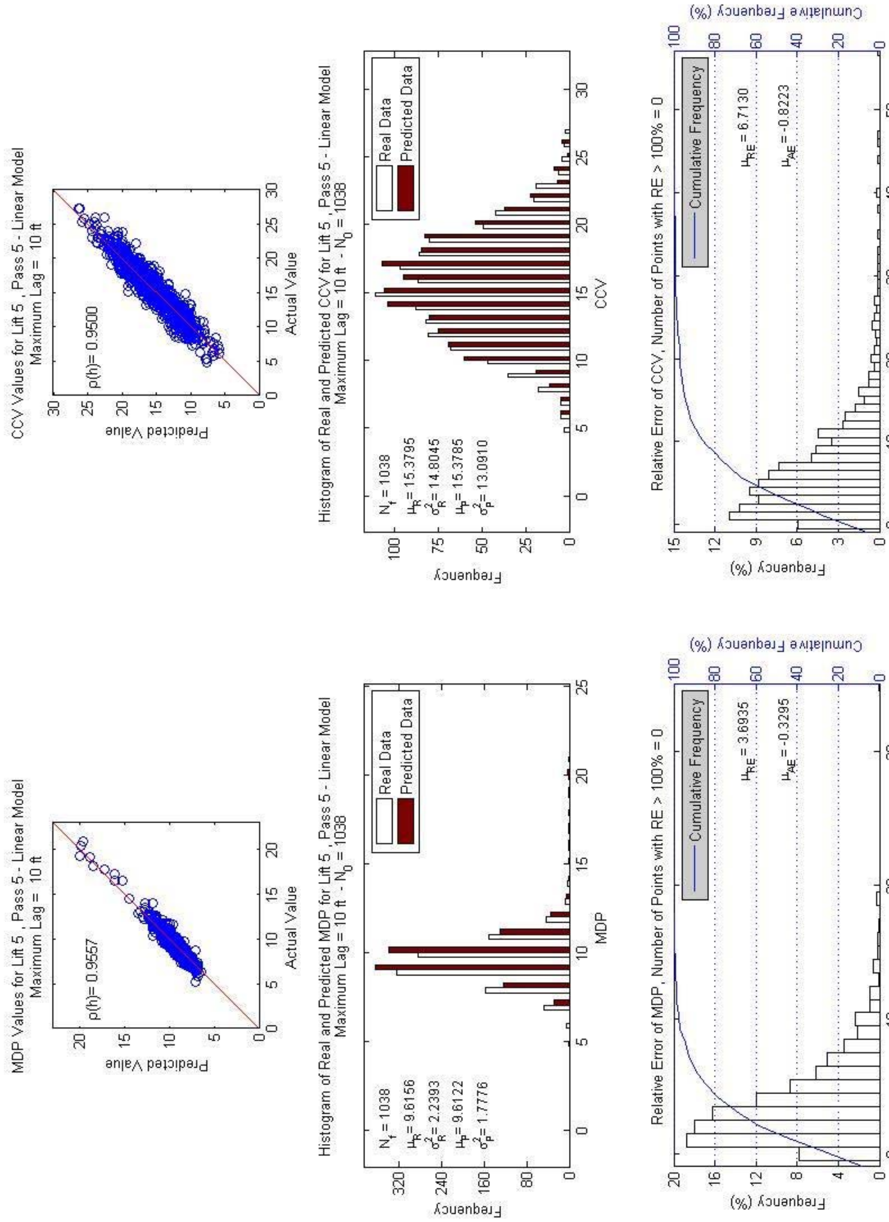

Figure C.100 Kriging results of CCC values for Lift 5, Pass 5/7, using Linear model and maximum lag of 3.0 (10 ft)

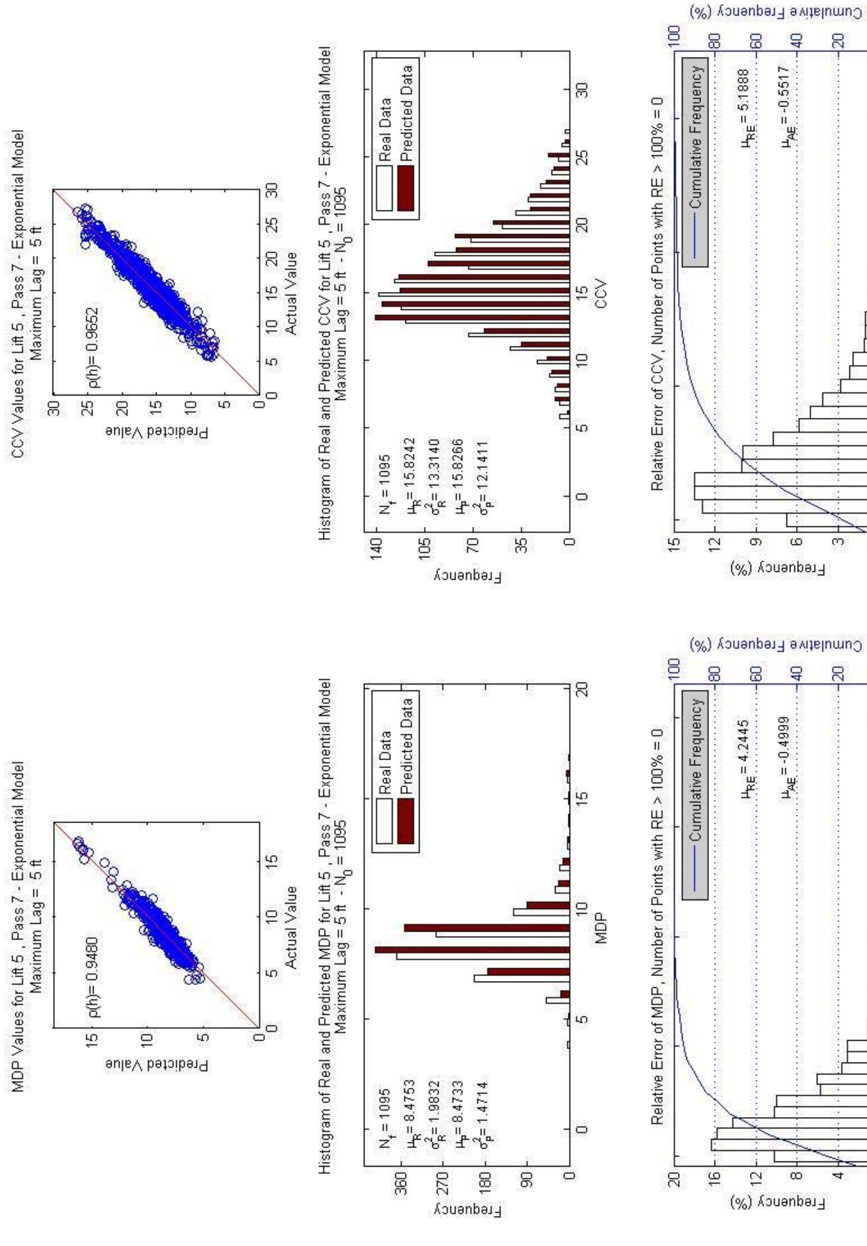

Figure C.101 Kriging results of CCC values for Lift 5, Pass 7/7, using Exponential model and maximum lag of 1.5 (5 ft)

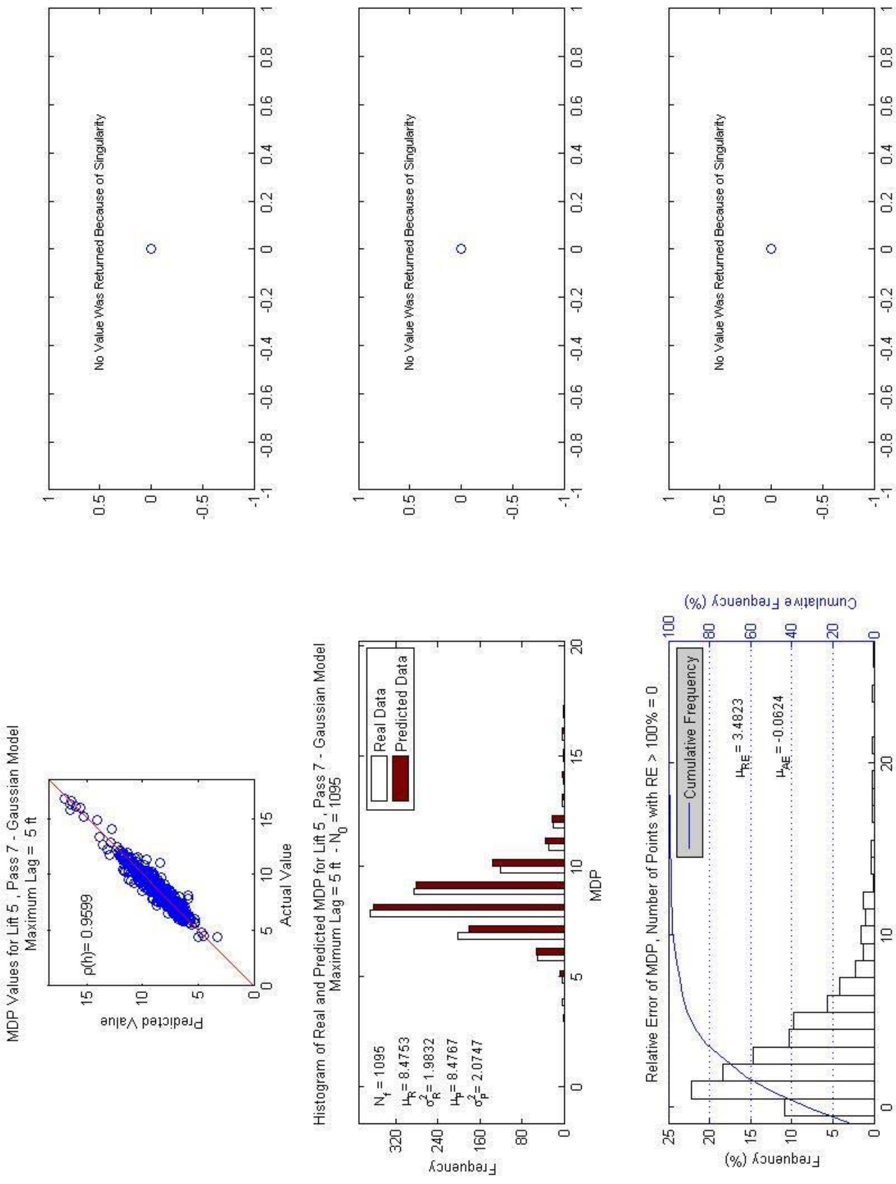

Figure C.102 Kriging results of CCC values for Lift 5, Pass 7/7, using Gaussian model and maximum lag of 1.5 (5 ft)

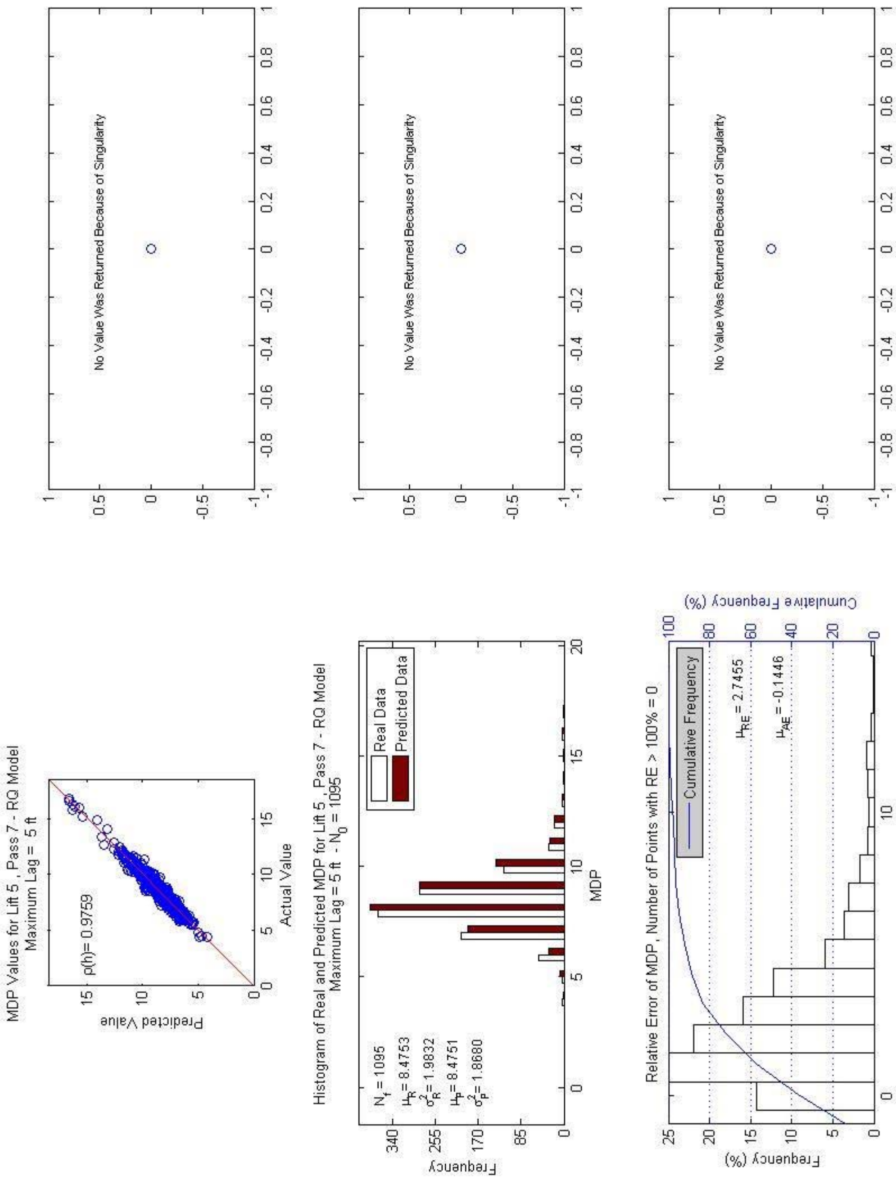

Figure C.103 Kriging results of CCC values for Lift 5, Pass 7/7, using Rational Quadratic (RQ) model and maximum lag of 1.5 (5 ft)

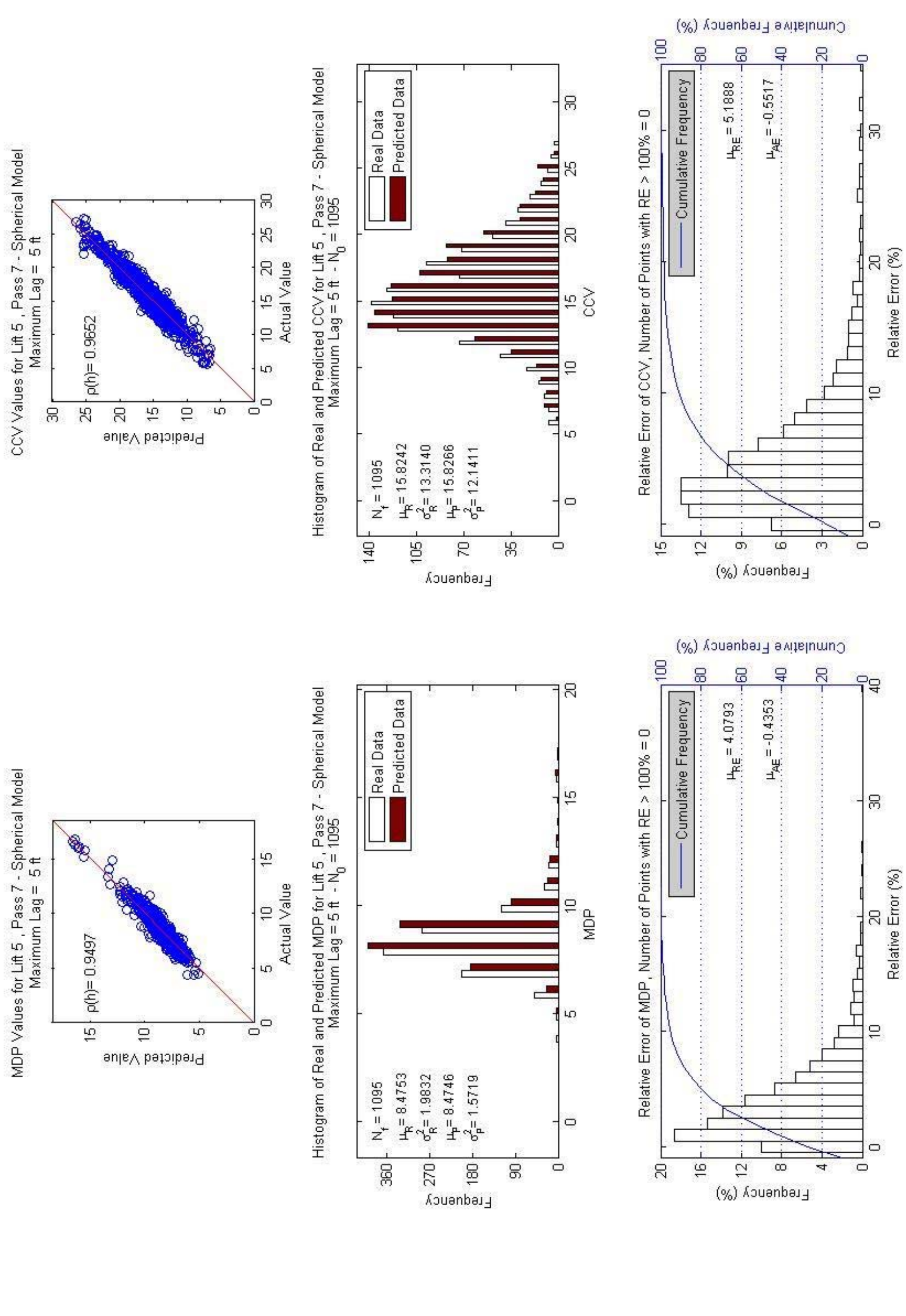

Figure C.104 Kriging results of CCC values for Lift 5, Pass 7/7, using Spherical model and maximum lag of 1.5 (5 ft)

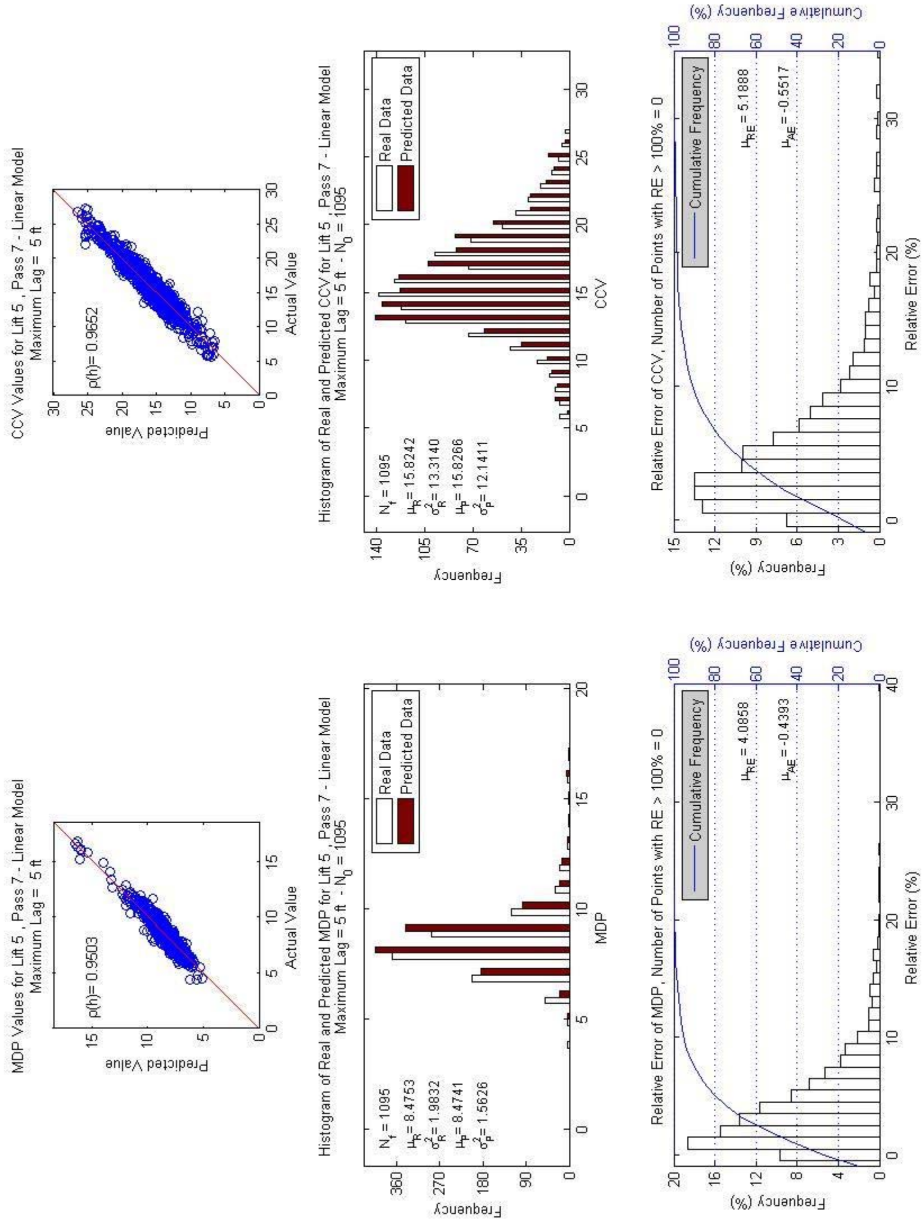

Figure C.105 Kriging results of CCC values for Lift 5, Pass 7/7, using Linear model and maximum lag of 1.5 (5 ft)

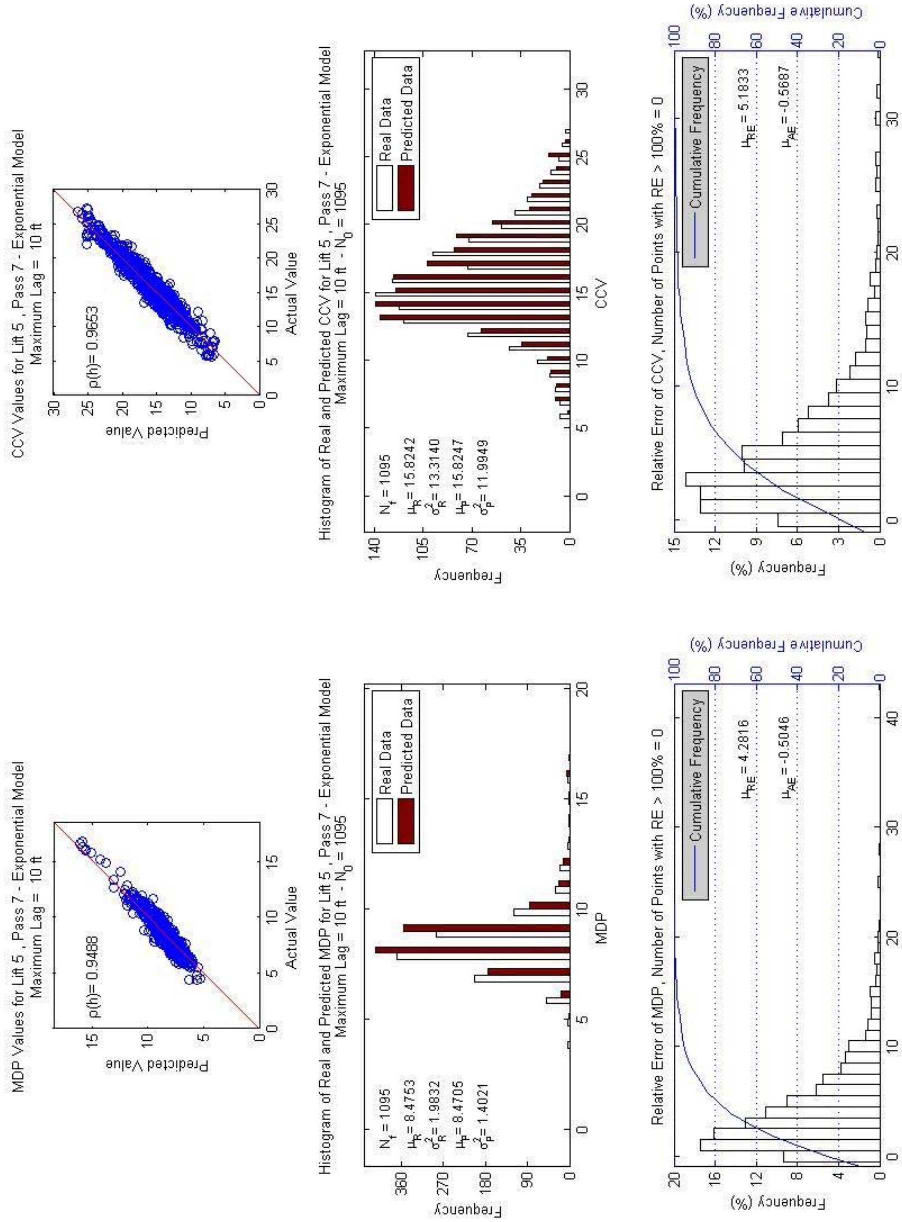

Figure C.106 Kriging results of CCC values for Lift 5, Pass 7/7, using Exponential model and maximum lag of 3.0 (10 ft)

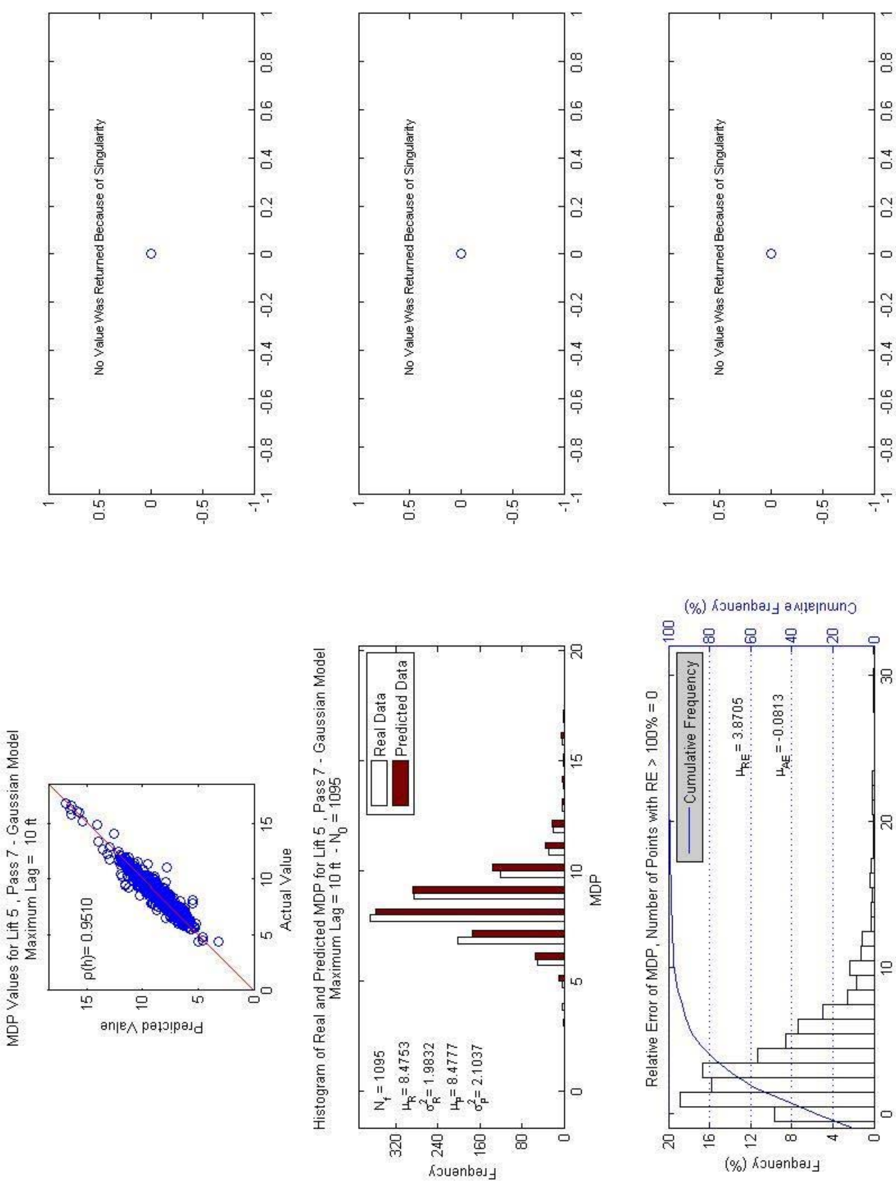

Figure C.107 Kriging results of CCC values for Lift 5, Pass 7/7, using Gaussian model and maximum lag of 3.0 (10 ft)

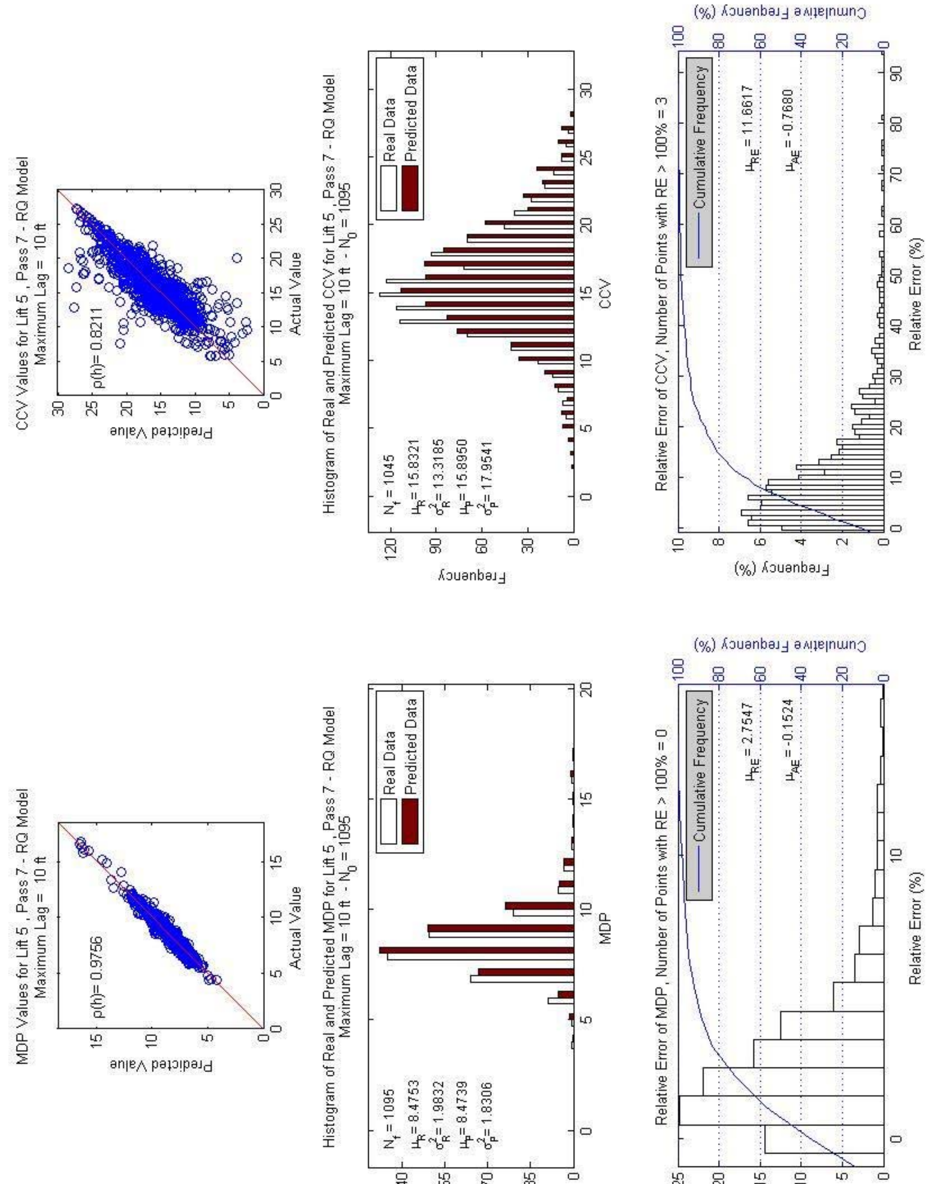

Figure C.108 Kriging results of CCC values for Lift 5, Pass 7/7, using Rational Quadratic (RQ) model and maximum lag of 3.0 (10 ft)

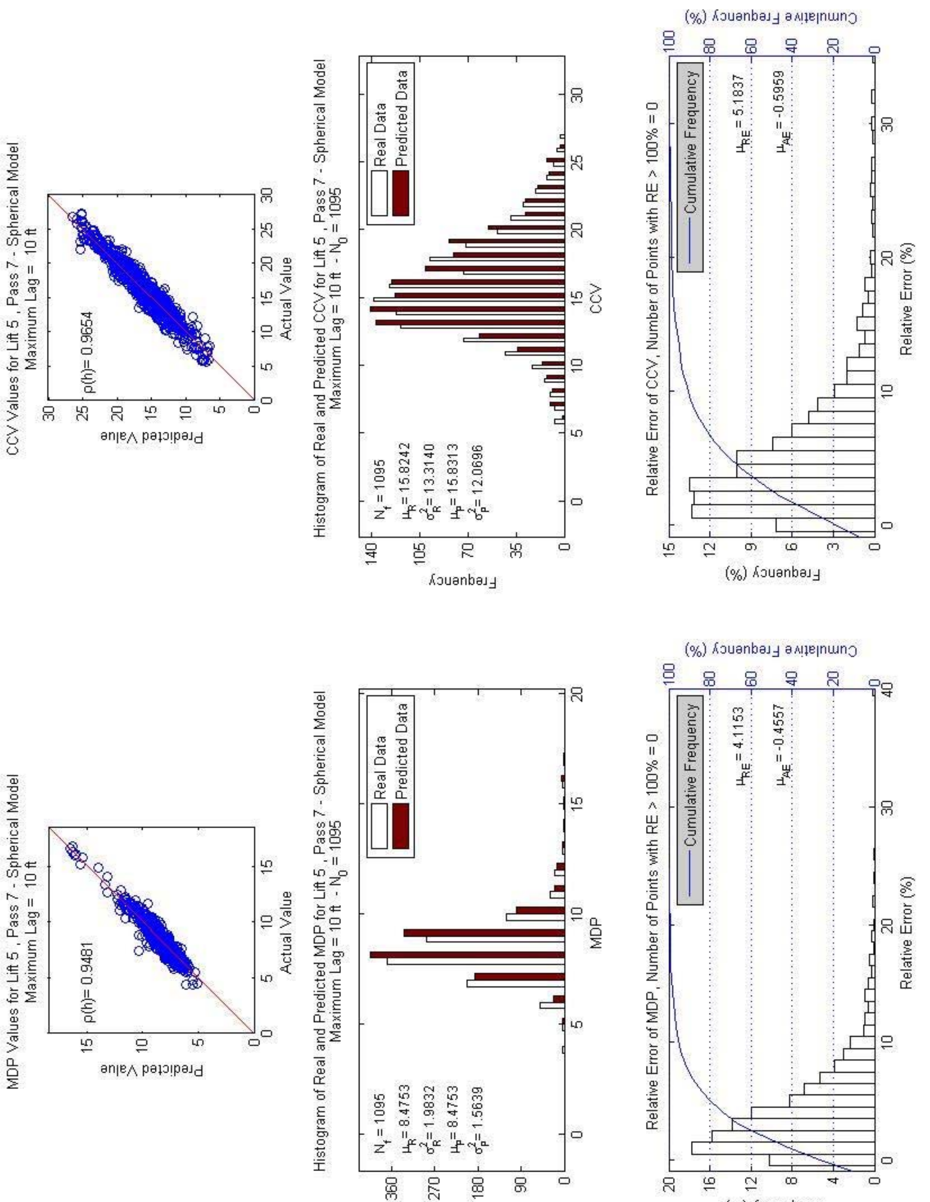

Figure C.109 Kriging results of CCC values for Lift 5, Pass 7/7, using Spherical model and maximum lag of 3.0 (10 ft)

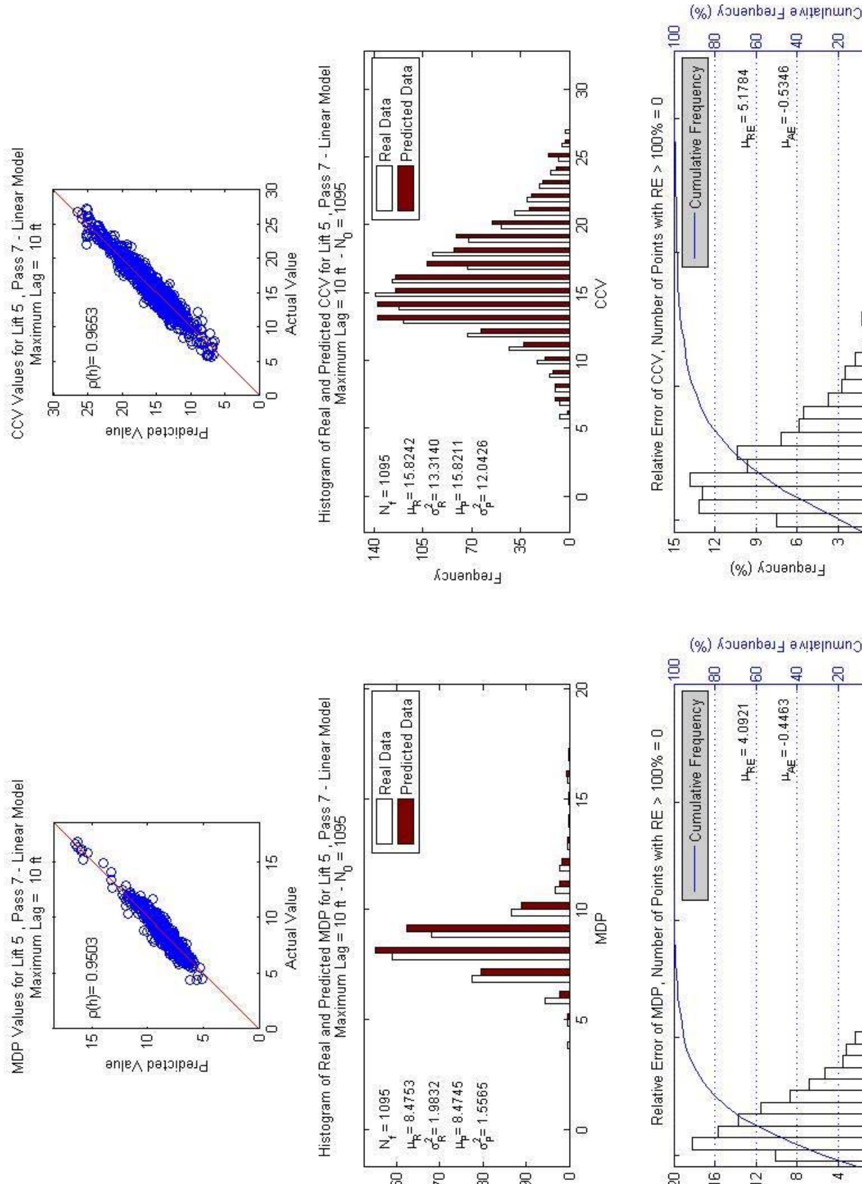

Figure C.110 Kriging results of CCC values for Lift 5, Pass 7/7, using Linear model and maximum lag of 3.0 (10 ft)

REFERENCES

AASHTO (2004). "Standard Method of Test for Family of Curves-One-Point Method." AASHTO T 272, American Association of State Highway and Transportation Officials, Washington, D.C.

Adam, D. (1997). "Continuous Compaction Control (CCC) with Vibratory Rollers." *Proceedings of GeoEnvironment 97*, Melbourne, Australia, Balkema, Rotterdam, 245–250.

Adam, D., and Brandl, H. (2003). "Sophisticated Roller Integrated Continuous Compaction Control." *12th Asian Regional Conference on Soil Mechanics and Geotechnical* Engineering - Geotechnical Infrastructure for the New Millennium, Singapore, 427-430.

Adam, D., and Kopf, F. (1998). "Application of Continuous Compaction Control (CCC) to Waste Disposal Liners." *Proceedings of 3rd International Congress on Environmental Geotechnics*, Lisbon, Portugal, 365-370.

Adam, D., and Kopf, F. (2004). "Operational Devices for Compaction Optimization and Quality Control (Continuous Compaction Control & Light Falling Weight Device)." *Proceedings of the International Seminar on Geotechnics in Pavement and Railway Design and Construction*, Athens, Greece, 97-106.

Alshibli, K. A., Abu-Farsakh, M., and Seyman, E. (2005). "Laboratory Evaluation of the Geogauge and Light Falling Weight Deflectometer as Construction Control Tools." *Journal of Materials in Civil Engineering,* ASCE, 17(5), 560-569.

Anderegg, R. (2000). "ACE Ammann Compaction Expert - Automatic Control of the Compaction." *Proceedings of European Workshop on Compaction of Soils and Granular Materials*, Paris, 229-236.

Anderegg R., and Kaufmann, K. (2004). "Intelligent Compaction with Vibratory Rollers - Feedback Control Systems in Automatic Compaction and Compaction Control." *Transportation Research Record 1868*, Journal of the Transportation Research Board, National Academy Press, 124-134.

Anderegg, R., von Felten, D., and Kaufmann, K. (2006). "Compaction Monitoring Using Intelligent Soil Compactors." *Proceedings of GeoCongress 2006: Geotechnical Engineering in the Information Technology Age*, Atlanta, CD-ROM.

ASTM (1993). "Standard Test Method for Nonrepetitive Static Plate Load Tests of Soils and Flexible Pavement Components, for Use in Evaluation and Design of Airport and Highway Pavements." ASTM D 1196, ASTM International, West Conshohocken, PA.

ASTM (2005). "Standard Test Methods for Density of Soil and Soil-Aggregate in Place by Nuclear Methods (Shallow Depth)." ASTM D 2922, ASTM International, West Conshohocken, PA.

ASTM (2005). "Standard Test Methods for Liquid Limit, Plastic Limit, and Plasticity Index of Soils." ASTM D 4318, ASTM International, West Conshohocken, PA.

ASTM (2005). "Standard Test Method for Water Content of Soil and Rock in Place by Nuclear Methods (Shallow Depth)." ASTM D 3017, ASTM International, West Conshohocken, PA.

ASTM (2006). "Standard Test Method for CBR (California Bearing Ratio) of Laboratory-Compacted Soils." ASTM D 1883, ASTM International, West Conshohocken, PA.

ASTM (2006). "Standard Practice for Classification of Soils for Engineering Purposes (Unified Soil Classification System)." ASTM D 2487, ASTM International, West Conshohocken, PA.

ASTM (2006). "Standard Test Method for Deflections with a Falling-Weight-Type Impulse Load Device ." ASTM D 4694, ASTM International, West Conshohocken, PA.

ASTM (2006). "Standard Test Method for Density and Unit Weight of Soil in Place by the Sand-Cone Method." ASTM D 1556, ASTM International, West Conshohocken, PA.

ASTM (2006). "Standard Test Methods for Laboratory Compaction Characteristics of Soil Using Modified Effort (56,000 ft-lbf/ft^3 (2,700 kN-m/m^3))." ASTM D 1557, ASTM International, West Conshohocken, PA.

ASTM (2006). "Standard Test Methods for Laboratory Compaction Characteristics of Soil Using Standard Effort (12,400 ft-lbf/ft^3(600 kN-m/m^3))." ASTM D 698, ASTM International, West Conshohocken, PA.

ASTM (2006). "Standard Test Method for Laboratory Determination of Water (Moisture) Content of Soil and Rock by Mass." ASTM D 2216, ASTM International, West Conshohocken, PA.

ASTM (2006). “Standard Test Method for Measuring Stiffness and Apparent Modulus of Soil and Soil-Aggregate In-Place by an Electro-Mechanical Method.” ASTM D 6758 , ASTM International, West Conshohocken, PA.

ASTM (2006). “Standard Test Methods for Particle Size (Sieve Analysis) of Plastic Materials.” ASTM D 1921, ASTM International, West Conshohocken, PA.

ASTM (2006). “Standard Test Method for Shear Strength (Dynamic Method) of Hook and Loop Touch Fasteners.” ASTM D 5169 , ASTM International, West Conshohocken, PA.

ASTM (2007). “Standard Practice for Measuring Deflections with a Light Weight Deflectometer (LWD).” ASTM E 2583, ASTM International, West Conshohocken, PA.

Baecher, G.B., Christian, J.T. (2003). *Reliability and Statistics in Geotechnical Engineering,* John Wiley & Sons, Inc., New York.

Bekker, M.G. (1969). *Introduction to Terrain-Vehicle Systems*. University of Michigan Press, Ann Arbor.

Boulanger, R.W. (2002). Geotechnical Engineering Photo Album, http://cee.engr.ucdavis.edu/faculty/boulanger/geo_photo_album/GeoPhoto.html

Brandl, H., and Adam, D. (1997). “Sophisticated Continuous Compaction Control of Soils and Granular Materials.” *Proceedings of 14th International Conference on Soil Mechanics and Foundation Engineering*, Hamburg, Germany, 1–6.

Brandl, H., Adam, D. (2004). “Continuous Compaction Control (CCC) for Fill Dams and Roller Compacted Concrete Dams.” *New Developments in Dam Engineering - Proceedings of 4th International Conference on Dam Engineering*, Nanjing, China, 17-44.

Briaud, J., and Seo, J. (2003). “Intelligent Compaction: Overview and Research Needs.” *Report*, Texas A&M Univ., College Station, Texas.

Camargo, F., Larsen, B., Chadbourn, B., Roberson, R., and Siekmeier, J. (2006). “Intelligent Compaction: a Minnesota Case History.” *Proceedings of 54th Annual Geotechnical Conference*, University of Minnesota, Minneapolis, CD-ROM.

Chang, G., Xu, Q., Merritt , D., White, D. J., Horan, B. (2009). "Accelerated Implementation of Intelligent Compaction Technology for Embankment Subgrade Soils, Aggregate Base, and Asphalt Pavement Materials", *Report*, Federal Highway Administration, Washington D.C.

Cressie, N. A. C. (1993). *Statistics for Spatial Data,* Revised Ed., John Wiley & Sons, Inc., New York.

De Beer, M. (1991). "Use of the Dynamic Cone Penetrometer (DCP) in the Design of Road Structures." *Geotechnics in the African Environment*, Blight et al. (Eds), Balkema, Rotterdam.

DelDOT (2001). *Division 200 Earthwork*, Delaware Department of Transportation.

Draper, N. R., Smith, H., (1998). *Applied Regression Analysis*, 3rd Ed., John Wiley & Sons, Inc., New York.

Forssblad, L. (1980). "Compaction Meter on Vibrating Rollers for Improved Compaction Control." *Proceedings of International Conference on Compaction*, Vol. II, Assoc. Amicale de Ingénieus, Paris, France, 541–546

Hoffmann, O., Guzina, B., and Drescher, A. (2003). *Stiffness Estimates Using Portable Deflectometers,* University of Minnesota ,Minneapolis, Minnesota.

Holtz, R. D., and Kovacs, W. D. (1981). *An Introduction to Geotechnical Engineering*, Prentice-Hall, Inc., Englewoods Cliffs, New Jersey.

Hossain, M., Mulandi, J., Keach, L., Hunt, M., and Romanoschi, S. (2006). "Intelligent Compaction Control." *Proceedings of 2006 Airfield and Highway Pavement Specialty Conference*, ASCE, Atlanta, Georgia, CD-ROM.

Humboldt Mfg. Co. (2000). *GeoGauge (Soil Stiffness/Modulus) user guide*, Version 3.8, Norridge, III.

Isaaks, E.H., and R. M. Srivastava. (1989). *An Introduction to Applied Geostatistics*, Oxford University Press, New York.

Kröber, W., Floss, E., Wallrath, W. (2001). "Dynamic Soil Stiffness as Quality Criterion for Soil Compaction." *Geotechnics for Roads, Rail Tracks and Earth Structures*, A.A.Balkema Publishers, Lisse /Abingdon/ Exton (Pa) /Tokyo, 189-199.

McVay, M.C., and Ko, J. (2005). "Evaluating Thick Lift Limerock-Base Course", *Report,* Florida Department of Transportation, Florida.

Minchin, R., Swanson, D., and Thomas, H. (2005). “Computer Methods in Intelligent Compaction.” *Proceedings of 2005 International Conference on Computing in Civil Engineering*, Cancun, Mexico, CD-ROM

Mooney, M. A., and Adam, D. (2007). “Vibratory Roller Integrated Measurement of Earthwork Compaction: An overview.” *Proceedings of 7th International Symposium on Field Measurements in Geomechanics - FMGM 2007*, ASCE, Boston, Massachusetts, CD-ROM.

Mooney, M. A. and Rinehart, R. (2007).”Field Monitoring of Roller Vibration during Compaction of Subgrade Soil.” *Journal of Geotechnical and Geoenvironmental Engineering*, ASCE, 133(3), 257-265.

Nohse, Y., Uchiyama, K., Kanamori, Y., Kase, J., Kawai, Y., Masumura, K., and Tateyama, K. (1999). “An Attempt Applying a New Control System for the Vibratory Compaction Using GPS and CMV in the Embankment Construction (Part 1).” *Proceedings of the 13th International Conference of the ISTVS*, Okinowa, Japan, 295-300.

Oetken N., Personal Communication, Design Engineer, Advanced Design Group, Caterpillar Global Paving – Minneapolis., 07/06/2009.

Petersen, D., Siekmeier, J., Nelson, C., and Peterson, R. (2006). “Intelligent Soil Compaction-Technology, Results and a Roadmap Toward Widespread Use.” *Proceedings of Annual Transportation Research Board Meeting*, Transportation Research Board, Washington, D.C., CD-ROM.

Rahman, F., Hossain, M., Hunt, M. M., Romanoschi, S. A. (2007). “Intelligent Compaction Control of Highway Embankment Soil.”, *86th Annual Meeting of the Transportation Research Board*, National Research Council, Washington, D.C., CD-ROM

Rawlings, J. O., Pantula, S. G., Dickey, D. A. (1998). *Applied Regression Analysis (A Research Tool)*, 2nd Ed., Springer, New York.

Rivoirard, J (1987).”Two Key Parameters When Choosing the Kriging Neighborhood.” *Journal of Mathematical Geology*, Springer, 19, 851-856.

Sandström, Å. (1993). “Oscillatory Compaction.” *Proceedings of 11th IRF World Road Congress*, Madrid, Spain, 957-961.

Sandström, A., and Pettersson, C. (2004). “Intelligent Systems for QA/QC in Soil Compaction.” *Proceedings of Annual Transportation Research Board Meeting*, Transportation Research Board, Washington, D.C., CD- ROM.

Schervish, M. J. (1996). "P Values: What They Are and What They Are Not." *The American Statistician*, American Statistical Association, 50 (3) 203-206

Schuring, D. J. (1966). "The Energy Loss of a Wheel." *Proceedings of 2nd International Terrain-Vehicle Systems*, Toronto University Press, Quebec City, Quebec, Canada.

Tehrani, F. S., Meehan, C. L. (2009), "Continuous Compaction Control: Preliminary Data from a Delaware Case Study", *8th International Conference on the Bearing Capacity of Roads, Railways, and Airfields*, Champaign, Illinois, 745-754.

Thompson, M., and White, D. J. (2007). "Field Calibration and Spatial Analysis of Compaction Monitoring Technology Measurements." *Transportation Research Record 2004*, Transportation Research Board, Washington, D.C., 69–79.

Thompson, M., and White, D. J. (2008). "Estimating Compaction of Cohesive Soils from Machine Drive Power." *Journal of Geotechnical Geoenvironmental Engineering*, ASCE, 134(12), 1771–1777.

Thurner, H. (1993). "Continuous Compaction Control - Specifications and Experience." *Proceedings of 11th IRF World Congress*, Madrid, Spain, 951-956.

Thurner, H., and Sandström, A. (1980). "A New Device for Instant Compaction Control." *Proceedings of International Conference on Compaction*, Vol. II, Assoc. Amicale de Ingénieus, Paris, 611–614.

Thurner, H., Sandström, Å. (2000). "Continuous Compaction Control, CCC." *Workshop on Compaction of Soils and Granular Materials, Modeling of Compacted Materials, Compaction Management and Continuous Control*, International Society of Soil Mechanics and Geotechnical Engineering (European Technical Committee), Paris, France, 237-246.

Uchiyama, K., Kanamori, Y., Nohse, Y., and Mitsui, A. (1998). "Influence of Soil Compaction of Vibrating Rollers with Different Vibration Mechanisms." *Proceedings of the 5th Asia-Pacific Regional Conference of the ISTVS*, Okinawa, Japan, 112-119.

White, D. J., and Thompson, M. (2008). "Relationships Between In-situ and Roller-Integrated Compaction Measurements for Granular Soils." *Journal of Geotechnical Geoenvironmental Engineering*, ASCE, 134(12), 1763–1770.

White, D. J., Jaselskis, E., Schaefer, V., and Cackler, E. (2005). "Real-time Compaction Monitoring in Cohesive Soils from Machine Response." *Transportation Research Record 1936*, Transportation Research Board, Washington, D.C., 173–180.

White, D. J., Thompson, M., and Vennapusa, P. (2007). "Field Validation of Intelligent Compaction Monitoring Technology for Unbound Materials." *Final Report*, Minnesota Department of Transportation, Maplewood, Minnesota.

White, D. J., Thopmson, M., Vennapusa, P., and Siekmeier, J. (2008). "Implementing Intelligent Compaction Specifications on Minnesota TH 64: Synopsis of Measurement Values, Data management, and Geostatistical Analysis." *Transportation Research Record 2045*, Transportation Research Board, 1-9.

White, D. J.., Vennapusa, P. K. R., Gieselman, H. H., Johanson, L., Siekmeier, J. (2009). "Alternatives to Heavy Test Rolling for Cohesive Subgrade Assessment", *8th International Conference on the Bearing Capacity of Roads, Railways, and Airfields*, Champaign, Illinois, 45-55.

Yoo, T-S., and Selig, E. T. (1979). "Dynamics of Vibratory-Roller Compaction." *Journal of Geotechnical Engineering Division*, 105(10), 1211–1231.

Delaware Center for Transportation
University of Delaware
Newark, Delaware 19716

AN EQUAL OPPORTUNITY/AFFIRMATIVE ACTION EMPLOYER
The University of Delaware is committed to assuring equal opportunity to all persons and does not discriminate on the basis of race, creed, color, gender, age, religion, national origin, veteran or handicapped status, or sexual orientation in its educational programs, activities, admissions or employment practices as required by Title IX of the Educational Amendments of 1972, Section 504 of the Rehabilitation Act of 1973, Title VII of the Civil Rights Act of 1964, and other applicable statutes. Inquiries concerning Section 504 compliance and information regarding campus accessibility should be referred to the Americans with Disabilities Act (ADA) Coordinator, 831-4643, located at 413 Academy Street. Inquiries concerning Title VII and Title IX should be referred to the Office of the Assistant Vice President for Affirmative Action, 831-8735, located at 124 Hullihen Hall.